University of Nevada, Reno

Molecular responses of grapevine to environmental stress

A dissertation submitted in partial fulfillment of the requirements for the degree of Doctor of Philosophy in Biochemistry

By

Haley S. Toups

Dr. Grant R. Cramer/ Dissertation Advisor

August 2021

THE GRADUATE SCHOOL

We recommend that the dissertation
prepared under our supervision by

HALEY S. TOUPS

entitled

Molecular responses of grapevine to environmental stress

be accepted in partial fulfillment of the
requirements for the degree of

DOCTOR OF PHILOSOPHY

Grant Cramer, Ph.D.
Advisor

Jeffrey Harper, Ph.D.
Committee Member

Dylan Kosma, Ph.D.
Committee Member

Ian Wallace, Ph.D.
Committee Member

Felipe Barrios Masias, Ph.D.
Graduate School Representative

David W. Zeh, Ph.D., Dean
Graduate School

August, 2021

ABSTRACT

In the past decade, advances in sequencing and transcript quantification technology have progressed science through the genomic era into the big data era, yielding thousands of studies examining plant gene expression in response to a vast assortment of conditions. Understanding and characterization of *Vitis* (grapevine) has been vastly improved with modern technology. Grapevines are a culturally and economically important crop susceptible to abiotic and biotic stresses. The *Vitis* genus consists of tens of thousands of varieties each belonging on a spectrum of tolerance and susceptibility to different stress conditions. Two genes (*VviERF6L1* and *NCED3*) were previously identified from microarray and RNA-Sequencing experiments and implicated in abiotic stress response but required further investigation and characterization in grapevine. The examination of these genes as hub genes in ABA signaling and stress response employed multi-level analyses of DNA, RNA, protein, and metabolite quantification in diverse *Vitis* species including *Vitis vinifera* cv. Cabernet Sauvignon (CS), *Vitis champinii* cv. Ramsey (RA), *Vitis riparia* cv. Riparia Gloire (RI), and *Vitis vinifera* x *Vitis girdiana* cv. SC2 (SC).

First, a bioinformatics approach was used to annotate ABA response elements (ABREs) across all promoter regions in the PN40024 reference genome. ABREs were highly abundant and in the majority of PN40024 promoter regions. Various ABREs were identified in the *ERF6L1* and *NCED3* promoter regions contributing to the understanding of previous transcriptional changes observed in response to abiotic stresses. Many novel and uncharacterized genes were also identified with high numbers of ABREs in respective

promoter regions that may provide valuable targets for future studies to improve grapevine breeding programs and abiotic stress tolerance.

Meta-data analysis of publicly available microarray and RNA-Sequencing data identified the *VviERF6L* clade to transcriptionally respond to numerous stimuli including water deficit, cold, salinity, pathogen infection, wounding, and berry ripening. *VviERF6Ls* were expressed in many tissues including leaves, roots, and berries. Although *VviERF6L1* overexpression vines did not have any obvious quantifiable morphological phenotype, the majority of genes differentially expressed in response to *VviERF6L1* overexpression were involved in pathogen response. Cis-acting elements like the WBOXATNPR1 in the *VviERF6L1* promoter region further implicated a role of *VviERF6L1* in pathogen response. This hypothesized function was also supported by known effects of *ERF5* and *ERF6 Arabidopsis thaliana* orthologs on pathogen susceptibility. To test the functional role of *VviERF6L1* in pathogen response, a grapevine-optimized *P. syringae* infection assay was established. *VviERF6L1* was demonstrated to have significantly higher transcript abundance in response to *P. syringae* infection than mock infection. Additionally, *VviERF6L1* overexpression vines had significantly fewer colony-forming units during *P. syringae* infection and thereby higher resistance to the pathogen than empty vector control vines.

NINE-CIS-EPOXYCAROTENOID DIOXYGENASE (*NCED3)* transcripts, NCED3 protein, and abscisic acid (ABA) concentration were quantified using RNA-Sequencing and RT-qPCR, western blots, and HPLC-MS/MS, respectively, in the leaves and roots of the four *Vitis* species in response to three different water deficit severities. *NCED3* was identified as the only ABA metabolism gene that was a hub gene during water deficit

response. *NCED3* and ABA metabolism were validated as a major part of the core water deficit responses in the four *Vitis* species. However, ABA metabolism was highly dependent on species, organ, stress severity, and stress duration during water deficit. Interestingly, *NCED3* transcript abundance paralleled ABA concentration, but this similarity was not maintained for NCED3 protein, concentrations of which did not significantly change in response to water deficit. Overall, the Texan grapevine, RA, was found to respond earlier and more sensitively during longer-term moderate and severe water deficits than the other more water deficit sensitive species.

Altogether, this work furthered the understanding of two genes involved in stress response in grapevine. *VviERF6L1* was identified to have a role in abiotic and biotic stress response, but the mechanism of *VviERF6L1* in pathogen response requires further investigation. *NCED3* was confirmed as an ABA signaling hub during water deficit with specific expression and downstream ABA concentrations being highly dependent upon species, organ, and stress conditions. However, NCED3 protein abundance response to water deficit requires further examination. These genes provide useful targets for future studies and may have applications in breeding programs to improve grapevine stress tolerance.

ACKNOWLEDGEMENTS

I would like to thank my family for their endless love and support. To my parents, John and Becky Toups, who made me who I am. You instilled in me a love of nature and a curiosity to understand how it works. I would not be where I am today without you. To my sister, Emily Toups, no one has ever fought harder for, with, or against me. I will be forever grateful for it all.

I would like to thank Dr. Grant Cramer for welcoming me into his lab as an undergraduate and offering me the opportunity to continue through graduate school to obtain my PhD. Thank you for pushing me to be an independent worker as well as lending me the chance to travel the world and work with amazing scientists. I would also like to thank my committee members for their time as well as the Biochemistry Department's laboratory managers and other graduate students for their assistance.

This dissertation would not have been possible without the guidance of the Post-Doctoral fellows I had the opportunity to work with and learn from throughout this time. To Dr. Ryan Ghan, Dr. Laurent Lamarque, and Dr. Noé Cochetel thank you. Finally, a special thanks to the many undergrads who have helped me through the years. I hope our lab was a place you always felt welcome and one from which you learned how to be good biochemists and better people.

TABLE OF CONTENTS

LIST OF TABLES

LIST OF FIGURES

CHAPTER 1: INTRODUCTION

CHAPTER 2: ABRES IN THE PN40024 GRAPEVINE REFERENCE GENOME PROMOTER REGIONS

CHAPTER 3: *VviERF6Ls*: AN EXPANDED CLADE IN *VITIS* RESPONDS TRANSCRIPTIONALLY TO ABIOTIC AND BIOTIC STRESSES AND BERRY DEVELOPMENT

CHAPTER 5: A MULTI-LEVEL ANALYSIS OF ABSCISIC ACID METABOLISM REVEALS SPECIES-SPECIFIC RESPONSES TO WATER DEFICIT IN GRAPEVINE

CHAPTER 1:

INTRODUCTION

1.1 The basis of the transcriptome

The central dogma of biochemistry is the flow of genetic information from DNA, to RNA, to protein (Crick, 1957). This dissertation investigates the biochemistry of two grapevine genes of interest during stress response with an emphasis on gene expression and transcript quantification, so the process of transcription, as well as descriptions of transcript quantification technologies, is outlined here. In the past forty years, sequencing technologies have advanced to make significant strides in improving the understanding of gene expression in the two-phase system of transcription and translation (Heather and Chain, 2016; Shendure et al., 2017). In the first step, transcription, DNA is copied into complementary messenger RNA (mRNA). The process of transcription entails three steps: initiation, elongation, and termination. Initiation is the rate-limiting step of transcription (Ptashne and Gann, 1997; Wade and Struhl, 2008), determining whether a transcript and thereby downstream protein is synthesized (or not).

Transcription initiation is controlled by many levels of regulation including epigenetics. The eukaryotic genome is marked with epigenetic modifications, wrapped around histones, and packed into nucleosomes to form chromatin (Kornberg, 1977). The complex layering of DNA folding poses a formidable obstacle for transcription factor (TF) binding and transcription initiation (Li et al., 2007). For transcription to initiate, DNA must be made accessible by chromatin remodeling complexes like SWI/SNF (Clapier and Cairns, 2009), histone-modifying enzymes, and histone chaperones (Sanematsu et al., 2006; Shandilya et al., 2007). Acetylation of select lysine residues of H3 and H4 histones relaxes DNA coiling, allowing accessibility for transcription machinery. Methylation of histones

at certain residues represses chromatin structure, obstructing transcription (Li et al., 2007). Additionally, multiple histone modifications can work cooperatively to effect transcription, and preliminary histone modifications may affect modifications made later (Briggs et al., 2002; Cheung et al., 2000). When DNA is accessible, transcription can initiate.

Transcription is initiated in eukaryotes when TF proteins bind to specific DNA sequences typically upstream (5') of the coding region of a gene (Fig. 1). The promoter is a DNA region where transcription is initiated. Generally, the first < 200 base pairs (bp) of a promoter are considered the core promoter, but promoters can extend tens of thousands of bp from the start codon of a gene (Griffiths et al., 2000). DNA looping allows distal promoter regions to regulate transcription proximal to a gene (Stadhouders et al., 2012). The promoter contains regulatory DNA sequences called cis-acting elements. Cis-acting elements include enhancers, silencers, and insulators. Enhancers are cis-elements that bind TFs to stimulate RNAP POLYMERASE II (RNAPII) binding and transcription (Pennacchio et al., 2013). Silencers are negative regulatory elements that act counterpart to enhancers to repress transcription (Ogbourne and Antalis, 1998). There are several universal core promoter cis-elements, including the TATA box (~ -30 bp from the transcription start site (TSS)), initiator, downstream promoter element, CCAAT box (~ -80 bp from the TSS), and GC box (~ -100 bp from the TSS), present in many eukaryotic core promoters (Dolfini et al., 2009). However, these cis-acting elements are not present in all promoters nor are universal motifs critical for transcription. Cis-element accessibility may be cell type, developmental stage, or stimuli specific. The same cis-acting element may also have different roles under a variety of conditions (Hernandez-Garcia and Finer, 2014; Pennacchio et al., 2013). Due to cis-acting element specificity, cis-acting elements

can be used to predict roles of the downstream gene. For example, abscisic acid (ABA) response elements (ABREs) are responsible for ABA-dependent gene expression in response to abiotic stress (Yoshida et al., 2015). The presence of a Gap box may indicate a gene is light responsive (Park et al., 1996), and a root hair element suggests the downstream gene may be involved in root morphogenesis (Cho, 2007). Additionally, cis-elements do not necessarily have fixed positions, orientations (Lis and Walther, 2016), or even sequences (Franco-Zorrilla et al., 2014; Worsley-Hunt et al., 2011) relative to downstream genes.

Complementary to cis-acting elements are trans-acting TFs. TFs bind to cis-acting elements and may promote or inhibit transcription. Transcription factors are one of the largest groups of proteins in eukaryotes, making up about 10% of coding genes within a plant genome (Franco-Zorrilla et al., 2014). Most TFs contain interaction, regulatory, and DNA-binding domains, but not all domains are present in all TFs, and even the definition of a TF varies from database to database (Davuluri et al., 2003; Guo et al., 2005; Iida et al., 2005; Mitsuda and Ohme-Takagi, 2009; Palaniswamy et al., 2006; Pérez-Rodríguez et al., 2010). Transcription factors bind to sequences in the major groove of DNA to elicit or repress transcription.

Transcription factors regulate gene expression of downstream genes in a signaling cascade often regulated by hub genes responding to stimuli. These genes are central to key aspects of the fitness of an organism in response to various stimuli and are often cores of signaling networks (Vandereyken et al., 2018). In grapevine, *ABRE BINDING FACTOR 2* (*VviABF2*) was identified as a hub gene in leaf dehydration and ethylene signaling, with many downstream target genes projected to be affected by VviABF2 activity (Hopper et

al., 2016). A few transcription factors *(ETHYLENE RESPONSE FACTOR 4* (*HvERF4*), *NAC DOMAIN CONTAINING PROTEIN 6* (*HvNAC6*), and *WRKY-DNA BINDING PROTEIN 42 (HvWRKY42*)) were also identified as hub genes in drought stress response in barley (Javadi et al., 2021) and others in rice (Lv et al., 2019).

There are thousands of TFs encoded in the genome of an organism, but no other kingdom has expanded TFs like plants (Lehti-Shiu et al., 2017; Shiu et al., 2005). The simple plant model, *Arabidopsis thaliana*, has four times as many TFs as other model species (*D. melanogaster* and *C. elegans*), and the same TF genome content as humans (Riechmann et al., 2000), hinting at the crucial role TFs play in plant diversity and adaptation. Usually, TF families are characterized by a DNA-binding domain. Major transcription factors are shared by all eukaryotes, but many plant-specific TF families exist as well.

Major transcription factors shared across eukaryotes include basic leucine zipper (bZIP), basic helix-loop-helix (bHLH), heat shock protein (HSP), and myeloblastosis (MYB) families (Hong, 2016). Additional plant transcription factor families include ABA RESPONSE FACTOR (ABF)/ABA RESPONSE FACTOR ELEMENT BINDING PROTEIN (AREB), NAM, ATAF1.2, CUC2 (NAC), WRKY, APPETELLA2/ETHYLENE RESPONSE FACTOR (AP2/ERF), AUXIN/INDOLE-3-ACETIC ACID (IAA/Aux), AUXIN RESPONSE (ARF), and JASMONATE ZIM-DOMAIN (JAZ) (Hong, 2016). These transcription factors regulate plant-specific responses and are often components of immense signaling cascades triggered by phytohormone production in response to stimuli. ABF/AREB and AP2/ERF TF families are key to this dissertation and will be discussed in more detail.

ABF/AREB TFs belong to Group-A bZIPs and act as signal transducers of the ABA signaling pathway in response to various abiotic stresses including water deficit, cold, and salt (Wang et al., 2018b). One *ABF/AREB*, *ABF2/AREB1*, a hub gene in the ABA signaling pathway, is responsible for activating the transcription of numerous downstream target TFs including NACs, WRKYs, and MYBs to effect stress tolerance, ripening, and dormancy (Pilati et al., 2017; Yoshida et al., 2015). ABF4/AREB2 is also considered a master transcription factor that regulates ABRE-dependent ABA signaling and drought tolerance (Yoshida et al., 2010).

AP2/ERFs contain a specific DNA binding domain and are divided into AP2, RAV, and ERF TFs based on the frequency of this domain; AP2 TFs contain duplicated DNA binding domains, ERF TFs contain a single DNA binding domain, and RAV contain a B3 + the AP2/ERF DNA binding domain (Licausi et al., 2013; Mizoi et al., 2012; Zhuang et al., 2009). The B3 domain is a pseudo-barrel protein motif, and this domain is also present in ARFs and the bZIP ABA INSENSITIVE 3 (ABI3) (Wang et al., 2012). ERFs can be further divided into the ERF and C-REPEAT BINDING FACTOR/ DEHYDRATION RESPONSE ELEMENT BINDING PROTEIN (CBF/DREB) subfamilies (Sakuma et al., 2002; Stockinger et al., 1997). CBF/DREB TFs bind dehydration response elements (DREs), cis-acting elements crucial for water deficit and cold responses (Maruyama et al., 2012; Narusaka et al., 2003). Some ERFs contain an ethylene-responsive element-binding factor-associated amphiphilic repression (EAR) motif, which elicits transcriptional repression and epigenetic changes through chromatin-modifying protein recruitment (Kagale and Rozwadowski, 2011; Kagale et al., 2010). AP2/ERF TFs like ERF1 play

important roles in senescence, ripening, and stress responses (Alexander and Grierson, 2002; Hopper et al., 2016; Iqbal et al., 2017).

General TFs (TFIIA, B, D-F, and H) bind to the core promoter recruit RNAPII and form the preinitiation complex to initiate transcription in all eukaryotes (Fig. 1). DNA-bound TFs interact with cofactors like the mediator complex to activate target promoters (Mathur et al., 2011). These transcriptional activators and associated cofactors bind to distant regulatory elements, facilitate chromatin remodeling, and finally recruit TFIID. TFIID binds to the TATA box, initiator, or downstream promoter element depending on the promoter sequence and other TFs present (Lawit et al., 2007; Workman and Roeder, 1987). TFIIB complexes with TFIID after binding to TFIIB recognition elements flanking the TATA box (Deng and Roberts, 2005). TFIIF binds next and facilitates RNAPII core promoter binding followed by TFIIE and TFIIH, resulting in a stable preinitiation complex (Chen et al., 2007; Dyke et al., 1988). The DNA helicase subunit of TFIIH hydrolyzes ATP to unwind the DNA, resulting in the formation of the open complex that enables template DNA to enter the active site of RNAPII and transition transcription into the elongation phase.

RNA elongation is the stepwise process of adding complementary nucleotides to a growing RNA transcript in the 5' to 3' direction. RNAPs are large (>500 kDa) enzymes consisting of ten to fourteen subunits (Parker, 2001) that actively transcribe DNA into RNA. RNAPs (I, II, III, IV, and V) are responsible for the synthesis of rRNA (Russell and Zomerdijk, 2006), mRNA and ncRNA (Djebali et al., 2012; Kornberg, 1999), tRNA (Turowski and Tollervey, 2016), and siRNA (Onodera et al., 2005). The siRNA pathway involving RNAPIV and V is plant-specific (Wierzbicki et al., 2008). Although each RNA

molecule has an important regulatory role, mRNA transcription is the most important control point for an organism experiencing environmental changes or stress (Hong, 2016).

Transcriptional elongation of mRNA and other RNA molecules entails three steps: promoter escape, promoter-proximal stalling, and finally productive elongation (Saunders et al., 2006) (Fig. 2). At the beginning of transcriptional elongation, an initial transcription bubble or open complex approximately 14 bp in length opens and separates the two strands of DNA, allowing for a DNA-RNA hybrid helix to form. However, RNAPII is still bound to the promoter and numerous associated TFs. As the initially transcribing complex establishes the first few nucleotides of a new transcript, RNAPII may experience abortive initiation. Abortive initiation occurs when TBIIB interferes with RNA exit from RNAPII (Bushnell et al., 2004). However, when RNAP passes the fourth nucleotide, the likelihood of abortive initiation decreases and the initially transcribing complex passes into escape commitment (Kugel and Goodrich, 2000).

During escape commitment, numerous protein-protein interactions are broken and new interactions are formed as RNAPII releases the promoter and processes along the DNA (Bushnell et al., 2004). The initial open complex collapses from the interaction of the RNA with TFIIB, resulting in the transcription bubble needed for productive elongation (Pal et al., 2005). Alternatively, transcription may be aborted (Keene and Luse, 1999) if all necessary components are not present and properly aligned. Promoter escape is the rate-limiting step of transcription elongation (Saunders et al., 2006). Once the promoter is cleared (~15 nucleotides transcribed), another round of initiation can begin (Kugel and Goodrich, 2000).

RNAPII stalling/pausing is another challenge that must be overcome early during elongation to achieve a stable initiation and a full-length transcript (Hong, 2016) (Fig. 2). RNAPII stalling is common among inducible and developmental promoters and acts as an additional checkpoint before RNAPII commits to productive elongation of a transcript (Levine, 2011). RNAPII pausing entails successful transcription initiation followed by discontinued elongation until necessary stimulus allows RNAPII to continue (Saunders et al., 2006). When the needed stimulus is not present to continue elongation, the net-transcription rate is reduced, and eventually, transcription is aborted (Steurer et al., 2018). Despite low rates of continued elongation after pausing, RNAPII pausing may play an important role in RNA capping, and capped RNA may be a requirement for continued elongation (Saunders et al., 2006). The capping enzyme associates with a phosphorylated serine in the C-terminal domain of RNAPII allowing the 5' end of the RNA transcript to be capped with 7-methylguanosine linked by a triphosphate bridge forming the complete m7G cap (Shatkin, 1976).

During productive elongation, RNAPII actively adds nucleotides to a growing mRNA chain based on template DNA (Fig. 1). DNA is guided into RNAPII via the RNAPII clamp and bridge structures and unwound before entering the active site (Landick, 2001). The RNAPII wall turns the template DNA in the active site and pairs each deoxynucleotide via the RNAPII trigger loop to a complementary ribonucleotide (Landick, 2001). Ribonucleotides enter the RNAPII active site through a tunnel and bind progressively to the entry, addition, and proofreading sites as a cycle of ribonucleotide addition is performed. As the mRNA chain grows, the RNAPII rudder separates the RNA-DNA hybrid helix, and

the bridge hinges to process the next deoxynucleotide, repeating the cycle (Kuznedelov et al., 2002).

In the case of damage, stalling, or mispairing, RNAPs backtrack to repair mistakes. However, if extensive damage is sustained, RNAPs stall, and the corrupted mRNA is hydrolytically cleaved by TFIIS and degraded. Despite the proofreading function, RNAPs still incorporate an incorrect ribonucleotide every 300 kb (Gout et al., 2017). Overall, the rate of transcription has been calculated to range from ~1-5 $kb \cdot min^{-1}$, but some groups have reported transcription exceeding 50 $kb \cdot min^{-1}$ (Maiuri et al., 2011). The exact rate of transcription is probably highly dependent on the gene being transcribed and the conditions of an organism; regardless of the exact number, the kb rate of transcription allows an organism to quickly adapt to a changing environment and respond to stress.

Transcriptional termination (Fig. 1) is generally conserved across eukaryotes, and one of the organisms the process is best described in is yeast (Porrua and Libri, 2015). In yeast, as transcription approaches termination, phosphorylation of serine-5 in the RNAP CTD that was crucial for elongation gradually shifts to include serine-2 (Peterlin and Price, 2006). Phosphorylated serine-2 of the RNAPII CTD recruits splicing and termination complexes including the cleavage and polyadenylation factor (CPF-CF) complex. The YEAST 73KD HOMOLOG 1 (Ysh1) subunit of the CPF-CF complex cleaves the RNA at the poly(A) site, and adenosines are added to the freed 3' hydroxyl group by the POLY(A) PHOSPHATASE 1 (Pap1) subunit (Hill et al., 2019). Poly(A)-binding proteins and shuttling factors escort the mRNA to the cytoplasm (Dunn et al., 2005; Hector et al., 2002). While the RNA is shuttled into the cytoplasm for further processing, RNAPII loses associated elongation factors (reducing processivity) (Ahn et al., 2004), and the CTD of

RNAPII is dephosphorylated, releasing RNAPII from the DNA (Hong, 2016). Other types of termination exist for different types of RNA (Schulz et al., 2013; Steinmetz et al., 2001), and variants of the CPF-CF depended termination also exist (Colin et al., 2014; Ghazal et al., 2009; Luo et al., 2006; Rondón et al., 2009). Finally, DNA loops around allowing spatial proximity of the terminal and promoter regions (Grzechnik et al., 2014). The hypophosphorylated RNAPII re-associates with promoter-bound general TFs, and another cycle of initiation begins.

During transcription and after transcriptional termination, eukaryotic precursor mRNA undergoes transcriptional modifications before becoming functional mature mRNA. Nearly 175 RNA post-transcriptional modifications have been identified (Boccaletto et al., 2018). However, the three main post-transcriptional modifications remain considered as the addition of a 5' cap, a 3' polyA tail, and splicing. All eukaryotic mRNA is capped with N7-methylated guanosine via a 5' to 5' triphosphate linkage between the first nucleotide and the m7G. This cap plays essential roles in protein synthesis, protection from exonucleases, and as a recruiting factor for polyadenylation, splicing, nuclear export (Sørensen et al., 2017), innate immune system self-recognition, and non-self-discrimination (Ramanathan et al., 2016). mRNA capping may occur co-transcriptionally (Price, 2018) or cytosolically (Mukherjee et al., 2014; Schoenberg and Maquat, 2009).

Polyadenylation is the addition of a poly(A) tail to the 3' end of pre-mRNA. The poly(A) tail, like the 5' cap, protects mRNA from degradation and allows for mRNA nuclear export and translation initiation (Hunt et al., 2008). The near-upstream element (Li and Hunt, 1995), far-upstream element (Lin et al., 2009), and poly(A) site are all cis-acting elements within mRNA that signal cleavage and poly(A) tail addition (Li and Hunt, 1997).

Plant polyadenylation signals differ from those in mammals and yeast (Graber et al., 1999), and less is understood in plant 3' end processing (Hunt et al., 2008). Poly(A) tail length can be highly variable. Alternative polyadenylation (APA) is the alternate use of various poly(A) sites at the 3'end of pre-mRNA, resulting in multiple transcript isoforms with varied sequence and length particularly in the 3' untranslated region (3' UTR). APA sites are found across 3' UTR as well as in introns and exons, allowing for a range of transcript isoforms to be translated, representing a unique level of gene expression regulation. APA and 3' UTRs represent an important regulatory mechanism controlling transcript localization, stability, function, and translation (Jalkanen et al., 2014; Preiss, 2013). Alternative 3' UTRs may code for different binding sites for RNA-binding proteins, which in turn affect the protein translation frequency and stability of the transcript (Miura et al., 2014). APA and 3'UTR isoforms also appear to have a role in tissue-specific transcript expression, stress response, and cell proliferation and differentiation (Srivastava et al., 2018; Vitting-Seerup and Sandelin, 2019; Zhang et al., 2017), but the link between APA and alternative 3'UTRs are less understood in plants.

Splicing entails the co-transcriptional removal of introns and the ligation of exons of a transcript to produce protein-coding mRNA. Up to 85% of plant genes contain at least one intron, but a gene may be interrupted > 40 times by as many introns (Lorković et al., 2000), making splicing essential to translate a functional protein. In plants, UA-rich introns can range from < 60 to > 10,000 nucleotides (Lorković et al., 2000). The splicing process, splice site consensus sequences, and complexes involved are similar in all eukaryotes (Lorković et al., 2000). Pre-mRNA splicing in the nucleus begins when the cap-binding complex associates with the spliceosome. snRNP base pairs with the 5' splice site, branch

point, and anchor the two exons (Meyer et al., 2015). The branch point is trans-esterified to the 5'splice site, creating a lariat loop. Transesterification of the 5' splice site to the 3' splice site allows for the intron lariat to be released and ligation of the two exons. The intron lariat is debranched and finally degraded while the mRNA goes on to be translated into protein (Lorković et al., 2000; Meyer et al., 2015).

Alternative splicing occurs when not every splice site of a pre-mRNA is used every time a gene is transcribed. Alternative splicing results in different mRNA isoforms and thereby protein variants of a single gene. Over 60% of genes in *Arabidopsis thaliana* produce more than one gene isoform (Marquez et al., 2012). Several alternative splicing events exist including exon skipping and intron retention. Alternatively spliced isoforms have also been linked to alternative polyadenylation and 3'UTR isoforms (Hu et al., 2020; Li et al., 2017b; Movassat et al., 2016), and these different isoforms may be organ, development, or stress-specific (MacDonald, 2019; Reddy, 2007; Reddy et al., 2013; Tack et al., 2019).

In addition to transcription, gene expression is regulated by RNA degradation. There are three main RNA decay pathways: mRNA de-capping, exosome-based degradation, and SUPPRESSOR OF VARICOSE (VCS) (SOV)/DIS3 LIKE 3'-5' EXORIBONUCLEASE 2 (DIS3L2) based degradation. mRNA de-capping is performed by DECAPPING (DCP) 1 and 2 (Coller and Parker, 2004). Once de-capped, mRNA is vulnerable to 5' to 3' exoribonuclease activity (Hsu and Stevens, 1993; Sorenson et al., 2018). The exosome hydrolytic ribonuclease activity degrades RNA in the 3' to 5' direction (Januszyk and Lima, 2014). Like the exosome, DIS32L degrades RNA via exonuclease activity from the 3' to 5' end of a transcript. Generally, cytoplasmic RNA decay is not well

characterized, and specific RNA substrates of each pathway remain unclear in Arabidopsis (Sorenson et al., 2018).

The transcriptome is the total RNA transcripts expressed by a sample at a certain time under specific conditions (Wang et al., 2009). Transcriptomic samples may be whole organisms, organs, or even a single cell. By definition, the transcriptome is fluid, varying between cells, organs, and across developmental stages (Wang et al., 2009). For example, no single gene was found to have the same transcriptional response in grapevine berries, shoot tips, leaves, roots, or callus after exogenous ABA application (Rattanakon et al., 2016). The transcriptome provides insight into the role of the functional elements of a genome. For example, *MYB121* transcripts uniquely accumulated in grapevine roots after exogenous ABA application, indicating this gene plays a role in the ABA signaling pathway in roots (Rattanakon et al., 2016). A transcriptome is a powerful tool used to quantify gene expression and identify gene isoforms and splicing patterns, but the final transcript abundance of each gene is a culmination of multiple levels of regulation.

Although the <u>focus of this dissertation is on transcriptional response</u>, other points of biochemical regulation are also considered in various chapters. In addition to transcriptional responses, this dissertation investigates DNA promoter region architecture, protein level, and metabolite concentration roles in stress response. Promoter region architecture or the composition, frequency, and location of cis-acting elements (Sanchez et al., 2011) affect transcription (Woo and Li, 2011). For example, NAC TFs that bind to E-box (CANNTG) motifs in promoter regions to activate transcription of *EARLY RESPONSIVE TO DEHYDRATION STRESS 1* (*ERD1*) during water deficit were unable to elicit reporter gene expression in the absence of this motif (Tran et al., 2004).

Protein abundance acts as another point of biochemical regulation. Just like mRNA, protein abundance is regulated by synthesis, various modifications, degradation, and transport in addition to mRNA abundance and accessibility (Vogel and Marcotte, 2012). Protein concentration can act as a feedback mechanism to regulate both transcription and translation of the same and other genes/proteins (and vice versa) (Ho et al., 2018; Moss Bendtsen et al., 2015).

Transcript abundance does not necessarily correlate to protein abundance (Jia et al., 2018; Liu and Aebersold, 2016; Liu et al., 2016). Only ~30-40% of the variation in protein concentration is explained by transcript abundance, but this value varies per gene and under different conditions (Vogel and Marcotte, 2012). Similarly, protein abundance does not necessarily reflect protein activity, which is another point of biochemical regulation. Protein activation is essential for the functionality and localization of many proteins (Eisenhaber and Eisenhaber, 2007) and generally entails post-translational modifications (Yang et al., 2017). Finally, metabolite concentrations and substrate/product concentrations have dynamic effects on numerous levels of biochemical regulation. For example, high concentrations of the phytohormone abscisic acid elicit conformational changes to receptors (Boneh et al., 2012) that trigger a signaling cascade (Wilkinson and Davies, 2002) touching numerous levels of biochemical regulation (Chinnusamy et al., 2008; Hirayama and Umezawa, 2010; Liu et al., 2020) that ultimately effect plant phenotypes (Duan et al., 2013; Pilati et al., 2017; Riboni et al., 2016). Overall, numerous other levels of regulation impact the overall phenotype of a plant particularly during stress responses, and this work explores only a few.

Since the establishment of the central dogma of biochemistry, many tangent steps and regulatory checkpoints for transcription and overall metabolic regulation have been discovered and found essential to organismal function and survival. Each gene in a transcriptome is uniquely regulated by all the factors described briefly here (epigenetics, cis- and trans-acting elements, RNAPII processivity, post-transcriptional modifications, and RNA degradation) and many more (e.g. RNA silencing, protein concentration, protein activity/modifications, and metabolite concentrations) to ensure an organism has the best fitness under any condition whether that be as a developing embryo or a fully mature organism confronting unavoidable stress. Transcript quantification is a measurement of the steady-state of a transcript, which is the culmination of numerous processes affecting transcription and mRNA decay. Today, transcript quantification is an entire field in biochemistry used to characterize all aspects of an organism as well as make assumptions about other levels of biochemistry (e.g. protein and metabolite). It is important to consider the many dynamic steps regulating transcript abundance (as well as all levels of biochemistry) and the interlinked factors involved in protein and metabolite regulation resulting in the phenotype of an organism.

1.2 A brief look into early transcript quantification

It was not until recently that transcripts were able to be identified and quantified. Numerous transcript quantification technologies have come and gone (differential colony

hybridization clones (Yamamoto et al., 1983), subtractive hybridization (Diatchenko et al., 1996), differential display (Liang and Pardee, 1992), etc.), but a few have had long-lasting effects on transcriptomics and will briefly be discussed.

The earliest technique for transcript detection is *in situ* hybridization (ISH) developed in the late 1960s. ISH is a technique that measures the localization and abundance of target nucleic acids in a cellular environment (Huber et al., 2018). Originally, ISH was used to label DNA with RNA-based (Gall and Pardue, 1969) and then DNA-based radioactive probes (Gall and Pardue, 1969) before safer fluorescent probes were adopted (Rudkin and Stollar, 1977) and improved (Bauman et al., 1980) for fluorescent *in situ* hybridization (FISH). Relative mRNA quantification via FISH was first performed in the early 1980s with biotin-labeled DNA probes to visualize actin mRNA in cell culture (Singer and Ward, 1982). FISH is still used today after many improvements including the utilization of short singly-labeled probes, image analysis software, background minimization, and optimization of the fluorophore-to-transcript ratios without quenching (Raj and van Oudenaarden, 2009; Raj et al., 2008). Variants of FISH include quantification of multiple target transcripts using different fluorophores (Chen et al., 2015; Eng et al., 2019; Raj and van Oudenaarden, 2009; Solanki et al., 2020) as well as pairing FISH with flow cytometry (for concurrent mRNA and protein quantification) (Arrigucci et al., 2017). FISH uses many harsh solvents and is highly temperature, salt, and pH-sensitive making optimization necessary for each probe (Cui et al., 2016; Young et al., 2020). To ensure comparability between samples, FISH entails long incubation times to establish a saturating signal (Huber et al., 2018). RNase contamination, autofluorescence, background, and tissue shrinkage are other concerns of FISH.

About a decade after the first ISH experiments, northern blotting was developed as another early technology for relative transcript quantification (Alwine et al., 1977). In addition to transcript abundance, northern blots divulge the length of the target transcript as well as the lengths and presence of any transcript isoforms present in a sample (Josefsen and Nielsen, 2011). Northern blots begin with mRNA extraction and purification. Uniform mRNA amounts of various samples are then loaded in individual lanes and size-fractionated by gel electrophoresis under denaturing conditions. Next, the fractionated mRNAs are transferred to a membrane (Josefsen and Nielsen, 2011). Once the mRNA is blotted on the membrane, labeled probes hybridize to immobilized target mRNA. Probes are commonly radioactively labeled, and transcript abundance can be compared between two samples as the radio signal intensity. Northern blots were favored for accessibility, and at one point required for validation of other transcript quantification techniques (Josefsen and Nielsen, 2011). However, northern blots are highly dependent on experimental parameters like RNA quality, RNA transfer efficiency (Josefsen and Nielsen, 2011), probe specificity and sensitivity, and target mRNA abundance (lowly expressed transcripts may not be detected). Additionally, Northern blots gels and buffers contain harmful solvents to denature the mRNA, making them less favorable than safer techniques for transcript quantification.

Finally, in the late 1980s, the field of single transcript quantification was revolutionized with the advent of real-time Reverse Transcription Quantitative Polymerase Chain Reaction (RT-qPCR) (Becker-André and Hahlbrock, 1989). The most common application of RT-qPCR is the quantification of transcript abundance for a gene of interest across multiple samples relative to stably expressed reference genes. This technique entails

extracting and purifying high-quality total RNA. The mRNA is reverse transcribed into cDNA. Diluted cDNA is mixed with a specific pair of primers, DNA polymerase, nucleotides, cofactors, and fluorescently labeled probes or an intercalating dye (VanGuilder et al., 2008). Fluorescently labeled probes have the added benefit of the possibility of multiplexing and quantifying multiple genes in a single reaction (Henegariu et al., 1997; Yi and Richards, 2007). The real-time reactions are performed in a thermocycler and fluorescence is measured after each cycle of amplification. The intensity of fluorescence above the background level at the earliest detectable cycle (C_t-value) is used to measure and quantify relative transcript abundance, which is normalized to stably expressed reference genes (and often a reference sample or condition) taking into account primer efficiencies (Hellemans et al., 2007). Absolute quantification can be calculated using standard curves (Wong and Medrano, 2005). RT-qPCR can measure transcript abundance across five (Schmittgen et al., 2000) to eight (Morrison et al., 1998) orders of magnitude. Today, RT-qPCR is used to measure the relative transcript abundance of genes of interest, validate microarray and RNA-Sequencing experiments, and monitor biomarkers (VanGuilder et al., 2008). However, RT-qPCR success is dependent on the quality of mRNA used, the amplification efficiency of the cDNA, and the primer efficiency of the RT-qPCR reaction (VanGuilder et al., 2008; Wong and Medrano, 2005). Numerous PCR inhibitors are used throughout RNA extraction and purification leading to false negatives and raising the limit of detection (VanGuilder et al., 2008). Primer dimers and primer mis-annealing can increase false positives (Bustin and Nolan, 2017; VanGuilder et al., 2008). Intrasample and technical replicate variation, as well as reference gene selection, can greatly impact data analysis of this highly sensitive technique. Despite these concerns,

RT-qPCR remains the gold standard for single (or limited number) gene transcript quantification due to its accessibility and low cost (VanGuilder et al., 2008; Zhu et al., 2020). RT-qPCR is largely accessible and highly specific when primers are properly designed. This user-friendly technology uses automated instrumentation and has a fast reaction time. FISH, northern blots, and RT-qPCR are all still relevant technologies today, but these techniques are only designed to quantify a minimal number of transcripts making them impractical for transcriptomic studies.

One of the earliest batch techniques of transcript profiling developed in and improved throughout the 1980s-2000s was expressed sequence tags (ESTs). ESTs are short fragments of mRNA sequences (200-800 nucleotides) generated from cDNA (Nagaraj et al., 2007; Parkinson and Blaxter, 2009). ESTs were considered a "poor man's genome" before whole-genome sequencing was more accessible (Rudd, 2003). ESTs played a crucial role in gene identification and verification throughout the human genome project (Adams et al., 1991). ESTs were generated from a cDNA library created by reverse transcribing 3' poly(A) tail enriched mRNA into cDNA *in vitro*. ESTs were sequenced from 5', 3', bidirectionally, and from mid-range cDNA open reading frames (Nagaraj et al., 2007; Neto et al., 2000; Parkinson and Blaxter, 2009). EST length was largely determined by sequencing technology (e.g. 454 Sequencing (~700 bp max length) was competitive in the early 2000s) (Parkinson and Blaxter, 2009). Raw trace data was processed to identify the underlying sequence (Bonaldo et al., 1996). The distribution of ESTs reflected the relative transcript abundance in a clone library. ESTs were then mapped to genomes to identify and verify genes (Zhu et al., 2003) and even used to compare genes between species (Ewing et al., 1999). Later, ESTs became useful in designing microarrays

(Gress et al., 1992). ESTs had several limitations including short and low-quality single-read sequences (Rudd, 2003). One major drawback of ESTs was the over-representation of highly abundant mRNAs (Parkinson and Blaxter, 2009) and the underrepresentation of lowly expressed transcripts (Nagaraj et al., 2007; Rudd, 2003). Another limitation is numerous ESTs share high sequence similarity and can match numerous paralogous genes. The National Center for Biotechnology Information (NCBI) officially retired this technology in 2019, but ESTs can still be used to confirm gene sequences.

In the 2000s microarrays emerged as the leading transcriptomic technology arising from colony hybridization in the mid-1970s (Grunstein and Hogness, 1975) and macroarrays in the early 1980s (Taub et al., 1983). Microarrays, unlike ESTs, were limited to probing known genes. Once an array design was decided upon, mRNA was converted to fluorescently or biotin-labeled cRNA or cDNA and amplified. The labeled cRNA or cDNA was hybridized to the microarray, and the array was washed. Fluorescence was measured in each well (usually with a confocal microscope) (Bumgarner, 2013) or fluorescent scanner (Miller and Tang, 2009). The signal intensity was an indirect measurement of the relative expression level of a gene. Microarrays quantified RNA over three orders of magnitude (Wang et al., 2019). However, highly expressed genes could saturate microarray signals and lowly expressed genes may go undetected. A major limitation of microarrays was the possibility of probe cross-hybridization. Array-to-array variation is another factor to consider with microarrays. Variations of microarrays include ChIP-chip for transcription factor binding site determination, single nucleotide polymorphism (SNP) genotyping, and more recently protein microarrays.

As science progressed through the genomic era, transcriptomic technologies advanced, and computer processing power increased and became more accessible. Older technologies died off, and new techniques like microarrays sprang up in their place. Throughout this era tens of thousands of genes were identified, the first complete genomes were released, and massive databases (Boguski et al., 1993) were created allowing for easy comparisons of transcripts between experiments and species. A host of limitations accompanied these early technologies including low throughput, low accuracy, low resolution, cross-hybridization of probes or primers, and 3' end bias. However, these technologies set the stage for the leading transcriptomic technology today: RNA-Sequencing.

1.3 Transcriptomics today and possibilities tomorrow

Today, science progresses in the big data era, wherein researchers are capable of producing overwhelming amounts of data including haplotype-specific transcriptomes from numerous species, samples, and conditions (Tilgner et al., 2014; Wang et al., 2016, 2018a). RNA-Sequencing (RNA-Seq) analysis can be performed at the sample, gene, transcript, and exon-level (Li and Li, 2018) to answer a host of biological questions. RNA-Seq yields whole transcriptomes of experimental samples and provides an invaluable resource for non-model species without a sequenced genome (Schliesky et al., 2012). The first RNA-Seq platforms utilized second-generation sequencing (SGS) technologies like 454/Roche (~100 and later up to 700 bp reads), Illumina HiSeq (125-250 bp reads) and

NextSeq (150-300 bp reads), SOLiD (60 bp reads), and Ion Torrent (200 bp reads) (Liu et al., 2012; Rhoads and Au, 2015). However, these short read-based RNA-Seq platforms are quickly becoming antiquated with the advent of third-generation sequencing and the rise of single-molecule real-time (SMRT) sequencing. Currently, PacBio's Iso-Seq is the leading technology for long-read RNA-Seq. Today, whole transcript (SMRT long-read <3kb-10kb) sequencings are paired with deeper short read sequencing in hybrid sequencing strategies for transcript quantification for the most accurate transcriptome (Au et al., 2012; Rhoads and Au, 2015; Tilgner et al., 2014).

Regardless of the platform used, RNA-Seq experiments follow a similar protocol. Workflow for Illumina SGS is briefly described here. First, RNA is extracted and undergoes rigorous quality control steps. Minimal RNA degradation is measured by an RNA integrity number (RIN). Next libraries are prepared. Before RNA-Seq can be performed rRNA, which constitutes > 90% of the RNA in a cell must be either depleted or excluded using poly(A) selection to enrich for mRNA (Pease and Sooknanan, 2012). The mRNA is fragmented and reverse transcribed using random primers with a 5'-tagging sequence (Pease and Sooknanan, 2012). 3'-tagging is accomplished by the terminal tagging reaction, resulting in single-stranded di-tagged cDNA fragments. The di-tagged single-strand cDNA is amplified with PCR, and final adaptors are added (Pease and Sooknanan, 2012). The amplified cDNA is hybridized to complementary adaptors attached to lanes on a flow cell for cluster generation. A polymerase creates a complement of the hybridized strand, and the double-strand molecule is denatured, allowing the original strand to wash away. Strands all across the flow cell are clonally amplified by bridge amplification using the adaptor regions, resulting in two complementary copies after a round of amplification

(Buermans and den Dunnen, 2014). Multiple rounds of amplification multiply all the clusters on the plate simultaneously. After sufficient amplification, a strand is cleaved and washed off the flow cell, depending on the type of sequencing to be employed. Two varieties of RNA-Seq can be performed: single or paired-end sequencing. Sequencing is performed using primers complementary to the adaptor and four uniquely fluorescently labeled nucleotides (Buermans and den Dunnen, 2014). After each cycle, excess nucleotides are washed away, and the fluorescent nucleotides incorporated into the growing strands are excited by light. The incorporated nucleotide, complementary to the cDNA fragment, is recorded based on the fluorescence emitted for all strands on the sequencing plate (Buermans and den Dunnen, 2014). After completion, the read product is washed away, and sequencing is complete for single-end reads. However, if a lab opts to utilize more accurate but costlier paired-end sequencing, sequencing begins with the forward strand and is performed the same as for single-end sequencing. After the read product is washed away, the forward strand undergoes a round of bridge amplification resulting in the complementary reverse strand. The previously sequenced forward strand is cleaved, and sequencing is repeated for the reverse strand. Paired-end reads are resultant of sequencing cDNA fragments from both ends, allowing for better read overlap and alignment. Sequencing platforms return raw reads to labs that process the data based on their experimental goal. Many informatics pipelines and numerous tools exist for RNA-Seq analysis (Corchete et al., 2020).

SMRT sequencing has several key differences from SGS. RNA processing and cDNA preparation are prepared as in SGS, but library preparation differs. SMRTbell libraries are created by ligating hairpin adaptors to both ends of cDNA, resulting in a single-

stranded circRNA (Rhoads and Au, 2015). Primer and proprietary long-read polymerase are added to the SMRTbells, and each SMRTbell is anchored by the polymerase in a zero-mode waveguide chamber on a SMRTcell for sequencing. SMRT sequencing uses fluorescently labeled nucleotides with linkage on the phosphate group (as opposed to base linkage like in SGS). This phosphate linkage allows the fluorescent group to be cleaved upon addition to the growing strand. The fluorescent signal resultant of nucleotide incorporation is measured in real-time as the fluorescent label is cleaved, increasing the speed of sequencing. Two modes of SMRT sequencing yield long reads. Circular consensus sequencing produces highly accurate HiFi long reads. Alternatively, continuous long-read sequencing can be used to generate the longest reads possible (at the cost of accuracy). After the sequencing is performed with SGS, SMRT, or hybrid sequencing platforms, the data is ready for analysis.

Major RNA-Seq analysis steps include trimming, quality checks, alignment/mapping, counting, normalization, and finally differential expression analysis. Trimming entails the removal of contamination sequences, adapters, low-quality bases, and low-quality reads (Schliesky et al., 2012) using tools like FastQC (Babraham Bioinformatics, 2010). Sequences are removed using a list of known adaptors/contaminants based on the sequencing technology used. Whole reads are discarded below a length threshold, and read ends may be trimmed if bases are below a quality threshold.

Alignment (also referred to as mapping) entails matching reads to a reference genome. Alignment is used for quality assessment of the RNA-Seq and used as input for normalization and differential expression analysis. Numerous tools exist for alignment;

among them, Bowtie2 (Langmead and Salzberg, 2012) and TopHat2 (Kim et al., 2013a) are commonly used and differ in the type of alignment performed (e.g. unsigned vs. spliced read alignment (Costa-Silva et al., 2017)). From mapping, several values can be reported to indicate the quality of the RNA-Seq. The longest read or unigene (sequence assembled from multiple sequential aligned reads), N50 (sequence length at half the total transcriptome) of unigenes or reads, and the total number of unigenes or unique reads are commonly reported for quality confirmation of RNA-Seq data series (Minio et al., 2018; Schliesky et al., 2012). The number of reference genes hit in a reference genome or the total number of expressed transcripts may also be used to indicate RNA-Seq quality (Minio et al., 2018; Schliesky et al., 2012). Aligning reads to a genome is normally the most time-consuming step of RNA-Seq analysis, but it can be sped up by quasi-mapping or pseudo-alignment. Normally >90% of reads should map to a reference genome for each sample.

Reads are counted by assigning overlapping reads (most commonly by breaking sequences into k-mers) and counting the number of aligned reads assigned to a gene (Schliesky et al., 2012) using tools like FeatureCounts (Liao et al., 2014). Counts can be considered as reads summarized across genes. As reads are assembled, divergent reads create a branch in the transcript assembly and may indicate a SNP, insertion or deletion (InDel), splice isoform, or a sequencing error. Identification of true differences is usually based on the k-mer coverage for each discrepancy and only those with high coverage are retained and counted.

Quasi-mapping and pseudo-alignment combine alignment and counting steps, and the advent of these techniques have created some distinction between “alignment” and “mapping”. Considering these techniques, alignment processes like those from Bowtie2

give exact read-to-genome correspondence at the nucleotide coordinate level and specify any insertions, deletions, or mismatches between the read and the reference genome. Mapping processes like quasi-mapping from Salmon (Patro et al., 2017) and pseudo-alignment from Kallisto (Bray et al., 2016) are less detailed and use less computing power to map a read to a genome since these tools do not consider exact alignments. Because RNA-Seq applications do not utilize all the details of the exact alignment, pseudo-alignments and quasi-mapping are faster than exact alignment methods, and mapping and counting can be performed in one step.

Normalization is performed using statistical and machine learning methods to remove sequencing bias, gene length effects, and batch effects (Costa-Silva et al., 2017; Li and Li, 2018). The most accurate normalization today is considered transcripts per million (TPM). Reads per kilobase per million mapped reads (RPKM) for single-end reads and fragments per kilobase per million mapped reads (FPKM) for paired-end reads are also common normalization methods. Both TPM and RPKM/FPKM normalize correct RNA-Seq biases in gene length and sequencing depth. The difference between TPM and RPKM/FPKM is the order of count/gene length division (performed first for TPM) and sample-scale factor determination (based on the length-normalized read counts for TPM) (Li and Li, 2018). Essentially, TPM of a gene is a representation of the proportion of RNA molecules of that gene in a sample (Li and Li, 2018). With RPKM it is difficult to compare the proportion of total reads that map to each gene because each sample has a different overall total sum of reads. This difference makes comparing RNA-Seq experiments and biological replicates within an experiment invalid; different gene transcript abundance can only be compared within a single sample using the FPKM/RPKM normalization. However,

with TPM the sums of total normalized reads are equivalent for all samples, allowing the transcript abundance of different biological samples to be compared to each other. The ability to accurately compare transcript abundance of a gene across biological samples that may correspond to different treatments, organs, or even species makes TPM a powerful normalization technique.

Differential expression analysis (DEA) identifies differentially expressed genes (DEGs) between conditions (Costa-Silva et al., 2017). DEA methods use distributions to model the normalized counts of an individual gene in different samples and determine if those values are statistically significant between samples (or groups) (Li and Li, 2018). DEA tools include limma+voom (Ritchie et al., 2015), NOIseq (Tarazona et al., 2015), and DESeq2 (Costa-Silva et al., 2017; Love et al., 2014). RNA-Seq has numerous applications in addition to transcript quantification including discovery of novel transcripts (Abdel-Ghany et al., 2016), alternative splicing events (Wang et al., 2016), alternative polyadenylation (Miura et al., 2014), fusion transcripts, circular (circ)RNAs, long non-coding (lnc)RNAs, isoform phasing, and genome annotation (Wang et al., 2019).

Additional steps of RNA-Seq analysis may include gene-co expression analysis performed using weighted gene co-expression network analysis (WGCNA) and gene ontology (GO) of WGCNA modules of interest (Langfelder and Horvath, 2008; Zhang and Horvath, 2005; Zhao et al., 2010). WGCNA detects gene groups called modules created based on expression pattern similarities across samples and experimental traits. Genes in modules are correlated to an Eigengene. Each Eigengene is a representative theoretical gene that is most correlated to an experimental trait. Genes that correlate to Eigengenes are ranked and considered linked to experimental traits. There is no consensus approach for

RNA-Seq analyses nor for the best tools to use. The many routes to identifying DEGs generally yield different but comparable results in terms of specificity and detection of true transcripts (Costa-Silva et al., 2017; Li and Li, 2018).

Still, third-generation sequencing is not perfected, containing raw read errors and limited throughput that enriches for more abundant and shorter transcripts (Wang et al., 2016). Usually less than half of the available zero-mode waveguides produce successful reads (Rhoads and Au, 2015), so polymerase anchoring and zero-mode waveguide loading can be improved. The high cost of RNA-Seq forces scientists to tradeoff between the number of biological replicates and the sequencing depth of samples, almost always sacrificing one or the other (Baccarella et al., 2018). Generally, read depth of 20-30 million reads per sample is considered sufficient coverage for error correction and gene expression quantification (Baccarella et al., 2018; Minio et al., 2019), but depths of up to 300 million have been reported to improve results (Baccarella et al., 2018). Often long-read sequencing is supplemented with short reads to fill gaps and increase depth, but this is an additional monetary and temporal cost. Short-read RNA-Seq does not sequence full-length transcripts, instead, it relies on short fragments, making it difficult to differentiate gene isoforms or highly similar or duplicated genes in complex genomes (Wang et al., 2016). One of the biggest hurdles RNA-Seq has yet to overcome is the task of the data analysis. Depending on the ploidy, sequencing depth, and the number of samples, computing space and storage may be a concern for some laboratories. One concern for single-molecule RNA-Seq is that pre-mRNA and decaying RNA are also detected. Another concern is proper library size selection; if improperly chosen, sequencing bias can be introduced for longer or shorter transcripts (Wang et al., 2019).

RNA-Seq has numerous advantages over other methods of transcript quantification. RNA-Seq provides precise measurement of transcripts over eight orders of magnitude (Owens et al., 2016). RNA-Seq differentiates transcript isoforms. RNA-Seq reads may be mapped to a reference genome or reads can be assembled *de novo* into a novel transcriptome (Schliesky et al., 2012). Additionally, RNA-Seq can be designed to investigate a certain type of RNA (mRNA, miRNA, circRNA), individual alleles, or gene isoforms. Although RNA-Seq analysis can be a daunting undertaking, technology is improving, the costs of powerful computers and storage space are decreasing, and more user-friendly pipelines are emerging (Seelbinder et al., 2019). For the next generation of bioscientists, RNA-Seq will likely be a common practice.

The future pushes science out of the big data era and into the insight era, where the power of the data produced will be harnessed and interpreted across disciplines. One emerging field that will benefit is systems biology, a powerful integrative approach to synthesize data from multiple levels of regulation to gain a more comprehensive understanding of the biochemistry of an organism. The novel ability of haplotype phasing genomes and transcriptomes will propel population genetics, breeding, ancestry, inheritance, and interpretation of allele functionality. As transcriptomes from various tissues, developmental stages, and stress conditions continue to be collected, larger studies of pan-transcriptomes (Jin et al., 2016; Ma et al., 2019; Petek et al., 2020) and comparative transcriptomics (Amrine et al., 2015; Güimil et al., 2005; Li et al., 2019b; Wang et al., 2018a) will provide deeper insight into trait variation and stress adaptations between species. For example, in grapevine allelic variation of a powdery mildew resistance locus (*Ren1*) was identified as being responsible for a range of different levels of disease

resistance (Amrine et al., 2015). Existing RNA-Seq experiments can be used and compared in meta-data analysis. Additionally, CRISPR experiments may help identify roles of unique transcript isoforms (Wang et al., 2006). The development of personal transcriptomes may allow for a better understanding of individual biology and disease progression, and additional third-generation sequencing technologies like Oxford Nanopore MinION will allow for faster data analysis at point-of-care or in field settings (Ashton et al., 2015).

The first plant RNA-Seq based plant transcriptome was created for *Arabidopsis thaliana* in 2007 (Weber et al., 2007). Since then transcriptomics has been used to identify markers for molecular plant breeding (Huang et al., 2012; Muñoz-Espinoza et al., 2016) and identify key genes in secondary metabolism pathways (Cramer et al., 2014; Deguchi et al., 2020; Desgagné-Penix et al., 2012; Sun et al., 2016). Transcriptomics has also been widely used in plants to quantify responses to biotic (Amrine et al., 2015; Blanco-Ulate et al., 2017; Massonnet et al., 2017) and abiotic stresses (Cochetel et al., 2020; Hopper et al., 2016; Iquebal et al., 2019; Rattanakon et al., 2016; Varoquaux et al., 2019). Grapevine gene expression has been widely studied using RNA-Sequencing. Transcriptomics is being used to unravel complex rootstock-scion interactions (Zombardo et al., 2020), pathogen susceptibility (Massonnet et al., 2017), and genes that improve drought resistance (Tu et al., 2020).

1.4 Grapevine, ABA, and water deficit

Grapevines (*Vitis*) are deeply rooted in human history and culture, and viticulture is as ancient as civilization itself (McGovern et al., 2017). Grapevines were domesticated almost 8,000 years ago, but evidence of winemaking dates back 1,000 years before grapevine domestication (Li et al., 2018). Grapevines have been divinified and worshipped for centuries (Hamilton, 2013) and are discussed in some of the most popular religious texts today (The Bible Genesis 8.4 and 9.20, The Holy Quran an-Nahl 67, The Torah Genesis 40:10 and Leviticus 25:5-11). Grapevine is linked to rituals and artifacts throughout the world across time and cultures (Damasco et al., 2020; Kumbaric and Caneva, 2014; Melillo, 1994), and some of the oldest pottery ever discovered are wine basins (McGovern et al., 2017).

North American history and modern culture are engrained with *Vitis*. For example, "Vinland", one of the earliest names for North America was given by Viking explorers including Leif Eriksson due to the proliferation of grapevine in the northeastern United States (McGovern et al., 2017). Thomas Jefferson and other founding fathers were responsible for some of the earliest Eurasian (*vinifera*)-North American species crosses that later led to an explosion in grapevine diversity in the 18th and 19th centuries in response to the phylloxera pandemic (Patrick E. McGovern, 2007).

Grapevines and wine are portrayed in famous art created by Leonardo Da Vinci and Claude Monet as well as songs from renowned performers including Johnny Cash, Neil Diamond, and Blake Shelton. Today, phrases like "heard it through the grapevine" and "sour grapes" decorate not only the English language, but also French, Italian, and Spanish.

Grape berries and raisins remain a popular snack, and wine is a staple beverage at many celebrations. Nutraceuticals like resveratrol and other grape berry-derived antioxidants are popular supplements with anti-aging and heart health improving properties (Baxter, 2008; Dyck et al., 2019). From culture to health, grapevines have been essential to human civilization and remain relevant today.

In addition to being a cornerstone of human culture, grapevines are one the most economically important horticultural crops in the world (Zhou et al., 2017). For at least the last seven years grapevines have been the non-citrus fruit crop with the highest utilized production value, and the value of grapevine increases nearly every year (United States Department of Agriculture, 2020) (Fig. 3). In 2019 the utilized production value of grape berries was $5.72 billion, far exceeding the value of any other non-citrus crop (United States Department of Agriculture, 2020) (Fig. 4). However, this sum fails to compare to the significance of the grapevine-product industry, which was valued at over $43.6 billion in California alone in 2019 (Wine Institute, 2020). In addition to being economically valuable, *Vitis* is becoming an increasingly powerful model organism with the release of numerous sequenced genomes. Each year more *Vitis* genomes become available (Fig. 5), which are a powerful tool in better identifying species-specific genes and traits. Still, the majority of *Vitis* remains largely uncharacterized.

Today, there are over 21,045 varieties, 10,000 cultivars, and 80 species of *Vitis* spanning every habited continent (International Organisation of Vine and Wine, 2017). Of these species, *Vitis vinifera* is the largest cultivated species used to produce fruit, juice, and wine. It is estimated cultivated grapevine diverged from wild relatives about 22,000 years ago (Zhou et al., 2017). Wild species including *V. champinii*, *V. riparia*, *V. rupestris*, and

V. sylvestris are used in breeding programs and as rootstock for stress tolerance and disease resistance. Interspecific hybridization rootstock breeding programs of evolutionarily distinct species and genetic mutations introduced from vegetative propagation make grapevine one of the most genetically diverse crops in the world (International Organisation of Vine and Wine, 2017). The spectrum of grapevine varieties with unique responses to a variety of stresses in combination with genomic and transcriptomic technologies allows for the identification of genes responsible for desirable traits like drought tolerance. *Vitis* makes a particularly strong model organism for studying water deficit response and drought tolerance because it is one of the few plants cultivated under water deficit to improve berry quality (Mirás-Avalos and Intrigliolo, 2017; Weiler et al., 2018).

Despite grapevine being considered as a moderately drought-tolerant crop (Fort et al., 2017; Heinitz et al., 2015), climate change is a threat to viticulture (Cabré and Nuñez, 2020; Monteverde and De Sales, 2020; Santos et al., 2020). As a woody perennial crop, grapevines are expected to survive and produce for decades, with old-vine vineyards held in high esteem and value. However, annual berry quality is highly dependent on temperature and water availability, and current projections of heatwaves, drought, and pathogen spread could exceed limits of grapevine productivity and survival (Charrier et al., 2018; Weiler et al., 2018). Current projections predict an 11% reduction of cropland due to water availability limitations by 2050 (Fitton et al., 2019) coinciding with a 1.5 ˚C increase in global temperatures and a 30% increase in global landmass experiencing severe drought by 2100 (Naumann et al., 2018). Much of the land used for viticulture will no longer be suitable under these conditions, and it is therefore essential not only to understand

drought tolerance and water deficit response in grapevine but also to identify genes and species that will ensure the survival and continuation of viticulture.

Drought tolerance is the ability of a vine to sustain physiological activity while minimizing or repairing damage during water deficit or drought (Gambetta, 2016). The drought tolerance of plants is in part associated with stomatal behaviors in response to water deficit and resultant use or preservation of available water. Grapevine responses to water deficit are characterized as belonging to a spectrum of stomatal reactions ranging from isohydric to anisohydric (Sade and Moshelion, 2014). Isohydric species maintain a relatively constant leaf water potential through early stomatal closure during water deficit (Tardieu and Simonneau, 1998), and anisohydric species experience decreasing leaf water potential and maintain open stomata during water deficit.

There are many other morphological differences between a drought-tolerant and drought-sensitive plant. For example, cutin, the waxy covering of a leaf that prevents excess water loss (Schreiber, 2010), is two orders of magnitude thicker in the drought-adapted cacti Opuntia (Jesse Mayer, 2018) than the model plants Arabidopsis (Franke et al., 2005), maize (Ristic and Jenks, 2002), and rice (Qin et al., 2011). Drought tolerant plants or plants that have simply experienced a water deficit generally have smaller leaf surface area than those that are well-watered (Ma, 1984). The difference in leaf size reflective of drought tolerance is exemplified by comparing the drought-sensitive grapevine species *Vitis riparia* that has leaves the size of dinner plates and the drought-tolerant Texan vine, *Vitis champinii*, the leaves of which easily fit in the palm of a hand under well-watered conditions. Drought tolerant leaves are also considered to have higher vein density, lower osmotic potential, and more mass per area (Fletcher et al., 2018;

RHIZOPOULOU and PSARAS, 2003). Plants with optimized canopy density and architecture or an overall lower number of leaves are generally more drought tolerant than a bushy plant due to reduced evaporative demand and higher water use efficiency (Devakumar et al., 1999; Digrado et al., 2020; Gao et al., 2020; Hatfield and Dold, 2019). Even plant height is a factor that effects overall drought tolerance (McGregor et al., 2020; Xu et al., 2018).

Stomatal density and location also affect drought tolerance with lower stomatal density associated with improved drought tolerance (Bertolino et al., 2019; Caine et al., 2019; Hughes et al., 2017). Reducing stomatal density improves water use efficiency (Hughes et al., 2017) and optimizes CO_2 uptake (Bertolino et al., 2019), and reduced stomatal density does not necessarily negatively impact crop yields (Bertolino et al., 2019; Dunn et al., 2019; Hughes et al., 2017). Most herbaceous plants have stomata on both the abaxial (bottom) and adaxial (top) sides of a leaf (Wang et al., 1998), but the stomata on either side of the leaf can have different sizes (Willmer and Fricker, 1996), densities (Fanourakis et al., 2015), and sensitivity to environmental stimuli (Lu et al., 1993). More drought-tolerant plants like grapevine generally have a lower adaxial stomatal density (Hardy et al., 1995). However, drought increased adaxial stomatal density in numerous rice cultivars (Ouyang et al., 2017).

There exists a fine balance between root and shoot mass allocation in plants with more drought-tolerant plants (and plants that have experienced water deficit) generally having higher root-to-shoot ratios (Hartmann et al., 2013; Kozlowski and Pallardy, 2002; Xu et al., 2015). The precise mechanism of mass reallocation appears species-dependent. For example, woody perennials grow longer roots to reach deep water reserves

(Markesteijn and Poorter, 2009; Mokany et al., 2006; Yıldırım et al., 2018). Cacti root systems are notoriously shallow to access scant precipitation that does not penetrate desert soils (Nobel, 1977; Nobel and Bobich, 2002; Reyes-Olivas et al., 2002). Some plants like beans have drought-tolerant varieties with deep and average root systems (Polania et al., 2017), and rice root biomass increase under drought is associated with higher root sugar concentrations (Xu et al., 2015). Root-based drought tolerance mechanisms for other species include increasing root diameter while decreasing root length (Zhou et al., 2018).

Xylem vessel diameter and abundance is another indicator of plant drought tolerance (Bauerle et al., 2011; Haworth et al., 2017; Jacobsen et al., 2012; Rosell et al., 2017; Torres-Ruiz et al., 2017). Wider xylem vessels allow for easier bulk water movement through a plant but make a plant more susceptible to embolism (Ryu et al., 2016; Scoffoni et al., 2017). Narrow xylem vessels are more resistant to water deficit and cold-induced cavitation (Rosell et al., 2017). Xylem vessel diameter and abundance directly factor into hydraulic conductance (Santiago et al., 2004; Tyree et al., 2002). Plants able to maintain higher hydraulic conductivity under water deficit also maintain higher photosynthesis and stomatal conductance (Brodribb and Feild, 2000). Additional mechanisms of drought tolerance include suberization (Vishal et al., 2019), biosynthesis of osmoprotectants (Hundertmark and Hincha, 2008), and changes to reproduction (Riboni et al., 2013), which will be briefly discussed in the following paragraphs.

Drought tolerance and involved genes are directly linked to the phytohormone abscisic acid. ABA, originally called ‘inhibitor ß’ (Williams, 1959), ‘abscisin II’ (Liu and Carns†, 1961; Ohkuma et al., 1963), and ‘dormin’(Cornforth et al., 1965), was first observed to have negative effects on plant growth in the 1920s (Oppenheimer, 1922), a

possible role in abscission, and effects on dormancy. It was not until the 1960s with the advent of paper chromatography that these compounds were identified as the same molecule and re-named 'abscisic acid' (Dörffling, 2015; Finkelstein, 2013). ABA is a 15-carbon terpenoid metabolite derived from carotenoids (Li et al., 2017a). Naturally occurring and active ABA is (+)-cis-ABA, referred to as 'ABA' throughout this manuscript. Early work that identified ABA as abscisin II, proposed this compound regulated leaf and fruit abscission (Ohkuma et al., 1963), lending this metabolite a misnomer. Later ethylene rather than ABA was discovered to regulate abscission (Morgan, 1984). However, ABA and ethylene have numerous points of crosstalk particularly throughout stress response, germination, and ripening that ultimately result in abscission and senescence (Hopper et al., 2016; Sharp, 2002; Sharp and LeNoble, 2002).

Although ABA was originally implied as a negative growth regulator, ABA-deficient mutants have a severely stunted phenotype across plant species (Sharp et al., 2000; Spollen et al., 2000). ABA is considered a ubiquitous phytohormone expressed in almost all cell types that contain a plastid such as a chloroplast or an amyloplast (Li et al., 2017a). ABA has also been found in various bacteria (Shahzad et al., 2017), fungi (Izquierdo-Bueno et al., 2018), and even humans (Bruzzone et al., 2007). ABA metabolism, signaling, and physiological responses are shared across plant species (Umezawa et al., 2010), and are well described in Arabidopsis, which will be used as an exemplary species to describe ABA metabolism and response in this section.

ABA concentration depends on ABA metabolism, which consists of biosynthesis, (de)conjugation, transport, and catabolism (Figs. 6 and 7). ABA biosynthesis, as well as that of cytokinins (Frébort et al., 2011), gibberellins (GAs) (Kasahara et al., 2002),

strigolactones (Alder et al., 2012), and brassinosteroids (Fujioka and Yokota, 2003) begins in a plastid with isopentenyl diphosphate (IPP) (Rodrı´guez-Concepción and Boronat, 2002). Condensation of three IPP and one dimethylallyl diphosphate molecules form the C_{20} molecule geranylgeranyl diphosphate (GGPP). Two GGPPs are condensed into phytoene (C_{40}) (Welsch et al., 2000, 2008), and then various desaturation, isomerization (Bartley et al., 1999; Linden et al., 1994; Ruiz-Sola and Rodríguez-Concepción, 2012) and cyclization (Zeng et al., 2015) steps yield ß-carotene. Hydroxylation of ß-carotene forms zeaxanthin (Du et al., 2010, 1999). Intermediate antheraxanthin and violaxanthin are formed by the reversible two-step epoxidation of zeaxanthin by ZEAXANTHIN EPOXIDASE/ABA DEFICIENT 1 (ZEP/ABA1) and NON-PHOTOQUENCHING 1 (NPQ1) (Eskling et al., 1997; Hieber et al., 2000; Niyogi, 1999). Violaxanthin can be isomerized by NEOXANTHIN SYNTHASE/ ABA DEFICIENT 4 (NXS/ABA4) and form neoxanthin (Dall'Osto et al., 2007; Perreau et al., 2020). Both violaxanthin and neoxanthin undergo the rate-limiting step of ABA biosynthesis perform by NINE-CIS-EPOXYCAROTENOID DIOXYGENASE (NCED) (Qin and Zeevaart, 1999; Schwartz, 1997; Tan et al., 1997).

There are five NCEDs in Arabidopsis involved in ABA biosynthesis (AtNCED2, 3, 5, 6, and 9) (Tan et al., 2003). The various AtNCEDs are specific for ABA biosynthesis in different tissues. For example, *AtNCED5*, *AtNCED6*, and *AtNCED9* are required for ABA biosynthesis during seed development, but *AtNCED6* is present at an earlier stage of development than the other *NCEDs* (Lefebvre et al., 2006; Tan et al., 2003). *AtNCED2* and *AtNCED3* are active in roots, flowers, and *AtNCED3* is the major stress-induced *NCED* in the leaves (Endo et al., 2008; Tan et al., 2003). AtNCED2, AtNCED3, and AtNCED5 are

considered the major contributors to increased ABA concentration in response to stress (Nambara and Marion-Poll, 2005). In grapevine, there are three NCEDs involved in ABA biosynthesis (VviNCED3, 5, and 6), and VviNCED3 (previously VviNCED1) is considered the major NCED contributing to ABA biosynthesis during abiotic stress (Cochetel et al., 2020).

Xanthoxin, the resulting C_{15} compound from the NCED reaction, moves out of the plastid to the cytoplasm where XANTHOXIN DEHYDROGENASE (ABA2) protonates the epoxy group of xanthoxin yielding ABA aldehyde (González-Guzmán et al., 2002). Finally, ABA aldehyde is oxidized to active ABA by ABA ALDEHYDE OXIDASE (AAO) (Seo et al., 2000) with a molybdenum cofactor sulfurase (ABA DEFICIENT 3 (ABA3)). Optimal ABA biosynthesis is not possible without all four of the ABA DEFICIENT proteins (ABA1, ABA2, ABA3, ABA4) (Bittner et al., 2001; González-Guzmán et al., 2002; Koornneef et al., 1984; North et al., 2007).

ABA is conjugated into an inactive storage form (Fig. 6) (Cutler and Krochko, 1999) via esterification with UDP-glucose (Xu et al., 2014). ABA glucose ester (ABA-GE) is the predominant storage form of ABA (Piotrowska and Bajguz, 2011). ABA esterification is performed by UDP-glucose glucosyltransferase (UGT) (Lim et al., 2005; Liu et al., 2015), and once conjugated, ABA-GE is stored in the vacuole (Bray and Zeevaart, 1985; Burla et al., 2013; Lehmann and Glund, 1986). When active ABA is needed, ABA-GE is readily de-esterified to active ABA via ß-d-glucosidases (BG or BGLU) (Lee et al., 2006; Xu et al., 2012). This pathway is thought to be important for quick ABA release and response as compared to ABA biosynthesis (Lee et al., 2006; Schroeder and Nambara, 2006; Wasilewska et al., 2008).

ABA catabolism (Fig. 6) consists of three pathways via hydroxylation of C-7', C-8', or C-9' (Nambara and Marion-Poll, 2005) performed by ABA hydroxylases (CYTOCHROME P450 (CYP707A)) (Krochko et al., 1998). ABA catabolites also function as signaling molecules affecting physiology, development, and environmental adaptation (Shimomura et al., 2007; Weng et al., 2016), but the distinct role of each catabolite remains unresolved. 8'-hydroxylation is considered the major ABA catabolism pathway (Cutler and Krochko, 1999). 8'-hydroxy ABA is isomerized into phaseic acid (PA) (Krochko et al., 1998) and further reduced to dihydrophaseic acid (DPA) (Gillard and Walton, 1976). Neophaseic acid (NeoPA) is formed from 9'-hydroxy ABA and is thought to be a minor catabolite.

Like any biological process, ABA metabolism is regulated by numerous factors. At the DNA level, epigenetics and DNA methylation affects ABA metabolism (Chinnusamy et al., 2008). For example, *NCED3* methylation via a histone H3 lysine methyltransferase was recently found to play a key role in promoting ABA biosynthesis (Chen et al., 2021). At the gene level, transcript abundance impacts ABA metabolism with ABA deficient mutants having lower ABA metabolite concentration even under abiotic stress (Dall'Osto et al., 2007; Koornneef et al., 1982). At the protein level, both protein concentration and protein activity are considered to impact ABA metabolism, but this aspect of metabolic regulation is not well developed compared to the importance of protein activation in ABA signaling (Kobayashi et al., 2005). Substrate availability also affects ABA metabolism. For example, exogenous ABA application is known to increase carotenoids, precursors for ABA biosynthesis (Barickman et al., 2014; Liu et al., 2020), and carotenoid biosynthesis mutants have reduced ABA concentrations (Romero et al., 2019).

In addition to being metabolized in most cells, ABA is also transported throughout a plant (Kuromori et al., 2018) (Fig. 7). ATP-BINDING CASSETTE G25 (ABCG25) is an ABA efflux transporter that removes ABA from vascular tissue and endosperm cells while ABCG40 is an influx transporter that moves ABA into the guard cell and seed embryo (Kang et al., 2010; Kuromori et al., 2010, 2014, 2018). ABA-vascular unloading and transport into guard cells (Kuromori et al., 2010) and endosperm-ABA unloading into the seed embryo (Kang et al., 2015) are well-established pathways. A pathway for ABA transport into the root from the shoot is also described (Ernst et al., 2010; Goodger and Schachtman, 2010; Ikegami et al., 2009). More recently nitrate transporters, NITRATE TRANSPORTER/PEPTIDE TRANSPORTER FAMILY 4.5 (NPF4.5) also known as ABA IMPORTING TRANSPORTER (AIT2) and NPF4.6 (AIT1) (Léran et al., 2020), were also demonstrated to transport ABA in seeds and vascular tissues. These nitrate/ABA transporters may link nitrogen status to ABA signaling and play an important role in modulating growth under stress (Kanno et al., 2012).

ABA signaling begins with ABA perception and binding via receptors (Fig. 8). ABA PYRABACTIN RESISTANCE/PYRABACTIN RESISTANCE-LIKE/REGULATORY COMPONENTS OF ABA RECEPTORS (PYR/PYL/RCARS) were simultaneously identified in Arabidopsis by two separate groups (Ma et al., 2009; Park et al., 2009). The first ABA receptors were identified with a yeast-two hybrid using the phosphoprotein phosphatase ABI2 as bait (Ma et al., 2009) and *PYRABACTIN RESISTANCE 1* (*Atpyr1*) mutants that were resistant to pyrabactin, an ABA agonist (Park et al., 2009). The binding of ABA by the PYR/PYL/RCARs induces conformational changes that expose a PHOSPHOPROTEIN PHOSPHATASE 2C (PP2C) interaction site

(Melcher et al., 2009). PP2Cs are negative regulators of ABA signaling (Gosti et al., 1999). The ABA-bound PYR/PYL/RCARs obstruct the active site of PP2Cs and prevent phosphatase activity (Melcher et al., 2009), which in turn relieves PP2C-mediated inhibition of SUCROSE NON-FERMENTING 1-RELATED PROTEIN KINASE 2s (SNRK2s), the positive regulators of ABA signaling (Hirayama and Umezawa, 2010). The various SNRK2s regulate different ABA responses (Fujii et al., 2007; Kim et al., 2013b; Yoshida et al., 2002). For example, SNRK2.6/OPEN STOMATA 1 (OST1) is key to regulating ABA-induced stomatal closure (Mustilli et al., 2002; Yoshida et al., 2002). Once PP2Cs interact with ABA-bound PYR/PYL/RCARS, SNRK2s undergo autophosphorylation (Zhang et al., 2016) or are activated by other kinases (Cai et al., 2014; Takahashi et al., 2020) and proceed to activate downstream transcription factors.

SNRK2 targets include ABI and ABRE-BINDING FACTOR/ABA RESPONSIVE ELEMENT BINDING FACTORS (ABF/AREB) TFs (Fig. 8) (Nakashima et al., 2009; Yoshida et al., 2015). *Atabi3*, *4*, and *5* mutants are insensitive to ABA. ABI3 is a TF that plays a critical role in seed development and dormancy with *Atabi3* mutants having defective, viviparous seeds (McCarty et al., 1989; Suzuki et al., 2001). ABI4 is an AP2/ERF TF with roles in seed development and germination (Finkelstein, 1994) as well as hormone crosstalk (Kerchev et al., 2011; Shkolnik-Inbar and Bar-Zvi, 2010; Shu et al., 2016), salt response (Quesada et al., 2000), and lateral root development (Shkolnik-Inbar and Bar-Zvi, 2010). *ABI5* encodes a bZIP TF considered a key gene in ABA signaling (Finkelstein and Lynch, 2000; Skubacz et al., 2016; Yang et al., 2011) due to diverse expression across tissues and conditions (Brocard, 2002; De Smet et al., 2003; Finkelstein, 1994; Finkelstein and Lynch, 2000; Skubacz et al., 2016) as well as at the abundant targets

of this TF including LEAs (Finkelstein and Lynch, 2000; Kim et al., 2002), CORs, and RABs (Brocard, 2002). ABFs/AREBs are in the same bZIP clade as ABI5 and considered as master TFs in ABA regulated drought tolerance (Li et al., 2017a) because disruption of these genes resulted in severely impaired ABA and stress responses (Yoshida et al., 2010, 2015).

ABI and ABF/AREB TFs target thousands of genes by binding to ABRE cis-acting elements (Gonzalez-Guzman et al., 2012; Song et al., 2016). There are numerous ABREs in plant promoter regions that bind unique TFs under specific conditions. ABREs have been identified and functionally validated throughout the promoter regions of several plant species including Arabidopsis, rice, (Gómez-Porras et al., 2007), soybean, cotton (Maruyama et al., 2012; Yamamoto et al., 2007), and more recently grapevine (Wong et al., 2017), indicating these motifs are conserved across plant species.

Through this signaling cascade, ABA regulates numerous physiological processes including seed maturation, dormancy, and germination. ABA concentrations oscillate throughout embryogenesis with a peak concentration at mid-maturation (Belin et al., 2009; Cheng et al., 2014; Karssen et al., 1983). The increase in ABA at this stage in embryogenesis prevents precocious germination (Karssen et al., 1983). After the embryo is fully mature ABA concentrations raise again in embryos as desiccation begins and the seeds transition into dormancy (Frey et al., 2004; Karssen et al., 1983; Kermode, 2005; Sondheimer et al., 1968). ABA induces desiccation tolerance by inducing antioxidant (Bailly, 2019; Jeevan Kumar et al., 2015; Lando et al., 2020) and LATE EMBRYOGENESIS ABUNDANT (LEA) protein (Dure, 1997; Maia et al., 2014; Zamora-Briseño and de Jiménez, 2016) accumulation to protect embryos over long periods. Maize

vivipary was one of the first phenotypes observed in ABA insensitive and deficient mutants, which played fundamental roles in identifying many genes involved in ABA metabolism and signaling (Li et al., 2017a). For example, *vp1* maize mutants (and *abi3* Arabidopsis mutants) do not experience seed dormancy (McCarty et al., 1989; Suzuki et al., 2001). Likewise, *Ataba1* and *Ataba2* mutants have reduced dormancy (del Carmen Rodríguez-Gacio et al., 2009). When a seed is imbibed, ABA is rapidly degraded by CYP707As, allowing a seed to germinate. Light and a chilling period followed by increased temperature result in decreased expression of ABA biosynthesis genes and an increase in ABA catabolism transcripts.

Although ABA is renowned as the central regulator of stress response, ABA is involved in plant growth and development processes outside of a stress context. Under well-watered control conditions, ABA is present in cells at a nanomolar concentration (Yoshida et al., 2019a), and ABA receptors and positive and negative regulators are expressed (Caldeira et al., 2014; Cochetel et al., 2020). Even at this low concentration, ABA is bound by receptors, interacts with PP2Cs, and elicits an ABA response (Tischer et al., 2017). Under non-stress conditions, ABA promotes lateral root growth in combination with auxin (Xing et al., 2016; Zhao et al., 2014). ABA also effects shoot and leaf growth under well-watered conditions. For example, ABA-deficient mutants of many plants grown in the dark have truncated hypocotyls (Barrero et al., 2008; Humplík et al., 2015), and these mutants have stunted growth under high humidity conditions (LeNoble et al., 2004; Sharp et al., 2000). ABA also regulates the rate of leaf emergence (Nakashima et al., 2009; Yoshida et al., 2019b) and stomatal development (Tanaka et al., 2013) under non-stress conditions.

ABA plays a role in flowering time, but less is known about the function of ABA in this process. Arabidopsis plants that experience water deficit under long-day conditions have accelerated flowering as a drought escape mechanism (Riboni et al., 2013), and exogenous ABA application induces flowering (Hwang et al., 2019). Conversely, under short-day conditions, water deficit represses flowering (Riboni et al., 2013). *Ataba1*, *Ataba2,* and *Ataba1/2/3/4* mutants have a late-flowering phenotype under well-watered conditions (Riboni et al., 2013, 2016; Yoshida et al., 2015), indicating the role of ABA in flowering time extends beyond a stress response. *GIGANTEA*, a key flowering gene that regulates the florigen *FLOWERING LOCUS T* (*FT*), is sensitive to ABA signaling (Riboni et al., 2016). The role of ABA in flowering time involving florigen regulation and *GIGANTEA* expression require testing (Martignago et al., 2020).

ABA is responsible for the ripening of non-climacteric fruits like grape berries (Kumar et al., 2014). ABA is involved in berry coloration (anthocyanin biosynthesis (Chung et al., 2019; Karppinen et al., 2018; Koyama et al., 2018)), sugar accumulation (Castellarin et al., 2016; Pilati et al., 2017), and softening (Castellarin et al., 2016). Climacteric and non-climacteric fruits treated with fluridone, an ABA biosynthesis inhibitor, retained firmness (Zhang et al., 2009) while nordihydroguaiaretic acid (NCED activity inhibitor) prevented coloration and reduced ABA concentrations (Li et al., 2019a). ABA levels are low early during non-climacteric fruit development and increase with coloration (Koyama et al., 2010, 2018), but different fruits have unique regulation of ABA during ripening (Fuentes et al., 2019).

In addition to being central to abiotic stress, ABA is also involved in pathogen response. There is a fine balance between abiotic and biotic stress response, and the two

pathways as well as the phytohormones involved (ABA vs. SA and JA) act antagonistically (Moeder et al., 2010). For example, *constitutive expresser of PR genes 22* (*Atcpr22*) mutants that constitutively express biotic defense responses and have enhanced resistance against pathogens also display ABA insensitive phenotypes including reduced stomatal closure and low expression of ABA-induced genes like *RD29B* (Mosher et al., 2010). Similarly, SA accumulation and SA biosynthetic gene expression were repressed with exogenous ABA application and salt (Yasuda et al., 2008). ABA application during pathogen susceptibility assays increases pathogen spread across plant species (Fan et al., 2009; Koga et al., 2004; Mohr and Cahill, 2003). Generally, ABA appears to have a negative impact on biotic stress response (Asselbergh et al., 2008a, 2008b; Cao et al., 2011). However, ABA plays an important role in stomatal closure in response to biotic stress (Melotto et al., 2006) with stomata acting as a major entry point for numerous phytopathogens (Zeng et al., 2010). ABA application also reduced *Cochliobolus miyabeanus* spread in rice mesophyll (Vleesschauwer et al., 2010) and the spread of other fungi in Arabidopsis (Ton and Mauch-Mani, 2004). *Ataba2-12* mutants produced lower JA concentration and were more susceptible to the necrotroph *P. irregulare* (Adie et al., 2007). Overall, the role of ABA in pathogen response appears pathogen (biotroph/necrotroph) and cell type specific.

ABA is the central regulator for plant response and tolerance to abiotic stresses including salt, cold, and water deficit (Cramer et al., 2011). ABA accumulates in response to salt stress, triggering a signaling cascade via ABF2, 3, and 4 (Choi et al., 2000) followed by other TFs. This signaling cascade prevents lateral root emergence, enhances Casparian strip deposition (Duan et al., 2013), and root suberization (Vishal et al., 2019) to limit salt

uptake into the shoot. In response to cold, ABA induces signaling via C-REPEAT BINDING FACTORS/DEHYDRATION-RESPONSIVE ELEMENT BINDING PROTEINS (CBFs/DREBs) and COLD RESPONSIVEs (CORs) (Pareek et al., 2017). This signaling cascade results in the accumulation of osmoprotectants like proline and sugars (Sharma et al., 2019) as well as LEA proteins (Huang et al., 2017; Hundertmark and Hincha, 2008; Sawicki et al., 2019) and lipids to protect plant tissues from ice crystal formation (Pareek et al., 2017).

ABA concentrations increase > 50-fold under water deficit, which is the most dramatic concentration change observed for any phytohormone in response to an environmental condition (Li et al., 2017a). Perhaps the most classic ABA-dependent response a plant has to water deficit is stomatal closure to prevent water loss (Fig. 9). ABA accumulation in guard cells triggers an increase of cytosolic Ca^{2+}, which causes depolarization and activates anion channels (Kim et al., 2010). The slow activating S-type anion channels and the rapid-transient R-type anion channels allow for the efflux of anions from the guard cells (Schroeder and Keller, 1992). The guard cell membrane is hyperpolarized by this efflux, resulting in an efflux of K^+ ions via K^+ channels (Schroeder et al., 2001). This mass efflux causes decreased guard cell turgor and volume, resulting in stomatal closure (Kim et al., 2010).

In addition to causing stomatal closure, ABA prevents stomatal opening. For stomatal opening to occur H^+-ATPases in the guard cell plasma membrane are activated by blue light (Shimazaki et al., 2007), resulting in hyperpolarization of the membrane and uptake of K^+ (Hamilton et al., 2000). This positive charge is balanced with anions like malate ($^{-2}$) (Bowling, 1976), Cl^- (MacRobbie et al., 1982), and NO_3^- (Guo et al., 2003; Qi et

al., 2018). Water is drawn into the guard cell due to the abundance of osmolytes, increasing the guard cell turgor and resulting in stomatal opening (Li et al., 2017a). ABA inhibits stomatal opening by downregulation of the K^+ channels and H^+-ATPase (Kim et al., 2010) necessary for the cation accumulation and hyperpolarization of the membrane.

ABA also affects plant growth under water deficit. Under mild water deficit, growth shifts to promote root development and inhibit shoot growth to better balance water uptake and water loss from photosynthesis (Munns and Cramer, 1996). However, when a plant experiences a severe or long-term water deficit, all growth comes to a halt. Water flow that regulates plant growth and is key to photosynthesis is controlled by plasma membrane intrinsic proteins (PIPs) and tonoplast intrinsic proteins (TIPs), commonly referred to as aquaporins. While some studies show upregulation of aquaporins to facilitate water transport during water deficit (Zargar et al., 2017), others indicate aquaporins, like those in Arabidopsis, are downregulated to prevent water loss (Alexandersson et al., 2005). Aquaporin gene expression in response to WD appears highly dependent upon the stress conditions, cell type, organ, and species in grapevine (Cochetel et al., 2020; Gambetta et al., 2012).

In the past several years, numerous advances have been made in improving understanding of water deficit response and drought tolerance in grapevine. Here a few examples of advances in grapevine water deficit research will be discussed related to work performed throughout this dissertation including physiological thresholds for drought-induced mortality and identification of water deficit response potential hub genes.

Recently, Charrier *et al*. investigated the critical embolism threshold in grapevine (Charrier et al., 2018). Upon experiencing a decrease in stem water potential resultant of

decreased water availability during water deficit, stomata close, and photosynthesis shuts down (Brodribb and Holbrook, 2003). Stomatal closure, resultant of ABA signaling, is essential to maintain xylem pressure above the onset of embolism (Jones and Sutherland, 1991; Tyree and Sperry, 1988). Plant embolism occurs when the chain of water molecules in xylem vessels is broken, allowing for air bubbles to block water flow killing the plant. Charrier *et al*. reported stomatal behaviors were linked to genotype-specific embolism vulnerabilities (i.e. a genotype that maintained open stomata could manage a lower stem water potential without embolism occurrence compared to a genotype with stomatal closure at a lower stress severity). For example, the drought-tolerant rootstock, 110 Richter, had a significantly lower stem water potential than Grenache for the same percentage loss of conductivity (Charrier et al., 2018). Significant differences in embolism vulnerability were also observed across the growing season and stages of plant development (50% loss in conductivity at -1.7 MPa in May vs. -2.07 MPa in July vs. -2.82 MPa in September) (Charrier et al., 2018). In most areas practicing viticulture, water is most available early in the growing season, and the likelihood of a vine experiencing this critical threshold of embolism is low. Although water availability decreases throughout a growing season, vascular tissues mature and lignify, pits thicken, and aquaporins are highly regulated to control water flow enabling a vine to adapt to the increasing stress. However, with the anticipated increase in drought duration and severity from climate change, the probability of a vine experiencing a critical level of stress early in the season increases as well as the likelihood the stress of a long-term drought may exceed the adaptations of mature vines.

One alluring solution to improved drought tolerance is increased ABA production. Tomato is another model plant species, and tomato and grapevine (representing climacteric

and non-climacteric fruits, respectively) genes and water deficit responses are often compared, (Fortes et al., 2017; Grimplet et al., 2016). Tomato plants overexpressing *LeNCED1* have increased ABA accumulation. Plants over producing ABA have improved water use efficiency (WUE) relative to wildtype (WT) plants while functioning at an overall lower stomatal conductance (Huang et al., 2018; Iuchi et al., 2001; Thompson et al., 2007). However, negative consequences like delayed germination and reduced growth and yield make over-production of ABA a less than ideal technique to improve drought tolerance in an agricultural setting. Lamarque *et al*. recently identified another consequence of overproduction of ABA: increased xylem embolism vulnerability (Lamarque et al., 2019). As observed in grapevine (Charrier et al., 2018), tomato plants had increased embolism resistance as plants matured, but surprisingly the overexpression of *LeNCED1* resulted in increased embolism susceptibility compared to WT (Lamarque et al., 2019). The increased embolism vulnerability may have been a result of decreased xylem vessel area (decreased up to 43% in *LeNCED1* overexpression plants). Although over-accumulation of ABA increased WUE under well-watered conditions, these plants had a higher risk of mortality under drought conditions due to a low hydraulic safety margin.

NCED is not the only gene under investigation for improving water deficit response and drought tolerance in grapevine. Numerous other potential target genes for introgression into breeding programs have been identified in the last decade from transcriptomic experiments (Cardone et al., 2019; Catacchio et al., 2019; Cramer et al., 2014; Hopper et al., 2016; Rattanakon et al., 2016; Yıldırım et al., 2018). Key genes identified in these experiments are potential hub genes for water deficit response. Hub genes are considered essential for the proper functioning of an organism in response to treatment or stress, and

disruption of these genes affects the expression of hundreds of other connected genes. Microarray and RNA-Seq experiments (Cochetel et al., 2020; Cramer et al., 2014; Rattanakon et al., 2016) led to the identification of ABA-responsive genes that were further investigated and characterized as potential water deficit response hub genes in this dissertation.

A microarray experiment that identified potential ABA-responsive hub genes was a berry ripening experiment performed to determine differences in gene expression in berry tissue across stages of development (Cramer et al., 2014). Throughout the experiment > 2,000 transcripts significantly changed in response to berry tissue and developmental stage including *NCEDs* and other genes involved in ABA metabolism and signaling, which have an important role in non-climacteric fruit ripening. A unique clade of uncharacterized ERF TFs, *ERF6Ls*, was specifically induced in berry skin as the CS berries ripened. These *ERF6Ls* had increased transcript abundance after ABA concentration was the highest during berry ripening (Alferez et al., 2021), indicating these genes may play a role in ABA response. Of particular interest was *VviERF6L1*, which had the greatest transcript increase of the *ERF6Ls* (Cramer et al., 2014). A rapid-dehydration microarray experiment provided additional evidence for a role of *ERF6Ls* in ABA signaling, as both *VviERF6L1* and *VviERF6L3* transcripts increased in Cabernet Sauvignon leaves within one hour of water deficit treatment (Hopper et al., 2016). The closest Arabidopsis ortholog, *AtERF6*, has established roles in reactive oxygen species (ROS) signaling, SA, cold (Sewelam et al., 2013), and pathogen responses (Meng et al., 2013), and *AtERF6* acts as a hub gene during water deficit (Dubois et al., 2013) providing further evidence this clade may have an important role during ABA signaling and water deficit in grapevine. The *ERF6L* clade and

specifically *VviERF6L1* were chosen for further investigation as an abiotic stress hub in grapevine.

More recently, an RNA-Seq experiment was performed to identify transcriptional similarities and differences of four diverse grapevine species in response to a one- and two-week moderate water deficit (Cochetel et al., 2020). The grapevines used in this experiment were previously shown to have differences in dehydration sensitivity and drought tolerance (Hopper et al., 2014; Lowe and Walker, 2006; Padgett-Johnson et al., 2003). *Vitis vinifera* cv. Cabernet Sauvignon (CS) a moderately water deficit tolerant vine, a drought-tolerant Texan vine, *Vitis champinii* cv. Ramsey (RA), drought-sensitive *Vitis riparia* cv. Riparia Gloire (RI), and an uncharacterized *Vitis vinifera* x *Vitis girdiana* hybrid SC2 (SC) were subjected to well-watered and water-deficit treatments. RNA-Seq identified *NCED3*, *RD29*, and *ABI1* as potential hub genes shared across species in response to water deficit (Cochetel et al., 2020). With the release of the Cabernet Sauvignon genome (Chin et al., 2016), this data set warranted re-analysis and confirmation of *NCED3* as a hub gene in ABA metabolism and water deficit response.

Regulation of gene expression is essential to link genotypes with phenotypes (Marguerat and Bähler, 2010). Today, it is known that the flow of genetic information to an observable phenotype is highly complex, encompassing numerous levels of regulation for DNA, RNA, protein, and metabolites. These previous works (Cochetel et al., 2020; Cramer et al., 2014; Hopper et al., 2016; Rattanakon et al., 2016) identified several potential hub genes responding to ABA including *VviERF6L1* and *VviNCED3*. The role of *VviERF6L1* in ABA signaling and abiotic stress required further investigation, and *NCED3* needed further validation as a water deficit response hub gene in grapevine. The goal of

this dissertation was to investigate these potential water deficit response genes at numerous levels of biochemical regulation (DNA, mRNA, protein, and metabolite) with an **emphasis on mRNA transcript response** to establish a more comprehensive understanding of water deficit in *Vitis*. **Specifically, the goal of this dissertation was to investigate the role of potential hub genes (*VviERF6L1* and *NCED3*) in ABA signaling and stress response at DNA, RNA, protein, and metabolite levels of biochemical regulation.** The results of this dissertation have applications in rootstock selection and targeted breeding programs to improve and expand viticulture in regions that experience abiotic stress like drought.

1.5 References

Abdel-Ghany, S.E., Hamilton, M., Jacobi, J.L., Ngam, P., Devitt, N., Schilkey, F., Ben-Hur, A., and Reddy, A.S.N. (2016). A survey of the sorghum transcriptome using single-molecule long reads. Nat. Commun. *7*, 11706.

Adams, M.D., Kelley, J.M., Gocayne, J.D., Dubnick, M., Polymeropoulos, M.H., Xiao, H., Merril, C.R., Wu, A., Olde, B., Moreno, R.F., et al. (1991). Complementary DNA sequencing: expressed sequence tags and human genome project. Science *252*, 1651–1656.

Adie, B.A.T., Pérez-Pérez, J., Pérez-Pérez, M.M., Godoy, M., Sánchez-Serrano, J.-J., Schmelz, E.A., and Solano, R. (2007). ABA Is an Essential Signal for Plant Resistance to Pathogens Affecting JA Biosynthesis and the Activation of Defenses in Arabidopsis. Plant Cell *19*, 1665–1681.

Ahn, S.H., Kim, M., and Buratowski, S. (2004). Phosphorylation of serine 2 within the RNA polymerase II C-terminal domain couples transcription and 3' end processing. Mol. Cell *13*, 67–76.

Alder, A., Jamil, M., Marzorati, M., Bruno, M., Vermathen, M., Bigler, P., Ghisla, S., Bouwmeester, H., Beyer, P., and Al-Babili, S. (2012). The Path from -Carotene to Carlactone, a Strigolactone-Like Plant Hormone. Science *335*, 1348–1351.

Alexander, L., and Grierson, D. (2002). Ethylene biosynthesis and action in tomato: a model for climacteric fruit ripening. J. Exp. Bot. *53*, 2039–2055.

Alexandersson, E., Fraysse, L., Sjövall-Larsen, S., Gustavsson, S., Fellert, M., Karlsson, M., Johanson, U., and Kjellbom, P. (2005). Whole gene family expression and drought stress regulation of aquaporins. Plant Mol. Biol. *59*, 469–484.

Alferez, F., de Carvalho, D.U., and Boakye, D. (2021). Interplay between Abscisic Acid and Gibberellins, as Related to Ethylene and Sugars, in Regulating Maturation of Non-Climacteric Fruit. Int. J. Mol. Sci. *22*, 669.

Alwine, J.C., Kemp, D.J., and Stark, G.R. (1977). Method for detection of specific RNAs in agarose gels by transfer to diazobenzyloxymethyl-paper and hybridization with DNA probes. Proc. Natl. Acad. Sci. U. S. A. *74*, 5350–5354.

Amrine, K.C.H., Blanco-Ulate, B., Riaz, S., Pap, D., Jones, L., Figueroa-Balderas, R., Walker, M.A., and Cantu, D. (2015). Comparative transcriptomics of Central Asian Vitis vinifera accessions reveals distinct defense strategies against powdery mildew. Hortic. Res. *2*.

Arrigucci, R., Bushkin, Y., Radford, F., Lakehal, K., Vir, P., Pine, R., Martin, D., Sugarman, J., Zhao, Y., Yap, G.S., et al. (2017). FISH-Flow, a protocol for the concurrent detection of mRNA and protein in single cells using fluorescence in situ hybridization and flow cytometry. Nat. Protoc. *12*, 1245–1260.

Ashton, P.M., Nair, S., Dallman, T., Rubino, S., Rabsch, W., Mwaigwisya, S., Wain, J., and O'Grady, J. (2015). MinION nanopore sequencing identifies the position and structure of a bacterial antibiotic resistance island. Nat. Biotechnol. *33*, 296–300.

Asselbergh, B., Achuo, A.E., Höfte, M., and Van Gijsegem, F. (2008a). Abscisic acid deficiency leads to rapid activation of tomato defence responses upon infection with Erwinia chrysanthemi. Mol. Plant Pathol. *9*, 11–24.

Asselbergh, B., De Vleesschauwer, D., and Höfte, M. (2008b). Global Switches and Fine-Tuning—ABA Modulates Plant Pathogen Defense. Mol. Plant-Microbe Interactions® *21*, 709–719.

Au, K.F., Underwood, J.G., Lee, L., and Wong, W.H. (2012). Improving PacBio Long Read Accuracy by Short Read Alignment. PLoS ONE *7*, e46679.

Babraham Bioinformatics (2010). Babraham Bioinformatics - FastQC A Quality Control tool for High Throughput Sequence Data.

Baccarella, A., Williams, C.R., Parrish, J.Z., and Kim, C.C. (2018). Empirical assessment of the impact of sample number and read depth on RNA-Seq analysis workflow performance. BMC Bioinformatics *19*, 423.

Bailly, C. (2019). The signalling role of ROS in the regulation of seed germination and dormancy. Biochem. J. *476*, 3019–3032.

Barickman, T.C., Kopsell, D.A., and Sams, C.E. (2014). Abscisic Acid Increases Carotenoid and Chlorophyll Concentrations in Leaves and Fruit of Two Tomato Genotypes. J. Am. Soc. Hortic. Sci. *139*, 261–266.

Barrero, J.M., Rodríguez, P.L., Quesada, V., Alabadí, D., Blázquez, M.A., Boutin, J.-P., Marion-Poll, A., Ponce, M.R., and Micol, J.L. (2008). The ABA1 gene and carotenoid biosynthesis are required for late skotomorphogenic growth in Arabidopsis thaliana. Plant Cell Environ. *31*, 227–234.

Bartley, G.E., Scolnik, P.A., and Beyer, P. (1999). Two Arabidopsis thaliana carotene desaturases, phytoene desaturase and zeta-carotene desaturase, expressed in Escherichia coli, catalyze a poly-cis pathway to yield pro-lycopene. Eur. J. Biochem. *259*, 396–403.

Bauerle, T.L., Centinari, M., and Bauerle, W.L. (2011). Shifts in xylem vessel diameter and embolisms in grafted apple trees of differing rootstock growth potential in response to drought. Planta *234*, 1045–1054.

Bauman, J.G.J., Wiegant, J., Borst, P., and van Duijn, P. (1980). A new method for fluorescence microscopical localization of specific DNA sequences by in situ hybridization of fluorochrome-labelled RNA. Exp. Cell Res. *128*, 485–490.

Baxter, R.A. (2008). Anti-aging properties of resveratrol: review and report of a potent new antioxidant skin care formulation. J. Cosmet. Dermatol. *7*, 2–7.

Becker-André, M., and Hahlbrock, K. (1989). Absolute mRNA quantification using the polymerase chain reaction (PCR). A novel approach by a PCR aided transcript titration assay (PATTY). Nucleic Acids Res. *17*, 9437–9446.

Belin, C., Megies, C., Hauserová, E., and Lopez-Molina, L. (2009). Abscisic Acid Represses Growth of the Arabidopsis Embryonic Axis after Germination by Enhancing Auxin Signaling. Plant Cell *21*, 2253–2268.

Bertolino, L.T., Caine, R.S., and Gray, J.E. (2019). Impact of Stomatal Density and Morphology on Water-Use Efficiency in a Changing World. Front. Plant Sci. *10*.

Bittner, F., Oreb, M., and Mendel, R.R. (2001). ABA3 is a molybdenum cofactor sulfurase required for activation of aldehyde oxidase and xanthine dehydrogenase in Arabidopsis thaliana. J. Biol. Chem. *276*, 40381–40384.

Blanco-Ulate, B., Hopfer, H., Figueroa-Balderas, R., Ye, Z., Rivero, R.M., Albacete, A., Pérez-Alfocea, F., Koyama, R., Anderson, M.M., Smith, R.J., et al. (2017). Red blotch disease alters grape berry development and metabolism by interfering with the transcriptional and hormonal regulation of ripening. J. Exp. Bot. *68*, 1225–1238.

Boccaletto, P., Machnicka, M.A., Purta, E., Piatkowski, P., Baginski, B., Wirecki, T.K., de Crécy-Lagard, V., Ross, R., Limbach, P.A., Kotter, A., et al. (2018). MODOMICS: a database of RNA modification pathways. 2017 update. Nucleic Acids Res. *46*, D303–D307.

Boguski, M.S., Lowe, T.M., and Tolstoshev, C.M. (1993). dbEST--database for "expressed sequence tags." Nat. Genet. *4*, 332–333.

Bonaldo, M.F., Lennon, G., and Soares, M.B. (1996). Normalization and subtraction: two approaches to facilitate gene discovery. Genome Res. *6*, 791–806.

Boneh, U., Biton, I., Zheng, C., Schwartz, A., and Ben-Ari, G. (2012). Characterization of potential ABA receptors in Vitis vinifera. Plant Cell Rep. *31*, 311–321.

Bowling, D.J.F. (1976). Malate-switch hypothesis to explain the action of stomata. Nature *262*, 393–394.

Bray, E.A., and Zeevaart, J.A.D. (1985). The Compartmentation of Abscisic Acid and β-d-Glucopyranosyl Abscisate in Mesophyll Cells. Plant Physiol. *79*, 719–722.

Bray, N.L., Pimentel, H., Melsted, P., and Pachter, L. (2016). Near-optimal probabilistic RNA-seq quantification. Nat. Biotechnol. *34*, 525–527.

Briggs, S.D., Xiao, T., Sun, Z.-W., Caldwell, J.A., Shabanowitz, J., Hunt, D.F., Allis, C.D., and Strahl, B.D. (2002). Trans -histone regulatory pathway in chromatin. Nature *418*, 498–498.

Brocard, I.M. (2002). Regulation and Role of the Arabidopsis Abscisic Acid-Insensitive 5 Gene in Abscisic Acid, Sugar, and Stress Response. PLANT Physiol. *129*, 1533–1543.

Brodribb, T.J., and Feild, T.S. (2000). Stem hydraulic supply is linked to leaf photosynthetic capacity: evidence from New Caledonian and Tasmanian rainforests. Plant Cell Environ. *23*, 1381–1388.

Brodribb, T.J., and Holbrook, N.M. (2003). Stomatal Closure during Leaf Dehydration, Correlation with Other Leaf Physiological Traits. Plant Physiol. *132*, 2166–2173.

Bruzzone, S., Moreschi, I., Usai, C., Guida, L., Damonte, G., Salis, A., Scarfì, S., Millo, E., Flora, A.D., and Zocchi, E. (2007). Abscisic acid is an endogenous cytokine in human granulocytes with cyclic ADP-ribose as second messenger. Proc. Natl. Acad. Sci. *104*, 5759–5764.

Buermans, H.P.J., and den Dunnen, J.T. (2014). Next generation sequencing technology: Advances and applications. Biochim. Biophys. Acta BBA - Mol. Basis Dis. *1842*, 1932–1941.

Bumgarner, R. (2013). DNA microarrays: Types, Applications and their future. Curr. Protoc. Mol. Biol. Ed. Frederick M Ausubel Al *0 22*, Unit-22.1.

Burla, B., Pfrunder, S., Nagy, R., Francisco, R.M., Lee, Y., and Martinoia, E. (2013). Vacuolar Transport of Abscisic Acid Glucosyl Ester Is Mediated by ATP-Binding Cassette and Proton-Antiport Mechanisms in Arabidopsis. Plant Physiol. *163*, 1446–1458.

Bushnell, D.A., Westover, K.D., Davis, R.E., and Kornberg, R.D. (2004). Structural basis of transcription: an RNA polymerase II-TFIIB cocrystal at 4.5 Angstroms. Science *303*, 983–988.

Bustin, S., and Nolan, T. (2017). Talking the talk, but not walking the walk: RT-qPCR as a paradigm for the lack of reproducibility in molecular research. Eur. J. Clin. Invest. *47*, 756–774.

Cabré, F., and Nuñez, M. (2020). Impacts of climate change on viticulture in Argentina. Reg. Environ. Change *20*, 12.

Cai, Z., Liu, J., Wang, H., Yang, C., Chen, Y., Li, Y., Pan, S., Dong, R., Tang, G., Barajas-Lopez, J. de D., et al. (2014). GSK3-like kinases positively modulate abscisic acid signaling through phosphorylating subgroup III SnRK2s in Arabidopsis. Proc. Natl. Acad. Sci. *111*, 9651–9656.

Caine, R.S., Yin, X., Sloan, J., Harrison, E.L., Mohammed, U., Fulton, T., Biswal, A.K., Dionora, J., Chater, C.C., Coe, R.A., et al. (2019). Rice with reduced stomatal density conserves water and has improved drought tolerance under future climate conditions. New Phytol. *221*, 371–384.

Caldeira, C.F., Bosio, M., Parent, B., Jeanguenin, L., Chaumont, F., and Tardieu, F. (2014). A Hydraulic Model Is Compatible with Rapid Changes in Leaf Elongation under Fluctuating Evaporative Demand and Soil Water Status. Plant Physiol. *164*, 1718–1730.

Cao, F.Y., Yoshioka, K., and Desveaux, D. (2011). The roles of ABA in plant–pathogen interactions. J. Plant Res. *124*, 489–499.

Cardone, M.F., Perniola, R., Catacchio, C.R., Alagna, F., Rotunno, S., Crupi, P., Antonacci, D., Velasco, R., Ventura, M., and Bergamini, C. (2019). Grapevine adaptation to drought: New candidate genes for the genotype-dependent response. BIO Web Conf. *15*, 01016.

del Carmen Rodríguez-Gacio, M., Matilla-Vázquez, M.A., and Matilla, A.J. (2009). Seed dormancy and ABA signaling. Plant Signal. Behav. *4*, 1035–1048.

Castellarin, S.D., Gambetta, G.A., Wada, H., Krasnow, M.N., Cramer, G.R., Peterlunger, E., Shackel, K.A., and Matthews, M.A. (2016). Characterization of major ripening events during softening in grape: turgor, sugar accumulation, abscisic acid metabolism, colour development, and their relationship with growth. J. Exp. Bot. *67*, 709–722.

Catacchio, C.R., Alagna, F., Perniola, R., Bergamini, C., Rotunno, S., Calabrese, F.M., Crupi, P., Antonacci, D., Ventura, M., and Cardone, M.F. (2019). Transcriptomic and

genomic structural variation analyses on grape cultivars reveal new insights into the genotype-dependent responses to water stress. Sci. Rep. *9*, 2809.

Charrier, G., Delzon, S., Domec, J.-C., Zhang, L., Delmas, C.E.L., Merlin, I., Corso, D., King, A., Ojeda, H., Ollat, N., et al. (2018). Drought will not leave your glass empty: Low risk of hydraulic failure revealed by long-term drought observations in world's top wine regions. Sci. Adv. *4*, eaao6969.

Chen, H.-T., Warfield, L., and Hahn, S. (2007). The positions of TFIIF and TFIIE in the RNA polymerase II transcription preinitiation complex. Nat. Struct. Mol. Biol. *14*, 696–703.

Chen, K., Du, K., Shi, Y., Yin, L., Shen, W.-H., Yu, Y., Liu, B., and Dong, A. (2021). H3K36 methyltransferase SDG708 enhances drought tolerance by promoting abscisic acid biosynthesis in rice. New Phytol. *n/a*.

Chen, K.H., Boettiger, A.N., Moffitt, J.R., Wang, S., and Zhuang, X. (2015). Spatially resolved, highly multiplexed RNA profiling in single cells. Science *348*.

Cheng, Z.J., Zhao, X.Y., Shao, X.X., Wang, F., Zhou, C., Liu, Y.G., Zhang, Y., and Zhang, X.S. (2014). Abscisic Acid Regulates Early Seed Development in Arabidopsis by ABI5-Mediated Transcription of SHORT HYPOCOTYL UNDER BLUE1[C][W][OPEN]. Plant Cell *26*, 1053–1068.

Cheung, P., Tanner, K.G., Cheung, W.L., Sassone-Corsi, P., Denu, J.M., and Allis, C.D. (2000). Synergistic coupling of histone H3 phosphorylation and acetylation in response to epidermal growth factor stimulation. Mol. Cell *5*, 905–915.

Chin, C.-S., Peluso, P., Sedlazeck, F.J., Nattestad, M., Concepcion, G.T., Clum, A., Dunn, C., O'Malley, R., Figueroa-Balderas, R., Morales-Cruz, A., et al. (2016). Phased diploid genome assembly with single-molecule real-time sequencing. Nat. Methods *13*, 1050–1054.

Chinnusamy, V., Gong, Z., and Zhu, J.-K. (2008). Abscisic Acid-mediated Epigenetic Processes in Plant Development and Stress Responses. J. Integr. Plant Biol. *50*, 1187–1195.

Cho, H.-T. (2007). A cis-Element for Root Hair Specificity Has Been Co-opted Repeatedly Through the Divergence of Upstream Fate-Determining Machineries. Plant Signal. Behav. *2*, 117.

Choi, H., Hong, J., Ha, J., Kang, J., and Kim, S.Y. (2000). ABFs, a family of ABA-responsive element binding factors. J. Biol. Chem. *275*, 1723–1730.

Chung, S.W., Yu, D.J., Oh, H.D., Ahn, J.H., Huh, J.H., and Lee, H.J. (2019). Transcriptional regulation of abscisic acid biosynthesis and signal transduction, and anthocyanin biosynthesis in 'Bluecrop' highbush blueberry fruit during ripening. PLOS ONE *14*, e0220015.

Clapier, C.R., and Cairns, B.R. (2009). The biology of chromatin remodeling complexes. Annu. Rev. Biochem. *78*, 273–304.

Cochetel, N., Ghan, R., Toups, H.S., Degu, A., Tillett, R.L., Schlauch, K.A., and Cramer, G.R. (2020). Drought tolerance of the grapevine, Vitis champinii cv. Ramsey, is associated with higher photosynthesis and greater transcriptomic responsiveness of abscisic acid biosynthesis and signaling. BMC Plant Biol. *20*.

Colin, J., Candelli, T., Porrua, O., Boulay, J., Zhu, C., Lacroute, F., Steinmetz, L.M., and Libri, D. (2014). Roadblock termination by reb1p restricts cryptic and readthrough transcription. Mol. Cell *56*, 667–680.

Coller, J., and Parker, R. (2004). Eukaryotic mRNA Decapping. Annu. Rev. Biochem. *73*, 861–890.

Corchete, L.A., Rojas, E.A., Alonso-López, D., De Las Rivas, J., Gutiérrez, N.C., and Burguillo, F.J. (2020). Systematic comparison and assessment of RNA-seq procedures for gene expression quantitative analysis. Sci. Rep. *10*, 19737.

Cornforth, J.W., Milborrow, B.V., Ryback, G., and Wareing, P.F. (1965). Chemistry and Physiology of 'Dormins' In Sycamore: Identity of Sycamore 'Dormin' with Abscisin II. Nature *205*, 1269–1270.

Costa-Silva, J., Domingues, D., and Lopes, F.M. (2017). RNA-Seq differential expression analysis: An extended review and a software tool. PLOS ONE *12*, e0190152.

Cramer, G.R., Urano, K., Delrot, S., Pezzotti, M., and Shinozaki, K. (2011). Effects of abiotic stress on plants: a systems biology perspective. BMC Plant Biol. *11*, 163.

Cramer, G.R., Ghan, R., Schlauch, K.A., Tillett, R.L., Heymann, H., Ferrarini, A., Delledonne, M., Zenoni, S., Fasoli, M., and Pezzotti, M. (2014). Transcriptomic analysis of the late stages of grapevine (Vitis vinifera cv. Cabernet Sauvignon) berry ripening reveals significant induction of ethylene signaling and flavor pathways in the skin. BMC Plant Biol. *14*.

Crick, F. (1957). On protein synthesis.

Cui, C., Shu, W., and Li, P. (2016). Fluorescence In situ Hybridization: Cell-Based Genetic Diagnostic and Research Applications. Front. Cell Dev. Biol. *4*.

Cutler, A.J., and Krochko, J.E. (1999). Formation and breakdown of ABA. Trends Plant Sci. *4*, 472–478.

Dall'Osto, L., Cazzaniga, S., North, H., Marion-Poll, A., and Bassi, R. (2007). The Arabidopsis aba4-1 Mutant Reveals a Specific Function for Neoxanthin in Protection against Photooxidative Stress. Plant Cell *19*, 1048–1064.

Damasco, G., Delpiano, D., Larcher, R., Nardin, T., Perra, M., and Lovicu, G. (2020). Confirming the function of a Final Bronze Age wine processing site in the Nuraghe Genna Maria in Villanovaforru (South Sardinia). VITIS - J. Grapevine Res. *59*, 93–100.

Davuluri, R.V., Sun, H., Palaniswamy, S.K., Matthews, N., Molina, C., Kurtz, M., and Grotewold, E. (2003). AGRIS: Arabidopsis Gene Regulatory Information Server, an information resource of Arabidopsis cis-regulatory elements and transcription factors. BMC Bioinformatics *4*, 25.

De Smet, I., Signora, L., Beeckman, T., Inzé, D., Foyer, C.H., and Zhang, H. (2003). An abscisic acid-sensitive checkpoint in lateral root development of *Arabidopsis*. Plant J. *33*, 543–555.

Deguchi, M., Kane, S., Potlakayala, S., George, H., Proano, R., Sheri, V., Curtis, W.R., and Rudrabhatla, S. (2020). Metabolic Engineering Strategies of Industrial Hemp (Cannabis sativa L.): A Brief Review of the Advances and Challenges. Front. Plant Sci. *11*.

Deng, W., and Roberts, S.G.E. (2005). A core promoter element downstream of the TATA box that is recognized by TFIIB. Genes Dev. *19*, 2418–2423.

Desgagné-Penix, I., Farrow, S.C., Cram, D., Nowak, J., and Facchini, P.J. (2012). Integration of deep transcript and targeted metabolite profiles for eight cultivars of opium poppy. Plant Mol. Biol. *79*, 295–313.

Devakumar, A.S., Gawai Prakash, P., Sathik, M.B.M., and Jacob, J. (1999). Drought alters the canopy architecture and micro-climate of Hevea brasiliensis trees. Trees *13*, 161–167.

Diatchenko, L., Lau, Y.F., Campbell, A.P., Chenchik, A., Moqadam, F., Huang, B., Lukyanov, S., Lukyanov, K., Gurskaya, N., Sverdlov, E.D., et al. (1996). Suppression subtractive hybridization: a method for generating differentially regulated or tissue-specific cDNA probes and libraries. Proc. Natl. Acad. Sci. U. S. A. *93*, 6025–6030.

Digrado, A., Mitchell, N.G., Montes, C.M., Dirvanskyte, P., and Ainsworth, E.A. (2020). Assessing diversity in canopy architecture, photosynthesis, and water-use efficiency in a cowpea magic population. Food Energy Secur. *9*, e236.

Djebali, S., Davis, C.A., Merkel, A., Dobin, A., Lassmann, T., Mortazavi, A., Tanzer, A., Lagarde, J., Lin, W., Schlesinger, F., et al. (2012). Landscape of transcription in human cells. Nature *489*, 101–108.

Dolfini, D., Zambelli, F., Pavesi, G., and Mantovani, R. (2009). A perspective of promoter architecture from the CCAAT box. Cell Cycle *8*, 12.

Dörffling, K. (2015). The Discovery of Abscisic Acid: A Retrospect. J. Plant Growth Regul. *34*, 795–808.

Du, H., Wang, N., Cui, F., Li, X., Xiao, J., and Xiong, L. (2010). Characterization of the β-Carotene Hydroxylase Gene DSM2 Conferring Drought and Oxidative Stress Resistance by Increasing Xanthophylls and Abscisic Acid Synthesis in Rice. Plant Physiol. *154*, 1304–1318.

Duan, L., Dietrich, D., Ng, C.H., Chan, P.M.Y., Bhalerao, R., Bennett, M.J., and Dinneny, J.R. (2013). Endodermal ABA Signaling Promotes Lateral Root Quiescence during Salt Stress in *Arabidopsis* Seedlings. Plant Cell *25*, 324–341.

Dubois, M., Skirycz, A., Claeys, H., Maleux, K., Dhondt, S., De Bodt, S., Vanden Bossche, R., De Milde, L., Yoshizumi, T., Matsui, M., et al. (2013). ETHYLENE RESPONSE FACTOR6 Acts as a Central Regulator of Leaf Growth under Water-Limiting Conditions in Arabidopsis. Plant Physiol. *162*, 319–332.

Dunn, E.F., Hammell, C.M., Hodge, C.A., and Cole, C.N. (2005). Yeast poly(A)-binding protein, Pab1, and PAN, a poly(A) nuclease complex recruited by Pab1, connect mRNA biogenesis to export. Genes Dev. *19*, 90–103.

Dunn, J., Hunt, L., Afsharinafar, M., Meselmani, M.A., Mitchell, A., Howells, R., Wallington, E., Fleming, A.J., and Gray, J.E. (2019). Reduced stomatal density in bread wheat leads to increased water-use efficiency. J. Exp. Bot. *70*, 4737–4748.

Dure, L. (1997). Lea Proteins and the Desiccation Tolerance of Seeds. In Cellular and Molecular Biology of Plant Seed Development, B.A. Larkins, and I.K. Vasil, eds. (Dordrecht: Springer Netherlands), pp. 525–543.

Dyck, G.J.B., Raj, P., Zieroth, S., Dyck, J.R.B., and Ezekowitz, J.A. (2019). The Effects of Resveratrol in Patients with Cardiovascular Disease and Heart Failure: A Narrative Review. Int. J. Mol. Sci. *20*.

Dyke, M.V., Roeder, R.G., and Sawadogo, M. (1988). Physical analysis of transcription preinitiation complex assembly on a class II gene promoter. Science *241*, 1335–1338.

Eisenhaber, B., and Eisenhaber, F. (2007). Posttranslational modifications and subcellular localization signals: indicators of sequence regions without inherent 3D structure? Curr. Protein Pept. Sci. *8*, 197–203.

Endo, A., Sawada, Y., Takahashi, H., Okamoto, M., Ikegami, K., Koiwai, H., Seo, M., Toyomasu, T., Mitsuhashi, W., Shinozaki, K., et al. (2008). Drought Induction of Arabidopsis 9-cis-Epoxycarotenoid Dioxygenase Occurs in Vascular Parenchyma Cells. PLANT Physiol. *147*, 1984–1993.

Eng, C.-H.L., Lawson, M., Zhu, Q., Dries, R., Koulena, N., Takei, Y., Yun, J., Cronin, C., Karp, C., Yuan, G.-C., et al. (2019). Transcriptome-scale super-resolved imaging in tissues by RNA seqFISH+. Nature *568*, 235–239.

Ernst, L., Goodger, J.Q.D., Alvarez, S., Marsh, E.L., Berla, B., Lockhart, E., Jung, J., Li, P., Bohnert, H.J., and Schachtman, D.P. (2010). Sulphate as a xylem-borne chemical signal precedes the expression of ABA biosynthetic genes in maize roots. J. Exp. Bot. *61*, 3395–3405.

Eskling, M., Arvidsson, P.-O., and Åkerlund, H.-E. (1997). The xanthophyll cycle, its regulation and components. Physiol. Plant. *100*, 806–816.

Ewing, R., Poirot, O., and Claverie, J.M. (1999). Comparative analysis of the Arabidopsis and rice expressed sequence tag (EST) sets. In Silico Biol. *1*, 197–213.

Fan, J., Hill, L., Crooks, C., Doerner, P., and Lamb, C. (2009). Abscisic acid has a key role in modulating diverse plant-pathogen interactions. Plant Physiol. *150*, 1750–1761.

Fanourakis, D., Giday, H., Milla, R., Pieruschka, R., Kjaer, K.H., Bolger, M., Vasilevski, A., Nunes-Nesi, A., Fiorani, F., and Ottosen, C.-O. (2015). Pore size regulates operating stomatal conductance, while stomatal densities drive the partitioning of conductance between leaf sides. Ann. Bot. *115*, 555–565.

Finkelstein, R. (2013). Abscisic Acid Synthesis and Response. Arab. Book Am. Soc. Plant Biol. *11*.

Finkelstein, R.R. (1994). Mutations at two new Arabidopsis ABA response loci are similar to the abi3 mutations. Plant J. *5*, 765–771.

Finkelstein, R.R., and Lynch, T.J. (2000). The Arabidopsis Abscisic Acid Response Gene ABI5 Encodes a Basic Leucine Zipper Transcription Factor. Plant Cell *12*, 599–609.

Fitton, N., Alexander, P., Arnell, N., Bajzelj, B., Calvin, K., Doelman, J., Gerber, J.S., Havlik, P., Hasegawa, T., Herrero, M., et al. (2019). The vulnerabilities of agricultural land and food production to future water scarcity. Glob. Environ. Change *58*, 101944.

Fletcher, L.R., Cui, H., Callahan, H., Scoffoni, C., John, G.P., Bartlett, M.K., Burge, D.O., and Sack, L. (2018). Evolution of leaf structure and drought tolerance in species of Californian Ceanothus. Am. J. Bot. *105*, 1672–1687.

Fort, K., Fraga, J., Grossi, D., and Walker, M.A. (2017). Early Measures of Drought Tolerance in Four Grape Rootstocks. J. Am. Soc. Hortic. Sci. *142*, 36–46.

Fortes, A.M., Granell, A., Pezzotti, M., and Bouzayen, M. (2017). Editorial: Molecular and Metabolic Mechanisms Associated with Fleshy Fruit Quality. Front. Plant Sci. *8*.

Franco-Zorrilla, J.M., López-Vidriero, I., Carrasco, J.L., Godoy, M., Vera, P., and Solano, R. (2014). DNA-binding specificities of plant transcription factors and their potential to define target genes. Proc. Natl. Acad. Sci. *111*, 2367–2372.

Franke, R., Briesen, I., Wojciechowski, T., Faust, A., Yephremov, A., Nawrath, C., and Schreiber, L. (2005). Apoplastic polyesters in Arabidopsis surface tissues – A typical suberin and a particular cutin. Phytochemistry *66*, 2643–2658.

Frébort, I., Kowalska, M., Hluska, T., Frébortová, J., and Galuszka, P. (2011). Evolution of cytokinin biosynthesis and degradation. J. Exp. Bot. *62*, 2431–2452.

Frey, A., Godin, B., Bonnet, M., Sotta, B., and Marion-Poll, A. (2004). Maternal synthesis of abscisic acid controls seed development and yield in Nicotiana plumbaginifolia. Planta *218*, 958–964.

Fuentes, L., Figueroa, C.R., and Valdenegro, M. (2019). Recent Advances in Hormonal Regulation and Cross-Talk during Non-Climacteric Fruit Development and Ripening. Horticulturae *5*, 45.

Fujii, H., Verslues, P.E., and Zhu, J.-K. (2007). Identification of Two Protein Kinases Required for Abscisic Acid Regulation of Seed Germination, Root Growth, and Gene Expression in Arabidopsis. Plant Cell *19*, 485–494.

Fujioka, S., and Yokota, T. (2003). Biosynthesis and Metabolism of Brassinosteroids. Annu. Rev. Plant Biol. *54*, 137–164.

Gall, J.G., and Pardue, M.L. (1969). Formation and Detection of Rna-Dna Hybrid Molecules in Cytological Preparations. Proc. Natl. Acad. Sci. *63*, 378–383.

Gambetta, G.A. (2016). Water Stress and Grape Physiology in the Context of Global Climate Change. J. Wine Econ. *11*, 168–180.

Gambetta, G.A., Manuck, C.M., Drucker, S.T., Shaghasi, T., Fort, K., Matthews, M.A., Walker, M.A., and McElrone, A.J. (2012). The relationship between root hydraulics and scion vigour across Vitis rootstocks: what role do root aquaporins play? J. Exp. Bot. *63*, 6445–6455.

Gao, X.-B., Guo, C., Li, F.-M., Li, M., and He, J. (2020). High Soybean Yield and Drought Adaptation Being Associated with Canopy Architecture, Water Uptake, and Root Traits. Agronomy *10*, 608.

Ghazal, G., Gagnon, J., Jacques, P.-E., Landry, J.-R., Robert, F., and Elela, S.A. (2009). Yeast RNase III triggers polyadenylation-independent transcription termination. Mol. Cell *36*, 99–109.

Gillard, D.F., and Walton, D.C. (1976). Abscisic Acid Metabolism by a Cell-free Preparation from Echinocystis lobata Liquid Endosperm. Plant Physiol *58*, 6.

Gómez-Porras, J.L., Riaño-Pachón, D.M., Dreyer, I., Mayer, J.E., and Mueller-Roeber, B. (2007). Genome-wide analysis of ABA-responsive elements ABRE and CE3 reveals divergent patterns in Arabidopsis and rice. BMC Genomics *8*, 260.

González-Guzmán, M., Apostolova, N., Bellés, J.M., Barrero, J.M., Piqueras, P., Ponce, M.R., Micol, J.L., Serrano, R., and Rodríguez, P.L. (2002). The Short-Chain Alcohol Dehydrogenase ABA2 Catalyzes the Conversion of Xanthoxin to Abscisic Aldehyde. Plant Cell *14*, 1833–1846.

Gonzalez-Guzman, M., Pizzio, G.A., Antoni, R., Vera-Sirera, F., Merilo, E., Bassel, G.W., Fernández, M.A., Holdsworth, M.J., Perez-Amador, M.A., Kollist, H., et al. (2012). Arabidopsis PYR/PYL/RCAR Receptors Play a Major Role in Quantitative Regulation of Stomatal Aperture and Transcriptional Response to Abscisic Acid. Plant Cell *24*, 2483–2496.

Goodger, J.Q., and Schachtman, D.P. (2010). Re-examining the role of ABA as the primary long-distance signal produced by water-stressed roots. Plant Signal. Behav. *5*, 1298–1301.

Gosti, F., Beaudoin, N., Serizet, C., Webb, A.A., Vartanian, N., and Giraudat, J. (1999). ABI1 protein phosphatase 2C is a negative regulator of abscisic acid signaling. Plant Cell *11*, 1897–1910.

Gout, J.-F., Li, W., Fritsch, C., Li, A., Haroon, S., Singh, L., Hua, D., Fazelinia, H., Smith, Z., Seeholzer, S., et al. (2017). The landscape of transcription errors in eukaryotic cells. Sci. Adv. *3*.

Graber, J.H., Cantor, C.R., Mohr, S.C., and Smith, T.F. (1999). In silico detection of control signals: mRNA 3′-end-processing sequences in diverse species. Proc. Natl. Acad. Sci. *96*, 14055–14060.

Gress, T.M., Hoheisel, J.D., Lennon, G.G., Zehetner, G., and Lehrach, H. (1992). Hybridization fingerprinting of high-density cDNA-library arrays with cDNA pools derived from whole tissues. Mamm. Genome *3*, 609–619.

Griffiths, A.J., Miller, J.H., Suzuki, D.T., Lewontin, R.C., and Gelbart, W.M. (2000). Transcription: an overview of gene regulation in eukaryotes. Introd. Genet. Anal. 7th Ed.

Grimplet, J., Agudelo-Romero, P., Teixeira, R.T., Martinez-Zapater, J.M., and Fortes, A.M. (2016). Structural and Functional Analysis of the GRAS Gene Family in Grapevine Indicates a Role of GRAS Proteins in the Control of Development and Stress Responses. Front. Plant Sci. *7*.

Grunstein, M., and Hogness, D.S. (1975). Colony hybridization: a method for the isolation of cloned DNAs that contain a specific gene. Proc. Natl. Acad. Sci. U. S. A. *72*, 3961–3965.

Grzechnik, P., Tan-Wong, S.M., and Proudfoot, N.J. (2014). Terminate and make a loop: regulation of transcriptional directionality. Trends Biochem. Sci. *39*, 319–327.

Güimil, S., Chang, H.-S., Zhu, T., Sesma, A., Osbourn, A., Roux, C., Ioannidis, V., Oakeley, E.J., Docquier, M., Descombes, P., et al. (2005). Comparative transcriptomics of

rice reveals an ancient pattern of response to microbial colonization. Proc. Natl. Acad. Sci. *102*, 8066–8070.

Guo, A., He, K., Liu, D., Bai, S., Gu, X., Wei, L., and Luo, J. (2005). DATF: a database of Arabidopsis transcription factors. Bioinforma. Oxf. Engl. *21*, 2568–2569.

Guo, F.-Q., Young, J., and Crawford, N.M. (2003). The Nitrate Transporter AtNRT1.1 (CHL1) Functions in Stomatal Opening and Contributes to Drought Susceptibility in Arabidopsis. Plant Cell *15*, 107–117.

Hamilton, E. (2013). Mythology (Hachette Book Group).

Hamilton, D.W.A., Hills, A., Köhler, B., and Blatt, M.R. (2000). Ca2+ channels at the plasma membrane of stomatal guard cells are activated by hyperpolarization and abscisic acid. Proc. Natl. Acad. Sci. U. S. A. *97*, 4967–4972.

Hardy, J.P., Anderson, V.J., and Gardner, J.S. (1995). Stomatal characteristics, conductance ratios, and drought-induced leaf modifications of semiarid grassland species. Am. J. Bot. *82*, 1–7.

Hartmann, H., Ziegler, W., and Trumbore, S. (2013). Lethal drought leads to reduction in nonstructural carbohydrates in Norway spruce tree roots but not in the canopy. Funct. Ecol. *27*, 413–427.

Hatfield, J.L., and Dold, C. (2019). Water-Use Efficiency: Advances and Challenges in a Changing Climate. Front. Plant Sci. *10*.

Haworth, M., Centritto, M., Giovannelli, A., Marino, G., Proietti, N., Capitani, D., De Carlo, A., and Loreto, F. (2017). Xylem morphology determines the drought response of two *Arundo donax* ecotypes from contrasting habitats. GCB Bioenergy *9*, 119–131.

Heather, J.M., and Chain, B. (2016). The sequence of sequencers: The history of sequencing DNA. Genomics *107*, 1–8.

Hector, R.E., Nykamp, K.R., Dheur, S., Anderson, J.T., Non, P.J., Urbinati, C.R., Wilson, S.M., Minvielle-Sebastia, L., and Swanson, M.S. (2002). Dual requirement for yeast hnRNP Nab2p in mRNA poly(A) tail length control and nuclear export. EMBO J. *21*, 1800–1810.

Heinitz, C.C., Fort, K., and Walker, M.A. (2015). DEVELOPING DROUGHT AND SALT RESISTANT GRAPE ROOTSTOCKS. Acta Hortic. 305–312.

Hellemans, J., Mortier, G., De Paepe, A., Speleman, F., and Vandesompele, J. (2007). qBase relative quantification framework and software for management and automated analysis of real-time quantitative PCR data. Genome Biol. *8*, R19.

Henegariu, O., Heerema, N. a., Dlouhy, S. r., Vance, G. h., and Vogt, P. h. (1997). Multiplex PCR: Critical Parameters and Step-by-Step Protocol. BioTechniques *23*, 504–511.

Hernandez-Garcia, C.M., and Finer, J.J. (2014). Identification and validation of promoters and cis-acting regulatory elements. Plant Sci. *217–218*, 109–119.

Hieber, A.D., Bugos, R.C., and Yamamoto, H.Y. (2000). Plant lipocalins: violaxanthin de-epoxidase and zeaxanthin epoxidase. Biochim. Biophys. Acta BBA - Protein Struct. Mol. Enzymol. *1482*, 84–91.

Hill, C.H., Boreikaitė, V., Kumar, A., Casañal, A., Kubík, P., Degliesposti, G., Maslen, S., Mariani, A., von Loeffelholz, O., Girbig, M., et al. (2019). Activation of the Endonuclease that Defines mRNA 3′ Ends Requires Incorporation into an 8-Subunit Core Cleavage and Polyadenylation Factor Complex. Mol. Cell *73*, 1217-1231.e11.

Hirayama, T., and Umezawa, T. (2010). The PP2C-SnRK2 complex. Plant Signal. Behav. *5*, 160–163.

Ho, B., Baryshnikova, A., and Brown, G.W. (2018). Unification of Protein Abundance Datasets Yields a Quantitative Saccharomyces cerevisiae Proteome. Cell Syst. *6*, 192-205.e3.

Hong, J.C. (2016). General Aspects of Plant Transcription Factor Families. In Plant Transcription Factors, (Elsevier), pp. 35–56.

Hopper, D.W., Ghan, R., and Cramer, G.R. (2014). A rapid dehydration leaf assay reveals stomatal response differences in grapevine genotypes. Hortic. Res. *1*.

Hopper, D.W., Ghan, R., Schlauch, K.A., and Cramer, G.R. (2016). Transcriptomic network analyses of leaf dehydration responses identify highly connected ABA and ethylene signaling hubs in three grapevine species differing in drought tolerance. BMC Plant Biol. *16*.

Hsu, C.L., and Stevens, A. (1993). Yeast cells lacking 5'-->3' exoribonuclease 1 contain mRNA species that are poly(A) deficient and partially lack the 5' cap structure. Mol. Cell. Biol. *13*, 4826–4835.

Hu, H., Yang, W., Zheng, Z., Niu, Z., Yang, Y., Wan, D., Liu, J., and Ma, T. (2020). Analysis of Alternative Splicing and Alternative Polyadenylation in Populus alba var. pyramidalis by Single-Molecular Long-Read Sequencing. Front. Genet. *11*.

Huang, J., Lu, X., Yan, H., Chen, S., Zhang, W., Huang, R., and Zheng, Y. (2012). Transcriptome characterization and sequencing-based identification of salt-responsive genes in Millettia pinnata, a semi-mangrove plant. DNA Res. Int. J. Rapid Publ. Rep. Genes Genomes *19*, 195–207.

Huang, X., Shi, H., Hu, Z., Liu, A., Amombo, E., Chen, L., and Fu, J. (2017). ABA Is Involved in Regulation of Cold Stress Response in Bermudagrass. Front. Plant Sci. *8*.

Huang, Y., Guo, Y., Liu, Y., Zhang, F., Wang, Z., Wang, H., Wang, F., Li, D., Mao, D., Luan, S., et al. (2018). 9-cis-Epoxycarotenoid Dioxygenase 3 Regulates Plant Growth and Enhances Multi-Abiotic Stress Tolerance in Rice. Front. Plant Sci. *9*.

Huber, D., Voith von Voithenberg, L., and Kaigala, G.V. (2018). Fluorescence in situ hybridization (FISH): History, limitations and what to expect from micro-scale FISH? Micro Nano Eng. *1*, 15–24.

Hughes, J., Hepworth, C., Dutton, C., Dunn, J.A., Hunt, L., Stephens, J., Waugh, R., Cameron, D.D., and Gray, J.E. (2017). Reducing Stomatal Density in Barley Improves Drought Tolerance without Impacting on Yield. Plant Physiol. *174*, 776–787.

Humplík, J.F., Bergougnoux, V., Jandová, M., Šimura, J., Pěnčík, A., Tomanec, O., Rolčík, J., Novák, O., and Fellner, M. (2015). Endogenous Abscisic Acid Promotes Hypocotyl Growth and Affects Endoreduplication during Dark-Induced Growth in Tomato (Solanum lycopersicum L.). PLOS ONE *10*, e0117793.

Hundertmark, M., and Hincha, D.K. (2008). LEA (Late Embryogenesis Abundant) proteins and their encoding genes in Arabidopsis thaliana. BMC Genomics *9*, 118.

Hunt, A.G., Xu, R., Addepalli, B., Rao, S., Forbes, K.P., Meeks, L.R., Xing, D., Mo, M., Zhao, H., Bandyopadhyay, A., et al. (2008). Arabidopsis mRNA polyadenylation machinery: comprehensive analysis of protein-protein interactions and gene expression profiling. BMC Genomics *9*, 220.

Hwang, K., Susila, H., Nasim, Z., Jung, J.-Y., and Ahn, J.H. (2019). Arabidopsis ABF3 and ABF4 Transcription Factors Act with the NF-YC Complex to Regulate SOC1 Expression and Mediate Drought-Accelerated Flowering. Mol. Plant *12*, 489–505.

Iida, K., Seki, M., Sakurai, T., Satou, M., Akiyama, K., Toyoda, T., Konagaya, A., and Shinozaki, K. (2005). RARTF: database and tools for complete sets of Arabidopsis transcription factors. DNA Res. Int. J. Rapid Publ. Rep. Genes Genomes *12*, 247–256.

Ikegami, K., Okamoto, M., Seo, M., and Koshiba, T. (2009). Activation of abscisic acid biosynthesis in the leaves of Arabidopsis thaliana in response to water deficit. J. Plant Res. *122*, 235–243.

International Organisation of Vine and Wine (2017). Distribution of the world's grapevine varieties (France: International Organisation of Vines and Wines).

Iqbal, N., Khan, N.A., Ferrante, A., Trivellini, A., Francini, A., and Khan, M.I.R. (2017). Ethylene Role in Plant Growth, Development and Senescence: Interaction with Other Phytohormones. Front. Plant Sci. *8*.

Iquebal, M.A., Sharma, P., Jasrotia, R.S., Jaiswal, S., Kaur, A., Saroha, M., Angadi, U.B., Sheoran, S., Singh, R., Singh, G.P., et al. (2019). RNAseq analysis reveals drought-responsive molecular pathways with candidate genes and putative molecular markers in root tissue of wheat. Sci. Rep. *9*, 13917.

Iuchi, S., Kobayashi, M., Taji, T., Naramoto, M., Seki, M., Kato, T., Tabata, S., Kakubari, Y., Yamaguchi-Shinozaki, K., and Shinozaki, K. (2001). Regulation of drought tolerance by gene manipulation of 9-cis-epoxycarotenoid dioxygenase, a key enzyme in abscisic acid biosynthesis in Arabidopsis. Plant J. Cell Mol. Biol. *27*, 325–333.

Izquierdo-Bueno, I., González-Rodríguez, V.E., Simon, A., Dalmais, B., Pradier, J.-M., Le Pêcheur, P., Mercier, A., Walker, A.-S., Garrido, C., Collado, I.G., et al. (2018). Biosynthesis of abscisic acid in fungi: identification of a sesquiterpene cyclase as the key enzyme in Botrytis cinerea. Environ. Microbiol. *20*, 2469–2482.

Jacobsen, A.L., Pratt, R.B., Tobin, M.F., Hacke, U.G., and Ewers, F.W. (2012). A global analysis of xylem vessel length in woody plants. Am. J. Bot. *99*, 1583–1591.

Jalkanen, A.L., Coleman, S.J., and Wilusz, J. (2014). Determinants and Implications of mRNA Poly(A) Tail Size - Does this Protein Make My Tail Look Big? Semin. Cell Dev. Biol. *0*, 24–32.

Januszyk, K., and Lima, C.D. (2014). The eukaryotic RNA exosome. Curr. Opin. Struct. Biol. *24*, 132–140.

Javadi, S.M., Shobbar, Z.-S., Ebrahimi, A., and Shahbazi, M. (2021). New insights on key genes involved in drought stress response of barley: gene networks reconstruction, hub, and promoter analysis. J. Genet. Eng. Biotechnol. *19*, 2.

Jeevan Kumar, S.P., Rajendra Prasad, S., Banerjee, R., and Thammineni, C. (2015). Seed birth to death: dual functions of reactive oxygen species in seed physiology. Ann. Bot. *116*, 663–668.

Jesse Mayer (2018). Opuntia ficus-indica: a climate-resilient biomass feedstock for low-input drylands agriculture. University of Nevada, Reno.

Jia, H., Sun, W., Li, M., and Zhang, Z. (2018). Integrated Analysis of Protein Abundance, Transcript Level, and Tissue Diversity To Reveal Developmental Regulation of Maize. J. Proteome Res. *17*, 822–833.

Jin, M., Liu, H., He, C., Fu, J., Xiao, Y., Wang, Y., Xie, W., Wang, G., and Yan, J. (2016). Maize pan-transcriptome provides novel insights into genome complexity and quantitative trait variation. Sci. Rep. *6*, 18936.

Jones, H.G., and Sutherland, R.A. (1991). Stomatal control of xylem embolism. Plant Cell Environ. *14*, 607–612.

Josefsen, K., and Nielsen, H. (2011). Northern Blotting Analysis. In RNA, H. Nielsen, ed. (Totowa, NJ: Humana Press), pp. 87–105.

Kagale, S., and Rozwadowski, K. (2011). EAR motif-mediated transcriptional repression in plants. Epigenetics *6*, 141–146.

Kagale, S., Links, M.G., and Rozwadowski, K. (2010). Genome-Wide Analysis of Ethylene-Responsive Element Binding Factor-Associated Amphiphilic Repression Motif-Containing Transcriptional Regulators in Arabidopsis. PLANT Physiol. *152*, 1109–1134.

Kang, J., Hwang, J.-U., Lee, M., Kim, Y.-Y., Assmann, S.M., Martinoia, E., and Lee, Y. (2010). PDR-type ABC transporter mediates cellular uptake of the phytohormone abscisic acid. Proc. Natl. Acad. Sci. *107*, 2355–2360.

Kang, J., Yim, S., Choi, H., Kim, A., Lee, K.P., Lopez-Molina, L., Martinoia, E., and Lee, Y. (2015). Abscisic acid transporters cooperate to control seed germination. Nat. Commun. *6*, 8113.

Kanno, Y., Hanada, A., Chiba, Y., Ichikawa, T., Nakazawa, M., Matsui, M., Koshiba, T., Kamiya, Y., and Seo, M. (2012). Identification of an abscisic acid transporter by functional screening using the receptor complex as a sensor. Proc. Natl. Acad. Sci. *109*, 9653–9658.

Karppinen, K., Tegelberg, P., Häggman, H., and Jaakola, L. (2018). Abscisic Acid Regulates Anthocyanin Biosynthesis and Gene Expression Associated With Cell Wall Modification in Ripening Bilberry (Vaccinium myrtillus L.) Fruits. Front. Plant Sci. *9*.

Karssen, C.M., Brinkhorst-van der Swan, D.L., Breekland, A.E., and Koornneef, M. (1983). Induction of dormancy during seed development by endogenous abscisic acid: studies on abscisic acid deficient genotypes of Arabidopsis thaliana (L.) Heynh. Planta *157*, 158–165.

Kasahara, H., Hanada, A., Kuzuyama, T., Takagi, M., Kamiya, Y., and Yamaguchi, S. (2002). Contribution of the mevalonate and methylerythritol phosphate pathways to the biosynthesis of gibberellins in Arabidopsis. J. Biol. Chem. *277*, 45188–45194.

Keene, R.G., and Luse, D.S. (1999). Initially Transcribed Sequences Strongly Affect the Extent of Abortive Initiation by RNA Polymerase II. J. Biol. Chem. *274*, 11526–11534.

Kerchev, P.I., Pellny, T.K., Vivancos, P.D., Kiddle, G., Hedden, P., Driscoll, S., Vanacker, H., Verrier, P., Hancock, R.D., and Foyer, C.H. (2011). The Transcription Factor ABI4 Is Required for the Ascorbic Acid–Dependent Regulation of Growth and Regulation of Jasmonate-Dependent Defense Signaling Pathways in Arabidopsis[C][W]. Plant Cell *23*, 3319–3334.

Kermode, A.R. (2005). Role of Abscisic Acid in Seed Dormancy. J. Plant Growth Regul. *24*, 319–344.

Kim, D., Pertea, G., Trapnell, C., Pimentel, H., Kelley, R., and Salzberg, S.L. (2013a). TopHat2: accurate alignment of transcriptomes in the presence of insertions, deletions and gene fusions. Genome Biol. *14*, R36.

Kim, S.Y., Ma, J., Perret, P., Li, Z., and Thomas, T.L. (2002). Arabidopsis ABI5 Subfamily Members Have Distinct DNA-Binding and Transcriptional Activities. Plant Physiol. *130*, 688–697.

Kim, T.-H., Böhmer, M., Hu, H., Nishimura, N., and Schroeder, J.I. (2010). Guard Cell Signal Transduction Network: Advances in Understanding Abscisic Acid, CO_2, and Ca^{2+} Signaling. Annu. Rev. Plant Biol. *61*, 561–591.

Kim, W., Lee, Y., Park, J., Lee, N., and Choi, G. (2013b). HONSU, a Protein Phosphatase 2C, Regulates Seed Dormancy by Inhibiting ABA Signaling in Arabidopsis. Plant Cell Physiol. *54*, 555–572.

Kobayashi, Y., Murata, M., Minami, H., Yamamoto, S., Kagaya, Y., Hobo, T., Yamamoto, A., and Hattori, T. (2005). Abscisic acid-activated SNRK2 protein kinases function in the gene-regulation pathway of ABA signal transduction by phosphorylating ABA response element-binding factors. Plant J. *44*, 939–949.

Koga, H., Dohi, K., and Mori, M. (2004). Abscisic acid and low temperatures suppress the whole plant-specific resistance reaction of rice plants to the infection of Magnaporthe grisea. Physiol. Mol. Plant Pathol. *65*, 3–9.

Koornneef, M., Jorna, M.L., Brinkhorst-van der Swan, D.L.C., and Karssen, C.M. (1982). The isolation of abscisic acid (ABA) deficient mutants by selection of induced revertants in non-germinating gibberellin sensitive lines of Arabidopsis thaliana (L.) heynh. Theor. Appl. Genet. *61*, 385–393.

Koornneef, M., Reuling, G., and Karssen, C.M. (1984). The isolation and characterization of abscisic acid-insensitive mutants of Arabidopsis thaliana. Physiol. Plant. *61*, 377–383.

Kornberg, R.D. (1977). Structure of Chromatin. Annu. Rev. Biochem. *46*, 931–954.

Kornberg, R.D. (1999). Eukaryotic transcriptional control. Trends Cell Biol. *9*, M46–M49.

Koyama, K., Sadamatsu, K., and Goto-Yamamoto, N. (2010). Abscisic acid stimulated ripening and gene expression in berry skins of the Cabernet Sauvignon grape. Funct. Integr. Genomics *10*, 367–381.

Koyama, R., Roberto, S.R., de Souza, R.T., Borges, W.F.S., Anderson, M., Waterhouse, A.L., Cantu, D., Fidelibus, M.W., and Blanco-Ulate, B. (2018). Exogenous Abscisic Acid Promotes Anthocyanin Biosynthesis and Increased Expression of Flavonoid Synthesis Genes in Vitis vinifera × Vitis labrusca Table Grapes in a Subtropical Region. Front. Plant Sci. *9*.

Kozlowski, T.T., and Pallardy, S.G. (2002). Acclimation and adaptive responses of woody plants to environmental stresses. Bot. Rev. *68*, 270–334.

Krochko, J.E., Abrams, G.D., Loewen, M.K., Abrams, S.R., and Cutler, A.J. (1998). (+)-Abscisic Acid 8′-Hydroxylase Is a Cytochrome P450 Monooxygenase. Plant Physiol. *118*, 849–860.

Kugel, J.F., and Goodrich, J.A. (2000). A Kinetic Model for the Early Steps of RNA Synthesis by Human RNA Polymerase II. J. Biol. Chem. *275*, 40483–40491.

Kumar, R., Khurana, A., and Sharma, A.K. (2014). Role of plant hormones and their interplay in development and ripening of fleshy fruits. J. Exp. Bot. *65*, 4561–4575.

Kumbaric, A., and Caneva, G. (2014). Updated outline of floristic richness in Roman iconography. Rendiconti Lincei *25*, 181–193.

Kuromori, T., Miyaji, T., Yabuuchi, H., Shimizu, H., Sugimoto, E., Kamiya, A., Moriyama, Y., and Shinozaki, K. (2010). ABC transporter AtABCG25 is involved in abscisic acid transport and responses. Proc. Natl. Acad. Sci. *107*, 2361–2366.

Kuromori, T., Sugimoto, E., and Shinozaki, K. (2014). Intertissue Signal Transfer of Abscisic Acid from Vascular Cells to Guard Cells. PLANT Physiol. *164*, 1587–1592.

Kuromori, T., Seo, M., and Shinozaki, K. (2018). ABA Transport and Plant Water Stress Responses. Trends Plant Sci. *23*, 513–522.

Kuznedelov, K., Korzheva, N., Mustaev, A., and Severinov, K. (2002). Structure-based analysis of RNA polymerase function: the largest subunit's rudder contributes critically to elongation complex stability and is not involved in the maintenance of RNA–DNA hybrid length. EMBO J. *21*, 1369–1378.

Lamarque, L.J., Delzon, S., Toups, H., Gravel, A.-I., Corso, D., Badel, E., Burlett, R., Charrier, G., Cochard, H., Jansen, S., et al. (2019). Over-accumulation of abscisic acid in transgenic tomato plants increases the risk of hydraulic failure. Plant Cell Environ.

Landick, R. (2001). RNA Polymerase Clamps Down. Cell *105*, 567–570.

Lando, A.P., Viana, W.G., da Silva, R.A., Costa, C.D.D., Fraga, H.P.F., Santos, M., Mioto, P.T., Guerra, M.P., and Steiner, N. (2020). The Physiological Relationship Between Abscisic Acid and Gibberellin During Seed Germination of Trichocline catharinensis (Asteraceae) Is Associated with Polyamine and Antioxidant Enzymes. J. Plant Growth Regul. *39*, 395–410.

Langfelder, P., and Horvath, S. (2008). WGCNA: an R package for weighted correlation network analysis. BMC Bioinformatics *9*, 559.

Langmead, B., and Salzberg, S.L. (2012). Fast gapped-read alignment with Bowtie 2. Nat. Methods *9*, 357–359.

Lawit, S.J., O'Grady, K., Gurley, W.B., and Czarnecka-Verner, E. (2007). Yeast two-hybrid map of Arabidopsis TFIID. Plant Mol. Biol. *64*, 73–87.

Lee, K.H., Piao, H.L., Kim, H.-Y., Choi, S.M., Jiang, F., Hartung, W., Hwang, I., Kwak, J.M., Lee, I.-J., and Hwang, I. (2006). Activation of Glucosidase via Stress-Induced Polymerization Rapidly Increases Active Pools of Abscisic Acid. Cell *126*, 1109–1120.

Lefebvre, V., North, H., Frey, A., Sotta, B., Seo, M., Okamoto, M., Nambara, E., and Marion-Poll, A. (2006). Functional analysis of Arabidopsis NCED6 and NCED9 genes indicates that ABA synthesized in the endosperm is involved in the induction of seed dormancy. Plant J. Cell Mol. Biol. *45*, 309–319.

Lehmann, H., and Glund, K. (1986). Abscisic acid metabolism-vacuolar/extravacuolar distribution of metabolites. Planta *168*, 559–562.

Lehti-Shiu, M.D., Panchy, N., Wang, P., Uygun, S., and Shiu, S.-H. (2017). Diversity, expansion, and evolutionary novelty of plant DNA-binding transcription factor families. Biochim. Biophys. Acta Gene Regul. Mech. *1860*, 3–20.

LeNoble, M.E., Spollen, W.G., and Sharp, R.E. (2004). Maintenance of shoot growth by endogenous ABA: genetic assessment of the involvement of ethylene suppression. J. Exp. Bot. *55*, 237–245.

Léran, S., Noguero, M., Corratgé-Faillie, C., Boursiac, Y., Brachet, C., and Lacombe, B. (2020). Functional Characterization of the Arabidopsis Abscisic Acid Transporters NPF4.5 and NPF4.6 in Xenopus Oocytes. Front. Plant Sci. *11*.

Levine, M. (2011). Paused RNA Polymerase II as a Developmental Checkpoint. Cell *145*, 502–511.

Li, Q., and Hunt, A.G. (1995). A near-upstream element in a plant polyadenylation signal consists of more than six nucleotides. Plant Mol. Biol. *28*, 927–934.

Li, Q., and Hunt, A.G. (1997). The Polyadenylation of RNA in Plants. Plant Physiol. *115*, 321–325.

Li, W.V., and Li, J.J. (2018). Modeling and analysis of RNA-seq data: a review from a statistical perspective. Quant. Biol. *6*, 195–209.

Li, B., Carey, M., and Workman, J.L. (2007). The Role of Chromatin during Transcription. Cell *128*, 707–719.

Li, D., Mou, W., Xia, R., Li, L., Zawora, C., Ying, T., Mao, L., Liu, Z., and Luo, Z. (2019a). Integrated analysis of high-throughput sequencing data shows abscisic acid-responsive genes and miRNAs in strawberry receptacle fruit ripening. Hortic. Res. *6*, 1–13.

Li, H., Wang, H., Li, H., Goodman, S., van der Lee, P., Xu, Z., Fortunato, A., and Yang, P. (2018). The worlds of wine: Old, new and ancient. Wine Econ. Policy *7*, 178–182.

Li, J., Wu, Y., Xie, Q., and Gong, Z. (2017a). Abscisic acid. In Hormone Metabolism and Signaling in Plants, (Elsevier), pp. 161–202.

Li, Q.Q., Liu, Z., Lu, W., and Liu, M. (2017b). Interplay between Alternative Splicing and Alternative Polyadenylation Defines the Expression Outcome of the Plant Unique OXIDATIVE TOLERANT-6 Gene. Sci. Rep. *7*, 2052.

Li, T., Zhang, W., Yang, H., Dong, Q., Ren, J., Fan, H., Zhang, X., and Zhou, Y. (2019b). Comparative transcriptome analysis reveals differentially expressed genes related to the tissue-specific accumulation of anthocyanins in pericarp and aleurone layer for maize. Sci. Rep. *9*, 2485.

Liang, P., and Pardee, A.B. (1992). Differential display of eukaryotic messenger RNA by means of the polymerase chain reaction. Science *257*, 967–971.

Liao, Y., Smyth, G.K., and Shi, W. (2014). featureCounts: an efficient general purpose program for assigning sequence reads to genomic features. Bioinforma. Oxf. Engl. *30*, 923–930.

Licausi, F., Ohme-Takagi, M., and Perata, P. (2013). APETALA2/Ethylene Responsive Factor (AP2/ERF) transcription factors: mediators of stress responses and developmental programs. New Phytol. *199*, 639–649.

Lim, E.-K., Doucet, C.J., Hou, B., Jackson, R.G., Abrams, S.R., and Bowles, D.J. (2005). Resolution of (+)-abscisic acid using an Arabidopsis glycosyltransferase. Tetrahedron Asymmetry *16*, 143–147.

Lin, H.-H., Huang, L.-F., Su, H.-C., and Jeng, S.-T. (2009). Effects of the multiple polyadenylation signal AAUAAA on mRNA 3'-end formation and gene expression. Planta *230*, 699–712.

Linden, H., Misawa, N., Saito, T., and Sandmann, G. (1994). A novel carotenoid biosynthesis gene coding for zeta-carotene desaturase: functional expression, sequence and phylogenetic origin. Plant Mol. Biol. *24*, 369–379.

Lis, M., and Walther, D. (2016). The orientation of transcription factor binding site motifs in gene promoter regions: does it matter? BMC Genomics *17*.

Liu, W.-C., and Carns†, H.R. (1961). Isolation of Abscisin, an Abscission Accelerating Substance. Science *134*, 384–385.

Liu, Y., and Aebersold, R. (2016). The interdependence of transcript and protein abundance: new data–new complexities. Mol. Syst. Biol. *12*.

Liu, L., Li, Y., Li, S., Hu, N., He, Y., Pong, R., Lin, D., Lu, L., and Law, M. (2012). Comparison of Next-Generation Sequencing Systems. J. Biomed. Biotechnol. *2012*, 1–11.

Liu, Y., Beyer, A., and Aebersold, R. (2016). On the Dependency of Cellular Protein Levels on mRNA Abundance. Cell *165*, 535–550.

Liu, Y., Dong, B., Zhang, C., Yang, L., Wang, Y., and Zhao, H. (2020). Effects of Exogenous Abscisic Acid (ABA) on Carotenoids and Petal Color in Osmanthus fragrans "Yanhonggui." Plants Basel Switz. *9*.

Liu, Z., Yan, J.-P., Li, D.-K., Luo, Q., Yan, Q., Liu, Z.-B., Ye, L.-M., Wang, J.-M., Li, X.-F., and Yang, Y. (2015). UDP-Glucosyltransferase71C5, a Major Glucosyltransferase, Mediates Abscisic Acid Homeostasis in Arabidopsis. Plant Physiol. *167*, 1659–1670.

Lorković, Z.J., Wieczorek Kirk, D.A., Lambermon, M.H.L., and Filipowicz, W. (2000). Pre-mRNA splicing in higher plants. Trends Plant Sci. *5*, 160–167.

Love, M.I., Huber, W., and Anders, S. (2014). Moderated estimation of fold change and dispersion for RNA-seq data with DESeq2. Genome Biol. *15*.

Lowe, K.M., and Walker, M.A. (2006). Genetic linkage map of the interspecific grape rootstock cross Ramsey (Vitis champinii) x Riparia Gloire (Vitis riparia). TAG Theor. Appl. Genet. Theor. Angew. Genet. *112*, 1582–1592.

Lu, Z., Quiñones, M.A., and Zeiger, E. (1993). Abaxial and adaxial stomata from Pima cotton (Gossypium barbadense L.) differ in their pigment content and sensitivity to light quality. Plant Cell Environ. *16*, 851–858.

Luo, W., Johnson, A.W., and Bentley, D.L. (2006). The role of Rat1 in coupling mRNA 3′-end processing to transcription termination: implications for a unified allosteric–torpedo model. Genes Dev. *20*, 954–965.

Lv, Y., Xu, L., Dossa, K., Zhou, K., Zhu, M., Xie, H., Tang, S., Yu, Y., Guo, X., and Zhou, B. (2019). Identification of putative drought-responsive genes in rice using gene co-expression analysis. Bioinformation *15*, 480–489.

Ma, F. (1984). Leaf size and shape variation associated with drought stress in Rumex acetosella L. (Polygonaceae). Am. Midl. Nat. *111*, 358–363.

Ma, Y., Szostkiewicz, I., Korte, A., Moes, D., Yang, Y., Christmann, A., and Grill, E. (2009). Regulators of PP2C phosphatase activity function as abscisic acid sensors. Science *324*, 1064–1068.

Ma, Y., Liu, M., Stiller, J., and Liu, C. (2019). A pan-transcriptome analysis shows that disease resistance genes have undergone more selection pressure during barley domestication. BMC Genomics *20*, 12.

MacDonald, C.C. (2019). Tissue-specific mechanisms of alternative polyadenylation: Testis, brain, and beyond (2018 update). WIREs RNA *10*, e1526.

MacRobbie, E.A.C., Keynes, R.D., and Ellory, J.C. (1982). Chloride transport in stomatal guard cells. Philos. Trans. R. Soc. Lond. B Biol. Sci. *299*, 469–481.

Maia, J., Dekkers, B.J.W., Dolle, M.J., Ligterink, W., and Hilhorst, H.W.M. (2014). Abscisic acid (ABA) sensitivity regulates desiccation tolerance in germinated Arabidopsis seeds. New Phytol. *203*, 81–93.

Maiuri, P., Knezevich, A., De Marco, A., Mazza, D., Kula, A., McNally, J.G., and Marcello, A. (2011). Fast transcription rates of RNA polymerase II in human cells. EMBO Rep. *12*, 1280–1285.

Marguerat, S., and Bähler, J. (2010). RNA-seq: from technology to biology. Cell. Mol. Life Sci. *67*, 569–579.

Markesteijn, L., and Poorter, L. (2009). Seedling root morphology and biomass allocation of 62 tropical tree species in relation to drought- and shade-tolerance. J. Ecol. *97*, 311–325.

Marquez, Y., Brown, J.W.S., Simpson, C., Barta, A., and Kalyna, M. (2012). Transcriptome survey reveals increased complexity of the alternative splicing landscape in Arabidopsis. Genome Res. *22*, 1184–1195.

Martignago, D., Siemiatkowska, B., Lombardi, A., and Conti, L. (2020). Abscisic Acid and Flowering Regulation: Many Targets, Different Places. Int. J. Mol. Sci. *21*, 9700.

Maruyama, K., Todaka, D., Mizoi, J., Yoshida, T., Kidokoro, S., Matsukura, S., Takasaki, H., Sakurai, T., Yamamoto, Y.Y., Yoshiwara, K., et al. (2012). Identification of Cis-Acting Promoter Elements in Cold- and Dehydration-Induced Transcriptional Pathways in Arabidopsis, Rice, and Soybean. DNA Res. Int. J. Rapid Publ. Rep. Genes Genomes *19*, 37–49.

Massonnet, M., Figueroa-Balderas, R., Galarneau, E.R.A., Miki, S., Lawrence, D.P., Sun, Q., Wallis, C.M., Baumgartner, K., and Cantu, D. (2017). Neofusicoccum parvum Colonization of the Grapevine Woody Stem Triggers Asynchronous Host Responses at the Site of Infection and in the Leaves. Front. Plant Sci. *8*.

Mathur, S., Vyas, S., Kapoor, S., and Tyagi, A.K. (2011). The Mediator Complex in Plants: Structure, Phylogeny, and Expression Profiling of Representative Genes in a Dicot (Arabidopsis) and a Monocot (Rice) during Reproduction and Abiotic Stress. Plant Physiol. *157*, 1609–1627.

McCarty, D.R., Carson, C.B., Stinard, P.S., and Robertson, D.S. (1989). Molecular Analysis of viviparous-1: An Abscisic Acid-Insensitive Mutant of Maize. Plant Cell *1*, 523–532.

McGovern, P., Jalabadze, M., Batiuk, S., Callahan, M.P., Smith, K.E., Hall, G.R., Kvavadze, E., Maghradze, D., Rusishvili, N., Bouby, L., et al. (2017). Early Neolithic wine of Georgia in the South Caucasus. Proc. Natl. Acad. Sci. *114*, E10309–E10318.

McGregor, I.R., Helcoski, R., Kunert, N., Tepley, A.J., Gonzalez-Akre, E.B., Herrmann, V., Zailaa, J., Stovall, A.E.L., Bourg, N.A., McShea, W.J., et al. (2020). Tree height and leaf drought tolerance traits shape growth responses across droughts in a temperate broadleaf forest. New Phytol. nph.16996.

Melcher, K., Ng, L.-M., Zhou, X.E., Soon, F.-F., Xu, Y., Suino-Powell, K.M., Park, S.-Y., Weiner, J.J., Fujii, H., Chinnusamy, V., et al. (2009). A gate–latch–lock mechanism for hormone signalling by abscisic acid receptors. Nature *462*, 602–608.

Melillo, L. (1994). Diuretic Plants in the Paintings of Pompeii. Am. J. Nephrol. *14*, 423–425.

Melotto, M., Underwood, W., Koczan, J., Nomura, K., and He, S.Y. (2006). Plant stomata function in innate immunity against bacterial invasion. Cell *126*, 969–980.

Meng, X., Xu, J., He, Y., Yang, K.-Y., Mordorski, B., Liu, Y., and Zhang, S. (2013). Phosphorylation of an ERF transcription factor by Arabidopsis MPK3/MPK6 regulates plant defense gene induction and fungal resistance. Plant Cell *25*, 1126–1142.

Meyer, K., Koester, T., and Staiger, D. (2015). Pre-mRNA Splicing in Plants: In Vivo Functions of RNA-Binding Proteins Implicated in the Splicing Process. Biomolecules *5*, 1717–1740.

Miller, M.B., and Tang, Y.-W. (2009). Basic Concepts of Microarrays and Potential Applications in Clinical Microbiology. Clin. Microbiol. Rev. *22*, 611–633.

Minio, A., Massonnet, M., Vondras, A., Figueroa-Balderas, R., Blanco-Ulate, B., and Cantu, D. (2018). Iso-Seq allows genome-independent transcriptome profiling of grape berry development (Genomics).

Minio, A., Massonnet, M., Figueroa-Balderas, R., Vondras, A.M., Blanco-Ulate, B., and Cantu, D. (2019). Iso-Seq Allows Genome-Independent Transcriptome Profiling of Grape Berry Development. G3 GenesGenomesGenetics *9*, 755–767.

Mirás-Avalos, J.M., and Intrigliolo, D.S. (2017). Grape Composition under Abiotic Constrains: Water Stress and Salinity. Front. Plant Sci. *8*.

Mitsuda, N., and Ohme-Takagi, M. (2009). Functional Analysis of Transcription Factors in Arabidopsis. Plant Cell Physiol. *50*, 1232–1248.

Miura, P., Sanfilippo, P., Shenker, S., and Lai, E.C. (2014). Alternative polyadenylation in the nervous system: to what lengths will 3′ UTR extensions take us? BioEssays News Rev. Mol. Cell. Dev. Biol. *36*, 766–777.

Mizoi, J., Shinozaki, K., and Yamaguchi-Shinozaki, K. (2012). AP2/ERF family transcription factors in plant abiotic stress responses. Biochim. Biophys. Acta BBA - Gene Regul. Mech. *1819*, 86–96.

Moeder, W., Ung, H., Mosher, S., and Yoshioka, K. (2010). SA-ABA antagonism in defense responses. Plant Signal. Behav. *5*, 1231–1233.

Mohr, P.G., and Cahill, D.M. (2003). Abscisic acid influences the susceptibility of Arabidopsis thaliana to Pseudomonas syringae pv. tomato and Peronospora parasitica. Funct. Plant Biol. *30*, 461–469.

Mokany, K., Raison, R.J., and Prokushkin, A.S. (2006). Critical analysis of root : shoot ratios in terrestrial biomes. Glob. Change Biol. *12*, 84–96.

Monteverde, C., and De Sales, F. (2020). Impacts of global warming on southern California's winegrape climate suitability. Adv. Clim. Change Res. *11*, 279–293.

Morgan, P.W. (1984). Is ethylene the Natural Regulator of Abscission? In Ethylene: Biochemical, Physiological and Applied Aspects, An International Symposium, Oiryat Anavim, Israel Held January 9–12 1984, Y. Fuchs, and E. Chalutz, eds. (Dordrecht: Springer Netherlands), pp. 231–240.

Morrison, T.B., Weis, J.J., and Wittwer, C.T. (1998). Quantification of low-copy transcripts by continuous SYBR Green I monitoring during amplification. BioTechniques *24*, 954–958, 960, 962.

Mosher, S., Moeder, W., Nishimura, N., Jikumaru, Y., Joo, S.-H., Urquhart, W., Klessig, D.F., Kim, S.-K., Nambara, E., and Yoshioka, K. (2010). The Lesion-Mimic Mutant cpr22 Shows Alterations in Abscisic Acid Signaling and Abscisic Acid Insensitivity in a Salicylic Acid-Dependent Manner1[W][OA]. Plant Physiol. *152*, 1901–1913.

Moss Bendtsen, K., Jensen, M.H., Krishna, S., and Semsey, S. (2015). The role of mRNA and protein stability in the function of coupled positive and negative feedback systems in eukaryotic cells. Sci. Rep. *5*, 13910.

Movassat, M., Crabb, T.L., Busch, A., Yao, C., Reynolds, D.J., Shi, Y., and Hertel, K.J. (2016). Coupling between alternative polyadenylation and alternative splicing is limited to terminal introns. RNA Biol. *13*, 646–655.

Mukherjee, C., Bakthavachalu, B., and Schoenberg, D.R. (2014). The Cytoplasmic Capping Complex Assembles on Adapter Protein Nck1 Bound to the Proline-Rich C-Terminus of Mammalian Capping Enzyme. PLoS Biol. *12*.

Munns, R., and Cramer, G.R. (1996). Is coordination of leaf and root growth mediated by abscisic acid? Opinion. Plant Soil *185*, 33–49.

Muñoz-Espinoza, C., Di Genova, A., Correa, J., Silva, R., Maass, A., González-Agüero, M., Orellana, A., and Hinrichsen, P. (2016). Transcriptome profiling of grapevine seedless segregants during berry development reveals candidate genes associated with berry weight. BMC Plant Biol. *16*, 104.

Mustilli, A.-C., Merlot, S., Vavasseur, A., Fenzi, F., and Giraudat, J. (2002). Arabidopsis OST1 Protein Kinase Mediates the Regulation of Stomatal Aperture by Abscisic Acid and Acts Upstream of Reactive Oxygen Species Production. Plant Cell *14*, 3089–3099.

Nagaraj, S.H., Gasser, R.B., and Ranganathan, S. (2007). A hitchhiker's guide to expressed sequence tag (EST) analysis. Brief. Bioinform. *8*, 6–21.

Nakashima, K., Fujita, Y., Kanamori, N., Katagiri, T., Umezawa, T., Kidokoro, S., Maruyama, K., Yoshida, T., Ishiyama, K., Kobayashi, M., et al. (2009). Three Arabidopsis SnRK2 Protein Kinases, SRK2D/SnRK2.2, SRK2E/SnRK2.6/OST1 and SRK2I/SnRK2.3, Involved in ABA Signaling are Essential for the Control of Seed Development and Dormancy. Plant Cell Physiol. *50*, 1345–1363.

Nambara, E., and Marion-Poll, A. (2005). ABSCISIC ACID BIOSYNTHESIS AND CATABOLISM. Annu. Rev. Plant Biol. *56*, 165–185.

Narusaka, Y., Nakashima, K., Shinwari, Z.K., Sakuma, Y., Furihata, T., Abe, H., Narusaka, M., Shinozaki, K., and Yamaguchi-Shinozaki, K. (2003). Interaction between two cis-acting elements, ABRE and DRE, in ABA-dependent expression of Arabidopsis rd29A gene in response to dehydration and high-salinity stresses. Plant J. Cell Mol. Biol. *34*, 137–148.

Naumann, G., Alfieri, L., Wyser, K., Mentaschi, L., Betts, R.A., Carrao, H., Spinoni, J., Vogt, J., and Feyen, L. (2018). Global Changes in Drought Conditions Under Different Levels of Warming. Geophys. Res. Lett. *45*, 3285–3296.

Neto, E.D., Correa, R.G., Verjovski-Almeida, S., Briones, M.R.S., Nagai, M.A., Silva, W. da, Zago, M.A., Bordin, S., Costa, F.F., Goldman, G.H., et al. (2000). Shotgun sequencing of the human transcriptome with ORF expressed sequence tags. Proc. Natl. Acad. Sci. *97*, 3491–3496.

Niyogi, K.K. (1999). PHOTOPROTECTION REVISITED: Genetic and Molecular Approaches. Annu. Rev. Plant Physiol. Plant Mol. Biol. *50*, 333–359.

Nobel, P.S. (1977). Water relations and photosynthesis of a barrel cactus, Ferocactus acanthodes, in the Colorado desert. Oecologia *27*, 117–133.

Nobel, P.S., and Bobich, E.G. (2002). Plant frequency, stem and root characteristics, and CO2 uptake for Opuntia acanthocarpa: elevational correlates in the northwestern Sonoran Desert. Oecologia *130*, 165–172.

North, H.M., De Almeida, A., Boutin, J.-P., Frey, A., To, A., Botran, L., Sotta, B., and Marion-Poll, A. (2007). The Arabidopsis ABA-deficient mutant aba4 demonstrates that the major route for stress-induced ABA accumulation is via neoxanthin isomers. Plant J. Cell Mol. Biol. *50*, 810–824.

Ogbourne, S., and Antalis, T.M. (1998). Transcriptional control and the role of silencers in transcriptional regulation in eukaryotes. Biochem. J. *331*, 1–14.

Ohkuma, K., Lyon, J.L., Addicott, F.T., and Smith, O.E. (1963). Abscisin II, an Abscission-Accelerating Substance from Young Cotton Fruit. Science *142*, 1592–1593.

Onodera, Y., Haag, J.R., Ream, T., Costa Nunes, P., Pontes, O., and Pikaard, C.S. (2005). Plant nuclear RNA polymerase IV mediates siRNA and DNA methylation-dependent heterochromatin formation. Cell *120*, 613–622.

Oppenheimer, H.R. (1922). Keimungshemmende Substanzen in der Frucht von Solanum Lycopersicum und in anderen Pflanzen: (Vorläufige Mitteilung); Aus d. pflanzenphysiolog. Institut d. Universität in Wien Nr 175 d. 2. Folge (A. Hölder).

Ouyang, W., Struik, P.C., Yin, X., and Yang, J. (2017). Stomatal conductance, mesophyll conductance, and transpiration efficiency in relation to leaf anatomy in rice and wheat genotypes under drought. J. Exp. Bot. *68*, 5191–5205.

Owens, N.D.L., Blitz, I.L., Lane, M.A., Patrushev, I., Overton, J.D., Gilchrist, M.J., Cho, K.W.Y., and Khokha, M.K. (2016). Measuring Absolute RNA Copy Numbers at High Temporal Resolution Reveals Transcriptome Kinetics in Development. Cell Rep. *14*, 632–647.

Padgett-Johnson, M., Williams, L.E., and Walker, M.A. (2003). Vine Water Relations, Gas Exchange, and Vegetative Growth of Seventeen Vitis Species Grown under Irrigated and Nonirrigated Conditions in California. J. Am. Soc. Hortic. Sci. *128*, 269–276.

Pal, M., Ponticelli, A.S., and Luse, D.S. (2005). The Role of the Transcription Bubble and TFIIB in Promoter Clearance by RNA Polymerase II. Mol. Cell *19*, 101–110.

Palaniswamy, S.K., James, S., Sun, H., Lamb, R.S., Davuluri, R.V., and Grotewold, E. (2006). AGRIS and AtRegNet. A Platform to Link cis-Regulatory Elements and Transcription Factors into Regulatory Networks. Plant Physiol. *140*, 818–829.

Pareek, A., Khurana, A., Sharma, A.K., and Kumar, R. (2017). An Overview of Signaling Regulons During Cold Stress Tolerance in Plants. Curr. Genomics *18*, 498–511.

Park, S.C., Kwon, H.B., and Shih, M.C. (1996). Cis-acting elements essential for light regulation of the nuclear gene encoding the A subunit of chloroplast glyceraldehyde 3-phosphate dehydrogenase in Arabidopsis thaliana. Plant Physiol. *112*, 1563.

Park, S.-Y., Fung, P., Nishimura, N., Jensen, D.R., Fujii, H., Zhao, Y., Lumba, S., Santiago, J., Rodrigues, A., Chow, T. -f. F., et al. (2009). Abscisic Acid Inhibits Type 2C Protein Phosphatases via the PYR/PYL Family of START Proteins. Science 1173041.

Parker, J. (2001). RNA Polymerase. In Encyclopedia of Genetics, (Elsevier), pp. 1746–1747.

Parkinson, J., and Blaxter, M. (2009). Expressed Sequence Tags: An Overview. In Expressed Sequence Tags (ESTs), J. Parkinson, ed. (Totowa, NJ: Humana Press), pp. 1–12.

Patrick E. McGovern (2007). Ancient Wine: The search for the origins of viticulture (Princeton University Press).

Patro, R., Duggal, G., Love, M.I., Irizarry, R.A., and Kingsford, C. (2017). Salmon provides fast and bias-aware quantification of transcript expression. Nat. Methods *14*, 417–419.

Pease, J., and Sooknanan, R. (2012). A rapid, directional RNA-seq library preparation workflow for Illumina ® sequencing. Nat. Methods *9*, i–ii.

Pennacchio, L.A., Bickmore, W., Dean, A., Nobrega, M.A., and Bejerano, G. (2013). Enhancers: five essential questions. Nat. Rev. Genet. *14*, 288–295.

Pérez-Rodríguez, P., Riaño-Pachón, D.M., Corrêa, L.G.G., Rensing, S.A., Kersten, B., and Mueller-Roeber, B. (2010). PlnTFDB: updated content and new features of the plant transcription factor database. Nucleic Acids Res. *38*, D822–D827.

Perreau, F., Frey, A., Effroy-Cuzzi, D., Savane, P., Berger, A., Gissot, L., and Marion-Poll, A. (2020). ABSCISIC ACID-DEFICIENT4 Has an Essential Function in Both cis-Violaxanthin and cis-Neoxanthin Synthesis. Plant Physiol. *184*, 1303–1316.

Petek, M., Zagorščak, M., Ramšak, Ž., Sanders, S., Tomaž, Š., Tseng, E., Zouine, M., Coll, A., and Gruden, K. (2020). Cultivar-specific transcriptome and pan-transcriptome reconstruction of tetraploid potato. Sci. Data *7*, 249.

Peterlin, B.M., and Price, D.H. (2006). Controlling the Elongation Phase of Transcription with P-TEFb. Mol. Cell *23*, 297–305.

Pilati, S., Bagagli, G., Sonego, P., Moretto, M., Brazzale, D., Castorina, G., Simoni, L., Tonelli, C., Guella, G., Engelen, K., et al. (2017). Abscisic Acid Is a Major Regulator of Grape Berry Ripening Onset: New Insights into ABA Signaling Network. Front. Plant Sci. *8*, 1093.

Piotrowska, A., and Bajguz, A. (2011). Conjugates of abscisic acid, brassinosteroids, ethylene, gibberellins, and jasmonates. Phytochemistry *72*, 2097–2112.

Polania, J., Rao, I.M., Cajiao, C., Grajales, M., Rivera, M., Velasquez, F., Raatz, B., and Beebe, S.E. (2017). Shoot and Root Traits Contribute to Drought Resistance in Recombinant Inbred Lines of MD 23–24 × SEA 5 of Common Bean. Front. Plant Sci. *8*.

Porrua, O., and Libri, D. (2015). Transcription termination and the control of the transcriptome: why, where and how to stop. Nat. Rev. Mol. Cell Biol. *16*, 190–202.

Preiss, T. (2013). The End in Sight: Poly(A), Translation and mRNA Stability in Eukaryotes (Landes Bioscience).

Price, D.H. (2018). Transient pausing by RNA polymerase II. Proc. Natl. Acad. Sci. *115*, 4810–4812.

Ptashne, M., and Gann, A. (1997). Transcriptional activation by recruitment. Nature *386*, 569–577.

Qi, G.-N., Yao, F.-Y., Ren, H.-M., Sun, S.-J., Tan, Y.-Q., Zhang, Z.-C., Qiu, B.-S., and Wang, Y.-F. (2018). The S-Type Anion Channel ZmSLAC1 Plays Essential Roles in Stomatal Closure by Mediating Nitrate Efflux in Maize. Plant Cell Physiol. *59*, 614–623.

Qin, X., and Zeevaart, J.A.D. (1999). The 9-cis-epoxycarotenoid cleavage reaction is the key regulatory step of abscisic acid biosynthesis in water-stressed bean. Proc. Natl. Acad. Sci. *96*, 15354–15361.

Qin, B.-X., Tang, D., Huang, J., Li, M., Wu, X.-R., Lu, L.-L., Wang, K.-J., Yu, H.-X., Chen, J.-M., Gu, M.-H., et al. (2011). Rice OsGL1-1 Is Involved in Leaf Cuticular Wax and Cuticle Membrane. Mol. Plant *4*, 985–995.

Quesada, V., Ponce, M.R., and Micol, J.L. (2000). Genetic Analysis of Salt-Tolerant Mutants in Arabidopsis thaliana. Genetics *154*, 421–436.

Raj, A., and van Oudenaarden, A. (2009). Single-Molecule Approaches to Stochastic Gene Expression. Annu. Rev. Biophys. *38*, 255–270.

Raj, A., van den Bogaard, P., Rifkin, S.A., van Oudenaarden, A., and Tyagi, S. (2008). Imaging individual mRNA molecules using multiple singly labeled probes. Nat. Methods *5*, 877–879.

Ramanathan, A., Robb, G.B., and Chan, S.-H. (2016). mRNA capping: biological functions and applications. Nucleic Acids Res. *44*, 7511–7526.

Rattanakon, S., Ghan, R., Gambetta, G.A., Deluc, L.G., Schlauch, K.A., and Cramer, G.R. (2016). Abscisic acid transcriptomic signaling varies with grapevine organ. BMC Plant Biol. *16*.

Reddy, A.S.N. (2007). Alternative splicing of pre-messenger RNAs in plants in the genomic era. Annu. Rev. Plant Biol. *58*, 267–294.

Reddy, A.S.N., Marquez, Y., Kalyna, M., and Barta, A. (2013). Complexity of the alternative splicing landscape in plants. Plant Cell *25*, 3657–3683.

Reyes-Olivas, A., García-Moya, E., and López–Mata, L. (2002). Cacti–shrub interactions in the coastal desert of northern Sinaloa, Mexico. J. Arid Environ. *52*, 431–445.

RHIZOPOULOU, S., and PSARAS, G.K. (2003). Development and Structure of Drought-tolerant Leaves of the Mediterranean Shrub Capparis spinosa L. Ann. Bot. *92*, 377–383.

Rhoads, A., and Au, K.F. (2015). PacBio Sequencing and Its Applications. Genomics Proteomics Bioinformatics *13*, 278–289.

Riboni, M., Galbiati, M., Tonelli, C., and Conti, L. (2013). GIGANTEA Enables Drought Escape Response via Abscisic Acid-Dependent Activation of the Florigens and SUPPRESSOR OF OVEREXPRESSION OF CONSTANS1. Plant Physiol. *162*, 1706–1719.

Riboni, M., Robustelli Test, A., Galbiati, M., Tonelli, C., and Conti, L. (2016). ABA-dependent control of *GIGANTEA* signalling enables drought escape via up-regulation of *FLOWERING LOCUS T* in *Arabidopsis thaliana*. J. Exp. Bot. *67*, 6309–6322.

Riechmann, J.L., Heard, J., Martin, G., Reuber, L., Jiang, C., Keddie, J., Adam, L., Pineda, O., Ratcliffe, O.J., Samaha, R.R., et al. (2000). Arabidopsis transcription factors: genome-wide comparative analysis among eukaryotes. Science *290*, 2105–2110.

Ristic, Z., and Jenks, M.A. (2002). Leaf cuticle and water loss in maize lines differing in dehydration avoidance. J. Plant Physiol. *159*, 645–651.

Ritchie, M.E., Phipson, B., Wu, D., Hu, Y., Law, C.W., Shi, W., and Smyth, G.K. (2015). limma powers differential expression analyses for RNA-sequencing and microarray studies. Nucleic Acids Res. *43*, e47–e47.

Rodríguez-Concepción, M., and Boronat, A. (2002). Elucidation of the Methylerythritol Phosphate Pathway for Isoprenoid Biosynthesis in Bacteria and Plastids. A Metabolic Milestone Achieved through Genomics. Plant Physiol. *130*, 1079–1089.

Romero, P., Lafuente, M.T., and Rodrigo, M.J. (2019). A sweet orange mutant impaired in carotenoid biosynthesis and reduced ABA levels results in altered molecular responses along peel ripening. Sci. Rep. *9*, 9813.

Rondón, A.G., Mischo, H.E., Kawauchi, J., and Proudfoot, N.J. (2009). Fail-Safe Transcriptional Termination for Protein-Coding Genes in S. cerevisiae. Mol. Cell *36*, 88–98.

Rosell, J.A., Olson, M.E., and Anfodillo, T. (2017). Scaling of Xylem Vessel Diameter with Plant Size: Causes, Predictions, and Outstanding Questions. Curr. For. Rep. *3*, 46–59.

Rudd, S. (2003). Expressed sequence tags: alternative or complement to whole genome sequences? Trends Plant Sci. *8*, 321–329.

Rudkin, G.T., and Stollar, B.D. (1977). High resolution detection of DNA–RNA hybrids in situ by indirect immunofluorescence. Nature *265*, 472–473.

Ruiz-Sola, M.Á., and Rodríguez-Concepción, M. (2012). Carotenoid Biosynthesis in Arabidopsis: A Colorful Pathway. Arab. Book Am. Soc. Plant Biol. *10*.

Russell, J., and Zomerdijk, J.C.B.M. (2006). The RNA polymerase I transcription machinery. Biochem. Soc. Symp. 203–216.

Ryu, J., Hwang, B.G., Kim, Y.X., and Lee, S.J. (2016). Direct observation of local xylem embolisms induced by soil drying in intact Zea mays leaves. J. Exp. Bot. *67*, 2617–2626.

Sade, N., and Moshelion, M. (2014). The dynamic isohydric–anisohydric behavior of plants upon fruit development: taking a risk for the next generation. Tree Physiol. *34*, 1199–1202.

Sakuma, Y., Liu, Q., Dubouzet, J.G., Abe, H., Shinozaki, K., and Yamaguchi-Shinozaki, K. (2002). DNA-Binding Specificity of the ERF/AP2 Domain of Arabidopsis DREBs, Transcription Factors Involved in Dehydration- and Cold-Inducible Gene Expression. Biochem. Biophys. Res. Commun. *290*, 998–1009.

Sanchez, A., Garcia, H.G., Jones, D., Phillips, R., and Kondev, J. (2011). Effect of Promoter Architecture on the Cell-to-Cell Variability in Gene Expression. PLOS Comput. Biol. *7*, e1001100.

Sanematsu, F., Takami, Y., Barman, H.K., Fukagawa, T., Ono, T., Shibahara, K., and Nakayama, T. (2006). Asf1 Is Required for Viability and Chromatin Assembly during DNA Replication in Vertebrate Cells. J. Biol. Chem. *281*, 13817–13827.

Santiago, L.S., Goldstein, G., Meinzer, F.C., Fisher, J.B., Machado, K., Woodruff, D., and Jones, T. (2004). Leaf photosynthetic traits scale with hydraulic conductivity and wood density in Panamanian forest canopy trees. Oecologia *140*, 543–550.

Santos, J.A., Fraga, H., Malheiro, A.C., Moutinho-Pereira, J., Dinis, L.-T., Correia, C., Moriondo, M., Leolini, L., Dibari, C., Costafreda-Aumedes, S., et al. (2020). A Review of the Potential Climate Change Impacts and Adaptation Options for European Viticulture. Appl. Sci. *10*, 3092.

Saunders, A., Core, L.J., and Lis, J.T. (2006). Breaking barriers to transcription elongation. Nat. Rev. Mol. Cell Biol. *7*, 557–567.

Sawicki, M., Rondeau, M., Courteaux, B., Rabenoelina, F., Guerriero, G., Gomès, E., Soubigou-Taconnat, L., Balzergue, S., Clément, C., Ait Barka, E., et al. (2019). On a Cold Night: Transcriptomics of Grapevine Flower Unveils Signal Transduction and Impacted Metabolism. Int. J. Mol. Sci. *20*.

Schliesky, S., Gowik, U., Weber, A.P.M., and Braeutigam, A. (2012). RNA-Seq Assembly – Are We There Yet? Front. Plant Sci. *3*.

Schmittgen, T.D., Zakrajsek, B.A., Mills, A.G., Gorn, V., Singer, M.J., and Reed, M.W. (2000). Quantitative Reverse Transcription–Polymerase Chain Reaction to Study mRNA Decay: Comparison of Endpoint and Real-Time Methods. Anal. Biochem. *285*, 194–204.

Schoenberg, D.R., and Maquat, L.E. (2009). Re-capping the message. Trends Biochem. Sci. *34*, 435–442.

Schreiber, L. (2010). Transport barriers made of cutin, suberin and associated waxes. Trends Plant Sci. *15*, 546–553.

Schroeder, J.I., and Keller, B.U. (1992). Two types of anion channel currents in guard cells with distinct voltage regulation. Proc. Natl. Acad. Sci. U. S. A. *89*, 5025–5029.

Schroeder, J.I., and Nambara, E. (2006). A Quick Release Mechanism for Abscisic Acid. Cell *126*, 1023–1025.

Schroeder, J.I., Allen, G.J., Hugouvieux, V., Kwak, J.M., and Waner, D. (2001). Guard cell signal transduction. Annu. Rev. Plant Physiol. Plant Mol. Biol. *52*, 627–658.

Schulz, D., Schwalb, B., Kiesel, A., Baejen, C., Torkler, P., Gagneur, J., Soeding, J., and Cramer, P. (2013). Transcriptome Surveillance by Selective Termination of Noncoding RNA Synthesis. Cell *155*, 1075–1087.

Schwartz, S.H. (1997). Specific Oxidative Cleavage of Carotenoids by VP14 of Maize. Science *276*, 1872–1874.

Scoffoni, C., Albuquerque, C., Brodersen, C.R., Townes, S.V., John, G.P., Cochard, H., Buckley, T.N., McElrone, A.J., and Sack, L. (2017). Leaf vein xylem conduit diameter influences susceptibility to embolism and hydraulic decline. New Phytol. *213*, 1076–1092.

Seelbinder, B., Wolf, T., Priebe, S., McNamara, S., Gerber, S., Guthke, R., and Linde, J. (2019). GEO2RNAseq: An easy-to-use R pipeline for complete pre-processing of RNA-seq data. BioRxiv 771063.

Seo, M., Peeters, A.J.M., Koiwai, H., Oritani, T., Marion-Poll, A., Zeevaart, J.A.D., Koornneef, M., Kamiya, Y., and Koshiba, T. (2000). The Arabidopsis aldehyde oxidase 3 (AAO3) gene product catalyzes the final step in abscisic acid biosynthesis in leaves. Proc. Natl. Acad. Sci. U. S. A. *97*, 12908–12913.

Sewelam, N., Kazan, K., Thomas-Hall, S.R., Kidd, B.N., Manners, J.M., and Schenk, P.M. (2013). Ethylene Response Factor 6 Is a Regulator of Reactive Oxygen Species Signaling in Arabidopsis. PLoS ONE *8*.

Shahzad, R., Khan, A.L., Bilal, S., Waqas, M., Kang, S.-M., and Lee, I.-J. (2017). Inoculation of abscisic acid-producing endophytic bacteria enhances salinity stress tolerance in Oryza sativa. Environ. Exp. Bot. *136*, 68–77.

Shandilya, J., Gadad, S., Swaminathan, V., and Kundu, T.K. (2007). Histone Chaperones in Chromatin Dynamics. In Chromatin and Disease, T.K. Kundu, R. Bittman, D. Dasgupta, H. Engelhardt, L. Flohe, H. Herrmann, A. Holzenburg, H.-P. Nasheuer, S. Rottem, M. Wyss, et al., eds. (Dordrecht: Springer Netherlands), pp. 111–124.

Sharma, A., Shahzad, B., Kumar, V., Kohli, S.K., Sidhu, G.P.S., Bali, A.S., Handa, N., Kapoor, D., Bhardwaj, R., and Zheng, B. (2019). Phytohormones Regulate Accumulation of Osmolytes Under Abiotic Stress. Biomolecules *9*.

Sharp, R.E. (2002). Interaction with ethylene: changing views on the role of abscisic acid in root and shoot growth responses to water stress. Plant Cell Environ. *25*, 211–222.

Sharp, R.E., and LeNoble, M.E. (2002). ABA, ethylene and the control of shoot and root growth under water stress. J. Exp. Bot. *53*, 33–37.

Sharp, R.E., LeNoble, M.E., Else, M.A., Thorne, E.T., and Gherardi, F. (2000). Endogenous ABA maintains shoot growth in tomato independently of effects on plant water balance: evidence for an interaction with ethylene. J. Exp. Bot. *51*, 1575–1584.

Shatkin, A. (1976). Capping of eucaryotic mRNAs. Cell *9*, 645–653.

Shendure, J., Balasubramanian, S., Church, G.M., Gilbert, W., Rogers, J., Schloss, J.A., and Waterston, R.H. (2017). DNA sequencing at 40: past, present and future. Nature *550*, 345–353.

Shimazaki, K., Doi, M., Assmann, S.M., and Kinoshita, T. (2007). Light Regulation of Stomatal Movement. Annu. Rev. Plant Biol. *58*, 219–247.

Shimomura, H., Etoh, H., Mizutani, M., Hirai, N., and Todoroki, Y. (2007). Effect of the minor ABA metabolite 7′-hydroxy-ABA on Arabidopsis ABA 8′-hydroxylase CYP707A3. Bioorg. Med. Chem. Lett. *17*, 4977–4981.

Shiu, S.-H., Shih, M.-C., and Li, W.-H. (2005). Transcription Factor Families Have Much Higher Expansion Rates in Plants than in Animals. Plant Physiol. *139*, 18–26.

Shkolnik-Inbar, D., and Bar-Zvi, D. (2010). ABI4 Mediates Abscisic Acid and Cytokinin Inhibition of Lateral Root Formation by Reducing Polar Auxin Transport in Arabidopsis. PLANT CELL ONLINE *22*, 3560–3573.

Shu, K., Chen, Q., Wu, Y., Liu, R., Zhang, H., Wang, P., Li, Y., Wang, S., Tang, S., Liu, C., et al. (2016). ABI4 mediates antagonistic effects of abscisic acid and gibberellins at transcript and protein levels. Plant J. Cell Mol. Biol. *85*, 348–361.

Singer, R.H., and Ward, D.C. (1982). Actin gene expression visualized in chicken muscle tissue culture by using in situ hybridization with a biotinated nucleotide analog. Proc. Natl. Acad. Sci. *79*, 7331–7335.

Skubacz, A., Daszkowska-Golec, A., and Szarejko, I. (2016). The Role and Regulation of ABI5 (ABA-Insensitive 5) in Plant Development, Abiotic Stress Responses and Phytohormone Crosstalk. Front. Plant Sci. *7*.

Solanki, S., Ameen, G., Zhao, J., Flaten, J., Borowicz, P., and Brueggeman, R.S. (2020). Visualization of spatial gene expression in plants by modified RNAscope fluorescent in situ hybridization. Plant Methods *16*, 71.

Sondheimer, E., Tzou, D.S., and Galson, E.C. (1968). Abscisic Acid Levels and Seed Dormancy. Plant Physiol. *43*, 1443–1447.

Song, L., Huang, S.C., Wise, A., Castanon, R., Nery, J.R., Chen, H., Watanabe, M., Thomas, J., Bar-Joseph, Z., and Ecker, J.R. (2016). A transcription factor hierarchy defines an environmental stress response network. Science *354*.

Sørensen, B.B., Ehrnsberger, H.F., Esposito, S., Pfab, A., Bruckmann, A., Hauptmann, J., Meister, G., Merkl, R., Schubert, T., Längst, G., et al. (2017). The Arabidopsis THO/TREX component TEX1 functionally interacts with MOS11 and modulates mRNA export and alternative splicing events. Plant Mol. Biol. *93*, 283–298.

Sorenson, R.S., Deshotel, M.J., Johnson, K., Adler, F.R., and Sieburth, L.E. (2018). Arabidopsis mRNA decay landscape arises from specialized RNA decay substrates, decapping-mediated feedback, and redundancy. Proc. Natl. Acad. Sci. *115*, E1485–E1494.

Spollen, W.G., LeNoble, M.E., Samuels, T.D., Bernstein, N., and Sharp, R.E. (2000). Abscisic Acid Accumulation Maintains Maize Primary Root Elongation at Low Water Potentials by Restricting Ethylene Production. Plant Physiol. *122*, 967–976.

Srivastava, A.K., Lu, Y., Zinta, G., Lang, Z., and Zhu, J.-K. (2018). UTR dependent control of gene expression in plants. Trends Plant Sci. *23*, 248–259.

Stadhouders, R., van den Heuvel, A., Kolovos, P., Jorna, R., Leslie, K., Grosveld, F., and Soler, E. (2012). Transcription regulation by distal enhancers. Transcription *3*, 181–186.

Steinmetz, E.J., Conrad, N.K., Brow, D.A., and Corden, J.L. (2001). RNA-binding protein Nrd1 directs poly(A)-independent 3′-end formation of RNA polymerase II transcripts. Nature *413*, 327–331.

Steurer, B., Janssens, R.C., Geverts, B., Geijer, M.E., Wienholz, F., Theil, A.F., Chang, J., Dealy, S., Pothof, J., Cappellen, W.A. van, et al. (2018). Live-cell analysis of endogenous GFP-RPB1 uncovers rapid turnover of initiating and promoter-paused RNA Polymerase II. Proc. Natl. Acad. Sci. *115*, E4368–E4376.

Stockinger, E.J., Gilmour, S.J., and Thomashow, M.F. (1997). Arabidopsis thaliana CBF1 encodes an AP2 domain-containing transcriptional activator that binds to the C-repeat/DRE, a cis-acting DNA regulatory element that stimulates transcription in response to low temperature and water deficit. Proc. Natl. Acad. Sci. U. S. A. *94*, 1035–1040.

Sun, L., Fan, X., Zhang, Y., Jiang, J., Sun, H., and Liu, C. (2016). Transcriptome analysis of genes involved in anthocyanins biosynthesis and transport in berries of black and white spine grapes (Vitis davidii). Hereditas *153*, 17.

Suzuki, M., Kao, C.Y., Cocciolone, S., and McCarty, D.R. (2001). Maize VP1 complements Arabidopsis abi3 and confers a novel ABA/auxin interaction in roots. Plant J. Cell Mol. Biol. *28*, 409–418.

Tack, D.C., Su, Z., Yu, Y., Bevilacqua, P.C., and Assmann, S.M. (2019). Tissue-specific changes in the RNA structurome mediate salinity response in Arabidopsis. 40.

Takahashi, Y., Zhang, J., Hsu, P.-K., Ceciliato, P.H.O., Zhang, L., Dubeaux, G., Munemasa, S., Ge, C., Zhao, Y., Hauser, F., et al. (2020). MAP3Kinase-dependent SnRK2-kinase activation is required for abscisic acid signal transduction and rapid osmotic stress response. Nat. Commun. *11*, 12.

Tan, B.C., Schwartz, S.H., Zeevaart, J.A.D., and McCarty, D.R. (1997). Genetic control of abscisic acid biosynthesis in maize. Proc. Natl. Acad. Sci. *94*, 12235–12240.

Tan, B.-C., Joseph, L.M., Deng, W.-T., Liu, L., Li, Q.-B., Cline, K., and McCarty, D.R. (2003). Molecular characterization of the Arabidopsis 9-cis epoxycarotenoid dioxygenase gene family. Plant J. *35*, 44–56.

Tanaka, Y., Nose, T., Jikumaru, Y., and Kamiya, Y. (2013). ABA inhibits entry into stomatal-lineage development in Arabidopsis leaves. Plant J. *74*, 448–457.

Tarazona, S., Furió-Tarí, P., Turrà, D., Pietro, A.D., Nueda, M.J., Ferrer, A., and Conesa, A. (2015). Data quality aware analysis of differential expression in RNA-seq with NOISeq R/Bioc package. Nucleic Acids Res. *43*, e140.

Tardieu, F., and Simonneau, T. (1998). Variability among species of stomatal control under fluctuating soil water status and evaporative demand: modelling isohydric and anisohydric behaviours. J. Exp. Bot. *49*, 419–432.

Taub, F., E., DeLEO, J.M., and Thompson, E.B. (1983). Sequential Comparative Hybridizations Analyzed by Computerized Image Processing Can Identify and Quantitate Regulated RNAs. DNA *2*, 309–327.

Thompson, A.J., Andrews, J., Mulholland, B.J., McKee, J.M.T., Hilton, H.W., Horridge, J.S., Farquhar, G.D., Smeeton, R.C., Smillie, I.R.A., Black, C.R., et al. (2007). Overproduction of Abscisic Acid in Tomato Increases Transpiration Efficiency and Root Hydraulic Conductivity and Influences Leaf Expansion. PLANT Physiol. *143*, 1905–1917.

Tilgner, H., Grubert, F., Sharon, D., and Snyder, M.P. (2014). Defining a personal, allele-specific, and single-molecule long-read transcriptome. Proc. Natl. Acad. Sci. *111*, 9869–9874.

Tischer, S.V., Wunschel, C., Papacek, M., Kleigrewe, K., Hofmann, T., Christmann, A., and Grill, E. (2017). Combinatorial interaction network of abscisic acid receptors and coreceptors from Arabidopsis thaliana. Proc. Natl. Acad. Sci. *114*, 10280–10285.

Ton, J., and Mauch-Mani, B. (2004). Beta-amino-butyric acid-induced resistance against necrotrophic pathogens is based on ABA-dependent priming for callose. Plant J. Cell Mol. Biol. *38*, 119–130.

Torres-Ruiz, J.M., Cochard, H., Fonseca, E., Badel, E., Gazarini, L., and Vaz, M. (2017). Differences in functional and xylem anatomical features allow Cistus species to co-occur and cope differently with drought in the Mediterranean region. Tree Physiol. *37*, 755–766.

Tran, L.-S.P., Nakashima, K., Sakuma, Y., Simpson, S.D., Fujita, Y., Maruyama, K., Fujita, M., Seki, M., Shinozaki, K., and Yamaguchi-Shinozaki, K. (2004). Isolation and Functional Analysis of Arabidopsis Stress-Inducible NAC Transcription Factors That Bind to a Drought-Responsive cis-Element in the early responsive to dehydration stress 1 Promoter. Plant Cell *16*, 2481–2498.

Tu, M., Wang, X., Yin, W., Wang, Y., Li, Y., Zhang, G., Li, Z., Song, J., and Wang, X. (2020). Grapevine VlbZIP30 improves drought resistance by directly activating VvNAC17 and promoting lignin biosynthesis through the regulation of three peroxidase genes. Hortic. Res. *7*, 1–15.

Turowski, T.W., and Tollervey, D. (2016). Transcription by RNA polymerase III: insights into mechanism and regulation. Biochem. Soc. Trans. *44*, 1367–1375.

Tyree, M.T., and Sperry, J.S. (1988). Do Woody Plants Operate Near the Point of Catastrophic Xylem Dysfunction Caused by Dynamic Water Stress?: Answers from a Model. Plant Physiol. *88*, 574–580.

Tyree, M.T., Vargas, G., Engelbrecht, B.M.J., and Kursar, T.A. (2002). Drought until death do us part: a case study of the desiccation-tolerance of a tropical moist forest seedling-tree, Licania platypus (Hemsl.) Fritsch. J. Exp. Bot. *53*, 2239–2247.

Umezawa, T., Nakashima, K., Miyakawa, T., Kuromori, T., Tanokura, M., Shinozaki, K., and Yamaguchi-Shinozaki, K. (2010). Molecular Basis of the Core Regulatory Network in ABA Responses: Sensing, Signaling and Transport. Plant Cell Physiol. *51*, 1821–1839.

United States Department of Agriculture (2020). Noncitrus Fruits and Nuts 2018 Summary (National Agricultural Statistics Service).

Vandereyken, K., Van Leene, J., De Coninck, B., and Cammue, B.P.A. (2018). Hub Protein Controversy: Taking a Closer Look at Plant Stress Response Hubs. Front. Plant Sci. *9*.

VanGuilder, H.D., Vrana, K.E., and Freeman, W.M. (2008). Twenty-five years of quantitative PCR for gene expression analysis. BioTechniques *44*, 619–626.

Varoquaux, N., Cole, B., Gao, C., Pierroz, G., Baker, C.R., Patel, D., Madera, M., Jeffers, T., Hollingsworth, J., Sievert, J., et al. (2019). Transcriptomic analysis of field-droughted sorghum from seedling to maturity reveals biotic and metabolic responses. Proc. Natl. Acad. Sci. *116*, 27124–27132.

Vishal, B., Krishnamurthy, P., Ramamoorthy, R., and Kumar, P.P. (2019). OsTPS8 controls yield-related traits and confers salt stress tolerance in rice by enhancing suberin deposition. New Phytol. *221*, 1369–1386.

Vitting-Seerup, K., and Sandelin, A. (2019). IsoformSwitchAnalyzeR: analysis of changes in genome-wide patterns of alternative splicing and its functional consequences. Bioinformatics *35*, 4469–4471.

Vleesschauwer, D.D., Yang, Y., Cruz, C.V., and Höfte, M. (2010). Abscisic Acid-Induced Resistance against the Brown Spot Pathogen Cochliobolus miyabeanus in Rice Involves MAP Kinase-Mediated Repression of Ethylene Signaling. Plant Physiol. *152*, 2036–2052.

Vogel, C., and Marcotte, E.M. (2012). Insights into the regulation of protein abundance from proteomic and transcriptomic analyses. Nat. Rev. Genet. *13*, 227–232.

Wade, J.T., and Struhl, K. (2008). The transition from transcriptional initiation to elongation. Curr. Opin. Genet. Dev. *18*, 130–136.

Wang, B., Tseng, E., Regulski, M., Clark, T.A., Hon, T., Jiao, Y., Lu, Z., Olson, A., Stein, J.C., and Ware, D. (2016). Unveiling the complexity of the maize transcriptome by single-molecule long-read sequencing. Nat. Commun. *7*, 11708.

Wang, B., Regulski, M., Tseng, E., Olson, A., Goodwin, S., McCombie, W.R., and Ware, D. (2018a). A comparative transcriptional landscape of maize and sorghum obtained by single-molecule sequencing. Genome Res. *28*, 921–932.

Wang, B., Kumar, V., Olson, A., and Ware, D. (2019). Reviving the Transcriptome Studies: An Insight Into the Emergence of Single-Molecule Transcriptome Sequencing. Front. Genet. *10*.

Wang, L., Hukin, D., Pritchard, J., and Thomas, C. (2006). Comparison of plant cell turgor pressure measurement by pressure probe and micromanipulation. Biotechnol. Lett. *28*, 1147–1150.

Wang, X.-Q., Wu, W.-H., and Assmann, S.M. (1998). Differential Responses of Abaxial and Adaxial Guard Cells of Broad Bean to Abscisic Acid and Calcium. Plant Physiol. *118*, 1421–1429.

Wang, Y., Deng, D., Zhang, R., Wang, S., Bian, Y., and Yin, Z. (2012). Systematic analysis of plant-specific B3 domain-containing proteins based on the genome resources of 11 sequenced species. Mol. Biol. Rep. *39*, 6267–6282.

Wang, Y., Zhang, Y., Zhou, R., Dossa, K., Yu, J., Li, D., Liu, A., Mmadi, M.A., Zhang, X., and You, J. (2018b). Identification and characterization of the bZIP transcription factor family and its expression in response to abiotic stresses in sesame. PLOS ONE *13*, e0200850.

Wang, Z., Gerstein, M., and Snyder, M. (2009). RNA-Seq: a revolutionary tool for transcriptomics. Nat. Rev. Genet. *10*, 57–63.

Wasilewska, A., Vlad, F., Sirichandra, C., Redko, Y., Jammes, F., Valon, C., Frey, N.F. dit, and Leung, J. (2008). An Update on Abscisic Acid Signaling in Plants and More …. Mol. Plant *1*, 198–217.

Weber, A.P.M., Weber, K.L., Carr, K., Wilkerson, C., and Ohlrogge, J.B. (2007). Sampling the Arabidopsis Transcriptome with Massively Parallel Pyrosequencing. Plant Physiol. *144*, 32–42.

Weiler, C.S., Merkt, N., and Graeff-Hönninger, S. (2018). Impact of Water Deficit during Fruit Development on Quality and Yield of Young Table Grape Cultivars. Horticulturae *4*, 45.

Welsch, R., Beyer, P., Hugueney, P., Kleinig, H., and von Lintig, J. (2000). Regulation and activation of phytoene synthase, a key enzyme in carotenoid biosynthesis, during photomorphogenesis. Planta *211*, 846–854.

Welsch, R., Wüst, F., Bär, C., Al-Babili, S., and Beyer, P. (2008). A Third Phytoene Synthase Is Devoted to Abiotic Stress-Induced Abscisic Acid Formation in Rice and Defines Functional Diversification of Phytoene Synthase Genes. Plant Physiol. *147*, 367–380.

Weng, J.-K., Ye, M., Li, B., and Noel, J.P. (2016). Co-evolution of Hormone Metabolism and Signaling Networks Expands Plant Adaptive Plasticity. Cell *166*, 881–893.

Wierzbicki, A.T., Haag, J.R., and Pikaard, C.S. (2008). Noncoding transcription by RNA Polymerase Pol IVb/Pol V mediates transcriptional silencing of overlapping and adjacent genes. Cell *135*, 635–648.

Wilkinson, S., and Davies, W.J. (2002). ABA-based chemical signalling: the co-ordination of responses to stress in plants. Plant Cell Environ. *25*, 195–210.

Williams, C.N. (1959). Action of Inhibitor- β on the Growth of Striga Seedlings. Nature *184*, 1577–1578.

Willmer, C., and Fricker, M. (1996). Stomatal responses to environmental factors. In Stomata, C. Willmer, and M. Fricker, eds. (Dordrecht: Springer Netherlands), pp. 126–191.

Wine Institute (2020). California Wine Sales Reach $43.6 Billion in U.S. Market in 2019.

Wong, M.L., and Medrano, J.F. (2005). Real-time PCR for mRNA quantitation. BioTechniques *39*, 75–85.

Wong, D.C.J., Lopez Gutierrez, R., Gambetta, G.A., and Castellarin, S.D. (2017). Genome-wide analysis of cis-regulatory element structure and discovery of motif-driven gene co-expression networks in grapevine. DNA Res. Int. J. Rapid Publ. Rep. Genes Genomes *24*, 311–326.

Woo, Y.H., and Li, W.-H. (2011). Gene clustering pattern, promoter architecture, and gene expression stability in eukaryotic genomes. Proc. Natl. Acad. Sci. *108*, 3306–3311.

Workman, J.L., and Roeder, R.G. (1987). Binding of transcription factor TFIID to the major late promoter during in vitro nucleosome assembly potentiates subsequent initiation by RNA polymerase II. Cell *51*, 613–622.

Worsley-Hunt, R., Bernard, V., and Wasserman, W.W. (2011). Identification of cis-regulatory sequence variations in individual genome sequences. Genome Med. *3*, 65.

Xing, L., Zhao, Y., Gao, J., Xiang, C., and Zhu, J.-K. (2016). The ABA receptor PYL9 together with PYL8 plays an important role in regulating lateral root growth. Sci. Rep. *6*, 27177.

Xu, P., Zhou, T., Yi, C., Fang, W., Hendrey, G., and Zhao, X. (2018). Forest drought resistance distinguished by canopy height. Environ. Res. Lett. *13*, 075003.

Xu, W., Cui, K., Xu, A., Nie, L., Huang, J., and Peng, S. (2015). Drought stress condition increases root to shoot ratio via alteration of carbohydrate partitioning and enzymatic activity in rice seedlings. Acta Physiol. Plant. *37*, 9.

Xu, Z.-Y., Lee, K.H., Dong, T., Jeong, J.C., Jin, J.B., Kanno, Y., Kim, D.H., Kim, S.Y., Seo, M., Bressan, R.A., et al. (2012). A Vacuolar β-Glucosidase Homolog That Possesses Glucose-Conjugated Abscisic Acid Hydrolyzing Activity Plays an Important Role in Osmotic Stress Responses in Arabidopsis. Plant Cell *24*, 2184–2199.

Xu, Z.-Y., Yoo, Y.-J., and Hwang, I. (2014). ABA Conjugates and Their Physiological Roles in Plant Cells. In Abscisic Acid: Metabolism, Transport and Signaling, D.-P. Zhang, ed. (Dordrecht: Springer Netherlands), pp. 77–87.

Yamamoto, M., Maehara, Y., Takahashi, K., and Endo, H. (1983). Cloning of sequences expressed specifically in tumors of rat. Proc. Natl. Acad. Sci. *80*, 7524–7527.

Yamamoto, Y.Y., Ichida, H., Matsui, M., Obokata, J., Sakurai, T., Satou, M., Seki, M., Shinozaki, K., and Abe, T. (2007). Identification of plant promoter constituents by analysis of local distribution of short sequences. BMC Genomics *8*, 67.

Yang, W., Zhang, W., and Wang, X. (2017). Post-translational control of ABA signalling: the roles of protein phosphorylation and ubiquitination. Plant Biotechnol. J. *15*, 4–14.

Yang, X., Yang, Y.-N., Xue, L.-J., Zou, M.-J., Liu, J.-Y., Chen, F., and Xue, H.-W. (2011). Rice ABI5-Like1 Regulates Abscisic Acid and Auxin Responses by Affecting the Expression of ABRE-Containing Genes. Plant Physiol. *156*, 1397–1409.

Yasuda, M., Ishikawa, A., Jikumaru, Y., Seki, M., Umezawa, T., Asami, T., Maruyama-Nakashita, A., Kudo, T., Shinozaki, K., Yoshida, S., et al. (2008). Antagonistic Interaction between Systemic Acquired Resistance and the Abscisic Acid–Mediated Abiotic Stress Response in Arabidopsis. Plant Cell *20*, 1678–1692.

Yi, H., and Richards, E.J. (2007). A Cluster of Disease Resistance Genes in Arabidopsis Is Coordinately Regulated by Transcriptional Activation and RNA Silencing. Plant Cell *19*, 2929–2939.

Yıldırım, K., Yağcı, A., Sucu, S., and Tunç, S. (2018). Responses of grapevine rootstocks to drought through altered root system architecture and root transcriptomic regulations. Plant Physiol. Biochem. PPB *127*, 256–268.

Yoshida, R., Hobo, T., Ichimura, K., Mizoguchi, T., Takahashi, F., Aronso, J., Ecker, J.R., and Shinozaki, K. (2002). ABA-activated SnRK2 protein kinase is required for dehydration stress signaling in Arabidopsis. Plant Cell Physiol. *43*, 1473–1483.

Yoshida, T., Fujita, Y., Sayama, H., Kidokoro, S., Maruyama, K., Mizoi, J., Shinozaki, K., and Yamaguchi-Shinozaki, K. (2010). AREB1, AREB2, and ABF3 are master transcription factors that cooperatively regulate ABRE-dependent ABA signaling involved in drought stress tolerance and require ABA for full activation. Plant J. *61*, 672–685.

Yoshida, T., Fujita, Y., Maruyama, K., Mogami, J., Todaka, D., Shinozaki, K., and Yamaguchi-Shinozaki, K. (2015). Four Arabidopsis AREB/ABF transcription factors function predominantly in gene expression downstream of SnRK2 kinases in abscisic acid signalling in response to osmotic stress. Plant Cell Environ. *38*, 35–49.

Yoshida, T., Christmann, A., Yamaguchi-Shinozaki, K., Grill, E., and Fernie, A.R. (2019a). Revisiting the Basal Role of ABA - Roles Outside of Stress. Trends Plant Sci. *24*, 625–635.

Yoshida, T., Obata, T., Feil, R., Lunn, J.E., Fujita, Y., Yamaguchi-Shinozaki, K., and Fernie, A.R. (2019b). The Role of Abscisic Acid Signaling in Maintaining the Metabolic

Balance Required for Arabidopsis Growth under Nonstress Conditions. Plant Cell *31*, 84–105.

Young, A.P., Jackson, D.J., and Wyeth, R.C. (2020). A technical review and guide to RNA fluorescence in situ hybridization. PeerJ *8*.

Zamora-Briseño, J.A., and de Jiménez, E.S. (2016). A LEA 4 protein up-regulated by ABA is involved in drought response in maize roots. Mol. Biol. Rep. *43*, 221–228.

Zargar, S.M., Nagar, P., Deshmukh, R., Nazir, M., Wani, A.A., Masoodi, K.Z., Agrawal, G.K., and Rakwal, R. (2017). Aquaporins as potential drought tolerance inducing proteins: Towards instigating stress tolerance. J. Proteomics *169*, 233–238.

Zeng, J., Wang, C., Chen, X., Zang, M., Yuan, C., Wang, X., Wang, Q., Li, M., Li, X., Chen, L., et al. (2015). The lycopene β-cyclase plays a significant role in provitamin A biosynthesis in wheat endosperm. BMC Plant Biol. *15*.

Zeng, W., Melotto, M., and He, S.Y. (2010). Plant stomata: a checkpoint of host immunity and pathogen virulence. Curr. Opin. Biotechnol. *21*, 599–603.

Zhang, B., and Horvath, S. (2005). A General Framework for Weighted Gene Co-Expression Network Analysis. Stat. Appl. Genet. Mol. Biol. *4*.

Zhang, M., Leng, P., Zhang, G., and Li, X. (2009). Cloning and functional analysis of 9-cis-epoxycarotenoid dioxygenase (NCED) genes encoding a key enzyme during abscisic acid biosynthesis from peach and grape fruits. J. Plant Physiol. *166*, 1241–1252.

Zhang, R., Calixto, C.P.G., Marquez, Y., Venhuizen, P., Tzioutziou, N.A., Guo, W., Spensley, M., Entizne, J.C., Lewandowska, D., ten Have, S., et al. (2017). A high quality Arabidopsis transcriptome for accurate transcript-level analysis of alternative splicing. Nucleic Acids Res. *45*, 5061–5073.

Zhang, X., Zhang, S., Wang, J., Zi, J., Wang, J., Chen, S., and Wan, Y. (2016). Expression, Purification, and Characterization of a Sucrose Nonfermenting 1-Related Protein Kinases 2 of Arabidopsis thaliana in E. coli-Based Cell-Free System (Hindawi).

Zhao, W., Langfelder, P., Fuller, T., Dong, J., Li, A., and Hovarth, S. (2010). Weighted gene coexpression network analysis: state of the art. J. Biopharm. Stat. *20*, 281–300.

Zhao, Y., Xing, L., Wang, X., Hou, Y.-J., Gao, J., Wang, P., Duan, C.-G., Zhu, X., and Zhu, J.-K. (2014). The ABA Receptor PYL8 Promotes Lateral Root Growth by Enhancing MYB77-Dependent Transcription of Auxin-Responsive Genes. Sci. Signal. *7*, ra53–ra53.

Zhou, G., Zhou, X., Nie, Y., Bai, S.H., Zhou, L., Shao, J., Cheng, W., Wang, J., Hu, F., and Fu, Y. (2018). Drought-induced changes in root biomass largely result from altered root morphological traits: Evidence from a synthesis of global field trials: Effects of drought on root traits. Plant Cell Environ. *41*, 2589–2599.

Zhou, Y., Massonnet, M., Sanjak, J.S., Cantu, D., and Gaut, B.S. (2017). Evolutionary genomics of grape (Vitis vinifera ssp. vinifera) domestication. Proc. Natl. Acad. Sci. *114*, 11715–11720.

Zhu, H., Zhang, H., Xu, Y., Laššáková, S., Korabečná, M., and Neužil, P. (2020). PCR past, present and future. Biotechniques *69*.

Zhu, W., Schlueter, S.D., and Brendel, V. (2003). Refined Annotation of the Arabidopsis Genome by Complete Expressed Sequence Tag Mapping. Plant Physiol. *132*, 469–484.

Zhuang, J., Peng, R.-H., Cheng, Z.-M. (Max), Zhang, J., Cai, B., Zhang, Z., Gao, F., Zhu, B., Fu, X.-Y., Jin, X.-F., et al. (2009). Genome-wide analysis of the putative AP2/ERF family genes in Vitis vinifera. Sci. Hortic. *123*, 73–81.

Zombardo, A., Crosatti, C., Bagnaresi, P., Bassolino, L., Reshef, N., Puccioni, S., Faccioli, P., Tafuri, A., Delledonne, M., Fait, A., et al. (2020). Transcriptomic and biochemical investigations support the role of rootstock-scion interaction in grapevine berry quality. BMC Genomics *21*, 468.

(1999). The zeaxanthin biosynthesis enzyme ^{2}-carotene hydroxylase is involved in myxoxanthophyll synthesis in Synechocystis sp. PCC 6803. FEBS Lett. *454*, 247–251.

Figures

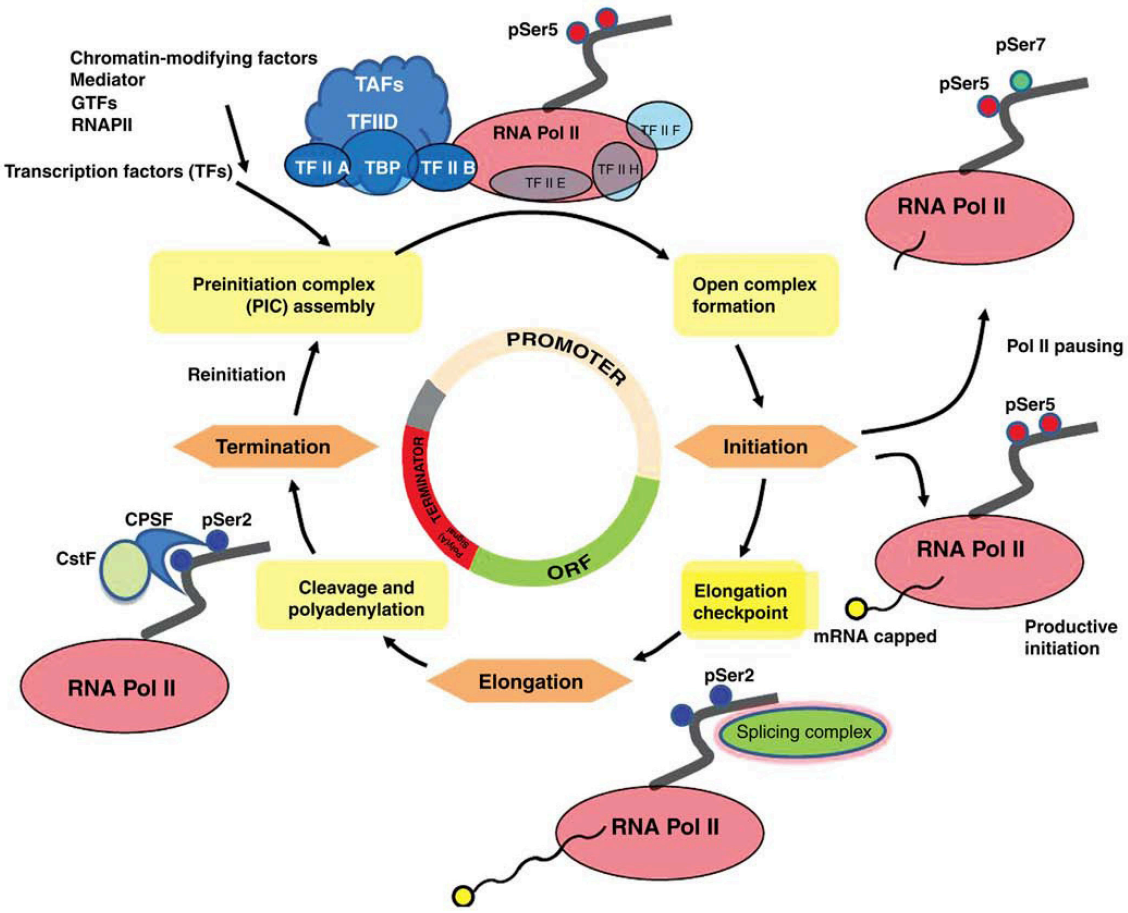

Figure 1: RNAPII transcription cycle from Hong 2016. Original image drawn according to Hahn (2004) and Shandilya and Roberts (2012) and derived from Hong, 2016 publication. The main phases of the transcription cycle (orange); key events of regulation (yellow). The circle in the middle depicts the occurrence of the events in relation to the position on the gene. GTFs, general TFs; ORF, open reading frame. RNAPII (pink) subunits (blue), C-terminal domain (CTD) phosphorylation of Ser-5P (red), Ser-2P (blue), and Ser-7P (light green).

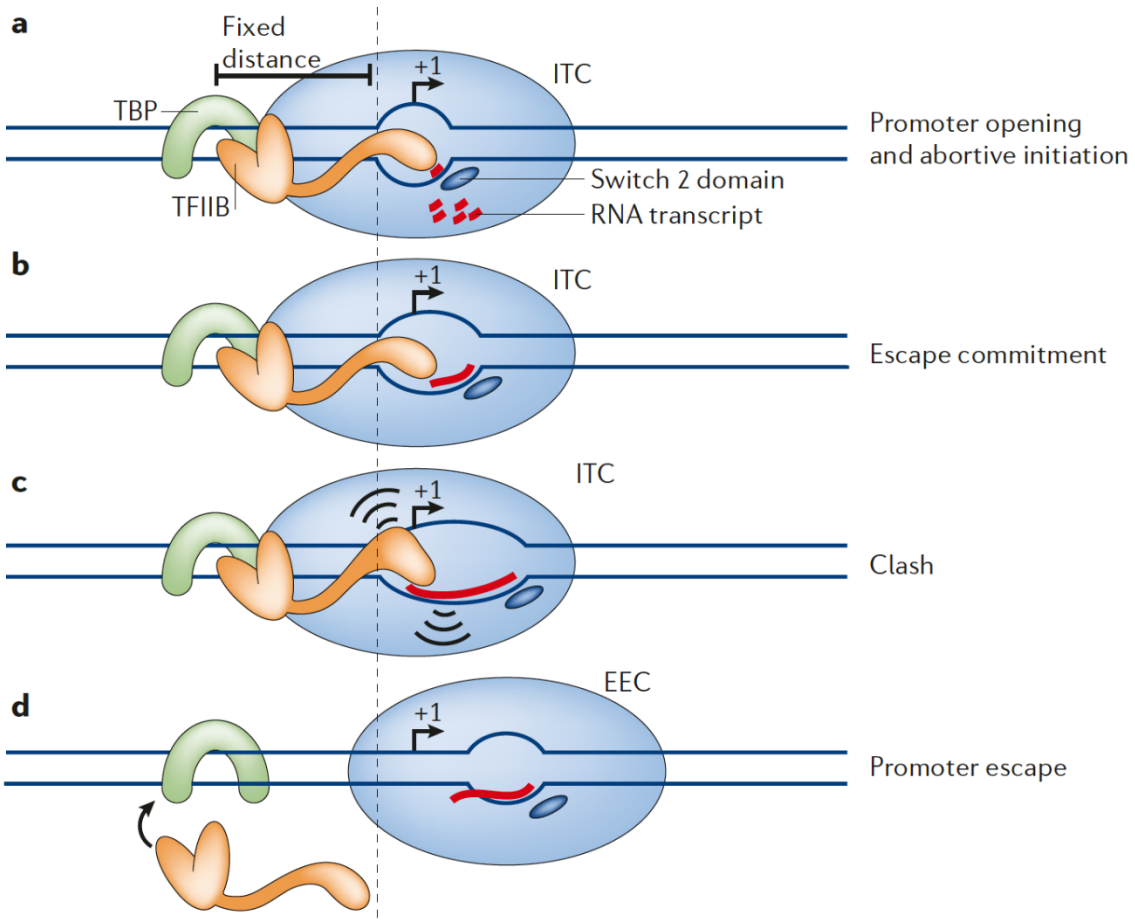

Figure 2: Promoter escape and the formation of an early elongation complex from Saunders 2006. a) The unwinding of promoter DNA to create a transcription bubble begins at a fixed position (~20 base pairs downstream from the binding site of the TATA-box-binding protein (TBP) or another cis-element). The upstream bubble edge (vertical dashed line) remains fixed until the end of promoter escape. The downstream bubble edge expands as transcription proceeds. The initially transcribing complex (ITC) undergoes abortive initiation. **b)** After synthesis of the first 4 nucleotides, the B-finger of TFIIB (orange) and a switch domain (dark blue oval) of Pol II (large blue oval) stabilize the short RNA, reducing abortive initiation **c)** After 5 nucleotides are transcribed, the nascent RNA collides with the B-finger of TFIIB, inducing stress resulting in increased abortive initiation, strong pausing, or transcript slippage. This step contributes to the rate-limiting step of promoter escape **d)** The transcription bubbles collapses from the stress of the growing RNA, providing the energy to remodel the transcription complex. The B-finger is ejected from the RNA-exit tunnel and TFIIB is released. The RNA–DNA hybrid contacts protein loops near the RNA-exit site. Abortive initiation stops, and transcript slippage is reduced. The transcription complex has changed into an early elongation complex (EEC). Figure derived from Saunders et al., 2006.

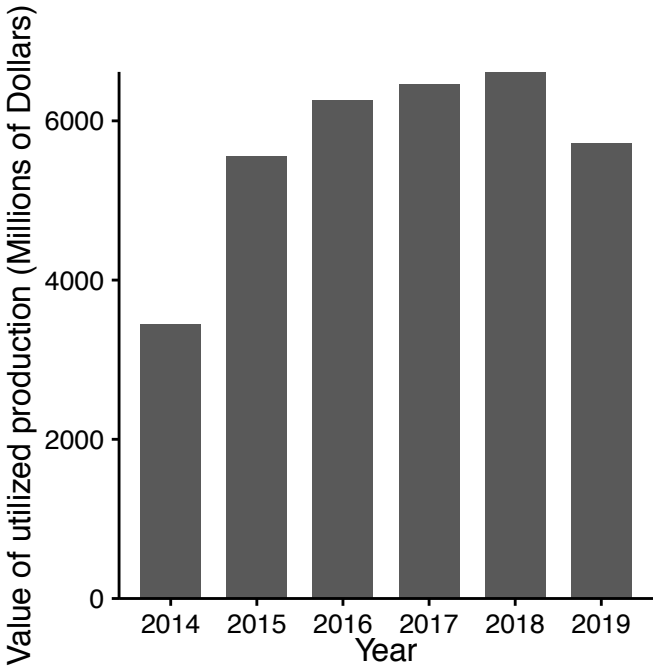

Figure 3: Utilized production value (millions of dollars) of grapevine in the USA from 2014-2019. Values obtained from the United States Department of Agriculture annual Non-citrus Fruits and Nuts Summary.

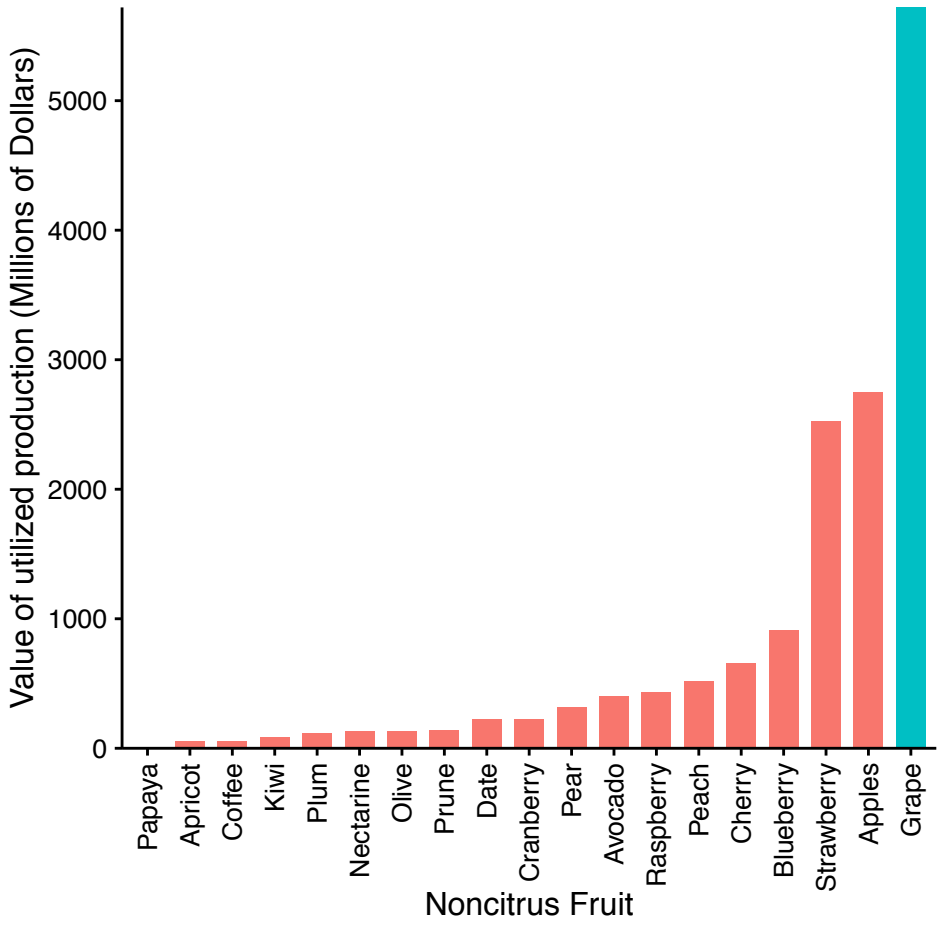

Figure 4: Utilized production value (millions of dollars) of non-citrus fruit crops in the USA from 2019. Values obtained from the United States Department of Agriculture annual Non-citrus Fruits and Nuts Summary (United States Department of Agriculture, 2020). Grapevine in blue and all other non-citrus crops in pink.

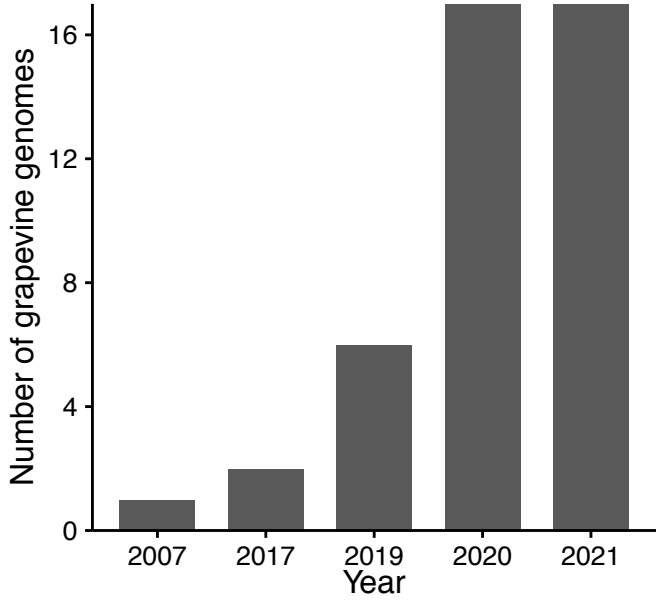

Figure 5: Number of released *Vitis* genomes. The cumulative number of available reference level *Vitis* genomes from 2007 to February 2021. Genomes include PN40024 (Canaguier et al., 2017), Cabernet Sauvignon (Chin et al., 2016), Carménère (Minio et al., 2019b), Riparia Gloire (Girollet et al., 2019), Riparia Manitoba 37 (Patel et al., 2020), Chardonnay (Zhou et al., 2019), Zinfandel (Vondras et al., 2019), *Vitis sylvestris* C1-2 (Badouin et al., 2020), black Corinth seeded, black Corinth seedless, Merlot, *Vitis sylvestris* (DVIT3351.27, DVIT3603.07, DVIT3603.16, and O34-16), *Vitis arizonica* (Massonnet et al., 2019), and *Muscadinia rotundifolia* (Cochetel et al., 2021).

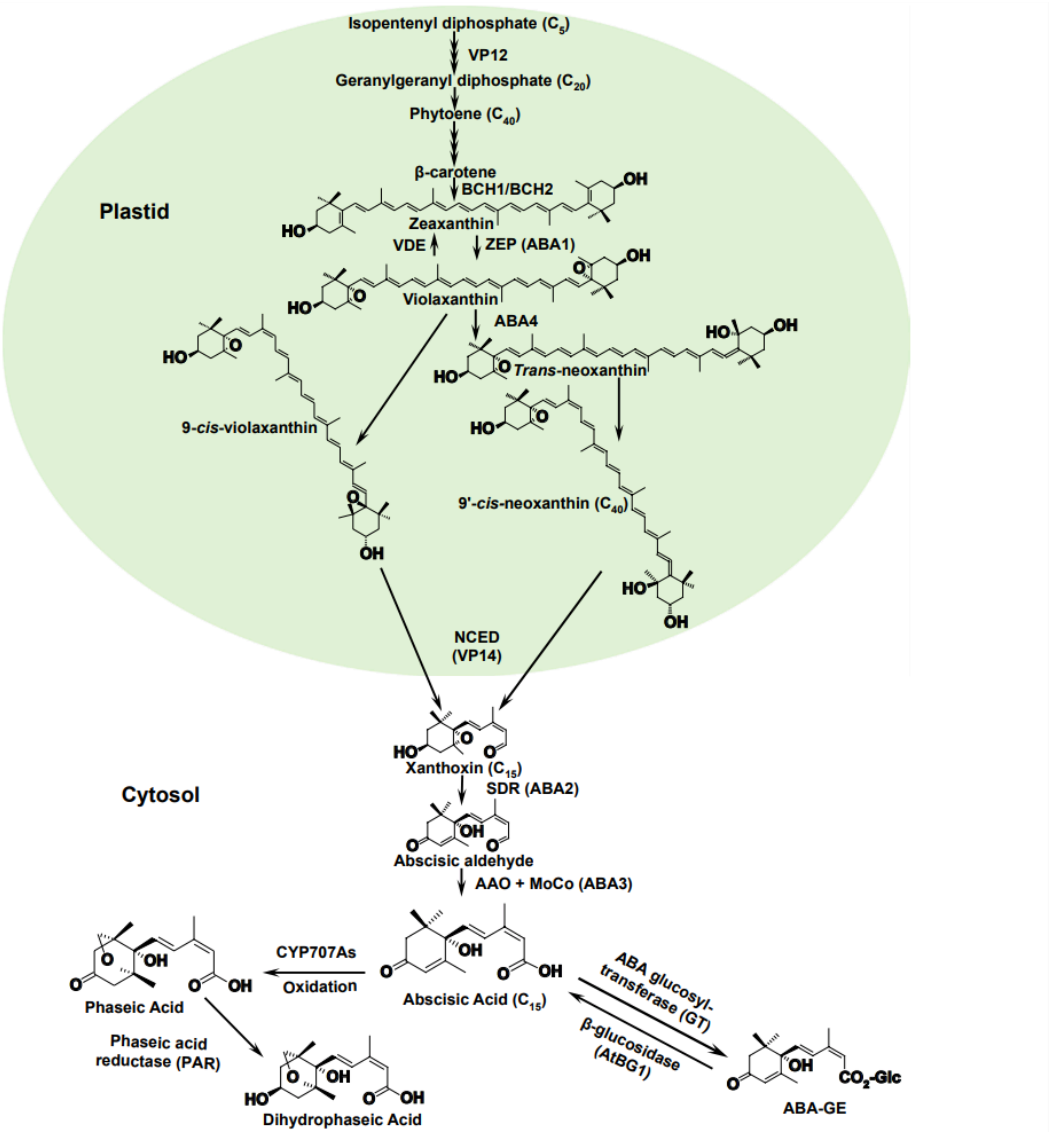

Figure 6: The abscisic acid (ABA) metabolic pathways in plants from Li et al. 2017. The ABA biosynthesis, degradation, and conjugation pathways are shown in respective cellular organelles where these events occur. Biosynthesis steps blocked in the Arabidopsis mutants (*aba1*, *aba2*, *aba3*, and *aba4*) and maize mutants (*vp12* and *vp14*) are indicated as in the original publication this figure is derived from Li et al., 2017.

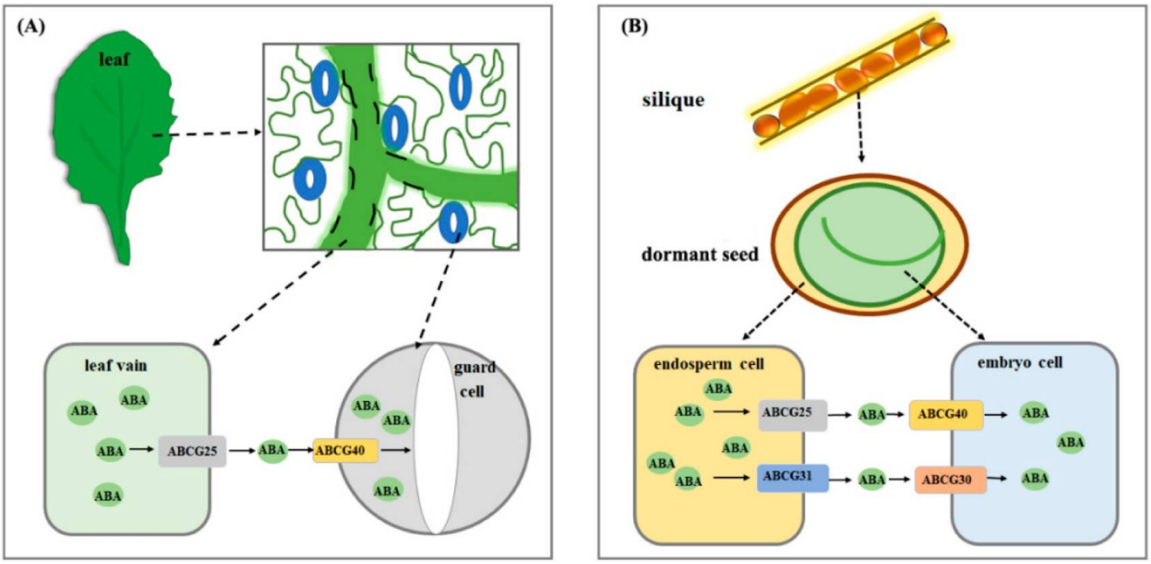

Figure 7: ABA transport system in leaf and dormant seed from Ma et al. 2018 (A) ABA transport in the leaf: under drought, ABCG25 transports ABA from leaf vein to the apoplast around guard cells, and subsequently ABA is taken up into guard cells by ABCG40, causing stomatal closure. **(B)** ABA transport during seed dormancy: ABCG25 and ABCG31 mediate ABA efflux from endosperm cells; ABCG30 and ABCG40 transport ABA from extracellular space into embryo cells to seed dormancy. Solid arrows indicate the direction of ABCG-mediated ABA transportation. Dotted arrows show local enlarged view of specific cells, tissues, and organs. Figure derived from original paper by Ma et al., 2018.

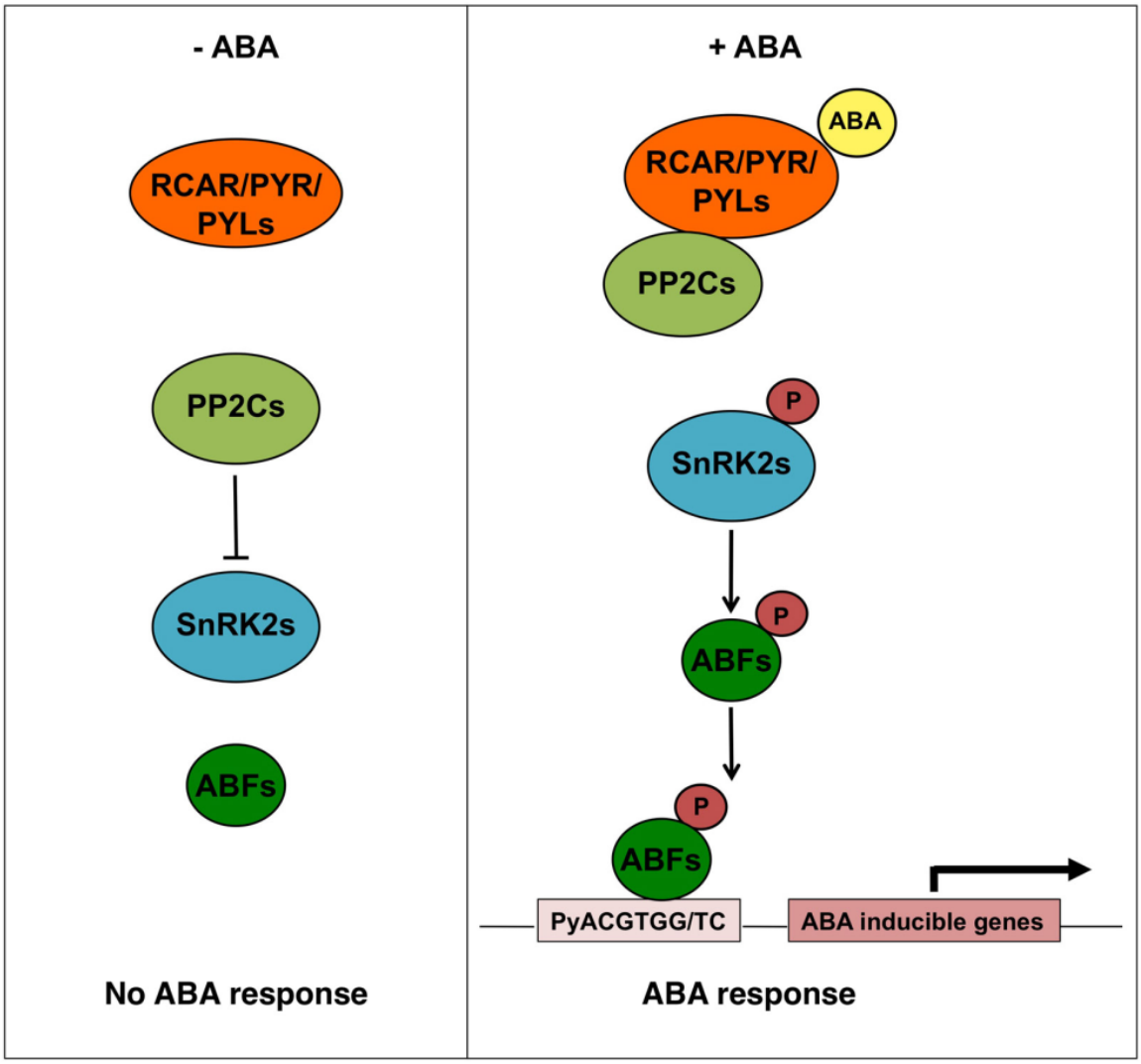

Figure 8: ABA signaling from the original manuscript from Fernando et. al 2016. The main ABA signaling components. In the absence of ABA, PP2Cs dephosphorylate SNRK2s preventing ABA signaling. In the presence of ABA, ABA PYR/PYL/RCAR receptors bind PP2Cs, freeing SNRK2s to activate target ABF/AREB TFs to induce ABA dependent gene expression. Figure from original paper by Fernando et al., 2016.

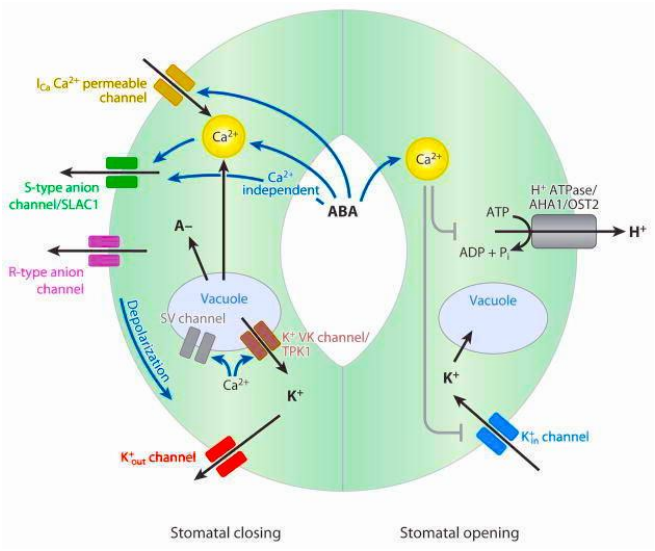

Figure 9: Summary of guard cell signaling and ion channel regulation from original work by Kim et al. 2010. Guard cell ion channel functions and ABA-induced signal transduction across the plasma membrane and vacuolar membrane of guard cells. Signaling events during stomatal closing (left), and major regulation steps for ABA-inhibition of stomatal opening mechanisms (right). Abbreviations: ABA, abscisic acid; ICa, inward Ca2+ current; S-type, slow-type; SLAC1, SLOW ANION CHANNEL ASSOCIATED 1; R-type, rapid-type; SV, slow vacuolar; VK, vacuolar K+ selective; TPK1, TWO PORE K+ CHANNEL 1; AHA1, ARABIDOPSIS H+ ATPASE 1; OST2, OPEN STOMATA 2. Figure from original paper by Kim et al., 2010.

CHAPTER 2:

ABRES IN THE PN40024 GRAPEVINE REFERENCE GENOME PROMOTER REGIONS

This chapter is unpublished work

2.0 Abstract

Abscisic acid (ABA) response elements (ABREs) are cis-acting elements involved in transcriptional activation during ABA signaling and abiotic stress response. Previously, cis-acting elements were annotated in grapevine, but since the original annotation, a novel reference genome annotation version was released, and the original cis-acting element analysis employed limited promoter region length and ABRE sequences. Here, ABREs were annotated in -3,000 bp promoter regions of the PN40024 v3 reference grapevine genome using a more comprehensive list of ABRE sequences than the previous analysis. Additionally, ABRE occurrences were compared for consensus and individual variants. ABREs were identified as being highly abundant throughout the promoter regions of the majority of annotated genes in the grapevine reference genome. The presence of ABREs was used to partially explain ABA signaling and abiotic stress responses previously observed for two genes of interest: *VviERF6L1* and *NCED3*. Additionally, this analysis identified novel potential genes involved in ABA signaling that require characterization and may be interesting targets for future studies.

2.1 Introduction

The ABA-responsive element (ABRE) is a conserved motif in ABA inducible genes (Guiltinan et al., 1990; Mundy et al., 1990), and many unique ABRE sequences have been identified. For example, ABREATCONSENSUS_1 and ABREATCONSENSUS_2

are among the first characterized ABREs, bound by bZIP TF EMBIGIN PSEUDOGENE 1 (EmBP1) in wheat (Guiltinan et al., 1990) and RAS RELATED PROTEIN (RAB12) in rice (Mundy et al., 1990), respectively. ABREZMRAB28 was another earlier discovered ABRE, regulating transcription of *RESPONSIVE TO ABA 28* (*RAB28*) in *Zea mays* during germination via binding by VIVIPAROUS 1 (VP1) (Busk and Pages, 1998). ABREZMRAB28 was characterized in poplar and Arabidopsis with roles in cold responses (Benedict et al., 2006; Suzuki et al., 2005).

Since the original identification of ABREs in wheat and rice (Guiltinan et al., 1990; Mundy et al., 1990), many more ABREs have been identified in numerous plant species including *Arabidopsis thaliana*, soybean, cotton (Maruyama et al., 2012; Yamamoto et al., 2007), and grapevine (Nicolas et al., 2014; Wong et al., 2017). For example, ABRELATERD1 was first discovered in the *EARLY RESPONSIVE TO DEHYDRATION 1* (*ERD1*) promoter region in *Arabidopsis thaliana* (Simpson et al., 2003). ABRE-related *Arabidopsis thaliana* calcium responsive (ABRERATCAL) motifs were first described as ABRE coupling elements with a role in transcriptional activation in response to cytosolic Ca^{2+}, a common response to stress and ABA (Kaplan et al., 2006). Additionally, ABRE-like binding site motif (ABRE-likebindingsitemotif) was first referenced in an ABRE review (Shinozaki and Yamaguchi-Shinozaki, 2000), but this consensus ABRE has also been referred to as the Classical ABRE (Leonhardt et al., 2004) and is enriched in E3 ligase promoter regions in Arabidopsis and grapevine (Wong et al., 2018). CGTGTSPHZMC1 is another cis-acting element sufficient for gene activation and transcription in the presence of ABA (Kao et al., 1996). There are many other ABREs with different lengths, sequences,

and regulatory functions that can be found on cis-acting element databases like PLACE (Higo et al., 1999), AGRIS (Davuluri et al., 2003), or plantCARE (Rombauts et al., 1999).

Some ABREs contain ambiguity codes. The ambiguity-codes of consensus ABREs are points in the ABRE sequence where more than one nucleotide can code for that position of the motif. For example, the consensus ABRE, ABRE-likebindingsitemotif (**B**ACGTG**KM**), has three ambiguity-code points that give rise to 12 different sequences (Table 1). The different ABRE sequences derived from consensus ABRE ambiguity codes are referred to as "ABRE variants" in this work. ABRE variants of the same consensus ABRE are delineated from one another with an underscore followed by a number. The term "ABREs" refers to ABREs that do not contain ambiguity points and each of the ABRE variants (e.g. 51 are examined in this work (Table 1)). ABREs that do not contain ambiguity points and the ABRE sequences reflective of all possible variants (e.g. **B**ACGTG**KM**) are referred to as "consensus ABREs" (e.g. 26 were examined in this work (Table 2)).

After TFs bind ABREs in response to ABA, target genes are transcribed to allow a plant to better adapt to stressful conditions. There are thousands of genes targeted by ABFs/AREBs or ABI TFs and transcriptionally activated by ABRE binding. For example, ABF2/AREB1 binds to ABREs in the promoter region of numerous genes including *RESPONSIVE TO DESICCATION 29B* (*RD29B*), *RAB18*, *RD20,* and *G-BOX BINDING FACTOR 3* (*GBF3*) (Fujita et al., 2005). ABF4/AREB2 also binds many promoter regions including that of *RD29B* to regulate transcriptional activation in response to ABA (Chinnusamy et al., 2005). The function of ABREs appears conserved across species (Nicolas et al., 2014; Pilati et al., 2017), but identification of ABREs in promoter regions is incomplete for many species including grapevine. Grapevine ABREs were identified

along with other cis-acting elements in a previous annotation version of the PN40024 genome (Wong et al., 2017). However, ABREs were not the focus of this work. Limited ABRE sequences were queried, and no distinction between ABRE variants was made. This work was expanded upon by utilizing the new annotation version of the PN40024 reference genome that yielded novel ABRE coordinates by querying more ABRE sequences and distinguishing ABRE variants in longer promoter regions.

Although many genes have been identified as ABA-responsive in grapevine (Cochetel et al., 2020; Cramer et al., 2014; Londo et al., 2018; Rattanakon et al., 2016), the precise activation mechanism for many genes has not been defined. Identification of ABREs in grapevine promoter regions is the next step for better understanding ABA-responsive genes and will provide insight into ABA signaling and abiotic stress response. Two ABA-responsive genes (*ERF6L1* and *NCED3*) may be valuable targets for abiotic stress tolerance improvement in grapevine breeding programs, but the activation of these genes in response to ABA requires further investigation. Identification of ABREs in the promoter regions of these genes would explain previously observed responsiveness to ABA and abiotic stresses as well as provide the basis to identify TFs targeting these genes in the future. Identification of specific ABRE sequences and future identification of TFs that target these cis-acting elements will improve the comprehensive understanding of ABA signaling.

Previously, *ERF6L1* was identified as a potential ABA-responsive hub gene in grapevine berry skin during ripening (Cramer et al., 2014). Additional analysis revealed *ERF6L1* along with 17 paralogs in PN40024 were differentially expressed in response to numerous ABA related processes including salt, cold, pathogen, and light intensity

responses in a variety of organs and tissues (Toups et al., 2020), but this gene and its paralogs required further characterization for a role in ABA response. Other studies showed *NCED3* may function as a water deficit response hub (Cochetel et al., 2020; Lamarque et al., 2019; Sussmilch et al., 2017), and *NCED3* transcripts are known to accumulate in response to abiotic stresses including water deficit (Cochetel et al., 2020).

Promoter architecture is a powerful tool to infer gene function (Higashi and Saito, 2013), and identification of genes with ABRE-containing promoter regions may prove valuable in breeding programs to improve crop abiotic stress response and tolerance. Cis-acting elements were previously identified in an earlier version of the PN40024 genome, but since then, with the release of the new annotation (Canaguier et al., 2017), additional ABREs may be identified. The previous work only considered the first 1,000 bp before the TSS and queried 39 ABRE sequences. In this work, promoter regions were extracted from each gene of the PN40024 V3 structural annotation of the V2 assembly Pinot Noir grapevine reference genome (Canaguier et al., 2017). Promoter regions are defined as -3000 base pairs (bp) from the transcription start site (TSS) (prior to the beginning of 5' UTR or start codon when no 5' UTR was annotated), and 51 ABRE sequences obtained from PLACE (Higo et al., 1999) and AGRIS (Davuluri et al., 2003; Palaniswamy et al., 2006) (Table 1) were queried in the PN40024 promoter regions. **The goal of this work was to quantify and substantiate the abundance of ABREs in the PN40024 grapevine reference genome and to use the presence of ABREs to further validate and explain ABA-responsive genes including potential hub genes *ERF6L1* and *NCED3* as well as identify novel potential ABA-responsive genes for future studies.**

2.2 Materials and Methods

PN40024 ABRE Identification

ABRE sequences were obtained from AGRIS (Davuluri et al., 2003; Palaniswamy et al., 2006) and PLACE (Higo et al., 1999) and confirmed in literature (Busk and Pages, 1998; Choi et al., 2000) in 2019. Consensus ABREs containing ambiguity codes were decoded using nomenclature from the Nomenclature Committee of the International Union of Biochemistry (Cornish-Bowden, 1985). ABRE sequences were compared to prevent repetitive inquiries for the same sequence with different names. So-named ABRE-likebindingsitemotif_2 (**C**ACGTG**GC**) and ABRE-likebindingsitemotif_10 (**T**ACGTG**GC**) overlapped in entirety with ABREATCONSENSUS_1 and ABREATCONSENSUS_2, respectively, and were excluded from the analysis to prevent repetitive ABREs. ABRE-likebindingsitemotif_12 was also a duplicate sequence and excluded. In total, 51 unique ABREs were used in this study.

Promoter regions of -3,000 bp were extracted from each gene of the PN40024 V3 structural annotation of the V2 assembly grapevine reference genome (Canaguier et al., 2017) using the complete genomic sequence and annotated gene files. Promoter regions used for ABRE identification were confirmed not to overlap with chromosome ends or neighboring genes using GenomicFeatures version 1.38.2 in R (Lawrence et al., 2013). Based on these limitations, not all promoter regions were -3,000 bp, but these regions were considered as complete proximal promoters of these genes. Promoter regions were

extracted upstream from the TSS and were confirmed not to include 5' UTRs of downstream genes nor 3' UTRs of upstream genes. If a 5' UTR was not annotated for a gene, the promoter region was extracted just before the start codon (translation start site).

The 51 ABRE sequences (Table 1) were queried in the 41,416 promoter regions of the PN40024 V2 assembly V3 structural annotation using GenomicFeatures version 1.38.2 in R (Lawrence et al., 2013). Completely overlapping ABREs (i.e., a shorter ABRE inside a longer ABRE) were identified and only the longest (highest ranking) ABRE was retained using GenomicFeatures in R (Lawrence et al., 2013). Partially overlapping ABREs (e.g., ABREs that overlapped in the middle but not at either end) were both retained and counted separately. ABREs were identified on both DNA strands. The start, end, strand, and identity of each ABRE in the promoter region of each gene were identified. The total number of occurrences of each ABRE was calculated (Table 2), and the total number of genes each ABRE was present in was also calculated (Table 2). All subsequent analyses were performed using this information.

RNA-Seq analysis

RNA-Seq analysis was performed on the PRJNA516950 (Cochetel et al., 2020) data series using the PN40024 V3 structural annotation of the V2 assembly grapevine reference genome (Canaguier et al., 2017), which was performed previously (Toups et al., 2020). Briefly, the data series was quality checked with fastqc (Babraham Bioinformatics, 2010) and trimmed with trimmomatic version 0.35 (Bolger et al., 2014). Transcript abundance was quantified with Salmon version 0.10.1 (Patro et al., 2017) using quasi-mapping, seqBias, gcBias, fldMean 50, fldSD 1, validateMappings, libType A, and

rageFactorizationBins 4. Tximport version 1.10.1 was used to generate the count matrix. Differential expression analysis was performed with DESeq2 version 1.22.2 (Love et al., 2014).

Statistical Analysis

One-way ANOVA and Tukey's HSD were performed to determine the relationship between ABRE occurrences and ABRE length (Fig. 2) after assumptions were met. Chi-squared Goodness of Fit Test assuming equal distribution was performed on the variants of the six consensus ABREs containing ambiguity codes individually (Fig. 3), ABRE sense and anti-sense strand distribution, and ABRE start position after assumptions were met. Non-normal data were box-cox transformed to meet normality and homoscedastic assumptions (Fox, 2020). Post Hoc tests were performed with Tukey's Test HSD for comparisons between species, treatments, and time points after assumptions were met. Asterisks indicate statistical significance from ANOVA (* = $p \leq 0.05$, ** = $p \leq 0.01$, *** = $p \leq 0.001$). Letters indicate statistical significance between the multiple comparisons. The error rate $\alpha = 0.05$ was used in all comparisons. Statistical analyses and all other R-based analyses were performed using R version 3.6.3 in RStudio version 1.2.13335 (R Core Team, 2018).

2.3 Results

ABRELATERD1 was a core ABRE

A total of 26 consensus ABREs were identified. Six of the consensus ABREs contained ambiguity codes (indicated in bold and underlined), yielding a total of 51 ABREs including 25 variant sequences, referred to as "variants" throughout this work (Table 1). The sequences (5-16 bp in length) of the ABREs were compared. The majority (33 of the ABREs) contained an ABRELATRD1 (ACGTG) core motif, while the remaining 17 ABREs did not include the entire sequence of any other ABRE (Fig. 1 and Table 1). The 33 ABREs containing the core motif were classified as primary, secondary, tertiary, and quaternary ABREs based on the sequence presence of shorter ABREs in sequentially longer ABREs (Table 1 and Fig. 1). For example, the ABRELATRD1 core (ACGTG) was present in the primary ABRE, ACGTABREMOTIFA2OSEM_1 (ACGTG**G**C), which was present in the secondary ABRE, ABREATCONSENSUS_2 (**T**ACGTGGC) that was present in three tertiary ABREs including ABREA2HVA1 (CCTACGTGGC), and ABREA2HVA1 was present in the only quaternary ABRE, ABRE2HVA1 (CCTACGTGGCGG) (Fig. 1). A total of 15, 9, 8, and 1 primary, secondary, tertiary, and quaternary ABRE variants were identified (Fig. 1). All 51 ABREs were queried in the PN40024 promoters.

ABREs were highly abundant in PN40024 promoter regions

A total of 93,852 ABRE occurrences were identified in the PN40024 promoter regions (Table 2). Almost all of the 51 ABREs were found in PN40024 promoter regions, except for the longest motif, CGTGTSPHZMC1 (CGTGTCGTCCATGCAT), which was not present in these PN40024 promoter regions (Table 2). ABRE occurrences were attributed to the longest possible ABRE (i.e. the highest-ranking ABRE class (Fig. 1 and Table 1)).

Therefore, although tens of thousands of promoters contained the ABRELATERD1 core, the promoter sequences that corresponded to higher ranking primary, secondary, tertiary, or quaternary ABREs were allocated thusly and not counted as a lower rank ABRE. After the ABRELATERD1 core, ABRERATCAL (**M**ACG**Y**G**B**) was the most abundant consensus ABRE, being present 32,016 times in the PN40024 promoter regions followed by ABRE-likebindingsitemotif (**B**ACGTG**KM**) and ACGTABREMOTIFA2OSEM (ACGTG**K**C) with 14,644 and 3,587 occurrences, respectively (Table 2). Numerous other consensus ABREs occurred hundreds and thousands of times in the PN40024 promoter regions (Table 2). Shorter ABRE variants had significantly ("significantly" meaning ≤ 0.05 unless otherwise specified throughout this work) more occurrences in the PN40024 promoter regions than longer ABRE variants (Fig. 2). For example, ABRELATERD1, the shortest ABRE, was the most abundant ABRE. ABRERATCAL and ABREOSRAB21 with a length of 7 and 8 bp, respectively, were significantly more abundant than ABREs with a length of ≥ 10 bp like and ABREATRD22 and ABRETAEM (Fig. 2). There was no significant difference in the number of occurrences of ABREs with a sequence length ≥ 9 bp (Fig. 2).

Specific ABRE variants were more abundant in PN40024 promoter regions

Of the 26 consensus ABREs, six contained ambiguity codes that gave rise to multiple ABRE variants. The abundance of the different variants for each of the six consensus ABREs were compared. ABRERATCAL variants are shown as an example (Fig. 3), but the numbers of occurrences of each variant for each consensus sequence can be found in Supplemental File 1. ABRERATCAL had 12 ABRE variant sequences. Of the 12

ABRERATCAL variants, ABRERATCAL_8 (**A**ACG**T**G**T**) had the highest number of occurrences in the PN40024 promoter regions, followed by ABRERATCAL_5 (**C**ACG**T**G**C**) and ABRERATCAL_7 (**A**ACG**G**G**T**) with 5,224; 4,357; and 4,001 occurrences, respectively (Fig. 3). Even ABRERATCAL_3 (**A**ACG**C**G**C**), the ABRERATCAL variant with the lowest abundance, had over 800 occurrences and was more prevalent than 16 of the consensus ABREs (Fig. 3 and Table 2).

Other consensus ABREs with sequence variations also had different numbers of occurrences for variant sequences. For example, ABREOSRAB21_2 (ACGT**GGG**C) was 2.4-fold more abundant than ABREOSRAB21_1 (ACGT**CCC**C) (Supplemental File 1). ABREATCONSENSUS_1 (**C**ACGTGGC) had 3.3-fold more abundance in PN40024 promoters than ABREATCONSENSUS_2 (**T**ACGTGGC) (Supplemental File 1). ABRE-likebindingsitemotif_4 (**C**ACGTG**TC**) ranged from ~1.4 – 5-fold higher occurrences than the other ABRE-likebindingsitemotif variants (Supplemental File 1). ABREATRD22 variants had the greatest difference between variant occurrences (Supplemental File 1). ABREATRD22_2 (**AC**ACGTGG**CA**) had ~17-fold more occurrences in PN40024 than the other three ABREATRD22 variants (Supplemental File 1). ACGTABREMOTIFA2OSEM variants had more similar abundance in PN40024 promoter regions (1,057 for ACGTABREMOTIFA2OSEM_1 vs. 1,026 for ACGTABREMOTIFA2OSEM_2) occurrences (Supplemental File 1). However, the observed proportions of the variants of each of these consensus ABREs were significantly not proportionally distributed, indicating some variants were more or less prevalent than others for the same consensus ABRE.

ABREs occurred abundantly -50 to -100 bp from the TSS

ABREs averaged 4,692.6 ± 299.21 (mean ± SE) occurrences per chromosome (Fig. 4). However, chromosome 18 contained the highest number of ABREs (7,952 ABREs) followed by chromosome 7 and chromosome 8 (6,806 and 5,677 ABREs, respectively) (Fig. 4 and Supplemental File 1). ABREs were significantly equally distributed on the positive (+) (46,718 occurrences) and minus (-) DNA strands (47,134 occurrences) (Supplemental File 1), and occurrences were counted regardless of the coding strand of the downstream gene. Interestingly, many of the ABREs on the positive strand (36.7%) had a partner-ABRE on the minus strand with starting coordinates within ±2 bp of the starting coordinates of the ABRE on the positive DNA strand (Supplemental File 1). Of these partner-ABREs, ~9% shared the exact starting coordinates on the + and – strands, and ~13% had starting coordinates 1 bp to the right on the minus strand relative to the starting coordinates on the + strand (Supplemental File 1). Another ~12% had starting coordinates 2 bp to the right on the minus strand relative to the starting coordinates on the + strand, and only ~2% had starting coordinates 1 bp to the left on the minus strand relative to the starting coordinates on the + strand (Supplemental File 1). More ABREs had partners on opposite strands with increased bp staggering (e.g. ± 3 bp). Of the 17,127 ABREs on the positive DNA strand that were partially overlapped by an ABRE on the negative DNA strand within 2 bps, only 4,917 were partially overlapped by the same ABRE on both strands (Supplemental File 1). All other instances of strand overlap were between two different ABREs. The ABRE partner combinations varied per shifted position (Supplemental File 1).

Additionally, per strand, some ABREs were staggered by a single base pair and partially overlapping (Supplemental File 1) (e.g. two ABREs sharing partially overlapping coordinates on the same DNA strand). For example, the promoter region of an uncharacterized gene (Vitvi08g00915) had an ABREZMRAB28 (CCACGTGG) begin at -62 bp from the TSS and an ABRE-likebindingsitemotif_1 (CACGTGGA) starting at -63 bp, both on the negative DNA strand (Supplemental File 1). The positive strand of this promoter region similarly had an ABREATCONSENSUS_1 (CACGTGGC) starting at -61 bp from the TSS and an ABREZMRAB28 (CCACGTGG) starting at -62 bp from the TSS (Supplemental File 1). This example demonstrated the partial overlapping of ABREs on the same DNA strand (e.g. ABREZMRAB28 and ABRE-likebindingsitemotif_1) as well as the staggering of ABREs on the positive and negative strands (e.g. ABREZMRAB28 and ABREATCONSENSUS_1).

ABREs started at every possible position in the -3,000 bp promoter regions (Supplemental File 1), but ABREs were significantly not proportionally distributed to each possible position. The -50 to -100 bp from the TSS range had the greatest number of ABRE occurrences (Fig. 5). The distribution of all ABREs from -1,000 to -3,000 bp from the TSS remained fairly constant and did not drop off with increasing distance from TSS until the last window from -2,775 to -3,000 bp. Although each ABRE demonstrated a similar distribution of occurrences to total ABREs farther from the TSS, the peak within the first hundred bps was not always present (Fig. 5). For example, neither ABRERATCAL_7 nor ABRE-bindingsitemotif_11 had a distinct increase in the number of occurrences within the first hundred bps (Fig. 5). However, the majority of individual ABREs did follow the same

distribution as total ABREs with a peak of ABRE occurrences in the first hundred bps and lower but comparable numbers of ABREs throughout the remainder of the promoter region.

The majority of PN40024 promoters contained at least one ABRE

Of the 41,416 annotated genes in the PN40024 reference genome, 30,085 gene promoter regions contained at least one ABRE (Fig. 6). A list of all genes containing ABREs, ABRE coordinates, and strand information, summarized total ABREs per gene, and summarized individual ABREs and variant occurrences per gene are in Supplemental File 1. Of the 30,085 promoter regions that contained ABRE(s), 29.8% contained a single ABRE, and 23.0% and 15.7% contain two and three ABREs, respectively (Fig. 7). Fewer and fewer promoter regions contained increasing numbers of ABREs (Fig. 7). After the ABRELATERD1 core, ABRERATCAL was the most predominant consensus ABRE being present at least one time in 18,816 promoter regions followed by ABRE-likebindingsitemotif and ABREATCONSENSUS present in 10,035 and 2,882 individual promoter regions respectively (Table 2).

The number of promoter regions each of the consensus ABREs was present in yielded similar results to the number of total consensus ABRE occurrences in the PN40024 promoter regions (Table 2). Overwhelmingly, the majority of ABRE-containing promoter regions contained a single ABRE, and those that contained multiple ABREs predominantly contained a single copy of each (Table 2 and Supplemental File 1). However, four consensus ABREs were significantly more repeated per promoter region than others (Fig. 8). ABREZMRAB28 had the significantly highest average number of repeats per PN40024 promoter region that this cis-acting element was present in (Fig. 8). ABRE-

likebindingsitemotif followed by ABRELATERD1 and then ABRERATCAL also had significantly a sequentially higher average number of repeated occurrences per PN40024 promoter region in which these cis-acting elements occurred (Fig. 8). The remaining 20 consensus ABREs did not have significantly different numbers of repeats per promoter region in which each consensus ABRE occurred (Fig. 8).

Although the average number of repeats for each consensus ABRE was low (due to the large number of promoter regions that contained a single occurrence), the number of repeated ABREs per PN40024 promoter region ranged from 1 to 33 (Supplemental File 1). The promoter regions of an uncharacterized gene (Vitvi11g01561) contained 33 ABRERATCAL repetitions, the highest number of any of the consensus ABREs for any of the 30,085 ABRE containing promoter regions. ABRERATCAL was also the second most repeated consensus ABRE, with 22 repetitions in the promoter regions of two uncharacterized genes (Vitivi05g02283 and Vitvi11g01562). Interestingly, ABRE3OSRAB16 occurred only a single time in the promoter region of another uncharacterized gene (Vitvi12g00446). ABRE2HVA1 and ABRECE3HVA1 were also rare ABREs, occurring once in *RING AND DOMAIN OF UNKNOWN FUNCTION 2* (*RDUF2;* Vitvi06g00502), *EMBRYO DEFECTIVE 1075* (*EMB1075*; Vitvi18g01299), and uncharacterized gene (Vitvi03g00579, Vitvi11g00613, and Vitvi11g01295) promoter regions, respectively.

Certain variants of consensus ABREs had significantly more occurrences in PN40024 promoter regions than others (Fig. 9 and Supplemental File 1). For example, ABRERATCAL_9 had significantly higher numbers of repeats per promoter region than any other ABRERATCAL variant (Fig. 9). ABRERATCAL_5, 6, 11, and 12 also had

significantly higher repeats per PN40024 promoter region than the seven remaining variants, but these four variants still had significantly lower repeats per promoter region on average than ABRERATCAL_9 (Fig. 9). Like ABRERATCAL, ABRE-likebindingsitemotif variants had significantly different numbers of repeats per promoter region that these cis-acting elements were present in. ABRE-likbindingsitemotif_4 had significantly more repeats per promoter region than any other ABRE-likebindingsitemotif variant followed by ABRE-likebindingsitemotif_1 (Supplemental File 1). ABREATCONSENSUS_1 also had significantly more repeats per promoter region than ABREATCONSENSUS_2. There was no significant difference between the number of repeats per promoter region for variants of ABREATRD22, ABREOSRAB21, and ACGTABREMOTIFA2OSEM individually (Supplemental File 1).

Promoter regions of known PN40024 ABA metabolism genes contained ABRE(s)

Numerous known ABA metabolism-related gene promoter regions contained at least one ABRE including those of *NCEDs* (Fig. 10), *CYP707As*, *BGs*, and *UGTs* (Supplemental File 1). Interestingly, not all ABA metabolism-related gene (Table 1) promoter regions contained a shared ABRE. However, ABRELATERD1 was in 17 of 31 ABA metabolism gene promoter regions involved in ABA biosynthesis, (de)conjugation, or catabolism considered here. *NCED* promoter regions were chosen as example ABA metabolism promoters to focus upon in this work because of the importance of *NCEDs* in ABA biosynthesis and because *NCED3* was identified as a potential water deficit hub gene in previous work (Cochetel et al., 2020). The *NCED6* promoter region had the most ABREs (13) followed by that of *NCED3* (9) and finally the promoter region of *NCED5* (7) (Fig.

10 and Supplemental File 1). ABRELATERD1 and ABRE-likebindingsitemotif_4 were the only ABREs present in all three N*CEDs* at least once (Fig. 10 and Supplemental File 1). Both *NCED3* and *NCED5* promoter regions contained all ABREs within the first ~1,500 bps, while the *NCED6* promoter region ABREs were extended past -2,500 bp (Fig. 10 and Supplemental File 1). Only the *NCED3* promoter region contained ABREs (ABRERATCAL_11 and ABREATCONSENSUS_1) within the -50 to -100 bp range (Fig. 10 and Supplemental File 1).

Promoter regions of PN40024 ABA-responsive genes contained ABRE(s)

Numerous known ABA signaling gene promoter regions contained at least one ABRE including those of *PP2Cs*, *SNRK2s*, *ABF/AREBs*, and *ABIs* (Supplemental File 1). The three PN40024 promoter regions with the most ABREs and functional annotations (*COP INTERACTING PROTEIN 8* (*CIP8*), *GBF3*, and *DICER-LIKE 3* (*DCL3*)) were chosen as an example to show here (Fig. 11). The top three annotated gene promoter regions containing the most ABREs all contained at least one ABREZRAB28, ABRELATERD1, ABRE-likbdingsitemotif_4, and ABRERATCAL_11. All three promoter regions had ABREs spread throughout the -3,000 bp promoter region, but the majority of *DCL3* ABREs were grouped from -700 to -1,600 bp (Fig. 11 and Supplemental File 1). Additionally, *DCL3* did not have an ABRE in the -50 to -100 bp range (Fig. 11 and Supplemental File 1). *CIP8* had one ABRE in the -50 to -100 bp range while *GBF3* had three ABREs in this range (Fig. 11 and Supplemental File 1). Nearly 40% of the ABREs of *GBF3* spanned a 200 bp region from -1,800 to -2,000 bp from the TSS, but this peak was not shared by *DCL3* (with the majority of ABREs spanning -700 to -1,700 bp) nor

CIP8 (did not demonstrate a specific grouping of ABREs) (Fig. 11 and Supplemental File 1).

The promoter region of the previously identified potential ABA-responsive hub gene, *ERF6L1*, also contained a few ABREs (Fig. 12 and Supplemental File 1). Of the 18 *ERF6Ls* in the PN40024 genome, 11 corresponding promoter regions contained ABREs. *ERF6L3*, *9*, *10*, *11*, *13*, *16*, and *18* promoter regions did not contain an ABRE. Although the *ERF6Ls* have highly similar gene sequences, the type, number, and coordinates of ABREs in *ERF6L* promoter regions were more diverse (Fig. 12 and Supplemental File 1). For example, the *ERF6L15* promoter region had the highest abundance of ABREs (6), while both ERF6L5 and ERF6L17 contained only a single ABRE, which were ABRE-likebindingsitemotif_11 and ABRERATCAL_8, respectively (Fig. 12 and Supplemental File 1). However, some of the *ERF6Ls* shared similar ABREs in promoter regions. For example, *ERF6L8* and *ERF6L14* both contained ABREATCONSENSUS_1, ABREATCONSENSUS_2, and ABRERATCAL_5 in the same order on the same strands, but the ABREs were shifted slightly closer to the TSS in the *ERF6L14* promoter region (Fig. 12 and Supplemental File 1). Interestingly, the only ABRE in *ERF6L15* was ABRELATERD1, and this ABRE was shifted by a single bp for all three occurrences on the positive DNA strand relative to the three occurrences on the negative strand (Supplemental File 1). Only *ERF6L1* and *ERF6L14* promoter regions contained ABREs in the -50 to -100 bp range (Fig. 12 and Supplemental File 1).

In addition to known ABA-responsive genes, numerous uncharacterized genes also had higher numbers of ABREs in promoter regions. 10 out of the top 25 promoter regions with the highest number of ABREs correspond to unannotated genes. The two genes

(Vitvi11g01561 and Vitvi05g02283) that had the highest number of ABREs (35) in respective promoter regions are functionally unannotated (Supplemental File 1).

Genes corresponding to ABRE-containing promoter regions were DEGs in response to water deficit.

The genes of ABRE-containing promoter regions were significantly differentially expressed in response to a moderate water deficit (WD) treatment. Previously, a moderate natural dry-down WD or daily irrigation Control treatment was performed on four *Vitis* species (*Vitis vinifera* cv. Cabernet Sauvignon (CS), *Vitis champinii* cv. Ramsey (RA), *Vitis riparia* cv. Riparia Gloire (RI), and *Vitis vinifera* x *Vitis girdiana* hybrid SC2 (SC)) for one- (W1) and two-weeks (W2). After W2 of treatment, leaves and roots were harvested and used for RNA-Seq, which was previously described (Cochetel et al., 2020). RNA-Seq analysis was performed previously based on the PN40024 V3 structural annotation of the V2 assembly grapevine reference genome (Toups et al., 2020). Of the 30,085 gene promoter regions containing at least one ABRE, 12,450 were also differentially expressed genes (DEGs) in response to two weeks WD in the leaves and/or the roots of at least one *Vitis* species. As was previously described numerous ABA metabolism and signaling genes were differentially expressed after W2 of water deficit treatment relative to Control treatment, including *CIP8*, *GBF3*, *NCED3*, and *ERF6L1* (Fig. 13). *CIP8* was only a DEG in RA leaves after W2 WD, relative to RA Control leaves (Fig. 13). *GBF3* was a DEG in response to W2 WD for CS and RA leaves and roots, RI leaves, and SC leaves (Fig. 13). Surprisingly, *DCL3*, the gene with the third most ABREs in the corresponding promoter region was not a DEG in any species or organ in response to 2W WD (Fig. 13). However,

ERF6L1 was a DEG (in CS roots and RA leaves) in response to 2W WD. Finally, *NCED3* was a DEG in the leaves and roots of all four species in response to 2W WD.

The log_2-fold change in transcript abundance in response to a two-week moderate water deficit treatment was compared to the number of ABREs in DEGs responding to WD. This comparison was performed to determine if there was a relationship between the number of ABREs in promoter regions and the change in gene expression from ABA signaling in response to water deficit (data not shown). There was not a linear relationship between the level of differential expression of a WD responsive DEG and the number of ABREs in the promoter region of that DEG.

2.4 Discussion

The results presented here are dependent upon the parameters employed

In this study, ABREs were identified in PN40024 promoter regions. ABREs were ranked as core, primary, secondary, tertiary, or quaternary ABREs based on the inclusivity of shorter motifs present in longer motif sequences (Table 1 and Fig. 1). ABRELATERD1 was identified as the core ABRE, but ABRELATERD1 was not present in all ABRE sequences (Fig. 1). ABRE sequence and function appear conserved across many plant species. ABREs of *Arabidopsis thaliana*, *Zea maize*, and *Oryza sativa* (from which the 51 ABREs queried in this study were derived) (Table 1 and Fig. 1) matched sequences in grapevine promoter regions (Table 2). Binding of ABREs by ABF/AREB TFs has previously been confirmed in grapevine (Nicolas et al., 2014; Pilati et al., 2017). Linking

the presence of ABREs in PN40024 promoter regions to water deficit-sourced ABA-induced gene expression in different grapevine cultivars as was performed here (Fig. 13) has also been performed on a smaller scale previously (Nicolas et al., 2014; Pilati et al., 2017), and like the results presented here (Fig. 13), authors found genes with ABRE-containing promoter regions were induced by ABA (Nicolas et al., 2014; Pilati et al., 2017).

Cis-acting elements were identified in a previous version of the PN40024 genome (Wong et al., 2017). The work here improved the previous analysis by employing a new version of the PN40024 reference grapevine genome (annotation V3 vs. V2), including longer promoter regions (-3,000 bp vs. -1,000 bp) and more ABRE sequences (51 vs. 39). In the previous study, 22,439 ABRE occurrences were identified in 9,997 promoter regions. In this study, there were 93,852 occurrences of ABREs in 30,085 PN40024 promoter regions (Fig. 6). This study more than quadrupled known ABRE occurrences and tripled the number of annotated genes with ABRE containing promoter regions in the PN40024 genome relative to the previous analysis. This difference was attributed to the longer promoter region and a more extensive list of ABREs queried in this analysis. A comparison of ABRE sequences queried and ABRE coordinates identified in this and the previous study is available upon request. This comparison does not include other cis-acting elements identified in the previous promoter region analysis.

Over 30,000 ABRE occurrences in the PN40024 promoter regions corresponded to the core ABRE and ABRELATERD1, (Table 2) indicating these ABRE occurrences did not coincide with any longer known ABRE sequences (primary – quaternary). These core ABRE occurrences may truly only contain the ABRE core motif or some may correspond to longer grapevine-specific or yet unidentified ABREs. Of the 51 ABREs queried here,

CGTGTSPHZMC1 (Kao et al., 1996) was the only ABRE not present in any PN40024 promoter region. The lack of CGTGTSPHZMC1 may be attributed to the fact that it had the longest sequence (16 bps). Shorter ABREs (5 – 8 bps) had significantly higher numbers of occurrences in PN40024 promoter regions than long ABREs (9 – 12 bps) (Fig. 2). However, identifying longer ABREs may provide better clues about the roles of individual ABREs and the effects of ambiguity codes. It is possible different TFs (or even different TF isoforms) have higher affinity for certain ABREs. Alternatively, individual ABREs or even variants of the same consensus ABRE may have different availability or activity under specific conditions. This hypothesis was supported by the different numbers of occurrences of variants of the same consensus ABRE observed here (Fig. 3). For example, ABRERATCAL_8 had 6.5-fold more occurrences than ABRERATCAL_3 (Fig. 3). Five of the six ABREs with variant sequences had different abundances (Supplemental File 1) and numbers of repeats per promoter region (Fig. 9 and Supplemental File 1) between variants, and the reason for the differences in ABRE variant abundances and functions requires resolution.

ABREs were not significantly equally distributed across all chromosomes (Fig. 4). Chromosome 18 had at least 1,000 more ABREs than any other chromosome (Fig. 4). Interestingly, chromosome 18 contains numerous ABA signaling genes including *ABF2* (Vitvi18g00784), *ARABIDOPSIS NAC DOMAIN CONTAINING PROTEIN* (*ATAF1*) (Vitvi18g00250), and *HIGHLY INDUCED BY ABA 1* (*HAI1*) (Vitivi18g02005). The high number of ABREs and the presence of ABA signaling genes may indicate there are ABA response loci located on this chromosome. The existence of such a locus would be a powerful tool for breeding programs aiming to improve abiotic stress tolerance.

Identification of promoter regions was dependent on knowledge of TSS, gene borders, and 5' UTR and 3'UTR lengths. Alternative 5' and 3' UTRs, multiple TSS, single nucleotide polymorphisms, and backward ABRE sequences were not considered in this analysis. The longest gene annotations were used to define the -3,000 bp promoter region, and these promoter regions were queried for exact matching ABRE sequences. Improved annotation or use of transcript isoforms of the PN40024 genome may change the results presented here. Validation of promoter regions was performed previously based on A:C:G:T content (Wong et al., 2017) and confirmed here for select promoters with EST data in GenomeViewer (Sterck et al., 2012). The selection of a -3,000 bp promoter region was based on previous work (Geisler et al., 2006; Timmerhaus et al., 2011; Yang et al., 2011) and justified here wherein ABRE occurrences remained at a constant level after the peak from -50 to -100 bp from the TSS and decreased for all ABREs in the last window of -2,775 to -3,000 bp (Fig. 5). Some promoter regions extend tens of thousands of bp upstream from the TSS (Griffiths et al., 2000), and DNA looping may allow non-sequential or distant regulatory elements to effect transcription proximal to a gene (Stadhouders et al., 2012). Including longer or complete promoter regions would likely increase the number of ABRE occurrences, but it would be difficult to predict the relevance and activity of highly distant ABREs (FitzGerald et al., 2004; Maruyama et al., 2012; Yamamoto et al., 2007).

Recently, additional grapevine genomes have been released (Chin et al., 2016; Girollet et al., 2019; Massonnet et al., 2019; Minio et al., 2019a). However, there is a large consortium for annotating the PN40024 grapevine reference genome (Sterck et al., 2012) that does not exist for any other grapevine genome at this time. Although the newer grapevine genomes have a higher sequencing and assembly quality than the PN40024

genome, the annotation of these diploid phased genomes is far from complete, making PN40024 the preferable reference genome for this analysis. Only ABREs were considered in this study, and other cis-acting elements involved in ABA signaling and stress response like DREs still need identification in the new PN40024 reference genome annotation and other grapevine genomes.

The G-box was a cis-acting element not investigated in this work. The G-box is a binding site for bZIP and bHLH TFs previously found in the promoter region of genes involved in abiotic and biotic stress (Wong et al., 2017). The G-box sequence (CACGTG) is highly similar to those of several ABREs, and the G-box was present in entirety in 13 of the 51 ABREs. The G-box was not specifically included in this study, but any occurrences are included in ABRELATERD1 (ACGTG) occurrences.

In the future, as the annotation of grapevine genomes improves, it will be interesting to compare promoter regions between species and relate the structure and composition of promoter regions to differences in gene expression. For example, comparing the promoter regions of key ABA response genes between different species (e.g. a drought-tolerant (RA) and drought-sensitive (RI) cultivars) may elucidate promoter composition as a key regulatory mechanism for abiotic stress response or drought tolerance. Keeping this in mind, the transcript abundances (Fig. 13) used to demonstrate the genes of ABRE-containing promoter regions are ABA-responsive (in this case as a result of WD) are imperfect because none of the species investigated in this experiment were PN40024. This limitation is exemplified with *CIP8,* which was only a DEG in RA leaves after W2 WD, relative to RA Control leaves (Fig. 13). It is possible the promoter region for *CIP8* in RA is different from that of PN40024, CS, RI, and SC, and the specific composition of the RA

CIP8 promoter region allows for significant differential expression of this gene in response to these WD conditions. Alternatively, one of the many other mechanisms regulating transcription (Chapter 1) may have been responsible for this discrepancy.

ABRE sequences appear highly functionally conserved across plant species (Maruyama et al., 2012), but there is also diversity in ABRE location and abundance per gene per species (Gómez-Porras et al., 2007). Comparing different species to a single reference genome is commonplace, and PN40024 is widely used as a reference genome (Minio et al., 2019b; Pilati et al., 2017; Pucker et al., 2020). The ABREs present in this reference genome (Supplemental File 1) is reflected in the ABA responsiveness of genes of at least some other grapevine species (Fig. 13).

Because the Riparia genome is available and overlaps with a species in the moderate water deficit experiment discussed here, the ABREs in the RI *NCED3* promoter region were identified as an example to compare ABRE distribution across *Vitis* species. The RI *NCED3* promoter region had more than double the ABREs in the PN40024 *NCED3* promoter region (20 vs. 9). ABRELATERD1 was the most abundant ABRE in the RI *NCED3* promoter region repeated seven times, followed by ABRERATCAL_11 with three occurrences. Interestingly, all ABREs in the PN40024 *NCED3* promoter region were also present in the RI *NCED3* promoter region, although most of the ABREs in the RI *NCED3* promoter were repeated more than the counterparts in the PN40024 *NCED3* promoter region. The RI *NCED3* promoter region also had ACGTABREMOTIFA2OSEM_1 and ACGTABREMOTIFA2OSEM_2 ABREs, which were not present in the PN40024 promoter region. This example demonstrates that different *Vitis* species have different ABRE distribution in the promoter regions of ABA-responsiveness, and this difference

may partially contribute to the different transcript abundances observed between the species in the moderate water deficit experiment. Gene expression is regulated by numerous factors (Banerjee and Roychoudhury, 2017a; Cruz et al., 2019; Jung et al., 2016; Li et al., 2005), and cis-acting elements are just one point of regulation.

It may be possible to identify additional cis-acting elements involved in ABA metabolism and signaling by performing motif enrichment (Bailey et al., 2009) using these ABRE-containing promoter regions as a query. Of course, with the identification of ABREs comes the necessity to determine the TF(s) that target these sequences. Numerous techniques exist to identify DNA-protein interactions like DNase footprinting (Zhang et al., 2012), electromobility shift assay (Nicolas et al., 2014), yeast one-hybrid (Deplancke et al., 2004), and CHIP-Seq (Cortijo et al., 2018; He et al., 2015), but few studies have identified ABRE-TF interactions in grapevine (Nicolas et al., 2014; Pilati et al., 2017). Different TFs likely bind different ABREs under different conditions or many TFs may compete for the same cis-acting element (Kribelbauer et al., 2019; Lebedeva et al., 2020; Sen et al., 2004), which may make DNA-protein interaction databases covering multiple stresses, developmental stages, and tissues necessary to have a more comprehensive understanding of the roles of ABREs and other cis-acting elements.

ABREs were present throughout -3,000 bp promoter regions

Like soybean, rice, Arabidopsis, and other species' cis-elements (FitzGerald et al., 2004; Maruyama et al., 2012; Yamamoto et al., 2007), PN40024 ABRE occurrences were most abundant between -50 and -100 bp from the TSS (Fig. 5). This observation is also

concurrent with findings for ABREs and other cis-elements in an earlier version of the PN40024 genome (Wong et al., 2017). Although many ABREs occur from -50 to -100 bp from the TSS (Fig. 5), ABREs occupied every possible start position in the -3,000 bp promoter regions when considering all 30,085 promoter regions that contained an ABRE(s). ABREs were also evenly spread between the positive and negative DNA strands. Most ABRE-containing promoter regions contained a single ABRE (Fig. 7), and the number of genes decreased with increasing numbers of ABREs in corresponding promoter regions. For example, fewer than 115 genes had 15 or more ABREs in corresponding promoter regions (Fig. 7). Although ABRELATERD1 had the highest number of occurrences, ABREZMRAB28 had significantly more repeats per promoter region than any other consensus ABRE (Fig. 8). However, there was no apparent pattern in the location of repeated ABREs across all relevant promoter regions. Both ABRE sequence and location likely play important roles in transcription regulation.

ABRE orientation, spatial distribution, and ambiguity points require further understanding

Cis-element orientation and strand specificity remain largely unstudied for ABREs, and the effects of orientation for other cis-acting elements appear to be relevant on a case-by-case basis. For example, the TATA-box (a core promoter element within 50 bp of the TSS (Deng and Roberts, 2005)) has strand-specific properties in Drosophila with the forward motif yielding transcription of the downstream gene via RNAPII and the reverse-complement motif resulting in transcription of the upstream gene by RNAPIII (Wang and Stumph, 1995). Hepatitis B virus promoter regions are orientation-specific (Moolla et al.,

2002). However, some human promoters like those of insulin receptors function regardless of motif orientation (Suwanickul et al., 1993). Similarly, anthocyanin pathway promoters in Arabidopsis and the common morning glory function with interchangeable cis-element orientation (Zhu et al., 2015). Currently, the consensus is cis-element orientation and strand are not considered as critical for transcription as the binding of TFs, and there is no pattern associated between cis-acting elements and transcriptional activity for all occurrences of a cis-acting element (Lis and Walther, 2016). However, the orientation (5' → 3' vs. 3' → 5') as well as the strand (+ vs. -) could have three-dimensional effects on TF binding that may, in turn, affect the recruitment of transcriptional machinery. It is possible the orientation, position, and sequence of ABREs play an important role in fine-tuning ABA signaling and metabolism in different organs, developmental stages, or in response to different concentrations of ABA, particularly when considering ABA-sensitivity gene promoter regions like those of *ELONGATED HYPOCOTYL 5* (*HY5*) (Chen and Xiong, 2008; Nawkar et al., 2017; Shin et al., 2013) and *ATAF1* (Garapati et al., 2015), which contained some of the highest numbers of ABREs (Supplemental File 1).

Here, 36% of ABREs on the positive strand had a partner ABRE on the minus strand starting within 2 bp of the start coordinates on the ABRE on the + strand. It is possible these ABREs that occur so close together on the positive or negative DNA strands have different functions, affinities for TFs, or are specific for different TFs. Alternatively, they may act cooperatively. One possible function for these partner-ABREs could be to provide alternative binding sites for different TFs that may function in different tissues, organs, developmental stages, or environmental conditions (Lebedeva et al., 2020).

Another possibility is the partner-ABREs function in balancing transcription via binding of transcriptional activators or repressors (Fujimoto et al.).

The staggering of multiple ABREs by 1 or 2 bps on the same DNA strand, such as was the case for Vitivi08g00915, may indicate the incomplete overlapping lower-ranking ABREs (like primary ABREs ABREZMRAB28 and ABRE-likebindingsitemotif_1 as was the case for Vitivi08g00915) can be combined into a higher ranking (secondary) novel ABRE. These potential novel ABREs would require validation *in vivo*. Alternatively, these partially overlapping ABREs may be specific for certain transcription factors in unique organs, developmental stages, or environmental conditions that require the same distance from the TSS.

ABA-responsive genes contain ABREs in promoter regions

Numerous ABA metabolism and signaling genes including *ABA1*, *ABA2*, *ATAF1*, and *SEUSS-LIKE 2* (*SLK2*) contained ABRE(s) (Supplemental File 1). However, not all ABA metabolism genes contained an ABRE like *AAO3* (Vitvi18g03177) and *BG3* (Vitvi14g00996). Because not all ABA metabolism gene promoter regions contained an ABRE, different aspects of ABA metabolism may not necessarily be ABA responsive. Alternatively, these genes may contain ABREs that have not been identified or respond to ABA at a different level of regulation.

ABA metabolism and signaling genes with ABRE-containing promoter regions were DEGs in response to WD (Figs. 10-13). The $\log_2$-fold change transcript abundance in response to W2 WD of individual genes with the same number of ABREs varied largely,

and it is more likely the position or composition of ABRE(s) that play a more important role in gene expression during WD.

The top ABRE containing promoter regions that corresponded to annotated genes belonged to *CIP8*, *GBF3*, and *DCL3* (Fig. 11 and Supplemental File 1). The expression of these genes may be highly dependent on ABA and could prove useful genes for breeding programs to alter ABA response to develop more stress-tolerant grapevines and crops. RNA-Seq performed on WD treated leaves and roots further corroborated *CIP8* and *GBF3* as ABA-responsive genes, because *CIP8* and *GBF3* were DEGs in response to WD (Fig. 13) (Cochetel et al., 2020; Toups et al., 2020), a highly ABA-dependent process (Daszkowska-Golec, 2016; Yoshida et al., 2010). However, *DCL3* was not a DEG in the leaves or roots of any of the four-grapevine species in response to WD (Fig. 13) despite the 25 ABREs in the corresponding promoter region (Fig. 11). The lack of differential expression may be linked to the lack of an ABRE in the -50 to -100 bp region, which appears to be an important range for cis-element occurrences (FitzGerald et al., 2004; Maruyama et al., 2012; Yamamoto et al., 2007). Like *DCL3*, not all genes with an ABRE(s) in the corresponding promoter region were DEGs in response to 2W moderate WD. The lack of differential expression of *DCL3* (and other ABRE-containing genes) in response to WD does not imply these genes are unresponsive to ABA. It is possible *DCL3* and other genes corresponding to ABRE-containing promoter regions respond to a different abiotic stress that involves ABA, or these genes may respond to WD at a different duration or severity of stress. Alternatively, *DCL3* may be a DEG in response to WD in a cell type, organ, or developmental stage that was not investigated in this study. Overall, the promoter

regions of *CIP8*, *GBF3*, and *DCL3* contain numerous ABREs, and the function of these ABREs and roles of these genes in ABA response require additional elucidation.

Interestingly, all three of the top annotated ABRE-containing genes are linked to ABA INSENSITIVE 5 (ABI5) in *Arabidopsis thaliana*. In Arabidopsis, CIP8 interacts with CONSTITUTIVE PHOTOMORPHOGENIC 1 (COP1) as well as UBIQUITIN CONJUGATING ENZYME 8 (UBC8), which ubiquitinates and causes the degradation of HY5. HY5 has roles in regulation of light-responsive genes (Nawkar et al., 2017) and anthocyanin accumulation (Shin et al., 2013), and *Athy5* mutants have ABA-resistant seeds (Chen and Xiong, 2008). *HY5* and another gene corresponding to a promoter region with one of the highest numbers of ABREs, *ATAF1*, have roles in ABA sensitivity and are both regulated by DYNAMIC INFLUENCER OF GENE EXPRESSION 1 (DIG1) (Song et al., 2016). HY5 is known to bind to the *ABA INSENSITIVE 5* (*ABI5*) promoter (Chen and Xiong, 2008) to affect the expression of numerous downstream genes. Similarly, GBF3, a master regulator of ABA signaling (Tarancón et al., 2017), is linked to ABI5. GBF3 binds G-box (CCACGTGG) cis-acting elements associated with environmental stimuli response (Katagiri and Chua, 1992; Lu et al., 1996). *GBF3* overexpression improved drought, salt, and osmotic stress tolerance in Arabidopsis (Dixit et al., 2019; Ramegowda et al., 2017). GBF3 is indicated to regulate ABI FIVE BINDING PROTEIN 1 (AFP1), which in turn regulates and interacts with *ABI5* (Lopez-Molina, 2003; Ramegowda et al., 2017). DCL3 is also connected to *ABI5*. DCL3 is a ribonuclease that creates siRNAs that function in RNA-directed DNA methylation and RNA-interference (Nagano et al., 2014). *Atdcl3* mutants are ABA-supersensitive and have increased *ABI3*, *ABI4*, and *ABI5* transcript abundance (Zhang et al., 2008).

Because some of the top ABRE-containing genes were linked to ABI5, ABI5 may be a central point of ABA signaling as was previously implicated (Finkelstein and Lynch, 2000; Skubacz et al., 2016; Yang et al., 2011). ABI5 is a member of the AREB clade that targets and regulates genes with ABRE-containing promoter regions (Finkelstein and Lynch, 2000; Finkelstein et al., 2005; Kim et al., 2002). ABI5 is a basic leucine zipper TF (Banerjee and Roychoudhury, 2017b) most well-known for a role in seed germination (Finkelstein, 1994), but ABI5 also regulates growth (Brocard, 2002; De Smet et al., 2003), ABA signaling (Finkelstein and Lynch, 2000), and abiotic stress response (Skubacz et al., 2016). ABI5 ABRE-containing targets related to seed development and germination include *LATE EMBRYOGENESIS ABUNDANT* (*LEAs*) (Finkelstein and Lynch, 2000; Kim et al., 2002). ABI5 ABRE-containing targets involved in abiotic stress response include *COLD RESPONSIVE 6.6* (*COR6.6*), *COR15a*, *RAB18* (Brocard, 2002), and *DIACYLGLYCEROL ACETYLTRANSFERASE 1* (*DGAT1*) (Kong et al., 2013). The large number and diversity of ABI5 targets support ABI5 as a possible hub for ABA signaling.

In this study, the ABI5 promoter region contained seven ABREs occurring from ~ -500 through -2,000 bps from the TSS (Supplemental File 1), indicating ABI5 is also regulated by other members of the ABA signaling pathway. TFs that target and regulate *ABI5* include ABI3 (Lopez-Molina et al., 2002), ABI4 (Bossi et al., 2009; Finkelstein and Lynch, 2000), MYB7 (Kim et al., 2015), PEROXISOME DEFECTIVE 3 (PED3) (Kanai et al., 2010), BRASSINOSTEROID INSENSITIVE 2 (BIN2) (Hu and Yu, 2014), and BRASSINOZOLE RESISTANT 1 (BZR1) (Yang et al., 2016) in addition to HY5 (Chen and Xiong, 2008). The interaction of *ABI5* with brassinosteroid signaling further elevates *ABI5* as a unique and intriguing ABA signaling gene that acts as a point of phytohormone

crosstalk and integration. ABI5 may prove a valuable target in breeding programs that requires further investigation.

Previous work identified *ERF6L1* (Cramer et al., 2014) and *NCED3* (Cochetel et al., 2020) as potential hub genes in ABA response. The presence of ABREs in these promoter regions (Fig. 10 and 12 and Supplemental File 1) supports these genes as ABA-responsive genes and provides further evidence they could function as hub genes in ABA responses. Validation of these genes as ABA-responsive was further demonstrated by the accumulation and significant differential expression of these transcripts in response to WD (Fig. 13).

Although these genes contain ABREs in respective promoter regions, it is important to consider the many other factors may be regulating these genes. NCED3 has potential post-translational modification sites, but none are well described at this time (Cruz et al., 2019). miRNAs regulate ERFs under a variety of stresses (Fu et al., 2017; Jeyaraj et al., 2017). Additionally, the presence of cis-acting elements in promoter regions is irrelevant if DNA modifications prevent transcription. Recently, histone H3 lysine 36 methyltransferases were found to play a key role in drought tolerance by activating *NCED3* and *NCED5* in rice (Chen et al., 2021), and epigenetics and DNA methylation are critical levels of regulation for abiotic stress response and drought tolerance (Banerjee and Roychoudhury, 2017a; Wang et al., 2016).

In addition to these annotated genes, many uncharacterized genes like Vitvi11g01561 and Vitvi05g02283 contained even higher numbers of ABREs in promoter regions (Supplemental File 1). Unfortunately, Vitvi11g01561 structural annotation appeared incomplete because the gene was only 48 bps, and the sequence did not yield any

BLAST results hits in other species. Vitvi11g01561 was a 408 bp gene, but there did not appear to be orthologous genes in other species because once again there were no BLAST hits. The closest genes in *Vitis* were also all unannotated, but all related genes and Vitvi11g01561 were near the ends of chromosomes. These genes highlight that although the PN40024 reference genome may have the most thorough annotation, this annotation is still incomplete. These genes and the many other uncharacterized genes with numerous ABREs in corresponding promoter regions may be highly responsive to ABA or even act as hub genes in ABA responses like WD. The uncharacterized genes with numerous ABRE occurrences in corresponding promoter regions warrant further investigation and characterization in the future.

Overall, this work improved the annotation of ABREs in the PN40024 grapevine reference genome using the new version of the genome and a more comprehensive list of ABREs than was used previously. ABREs were determined to be predominant throughout promoter regions in this grapevine reference genome. The presence of ABREs in promoter regions validated and explained ABA responses of numerous genes including potential hub genes, *ERF6L1* and *NCED3*. Additionally, this analysis identified novel potential ABA-responsive genes that are currently uncharacterized. These uncharacterized genes with high ABRE occurrences in respective promoter regions may prove valuable targets for future studies of ABA signaling and breeding programs seeking to improve abiotic stress tolerance.

2.5 References

Babraham Bioinformatics (2010). Babraham Bioinformatics - FastQC A Quality Control tool for High Throughput Sequence Data.

Bailey, T.L., Boden, M., Buske, F.A., Frith, M., Grant, C.E., Clementi, L., Ren, J., Li, W.W., and Noble, W.S. (2009). MEME Suite: tools for motif discovery and searching. Nucleic Acids Res. *37*, W202–W208.

Banerjee, A., and Roychoudhury, A. (2017a). Epigenetic regulation during salinity and drought stress in plants: Histone modifications and DNA methylation. Plant Gene *11*, 199–204.

Banerjee, A., and Roychoudhury, A. (2017b). Abscisic-acid-dependent basic leucine zipper (bZIP) transcription factors in plant abiotic stress. Protoplasma *254*, 3–16.

Benedict, C., Skinner, J.S., Meng, R., Chang, Y., Bhalerao, R., Huner, N.P.A., Finn, C.E., Chen, T.H.H., and Hurry, V. (2006). The CBF1-dependent low temperature signalling pathway, regulon and increase in freeze tolerance are conserved in Populus spp. Plant Cell Environ. *29*, 1259–1272.

Bolger, A.M., Lohse, M., and Usadel, B. (2014). Trimmomatic: a flexible trimmer for Illumina sequence data. Bioinformatics *30*, 2114–2120.

Bossi, F., Cordoba, E., Dupré, P., Mendoza, M.S., Román, C.S., and León, P. (2009). The Arabidopsis ABA-INSENSITIVE (ABI) 4 factor acts as a central transcription activator of the expression of its own gene, and for the induction of ABI5 and SBE2.2 genes during sugar signaling. Plant J. Cell Mol. Biol. *59*, 359–374.

Brocard, I.M. (2002). Regulation and Role of the Arabidopsis Abscisic Acid-Insensitive 5 Gene in Abscisic Acid, Sugar, and Stress Response. PLANT Physiol. *129*, 1533–1543.

Busk, P.K., and Pages, M. (1998). Regulation of abscisic acid-induced transcription. 11.

Canaguier, A., Grimplet, J., Di Gaspero, G., Scalabrin, S., Duchêne, E., Choisne, N., Mohellibi, N., Guichard, C., Rombauts, S., Le Clainche, I., et al. (2017). A new version of the grapevine reference genome assembly (12X.v2) and of its annotation (VCost.v3). Genomics Data *14*, 56–62.

Chen, H., and Xiong, L. (2008). Role of HY5 in abscisic acid response in seeds and seedlings. Plant Signal. Behav. *3*, 986–988.

Chen, K., Du, K., Shi, Y., Yin, L., Shen, W.-H., Yu, Y., Liu, B., and Dong, A. (2021). H3K36 methyltransferase SDG708 enhances drought tolerance by promoting abscisic acid biosynthesis in rice. New Phytol. *n/a*.

Chin, C.-S., Peluso, P., Sedlazeck, F.J., Nattestad, M., Concepcion, G.T., Clum, A., Dunn, C., O'Malley, R., Figueroa-Balderas, R., Morales-Cruz, A., et al. (2016). Phased diploid genome assembly with single-molecule real-time sequencing. Nat. Methods *13*, 1050–1054.

Chinnusamy, V., Jagendorf, A., and Zhu, J.-K. (2005). Understanding and Improving Salt Tolerance in Plants. Crop Sci. *45*, 437–448.

Choi, H., Hong, J., Ha, J., Kang, J., and Kim, S.Y. (2000). ABFs, a family of ABA-responsive element binding factors. J. Biol. Chem. *275*, 1723–1730.

Cochetel, N., Ghan, R., Toups, H.S., Degu, A., Tillett, R.L., Schlauch, K.A., and Cramer, G.R. (2020). Drought tolerance of the grapevine, Vitis champinii cv. Ramsey, is associated with higher photosynthesis and greater transcriptomic responsiveness of abscisic acid biosynthesis and signaling. BMC Plant Biol. *20*.

Cornish-Bowden, A. (1985). Nomenclature for incompletely specified bases in nucleic acid sequences: recommendations 1984. Nucleic Acids Res. *13*, 3021–3030.

Cortijo, S., Charoensawan, V., Roudier, F., and Wigge, P.A. (2018). Chromatin Immunoprecipitation Sequencing (ChIP-Seq) for Transcription Factors and Chromatin Factors in Arabidopsis thaliana Roots: From Material Collection to Data Analysis. Methods Mol. Biol. Clifton NJ *1761*, 231–248.

Cramer, G.R., Ghan, R., Schlauch, K.A., Tillett, R.L., Heymann, H., Ferrarini, A., Delledonne, M., Zenoni, S., Fasoli, M., and Pezzotti, M. (2014). Transcriptomic analysis of the late stages of grapevine (Vitis vinifera cv. Cabernet Sauvignon) berry ripening reveals significant induction of ethylene signaling and flavor pathways in the skin. BMC Plant Biol. *14*.

Cruz, E.R., Nguyen, H., Nguyen, T., and Wallace, I.S. (2019). Functional analysis tools for post-translational modification: a post-translational modification database for analysis of proteins and metabolic pathways. Plant J. *99*, 1003–1013.

Daszkowska-Golec, A. (2016). The Role of Abscisic Acid in Drought Stress: How ABA Helps Plants to Cope with Drought Stress. In Drought Stress Tolerance in Plants, Vol 2, M.A. Hossain, S.H. Wani, S. Bhattacharjee, D.J. Burritt, and L.-S.P. Tran, eds. (Cham: Springer International Publishing), pp. 123–151.

Davuluri, R.V., Sun, H., Palaniswamy, S.K., Matthews, N., Molina, C., Kurtz, M., and Grotewold, E. (2003). AGRIS: Arabidopsis Gene Regulatory Information Server, an information resource of Arabidopsis cis-regulatory elements and transcription factors. BMC Bioinformatics *4*, 25.

De Smet, I., Signora, L., Beeckman, T., Inzé, D., Foyer, C.H., and Zhang, H. (2003). An abscisic acid-sensitive checkpoint in lateral root development of *Arabidopsis*. Plant J. *33*, 543–555.

Deng, W., and Roberts, S.G.E. (2005). A core promoter element downstream of the TATA box that is recognized by TFIIB. Genes Dev. *19*, 2418–2423.

Deplancke, B., Dupuy, D., Vidal, M., and Walhout, A.J.M. (2004). A Gateway-Compatible Yeast One-Hybrid System. Genome Res. *14*, 2093–2101.

Dixit, S.K., Gupta, A., Fatima, U., and Senthil-Kumar, M. (2019). AtGBF3 confers tolerance to Arabidopsis thaliana against combined drought and Pseudomonas syringae stress. Environ. Exp. Bot. *168*, 103881.

Finkelstein, R.R. (1994). Mutations at two new Arabidopsis ABA response loci are similar to the abi3 mutations. Plant J. *5*, 765–771.

Finkelstein, R.R., and Lynch, T.J. (2000). The Arabidopsis Abscisic Acid Response Gene ABI5 Encodes a Basic Leucine Zipper Transcription Factor. Plant Cell *12*, 599–609.

Finkelstein, R., Gampala, S.S.L., Lynch, T.J., Thomas, T.L., and Rock, C.D. (2005). Redundant and Distinct Functions of the ABA Response Loci ABA-INSENSITIVE(ABI)5 and ABRE-BINDING FACTOR (ABF)3. Plant Mol. Biol. *59*, 253–267.

FitzGerald, P.C., Shlyakhtenko, A., Mir, A.A., and Vinson, C. (2004). Clustering of DNA Sequences in Human Promoters. Genome Res. *14*, 1562–1574.

Fox, J. (2020). An R Companion to Applied Regression (Thousand Oaks CA: Sage).

Fu, R., Zhang, M., Zhao, Y., He, X., Ding, C., Wang, S., Feng, Y., Song, X., Li, P., and Wang, B. (2017). Identification of Salt Tolerance-related microRNAs and Their Targets in Maize (Zea mays L.) Using High-throughput Sequencing and Degradome Analysis. Front. Plant Sci. *8*.

Fujimoto, S.Y., Ohta, M., Usui, A., Shinshi, H., and Ohme-Takagi, M. Arabidopsis Ethylene-Responsive Element Binding Factors Act as Transcriptional Activators or Repressors of GCC Box–Mediated Gene Expression. 12.

Fujita, Y., Fujita, M., Satoh, R., Maruyama, K., Parvez, M.M., Seki, M., Hiratsu, K., Ohme-Takagi, M., Shinozaki, K., and Yamaguchi-Shinozaki, K. (2005). AREB1 Is a Transcription Activator of Novel ABRE-Dependent ABA Signaling That Enhances Drought Stress Tolerance in Arabidopsis. Plant Cell *17*, 3470–3488.

Garapati, P., Xue, G.-P., Munné-Bosch, S., and Balazadeh, S. (2015). Transcription Factor ATAF1 in Arabidopsis Promotes Senescence by Direct Regulation of Key Chloroplast Maintenance and Senescence Transcriptional Cascades. Plant Physiol. *168*, 1122–1139.

Geisler, M., Kleczkowski, L.A., and Karpinski, S. (2006). A universal algorithm for genome-wide in silicio identification of biologically significant gene promoter putative cis-regulatory-elements; identification of new elements for reactive oxygen species and sucrose signaling in Arabidopsis. Plant J. Cell Mol. Biol. *45*, 384–398.

Girollet, N., Rubio, B., Lopez-Roques, C., Valière, S., Ollat, N., and Bert, P.-F. (2019). De novo phased assembly of the Vitis riparia grape genome. Sci. Data *6*, 1–8.

Gómez-Porras, J.L., Riaño-Pachón, D.M., Dreyer, I., Mayer, J.E., and Mueller-Roeber, B. (2007). Genome-wide analysis of ABA-responsive elements ABRE and CE3 reveals divergent patterns in Arabidopsis and rice. BMC Genomics *8*, 260.

Griffiths, A.J., Miller, J.H., Suzuki, D.T., Lewontin, R.C., and Gelbart, W.M. (2000). Transcription: an overview of gene regulation in eukaryotes. Introd. Genet. Anal. 7th Ed.

Guiltinan, M.J., Marcotte, W.R., and Quatrano, R.S. (1990). A plant leucine zipper protein that recognizes an abscisic acid response element. Science *250*, 267–271.

He, Q., Johnston, J., and Zeitlinger, J. (2015). ChIP-nexus enables improved detection of in vivo transcription factor binding footprints. Nat. Biotechnol. *33*, 395–401.

Higashi, Y., and Saito, K. (2013). Network analysis for gene discovery in plant-specialized metabolism. Plant Cell Environ. *36*, 1597–1606.

Higo, K., Ugawa, Y., Iwamoto, M., and Korenaga, T. (1999). Plant cis-acting regulatory DNA elements (PLACE) database: 1999. Nucleic Acids Res. *27*, 297–300.

Hu, Y., and Yu, D. (2014). BRASSINOSTEROID INSENSITIVE2 interacts with ABSCISIC ACID INSENSITIVE5 to mediate the antagonism of brassinosteroids to abscisic acid during seed germination in Arabidopsis. Plant Cell *26*, 4394–4408.

Jeyaraj, A., Liu, S., Zhang, X., Zhang, R., Shangguan, M., and Wei, C. (2017). Genome-wide identification of microRNAs responsive to Ectropis oblique feeding in tea plant (Camellia sinensis L.). Sci. Rep. *7*, 13634.

Jung, I., Ahn, H., Shin, S.-J., Kim, J., Kwon, H.-B., Jung, W., and Kim, S. (2016). Clustering and evolutionary analysis of small RNAs identify regulatory siRNA clusters induced under drought stress in rice. BMC Syst. Biol. *10*, 115.

Kanai, M., Nishimura, M., and Hayashi, M. (2010). A peroxisomal ABC transporter promotes seed germination by inducing pectin degradation under the control of ABI5. Plant J. Cell Mol. Biol. *62*, 936–947.

Kao, C.Y., Cocciolone, S.M., Vasil, I.K., and McCarty, D.R. (1996). Localization and interaction of the cis-acting elements for abscisic acid, VIVIPAROUS1, and light activation of the C1 gene of maize. Plant Cell *8*, 1171–1179.

Kaplan, B., Davydov, O., Knight, H., Galon, Y., Knight, M.R., Fluhr, R., and Fromm, H. (2006). Rapid Transcriptome Changes Induced by Cytosolic Ca2+ Transients Reveal ABRE-Related Sequences as Ca2+-Responsive cis Elements in Arabidopsis. Plant Cell *18*, 2733–2748.

Katagiri, F., and Chua, N.H. (1992). Plant transcription factors: present knowledge and future challenges. Trends Genet. TIG *8*, 22–27.

Kim, J.H., Hyun, W.Y., Nguyen, H.N., Jeong, C.Y., Xiong, L., Hong, S.-W., and Lee, H. (2015). AtMyb7, a subgroup 4 R2R3 Myb, negatively regulates ABA-induced inhibition of seed germination by blocking the expression of the bZIP transcription factor ABI5. Plant Cell Environ. *38*, 559–571.

Kim, S.Y., Ma, J., Perret, P., Li, Z., and Thomas, T.L. (2002). Arabidopsis ABI5 Subfamily Members Have Distinct DNA-Binding and Transcriptional Activities. Plant Physiol. *130*, 688–697.

Kong, Y., Chen, S., Yang, Y., and An, C. (2013). ABA-insensitive (ABI) 4 and ABI5 synergistically regulate DGAT1 expression in Arabidopsis seedlings under stress. FEBS Lett. *587*, 3076–3082.

Kribelbauer, J.F., Rastogi, C., Bussemaker, H.J., and Mann, R.S. (2019). Low-Affinity Binding Sites and the Transcription Factor Specificity Paradox in Eukaryotes. Annu. Rev. Cell Dev. Biol. *35*, 357–379.

Lamarque, L.J., Delzon, S., Toups, H., Gravel, A.-I., Corso, D., Badel, E., Burlett, R., Charrier, G., Cochard, H., Jansen, S., et al. (2019). Over-accumulation of abscisic acid in transgenic tomato plants increases the risk of hydraulic failure. Plant Cell Environ.

Lawrence, M., Huber, W., Pagès, H., Aboyoun, P., Carlson, M., Gentleman, R., Morgan, M.T., and Carey, V.J. (2013). Software for Computing and Annotating Genomic Ranges. PLOS Comput. Biol. *9*, e1003118.

Lebedeva, M.A., Dodueva, I.E., Gancheva, M.S., Tvorogova, V.E., Kuznetsova, K.A., and Lutova, L.A. (2020). The Evolutionary Aspects of Flowering Control: Florigens and Anti-Florigens. Russ. J. Genet. *56*, 1323–1344.

Leonhardt, N., Kwak, J.M., Robert, N., Waner, D., Leonhardt, G., and Schroeder, J.I. (2004). Microarray Expression Analyses of Arabidopsis Guard Cells and Isolation of a Recessive Abscisic Acid Hypersensitive Protein Phosphatase 2C Mutant. Plant Cell *16*, 596–615.

Li, J., Yang, Z., Yu, B., Liu, J., and Chen, X. (2005). Methylation protects miRNAs and siRNAs from a 3'-end uridylation activity in Arabidopsis. Curr. Biol. CB *15*, 1501–1507.

Lis, M., and Walther, D. (2016). The orientation of transcription factor binding site motifs in gene promoter regions: does it matter? BMC Genomics *17*.

Londo, J.P., Kovaleski, A.P., and Lillis, J.A. (2018). Divergence in the transcriptional landscape between low temperature and freeze shock in cultivated grapevine (Vitis vinifera). Hortic. Res. *5*.

Lopez-Molina, L. (2003). AFP is a novel negative regulator of ABA signaling that promotes ABI5 protein degradation. Genes Dev. *17*, 410–418.

Lopez-Molina, L., Mongrand, S., McLachlin, D.T., Chait, B.T., and Chua, N.-H. (2002). ABI5 acts downstream of ABI3 to execute an ABA-dependent growth arrest during germination. Plant J. *32*, 317–328.

Love, M.I., Huber, W., and Anders, S. (2014). Moderated estimation of fold change and dispersion for RNA-seq data with DESeq2. Genome Biol. *15*.

Lu, G., Paul, A.L., McCarty, D.R., and Ferl, R.J. (1996). Transcription factor veracity: is GBF3 responsible for ABA-regulated expression of Arabidopsis Adh? Plant Cell *8*, 847–857.

Maruyama, K., Todaka, D., Mizoi, J., Yoshida, T., Kidokoro, S., Matsukura, S., Takasaki, H., Sakurai, T., Yamamoto, Y.Y., Yoshiwara, K., et al. (2012). Identification of Cis-Acting Promoter Elements in Cold- and Dehydration-Induced Transcriptional Pathways in Arabidopsis, Rice, and Soybean. DNA Res. Int. J. Rapid Publ. Rep. Genes Genomes *19*, 37–49.

Massonnet, M., Cochetel, N., Minio, A., Vondras, A.M., Muyle, A., Lin, J., Garcia, J.F., Zhou, Y., Delledonne, M., Riaz, S., et al. (2019). The genetic basis of sex determination in grapevines (*Vitis spp.*) (Evolutionary Biology).

Minio, A., Massonnet, M., Figueroa-Balderas, R., Castro, A., and Cantu, D. (2019a). Diploid Genome Assembly of the Wine Grape Carménère. G3 GenesGenomesGenetics *9*, 1331–1337.

Minio, A., Massonnet, M., Figueroa-Balderas, R., Vondras, A.M., Blanco-Ulate, B., and Cantu, D. (2019b). Iso-Seq Allows Genome-Independent Transcriptome Profiling of Grape Berry Development. G3 GenesGenomesGenetics *9*, 755–767.

Moolla, N., Kew, M., and Arbuthnot, P. (2002). Regulatory elements of hepatitis B virus transcription. J. Viral Hepat. *9*, 323–331.

Mundy, J., Yamaguchi-Shinozaki, K., and Chua, N.H. (1990). Nuclear proteins bind conserved elements in the abscisic acid-responsive promoter of a rice rab gene. Proc. Natl. Acad. Sci. *87*, 1406–1410.

Nagano, H., Fukudome, A., Hiraguri, A., Moriyama, H., and Fukuhara, T. (2014). Distinct substrate specificities of Arabidopsis DCL3 and DCL4. Nucleic Acids Res. *42*, 1845–1856.

Nawkar, G.M., Kang, C.H., Maibam, P., Park, J.H., Jung, Y.J., Chae, H.B., Chi, Y.H., Jung, I.J., Kim, W.Y., Yun, D.-J., et al. (2017). HY5, a positive regulator of light signaling, negatively controls the unfolded protein response in Arabidopsis. Proc. Natl. Acad. Sci. *114*, 2084–2089.

Nicolas, P., Lecourieux, D., Kappel, C., Cluzet, S., Cramer, G., Delrot, S., and Lecourieux, F. (2014). The Basic Leucine Zipper Transcription Factor ABSCISIC ACID RESPONSE ELEMENT-BINDING FACTOR2 Is an Important Transcriptional Regulator of Abscisic Acid-Dependent Grape Berry Ripening Processes. Plant Physiol. *164*, 365–383.

Palaniswamy, S.K., James, S., Sun, H., Lamb, R.S., Davuluri, R.V., and Grotewold, E. (2006). AGRIS and AtRegNet. A Platform to Link cis-Regulatory Elements and Transcription Factors into Regulatory Networks. Plant Physiol. *140*, 818–829.

Patro, R., Duggal, G., Love, M.I., Irizarry, R.A., and Kingsford, C. (2017). Salmon provides fast and bias-aware quantification of transcript expression. Nat. Methods *14*, 417–419.

Pilati, S., Bagagli, G., Sonego, P., Moretto, M., Brazzale, D., Castorina, G., Simoni, L., Tonelli, C., Guella, G., Engelen, K., et al. (2017). Abscisic Acid Is a Major Regulator of Grape Berry Ripening Onset: New Insights into ABA Signaling Network. Front. Plant Sci. *8*, 1093.

Pucker, B., Schwandner, A., Becker, S., Hausmann, L., Viehöver, P., Töpfer, R., Weisshaar, B., and Holtgräwe, D. (2020). RNA-Seq Time Series of Vitis vinifera Bud Development Reveals Correlation of Expression Patterns with the Local Temperature Profile. BioRxiv 2020.10.18.344176.

R Core Team (2018). R: The R Project for Statistical Computing.

Ramegowda, V., Gill, U.S., Sivalingam, P.N., Gupta, A., Gupta, C., Govind, G., Nataraja, K.N., Pereira, A., Udayakumar, M., Mysore, K.S., et al. (2017). GBF3 transcription factor imparts drought tolerance in Arabidopsis thaliana. Sci. Rep. *7*, 9148.

Rattanakon, S., Ghan, R., Gambetta, G.A., Deluc, L.G., Schlauch, K.A., and Cramer, G.R. (2016). Abscisic acid transcriptomic signaling varies with grapevine organ. BMC Plant Biol. *16*.

Rombauts, S., Dehais, P., Van Montagu, M., and Rouze, P. (1999). PlantCARE, a plant cis-acting regulatory element database. Nucleic Acids Res. *27*, 295–296.

Sen, E., Alam, S., and Meyers, C. (2004). Genetic and Biochemical Analysis of cis Regulatory Elements within the Keratinocyte Enhancer Region of the Human Papillomavirus Type 31 Upstream Regulatory Region during Different Stages of the Viral Life Cycle. J. Virol. *78*, 612–629.

Shin, D.H., Choi, M., Kim, K., Bang, G., Cho, M., Choi, S.-B., Choi, G., and Park, Y.-I. (2013). HY5 regulates anthocyanin biosynthesis by inducing the transcriptional activation of the MYB75/PAP1 transcription factor in Arabidopsis. FEBS Lett. *587*, 1543–1547.

Shinozaki, K., and Yamaguchi-Shinozaki, K. (2000). Molecular responses to dehydration and low temperature: differences and cross-talk between two stress signaling pathways. Curr. Opin. Plant Biol. *3*, 217–223.

Simpson, S.D., Nakashima, K., Narusaka, Y., Seki, M., Shinozaki, K., and Yamaguchi-Shinozaki, K. (2003). Two different novel cis-acting elements of erd1, a clpA homologous Arabidopsis gene function in induction by dehydration stress and dark-induced senescence. Plant J. *33*, 259–270.

Skubacz, A., Daszkowska-Golec, A., and Szarejko, I. (2016). The Role and Regulation of ABI5 (ABA-Insensitive 5) in Plant Development, Abiotic Stress Responses and Phytohormone Crosstalk. Front. Plant Sci. *7*.

Song, L., Huang, S.C., Wise, A., Castanon, R., Nery, J.R., Chen, H., Watanabe, M., Thomas, J., Bar-Joseph, Z., and Ecker, J.R. (2016). A transcription factor hierarchy defines an environmental stress response network. Science *354*.

Stadhouders, R., van den Heuvel, A., Kolovos, P., Jorna, R., Leslie, K., Grosveld, F., and Soler, E. (2012). Transcription regulation by distal enhancers. Transcription *3*, 181–186.

Sterck, L., Billiau, K., Abeel, T., Rouzé, P., and Van de Peer, Y. (2012). ORCAE: online resource for community annotation of eukaryotes. Nat. Methods *9*, 1041.

Sussmilch, F.C., Brodribb, T.J., and McAdam, S.A.M. (2017). Up-regulation of NCED3 and ABA biosynthesis occur within minutes of a decrease in leaf turgor but AHK1 is not required. J. Exp. Bot. *68*, 2913–2918.

Suwanickul, A., Morris, S.L., and Powell, D.R. (1993). Identification of an insulin-responsive element in the promoter of the human gene for insulin-like growth factor binding protein-1. J. Biol. Chem. *268*, 17063–17068.

Suzuki, M., Ketterling, M.G., and McCarty, D.R. (2005). Quantitative Statistical Analysis of cis-Regulatory Sequences in ABA/VP1- and CBF/DREB1-Regulated Genes of Arabidopsis. Plant Physiol. *139*, 437–447.

Tarancón, C., González-Grandío, E., Oliveros, J.C., Nicolas, M., and Cubas, P. (2017). A Conserved Carbon Starvation Response Underlies Bud Dormancy in Woody and Herbaceous Species. Front. Plant Sci. *8*.

Timmerhaus, G., Hanke, S.T., Buchta, K., and Rensing, S.A. (2011). Prediction and Validation of Promoters Involved in the Abscisic Acid Response in Physcomitrella patens. Mol. Plant *4*, 713–729.

Toups, H.S., Cochetel, N., Gray, D., and Cramer, G.R. (2020). VviERF6Ls: an expanded clade in Vitis responds transcriptionally to abiotic and biotic stresses and berry development. BMC Genomics *21*.

Wang, Y., and Stumph, W.E. (1995). RNA polymerase II/III transcription specificity determined by TATA box orientation. Proc. Natl. Acad. Sci. U. S. A. *92*, 8606–8610.

Wang, W., Qin, Q., Sun, F., Wang, Y., Xu, D., Li, Z., and Fu, B. (2016). Genome-Wide Differences in DNA Methylation Changes in Two Contrasting Rice Genotypes in Response to Drought Conditions. Front. Plant Sci. *7*.

Wong, D.C.J., Lopez Gutierrez, R., Gambetta, G.A., and Castellarin, S.D. (2017). Genome-wide analysis of cis-regulatory element structure and discovery of motif-driven gene co-expression networks in grapevine. DNA Res. Int. J. Rapid Publ. Rep. Genes Genomes *24*, 311–326.

Wong, D.C.J., Ariani, P., Castellarin, S., Polverari, A., and Vandelle, E. (2018). Co-expression network analysis and cis-regulatory element enrichment determine putative functions and regulatory mechanisms of grapevine ATL E3 ubiquitin ligases. Sci. Rep. *8*, 3151.

Yamamoto, Y.Y., Ichida, H., Matsui, M., Obokata, J., Sakurai, T., Satou, M., Seki, M., Shinozaki, K., and Abe, T. (2007). Identification of plant promoter constituents by analysis of local distribution of short sequences. BMC Genomics *8*, 67.

Yang, X., Yang, Y.-N., Xue, L.-J., Zou, M.-J., Liu, J.-Y., Chen, F., and Xue, H.-W. (2011). Rice ABI5-Like1 Regulates Abscisic Acid and Auxin Responses by Affecting the Expression of ABRE-Containing Genes. Plant Physiol. *156*, 1397–1409.

Yang, X., Bai, Y., Shang, J., Xin, R., and Tang, W. (2016). The antagonistic regulation of abscisic acid-inhibited root growth by brassinosteroids is partially mediated via direct suppression of ABSCISIC ACID INSENSITIVE 5 expression by BRASSINAZOLE RESISTANT 1. Plant Cell Environ. *39*, 1994–2003.

Yoshida, T., Fujita, Y., Sayama, H., Kidokoro, S., Maruyama, K., Mizoi, J., Shinozaki, K., and Yamaguchi-Shinozaki, K. (2010). AREB1, AREB2, and ABF3 are master transcription factors that cooperatively regulate ABRE-dependent ABA signaling involved in drought stress tolerance and require ABA for full activation. Plant J. *61*, 672–685.

Zhang, J.-F., Yuan, L.-J., Shao, Y., Du, W., Yan, D.-W., and Lu, Y.-T. (2008). The disturbance of small RNA pathways enhanced abscisic acid response and multiple stress responses in Arabidopsis. Plant Cell Environ. *31*, 562–574.

Zhang, W., Zhang, T., Wu, Y., and Jiang, J. (2012). Genome-Wide Identification of Regulatory DNA Elements and Protein-Binding Footprints Using Signatures of Open Chromatin in Arabidopsis. Plant Cell *24*, 2719–2731.

Zhu, Z., Wang, H., Wang, Y., Guan, S., Wang, F., Tang, J., Zhang, R., Xie, L., and Lu, Y. (2015). Characterization of the cis elements in the proximal promoter regions of the anthocyanin pathway genes reveals a common regulatory logic that governs pathway regulation. J. Exp. Bot. *66*, 3775–3789.

Tables

Table 1: ABREs. ABRE motif name, variant number (indicated by "_#" in text), sequence, type (determined by sequence overlap of shorter ABRE sequences in longer ABRE sequences), ID from source, and source of ABRE (PLACE (Higo et al., 1999) or AGRIS (Davuluri et al., 2003; Palaniswamy et al., 2006)). Ambiguity-code points are indicated in bold and underlined for ABRE variants.

Motif	Variant	Sequence	Class	Length	ID	Source
ABRE-likebindingsitemotif	1	**C**ACGTG**GA**	Primary	8	3	AGRIS
ABRE-likebindingsitemotif	3	**C**ACGTG**TA**	Secondary	8	5	AGRIS
ABRE-likebindingsitemotif	4	**C**ACGTG**TC**	Secondary	8	6	AGRIS
ABRE-likebindingsitemotif	5	**G**ACGTG**GA**	Primary	8	7	AGRIS
ABRE-likebindingsitemotif	6	**G**ACGTG**GC**	Secondary	8	8	AGRIS
ABRE-likebindingsitemotif	7	**G**ACGTG**TA**	Primary	8	9	AGRIS
ABRE-likebindingsitemotif	8	**G**ACGTG**TC**	Secondary	8	10	AGRIS
ABRE-likebindingsitemotif	9	**T**ACGTG**GA**	Primary	8	11	AGRIS
ABRE-likebindingsitemotif	11	**T**ACGTG**TA**	Primary	8	13	AGRIS
ABRE2HVA1		CCTACGTGGCGG	Quaternary	12	S000134	PLACE
ABRE2HVA22		CGCACGTGTC	Tertiary	10	S000117	PLACE
ABRE3HVA1		GCAACGTGTC	Secondary	10	S000135	PLACE
ABRE3HVA22		GCCACGTACA		10	S000118	PLACE
ABRE3OSRAB16		GTACGTGGCGC	Tertiary	11	S000120	PLACE
ABREA2HVA1		CCTACGTGGC	Tertiary	10	S000140	PLACE
ABREATCONSENSUS	1	**C**ACGTGGC	Secondary	8	S000406	PLACE
ABREATCONSENSUS	2	**T**ACGTGGC	Secondary	8	S000406	PLACE
ABREATRD22	1	**GC**ACGTGG**CG**	Tertiary	10	S000013	PLACE
ABREATRD22	2	**AC**ACGTGG**CA**	Tertiary	10	S000013	PLACE
ABREATRD22	3	**GT**ACGTGG**TG**	Primary	10	S000013	PLACE
ABREATRD22	4	**AT**ACGTGG**TA**	Primary	10	S000013	PLACE
ABREAZMRAB28		GCCACGTGGG	Secondary	10	S000218	PLACE
ABREBNNAPA		CGCCACGTGTCC	Tertiary	12	S000145	PLACE
ABREBZMRAB28		TCCACGTCTC		10	S000219	PLACE
ABRECE1HVA22		TGCCACCGG		9	S000014	PLACE

ABRECE3HVA1		ACGCGTGTCCTC		12	S000141	PLACE
ABRECE3ZMRAB28		ACGCGCCTCCTC		12	S000221	PLACE
ABREDISTBBNNAPA		GCCACTTGTC		10	S000262	PLACE
ABRELATERD1		ACGTG	CORE	5	S000414	PLACE
ABREMOTIFAOSOSEM		TACGTGTC	Secondary	8	S000299	PLACE
ABREMOTIFIIIOSRAB16B		GCCGCGTGGC		10	S000291	PLACE
ABREMOTIFIOSRAB16B		AGTACGTGGC	Tertiary	10	S000290	PLACE
ABREOSRAB21	1	ACGT**CCC**C		8	S000012	PLACE
ABREOSRAB21	2	ACGT**GGG**C	Primary	8	S000012	PLACE
ABRERATCAL	1	**A**ACG**G**G**C**		7	S000507	PLACE
ABRERATCAL	2	**A**ACG**T**G**C**	Primary	7	S000507	PLACE
ABRERATCAL	3	**A**ACG**C**G**C**		7	S000507	PLACE
ABRERATCAL	4	**C**ACG**G**G**C**		7	S000507	PLACE
ABRERATCAL	5	**C**ACG**T**G**C**	Primary	7	S000507	PLACE
ABRERATCAL	6	**C**ACG**C**G**C**		7	S000507	PLACE
ABRERATCAL	7	**A**ACG**G**G**T**		7	S000507	PLACE
ABRERATCAL	8	**A**ACG**T**G**T**	Primary	7	S000507	PLACE
ABRERATCAL	9	**A**ACG**C**G**T**		7	S000507	PLACE
ABRERATCAL	10	**C**ACG**G**G**T**		7	S000507	PLACE
ABRERATCAL	11	**C**ACG**T**G**T**	Primary	7	S000507	PLACE
ABRERATCAL	12	**C**ACG**C**G**T**		7	S000507	PLACE
ABRETAEM		GGACACGTGGC	Tertiary	11	S000015	PLACE
ABREZMRAB28		CCACGTGG	Primary	8	S000133	PLACE
ACGTABREMOTIFA2OSEM	1	ACGTG**G**C	Primary	7	S000394	PLACE
ACGTABREMOTIFA2OSEM	2	ACGTG**T**C	Primary	7	S000394	PLACE
CGTGTSPHZMC1		CGTGTCGTCCATGCAT		16	S000294	PLACE

Table 2: Consensus ABRE Occurrences. The number of total occurrences and the total number of promoter regions the consensus ABREs were present in at least once in the PN40024 promoter regions. Consensus ABREs are ordered by increasing number of occurrences.

Consensus ABRE	Total Number of Occurrences	Total Number of Promoters
ABRE3OSRAB16	1	1
ABRE2HVA1	2	2
ABRECE3HVA1	3	3
ABRECE3ZMRAB28	14	14
ABREMOTIFIIIOSRAB16B	25	25
ABRE2HVA22	33	33
ABREMOTIFIOSRAB16B	44	44
ABRE3HVA22	50	50
ABREBNNAPA	67	66
ABRE3HVA1	97	97
ABREA2HVA1	98	97
ABREBZMRAB28	105	104
ABRECE1HVA22	116	115
ABREDISTBBNNAPA	163	163
ABREAZMRAB28	172	170
ABRETAEM	195	193
ABREMOTIFAOSOSEM	1005	964
ABREATRD22	1016	916
ABREOSRAB21	1433	1371
ACGTABREMOTIFA2OSEM	2083	1980
ABREZMRAB28	2830	1393
ABREATCONSENSUS	3587	2882
ABRE-likebindingsitemotif	14644	10035
ABRERATCAL	32016	18816
ABRELATERD1	34053	20356

Figures

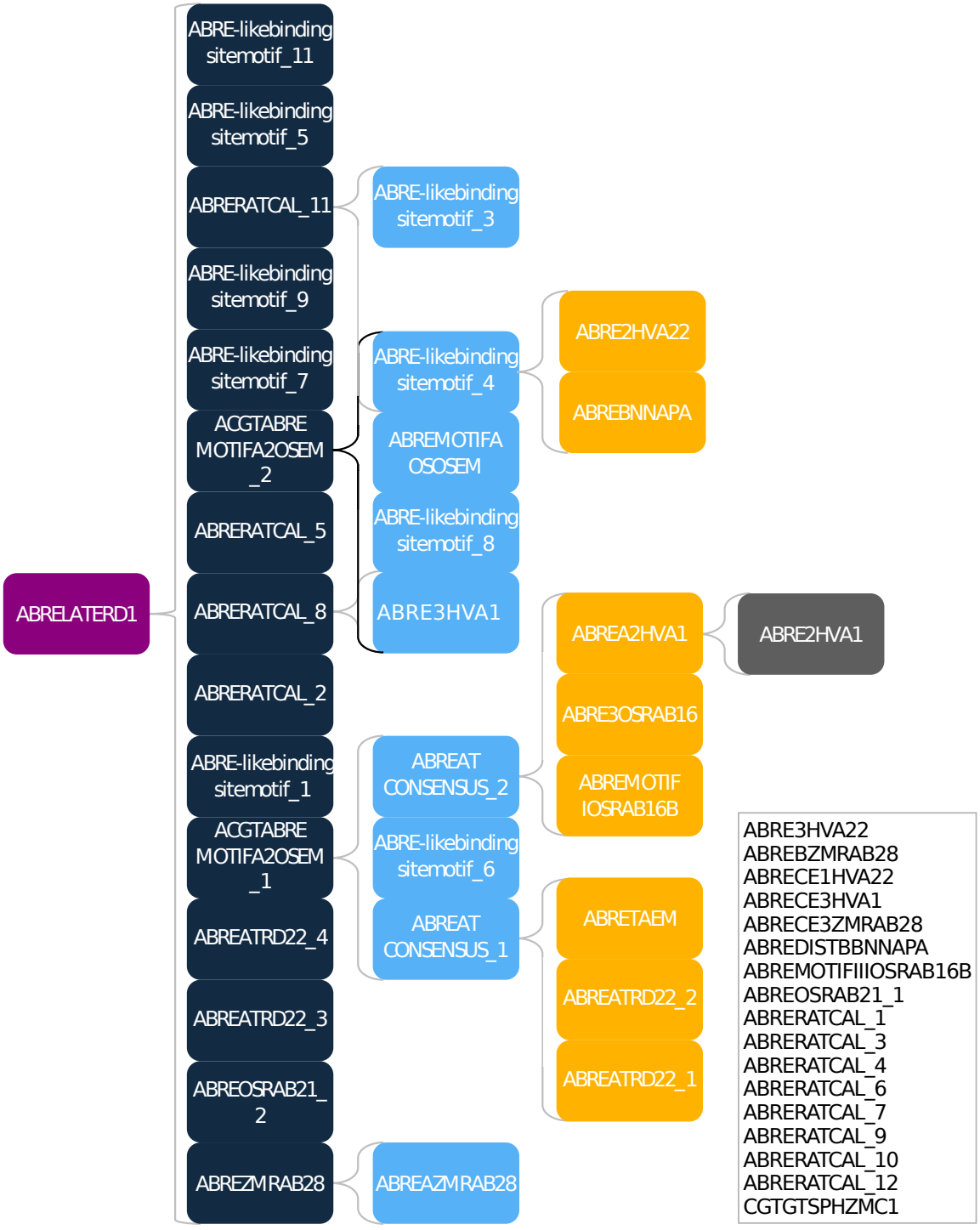

Figure 1: ABRELATERD1 is a core ABRE. A diagram of ABREs is shown with ABRELATERD1 (ACGTG) at the core. The core ABRE sequence was present in entirety

in primary ABRE sequences: ABRERATCAL_8, ACGTABREMOTIFA2OSEM, ABRERATCAL_11, ABRE-likebindingsitemotif_1, ABRE-likebindingsitemotif_5, ABRE-likebindingsitemotif_7, ABRE-likebindingsitemotif_9, ABRE-likebindingsitemotif_11, ABREOSRAB12_2, ABREATCAL_5, ABREATCAL_2, ABREATRD22_4, ABREATRD22_3, ABREZMRAB28, and ACGTABREMOTIFA20SEM_1 (in dark blue). The core ABRE and specific primary ABRE sequences were present in secondary ABREs: ABREAZMRAB28, ABRE-likebindingsitemotif_6, ABREATCONSENSUS_1, ABREATCONSENSUS_2, ABRE3HVA1, ABRE-likebindingsitemotif_8, ABRE-likebindingsitemotif_4, ABREMOTIFAOSOSEM, and ABRE-likebindingsitemotif_3 (light blue). Tertiary ABREs containing the core, specific primary, and specific secondary ABRE sequences included ABREATRD22_1, ABREATRD22_2, ABRETAEM, ABREMOTIFIOSRAB16B, ABRE30SRAB16, ABREA2HVA1, ABRENNAPA, and ABRE2HVA22 (yellow). A single tertiary ABRE contained the core ABRE motif and a specific primary, secondary, and tertiary ABRE sequences (grey). Core and sequentially ranked ABREs (primary, secondary, tertiary, quaternary) from left to right. An Additional 18 ABREs did not contain the entirety of any other ABRE sequence (box). Brackets in grey or black to distinguish overlapping groups.

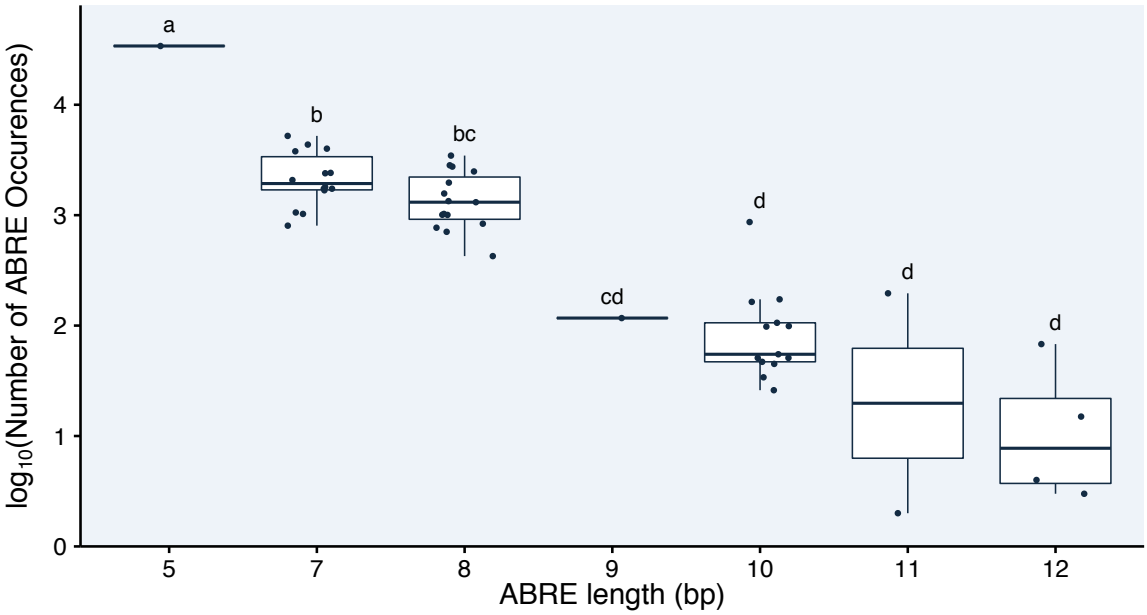

Figure 2: Short ABREs have significantly higher occurrences in PN40024 promoter regions. The number of ABRE occurrences is shown $\log_{10}$ transformed (for visualization purposes) for each of the ABREs present in the PN40024 promoter regions. ABREs are grouped by length (bp). One-way ANOVA Tukey's HSD ($p \leq 0.05$) letters for ABRE length. Each point represents an individual ABRE.

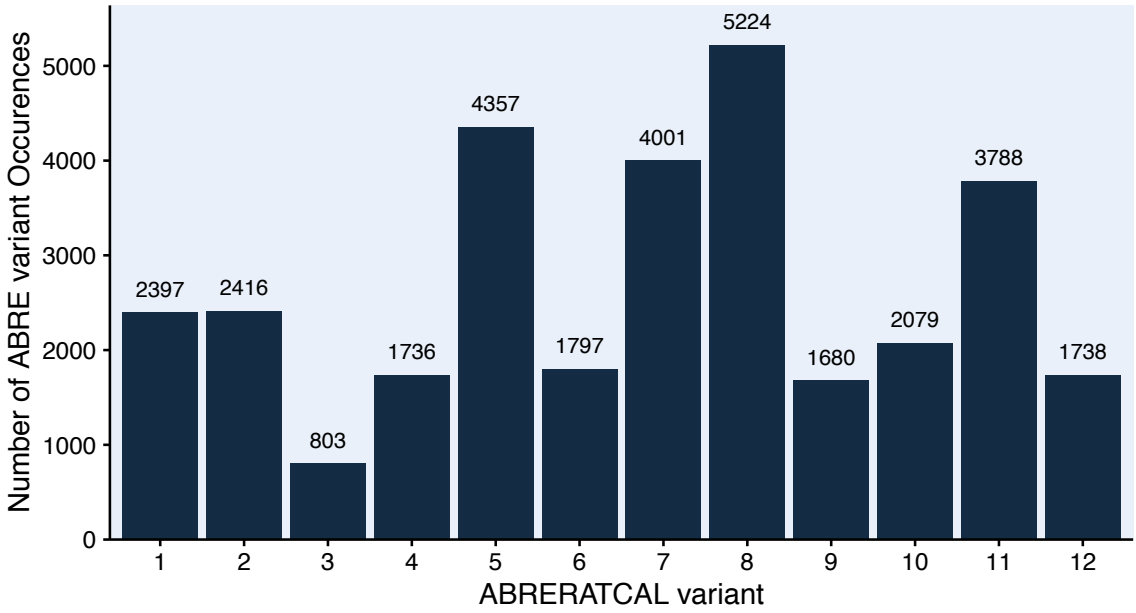

Figure 3: ABRERATCAL variant Occurrences. The distribution of the 32,016 occurrences of the ABRERATCAL consensus ABRE per variant sequence (from 1 to 12). Variant specific details are in Table 1. Exact ABRERATCAL variant occurrence numbers above each bar.

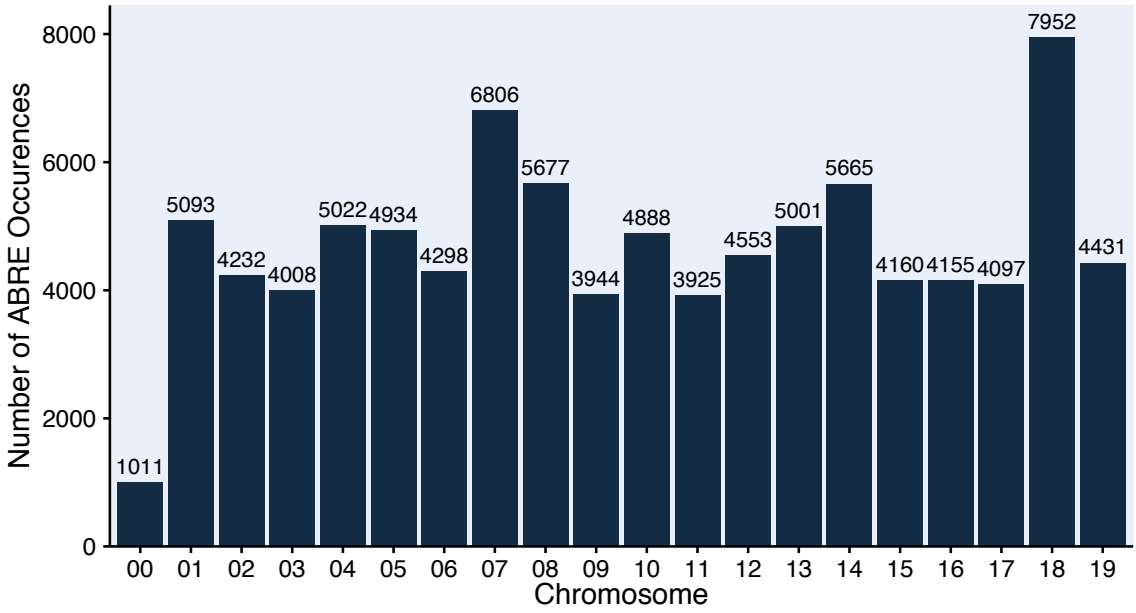

Figure 4: ABREs per chromosome. The number of ABREs present in each chromosome (00-19). Chromosome 00 represents the unplaced sequence pseudo-chromosome. Exact number of ABREs present in each chromosome indicated above each bar.

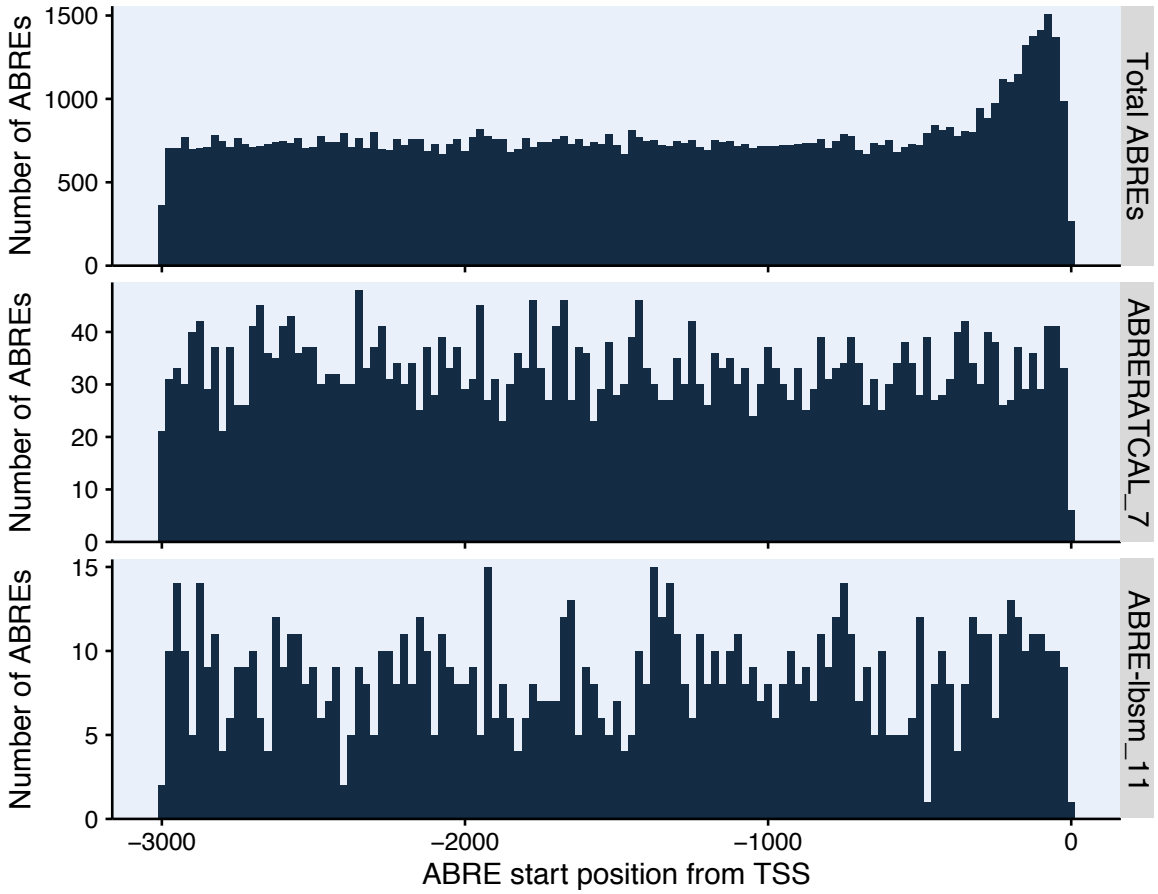

Figure 5: ABREs distribution along promoter region. The number of total ABRE occurrences of all ABREs, the number of ABRERATCAL_7 variant occurrences, and the number of ABRE-likebindingsitemotif (lbsm)_11 variant (top to bottom) occurrences present in a 25 bp window from 0 to -3,000 bp from the TSS. Each bar corresponds to a 25 bp window.

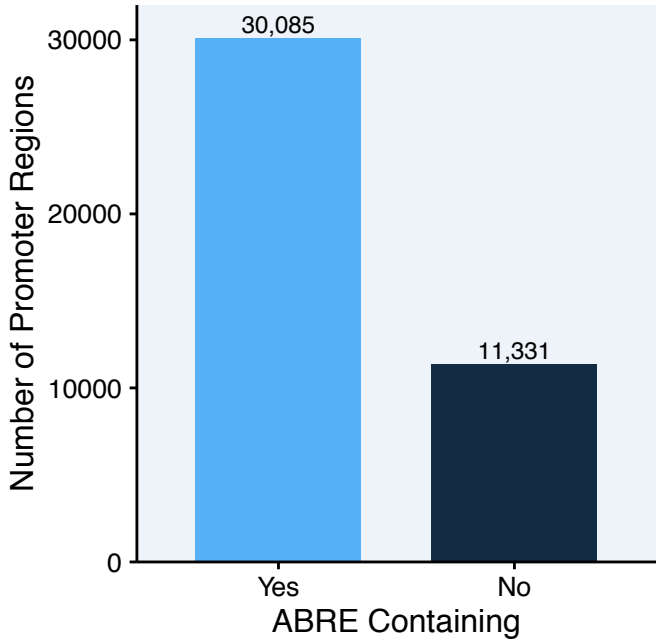

Figure 6: Number of ABRE containing promoter regions. The number of PN40024 promoters containing at least one ABRE (light blue (Yes)) and the number of promoter regions that do not contain an ABRE (dark blue (No)).

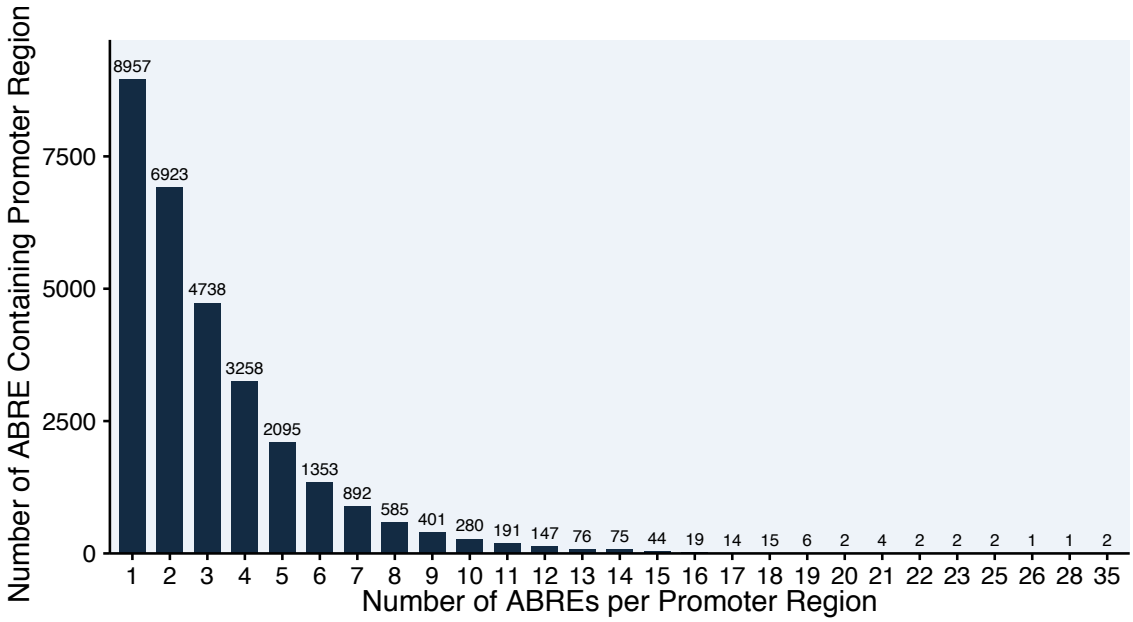

Figure 7: Number of ABREs per promoter region of the total promoter regions containing ABRE(s). The number of ABRE containing promoter regions that contain a certain number (1-23, 25, 26, 28, or 35) of ABREs. Exact numbers indicated over bars.

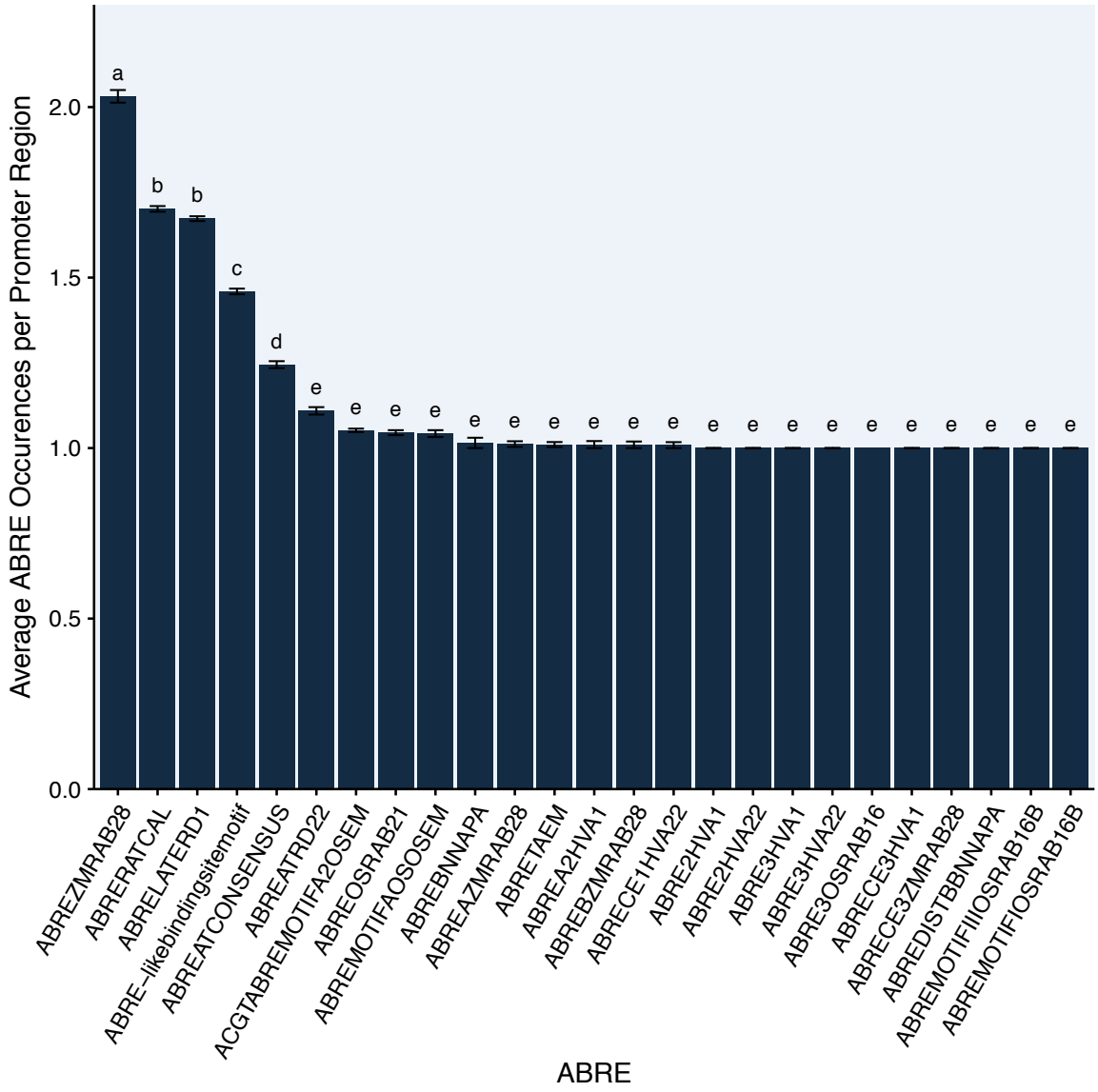

Figure 8: Average consensus ABRE occurrences per promoter region. The average number of occurrences of each consensus ABRE in each promoter region that contained that consensus ABRE. All ABRE variants were combined in consensus ABREs for ABRE-likebindingsitemotif, ABREATCONSENSUS, ABREATRD22, ABREOSRAB21, ABRERATCAL, and ACGTABREMOTIFA2OSEM individually. One-way ANOVA Tukey's HSD ($p \leq 0.05$) letters for consensus ABRE. Mean ± SE, n =1 – 20,356 promoter regions.

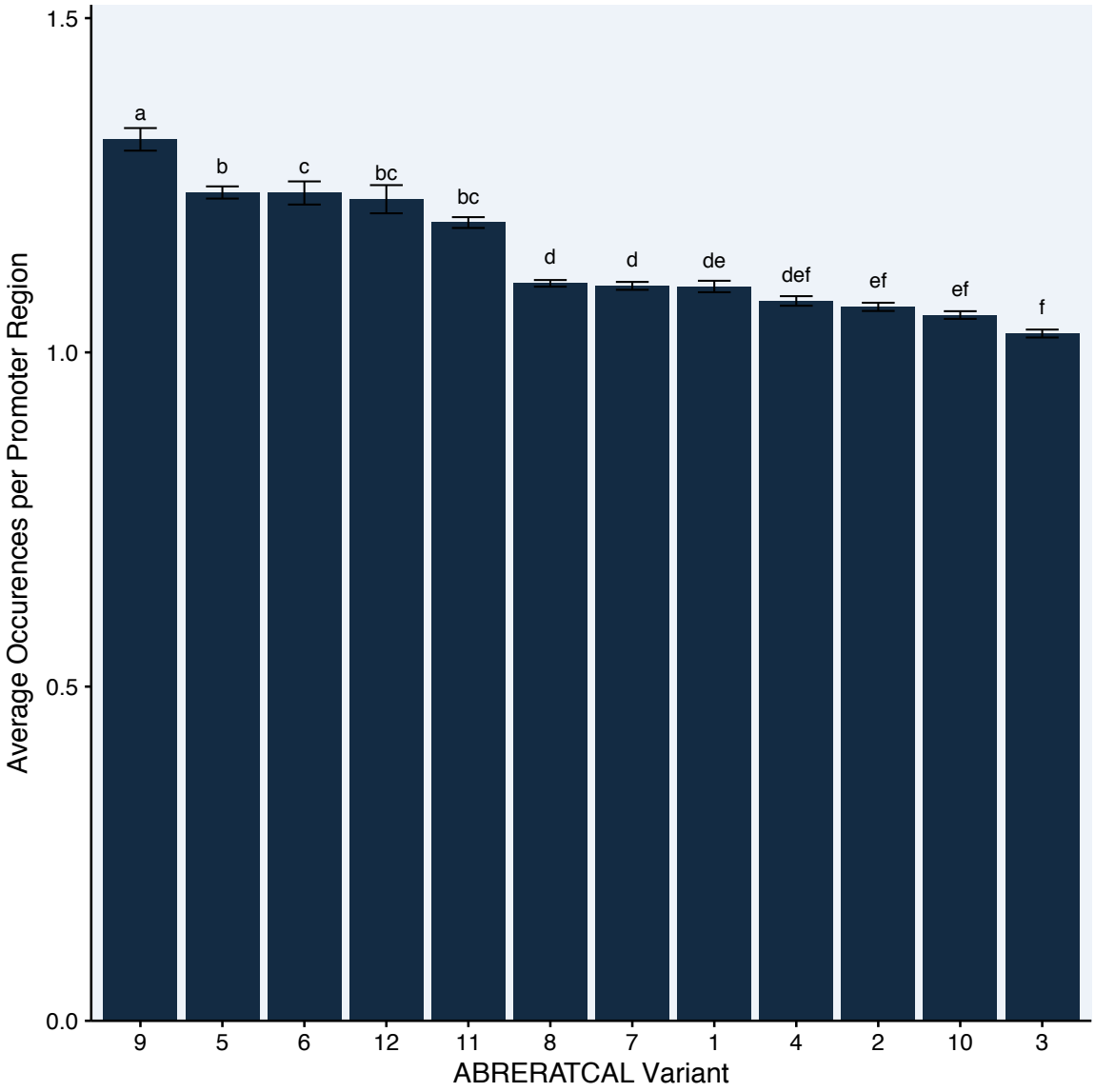

Figure 9: Average occurrences per promoter region for ABRERATCAL variants. The average number of occurrences of each ABRERATCAL variant in each promoter region that contained that ABRERATCAL variant. One-way ANOVA Tukey's HSD ($p \leq 0.05$) letters for ABRERATCAL variant. Mean ± SE, n =781- 4735 promoter regions.

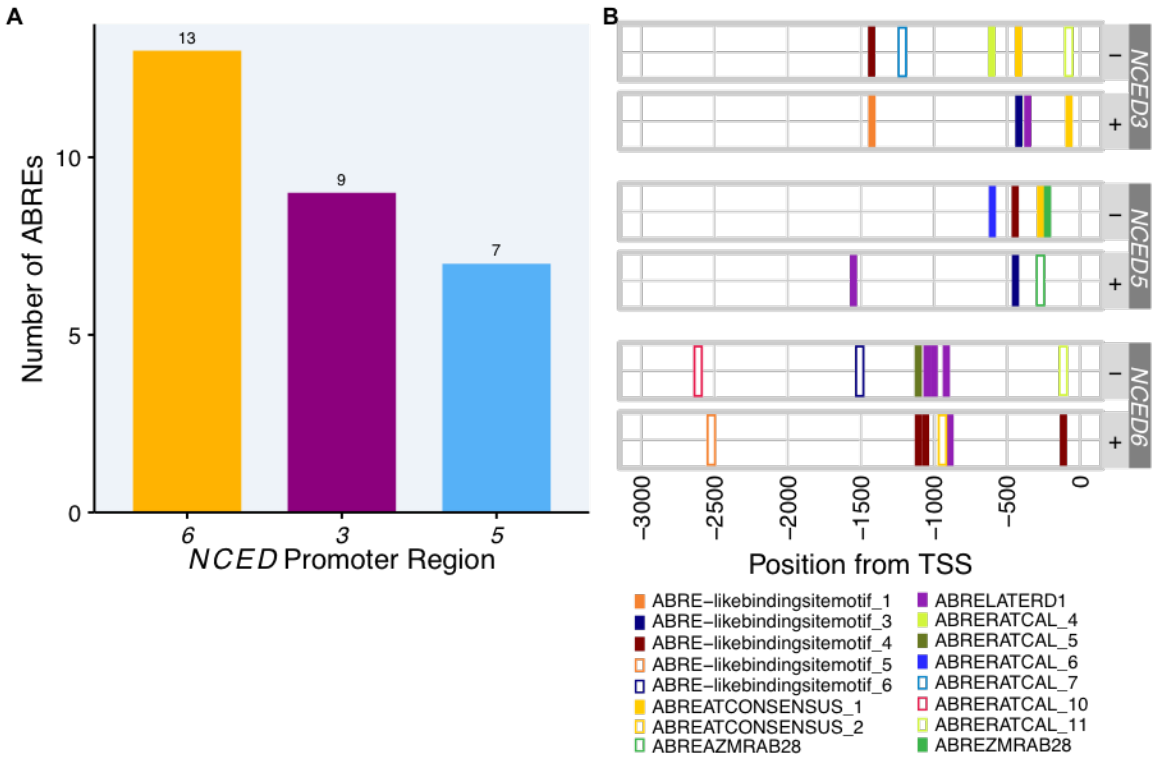

Figure 10: *NCED* Promoter Region ABREs. A) The total number of ABRES in *NCED3*, *NCED5*, and *NCED6* promoter regions. Colors correspond to number of ABREs in each promoter region. **B)** The location and type of each ABRE on the – and + strands of each *NCED* promoter region from 0 (TSS) to -3,000 bp from the TSS. Colors indicate type of ABRE. Partially overlapping ABREs are spread for visualization purposes here. Exact ABRE coordinates are in Supplemental File 1.

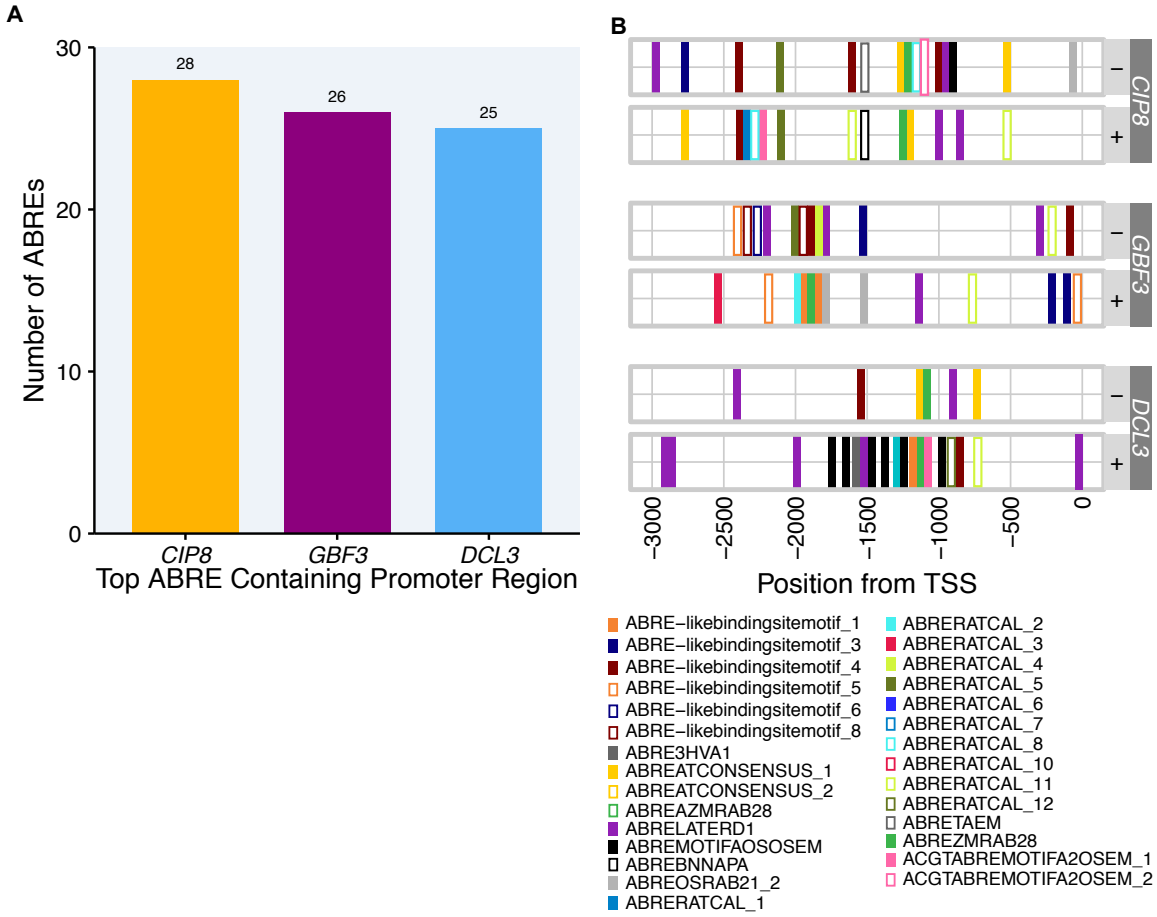

Figure 11: Top ABRE Containing Promoter Regions. A) The total number of ABREs in *CIP8*, *GBF3*, and *DCL3* promoter regions. Colors correspond to number of ABREs in each promoter region. **B)** The location and type of each ABRE on the – and + strands of *CIP8*, *GBF3*, and *DCL3* promoter regions from 0 (TSS) to -3,000 bp from the TSS. Colors indicate type of ABRE. Partially overlapping ABREs are spread for visualization purposes here. Exact ABRE coordinates are in Supplemental File 1.

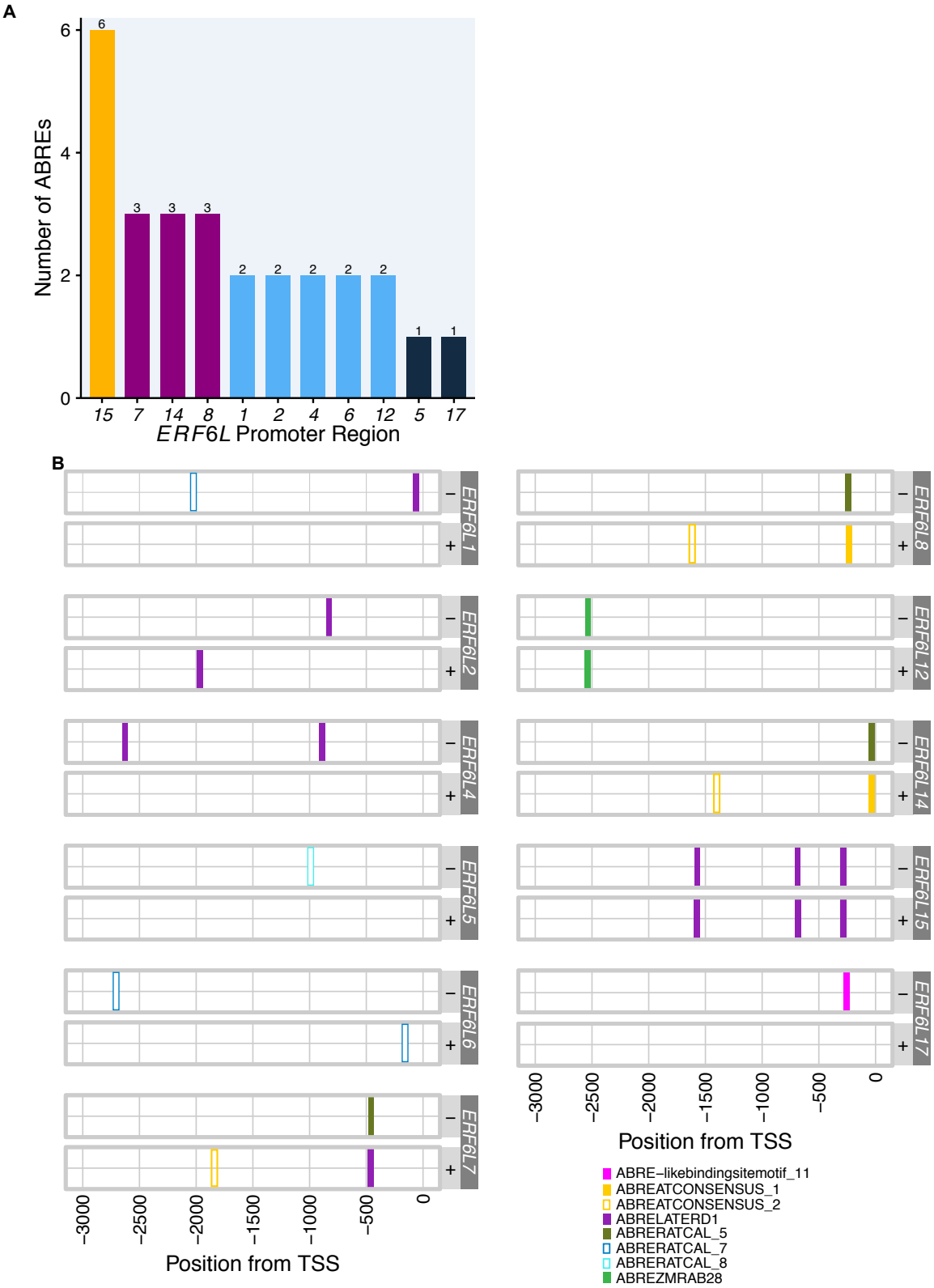
A
Number of ABREs
6
4
2
0
6
3
3
3
2
2
2
2
2
1
1
15 7 14 8 1 2 4 6 12 5 17
ERF6L Promoter Region
B
ERF6L1
ERF6L2
ERF6L4
ERF6L5
ERF6L6
ERF6L7
ERF6L8
ERF6L12
ERF6L14
ERF6L15
ERF6L17
−3000 −2500 −2000 −1500 −1000 −500 0
Position from TSS
ABRE−likebindingsitemotif_11
ABREATCONSENSUS_1
ABREATCONSENSUS_2
ABRELATERD1
ABRERATCAL_5
ABRERATCAL_7
ABRERATCAL_8
ABREZMRAB28

Figure 12: *ERF6Ls* Promoter Region ABREs. A) The total number of ABREs in the *ERF6L* promoter regions. Colors correspond to number of ABREs in each promoter region. **B)** The location and type of each ABRE on the – and + strands of the *ERF6L* promoter regions from 0 (TSS) to -3,000 bp from the TSS. Colors indicate type of ABRE. Partially overlapping ABREs are spread for visualization purposes here. Exact ABRE coordinates are in Supplemental File 1.

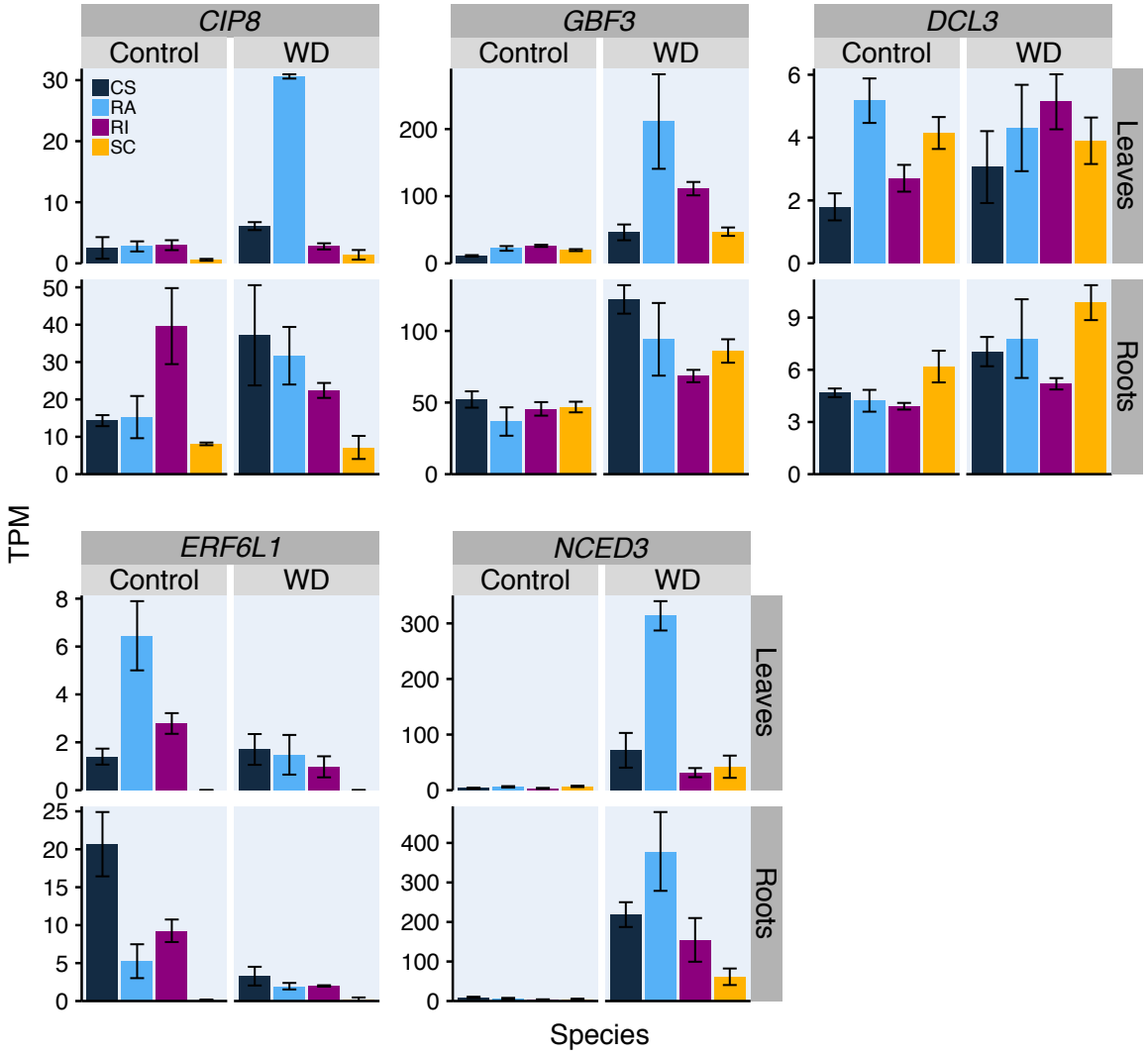

Figure 13: Differentially expressed ABA responsive genes with ABRE containing promoter regions. The expression levels (transcripts per million = TPM) of *CIP8*, *GBF3*, *DCL3* (top from left to right), *ERF6L1*, and *NCED3* (bottom from left to right) in leaves (top) and roots (bottom) for control (left) and water deficit (WD) (right) treated vines after two weeks of treatment. Mean ± SE; n = 3-5 individual vines. Exact expression levels are in Cochetel et al., 2020.

CHAPTER 3:

VviERF6LS: AN EXPANDED CLADE IN *VITIS* RESPONDS TRANSCRIPTIONALLY TO ABIOTIC AND BIOTIC STRESSES AND BERRY DEVELOPMENT

This chapter is based on a manuscript published in *BMC Genomics.*

Toups, H.S., Cochetel, N., Gray, D., and Cramer, G.R. (2020). VviERF6Ls: an expanded clade in Vitis responds transcriptionally to abiotic and biotic stresses and berry development. BMC Genomics *21*.

3.0 Abstract

VviERF6Ls are an uncharacterized gene clade in *Vitis* with only distant *Arabidopsis* orthologs. Preliminary data indicated these transcription factors may play a role in berry development and extreme abiotic stress responses. To better understand this highly duplicated, conserved clade, additional members of the clade were identified in four *Vitis* genotypes. A meta-data analysis was performed on publicly available microarray and RNA-Seq data (confirmed and expanded with RT-qPCR), and *Vitis VviERF6L1* overexpression lines were established and characterized with phenotyping and RNA-Seq. A total of 18 PN40024 *VviERF6Ls* were identified; additional *VviERF6Ls* were identified in Cabernet Sauvignon, Chardonnay, and Carménère. The amino acid sequences of VviERF6Ls were found to be highly conserved. *VviERF6L* transcripts were detected in numerous plant organs and were differentially expressed in response to numerous abiotic stresses including water deficit, salinity, and cold as well as biotic stresses such as red blotch virus, *N. parvum*, and *E. necator*. *VviERF6Ls* were differentially expressed across stages of berry development, peaking in the pre-veraison/veraison stage and retaining conserved expression patterns across different vineyards, years, and *Vitis* cultivars. Co-expression network analysis identified a scarecrow-like transcription factor and a calmodulin-like gene with highly similar expression profiles to the *VviERF6L* clade. Overexpression of *VviERF6L1* in a Seyval Blanc background did not result in detectable morphological phenotypes. Genes differentially expressed in response to *VviERF6L1* overexpression were associated with abiotic and biotic stress responses. VviERF6Ls represent a large and distinct clade of ERF transcription factors in grapevine. The high conservation of protein sequence between these 18 transcription factors may indicate these

genes originate from a duplication event in *Vitis*. Despite high sequence similarity and similar expression patterns, *VviERF6Ls* demonstrate unique levels of expression supported by similar but heterogeneous promoter sequences. *VviERF6L* gene expression differed between *Vitis* species, cultivars, and organs including roots, leaves, and berries. These genes respond to berry development and abiotic and biotic stresses. *VviERF6L1* overexpression in *Vitis vinifera* results in differential expression of genes related to phytohormone and immune system signaling. Further investigation of this interesting gene family is warranted.

3.1 Introduction

Ethylene is a key phytohormone with roles in plant growth and development (Iqbal et al., 2017) as well as abiotic and biotic stress responses (Licausi et al., 2010, 2013; Zhu et al., 2013). *Vitis vinifera* (grapevine) is a non-climacteric fruit that does not ripen with a respiratory burst of ethylene, instead maturing with increased abscisic acid (ABA) concentration. However, ethylene plays an important role in fruit development as berries transition into veraison, the beginning stage of color development and berry softening, initiating ethylene signaling and activating Ethylene Response Factors (ERFs) (Chervin et al., 2004; Leida et al., 2016; Ma et al., 2015). ERFs regulate gene expression of targets including transcription factors like *RESPONSIVE TO DEHYDRATION 29B* (*RD29B*), *LATE EMBRYOGENESIS 4-5* (*LEA4-5*), *HEAT SHOCK PROTEIN 101* (*HSP101*), and other *ERFs*, resulting in physiological responses and adaptations that allow a plant to better

survive under specific environmental conditions like water deficit and high temperature (Müller and Munné-Bosch, 2015). These transcription factors act as major signaling hubs that integrate cross-talk between ethylene and other phytohormones to mediate gene expression (Burg and Burg, 1966; Deslauriers and Larsen, 2010; Divi et al., 2010; Kunkel and Brooks, 2002; Saithong et al., 2015; Sharp, 2002). ERFs belong to the APETELA2/ERF Family consisting of over 122 and 149 genes in Arabidopsis (Nakano et al., 2006) and *Vitis* (Licausi et al., 2010), respectively. This family is divided into 12 subfamilies based on regulatory elements and DNA-binding domains.

Previously, a unique *Vitis* clade was identified in subfamily IX, consisting of 12 members with no Arabidopsis ortholog (Cramer et al., 2014). Sequence analysis revealed these genes most closely resembled *AtERF6*. This clade was named *ERF6-like* (*ERF6L*) after the closest Arabidopsis ortholog, and the genes were numbered from one through twelve based on chromosomal coordinates of the V1 structural annotation V2 assembly of PN40024 (Cramer et al., 2014). Affymetrix and NimbleGen grapevine microarrays with limited probe sets hybridizing to some of the *VviERF6L* genes revealed *VviERF6L* transcription were differentially expressed in berry skins across berry ripening (Cramer et al., 2014) and in leaves in response to severe leaf dehydration (Hopper et al., 2016).

Recently, a new improved structural annotation (V3) of the PN40024 genome (V2 assembly) was released, providing additional gene loci names (Canaguier et al., 2017). In this report, the early observations of the *VviERF6L* clade are investigated further**. These genes were analyzed using the new structural annotation of PN40024 (Canaguier et al., 2017); to better understand the role of this clade in *Vitis*, gene expression patterns were queried in a meta-data analysis, and novel experimental treatments were**

performed. *VviERF6L1* overexpression lines were established and phenotyped. Manual curation of the new structural annotations resulted in the discovery of additional *VviERF6Ls* not previously identified. *VviERF6L* expression was dependent on cultivar, species, organ, hormone, and stress treatments.

3.2 Materials and Methods

Phylogenetic analysis and cis-regulatory element identification of the *ERF6-like* clade

DNA sequences from the *VviERF6-like* clade and *Arabidopsis thaliana* orthologs were obtained from ORCAE and Araport11 and compared to CRIBI and TAIR identifiers, respectively (Berardini et al., 2015; Canaguier et al., 2017; Cheng et al., 2017; Vitulo et al., 2014). Sequences were aligned with MUSCLE using the msa R package and a phylogenetic tree was drawn using a clustal omega alignment in Mega X (Bodenhofer et al., 2015; Kumar et al., 2018). A maximum likelihood method and Jones-Taylor-Thornton matrix-based model with Bootstrapping n=1,000 replicates were used to create a consensus tree consisting of PN40024, CS, CH, and CA VviERF6Ls and PN40024 ERFs. Branches present in <50% bootstrap replicates are collapsed. The initial tree for the heuristic search was generated from the maximum parsimony method. The Subtree-Pruning-Regraftings - Fast (SPR level 3) was used.

Conserved motifs were identified and confirmed in MEME using the standard settings (motif limit at 50 amino acid residues) (Bailey and Elkan, 1994; Bailey et al., 2009). Motifs were characterized with InterPro and modeled in SWISS-Model using standard

settings (Mitchell et al., 2019; Waterhouse et al., 2018). *VviERF6L1* gene upstream regions (-3,000 bp) were obtained with the R package GenomicFeatures (Lawrence et al., 2013). Cis-element enrichment and identification analysis were performed with PLACE (Higo et al., 1999). Promoter regions were aligned, and a phylogenetic tree was made in clustal omega.

Meta-data analysis

RNA-Seq and microarray data sets were downloaded from NCBI GEO (Edgar, 2002) and SRA (Leinonen et al., 2011) with GEOquery (Davis and Meltzer, 2007) version 2.50.5 and the SRA Toolkit version 2.9.2, respectively. Data series that were re-analyzed with the V3 PN40024 annotation were quality checked with fastqc (Babraham Bioinformatics, 2010) and trimmed with trimmomatic version 0.35 (Bolger et al., 2014). Transcript abundance was quantified with Salmon version 0.10.1 (Patro et al., 2017) using quasi-mapping, seqBias, gcBias, fldMean 50, fldSD 1, validateMappings, libType A, and rageFactorizationBins 4. Tximport version 1.10.1 was used to generate the count matrix. Differential expression analysis was performed with DESeq2 version 1.22.2 (Love et al., 2014). Co-expression analysis was performed using WGCNA version 1.68 for all 18 *VviERF6Ls* as a clade as well as for each *VviERF6L* individually using the five data series that were re-analyzed with the V3 annotation of PN40024. The top 100 genes most connected to the *VviERF6L* clade were used to make a Venn diagram (Fig. 13).

Plant transformation

VviERF6L1 CDS was inserted into pECBC under the control of a bi-directional duplex 35S promoter with two PR1B enhancers and fused to EGFP/NPTII (Gray and Zhijian, Li, 2006). Seyval Blanc cell cultures were transformed with *Agrobacterium tumefaciens* and grown under kanamycin selection. The empty vector was also inserted into cells to be used for control plant generation. Transgenic lines were created at the Mid-Florida Research and Education Center for the Institute of Food and Agricultural Sciences. Transgenic cells were confirmed with GFP screening performed with confocal microscopy. Four overexpression lines (L12-1, L12-2, L12-3, L12-11, and L12-23) and one control line (G1) were regenerated into full plants grown under greenhouse conditions.

Plant materials and growth conditions

Own-rooted *Vitis vinifera* (L.) cv. Cabernet Sauvignon clone 8 (CS) was obtained from Inland Desert Nursery (Benton City, Washington, USA). *Vitis champinii* cv. Ramsey (RA), *Vitis riparia cv.* Riparia Gloire (RI), and *Vitis vinifera x girdiana* SC2 (SC) were obtained from the Plant Foundation Services at UC Davis (Davis, CA USA). Mature plants of the five transgenic lines and the four genotypes CS, RA, RI, and SC were grown in Stuewe and Son's tree pots TP915R (22.9 cm x 39.4 cm) containing 1:1:1:2 perlite:peat moss:Grow Mulch (Kellogg):washed sand. Each pot contained ~8.0 kg of soil mix. Mature plants were irrigated with ~1.2 L of pH 5.5 water bi-weekly. Propagates were generated from single-node cuttings of mature plants and transferred in trays containing pH 5.5 water with an air-stone until roots emerged. Plants were transferred to Stuewe and Son's Anderson AB39 pots (7.3 cm x 22.9 cm) consisting of ~1.0 kg quikrete medium grain sand and ~40 g of 50:50 perlite-vermiculite mix. Plants were covered for one week to increase relative

humidity and slowly acclimated to greenhouse humidity conditions for two weeks. Greenhouse conditions were maintained at approximately 21-26.5 °C and 20-50% relative humidity. All pots were elevated 7.5 cm off the floor with perforated black plastic flats. Light was supplemented with 1,000 W high-pressure sodium light bulbs approximately 4.5 m above the floor directly over the center of the experimental area. Supplemental light had a 16:8-hour light-dark cycle. The mid-day light intensity of the greenhouse averaged 1200 $\mu E\ m^{-2}\ s^{-1}$. Propagates were irrigated every other day (until they reached approximately 70 cm height at which point the experimental treatment began) with Cramer's complete nutrient solution (1.5 mM $Ca(NO_3)_2$, 2 mM KNO_3, 0.6 mM $MgSO_4$, 1 mM KH_2PO_4, 1.5 mM $CaCl_2$, 36 µM Fe_2^+ Sprint 330, 1 µM $MnSO_4$, 0.5 µM $CuSO_4$, 20 µM $ZnSO_4$, 20 µM H_3BO_3, and 0.01 µM $(NH_4)_6Mo_7O$).

Phenotypic characterization of *ERF6L1* overexpressing lines

Mature transgenic plants were grown as a single shoot. Weekly measurements were taken for stem length, number of nodes, internode length, number of leaves, leaf length (from petiole attachment point to the tip of the leaf down the midvein), leaf width (from one side of the leaf to the other at the widest point perpendicular to the midvein), leaf lobe sinus lengths and angles, leaf surface area, tendril emergence, and berry development (berry occurrence and circumference). Berry occurrence, number, and circumference were photographed and quantified with ImageJ. Stem elongation rate was calculated from repeated stem length measurements. Leaf surface area was obtained from photographs using ImageJ version 1.52h (Schneider et al., 2012). Leaf measurements were performed weekly on at least ten plants per line and repeated continuously over at least six months.

All measurements were performed on similar nodes to ensure uniform developmental stages. Shoots were pruned when the plant height reached one meter, at which time, measurements were repeated as a new shoot emerged at the cane. Leaf length measurements were repeated over three years. To phenotype roots, overexpression line propagates were transferred to 12 L hydroponic tubs containing an air-stone and 0.5x strength Cramer's complete nutrient solution when roots were ~5 cm. Propagates were placed in tight-fitting lids and allowed to grow for twenty days under greenhouse conditions. Roots were imaged and analyzed with WinRHIZO every five days. Measurements included total root length, total root surface area, number of primary lateral roots, number of adventitious roots, and plant fresh weight. Two mature leaves at a similar developmental stage from each transgenic line from three individual cloned plants were excised from mature plants and frozen in liquid nitrogen for RNA sequencing.

Abiotic stress and hormone treatments

Treatments consisted of control treatment that entailed irrigating plants daily with 100 mL complete nutrient solution under greenhouse conditions (control); a salinity treatment: that was irrigating plants daily with 100 mL complete nutrient solution with 100 mM NaCl and 20 mM $CaCl_2$ added; a cold treatment: that was growing plants in a 10 °C growth chamber with a light intensity 250 μE and irrigating daily with 100 mL 10 °C complete nutrient solution; a water deficit treatment: that was maintaining pots at a low 30% relative water content. Water deficit pots were dried down to 30% relative water content by withholding irrigation at which point they were maintained daily at 30% pot relative water content, for one and two weeks. Control plants were watered in excess daily. After twenty days of salt,

cold, and control treatment, four experimental replicates of individual G1, L12-1, L12-2, L12-3, L12-11, and L12-23 vines were harvested. After one and two weeks of control and water deficit treatment, five experimental replicates of G1, L12-1, L12-2, L12-3, L12-11, and L12-23 individual vines were harvested. Shoot, stem, leaf, and root fresh and dry weights were measured in addition to total canopy surface area measured from photographs with ImageJ.

To examine *VviERF6L1* response to hormones, CS leaves were sprayed with 10 µM ProTone (s-ABA) (Valent BioSciences LLC) or water (control) for 1 hour. All sprays contained 0.5% Tween20. For spray treatments, mature leaves were selected and sprayed to saturation (solution dripping from leaves) on both sides of the leaf (Rattanakon et al., 2016). All samples were frozen in liquid nitrogen for all treatments. These experiments were performed in triplicate with each round consisting of three individual leaves of similar developmental stage from separate plants per genotype per harvest-time. Different sprays were made for each round.

Chilling treatments were performed on CS, RA, RI, and SC plants placed in a 4 °C growth chamber with a light intensity of ~200 µmol m^{-2} s^{-1} in a randomized block experimental design. Eight thermometers were placed evenly throughout pots in the growth chamber. Pot temperature was recorded before each harvest time. Control plants were kept under greenhouse conditions. Total leaves were harvested within two minutes after two hours of chilling treatment and frozen in liquid nitrogen. These experiments were performed in triplicate with each round consisting of three individual plants per genotype per harvest-time per treatment. Additional chilling treatments were performed in a 4 °C refrigerator. RA and CS leaves of comparable age and size were placed on a wire support

in pre-chilled or control Tupperware boxes containing 200 mL DI water similar to what has been described previously (Hopper et al., 2014). Petioles were placed in the water and lamina was supported by the wire rack above the water. A light-proof cardboard box was placed over the leaf-containing Tupperware box to prevent light intrusion. Control samples were placed under a light-proof box at 23 °C. Leaves were harvested within two minutes after two hours of temperature treatment and frozen in liquid nitrogen.

RNA extraction

All samples were ground with a mortar and pestle under liquid nitrogen. RNA extraction for RNA-Seq samples was performed with a CTAB-based method including an RNase-free DNase treatment as previously described (Ghan et al., 2017). RNA-Seq samples were prepared from 1.3 µg RNA. Quality and concentration were confirmed with Ribogreen technology performed by the Nevada Genomics Center and Experion RNA StdSens Chips (Bio-Rad).

RNA from leaves of the plants treated with either abiotic or hormone treatment was extracted with a Spectrum Total Plant RNA kit (Sigma-Aldrich) modified protocol (Cookson et al., 2013). All RNA extractions were treated with RNAse-free DNase I (Qiagen) to remove genomic DNA contamination. RNA concentration, quantity, and purity for all samples were confirmed with a Nanodrop spectrophotometer, a 1.2% quality gel loaded with 400 ng RNA from each sample, and a 2% gel loaded with 10 µL LAR intron PCR product. LAR PCR products were amplified from a 10 µL GoTaq Green Master Mix (Promega) containing 250 ng RNA and 0.5 µM forward and reverse primers specific for a LAR intron. The PCR reaction included 95 °C for 2 min, 35 cycles of 95 °C for 30 s, 62

°C for 25 s, and 72 °C for 25 s. Purified samples demonstrating two bands corresponding to ribosomal subunit RNA, no band corresponding to the LAR intron, and sufficient concentration were utilized for RT-qPCR.

PCR and RT-qPCR

All samples from cold and hormone spray experiments were reverse transcribed with iScript Reverse Transcriptase Supermix (Bio-Rad) according to the manufacturer's instructions from 2 µg RNA. Primers were designed using NCBI Primer-BLAST. Primer sequences are provided in Appendix 18. Primer efficiencies were verified on purified PCR products (Machery-Nagel NucleoSpin® Gel and PCR Clean-up kit) and will be considered at 100% for the gene expression calculations. All reactions were performed on a Bio-Rad Real-Time thermal cycler CFX96 with the following protocol: 95 °C for 3 mins; 40 cycles of 95 °C for 10 s, 60 °C for 15 s. Fluorescence was recorded after each cycle, and melting curve analysis was performed from 65 °C to 95 °C. Reference genes were selected based on a low coefficient of variation of expression reported in literature and uniform expression for all cDNA samples for each of the above-described experiments.

VviERF6L1 overexpression was tested upon receival of transgenic plants with PCR of GFP and semi-quantitative PCR of *VviERF6L1*. GFP expression was confirmed with PCR (95 °C for 2 min, 35 cycles of 95 °C for 30 s, 58 °C for 30 s, 72 °C for 30 s) using GFP specific primers. Semi-quantitative PCR was performed on 1.0 µg of reverse-transcribed RNA from two leaves of three individual plants per line with gene-specific primers. The reaction consisted of 7 µL 10-fold diluted cDNA, 3.5 µL each 10µM forward and reverse primers, 35 µL GoTaq Green Master Mix (Promega), and 21 µL DEPC water.

Samples collected at cycles 23, 26, 29, 32, and 35 were run on 2% agarose gels stained with ethidium bromide to compare *VviERF6L1* amplification in overexpression lines relative to the empty vector control normalized to a ubiquitin reference gene. Several years after receival of the transgenic lines, stable overexpression was confirmed by RT-qPCR performed on 1.5 µg cDNA from three individual leaves harvested on 3 separate plants for each line with gene-specific primers as before (Rattanakon et al., 2016). RT-qPCR was performed on cDNA samples reverse transcribed from 1.3 µg template RNA with iScript reverse transcriptase supermix (Bio-Rad) according to the manufacturer's instructions using *VviGAPDH* and *VviACT7* as reference genes. RT-qPCR was conducted with SYBR Green Master Mix (Bio-Rad) for initial confirmation of overexpression lines and to confirm results on the same samples analyzed with RNA-Seq. All other RT-qPCR was performed with 2 µg of RNA reverse transcribed to cDNA with iScript Reverse Transcriptase Supermix (Bio-Rad) according to the manufacturer's instructions. RT-qPCR was conducted for overexpression confirmation, chilling, ABA, and respective control treatments with SYBR Green Master Mix (Bio-Rad). RT-qPCR was conducted to confirm *VviERF6L1* expression and for cold treatments and controls with GoTaq® qPCR Master Mix (Promega). Normalized relative quantity was calculated according to Hellemans *et al*. (Hellemans et al., 2007). *VviACT7* and *VviGAPDH* were used as reference genes for the ABA treatment. *VviABF2* was used as a positive control gene for the ABA treatment. *VviUbi* and *VviACT7* were used as reference genes, and V*viCBF1* was used as a positive control gene.

RNA-Seq analysis of *VviERF6L1* overexpression lines

Leaf RNA samples from three individual L12-3, L12-11, L12-23, and G1 vines were sequenced with Illumina TruSeq 2500 at the University of California, Los Angeles Genomic Center, to produce 36 bp single-end reads. Each sample was sequenced on two different lanes (technical replicates). Read quality for each sample was verified with FastQC version 0.11.8 before and after trimming adaptors based on released adaptor sequences (Babraham Bioinformatics, 2010). Sample 12-23-2_S8 had ~4.4 % library size compared to the average library size of the other samples and was excluded from further analysis. Over-represented sequences were extracted and identified with blast+ version 2.8.0 alpha (Camacho et al., 2009). Reads from both sequencing lanes were concatenated per sample. Transcript abundance was quantified with Salmon with standard settings for single-end reads (Patro et al., 2017). Tximport version 1.8.0 (Soneson et al., 2015) followed by DESeq2 version 1.20.0 (Love et al., 2014) were implemented to perform differential expression analysis. Venn diagrams were created in R with the package limma version 3.36.5 (Ritchie et al., 2015). Heatmaps were created in R with ComplexHeatmap (Gu et al., 2016).

Statistical analysis

Statistical analysis performed to compare multiple means included the student t-test, one- and two-way ANOVA's followed by Tukey's HSD test after assumptions were met. Letters or asterisks indicate statistical significance between the specified comparisons. The error rate $\alpha = 0.05$ was used in all comparisons. Statistical analyses were performed using R version 3.4.3.

3.3 Results

The *VviERF6L* clade was expanded to 18 members in the PN40024 reference genome

Novel *VviERF6Ls* genes were discovered by manually searching for conserved amino acid (AA) motifs in the newly annotated PN40024 genome. Along with the 12 previously identified *VviERF6L* genes (Cramer et al., 2014), five additional genes were first identified (Table 1) from this manual curation. These additional genes were identified in unannotated sections of chromosome sequences by searching for specific AA motifs across the individual chromosomes using tools in ORCAE (Sterck et al., 2012) where the reference grape genome sequence, PN40024, is stored. Structural models were confirmed in ORCAE using both mRNA (Jaillon et al., 2007) and expressed sequence tag (EST) data to confirm 5' and 3' ends of annotated sequences (Grimplet et al., 2012).

An additional VviERF6L was identified with an *in-silico* detection strategy. The manually curated VviERF6Ls were confirmed and substantiated as members of this clade from protein motifs identified in MEME (Bailey et al., 2009; Gupta et al., 2007). MEME revealed VviERF6L proteins consist of nine highly conserved AA motifs (Fig. 1, Supplemental File 1 and Appendix 1). The nine motifs are referred to in order of E-value with the lowest value motif corresponding to Motif 1 (Appendix 1). To identify additional novel *VviERF6Ls* that may have been overlooked with the manual annotation, an *in-silico* detection strategy was devised using the first (Motif 5) and last (Motif 4) spatial AA motifs to query the *Vitis* proteome. Genome coordinates that contained either the first, last, or both

motifs were extracted corresponding to the potential proteins containing the motif(s) of interest. When only the first or the last motif was detected, the putative protein sequence was extended to 280 AA to obtain the potential full-length protein. This strategy confirmed the five novel *VviERF6L* genes from the manual curation and identified a sixth, increasing the members of the *VviERF6L* clade from 12 in the V1 annotation to 18 in the V2 assembly of PN40024 (Table 1).

The nine VviERF6L protein motifs were detected as being significantly present ($p < 1.73x10^{-179}$) and conserved ($E < 8.8x10^{-14}$) among the 18 VviERF6Ls (Appendix 1). These proteins had an average length of ~280 AA with the longest and shortest motifs (Motif 1 and Motif 9) having lengths of 50 and 7 AA, respectively (Appendix 1), resultant of the MEME settings used. Specific VviERF6L protein motif sequence and location per VviERF6L can be found in Appendix 2. Four protein motifs were identifiable and had previously been characterized as regulatory domains of other ERF Group IX TFs (Fig. 1) (Nakano et al., 2006). These protein motifs included the AP2/ERF domain (DNA-binding; Motifs 1 and 2), the CMIX-2 (N-terminal acidic transactivation; Motif 5) the CMIX-5 (MAP kinase phosphorylation site; Motif 4), and the CMIX-6 (MAP kinase phosphorylation site; Motif 9) domains (Fig. 1). Motifs 1, 2, and 7 were present in all eighteen VviERF6Ls. Motifs 3, 4, 5, 6, and 9 were present in 77.8% of VviERF6L proteins, and Motif 8 was present in nine of the 18 VviERF6Ls (calculated from Supplemental File 3).

The VviERF6L AP2/ERF domain is homologous to that of Arabidopsis (At)ERF1 and 096. To identify VviERF6L sequence conservation with proteins in *Arabidopsis thaliana*, the nine motifs were queried in InterPro and the AP2/ERF domain was modeled

in SWISS-model (Mitchell et al., 2019; Waterhouse et al., 2018). The AP2/ERF domain (Motifs 1 and 2) of VviERF6L1, 2, 3, 4, 5, 6, 7, and 13 had the closest identity with that of AtERF1 with an average identity of 75.5% (Appendix 3). VviERF6L8, 9, 10, 11, 12, 15, 16, 17, and 18 had an average identity of 70.8% with the AtERF096 AP2/ERF domain, identified as the closest ortholog (Appendix 3).

VviERF6L12 and 14 appear to be truncated proteins. VviERF6L14 lacks the first 4 N-terminal motifs (Fig. 1), with no matching publicly available RNA-Seq or EST reads and insufficient sequence information in this region of the PN40024 genome in ORCAE. Besides *VviERF6L15*, *VviERF6L14* is the only other non-mono-exonal *VviERF6L*. The true start codon of *VviERF6L14* may exist in what is currently the un-sequenced region that is presently annotated as an intron and can be viewed in ORCAE (Sterck et al., 2012). Despite potential mis-annotation of *VviERF6L14* gene coordinates, promoter (see later) and protein motif analysis (Fig. 1, Supplemental File 1, and Appendix 1) validate this gene as a *VviERF6L*. VviERF6L12 appears to be a functional truncated protein (Fig. 1), supported by mRNA and EST read mapping across the length of the transcript in ORCAE. VviERF6L12 lacks the first 4 N-terminal motifs, which correspond to potential regulatory domains including the CMIX-2 domain (Fig. 1). VviERF6L12 is also missing Motif 4 corresponding to a CMIX-5 domain. VviERF6L3, 6, 9, 11, 13, 16, and 18 do not share consensus Motif 8 (Fig. 1). These proteins have higher amino acid variability in this region. VviERF6L10, 15, and 17 are also missing Motif 4 (Fig. 1).

The 18 VviERF6L proteins are a conserved clade. A multiple sequence comparison by log-expectation (MUSCLE) multiple sequence alignment (MSA) was performed to better understand the diversity within the VviERF6L clade. Percent identity was extracted

from a MUSCLE alignment (Fig. 2). The 18 VviERF6Ls share high sequence conservation (average of 73.8%), with VviERF6L12, one of the truncated VviERF6Ls, diverging the most with an average percent identity of 50.9% (calculated from Fig. 2).

The *VviERF6L* clade is expanded in *Vitis vinifera* relative to other plant species. The number of *ERF6L* paralogs was identified in the species that had the genes with the highest orthology to *VviERF6L1* from the Pan-taxonomic Compara Gene Tree in Gramene update 2018 containing 44 genomes (Tello-Ruiz et al., 2018) including the V1 annotation of PN40024 (Jaillon et al., 2007). The number of potential *ERF6L* orthologs was quantified in carrot (*D. carota*), soybean (*G. max*), tomato (*S. lycopersicum*), and potato (*S. tuberosum*) (Supplemental File 2). *Vitis vinifera* had 4.5-fold more *ERF6L* paralogs than tomato and potato, 9-fold more than soybean, and 17 more potential *ERF6L* genes than carrot (Supplemental File 2).

The *VviERF6L* clade is expanded across *Vitis* genotypes

Additional *VviERF6L*s were identified in the translated Cabernet Sauvignon (CS) genome (Chin et al., 2016) indicating the *VviERF6L* clade members vary with grape genotypes. The nine PN40024 VviERF6L protein motifs were utilized to detect *VviERF6Ls* in the proteome sequence of CS using TOMTOM (Gupta et al., 2007). Translated genes that contained at least three of the nine PN40024 VviERF6L protein motifs were extracted and analyzed with MEME as potential VviERF6Ls. These genes were used to identify CS-specific VviERF6L protein motifs. TOMTOM used the CS cultivar specific VviERF6L protein motifs to identify additional potential CS VviERF6Ls that were missed using the nine PN40024 motifs (Appendix 2 and Supplemental Files 3-5 and Appendix 4). Thirteen

highly conserved ($E < 1.3x10^{-2}$) CS protein motifs (Appendix 1) were identified. The CS protein motifs were very similar to those of PN40024 (Supplemental Files 1, 4, and 5 and Appendix 5). Homology between PN40024 and CS VviERF6L protein motifs was quantified with protein BLAST (Altschul et al., 1990) (Appendix 5). CS Motifs 1-6 shared 100% identity with corresponding PN40024 motifs, and CS Motif 7 shared ~71% with PN40024 Motif 9 (Appendix 5). In total, 26 CS VviERF6Ls were identified (Appendix 4 and 6 and Supplemental File 5). Interestingly, unique *VviERF6L* sequences were identified in CS like VvCabSauv08_H0036F_008.ver1.0.g139880, which appears to be a novel *VviERF6L* not conserved in PN40024 (Supplemental File 6 and Appendix 7). Lengths of CS VviERF6L proteins are in Appendix 6. CS VviERF6Ls (~300 AA residues) were on average 20 AA residues longer than PN40024 VviERF6Ls (~280 AA residues) (Table 1 and Appendix 6). CS lacked paralogs similar to PN40024 VviERF6L3, 8, 11, and 14 and had distinct VviERF6Ls (like VvCabSauv08_P0367F.ver1.0.g601540 and VvCabSauv08_H0036F_008.ver1.0.g139880), without a clearly distinguishable PN40024 equivalent. VvCabSauv08_H0036F_008.ver1.0.g139910 (596 AA residues) contained duplicated Motif 1-4, 5-9, and 11 (Supplemental File 3 and 9). VvCabSauv08_H0036F_008.ver1.0.g139950 (839 AA residues) consisted of duplicate Motif 1, 2, 7, and 12 and triplicate Motif 3, 5, 6, and 11. These two genes were about two and three times the length of the average CS VviERF6L (~300 AA residues (calculated from Appendix 5)), respectively. VvCabSauv08_H0036F_008.ver1.0.g139990 was a severely truncated VviERF6L (106 AA residues), completely lacking any conserved N-terminal motif (Supplemental Files 3 and 5). VvCabSauv08_P0070F.ver1.0.g450750 was of comparable length (243 AA residues) to the average CS VviERF6L, but this gene had a

more variable sequence, containing only four of the thirteen conserved motifs (Supplemental Files 3 and 5).

Chardonnay (CH) (Zhou et al., 2019) and Carménère (CA) (Minio et al., 2019a) also have expanded *VviERF6L* clades with 15 and 14 *VviERF6Ls* respectively (Supplemental File 6 and Appendix 7). VviERF6Ls from PN40024 and CS were queried in protein BLAST in genome sequences of CH and CA to identify VviERF6Ls in these genotypes. The genomes of CH and CA were not released at this time; only BLAST was publicly available. Additional novel *VviERF6Ls* may exist in these genotypes, which may be identified using the motif detection strategy described for PN40024 and CS when the genomes become fully available.

The PN40024, CS, CH, and CA VviERF6Ls were more similar across *Vitis vinifera* genotypes than to other VviERF proteins (Supplemental File 6). To distinguish relationships between the highly homologous members of the VviERF6L clade in the AP2/ERF subfamily IX (Cramer et al., 2014), a maximum likelihood phylogenetic tree was generated from *Vitis vinifera* PN40024, CS, CH, and CA VviERF6L paralogs and PN40024 VviERF proteins (gene names and protein sequences available in Appendix 7). The tree was created using the Jones-Taylor-Thornton model with the Bootstrap method test in MEGA X (Kumar et al., 2018). Sequences were extracted from the PN40024 V2 assembly V3 structural annotation (Canaguier et al., 2017), CS genome (Chin et al., 2016), CH BLAST-tool (Zhou et al., 2019), and the CA BLAST tool (Minio et al., 2019a). All predicted VviERF6L proteins grouped together from the four genotypes examined (Supplemental File 6). Vitvi05g01525, corresponding to a putative disease-related PRF protein (Grimplet et al., 2012), clustered with CH and CA VviERF6Ls in the multi-

genotype VviERF6L clade. This gene is inadequately sequenced on ORCAE, having 4,512 N's in the coding sequence, and it is unclear if this gene is correctly positioned or annotated. The *VviERF6L* clade is distinct from other members of the AP2/ERF family (Supplemental File 6), and the VviERF6L protein sequences are highly conserved.

VviERF6L promoter regions are distinct with several conserved motifs

The PN40224 *VviERF6Ls* have variable promoter regions with several conserved and repeated cis-acting elements. To gain insight into the transcriptional regulation of the highly conserved *VviERF6L* genes in the PN40024 genome, -3000 bp upstream from the transcription start site (TSS) for the 18 PN40024 *VviERF6Ls* was analyzed with PLACE (Higo et al., 1999), and a multiple sequence alignment was performed to compare the putative promoter regions (Fig. 3). These regions showed greater diversity than VviERF6L protein sequences, averaging 48.7% relative to 81.05% identity (calculated from DNA sequences). PN40024 *VviERF6L* promoter region motif coordinates are in Appendix 8. A total of 200 known motifs were identified in the *VviERF6L* -3,000 bp putative promoter regions (calculated from Appendix 8). Of these cis-elements, 42 were present in all *VviERF6L* upstream regions (Appendix 9). The CAATBOX1 was the most over-represented motif across *VviERF6L* putative promoters, repeated 885 times, followed by DOFCOREZM (864 repetitions) and CACTFTPPCA1 (845 repetitions) (Appendix 9). These three motifs had an average of ~46 repeats per *VviERF6L* promoter. Numerous other cis-elements were repeated hundreds of times including ARR1AT and MYCCONSENSUSAT motifs.

Although the *VviERF6Ls* shared several highly repeated cis-regulatory elements, there were numerous differences across the *VviERF6L* promoter regions. The *VviERF6L12* promoter region contained the highest number of ROOTMOTIFTAPOX1 (82 repeats), with the closest *VviERF6L*, *VviERF6L14* having 41 repeats, and the other *VviERF6Ls* having even fewer. The *VviERF6L12* promoter region also had the most duplication of TATABOX3, ACGTATERD1 (analogous with *VviERF6L1*), SEF1MOTIF, SEF4MOTIFGM7S, WBOXATNPR1, and LECPLEACS2 (Supplemental File 7 and Appendix 9). Three unique motifs were detected in the promoter region of *VviERF6L12* that were not present in any other *VviERF6L* promoter: ABREZMRAB28, PALBOXLPC, and UP1ATMASD (Appendix 8). Although the VviERF6L protein sequences are highly conserved, there is considerable variation in the *VviERF6L* promoter regions, indicating these genes are under unique transcriptional regulation.

VviERF6L **genes are expressed in many organs and tissues**

Examining the grapevine gene atlas (Fasoli et al., 2012), *VviERF6Ls* were expressed in numerous grapevine organs, across developmental stages, and in tissues including berries, stamen, buds, tendrils, flowers, pollen, seeds, leaves, and roots (Appendix 10). *VviERF6L1*, *5*, and *12* were the most commonly expressed *VviERF6Ls* across various tissues. *VviERF6L6*, *10*, and *11* were less broadly expressed across tissues. *VviERF6L6* was only expressed in the rachis, carpel, petal, leaves, roots, and buds while *VviERF6L10* and *11* were expressed in these tissues as well as berry flesh. *VviERF6L8* was expressed in the same number of tissues as *VviERF6L2* and *3* and comparable to *VviERF6L4* and *7*. Breaking down the berry into pulp, seed, and skin *VviERF6Ls* generally

had significantly higher expression in the skin at pre-veraison and seed at maturity when the berries are red, soft, and ready to harvest (RSH) (Supplemental File 8) [GSE49569] (Gouthu et al., 2014). *VviERF6L12* was the only *VviERF6L* to increase signal intensity in the pulp as berries developed, and this gene maintained the highest expression level in all berry tissues at all developmental stages.

VviERF6L meta-data analysis parameters

VviERF6L expression was extensively examined across existing transcriptomic data in the literature. To better differentiate and understand the potential functional roles of *VviERF6L* genes in *Vitis*, *VviEFRF6L* gene expression was examined in a meta-data analysis of *VviERF6L* gene expression performed using 75 publicly available microarray and 24 RNA-Seq data series downloaded from NCBI Gene Expression Omnibus (GEO) (Edgar, 2002) and Sequence Read Archive (Leinonen et al., 2011) databases. The following data are examples of results found, but many other datasets demonstrate similar patterns. The example data series selected are simplified for visualization purposes. The data series (Appendix 11) investigated for *VviERF6L* gene expression met the following criteria: the experiment contained at least three individual biological or experimental replicates, *VviERF6L* gene expression was detectable, and at least one *VviERF6L* was a differentially expressed gene (DEG) in the author's original differential expression analysis (DEA). Results are discussed based on the author's original DEA and statistical analysis unless otherwise specified.

Four and twelve probe sets were utilized on the grape Affymetrix and NimbleGen microarrays, respectively, with possible cross-hybridization occurring amongst the 18

PN40024 *VviERF6L*s (Cramer et al., 2014). Numerous occurrences of probe cross-hybridization for NimbleGen microarrays of the *VviERF6L* genes were previously determined (Cramer et al., 2014) (Appendix 12), making it important to consider these results in terms of the *VviERF6L* clade response as opposed to individual gene responses. With the short-read length of the RNA-Seq data sets analyzed here and the high homology of the *VviERF6Ls*, it is unclear how distinguishable *VviERF6Ls* are individually in the RNA-Seq analysis.

Data series are referred to as in original publications. SRP117281, PRJNA516950, GSE67191, GSE62744, and GSE62745 were chosen as representative RNA-Seq data series of abiotic stress, berry development, and biotic stress to re-analyze with the V3 structural annotation of PN40024. The data series selected for re-analysis with the V3 structural annotation of PN40024 were used for weighted gene co-expression network analysis (WGCNA) to identify genes that share the same expression pattern as the *VviERF6Ls* under various stress conditions and developmental stages. All other data series demonstrated in the figures were graphed based on the original author's transcript abundance quantification and statistics.

***VviERF6L* genes are involved in multiple abiotic stress responses**

***VviERF6L* genes respond to water deficit and salinity**

VviERF6Ls were differentially expressed in response to numerous abiotic stresses including water deficit and salinity. *VviERF6Ls* were significantly differentially expressed in CS leaves exposed to rapid dehydration for one hour (Fig. 4) [GSE78920] (Hopper et al., 2016). The *VviERF6Ls* shared the same general expression pattern in response to rapid

dehydration with a significant increase in transcript abundance early in the experiment followed by decreased transcript abundance and plateauing thereafter. *VviERF6L12* and *9* demonstrated the highest and lowest levels of expression respectively. *VviERF6L1* was among the most responsive *VviERF6Ls*, increasing quickly to the severe stress within one hour of treatment and decreasing at all time points after that to eventually be at the same level of expression as control plants after 24 hours of treatment. *VviERF6L1* was chosen as a representative gene of the *VviERF6L* clade for subsequent RT-qPCR and overexpression experiments. RT-qPCR was performed for *VviERF6L1* on CS leaves treated with 10 µM Protone (s-ABA). *VviERF6L1* transcript abundance in CS leaves did not respond to ABA treatment (Supplemental File 9), indicating the water deficit response may follow an ABA-independent pathway.

CS shoot tips exposed to a severe 16-day salt and water deficit treatment also show significantly increased *VviERF6L* transcript abundance (Fig. 5) (Cramer et al., 2007). Probe sets 1618661_s_at (*VviERF6L12*) and 1619390_at (*VviERF6L11*) were highly induced by extreme water deficit and salt stress, but 1613698_at (cross-hybridizes to *VviERF6L2 and VviERF4*) and 1613799_at (*VviERF6L3*) were not induced. The accumulation of *VviERF6L* transcripts on day 16, the point at which both abiotic stresses were most severe indicates some *VviERF6Ls* may play a role in extreme salt and water deficit responses in grapevine.

VviERF6L differential expression in response to water deficit is supported by recent more comprehensive RNA-Seq data in which four *Vitis* species (*Vitis vinifera* cv. CS, *Vitis champinii* cv. Ramsey (RA), *Vitis riparia* cv. Riparia Gloire (RI), and *Vitis vinifera x Vitis girdiana* cv. SC2 (SC)) were treated with well-watered and moderate water deficit (WD)

conditions in the form of a natural dry-down for two weeks (Cochetel et al., 2020). The grapevines demonstrated significantly differential *VviERF6L* expression patterns within each species (Fig. 6). For example, *VviERF6L1* was not expressed in SC, but it was expressed in the three other species. Within each Species x Organ x Treatment group, the 18 *VviERF6Ls* followed similar expression patterns to each other (Fig. 6). *VviERF6Ls* were differentially expressed in leaves and roots in response to the WD (Fig. 6). *VviERF6Ls* were significantly more highly expressed in roots than in leaves. Consistently, the *VviERF6Ls* had higher expression in roots than leaves under both Control and WD conditions (13 average TPM (standard error of the mean (SEM) = ± 1.5) vs 4.6 average TPM (SEM = ± 0.51) for roots and leaves, respectively). As a general trend *VviERF6L* transcripts were decreased in response to WD (e.g. *VviERF6L1*). The majority of *VviERF6Ls* have relatively low expression levels apart from *VviERF6L12* that demonstrated a significantly higher level of expression (Z-score for two population proportions $p < 0.00001$). *VviERF6L8* was consistently the lowest expressed *VviERF6L* across organs and treatments. Interestingly, leaves from RA (a drought-tolerant rootstock originating from Texas, USA) had a significantly higher accumulation of *VviERF6L12* transcripts in week 2 WD relative to RA Control leaves as well as compared to 2 WD treatment leaves of the other three species. The other species, which are more drought sensitive, did not exhibit an increase or as high of an increase in *VviERF6L12* transcripts in the leaves in response to two weeks of WD.

Amongst the *VviERF6L* clade, DEA showed *VviERF6L1* and 18 were the most common DEGs in DEA contrasts of interest. DEA was performed for each genotype for WD vs. Control and for each WD treated species to the others for weeks one and two for

roots and leaves individually. A list of DEA contrasts of interest for this data set is located in Appendix 13. The frequency at which each *VviERF6L* was a DEG in the DEA contrasts of interest was quantified (Supplemental File 10). *VviERF6L1* was identified as the most responsive *VviERF6L*, being a DEG in 14 DEA contrasts of interest followed by *VviERF6L18* (a DEG in 10 DEA contrasts of interest); however, both genes were expressed at relatively low levels (Fig. 6). The other *VviERF6Ls* varied in DEG frequency in the DEA contrasts of interest (Supplemental File 10). *VviERF6L7* and *8* were not DEGs in any contrast of interest. The range of frequencies each *VviERF6L* was a DEG in the DEA contrasts of interest was consistent with the results of the promoter analysis, indicating that while these genes are highly conserved, they are under distinct regulation.

VviERF6L genes respond to chilling and cold

VviERF6Ls were differentially expressed in leaves in response to chilling, cold, and freezing in the meta-data analysis. Many of the *VviERF6Ls* responded with analogous expression patterns. Recent RNA-Seq data in which five *Vitis vinifera* cultivars (Cabernet Franc, Chardonnay, Riesling, Sangiovese, and Tocai Friulano) were treated with chilling (ACC), freezing (FRZ), or a chilling acclimation followed by the freeze treatment (A+F) demonstrate significant *VviERF6L* differential expression (Fig. 7) (Londo et al., 2018). As with WD response, various *V. vinifera* cultivars demonstrated unique *VviERF6L* expression in leaves in response to cold treatments. For example, comparing freezing vs. control DEA across cultivars, Chardonnay had the highest significant increase in *VviERF6L1* transcript abundance while Tocai Friulano and Sangiovese did not demonstrate *ERF6L1* differential expression (Fig. 7 and DEA from the original

publication (Londo et al., 2018)). All cultivars had a decrease in transcript abundance of *VviERF6L1* in the chilling vs. control treatment comparison (Fig. 7). The transcript abundance of *VviERF6L11 and VviERF6L12* was increased in all genotypes in response to the freezing treatment (Fig. 7). The results in Figure 7 are supported by microarray data in which *VviERF6Ls* were differentially expressed in CS shoot tips exposed to a chilling treatment for 0, 4, and 8 hours (Supplemental File 11) (Tattersall et al., 2007). To confirm these results, RT-qPCR was performed on *VviERF6L1* for RA, RI, CS, and SC whole canopy and single leaves treated with 4°C chilling for 0-2 hours. In contrast to the previous freezing and chilling treatments, these chilling experiments did not result in a significant difference in *VviERF6L1* transcript abundance relative to control; there was, however, a significant increase in *CBF1* transcript abundance used as a positive control in chilled samples (Supplemental File 12). It is possible *VviERF6L1* was not the most responsive *VviERF6L* in these species under these conditions. Together these examples from the meta-data analysis reveal *VviERF6Ls* are differentially expressed with complex responses to temperature reduction in cultivar-, temperature- and time-dependent manners and may play a role in cold response in grapevine.

***VviERF6L* genes respond to light intensity**

VviERF6Ls were significantly differentially expressed in response to increased light exposure. CS berries exposed to varying light intensity through leaf removal or leaf movement at veraison demonstrated reduced *VviERF6L12* transcript abundance in de-seeded berries (pulp and skin only) at late veraison and harvest. The majority of the other *VviERF6Ls* (all with lower transcript abundance than *VviERF6L12*) had enhanced

transcript accumulation at harvest (particularly with leaf removal) relative to control conditions in which no leaves were (re)moved (Sun et al., 2017) (Fig. 8) [GSE121146]. In this experiment, leaves were cut off vines for the leaf removal treatment and physically bound in place for the leaf moving treatment. These actions may have elicited a wounding response. However, as the berries remained intact on the vine and only the leaves were removed, the increased *VviERF6L* transcript abundance in the berries is likely associated with increased light exposure and not a wounding response. The accumulation of *VviERF6L* transcripts with enhanced light exposure at harvest in combination with the abundance of *VviERF6L* promoter motifs associated with light response indicates *VviERF6Ls* may play a role in grapevine response to light intensity. Supportive of these data and *VviERF6L* light response, *VviERF6Ls* were also differentially expressed in berries grown under a double-cropping system with summer and winter harvests [GSE103226] (Chen et al., 2017). In the summer, CS berries grown in this system had the highest level of *VviERF6L* expression at the end of veraison (EL36), while there was a distinct depression in *VviERF6L* transcript level for winter berries (Supplemental File 13). These data sets support the hypothesis that *VviERF6Ls* have a cultivar-specific response to abiotic stress and may play a role in response to light intensity.

***VviERF6L* genes are involved in various biotic stress responses**

VviERF6L* genes respond to *Neofusicoccum parvum

VviERF6Ls are differentially expressed in response to *Neofusicoccum parvum*. CS plants inoculated with *N. parvum* had significantly enhanced *VviERF6L* transcript accumulation in woody stems two weeks after treatment (Fig. 9) [GSE97900] (Massonnet

et al., 2017a). Interestingly, *VviERF6Ls* also responded to the wounding aspect of this treatment, which consisted of taking a power drill to the woody stem. The wounding response remained significant for the majority of *VviERF6Ls* up to two weeks after the treatment (Fig. 9). *VviERF6L12* and *8* consistently demonstrated the highest and lowest expression levels, respectively (Fig. 9).

In general, *VviERF6L* expression levels significantly increased in response to *E. necator* inoculation in leaves of *V. vinifera* cv. Carignane and six partially resistant Asian accessions (DVIT3351.27 (DVIT3351), Hussiene, Karadzhandal, Khalchii, O34-16, Sochal, and Vavilov) [GSE67191] (Amrine et al., 2015). The cultivars showed similar expression patterns with differences in expression levels of the *VviERF6Ls* (Supplemental File 14). *VviERF6L12* and *16* generally had the highest expression in response to the powdery mildew inoculation (Supplemental File 14). *VviERF6L8* generally had a low, but detectable expression except in DVIT3351, which *VviERF6L8* had higher expression levels in, similar to those of *VviERF6L3-7*, and Vavilov that did not demonstrate any *VviERF6L8* expression at either time point or treatment. It is possible *VviERF6Ls* play diverging roles in response to various pathogens.

Whole Zinfandel berries had high levels of *VviERF6L12* counts across berry development in both control and red blotch-associated virus treatment in two separate vineyards (Fig. 10) [GSE85812] (Blanco-Ulate et al., 2017). In control berries, the expression of the *VviERF6L* clade was highest in the pre-veraison (PRV) stage with a subsequent decline in transcript abundance as the berry maturity stage increased. *VviERF6L8* expression was only detectable in one vineyard at pre-veraison; in all other cases, it does not appear to be expressed (Fig. 10). *VviERF6L* expression at pre-veraison

significantly decreased in response to red blotch-associated virus in at least one vineyard (Fig. 10) (Blanco-Ulate et al., 2017). *VviERF6Ls* showed variable expression across the vineyards in response to red blotch-associate virus, particularly at pre-veraison. *VviERF6L5*, *7*, and *10* had increased counts in infected samples at veraison (Fig. 10). At post-veraison, *VviERF6L1*, *5*, and *11* had higher expression in red blotch-associated virus samples in both vineyards, and at harvest, *VviERF6L3* had lower counts in infected berry tissue (Fig. 10). While various *VviERF6Ls* were significantly differentially expressed in response to these pathogens (Figs. 9-10 and Supplemental File 14), the pattern and degree of expression across genotypes were not consistent.

***VviERF6L* genes are involved in berry development**

Unlike abiotic and biotic stress responses, *VviERF6L* gene expression patterns and levels show general conservation across cultivars with *VviERF6L12* consistently having the highest transcript abundance in red and white berries (Massonnet et al., 2017b). One study examining red and white berry development over four developmental stages (pea-sized (Pea), touching (Touch), softening (Soft), and harvest (Harv)) showed differential expression of *VviERF6Ls* across berry ripening, but at a low expression level (Fig. 11). *VviERF6Ls* had the highest number of *VviERF6L* transcripts at the pea-sized and touching stages of berry development. *VviERF6L* transcript abundance decreased as berries softened and was even lower at harvest (Fig. 11). *VviERF6L2*, *12*, and *13* were among the highest expressed *VviERF6Ls* in white berries with the addition of *VviERF6L5*, *15*, and *16* for red cultivars in the early stages of berry development. In the later stages of berry development, *VviERF6L12* had the highest transcript abundance (Fig. 11). From pea-sized to touching

berries, *VviERF6L8* was expressed in white berries (except Passerina) to a comparable level with other *VviERF6Ls*, including *VviERF6L7* and *9*. At all other developmental stages, *VviERF6L8* was negligibly expressed. In red berries, *VviERF6L8* was only expressed in Barbera in pea-sized berries. *VviERF6L* expression across berry development is also consistent across vineyards and years [GSE97578] (Dal Santo et al., 2018) [GSE41633] (Dal Santo et al., 2013) (Supplemental Files 15-16). *VviERF6L* signal intensity peaked significantly at pre-veraison and generally declined as berries approached full ripening (FR) (Supplemental File 15). There were subtle changes in signal intensity level over the years and vineyards (Supplemental File 16), but generally, expression levels were similar and the *VviERF6L* expression pattern remained conserved, indicating these genes may not be strongly influenced by the environment during berry development.

VviLISCL3 and *VviCML45* were the most connected genes to the *VviERF6Ls*

Two genes share a similar expression pattern as the 18 *VviERF6Ls* across various cultivars, organs, and treatments. The meta-data analysis was completed with a gene co-expression analysis to identify genes sharing expression patterns for all *VviERF6Ls* as a clade between the five data series that were re-analyzed with the V3 annotation of PN40024 (SRP117281, PRJNA516950, GSE67191, GSE62744, and GSE62745). The top 100 genes most connected to each *VviERF6L* were extracted from the TOM (Topological Overlap Matrix) for each WGCNA. Common co-expressed genes were identified by comparing these sets of genes. In total, two genes were identified in all five data series that were the most connected to the *VviERF6L* clade across the various conditions and variables of each data series (Supplemental File 17). The two co-expressed genes were a Scarecrow-like

transcription factor, *VviLISCL3* (Vitvi06g00489), and a calmodulin-like protein, *VviCML45* (Vitvi14g01975). Several other genes shared expression patterns with the *VviERF6L* clade in four out of the five data series including *VviERF1* and *VviWRKY33* (Appendix 14). The full list of genes co-expressed with the *VviERF6L* clade in four of the five data series is in Appendix 14. Six of the 16 genes sharing the *VviERF6L* expression pattern were unannotated.

After analyzing the *VviERF6L* clade as a whole, the co-expression analysis was repeated for each *VviERF6L* individually. Surprisingly, no gene was connected to any *VviERF6L* in all five data series in this individual analysis, not even the other *VviERF6Ls*. Because no genes were co-expressed with any *VviERF6L* individually, genes co-expressed in four out of the five RNA-Seq data series were considered. *VviWRKY33* was the only gene to be co-expressed in four out of the five data series in this individual *VviERF6L* gene co-expression analysis but only for *VviERF6L11* and *16*. The low number of genes co-expressed with *VviERF6Ls* in all five RNA-Seq series (16 for the clade co-expression analysis (Appendix 14) and 0 for the individual *VviERF6L* co-expression analysis) may be a result of the diverse RNA-Seq series utilized that examined various organs, genotypes, developmental stages, and stresses.

Summary of the meta-analysis

Generally, *VviERF6Ls* were lowly expressed in all data sets, but these genes demonstrate striking fold changes in expression levels and significant differential expression under numerous conditions. *VviERF6Ls* are broadly expressed across grapevine organs, tissues and in response to various abiotic and biotic stresses as well as throughout

berry development (Fig. 12). *VviERF6Ls* appear to increase in expression in response to severe water deficit and salinity. However, over more long-term moderate water deficit, *VviERF6Ls* are generally decreased. *VviERF6Ls* have distinct differential expression in response to cold and light in different cultivars. *VviERF6Ls* are differentially expressed in response to various pathogens, but the level of expression varies depending on the pathogen and cultivar. *VviERF6Ls* are also differentially expressed across berry development with the highest expression levels as berries transition into veraison. *VviERF6L* expression patterns are highly conserved across cultivars, vineyards, and years. The broad range of *VviERF6L* expression across tissues and expression patterns are conserved throughout numerous data series. The transcriptional response for each member of the *VviERF6L* clade was dependent on numerous factors (organ, time, treatment, duration, severity, genotype, etc.). The transcriptomic response for each experimental design, while generally conserved, was unique for each *VviERF6L* (i.e. some members of the clade increased in transcript abundance, some decreased, and others did not respond under a specific condition). The individuality emerging in the *VviERF6L* clade as well as divergent observations for different severities of similar treatments makes it difficult to generalize common responses. However, a diagram (Fig. 12) was constructed to summarize the conditions that elicited *VviERF6Ls* responses as well as conditions requiring additional data to further elucidate the role *VviERF6Ls* play in grapevine. As transcriptomic technology evolves, the *VviERF6Ls* will be able to be better differentiated and understanding of the clade will be improved.

Two results are clear, first, in all the data series discussed, *VviERF6L12,* one of the truncated *VviERF6Ls*, repeatedly demonstrated significantly higher expression than any of

the other *VviERF6Ls*. *VviERF6L12* had 2–228 times more transcript abundance than the average of all other *VviERF6Ls*. Across the treatments and conditions of the selected data sets, the transcript abundance of *VviERF6L12* averaged 25.6-times more RMA-normalized signal intensity, counts, FPKM, or TPM than the average expression of the other *VviERF6Ls* (Appendix 15). Second, *VviERF6L8* was frequently the lowest expressed *VviERF6L* with no detectable expression in certain cultivars. The vast range of *VviERF6L* expression levels made it necessary to $\log_2$ transform the data in the meta-data analysis, so each *VviERF6L* expression was visible. Although the *VviERF6L* clade is highly conserved, each *VviERF6L* is under unique transcriptional regulation.

Overexpressing *VviERF6L1* in *Vitis* had a minor impact on the transcriptome and phenotype

In previous microarray studies, *VviERF6L1* appeared to be the most responsive *VviERF6L*, with transcript abundance increasing in CS in response to severe leaf dehydration (Hopper et al., 2016) and with changing sugar levels in a study of the late stages of berry ripening (Cramer et al., 2014). Further investigation of *ERF6L1* function was investigated with *VviERF6L1* overexpression and knockdown lines. Attempts to establish *Vvierf6l1* knock-down lines failed; plants were unable to be re-established after transformation with a T-DNA insertion. An empty vector control (G1) and *VviERF6L1* overexpression lines (L12-1, L12-2, L12-3, L12-11, and L12-23) were created in a Seyval Blanc background under the control of a bi-directional duplex 35S promoter fused to EGFP/NPTII in pECBC (Gray and Zhijian, Li, 2006). Overexpression was confirmed with semi-quantitative PCR and RT-qPCR to verify stable overexpression (Supplemental File

18). Extensive phenotyping revealed *VviERF6L1* overexpression lines did not exhibit a morphological phenotype under control conditions, or in response to salinity, water deficit or pathogen spread treatments (Appendix 16).

Potential downstream targets of *VviERF6L1* were determined with differential expression analysis on RNA-Seq data from leaves of the empty vector control (G1) and *VviERF6L1* overexpression lines (L12-3, L12-11, and L12-23). *VviERF6L1* was the only *VviERF6L* gene with significantly higher expression in the overexpression lines compared with G1 (Supplemental File 19). In total, only fourteen genes were significantly differentially expressed in all three overexpression lines relative to G1 (Supplemental File 20 and Appendix 17). Up-regulated genes included: *VviERF6L1* (Vitvi16g00350), *CYP722A1* (Vitvi04g01352), *CRK8* (Vitvi11g01160), *LAC14* (Vitvi18g01479). Down-regulated genes included: three *PRB1* (pathogenesis-related protein 1) genes (Vitvi03g00757, Vitvi03g01649, Vitvi03g01651), unannotated genes (Vitvi03g01650, Vitvi07g01985, Vitvi11g01692, Vitvi18g02319), *MET1* (Vitvi12g02119), *WAKL1* (Vitvi18g00024), and *LIMYB* (Vitvi01g01444).

3.4 Discussion

The *VviERF6L* clade was expanded and conserved

VviERF6L genes with no previously known functions were identified to be an expanded clade in *Vitis* in comparison with other plant species. Using protein and promoter motifs and a meta-data analysis, this work shows *VviERF6Ls* are highly conserved proteins.

Manual and *in silico* techniques identified and confirmed 18, 26, 15, and 14 members of the *VviERF6L* clade in PN40024, CS, CH, and CA, respectively (Supplemental File 6). The high sequence and spatial conservation of amino acid motifs validate these sequences as members of the *VviERF6L* clade in the AP2/ERF subfamily IX. The small differences in protein motif sequence and position may contribute to the differential regulation of the *VviERF6Ls* observed in the publicly available microarray and RNA-Seq analysis. Four known protein domains identified (Fig. 1) in the VviERF6L proteins coincide with those in Arabidopsis ERF IXb transcription factors including ERF5 (At5g47230), ERF6 (At4g17490), ERF104 (At5g61600), and ERF105 (At5g511290) (Nakano et al., 2006). The VviERF6Ls contain CMIX-2, 5, and 6 domains (putative post-translational modification sites) as well as the AP2/ERF domain (DNA-binding) (Fig. 1). While VviERF6L1 has the highest orthology to AtERF6, it contains an additional domain, CMIX6, found in AtERF104, but not present in AtERF6. This domain is thought to contain a MAP kinase phosphorylation site (Nakano et al., 2006).

Four motifs located near the amino and carboxyl ends of the VviERF6L proteins were unable to be identified. ERF transcription factors interact with numerous other proteins including regulatory enzymes, coactivators, repressors, and other transcription factors (Alves et al., 2014; Phukan et al., 2017; Wang et al., 2018a). These interactions regulate stability and activity as well as localization of ERFs. The unidentified VviERF6L protein domains may play roles in post-translational regulation and/or interactions with other proteins. One such interaction occurs with AtERF104, which is phosphorylated by MPK6 and released from this interaction in the presence of the flg22-peptide to influence ethylene signaling and pathogen susceptibility (Bethke et al., 2009).

Vitis vinifera had the highest number of *VviERF6L* paralogs compared to species with the closest related genes (Supplemental File 2), marking this as an expanded clade in grapevine. The VviERF6L clade consists of nearly consecutive genes on chromosome 16. The *VviERF6L* paralogs likely originate from gene duplications. Duplication events are common and frequent in plants contributing to gene evolution and diversification (Panchy et al., 2016). Recent whole-genome duplications in cotton (Renny-Byfield et al., 2014), wheat (Brenchley et al., 2012), and soybean (Schmutz et al., 2010) and dispersed duplication in corn (Schnable et al., 2011) gave rise to agronomically valuable traits of 4 of the top 10 produce crops in the United States. Exploring *VviERF6L* evolution in wild grapevine as well as the ancestor of domesticated grapevine may provide more evidence and a timeline for the hypothesized duplication event. The contiguous *VviERF6Ls* may be tandem array genes, arising from tandem duplication of an ancestral gene. The significance of tandem ERF duplication was recently described in *Fragaria vesca* (Wang et al., 2019). Tandem *Fve*ERFs are differentially expressed from one another in response to abiotic stress, suggesting gene divergence occurring after tandem duplication(s) (Wang et al., 2019). A similar event may have occurred with grapevine *VviERF6Ls*. The possibility of *ERF6L* duplication in *Vitis* is supported by the expansive ERF family in pear (155 members) (Li et al., 2018), another woody perennial, as well as *Arabidopsis* (122 members) and rice (139 members) (Nakano et al., 2006).

Individual *VviERF6Ls* had unique gene expression

The *VviERF6L* clade is under unique transcriptional regulation in response to numerous conditions (Fig. 12). Contrasting the high similarity in protein sequence, *VviERF6L*

putative promoter regions (Fig. 3) showed greater diversity than VviERF6L protein sequences (Fig. 1), indicating these genes are under distinct transcriptional regulation. However, strong patterns and conserved motifs were detected across the promoter regions. The CAATBOX1 motif was the most abundant in the 18 *VviERF6L* upstream regions (Appendix 9), which may play a role in tissue-specific gene expression (Shirsat et al., 1989) and contribute to *VviERF6L* expression across the broad range of tissues observed in the meta-data analysis. The MYB1AT motif is present in dehydration-responsive genes like *RD22* (Alves et al., 2017). This motif was present in all *VviERF6L* promoters, but with fewer repetitions, supporting the transcriptomic data that *ERF6Ls* are only responding to severe water stress (Fig. 5). DOFCOREZM, another abundantly present cis-regulatory element in the *VviERF6L* promoter regions (Appendix 9), is the binding motif for Dof proteins, a diverse group of transcription factors with roles in defense and phytohormone responses, light, and development (Yanagisawa, 2002). Interestingly, numerous *VviERF6L* promoter motifs associated with light responses were identified including the CACTFTPPCA1, DOFCOREZM, GATABOX, GT1CONSENSUS, with responses supported by the results from the meta-data analysis (Fig. 8 and Supplemental File 13). AtERF5 has also been linked to light responses (Giraud et al., 2008). The light response of VviERF6Ls may be tissue-specific and was not well identified in the berry-centric microarrays and RNA-Seq data sets, requiring further investigation in other tissues. Several motifs associated with biotic stress responses were also present in the promoter including WBOXATNPR1, which had the highest number of repeats in *VviERF6L12*. Together, the presence of these motifs supports the proposed roles of *VviERF6Ls* in extreme water deficit, cold, light, and pathogen responses.

The diverse promoter sequences partially explain the distinct *VviERF6L* expression levels and patterns observed across the RNA-Seq and microarray series. *VviERF6L12* had one of the most variable promoter sequences (Supplemental File 7) along with *VviERF6L1* and *VviERF6L6*. Putative promoter regions of *VviERF6L12* (and other *VviERF6Ls*) contained unique cis-regulatory elements as well as distinctive motif placement and replication. The distinct conditions in which certain *VviERF6Ls* are DEGs (Supplemental File 10) in the meta-data analysis may be partially explained by the diversity in upstream sequences.

Additional differences in transcriptional regulation may be contributed to by epigenetics. ERFs have been demonstrated to regulate one another and affect epigenetic regulation through the ethylene-responsive element binding factor-associated amphiphilic repression (EAR). The EAR motif is a short peptide sequence comprised of charged and polar residues (LxLxLx or DNLxxP) that are proposed to confer gene silencing via histone modification and chromatin remodeling through an unresolved mechanism (Kagale et al., 2010; Licausi et al., 2013). AtERF3, 4, and 7 contain EAR motifs that act as active repressors of target and reporter genes (McGrath, 2005; Ohta et al., 2001; Song, 2005; Yang et al., 2005). Epigenetic regulation and upstream effectors of *VviERF6L* expression require further investigation to determine interactions with EAR-containing ERFs.

VviERF6L1 expression was independent of ABA treatment

The transcript abundance of *VviERF6Ls* was shown to increase in response to severe osmotic stress and at pre-veraison in berry develop in preliminary microarrays that originally brought attention to the *VviERF6L* clade (Cramer et al., 2014; Hopper et al.,

2016). Although ERFs are traditionally associated with ethylene signaling, these ERF transcription factors are well documented to act as hubs for hormone-crosstalk and signaling integration (Berens et al., 2019; Kunkel and Brooks, 2002; Mao et al., 2016; Saithong et al., 2015). ABA is a key phytohormone in abiotic stress responses and berry ripening in grapevine. Water deficit responses are ABA-dependent and/or ABA-independent (Yoshida et al., 2014). However, *VviERF6L1* expression was not significantly different in CS leaves treated with exogenous ABA relative to control (Supplemental File 9). Interestingly, *AtERF5* is also not associated with ABA signaling (Wang et al., 2018b). Other *VviERF6L* transcripts may increase or decrease in response to ABA treatment, as the *VviERF6Ls* are distinctly regulated (Appendix 9). Alternatively, a *VviERF6L* ABA response may be tissue-specific (e.g. berries transitioning into veraison). The increased expression of *VviERF6L1* in response to various abiotic stresses and berry development in the meta-data analysis, but the lack of induction in response to ABA foliar spray indicates the *VviERF6L1* abiotic-stressed-based induction may be independent of the ABA signaling pathway. RT-qPCR along with microarrays and short-read RNA-Seq were determined to be less than ideal techniques for quantifying *VviERF6L* transcripts due to the high sequence similarity of these genes; primers and probes could hybridize to (and short reads could be attributed to) multiple *VviERF6Ls* resulting in inflated transcript levels and difficulty separating the *VviERF6Ls* independently. With the advent of Iso-Seq and the ability to quantify full-length transcript reads, the future of distinguishing *VviERF6Ls* individually will be more reliable and accurate (Minio et al., 2019b).

VviERF6Ls **were differentially expressed in response to water deficit, salt, and cold**

VviERF6L expression significantly increased in response to extreme water deficit and salt (Figs. 4-5). However, exposing CS, RA, RI, and SC vines to a moderate one- and two-week natural dry down revealed *ERF6Ls* were generally significantly decreased in transcript abundance (Fig. 6). Each *VviERF6L* had a unique expression level that responded differently in each species and organ examined in this experiment, further distinguishing the *VviERF6Ls* individually and supporting the hypothesis each *VviERF6L* is under specific transcriptional regulation.

The uniqueness of *VviERF6Ls* across tissues and cultivars is further demonstrated with significant differential *VviERF6L* expression in response to cold (Fig. 7, Supplemental File 6, and Appendix 6). Again, each *VviERF6L* in the different cultivars had varied responses to the cold (Fig. 7). There were also differences between the leaves and shoot tips investigated in the different data series. *VviERF6Ls* generally followed similar expression patterns within treatments but to different degrees of expression across cultivars and *Vitis* species indicating differential *ERF6L* regulation across these divisions of *Vitis*. Differences in *ERF6L* regulation may contribute to differences in abiotic stress tolerance across various grapevine cultivars.

VviERF6Ls **were differentially expressed in response to biotic stresses**

Differential expression analysis performed on *VviERF6L1 Vitis* overexpression relative to control vines revealed three *PRB1* paralogs, one putative *PR1*, and a putative mildew resistance locus that were significantly downregulated in the overexpression lines. *PR1* is a common SA signaling marker gene up-regulated in response to certain pathogens including *Pseudomonas syringae* (Ali et al., 2018; Bowling et al., 1997; Ford et al., 2010;

Laird et al., 2004). The distinct downregulation of this gene and its paralogs in *VviERF6L1* overexpression lines is consistent with the enhanced susceptibility to *Pseudomonas syringae documented in the AtERF6 and AtERF5* overexpressors (Moffat et al., 2012). It is possible VviERF6L1 works in combination with other TFs to impact grapevine susceptibility to various pathogens. Another DEG in OX *VviERF6L1* lines, *LAC14*, may also be linked to biotic stress response. This gene encodes a laccase that is part of secondary metabolism responsible for lignin degradation or polymerization (Berthet et al., 2012) and was significantly upregulated in the OX *VviERF6L1* lines. Lignin biosynthesis and accumulation aids in plant resistance to insect pests. Lignin deposition is also associated with abiotic stress response and antagonization with plant growth (Fan et al., 2006; Lee et al., 2007). The duality of the DEGs' roles in both abiotic and biotic stress response further strengthens the hypothesis of broad functionality of *VviERF6Ls*. *VviERF6Ls* were differentially expressed in response to various pathogens in the meta-data analysis (Figs. 9-10 and Supplemental File 14). The level of *VviERF6L* expression and specific *VviERF6Ls* that were DEGs were pathogen and tissue-specific.

VviERF6Ls response to pathogens is conserved in Arabidopsis. AtERF5, one of the closest orthologs to the VviERF6L clade, directly interacts with AtERF6 and 8 as well as SCL13 and MPK3 and 6 in unique combinations to respond differentially to *Pseudomonas syringae* (Son et al., 2012), *Botrytis cinerea* (Moffat et al., 2012), *Alternaria brassicicola* (Son et al., 2012), and *Meloidogyne incognita* (Warmerdam et al., 2018). *Aterf5/6* double mutants have enhanced susceptibility to *V. longisporum*, a fungus that induces severe wilting and plant death (Fröschel et al., 2019). Another pathogen-related example of a potential role in pathogen response shows decreased *VviERF6L* expression in response to

Plasmopera viticola (downy mildew) in more susceptible vines and either an increase or no significant change in transcript abundance in more tolerant vines (Eisenmann et al., 2019; Rienth et al., 2019).

VviERF6Ls **were differentially expressed throughout berry development**

The *VviERF6Ls* had a consistent significant differential expression pattern during berry development. *VviERF6L* transcript abundance was significantly increased at pre-veraison as the berries transitioned into ripening and decreased as the berries approached full ripening and harvest (Fig. 11). The *VviERF6L* expression pattern over berry development was conserved across red and white berries (Fig. 11), vineyards, and years (Supplemental Files 15-16).

The *VviERF6L* ortholog *Solyc08g078190* identified from the Pan-taxonomic Compara Gene Tree in Gramene follows a similar expression pattern as *VviERF6Ls.* This gene, annotated as SlERF.B13 (Liu et al., 2016) or ERF1a (Fernandez-Pozo et al., 2017), increases in the breaker stage (equivalent to veraison in grapevine) of berry development in tomato and decreases in transcript abundance as berries ripen (Liu et al., 2016). Another *VviERF6L* tomato ortholog, *Sl-ERF.B3* (Solyc05g052030), also plays a role in berry development (Liu et al., 2014). Like grapevine, tomato *ERFs* can have increased or decreased transcript abundance under certain conditions (Liu et al., 2016). This similarity between non-climacteric grapevine and climacteric tomato along with the significant transcriptomic responses in the meta-data analysis support a potential role of *VviERF6Ls* in berry development requiring further investigation.

VviLISCL3 and *VviCML45* were genes connected to the *VviERF6L* clade

Little is known about *VviLISCL3* and *VviCML45* that were co-expressed with the *VviERF6L* clade. VviLISCL3 is a GRAS transcription factor with roles in plant development, abiotic stress, and disease response (Benfey et al., 1993; Pysh et al., 1999) similar to the *VviERF6L* expression profile identified from the meta-data analysis. *VviLISCL3*, like the *VviERF6Ls*, appears to be ubiquitously expressed across plant tissues except for pollen (Grimplet et al., 2016). *VviLISCL3* was differentially expressed over berry development and likely plays a role in berry set and the early stages of berry development (Grimplet et al., 2016). However, unlike the *VviERF6Ls*, *VviLISCL3* had high expression levels at ripe, harvest, and post-harvest stages of berry development (Grimplet et al., 2016). *SlGRAS13*, the *VviLISCL3* ortholog in tomato, shows the same expression pattern and role in fruit ripening (Huang et al., 2015). *AtCML45*, the Arabidopsis ortholog of *VviCML45*, is differentially expressed in *nrp1 nrp2* Arabidopsis double mutants that lack these histone chaperones associated with root growth (Zhu et al., 2006) and may provide a very loose link of VviERF6Ls to epigenetic modification that ERFs are known to play a role in (Kagale et al., 2010; Licausi et al., 2013). The link between VviERF6Ls, VviLISCL3, and VviCML45 was discovered but remains unresolved, requiring further clarification.

Overexpressing *VviERF6L1* had a minimal impact on grapevine

Overexpressing *VviERF6L1* in *Vitis vinifera* did not result in a detected morphological phenotype. This observation may be attributed to the limited number of genes *VviERF6L1* overexpression effected (Supplemental File 17). It is possible a

VviERF6L1 overexpression phenotype is only detectable under specific conditions not tested in this work. *VviERF6L1* was the only member of the *VviERF6L* clade with enhanced gene expression in the *VviERF6L1* overexpression lines (Supplemental File 19). The other *VviERF6L* genes may share similar functions and could have been downregulated in response to the overexpression of *VviERF6L1*. The hypothesis that *VviERF6L* genes share similar functions is supported by the redundant gene and promoter sequences of *VviERF6L* genes (Figs. 2 and 3). Paralog downregulation in response to overexpression is observed in plants. For example, *CYP78A8*, one of the closest paralogs to *CYP78A9*, is downregulated in response to *CYP78A9* overexpression (Sotelo-Silveira et al., 2013). However, this does not appear to be the case in the overexpression of *VviERF6L1*. The promoter and meta-data analysis support this conclusion. Although the *VviERF6Ls* share similar expression patterns, expression levels, and transcriptional regulation are unique for each *VviERF6L*, and the overexpression of *VviERF6L1* does not appear to influence the transcription of the other *VviERF6Ls*. Further studies are needed to identify and confirm specific VviERF6L downstream targets.

The *VviERF6L* in grapevine is distinct from Arabidopsis *ERFs*

Arabidopsis thaliana ERFs do not have strong orthology to *VviERF6Ls*. AtERF5 and AtERF6 are the closest orthologs to VviERF6L1. *AtERF6* and *AtERF5* are rapidly induced in growing tissues and effectively arrest cell cycle progression and plant growth in response to osmotic stress (Skirycz et al., 2011). *AtERF5* is involved in karrikin signaling (Wang et al., 2018b), water deficit and osmotic stress (Dubois et al., 2013), programmed cell death (Mase et al., 2013), and immunity response (Moffat et al., 2012). *AtERF6*

overexpression lines are hypersensitive to osmotic stress (Dubois et al., 2013). *VviERF6L1* overexpression vines exposed to chilling, water deficit, and salinity demonstrated no significant differences from controls in the reduction in growth, carbon assimilation, or canopy surface area relative to empty vector control plants (Appendix 16). *VviERF6Ls* were shown to respond transcriptionally to osmotic stress (Fig. 5), but no link was made to cell cycle regulation. AtERF6 is also a positive regulator of antioxidant production with *Aterf6* mutants having stunted growth and enhanced levels of ROS and anthocyanin content (Sewelam et al., 2013). AtERF6 is an inductor of stress tolerance genes and a key activator of leaf growth inhibition (Dubois et al., 2015). *VviERF6L1* overexpression lines had no reduction in growth or development relative to empty vector controls (Appendix 16), and no connection was made specifically to antioxidants and anthocyanins.

In Arabidopsis, *AtERF6* acts as a regulatory hub favoring stress defense mechanisms at the cost of plant growth through DELLA protein stabilization via ethylene and gibberellin crosstalk (Dubois et al., 2015; Rieu et al., 2008). *VviERF6Ls* were found to respond to various pathogens (Figs. 10-11 and Supplemental File 14), but no negative impact on growth was found at least in the case of *VviERF6L1* (Appendix 16). It is possible other *VviERF6Ls* could impact growth. *VviERF6L1* overexpression lines did, however, have significantly decreased transcript abundance of several *PR1B* genes, associated with pathogen stress response (Appendix 17). AtERF6 and AtERF5 function redundantly in response to biotic stresses and act as a point of crosstalk between ethylene and JA signaling, providing enhanced resistance to *Botrytis cinerea,* but increased susceptibility to *Pseudomonas syringae* in *AtERF5* and *AtERF6* constitutive plants. *Aterf5/Aterf6* double mutants demonstrate enhanced susceptibility to *Botrytis cinerea* (Moffat et al., 2012).

Preliminary pathogen spread assays did not show significant differences in OX *VviERF6L1* leaves relative to empty vector control (Appendix 16). Further investigation of *VviERF6L1* overexpression susceptibility to various pathogens is ongoing and may reveal a more definite role in biotic stress response.

AtERF6 overexpression lines demonstrate extreme dwarfism (Dubois et al., 2013). AtERF6 activates *AtERF11* transcription, which in turn competes with AtERF6 for DNA-binding sites as a balancing mechanism between stress response and growth (Dubois et al., 2015). *AtERF11* overexpression rescues the dwarf phenotype in *AtERF6* overexpression plants (Dubois et al., 2015). A VviERF6L1-ERF11 antagonism was not detected in the DEA of the *VviERF6L1* overexpression lines. It is possible a different VviERF6L is responsible for this regulatory mechanism or that this interaction is not present in *Vitis*.

AtERF6 is also documented to activate *MYB51*, *WRKY33*, and *STZ* (Dubois et al., 2013), all genes with roles in biotic (Birkenbihl et al., 2012; Gigolashvili et al., 2007) and abiotic (Li et al., 2011; Sakamoto et al., 2004; Wang et al., 2013) stress responses. *VviERF6Ls* are co-expressed with *VviWRKY33* (Appendix 14), linking the two species in this signaling pathway, but at least *VviERF6L1* does not appear responsible for *VviWRKY33* activation (Appendix 16). The distinction of the *Vitis* ERF6L clade from the closest *Arabidopsis* orthologs is supported by the work presented here including the lack of comparable phenotypes in overexpression lines and transcriptomic responses from the meta-data analysis. However, while *Vitis ERF6L* genes are unique, they may functionally overlap with the distant Arabidopsis orthologs to an extent with associated abiotic and biotic stress responses. ERF TFs in Arabidopsis and *Vitis* are differentially regulated by abiotic stresses (Klay et al., 2018) including cold, salinity (Yamaguchi-Shinozaki and

Shinozaki, 2005), and water deficit as well as biotic stresses such as wounding and pathogen attack (Ecker and Davis, 1987; van Loon et al., 2006).

VviERF6Ls are an expanded and highly conserved *Vitis* clade. *VviERF6L* expression was increased in berries at the pre-veraison stage and was found to be induced in leaves by extreme abiotic stress including salt, cold, and water deficit (Fig. 12). *VviERF6L1* was not induced by ABA, indicating a role in water deficit responses through an ABA-independent pathway. Overexpression of *VviERF6L1* in a Seyval Blanc background did not yield a detectable morphological phenotype, emphasizing the separation of this clade from the Arabidopsis orthologs *ERF6* and *ERF5*, overexpression of which results in extreme dwarfism and osmotic stress sensitivity. DEA performed on RNA-Seq from the *VviERF6L1* overexpression lines identified 14 DEGs involved in abiotic and biotic stress responses. Overall, *VviERF6Ls* have versatile functions and are expressed in numerous tissues in response to abiotic and biotic stress and may play multiple roles in these processes that require further elucidation.

3.5 References

Ali, S., Mir, Z.A., Bhat, J.A., Tyagi, A., Chandrashekar, N., Yadav, P., Rawat, S., Sultana, M., and Grover, A. (2018). Isolation and characterization of systemic acquired resistance marker gene PR1 and its promoter from Brassica juncea. 3 Biotech *8*.

Altschul, S.F., Gish, W., Miller, W., Myers, E.W., and Lipman, D.J. (1990). Basic local alignment search tool. J. Mol. Biol. *215*, 403–410.

Alves, G.S.C., Torres, L.F., Déchamp, E., Breitler, J.-C., Joët, T., Gatineau, F., Andrade, A.C., Bertrand, B., Marraccini, P., and Etienne, H. (2017). Differential fine-tuning of gene

expression regulation in coffee leaves by CcDREB1D promoter haplotypes under water deficit. J. Exp. Bot. *68*, 3017–3031.

Alves, M., Dadalto, S., Gonçalves, A., de Souza, G., Barros, V., and Fietto, L. (2014). Transcription Factor Functional Protein-Protein Interactions in Plant Defense Responses. Proteomes *2*, 85–106.

Amrine, K.C.H., Blanco-Ulate, B., Riaz, S., Pap, D., Jones, L., Figueroa-Balderas, R., Walker, M.A., and Cantu, D. (2015). Comparative transcriptomics of Central Asian Vitis vinifera accessions reveals distinct defense strategies against powdery mildew. Hortic. Res. *2*.

Babraham Bioinformatics (2010). Babraham Bioinformatics - FastQC A Quality Control tool for High Throughput Sequence Data.

Bailey, T.L., and Elkan, C. (1994). Fitting a mixture model by expectation maximization to discover motifs in biopolymers. Proc. Int. Conf. Intell. Syst. Mol. Biol. *2*, 28–36.

Bailey, T.L., Boden, M., Buske, F.A., Frith, M., Grant, C.E., Clementi, L., Ren, J., Li, W.W., and Noble, W.S. (2009). MEME Suite: tools for motif discovery and searching. Nucleic Acids Res. *37*, W202–W208.

Benfey, P.N., Linstead, P.J., Roberts, K., Schiefelbein, J.W., Hauser, M.T., and Aeschbacher, R.A. (1993). Root development in Arabidopsis: four mutants with dramatically altered root morphogenesis. Development *119*, 57–70.

Berardini, T.Z., Reiser, L., Li, D., Mezheritsky, Y., Muller, R., Strait, E., and Huala, E. (2015). The arabidopsis information resource: Making and mining the "gold standard" annotated reference plant genome: Tair: Making and Mining the "Gold Standard" Plant Genome. Genesis *53*, 474–485.

Berens, M.L., Wolinska, K.W., Spaepen, S., Ziegler, J., Nobori, T., Nair, A., Krüler, V., Winkelmüller, T.M., Wang, Y., Mine, A., et al. (2019). Balancing trade-offs between biotic and abiotic stress responses through leaf age-dependent variation in stress hormone cross-talk. Proc. Natl. Acad. Sci. *116*, 2364–2373.

Berthet, S., Thevenin, J., Baratiny, D., Demont-Caulet, N., Debeaujon, I., Bidzinski, P., Leple, J.-C., Huis, R., Hawkins, S., Gomez, L.-D., et al. (2012). Role of Plant Laccases in Lignin Polymerization. In Advances in Botanical Research, (Elsevier), pp. 145–172.

Bethke, G., Unthan, T., Uhrig, J.F., Poschl, Y., Gust, A.A., Scheel, D., and Lee, J. (2009). Flg22 regulates the release of an ethylene response factor substrate from MAP kinase 6 in Arabidopsis thaliana via ethylene signaling. Proc. Natl. Acad. Sci. *106*, 8067–8072.

Birkenbihl, R.P., Diezel, C., and Somssich, I.E. (2012). Arabidopsis WRKY33 Is a Key Transcriptional Regulator of Hormonal and Metabolic Responses toward Botrytis cinerea Infection. PLANT Physiol. *159*, 266–285.

Blanco-Ulate, B., Hopfer, H., Figueroa-Balderas, R., Ye, Z., Rivero, R.M., Albacete, A., Pérez-Alfocea, F., Koyama, R., Anderson, M.M., Smith, R.J., et al. (2017). Red blotch disease alters grape berry development and metabolism by interfering with the transcriptional and hormonal regulation of ripening. J. Exp. Bot. *68*, 1225–1238.

Bodenhofer, U., Bonatesta, E., Horejš-Kainrath, C., and Hochreiter, S. (2015). msa: an R package for multiple sequence alignment.

Bolger, A.M., Lohse, M., and Usadel, B. (2014). Trimmomatic: a flexible trimmer for Illumina sequence data. Bioinformatics *30*, 2114–2120.

Bowling, S.A., Clarke, J.D., Liu, Y., Klessig, D.F., and Dong, X. (1997). The cpr5 Mutant of Arabidopsis Expresses Both NPRl-Dependent and NPRl-1ndependent Resistance. Plant Cell *9*, 1573–1584.

Brenchley, R., Spannagl, M., Pfeifer, M., Barker, G.L.A., D'Amore, R., Allen, A.M., McKenzie, N., Kramer, M., Kerhornou, A., Bolser, D., et al. (2012). Analysis of the bread wheat genome using whole-genome shotgun sequencing. Nature *491*, 705–710.

Burg, S.P., and Burg, E.A. (1966). The interaction between auxin and ethylene and its role in plant growth. Proc. Natl. Acad. Sci. U. S. A. *55*, 262–269.

Camacho, C., Coulouris, G., Avagyan, V., Ma, N., Papadopoulos, J., Bealer, K., and Madden, T.L. (2009). BLAST+: architecture and applications. BMC Bioinformatics *10*.

Canaguier, A., Grimplet, J., Di Gaspero, G., Scalabrin, S., Duchêne, E., Choisne, N., Mohellibi, N., Guichard, C., Rombauts, S., Le Clainche, I., et al. (2017). A new version of the grapevine reference genome assembly (12X.v2) and of its annotation (VCost.v3). Genomics Data *14*, 56–62.

Chen, W.-K., Bai, X.-J., Cao, M.-M., Cheng, G., Cao, X.-J., Guo, R.-R., Wang, Y., He, L., Yang, X.-H., He, F., et al. (2017). Dissecting the Variations of Ripening Progression and Flavonoid Metabolism in Grape Berries Grown under Double Cropping System. Front. Plant Sci. *8*.

Cheng, C.-Y., Krishnakumar, V., Chan, A.P., Thibaud-Nissen, F., Schobel, S., and Town, C.D. (2017). Araport11: a complete reannotation of the *Arabidopsis thaliana* reference genome. Plant J. *89*, 789–804.

Chervin, C., El-Kereamy, A., Roustan, J.-P., Latché, A., Lamon, J., and Bouzayen, M. (2004). Ethylene seems required for the berry development and ripening in grape, a non-climacteric fruit. Plant Sci. *167*, 1301–1305.

Chin, C.-S., Peluso, P., Sedlazeck, F.J., Nattestad, M., Concepcion, G.T., Clum, A., Dunn, C., O'Malley, R., Figueroa-Balderas, R., Morales-Cruz, A., et al. (2016). Phased diploid genome assembly with single-molecule real-time sequencing. Nat. Methods *13*, 1050–1054.

Cochetel, N., Ghan, R., Toups, H.S., Degu, A., Tillett, R.L., Schlauch, K.A., and Cramer, G.R. (2020). Drought tolerance of the grapevine, Vitis champinii cv. Ramsey, is associated with higher photosynthesis and greater transcriptomic responsiveness of abscisic acid biosynthesis and signaling. BMC Plant Biol. *20*.

Cookson, S.J., Clemente Moreno, M.J., Hevin, C., Nyamba Mendome, L.Z., Delrot, S., Trossat-Magnin, C., and Ollat, N. (2013). Graft union formation in grapevine induces transcriptional changes related to cell wall modification, wounding, hormone signalling, and secondary metabolism. J. Exp. Bot. *64*, 2997–3008.

Cramer, G.R., Ergül, A., Grimplet, J., Tillett, R.L., Tattersall, E.A.R., Bohlman, M.C., Vincent, D., Sonderegger, J., Evans, J., Osborne, C., et al. (2007). Water and salinity stress in grapevines: early and late changes in transcript and metabolite profiles. Funct. Integr. Genomics *7*, 111–134.

Cramer, G.R., Ghan, R., Schlauch, K.A., Tillett, R.L., Heymann, H., Ferrarini, A., Delledonne, M., Zenoni, S., Fasoli, M., and Pezzotti, M. (2014). Transcriptomic analysis of the late stages of grapevine (Vitis vinifera cv. Cabernet Sauvignon) berry ripening reveals significant induction of ethylene signaling and flavor pathways in the skin. BMC Plant Biol. *14*.

Dal Santo, S., Tornielli, G.B., Zenoni, S., Fasoli, M., Farina, L., Anesi, A., Guzzo, F., Delledonne, M., and Pezzotti, M. (2013). The plasticity of the grapevine berry transcriptome. Genome Biol. *14*.

Dal Santo, S., Zenoni, S., Sandri, M., De Lorenzis, G., Magris, G., De Paoli, E., Di Gaspero, G., Del Fabbro, C., Morgante, M., Brancadoro, L., et al. (2018). Grapevine field experiments reveal the contribution of genotype, the influence of environment and the effect of their interaction (G×E) on the berry transcriptome. Plant J. *93*, 1143–1159.

Davis, S., and Meltzer, P.S. (2007). GEOquery: a bridge between the Gene Expression Omnibus (GEO) and BioConductor. Bioinformatics *23*, 1846–1847.

Deslauriers, S.D., and Larsen, P.B. (2010). FERONIA Is a Key Modulator of Brassinosteroid and Ethylene Responsiveness in Arabidopsis Hypocotyls. Mol. Plant *3*, 626–640.

Divi, U.K., Rahman, T., and Krishna, P. (2010). Brassinosteroid-mediated stress tolerance in Arabidopsis shows interactions with abscisic acid, ethylene and salicylic acid pathways. BMC Plant Biol. *10*.

Dubois, M., Skirycz, A., Claeys, H., Maleux, K., Dhondt, S., De Bodt, S., Vanden Bossche, R., De Milde, L., Yoshizumi, T., Matsui, M., et al. (2013). ETHYLENE RESPONSE FACTOR6 Acts as a Central Regulator of Leaf Growth under Water-Limiting Conditions in Arabidopsis. Plant Physiol. *162*, 319–332.

Dubois, M., Van den Broeck, L., Claeys, H., Van Vlierberghe, K., Matsui, M., and Inzé, D. (2015). The ETHYLENE RESPONSE FACTORs ERF6 and ERF11 Antagonistically Regulate Mannitol-Induced Growth Inhibition in Arabidopsis. Plant Physiol. *169*, 166–179.

Ecker, J.R., and Davis, R.W. (1987). Plant defense genes are regulated by ethylene. Proc. Natl. Acad. Sci. *84*, 5202–5206.

Edgar, R. (2002). Gene Expression Omnibus: NCBI gene expression and hybridization array data repository. Nucleic Acids Res. *30*, 207–210.

Eisenmann, B., Czemmel, S., Ziegler, T., Buchholz, G., Kortekamp, A., Trapp, O., Rausch, T., Dry, I., and Bogs, J. (2019). Rpv3–1 mediated resistance to grapevine downy mildew is associated with specific host transcriptional responses and the accumulation of stilbenes. BMC Plant Biol. *19*.

Fan, L., Linker, R., Gepstein, S., Tanimoto, E., Yamamoto, R., and Neumann, P.M. (2006). Progressive Inhibition by Water Deficit of Cell Wall Extensibility and Growth along the Elongation Zone of Maize Roots Is Related to Increased Lignin Metabolism and Progressive Stelar Accumulation of Wall Phenolics. Plant Physiol. *140*, 603–612.

Fasoli, M., Dal Santo, S., Zenoni, S., Tornielli, G.B., Farina, L., Zamboni, A., Porceddu, A., Venturini, L., Bicego, M., Murino, V., et al. (2012). The Grapevine Expression Atlas Reveals a Deep Transcriptome Shift Driving the Entire Plant into a Maturation Program. Plant Cell *24*, 3489–3505.

Fernandez-Pozo, N., Zheng, Y., Snyder, S.I., Nicolas, P., Shinozaki, Y., Fei, Z., Catala, C., Giovannoni, J.J., Rose, J.K.C., and Mueller, L.A. (2017). The Tomato Expression Atlas. Bioinformatics *33*, 2397–2398.

Ford, K.A., Casida, J.E., Chandran, D., Gulevich, A.G., Okrent, R.A., Durkin, K.A., Sarpong, R., Bunnelle, E.M., and Wildermuth, M.C. (2010). Neonicotinoid insecticides induce salicylate-associated plant defense responses. Proc. Natl. Acad. Sci. *107*, 17527–17532.

Fröschel, C., Iven, T., Walper, E., Bachmann, V., Weiste, C., and Dröge-Laser, W. (2019). A Gain-of-Function Screen Reveals Redundant ERF Transcription Factors Providing Opportunities for Resistance Breeding Toward the Vascular Fungal Pathogen Verticillium longisporum. Mol. Plant-Microbe Interact. MPMI *32*, 1095–1109.

Ghan, R., Petereit, J., Tillett, R.L., Schlauch, K.A., Toubiana, D., Fait, A., and Cramer, G.R. (2017). The common transcriptional subnetworks of the grape berry skin in the late stages of ripening. BMC Plant Biol. *17*.

Gigolashvili, T., Berger, B., Mock, H.-P., Müller, C., Weisshaar, B., and Flügge, U.-I. (2007). The transcription factor HIG1/MYB51 regulates indolic glucosinolate biosynthesis in Arabidopsis thaliana: HIG1 and glucosinolate biosynthesis. Plant J. *50*, 886–901.

Giraud, E., Ho, L.H.M., Clifton, R., Carroll, A., Estavillo, G., Tan, Y.-F., Howell, K.A., Ivanova, A., Pogson, B.J., Millar, A.H., et al. (2008). The Absence of ALTERNATIVE OXIDASE1a in Arabidopsis Results in Acute Sensitivity to Combined Light and Drought Stress. Plant Physiol. *147*, 595–610.

Gouthu, S., O'Neil, S.T., Di, Y., Ansarolia, M., Megraw, M., and Deluc, L.G. (2014). A comparative study of ripening among berries of the grape cluster reveals an altered transcriptional programme and enhanced ripening rate in delayed berries. J. Exp. Bot. *65*, 5889–5902.

Gray, D., and Zhijian, Li (2006). pECBC Patent (Gainesville, Florida).

Grimplet, J., Van Hemert, J., Carbonell-Bejerano, P., Díaz-Riquelme, J., Dickerson, J., Fennell, A., Pezzotti, M., and Martínez-Zapater, J.M. (2012). Comparative analysis of grapevine whole-genome gene predictions, functional annotation, categorization and integration of the predicted gene sequences. BMC Res. Notes *5*.

Grimplet, J., Agudelo-Romero, P., Teixeira, R.T., Martinez-Zapater, J.M., and Fortes, A.M. (2016). Structural and Functional Analysis of the GRAS Gene Family in Grapevine Indicates a Role of GRAS Proteins in the Control of Development and Stress Responses. Front. Plant Sci. *7*.

Gu, Z., Eils, R., and Schlesner, M. (2016). Complex heatmaps reveal patterns and correlations in multidimensional genomic data. Bioinforma. Oxf. Engl. *32*, 2847–2849.

Gupta, S., Stamatoyannopoulos, J.A., Bailey, T.L., and Noble, W.S. (2007). Quantifying similarity between motifs. Genome Biol. *8*, R24.1-R24.9.

Hellemans, J., Mortier, G., De Paepe, A., Speleman, F., and Vandesompele, J. (2007). qBase relative quantification framework and software for management and automated analysis of real-time quantitative PCR data. Genome Biol. *8*, R19.

Higo, K., Ugawa, Y., Iwamoto, M., and Korenaga, T. (1999). Plant cis-acting regulatory DNA elements (PLACE) database: 1999. Nucleic Acids Res. *27*, 297–300.

Hopper, D.W., Ghan, R., and Cramer, G.R. (2014). A rapid dehydration leaf assay reveals stomatal response differences in grapevine genotypes. Hortic. Res. *1*.

Hopper, D.W., Ghan, R., Schlauch, K.A., and Cramer, G.R. (2016). Transcriptomic network analyses of leaf dehydration responses identify highly connected ABA and ethylene signaling hubs in three grapevine species differing in drought tolerance. BMC Plant Biol. *16*.

Huang, W., Xian, Z., Kang, X., Tang, N., and Li, Z. (2015). Genome-wide identification, phylogeny and expression analysis of GRAS gene family in tomato. BMC Plant Biol. *15*, 209.

Iqbal, N., Khan, N.A., Ferrante, A., Trivellini, A., Francini, A., and Khan, M.I.R. (2017). Ethylene Role in Plant Growth, Development and Senescence: Interaction with Other Phytohormones. Front. Plant Sci. *8*.

Jaillon, O., Aury, Jean-Marc, Noel, Benjamin, Policriti, Alberto, Clepet, Christian, Casagrande, Alberto, Choisne, Nathalie, Aubourg, Sébastien, Vitulo, Nicola, Jubin, C., et al. (2007). The grapevine genome sequence suggests ancestral hexaploidization in major angiosperm phyla. Nature *449*, 463–467.

Kagale, S., Links, M.G., and Rozwadowski, K. (2010). Genome-Wide Analysis of Ethylene-Responsive Element Binding Factor-Associated Amphiphilic Repression Motif-Containing Transcriptional Regulators in Arabidopsis. PLANT Physiol. *152*, 1109–1134.

Klay, I., Gouia, S., Liu, M., Mila, I., Khoudi, H., Bernadac, A., Bouzayen, M., and Pirrello, J. (2018). Ethylene Response Factors (ERF) are differentially regulated by different abiotic stress types in tomato plants. Plant Sci. *274*, 137–145.

Kumar, S., Stecher, G., Li, M., Knyaz, C., and Tamura, K. (2018). MEGA X: Molecular Evolutionary Genetics Analysis across Computing Platforms. Mol. Biol. Evol. *35*, 1547–1549.

Kunkel, B.N., and Brooks, D.M. (2002). Cross talk between signaling pathways in pathogen defense. Curr. Opin. Plant Biol. *5*, 325–331.

Laird, J., Armengaud, P., Giuntini, P., Laval, V., and Milner, J.J. (2004). Inappropriate annotation of a key defence marker in Arabidopsis: will the real PR-1 please stand up? Planta *219*, 1089–1092.

Lawrence, M., Huber, W., Pagès, H., Aboyoun, P., Carlson, M., Gentleman, R., Morgan, M.T., and Carey, V.J. (2013). Software for Computing and Annotating Genomic Ranges. PLoS Comput. Biol. *9*.

Lee, B.-R., Kim, K.-Y., Jung, W.-J., Avice, J.-C., Ourry, A., and Kim, T.-H. (2007). Peroxidases and lignification in relation to the intensity of water-deficit stress in white clover (Trifolium repens L.). J. Exp. Bot. *58*, 1271–1279.

Leida, C., Dal Rì, A., Dalla Costa, L., Gómez, M.D., Pompili, V., Sonego, P., Engelen, K., Masuero, D., Ríos, G., and Moser, C. (2016). Insights into the Role of the Berry-Specific Ethylene Responsive Factor VviERF045. Front. Plant Sci. *7*.

Leinonen, R., Sugawara, H., Shumway, M., and International Nucleotide Sequence Database Collaboration (2011). The Sequence Read Archive. Nucleic Acids Res. *39*, D19–D21.

Li, S., Fu, Q., Chen, L., Huang, W., and Yu, D. (2011). Arabidopsis thaliana WRKY25, WRKY26, and WRKY33 coordinate induction of plant thermotolerance. Planta *233*, 1237–1252.

Li, X., Tao, S., Wei, S., Ming, M., Huang, X., Zhang, S., and Wu, J. (2018). The mining and evolutionary investigation of AP2/ERF genes in pear (Pyrus). BMC Plant Biol. *18*.

Licausi, F., Giorgi, F.M., Zenoni, S., Osti, F., Pezzotti, M., and Perata, P. (2010). Genomic and transcriptomic analysis of the AP2/ERF superfamily in Vitis vinifera. BMC Genomics *11*.

Licausi, F., Ohme-Takagi, M., and Perata, P. (2013). APETALA2/Ethylene Responsive Factor (AP2/ERF) transcription factors: mediators of stress responses and developmental programs. New Phytol. *199*, 639–649.

Liu, M., Diretto, G., Pirrello, J., Roustan, J.-P., Li, Z., Giuliano, G., Regad, F., and Bouzayen, M. (2014). The chimeric repressor version of an Ethylene Response Factor (ERF) family member, Sl-ERF.B3, shows contrasting effects on tomato fruit ripening. New Phytol. *203*, 206–218.

Liu, M., Gomes, B.L., Mila, I., Purgatto, E., Peres, L.E.P., Frasse, P., Maza, E., Zouine, M., Roustan, J.-P., Bouzayen, M., et al. (2016). Comprehensive Profiling of Ethylene Response Factor Expression Identifies Ripening-Associated ERF Genes and Their Link to Key Regulators of Fruit Ripening in Tomato. Plant Physiol. *170*, 1732–1744.

Londo, J.P., Kovaleski, A.P., and Lillis, J.A. (2018). Divergence in the transcriptional landscape between low temperature and freeze shock in cultivated grapevine (Vitis vinifera). Hortic. Res. *5*.

van Loon, L.C., Geraats, B.P.J., and Linthorst, H.J.M. (2006). Ethylene as a modulator of disease resistance in plants. Trends Plant Sci. *11*, 184–191.

Love, M.I., Huber, W., and Anders, S. (2014). Moderated estimation of fold change and dispersion for RNA-seq data with DESeq2. Genome Biol. *15*.

Ma, Q., Zhang, G., Hou, L., Wang, W., Hao, J., and Liu, X. (2015). Vitis vinifera VvWRKY13 is an ethylene biosynthesis-related transcription factor. Plant Cell Rep. *34*, 1593–1603.

Mao, J.-L., Miao, Z.-Q., Wang, Z., Yu, L.-H., Cai, X.-T., and Xiang, C.-B. (2016). Arabidopsis ERF1 Mediates Cross-Talk between Ethylene and Auxin Biosynthesis during Primary Root Elongation by Regulating ASA1 Expression. PLOS Genet. *12*, e1005760.

Mase, K., Ishihama, N., Mori, H., Takahashi, H., Kaminaka, H., Kodama, M., and Yoshioka, H. (2013). Ethylene-Responsive AP2/ERF Transcription Factor MACD1 Participates in Phytotoxin-Triggered Programmed Cell Death. Mol. Plant. Microbe Interact. *26*, 868–879.

Massonnet, M., Figueroa-Balderas, R., Galarneau, E.R.A., Miki, S., Lawrence, D.P., Sun, Q., Wallis, C.M., Baumgartner, K., and Cantu, D. (2017a). Neofusicoccum parvum

Colonization of the Grapevine Woody Stem Triggers Asynchronous Host Responses at the Site of Infection and in the Leaves. Front. Plant Sci. *8*.

Massonnet, M., Fasoli, M., Tornielli, G.B., Altieri, M., Sandri, M., Zuccolotto, P., Paci, P., Gardiman, M., Zenoni, S., and Pezzotti, M. (2017b). Ripening Transcriptomic Program in Red and White Grapevine Varieties Correlates with Berry Skin Anthocyanin Accumulation. Plant Physiol. *174*, 2376–2396.

McGrath, K.C. (2005). Repressor- and Activator-Type Ethylene Response Factors Functioning in Jasmonate Signaling and Disease Resistance Identified via a Genome-Wide Screen of Arabidopsis Transcription Factor Gene Expression. PLANT Physiol. *139*, 949–959.

Minio, A., Massonnet, M., Figueroa-Balderas, R., Castro, A., and Cantu, D. (2019a). Diploid Genome Assembly of the Wine Grape Carménère. G3 GenesGenomesGenetics *9*, 1331–1337.

Minio, A., Massonnet, M., Figueroa-Balderas, R., Vondras, A.M., Blanco-Ulate, B., and Cantu, D. (2019b). Iso-Seq Allows Genome-Independent Transcriptome Profiling of Grape Berry Development. G3 GenesGenomesGenetics *9*, 755–767.

Mitchell, A.L., Attwood, T.K., Babbitt, P.C., Blum, M., Bork, P., Bridge, A., Brown, S.D., Chang, H.-Y., El-Gebali, S., Fraser, M.I., et al. (2019). InterPro in 2019: improving coverage, classification and access to protein sequence annotations. Nucleic Acids Res. *47*, D351–D360.

Moffat, C.S., Ingle, R.A., Wathugala, D.L., Saunders, N.J., Knight, H., and Knight, M.R. (2012). ERF5 and ERF6 Play Redundant Roles as Positive Regulators of JA/Et-Mediated Defense against Botrytis cinerea in Arabidopsis. PLoS ONE *7*.

Müller, M., and Munné-Bosch, S. (2015). Ethylene Response Factors: A Key Regulatory Hub in Hormone and Stress Signaling. Plant Physiol. *169*, 32–41.

Nakano, T., Suzuki, K., Fujimura, T., and Shinshi, H. (2006). Genome-Wide Analysis of the ERF Gene Family in Arabidopsis and Rice. Plant Physiol. *140*, 411–432.

Ohta, M., Matsui, K., Hiratsu, K., Shinshi, H., and Ohme-Takagi, M. (2001). Repression Domains of Class II ERF Transcriptional Repressors Share an Essential Motif for Active Repression. Plant Cell *13*, 1959–1968.

Panchy, N., Lehti-Shiu, M.D., and Shiu, S.-H. (2016). Evolution of gene duplication in plants. Plant Physiol. *171*, 2294–2316.

Patro, R., Duggal, G., Love, M.I., Irizarry, R.A., and Kingsford, C. (2017). Salmon provides fast and bias-aware quantification of transcript expression. Nat. Methods *14*, 417–419.

Phukan, U.J., Jeena, G.S., Tripathi, V., and Shukla, R.K. (2017). Regulation of Apetala2/Ethylene Response Factors in Plants. Front. Plant Sci. *8*.

Pysh, L.D., Wysocka-Diller, J.W., Camilleri, C., Bouchez, D., and Benfey, P.N. (1999). The GRAS gene family in Arabidopsis: sequence characterization and basic expression analysis of the SCARECROW-LIKE genes. Plant J. *18*, 111–119.

Rattanakon, S., Ghan, R., Gambetta, G.A., Deluc, L.G., Schlauch, K.A., and Cramer, G.R. (2016). Abscisic acid transcriptomic signaling varies with grapevine organ. BMC Plant Biol. *16*.

Renny-Byfield, S., Gallagher, J.P., Grover, C.E., Szadkowski, E., Page, J.T., Udall, J.A., Wang, X., Paterson, A.H., and Wendel, J.F. (2014). Ancient Gene Duplicates in Gossypium (Cotton) Exhibit Near-Complete Expression Divergence. Genome Biol. Evol. *6*, 559–571.

Rienth, M., Crovadore, J., Ghaffari, S., and Lefort, F. (2019). Oregano essential oil vapour prevents Plasmopara viticola infection in grapevine (Vitis Vinifera) and primes plant immunity mechanisms. PLOS ONE *14*.

Rieu, I., Eriksson, S., Powers, S.J., Gong, F., Griffiths, J., Woolley, L., Benlloch, R., Nilsson, O., Thomas, S.G., Hedden, P., et al. (2008). Genetic Analysis Reveals That C19-GA 2-Oxidation Is a Major Gibberellin Inactivation Pathway in Arabidopsis. PLANT CELL ONLINE *20*, 2420–2436.

Ritchie, M.E., Phipson, B., Wu, D., Hu, Y., Law, C.W., Shi, W., and Smyth, G.K. (2015). limma powers differential expression analyses for RNA-sequencing and microarray studies. Nucleic Acids Res. *43*, e47–e47.

Saithong, T., Saerue, S., Kalapanulak, S., Sojikul, P., Narangajavana, J., and Bhumiratana, S. (2015). Gene Co-Expression Analysis Inferring the Crosstalk of Ethylene and Gibberellin in Modulating the Transcriptional Acclimation of Cassava Root Growth in Different Seasons. PLoS ONE *10*.

Sakamoto, H., Maruyama, K., Sakuma, Y., Meshi, T., Iwabuchi, M., Shinozaki, K., and Yamaguchi-Shinozaki, K. (2004). Arabidopsis Cys2/His2-Type Zinc-Finger Proteins Function as Transcription Repressors under Drought, Cold, and High-Salinity Stress Conditions. PLANT Physiol. *136*, 2734–2746.

Schmutz, J., Cannon, S.B., Schlueter, J., Ma, J., Mitros, T., Nelson, W., Hyten, D.L., Song, Q., Thelen, J.J., Cheng, J., et al. (2010). Genome sequence of the palaeopolyploid soybean. Nature *463*, 178–183.

Schnable, J.C., Springer, N.M., and Freeling, M. (2011). Differentiation of the maize subgenomes by genome dominance and both ancient and ongoing gene loss. Proc. Natl. Acad. Sci. *108*, 4069–4074.

Schneider, C.A., Rasband, W.S., and Eliceiri, K.W. (2012). NIH Image to ImageJ: 25 years of Image Analysis. Nat. Methods *9*, 671–675.

Sewelam, N., Kazan, K., Thomas-Hall, S.R., Kidd, B.N., Manners, J.M., and Schenk, P.M. (2013). Ethylene Response Factor 6 Is a Regulator of Reactive Oxygen Species Signaling in Arabidopsis. PLoS ONE *8*.

Sharp, R.E. (2002). Interaction with ethylene: changing views on the role of abscisic acid in root and shoot growth responses to water stress. Plant Cell Environ. *25*, 211–222.

Shirsat, A., Wilford, N., Croy, R., and Boulter, D. (1989). Sequences responsible for the tissue specific promoter activity of a pea legumin gene in tobacco. MGG Mol. Gen. Genet. *215*, 326–331.

Skirycz, A., Claeys, H., De Bodt, S., Oikawa, A., Shinoda, S., Andriankaja, M., Maleux, K., Eloy, N.B., Coppens, F., Yoo, S.-D., et al. (2011). Pause-and-Stop: The Effects of Osmotic Stress on Cell Proliferation during Early Leaf Development in *Arabidopsis* and a Role for Ethylene Signaling in Cell Cycle Arrest. Plant Cell *23*, 1876–1888.

Son, G.H., Wan, J., Kim, H.J., Nguyen, X.C., Chung, W.S., Hong, J.C., and Stacey, G. (2012). Ethylene-Responsive Element-Binding Factor 5, ERF5, Is Involved in Chitin-Induced Innate Immunity Response. Mol. Plant. Microbe Interact. *25*, 48–60.

Soneson, C., Love, M.I., and Robinson, M.D. (2015). Differential analyses for RNA-seq: transcript-level estimates improve gene-level inferences. F1000Research *4*.

Song, C.-P. (2005). Role of an Arabidopsis AP2/EREBP-Type Transcriptional Repressor in Abscisic Acid and Drought Stress Responses. PLANT CELL ONLINE *17*, 2384–2396.

Sotelo-Silveira, M., Cucinotta, M., Chauvin, A.-L., Chavez Montes, R.A., Colombo, L., Marsch-Martinez, N., and de Folter, S. (2013). Cytochrome P450 CYP78A9 Is Involved in Arabidopsis Reproductive Development. PLANT Physiol. *162*, 779–799.

Sterck, L., Billiau, K., Abeel, T., Rouzé, P., and Van de Peer, Y. (2012). ORCAE: online resource for community annotation of eukaryotes. Nat. Methods *9*, 1041.

Sun, R.-Z., Cheng, G., Li, Q., He, Y.-N., Wang, Y., Lan, Y.-B., Li, S.-Y., Zhu, Y.-R., Song, W.-F., Zhang, X., et al. (2017). Light-induced Variation in Phenolic Compounds in Cabernet Sauvignon Grapes (Vitis vinifera L.) Involves Extensive Transcriptome Reprogramming of Biosynthetic Enzymes, Transcription Factors, and Phytohormonal Regulators. Front. Plant Sci. *8*.

Tattersall, E.A.R., Grimplet, J., DeLuc, L., Wheatley, M.D., Vincent, D., Osborne, C., Ergül, A., Lomen, E., Blank, R.R., Schlauch, K.A., et al. (2007). Transcript abundance profiles reveal larger and more complex responses of grapevine to chilling compared to osmotic and salinity stress. Funct. Integr. Genomics *7*, 317–333.

Tello-Ruiz, M.K., Naithani, S., Stein, J.C., Gupta, P., Campbell, M., Olson, A., Wei, S., Preece, J., Geniza, M.J., Jiao, Y., et al. (2018). Gramene 2018: unifying comparative genomics and pathway resources for plant research. Nucleic Acids Res. *46*, D1181–D1189.

Vitulo, N., Forcato, C., Carpinelli, E.C., Telatin, A., Campagna, D., D'Angelo, M., Zimbello, R., Corso, M., Vannozzi, A., Bonghi, C., et al. (2014). A deep survey of alternative splicing in grape reveals changes in the splicing machinery related to tissue, stress condition and genotype. BMC Plant Biol. *14*.

Wang, L., Sun, Y., Xia, X.-L., and Jiang, T.-B. (2018a). Screening of proteins interacting with ERF transcriptional factor from *Populus simonii* × *P.nigra* by yeast two-hybrid method. Biotechnol. Biotechnol. Equip. *32*, 543–549.

Wang, L., Waters, M.T., and Smith, S.M. (2018b). Karrikin-KAI2 signalling provides Arabidopsis seeds with tolerance to abiotic stress and inhibits germination under conditions unfavourable to seedling establishment. New Phytol. *219*, 605–618.

Wang, X., Du, B., Liu, M., Sun, N., and Qi, X. (2013). Arabidopsis Transcription Factor WRKY33 Is Involved in Drought by Directly Regulating the Expression of CesA8. Am. J. Plant Sci. *4*, 21–27.

Wang, X., Lin, S., Liu, D., Wang, Q., McAvoy, R., Ding, J., and Li, Y. (2019). Characterization and Expression Analysis of ERF Genes in Fragaria vesca Suggest Different Divergences of Tandem ERF Duplicates. Front. Genet. *10*.

Warmerdam, S., Sterken, M.G., Van Schaik, C., Oortwijn, M.E.P., Lozano-Torres, J.L., Bakker, J., Goverse, A., and Smant, G. (2018). Mediator of tolerance to abiotic stress ERF6 regulates susceptibility of Arabidopsis to Meloidogyne incognita. Mol. Plant Pathol. *20*, 137–152.

Waterhouse, A., Bertoni, M., Bienert, S., Studer, G., Tauriello, G., Gumienny, R., Heer, F.T., de Beer, T.A.P., Rempfer, C., Bordoli, L., et al. (2018). SWISS-MODEL: homology modelling of protein structures and complexes. Nucleic Acids Res. *46*, W296–W303.

Yamaguchi-Shinozaki, K., and Shinozaki, K. (2005). Organization of cis-acting regulatory elements in osmotic- and cold-stress-responsive promoters. Trends Plant Sci. *10*, 88–94.

Yanagisawa, S. (2002). The Dof family of plant transcription factors. Trends Plant Sci. *7*, 555–560.

Yang, Z., Tian, L., Latoszek-Green, M., Brown, D., and Wu, K. (2005). Arabidopsis ERF4 is a transcriptional repressor capable of modulating ethylene and abscisic acid responses. Plant Mol. Biol. *58*, 585–596.

Yoshida, T., Mogami, J., and Yamaguchi-Shinozaki, K. (2014). ABA-dependent and ABA-independent signaling in response to osmotic stress in plants. Curr. Opin. Plant Biol. *21*, 133–139.

Zhou, Y., Minio, A., Massonnet, M., Solares, E., Lv, Y., Beridze, T., Cantu, D., and Gaut, B.S. (2019). The population genetics of structural variants in grapevine domestication. Nat. Plants *5*, 965–979.

Zhu, Y., Dong, A., Meyer, D., Pichon, O., Renou, J.-P., Cao, K., and Shen, W.-H. (2006). Arabidopsis NRP1 and NRP2 Encode Histone Chaperones and Are Required for Maintaining Postembryonic Root Growth. Plant Cell *18*, 2879–2892.

Zhu, Z., Shi, J., Xu, W., Li, H., He, M., Xu, Y., Xu, T., Yang, Y., Cao, J., and Wang, Y. (2013). Three ERF transcription factors from Chinese wild grapevine Vitis pseudoreticulata participate in different biotic and abiotic stress-responsive pathways. J. Plant Physiol. *170*, 923–933.

Tables

Table 1: PN40024 VviERF6L gene names and coordinates. Common gene names, V2 and V3 PN40024 loci annotation names, start and stop gene chromosome coordinates, coding strands, and total protein lengths in amino acid residues of the 18 identified *VviERF6Ls* in PN40024.

PN40024 *VviERF6Ls*						
Gene Name	**Loci name V3**	**Loci name V2**	**start**	**stop**	**strand**	**Length (AA)**
VviERF6L1	Vitvi16g00350	VIT_16s0013g00900	6283579	6284605	+	278
VviERF6L2	Vitvi16g01429	VIT_16s0013g00950	6323868	6324845	+	278
VviERF6L3	Vitvi16g01438	VIT_16s0013g00970	6340458	6341282	+	275
VviERF6L4	Vitvi16g01430	VIT_16s0013g00980	6353674	6354603	+	276
VviERF6L5	Vitvi16g01424	VIT_16s0013g00990	6374230	6375289	+	278
VviERF6L6	Vitvi16g01432	VIT_16s0013g01000	6390945	6391977	-	269
VviERF6L7	Vitvi16g00362	VIT_16s0013g01050	6495312	6496325	+	278
VviERF6L8	Vitvi16g00363	VIT_16s0013g01060	6518283	6519283	+	278
VviERF6L9	Vitvi16g00370	VIT_16s0013g01070	6550999	6552087	+	276
VviERF6L10	Vitvi16g01437	VIT_16s0013g01090	6626070	6627309	-	265
VviERF6L11	Vitvi16g01434	VIT_16s0013g01110	6659232	6660318	-	279
VviERF6L12	Vitvi16g00380	VIT_16s0013g01120	6692405	6693620	+	243
VviERF6L13	Vitvi16g01423	NA	6387963	6388894	+	275
VviERF6L14	Vitvi16g00360	NA	6460898	6461806	+	191
VviERF6L15	Vitvi16g01442	NA	6530589	6531483	+	275
VviERF6L16	Vitvi16g01444	NA	6621652	6622826	-	283
VviERF6L17	Vitvi16g01443	NA	6662810	6663750	-	265
VviERF6L18	Vitvi16g01435	NA	6667987	6669132	-	279

Figures

Figure 1: PN40024 VviERF6L protein motif relative presence and order. The relative order of the nine highly conserved amino acid motifs (top) in the 18 PN40024 VviERF6L proteins from N-terminus (left) to C-terminus (right) spanning in total an average of ~280 amino acid residues. White spaces indicate absence of a motif. Previously identified motifs are labeled (bottom). Exact motif coordinates are in Appendix 2.

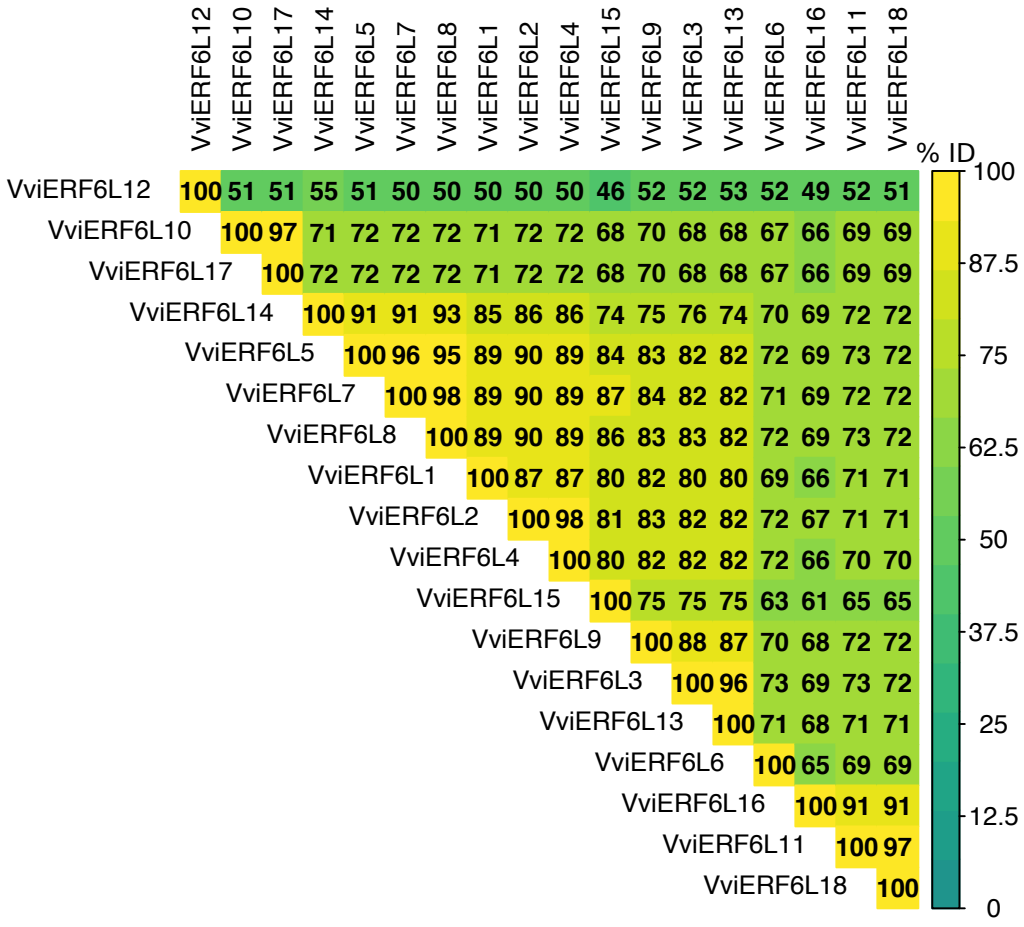

Figure 2: Percent identity of the 18 PN40024 *VviERF6L* proteins. Sequences were aligned with a MUSCLE multiple sequence alignment and compared to all other sequences with blue representing lower and yellow representing higher percent identity (% ID).

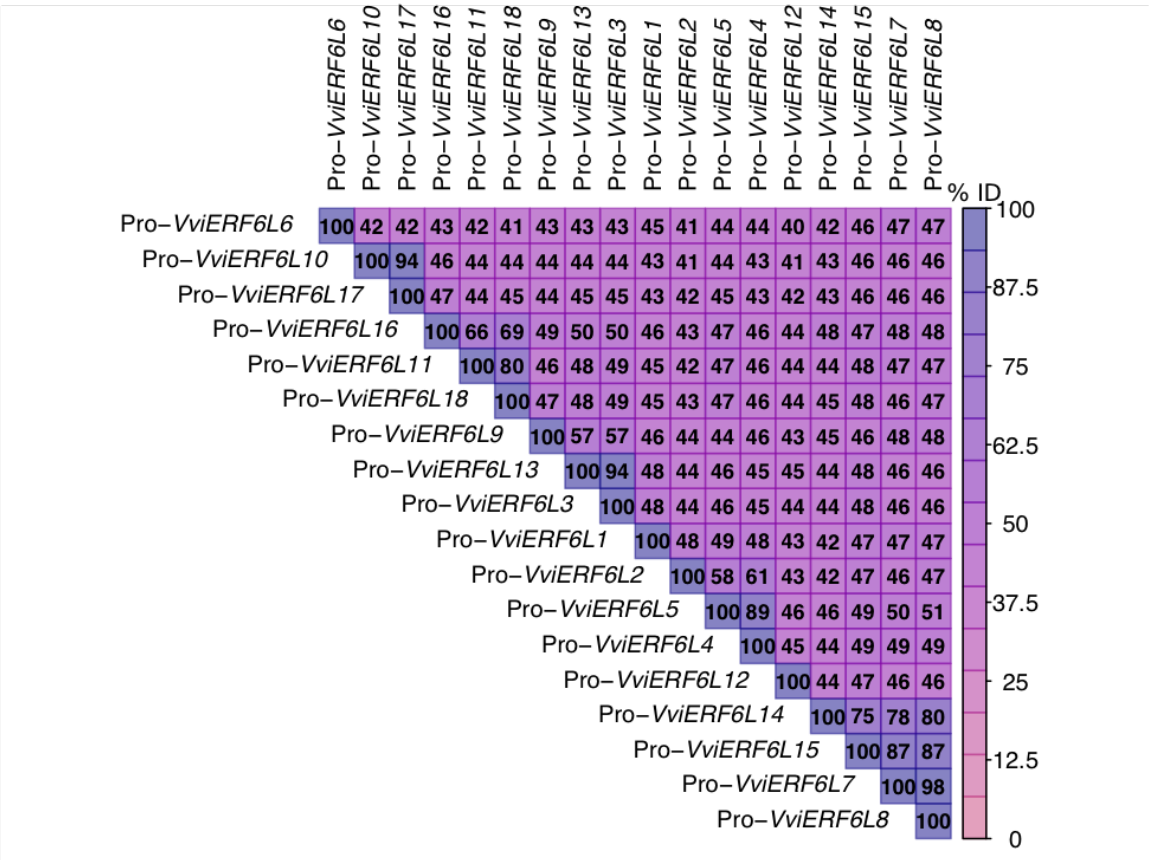

Figure 3: Percent identity of the 18 PN40024 *VviERF6L* putative promoter regions (-3,000 bp). Promoter (Pro-) sequences (-3,000 bp) were aligned with a MUSCLE multiple sequence alignment and compared to all other sequences with pink representing lower and purple representing higher percent identity (% ID)

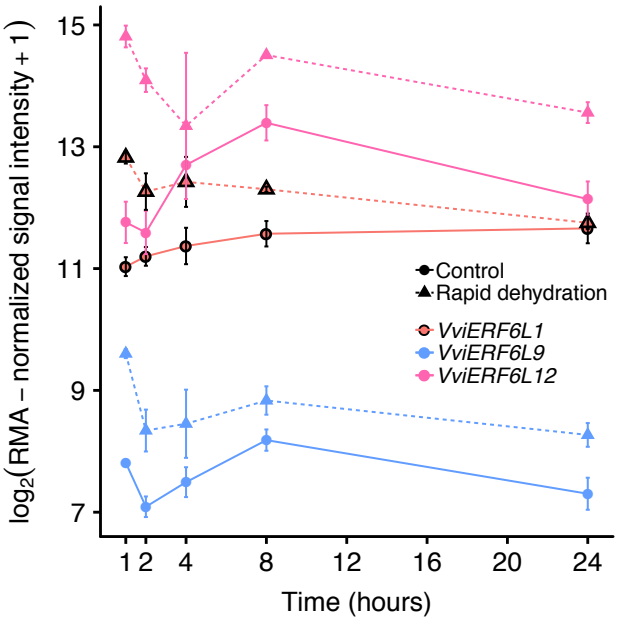

Figure 4: *VviERF6L* gene expression in response to rapid dehydration CS leaves. Log_2(RMA-normalized signal intensity+1) gene expression of three *VviERF6Ls* in CS leaves treated with control (solid lines and circles) or detached and allowed to rapidly dehydrate under regulated conditions (dotted lines and triangles) for 1, 2, 4, 8, or 24 hours. *VviERF6L1* in red with black outline, *VviERF6L9* in blue, and *VviERF6L12* in pink [GSE78920]; mean ± SE.

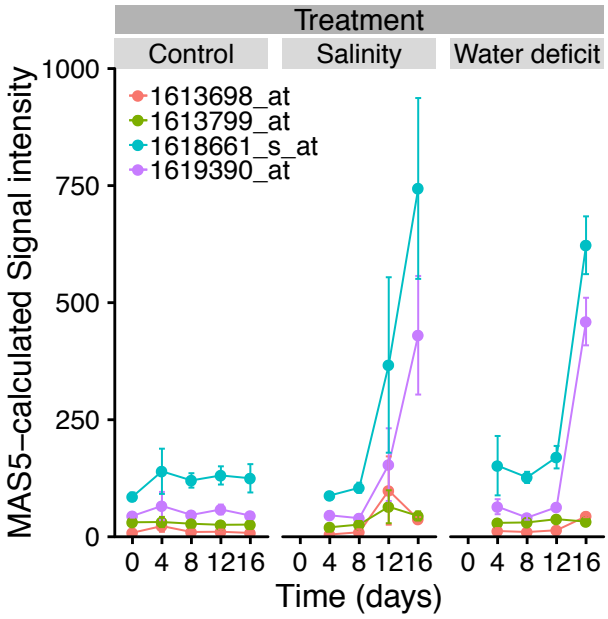

Figure 5: *VviERF6L* gene expression in response to salinity and water deficit in CS shoot tips. MAS5-calculated signal intensity of four *VviERF6L* probes in which CS vine were treated with a control nutrient solution, a progressive ramp of NaCl + $CaCl_2$, or a natural dry down for 16 days [GSE31677]; mean ± SE.

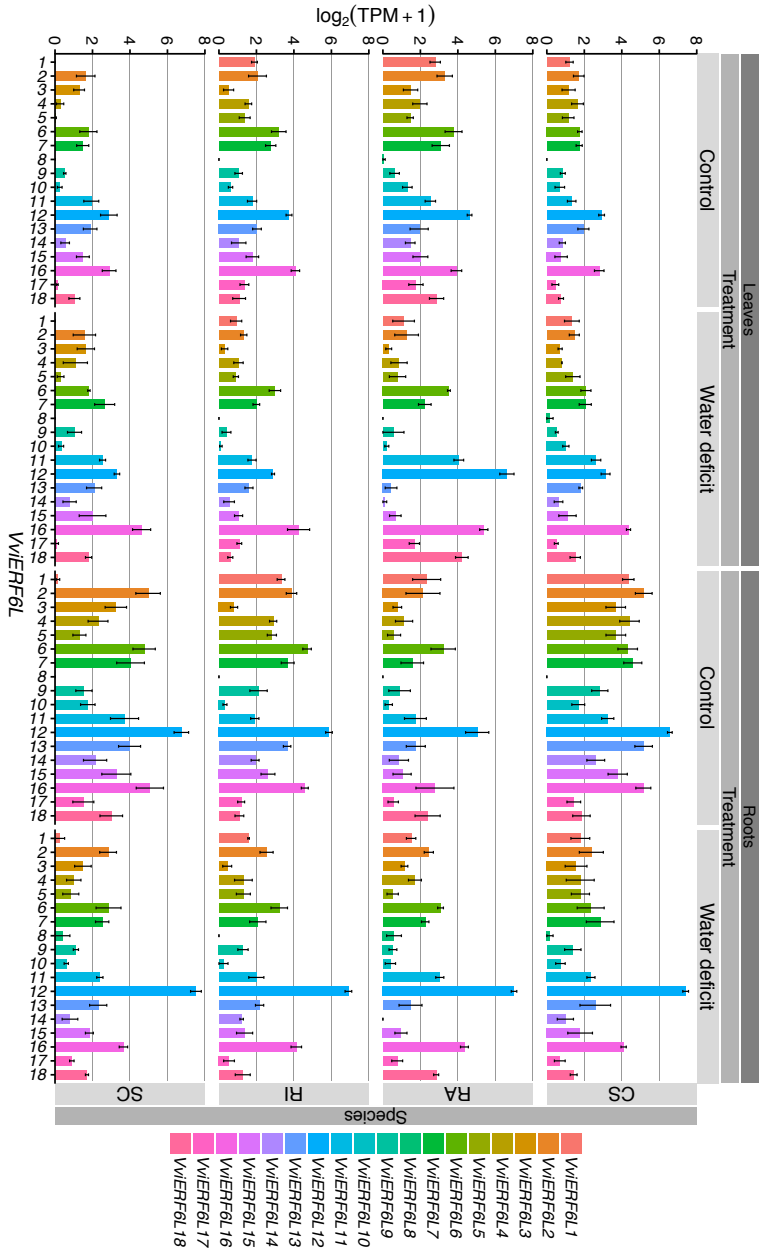

Figure 6: *VviERF6L* gene expression in response to two weeks of water deficit in leaves and roots of four *Vitis* species. Log_2(Transcripts per million (TPM)+1) of 18 *VviERF6Ls* treated with well-watered control and water deficit for two weeks in leaves (left) and roots (right) in CS, RA, RI, and SC [PRJNA516950]; mean ± SE.

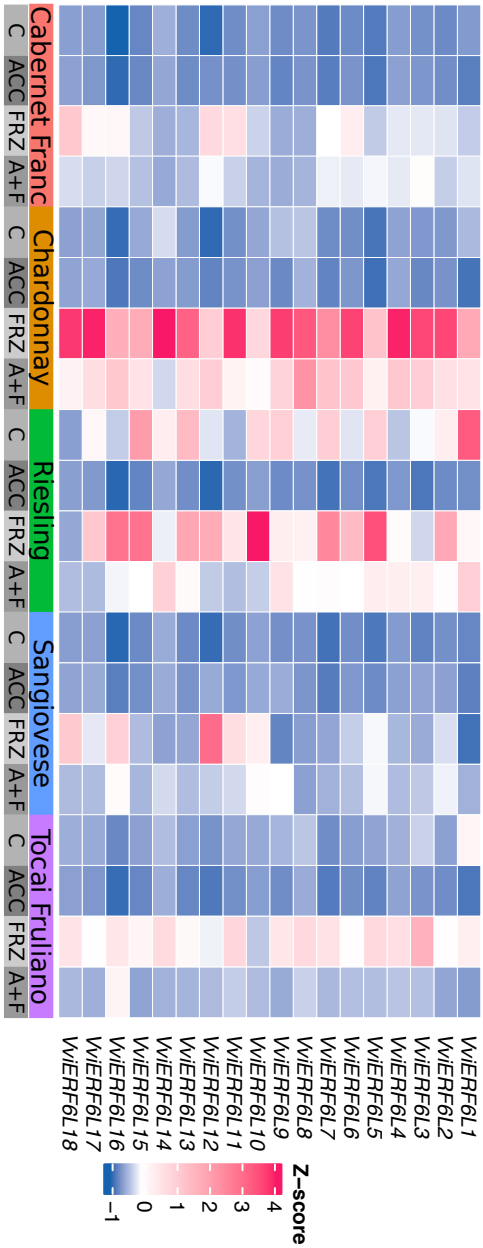

Figure 7: Heatmap representation of the gene expression of *VviERF6Ls* in response to cold. Average TPM of 18 *VviERF6Ls* were $\log_2$ transformed and represented as Z-scores (calculated per gene) with pink representing higher and blue representing lower values from leaves of whole vines treated with chilling acclimation (ACC), acclimation followed by freezing (A+F), control (C), and freezing (FRZ) from Cabernet Franc (pink), Chardonnay (orange), Riesling (green), Sangiovese (blue), and Tocai Friulano (purple) [SRP117281].

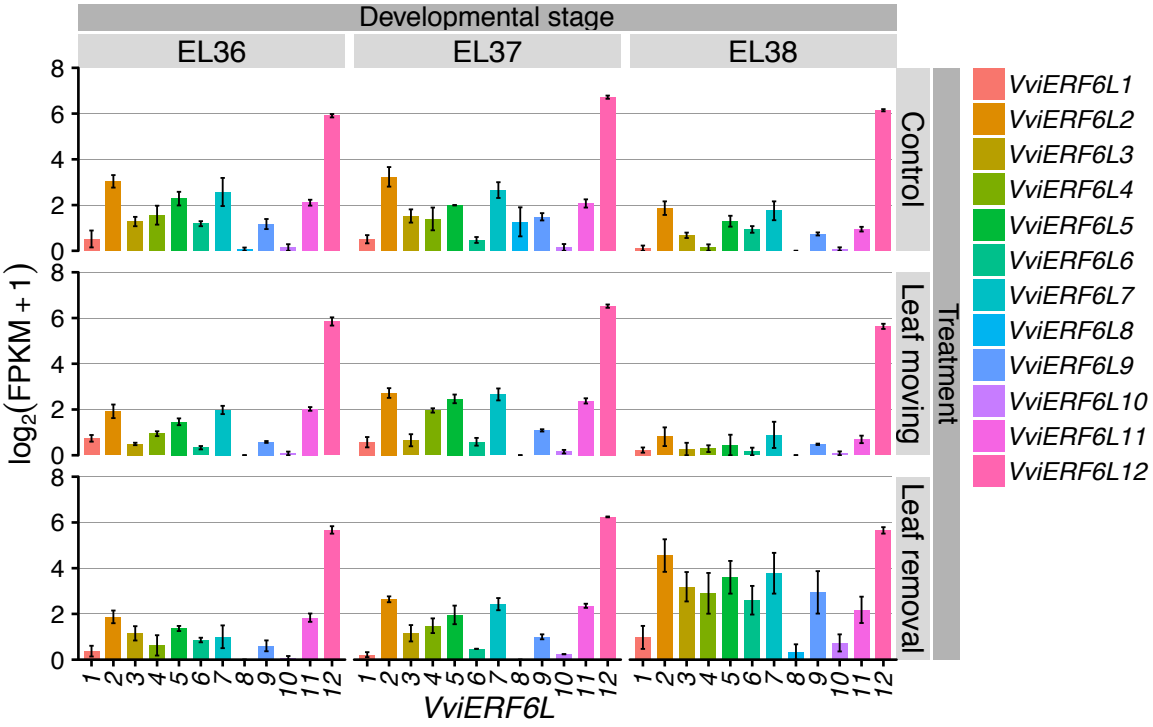

Figure 8: *VviERF6L* gene expression in response to light exposure. Log_2(FPKM+1) gene expression of 12 *VviERF6Ls* from berry pericarp at three stages of ripening (EL36-38) under control, leaf movement, and leaf removal light exposure treatments [GSE121146]; mean ± SE.

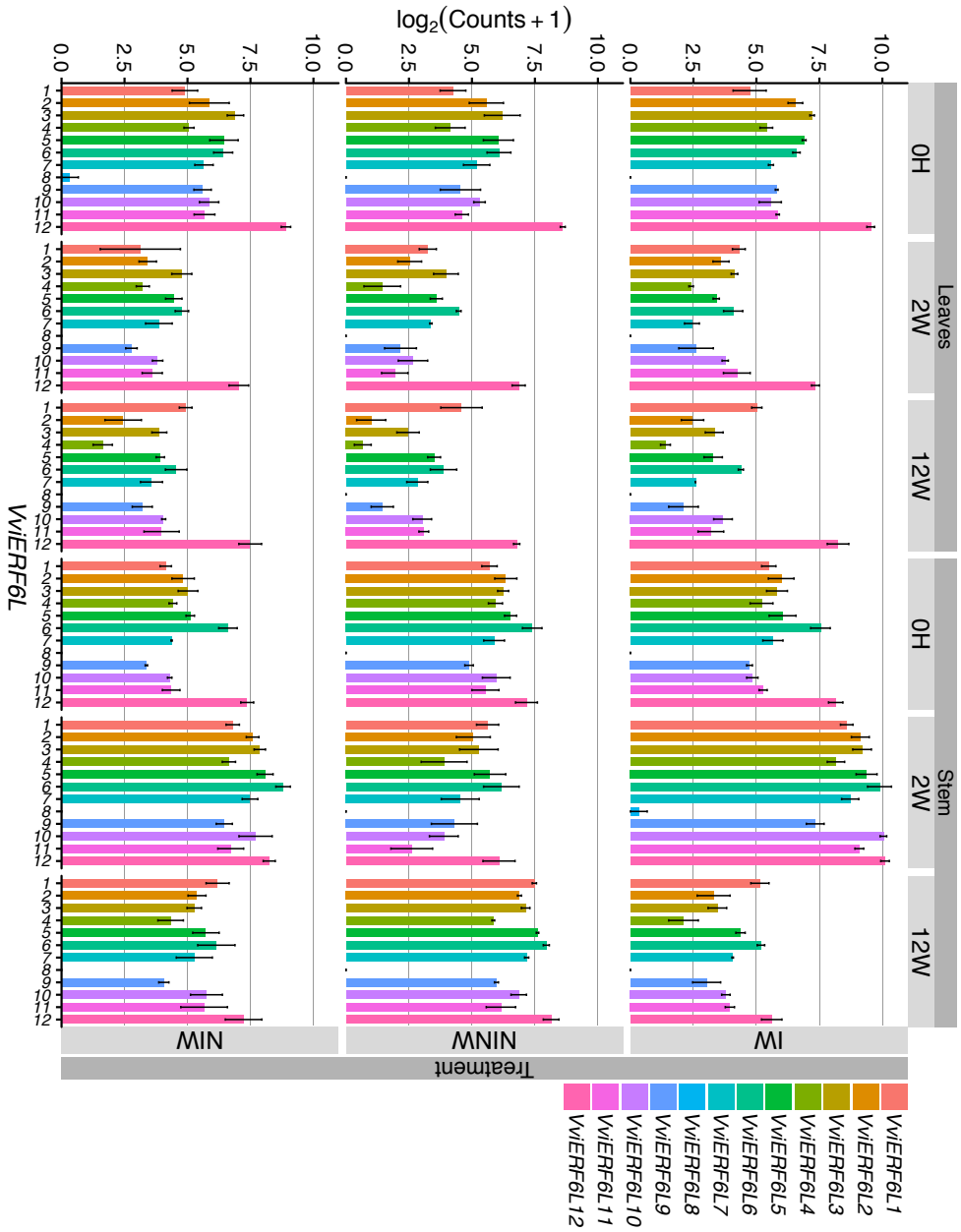

Figure 9: *VviERF6L* gene expression in response to *Neofusicoccum parvum* infection. Log_2(Counts+1) gene expression of 12 *VviERF6Ls* from leaves and stems treated with control, non-infected – non-wounded (NINW), *Neofusicoccum parvum* infected and wounded (IW), and non-infected – wounded (NIW) after 0 hours, and 2 and 12 weeks [GSE97900]; mean ± SE.

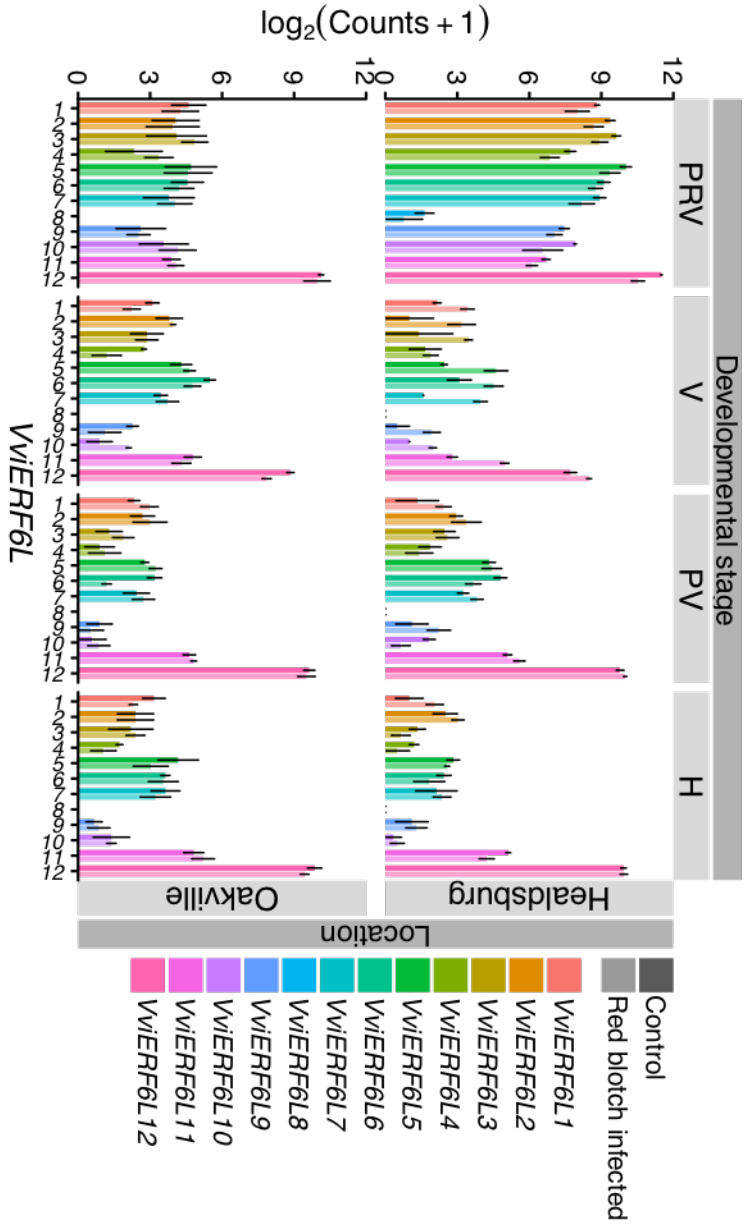

Figure 10: *VviERF6L* gene expression in response to red blotch-associated virus infection. Log_2(Counts+1) gene expression of 12 *VviERF6Ls* from whole Zinfandel berries across four stages of berry development: pre-veraison (PRV), veraison (V), post-veraison (PV), and harvest (H) treated with control mock inoculation (dark) or red blotch associated virus infection (light) from two vineyards (Healdsburg and Oakville) [GSE85812]; mean ± SE.

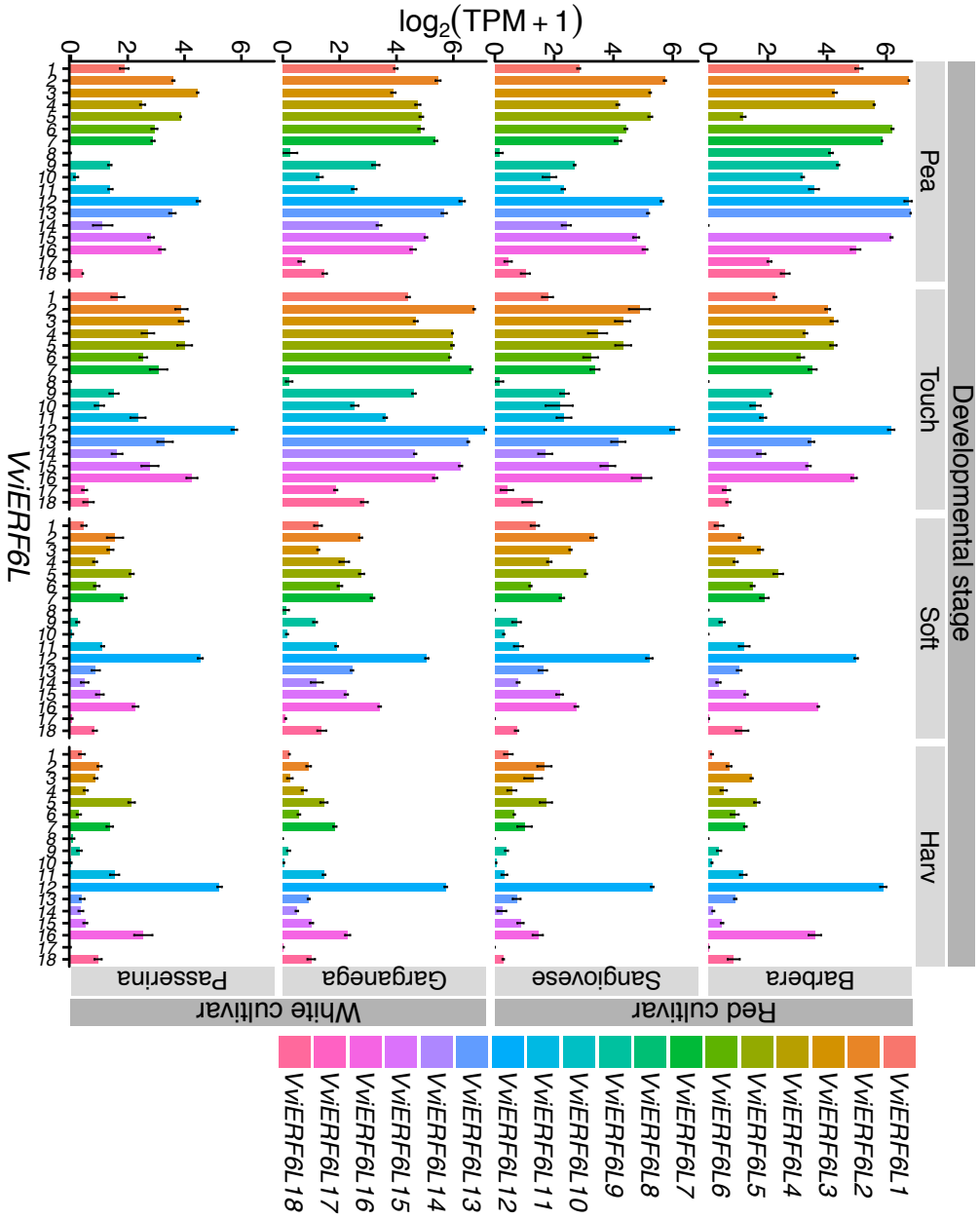

Figure 11: *VviERF6L* gene expression in response to berry development in red and white berries. Log_2(Transcripts per million (TPM)+1) of 18 *VviERF6Ls* from red cultivar berries (Barbera and Sangiovese) and white berries (Garganega and Passerina) at the pea-size (Pea), touching (Touch), softening (Soft), and harvest (Harv) stages of berry development [GSE62744 and GSE62745]; mean ± SE.

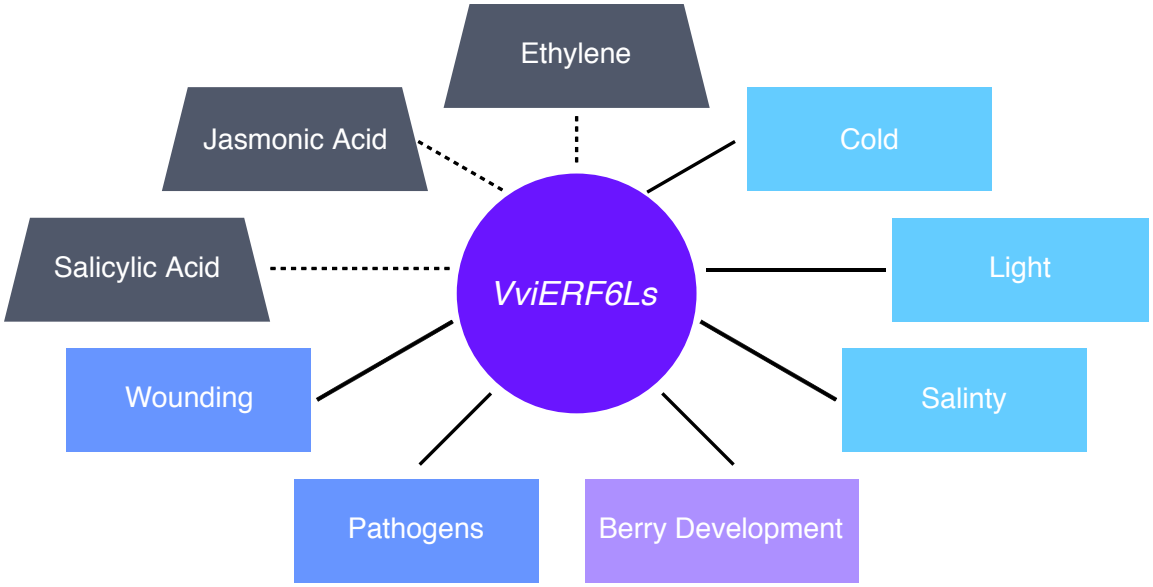

Figure 12: *VviERF6L* clade transcriptional response model. A summary model of conditions *VviERF6Ls* transcriptionally responded to in the meta-data analysis are connected with solid lines. Conditions linked to those investigated in the meta-data analysis requiring further confirmation are connected with dotted lines. Phytohormones are shown in grey. Developmental stages are shown in purple. Abiotic stresses are shown in light blue, and biotic stresses are shown in darker blue.

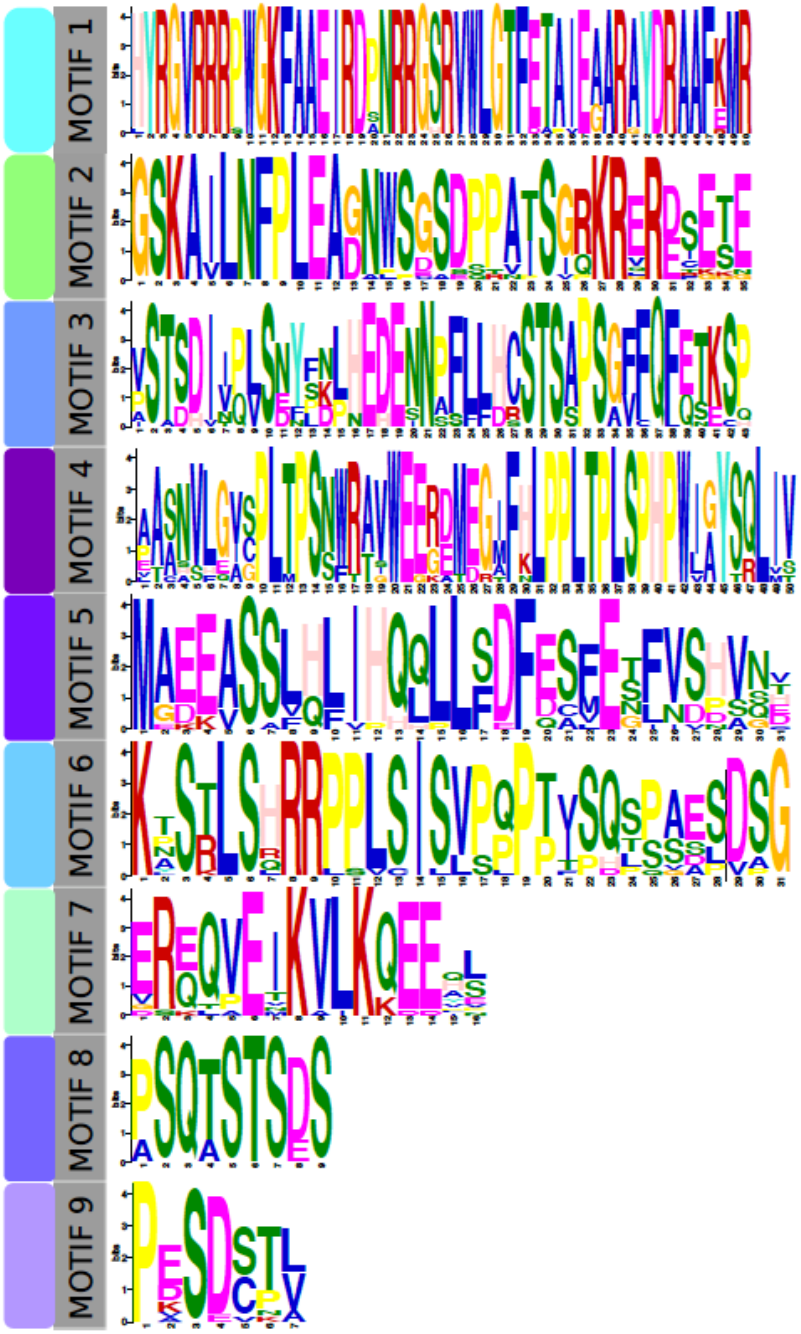

Supplemental File 1: PN40024 VviERF6L protein motif logos. Protein motif logos of PN40024 VviERF6Ls determined by MEME. X-axis represents relative residue position in motif. Y-axis letter height (bits) indicates relative frequency of a residue at a given position in the motif across the VviERF6L proteins. Left side colors correspond to Figure 1.

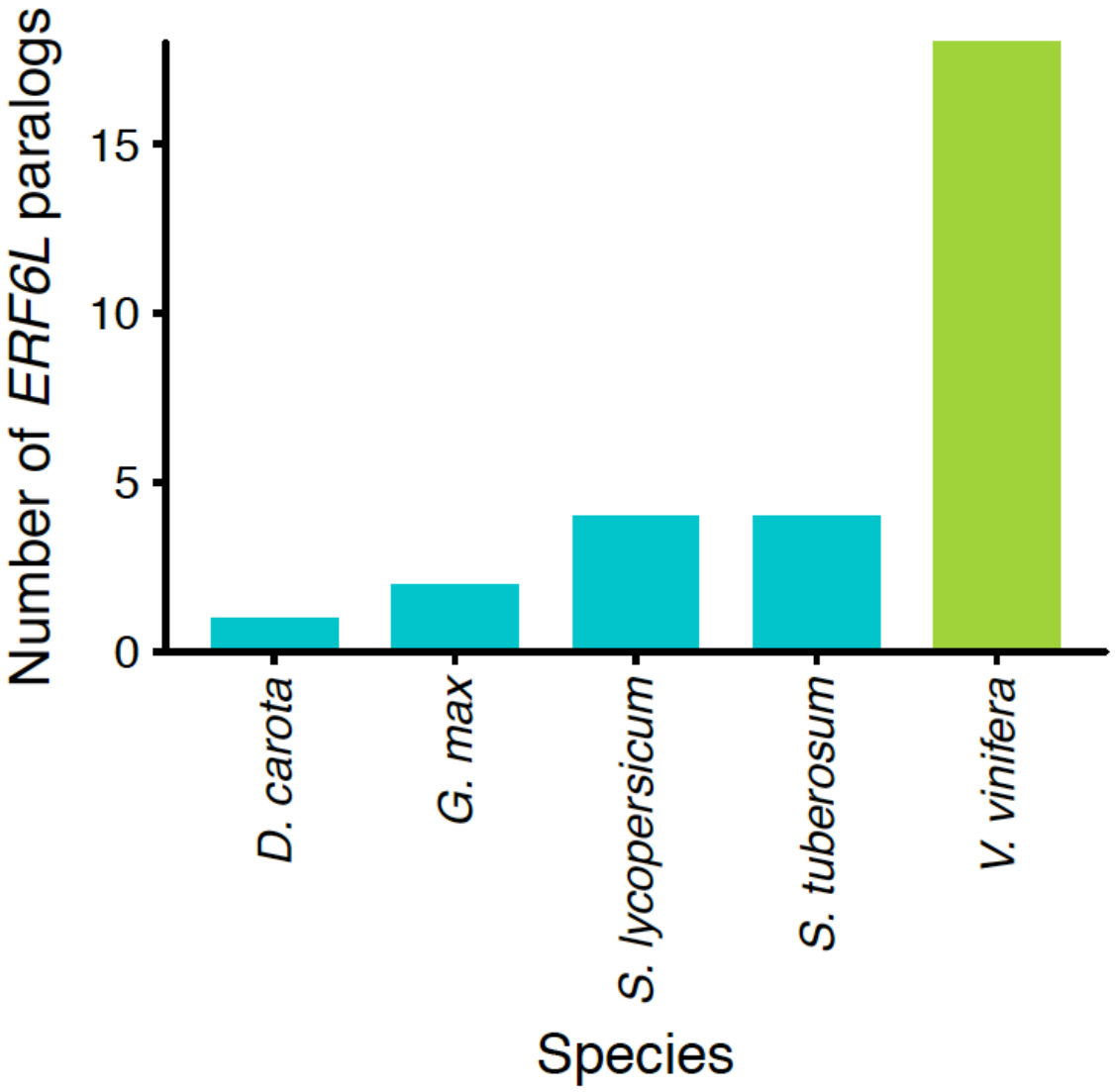

Supplemental File 2: The number of ERF6L paralogs across species. The number of ERF6Ls in species (carrot (*D. carota*), soybean (*G. max*), tomato (*S. lycopersicum*), and potato (*S. tuberosum*)) identified being closely related to *VviERF6L1* from the Pantaxonomic Compara Gene Tree on Gramene (2018 version containing 44 species) using the V3 annotation of PN40024.

Supplemental File 3: Cabernet Sauvignon (CS) VviERF6L protein motif presence and abundance.

The frequency of the 13 highly conserved amino acid motifs (right) in the 26 translated CS *VviERF6L* genes (bottom). Exact motif coordinates are in Appendix 4.

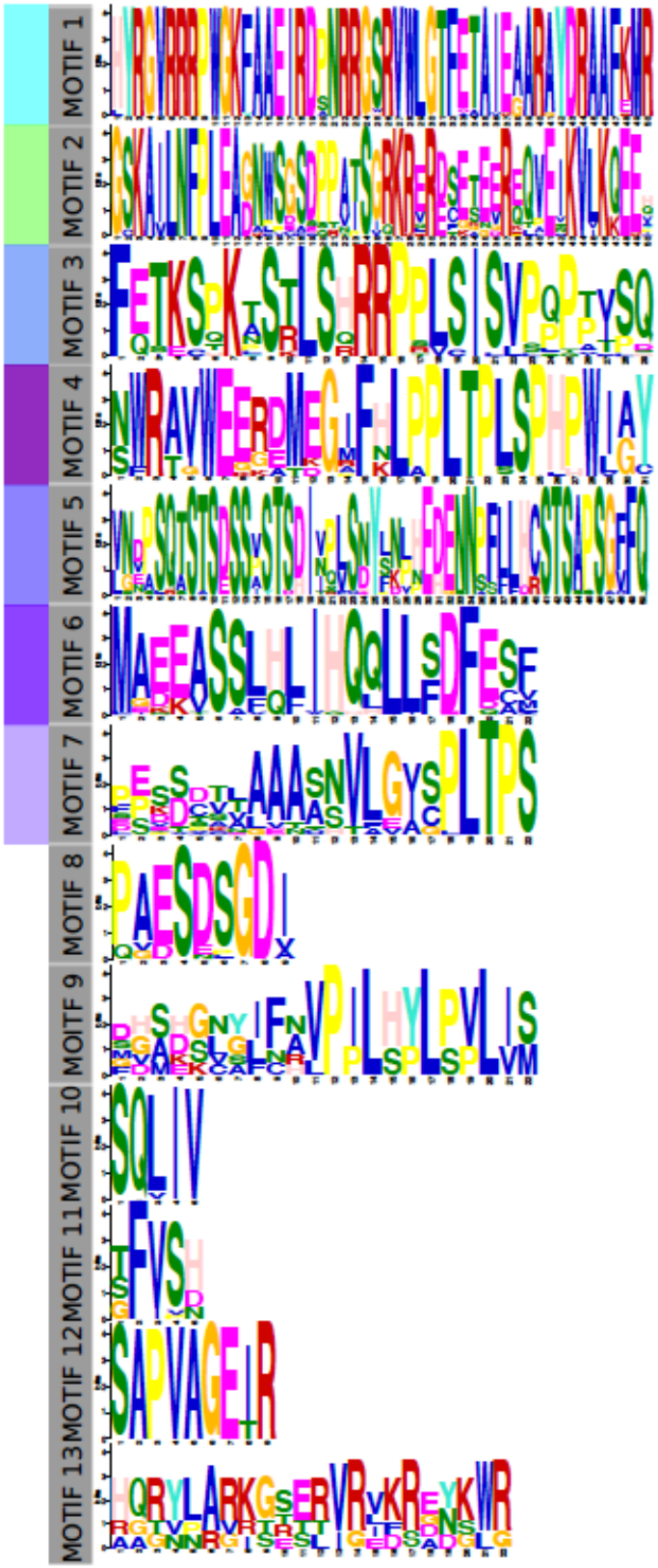
MOTIF 1
MOTIF 2
MOTIF 3
MOTIF 4
MOTIF 5
MOTIF 6
MOTIF 7
MOTIF 8
MOTIF 9
MOTIF 10
MOTIF 11
MOTIF 12
MOTIF 13

Supplemental File 4: Cabernet Sauvignon (CS) VviERF6L protein motif logos. Protein motif logos of CS VviERF6Ls determined by MEME. X-axis represents relative residue position in motif. Y-axis letter height (bits) indicates relative frequency of a residue at a given position in the motif across the VviERF6L proteins. Left side colors corresponding to PN40024 motifs based on percent identity.

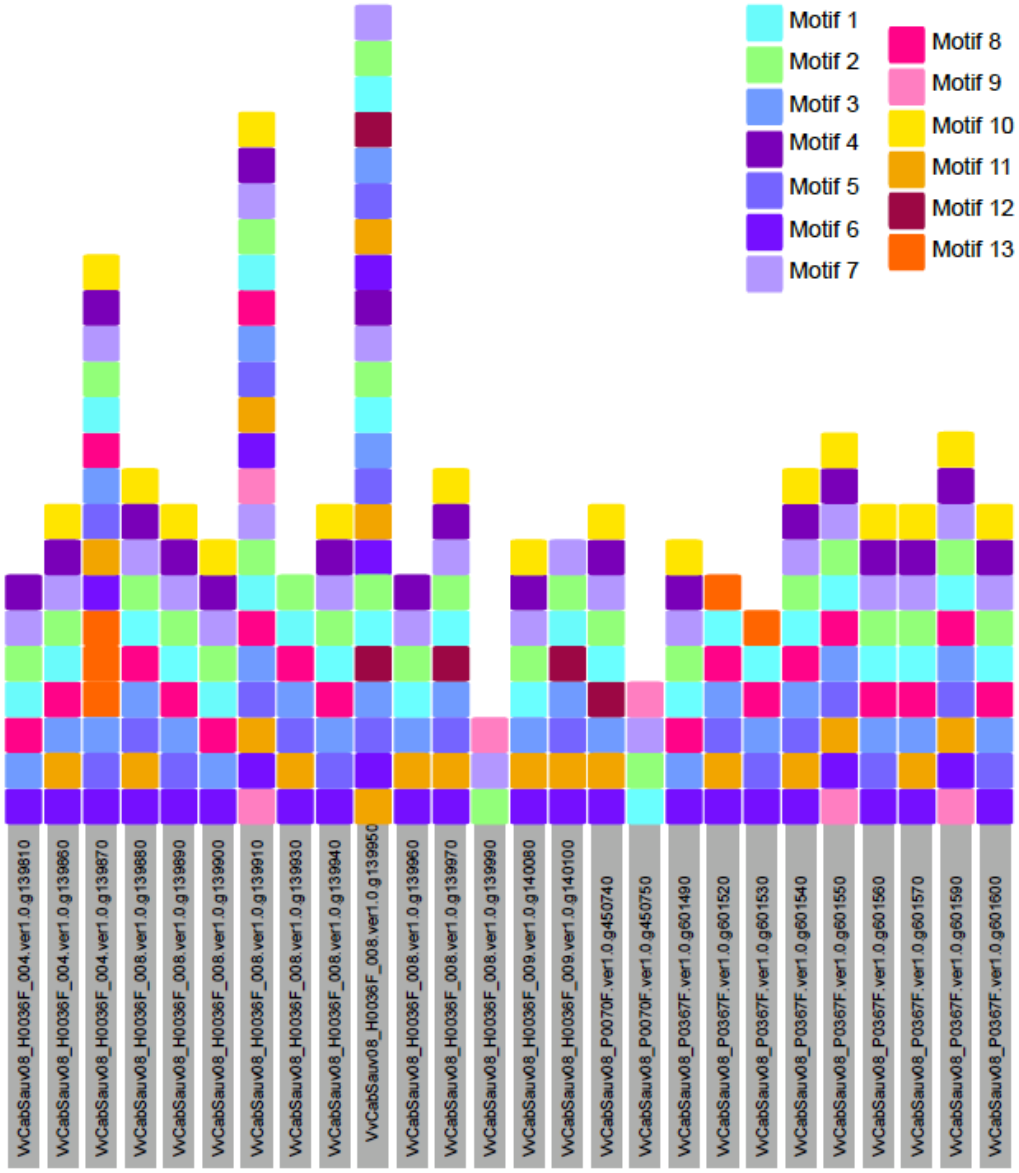

Supplemental File 5: CS VviERF6L protein motifs. Relative position of protein motifs from N-terminus (bottom) to C-terminus (top) of CS VviERF6Ls determined by MEME. Motif number based on E-value and sequence from Appendix 1 represented by colors (upper right). For exact motif coordinates of each CS VviERF6L see Appendix 5. CS VviERF6L motifs with corresponding PN40024 motifs share colors with Fig. 1.

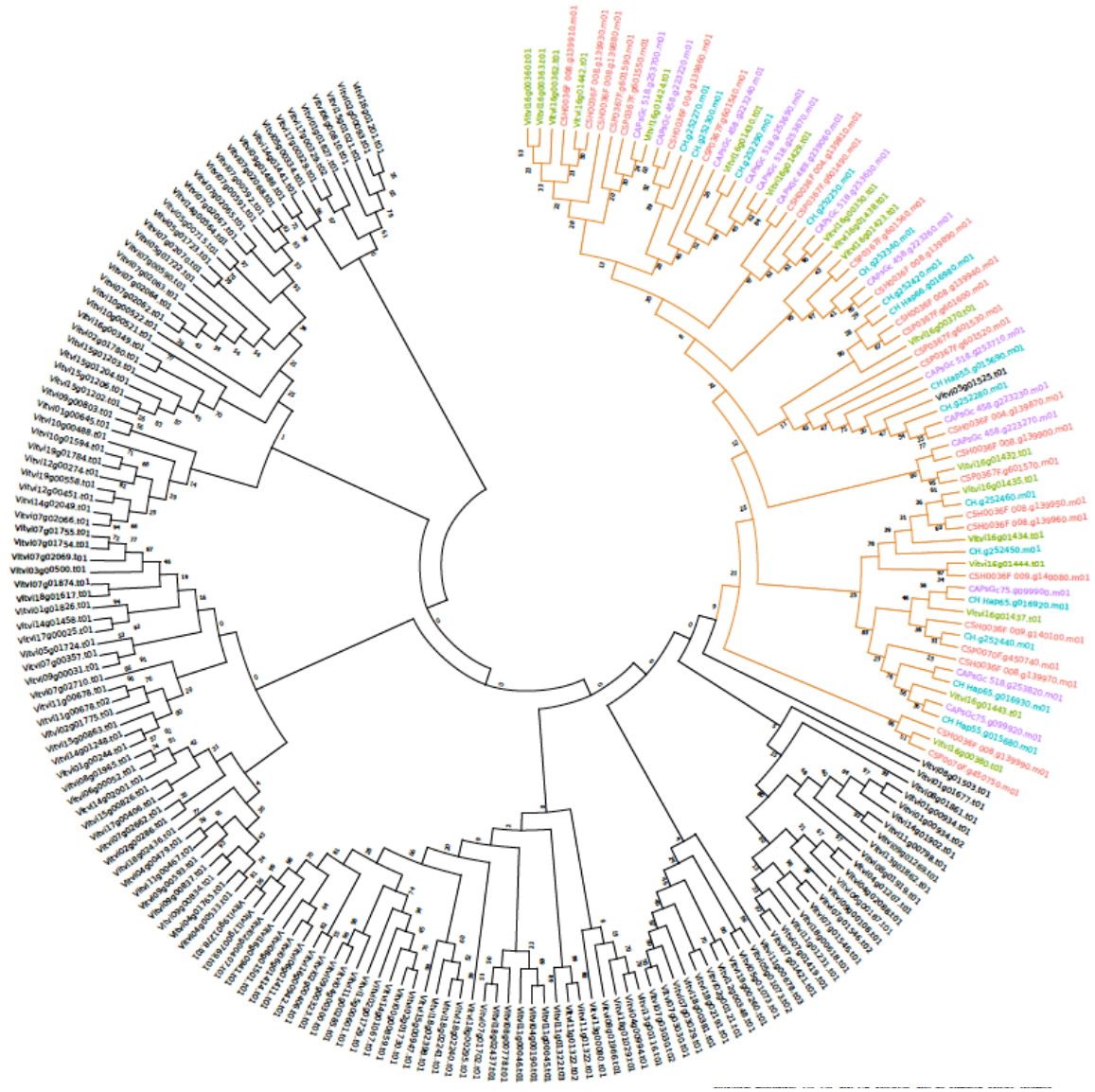

Supplemental File 6: Maximum likelihood phylogenetic tree of PN40024 V2 assembly V3 structural annotation, CS, CH, and CA VviERF6L and all PN40024 VviERF proteins. Maximum likelihood method and Jones-Taylor-Thornton matrix-based model; Bootstrap consensus tree inferred from n=1,000 replicates. The percentage of bootstrap replicates in which associated proteins clustered together are shown as numbers next to the branches. The initial tree for the heuristic search generated from the maximum parsimony method. n= 217 amino acid sequences and 1886 positions in the final data set. Evolutionary analysis from MEGA X; Subtree-Pruning-Regrafting - Fast (SPR level 3).

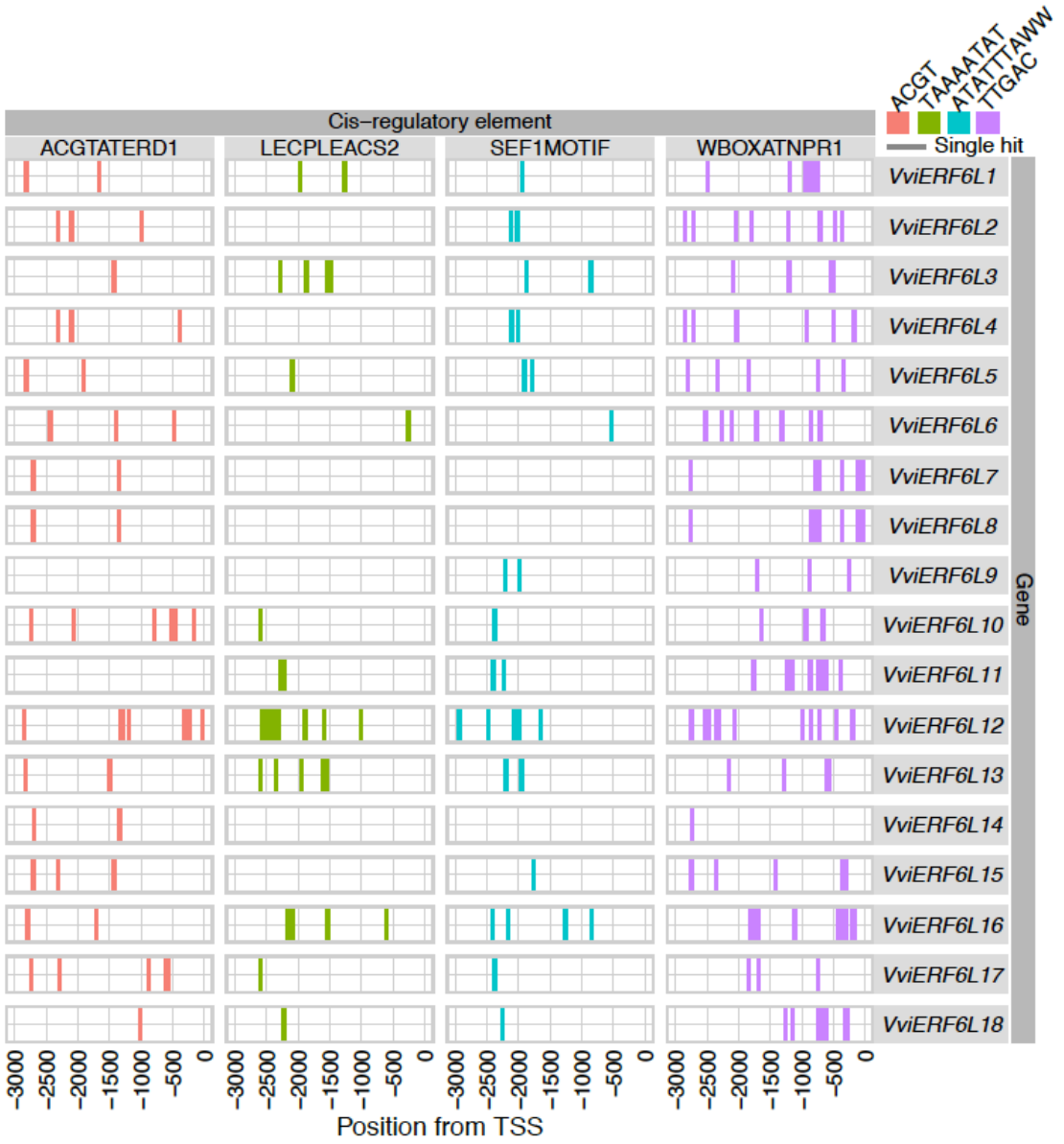

Supplemental File 7: Number and location of PN40024 cis-regulatory elements most abundant in *VviERF6L12* relative to all other *VviERF6L* promoter regions. The ACGTATERD1 (red), LECPLEACS2 (green), SEF1MOTIF (blue), and WBOXATNPR1 (purple) were amongst the most abundant promoter motifs in *VviERF6L12*. Each occurrence of a motif is marked as a single hit at its appropriate position from the transcription start site (TSS) at position 0. Motif nucleotide sequence denoted in corresponding color to hits. Complete cis-regulatory element data is located in Appendices 8 and 9.

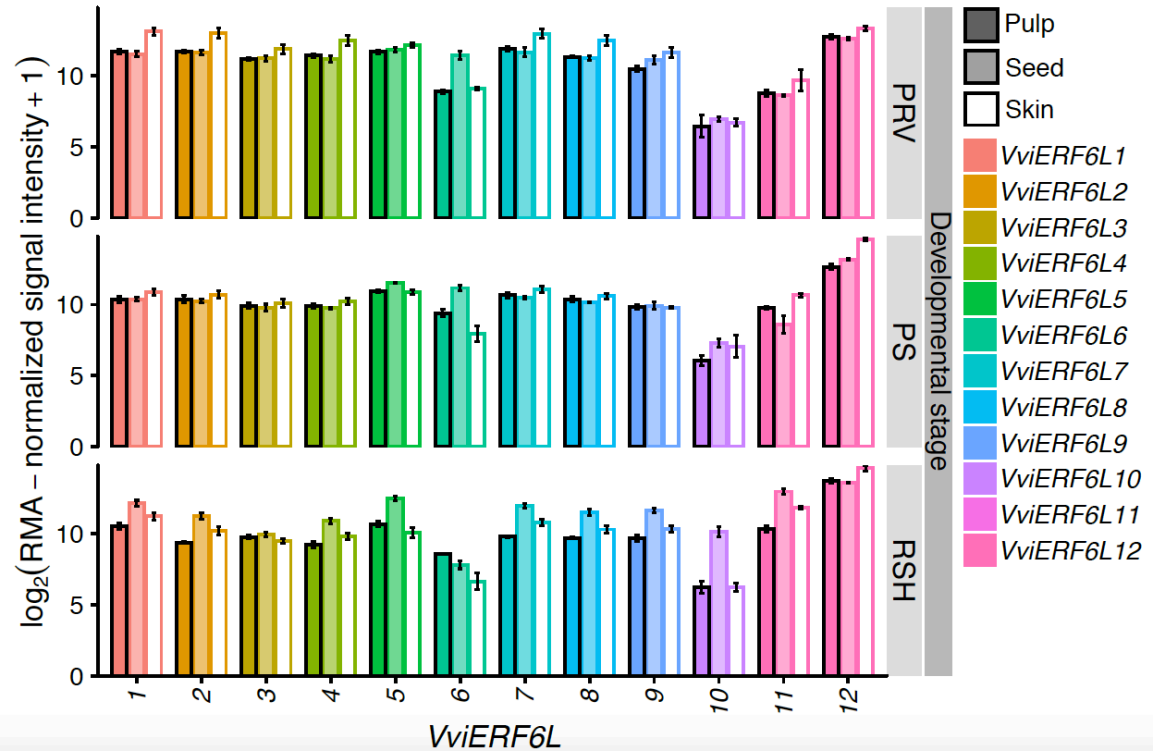

Supplemental File 8: VviERF6L gene expression in berry pulp, seed, and skin across berry development. Log2(RMA-normalized signal intensity+1) gene expression of 12 *VviERF6Ls* from Pinot Noir clone Pommard berry pulp (dark), seed (light), and skin (white) at pre-veraison (PRV), pink-soft (PS) berries at mid-ripening, and red-soft (RSH) berries at maturity [GSE49569]; mean ± SE.

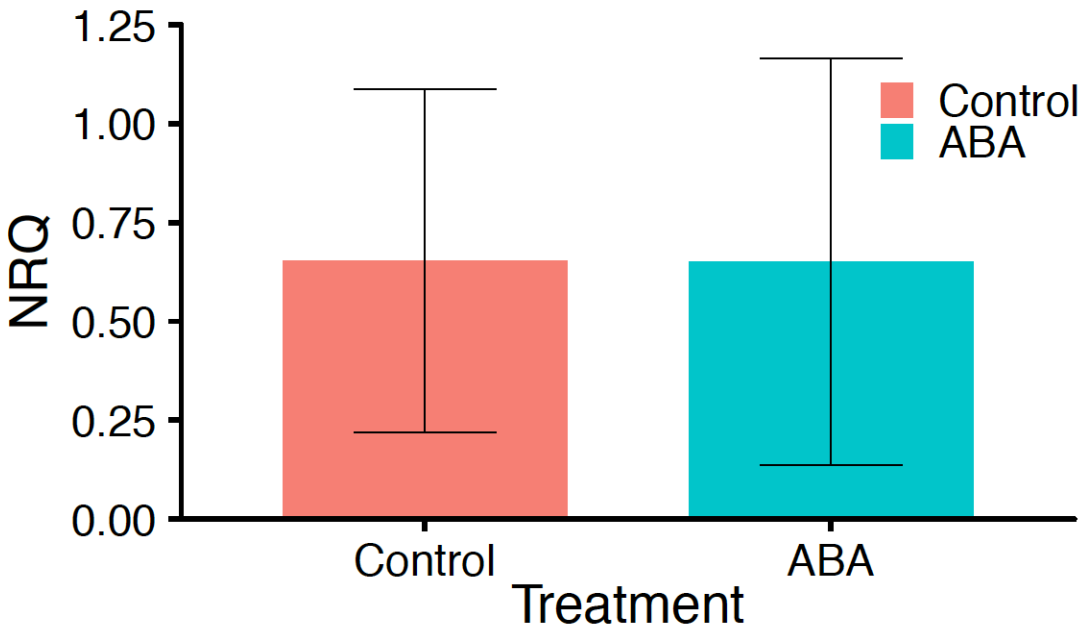

Supplemental File 9: RT-qPCR results of exogenous ABA application. Mature detached CS leaves were sprayed with exogenous 10 µM ABA (protone) or water control. Leaves were collected one hour after treatment. Control in pink and ABA treated in blue with bars as mean ± SE; n = 3.

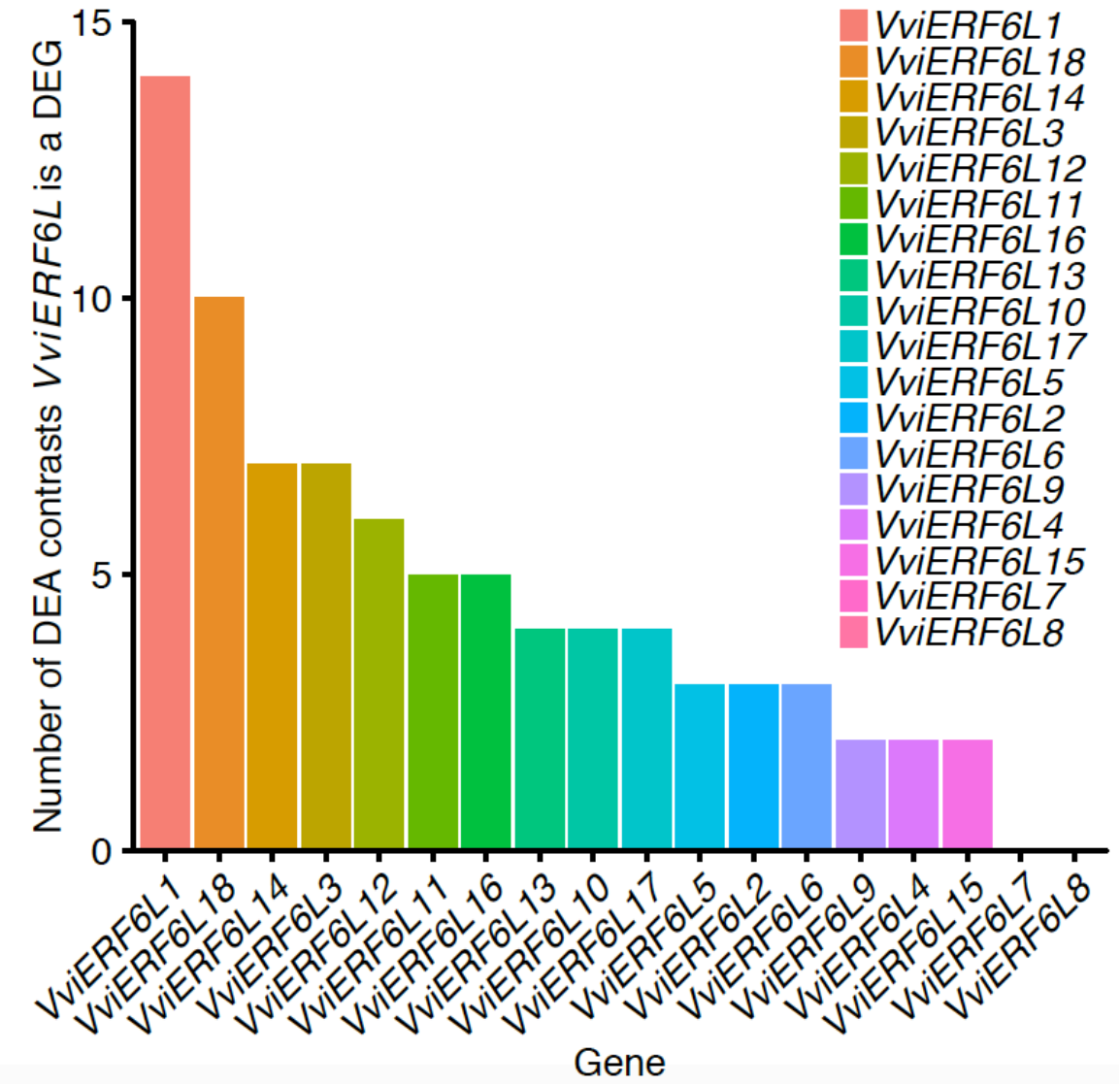

Supplemental File 10: The number of differential expression analysis (DEA) contrasts of interest (COI) in which a *VviERF6L* was a differentially expressed gene (DEG) in PRJNA516950. *VviERF6Ls* are ordered from highest to lowest number of COI in which a *VviERF6L* is a DEG. COI are listed in Appendix 13.

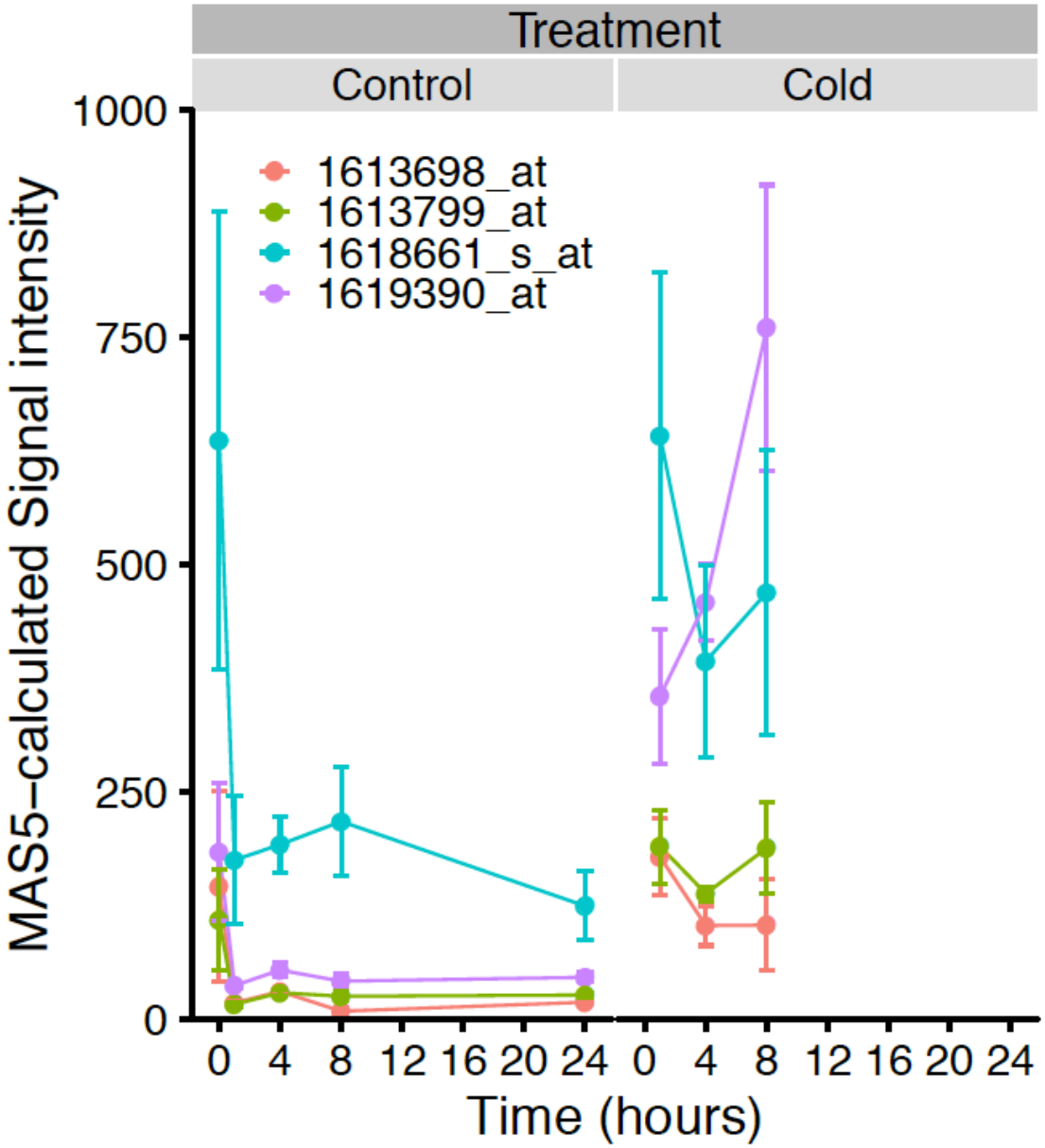

Supplemental File 11: *VviERF6L* gene expression in response to chilling. MAS5 calculated signal intensity of *VviERF6Ls* in CS shoot tips of vines exposed to 22 °C control or 5 °C chilling treatment for 0, 4, and 8 hours [GSE31594];mean ± SE.

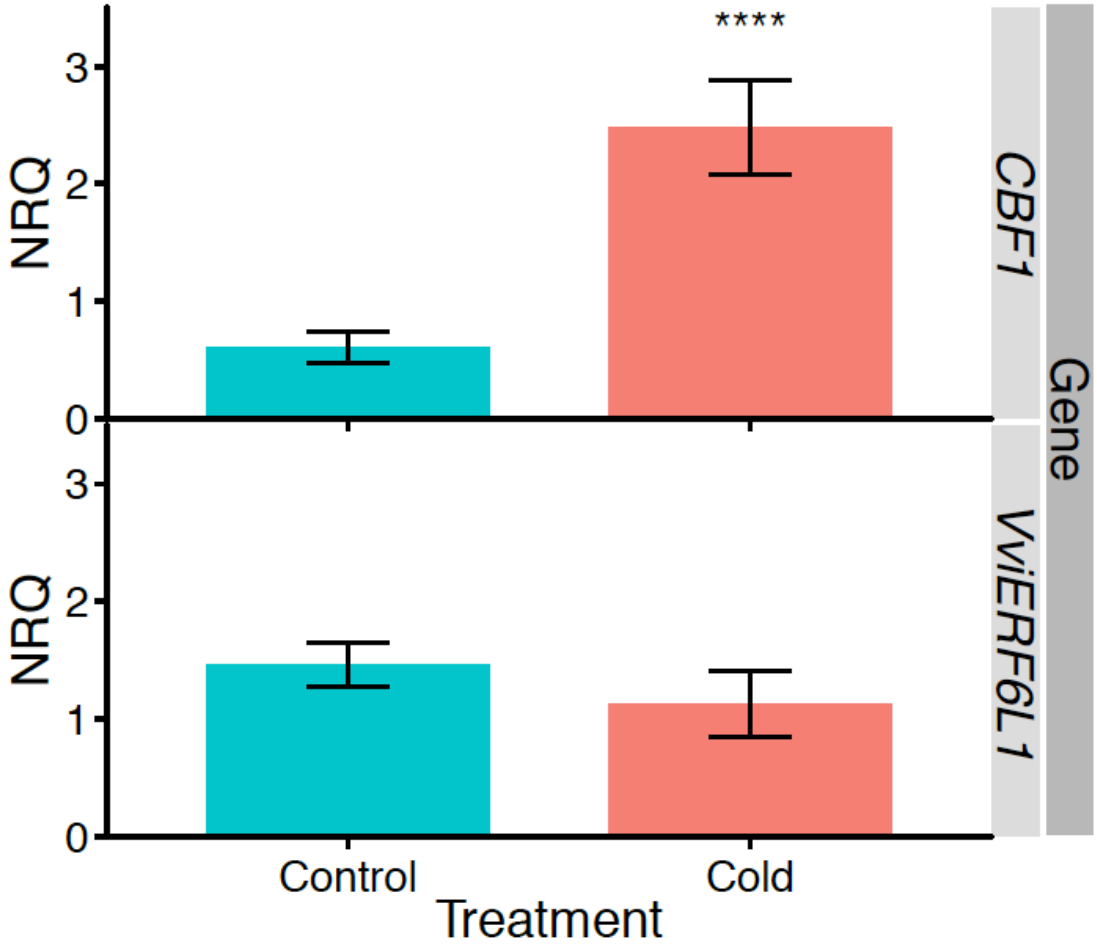

Supplemental File 12*: VviERF6L1* did not respond to cold in Cabernet Sauvignon leaves. Expression of *CBF1* (top) and *VviERF6L1* (bottom) in CS leaves after 2 hours of 4° C chilling treatment represented as NRQ measured with RT-qPCR, mean ± SE, n = 5 rounds of three individual leaves from individual plants. Control and chilling are represented as blue and pink respectively.

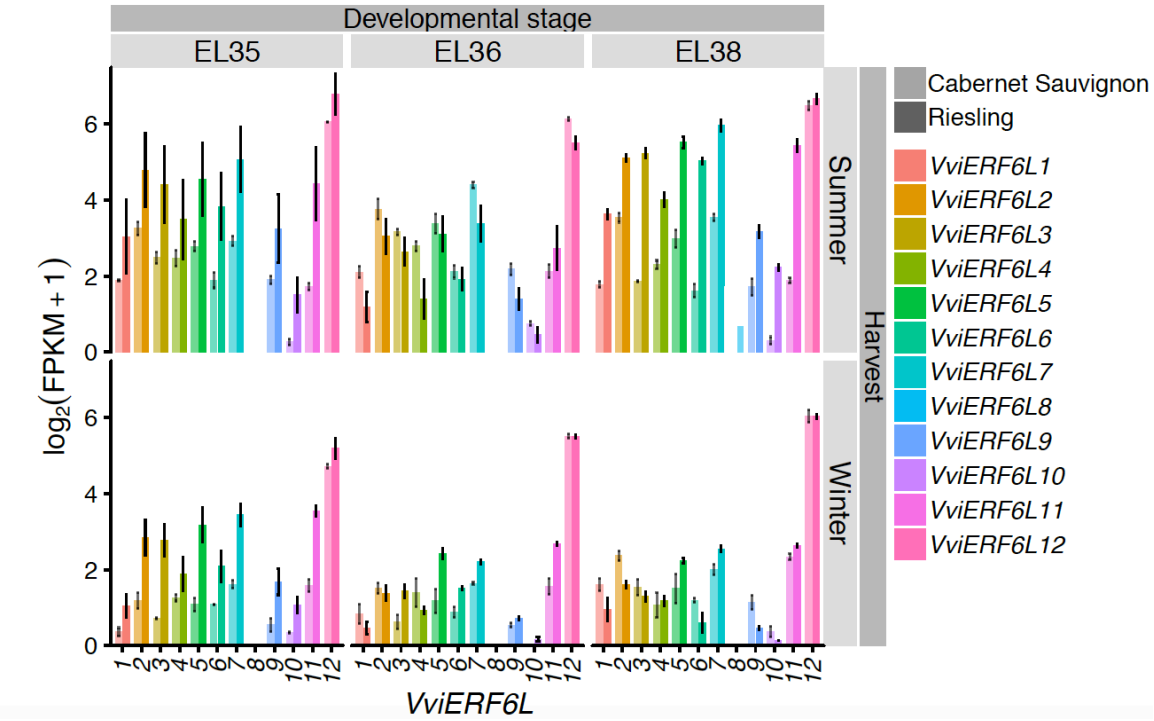

Supplemental File 13: *VviERF6L* gene expression in response to summer and winter harvest. Log2(FPKM+1) gene expression of 12 *VviERF6Ls* from berry pericarp of CS (light) and Riesling (dark) at three stages of ripening (EL35, 36, and 38) under a dual cropping system with harvesting in summer and winter [GSE103226]; mean ± SE.

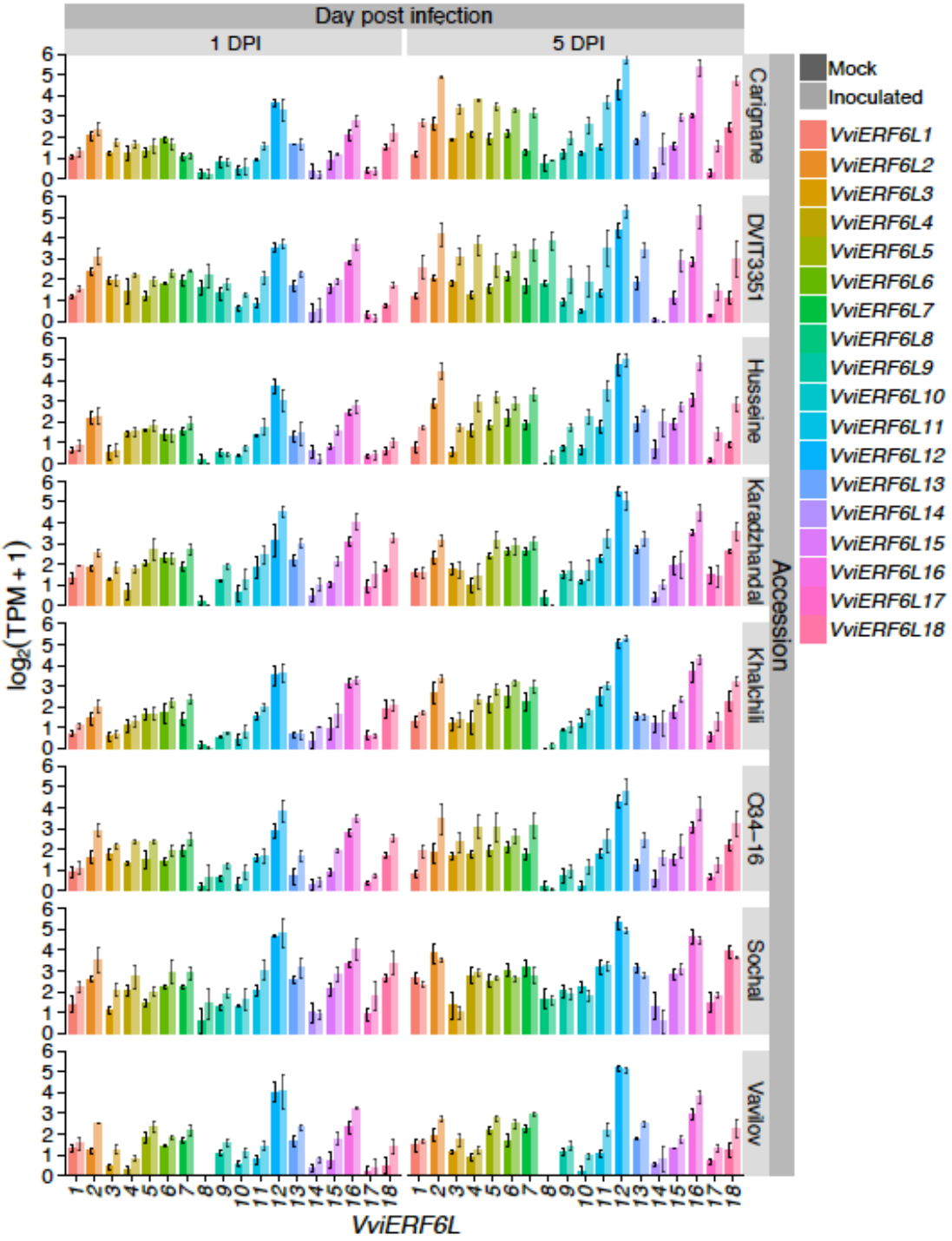

Supplemental File 14: *VviERF6L* gene expression in response to Erysiphe necator infection. Log2(TPM+1) gene expression of 18 *VviERF6Ls* from leaves of *Vitis vinifera* cv. Carignan and Chinese *Vitis* accession DVIT3351.27 (DVIT3351), Husseine, Karadshandal, Khalchii, O34-16, Sochal, and Valilov mock (dark) or inoculated (light) with Erysiphe necator 1- and 5-days post infection (DPI) [GSE67191]; mean ± SE.

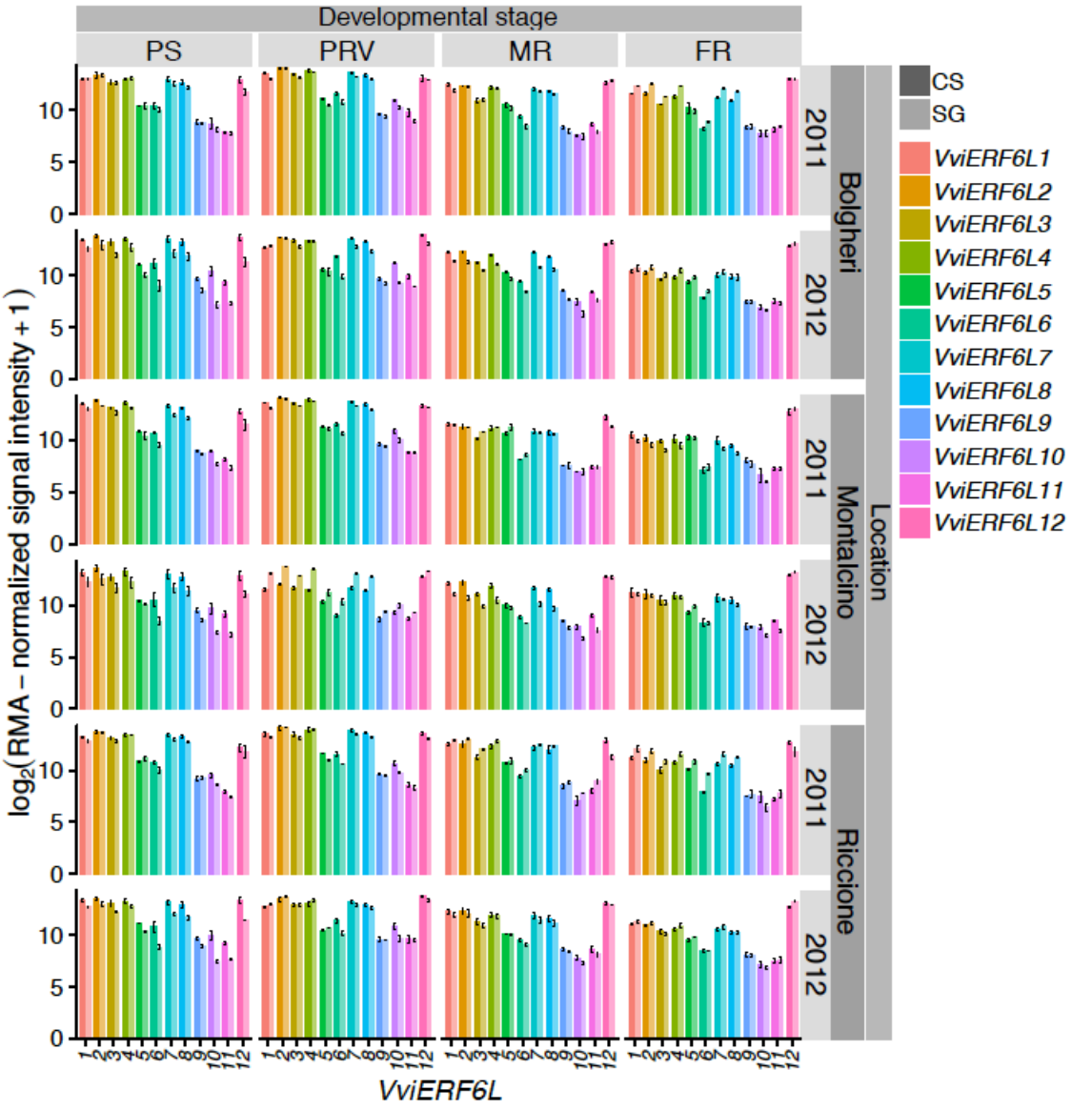

Supplemental File 15: *VviERF6L* gene expression in CS and SG pericarp over berry development across vineyards and years. Log2(RMA-normalized signal intensity+1) gene expression of 12 *VviERF6Ls* from Cabernet Sauvignon (CS (dark)) and Sangiovese (SG (light)) berry pericarp from three vineyards located in Bolgheri, Montalcino, and Riccone Italy in 2011 and 2012 over pea-size (PS), pre-veraison (PV), mid-ripening (MR), and fully ripened (FR) stages of development; mean ± SE.

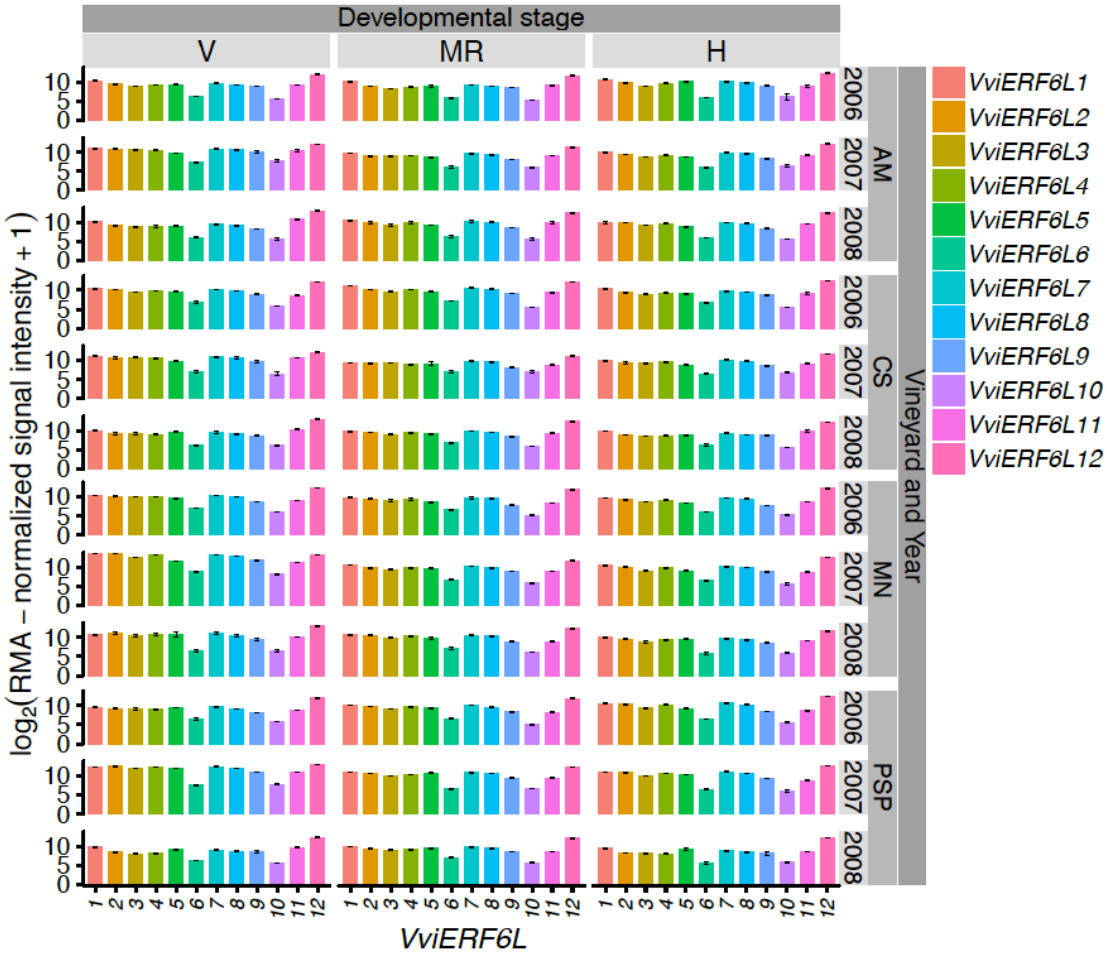

Supplemental File 16: *VviERF6L* gene expression in Corvina pericarp over berry development across vineyards and years. Log2(RMA-normalized signal intensity+1) gene expression of 12 *VviERF6Ls* from Corvina pericarp from four representative Italian vineyards (abbreviated names from original paper; meaning nondisclosed) from 2006-2008 at veraison (V), mid-ripening (MR), and harvest (H) [GSE41633]; mean ± SE.

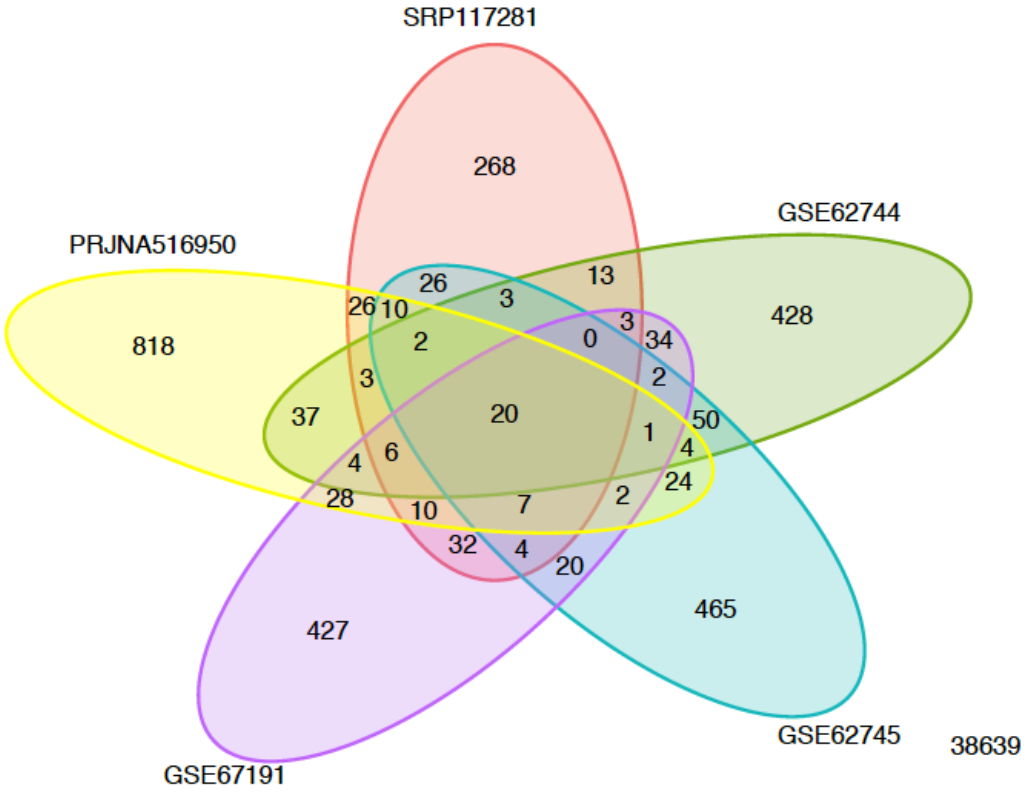

Supplemental File 17: Venn diagram of gene co-expression analysis. Co-expression analysis was performed on the 18-member *VviERF6L* clade in the five data series reanalyzed with the PN40024 V3 annotation. Number of genes sharing expression patterns for data series represented in cross-sections from top 100 co-expressed genes. Number at bottom indicates genes that did not share expression pattern with the *VviERF6L* clade.

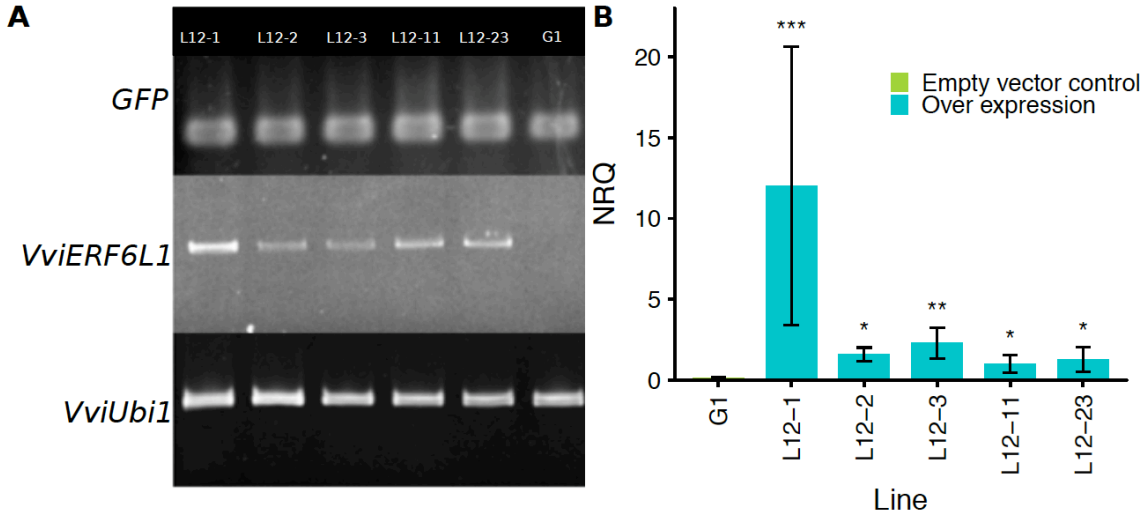

Supplemental File 18: Verification of *VviERF6L1* overexpression lines. (A) Semi-quant RTqPCR of GFP, *VviERF6L1*, and *VviUbi1* from leaves at cycle 32. **(B)** Verification of *VviERF6L1* overexpression with RT-qPCR with *VviGAPDH* and *VviACT7* reference genes from individual leaves represented as a normalized relative quantity, mean ± SE, n = 3 individual leaves from 3 individual plants. Stars indicate significance between G1 (empty vector control) and *VviERF6L1* overexpression lines (p-value < 0.05) using student's T-test. Blue and green corresponding to *VviERF6L1* overexpression lines and empty vector control, respectively.

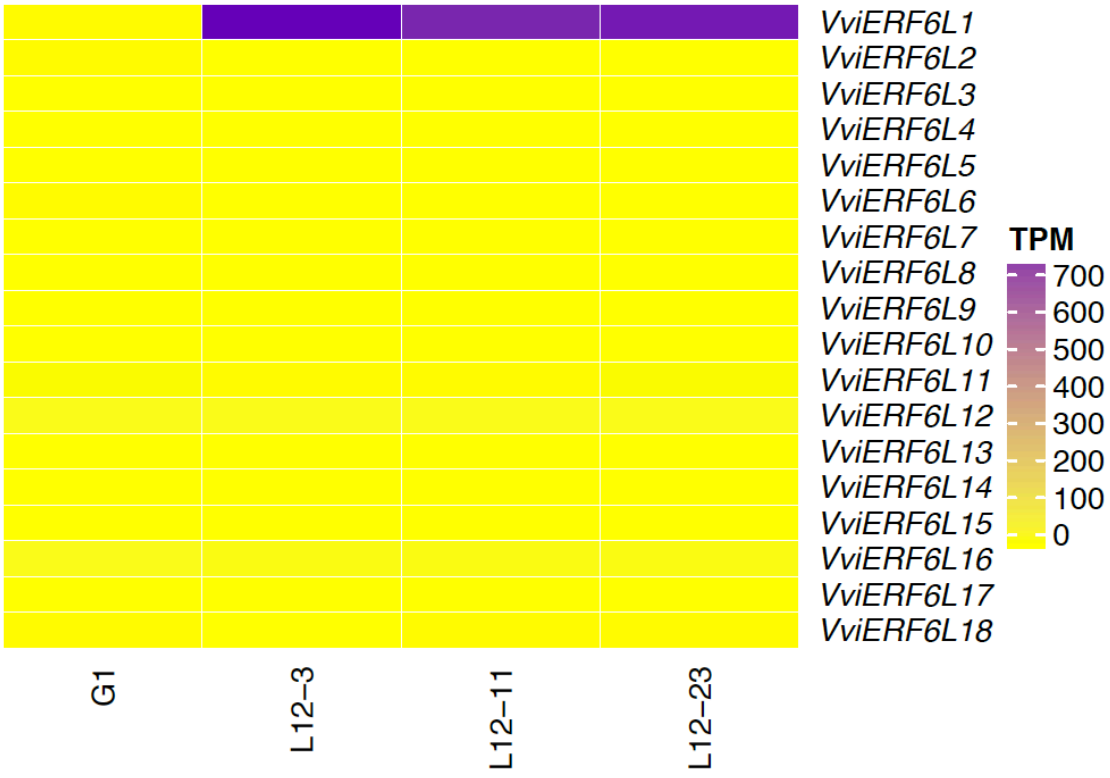

Supplemental File 19: *VviERF6L* expression in *VviERF6L1* overexpression lines. For each overexpression line (L12-3, L12-11, L12-23) and the empty vector control (G1), an average TMP value was calculated and $\log_2$ transformed and colored from yellow (low value) to purple (high value) for each of the 18 *VviERF6Ls*, n= 3.

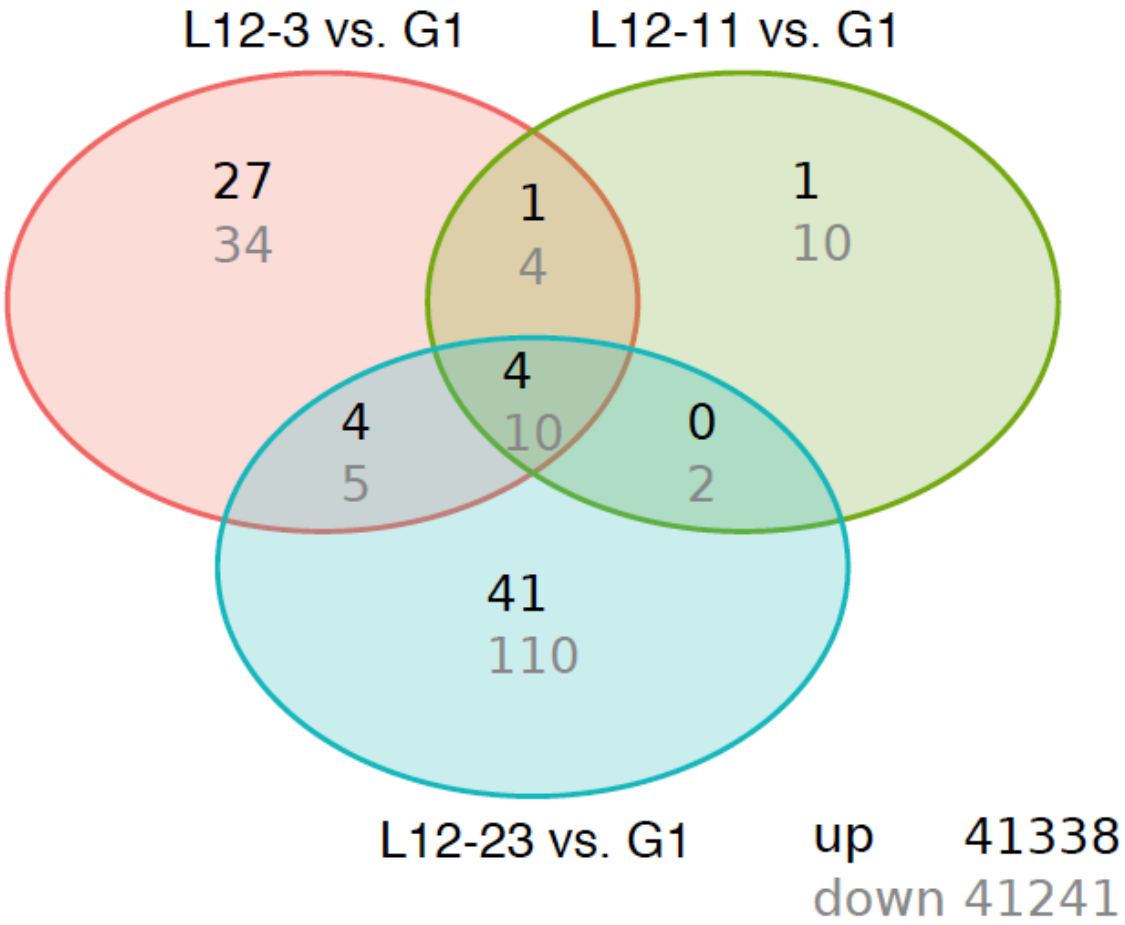

Supplemental File 20: Venn Diagram of differentially expressed genes between L12-3, -11, and -23 *VviERF6L1* overexpression lines relative to G1 empty vector control. Number of upregulated genes presented in black and down regulated genes presented as grey.

CHAPTER 4:

A *PSEUDOMONAS SYRINGAE* INFECTION ASSAY FOR *VITIS* LEAVES IDENTIFIES *VviERF6L1* OVEREXPRESSION MAY REDUCE PSEUDOMONAS SYRNINGAE SUSCEPTIBILITY

This chapter is unpublished work.

4.0 Abstract

Pseudomonas syringae is a gram-negative hemibiotroph that poses a threat to agriculture and is a novel danger to grapevine. Although numerous *P. syringae* infection techniques exist for *Arabidopsis thaliana* none have ever been optimized for grapevine. This work describes a simple and reproducible *P. syringae* infection assay for detached grapevine leaves that is scalable to whole potted vines and adaptable to other plant species. This grapevine-optimized *P. syringae* infection assay was implemented on detached Cabernet Sauvignon and *VviERF6L1* overexpression vine leaves. *VviERF6L1* transcript abundance significantly increased in detached Cabernet Sauvignon leaves one day after *P. syringae* infection relative to mock infection Control leaves. *VviERF6L1* overexpression vines had lower colony forming units per leaf surface area and increased resistance to *P. syringae* than empty vector control vines. This assay and *VviERF6L1* have future applications in identifying *P. syringae* resistant grapevines.

4.1 Introduction

In addition to increased abiotic stresses resultant of climate change, temperature fluctuation, increased atmospheric CO_2, and changes in wind and precipitation patterns are affecting phytopathogen spread and plant susceptibility (Pautasso et al., 2012; Zhu et al., 2010). Today, global crop yield losses to pests and pathogens range from 20-30% (Savary et al., 2019), and plant disease is projected to be a major limiting factor of crop productivity for the 21st century (Savary et al., 2019).

P. syringae is a gram-negative hemibiotrophic bacteria that infects a broad range of plants including Arabidopsis (Katagiri et al., 2002), tomato (Xin and He, 2013), and grapevine (Gerin et al., 2019; Hall et al., 2002, 2019; Porotikova et al., 2016; Whitelaw-Weckert et al., 2011). However, *P. syringae* infection in grapevine is a fairly contemporary problem with the first incident of disease reported in the late 1960s (Klingner et al., 1976). Since the initial report, cases of *P. syringae* infection have increased all across the world in a variety of grapevine organs including leaves (Hall et al., 2002; Porotikova et al., 2016), berries (Gerin et al., 2019), and inflorescence (Hall et al., 2019; Whitelaw-Weckert et al., 2011).

P. syringae is carried on air currents and disseminated in precipitation and through bodies of water (Morris et al., 2013). Already, *P. syringae* is present in 65% of rainfalls in southern France, an important region for viticulture. Airmasses and clouds containing *P. syringae* can transverse continents in days (Morris et al., 2013), and projected global temperature increases (Naumann et al., 2018) correspond to more favorable *P. syringae* growth conditions and reduced plant pathogen resistance (Zhu et al., 2010). The potential for *P. syringae* spread and epidemics in grapevine are unprecedented. Because of the novelty of *P. syringae* infection in grapevine, there is concern grapevine may not have high immunity or resistance to this pathogen particularly with compounding abiotic stress (Gerin et al., 2019).

P. syringae enters a plant host through wounds or natural openings like stomata (Melotto et al., 2006). Once in a plant, this hemibiotroph multiplies, eventually leading to leaf chlorosis, necrosis, canker or gall formation, and ultimately plant death (Katagiri et al., 2002). Plants prevent disease symptoms by minimizing *P. syringae* reproduction via

localized programmed cell death of infected cells in a defensive hypersensitive response (HR) (Dangl et al., 1996). Plant resistance to a *P. syringae* strain is determined on a gene-for-gene basis (Whalen et al., 1991) with resistance arising when a plant has a resistance (*R*) gene corresponding to an avirulent (*avr*) pathogen gene. For example, Arabidopsis and soybean ecotypes that express *RESISTANT TO P. SYRINGAE 2* (*RPS2*) are resistant to *P. syringae* strains with the *avrRpt2* avirulence effector loci, but the same plants are susceptible to *P. syringae* strains lacking this *avr* gene or expressing a different *avr* gene (Chen et al., 2000; Katagiri et al., 2002; Whalen et al., 1991).

Ethylene plays a positive role in *P. syringae* resistance in Arabidopsis with *aminocyclopropane-1-carboxylate synthase* (*acs*) mutants having enhanced susceptibility (Guan et al., 2015). Ethylene biosynthesis is highly induced by salicylic acid (SA), pathogen-associated molecular pattern (PAMP)-triggered immunity (PTI), and effector-triggered immunity (ETI) (Guan et al., 2015). After a pathogen triggers an immune response in a plant, mitogen-activated kinases (MAPKs) stabilize ACS that catalyzes the first committed and rate-limiting step of ethylene biosynthesis (Xu and Zhang, 2014, 2015). Additionally, Arabidopsis seedlings inoculated with *P. syringae* containing *avrRpt2* produced higher ethylene than pathovars lacking this effector (Guan et al., 2015). However, the exact ethylene signaling response in plants leading to increased resistance is unclear.

Previously *VviERF6Ls* were identified to be significantly differentially expressed in response to wounding, *Neofusicoccum parvum*, red blotch associated virus, and *Erysiphe necator* in various grapevine organs (Toups et al., 2020). Downy mildew (*Plasmopera viticola*) susceptible grapevines have a marked reduction in *VviERF6L* expression than more resistant cultivars (Eisenmann et al., 2019; Rienth et al., 2019). *VviERF6Ls* also have

numerous pathogen response cis-acting elements like the WBOXATNPR1 in respective promoter regions (Toups et al., 2020). Most compellingly, the only genes differentially expressed in *VviERF6L1* overexpression lines (PATHOGENESIS-RELATED PROTEINS (PR1 and PR1B) (Goto et al., 2016), CYSTEINE RICH RECEPTOR LIKE KINASES (CRK8) (Quezada et al., 2019), CYTOCHROME P450 722 (CYP722A1), WALL ASSOCIATED RECEPTOR KINASE-LIKE 1 (WAKL1) (Li et al., 2020), L10-INTERACTING MYB DOMAIN-CONTAINING PROTEIN (LIMYB) (Zorzatto et al., 2015), AND LACCASE 14 (LAC14)) (Lu et al., 2013) are all involved in pathogen resistance and the HR (Toups et al., 2020). Although preliminary spread assays with *Botrytis cinerea* and *Alternaria brassicicola* did not demonstrate *VviERF6L1* overexpression effected grapevine leaf resistance (Toups et al., 2020), it was hypothesized *VviERF6L1* had a role in pathogen response.

The potential role of *VviERF6L1* in pathogen response was supported by ERF5 and ERF6 orthologs in Arabidopsis. *AtERF5* and *AtERF6* overexpression increase *Botrytis cinerea* resistance (Moffat et al., 2012; Son et al., 2012), while reduced expression of *AtERF5* or *AtERF6,* as well as *aterf5*/*aterf6* double mutants, have enhanced susceptibility to necrotrophic fungi (*V. longisporum* (Fröschel et al., 2019), *Botrytis cinerea* (Moffat et al., 2012), and *Alternaria brassicicola* (Son et al., 2012)) and nematodes (*Meloidogyne incognita*) (Fröschel et al., 2019; Warmerdam et al., 2018). However, the effect of *AtERF5* and *AtERF6* on *P. syringae* susceptibility has opposing reports: Moffat *et al*. identify constitutive *AtERF5* and *AtERF6* expression enhances Arabidopsis susceptibility to *P. syringae* (Moffat et al., 2012), but Fröschel *et al*. conclude ERF5 positively regulates salicylic acid (SA) signaling and *P. syringae* resistance (Fröschel et al., 2019).

Quantification of pathogen growth after infection provides insight into immune response and relative susceptibility or resistance of organisms to a pathogen, and *P. syringae* infection assays are highly optimized for Arabidopsis (Liu et al., 2015). However, no such system has been optimized for grapevine. *P. syringae* delivery in Arabidopsis systems include syringe and vacuum infiltration as well as dip and spray inoculation techniques (Katagiri et al., 2002; Liu et al., 2015; Tornero and Dangl, 2001). As an annual plant, Arabidopsis has the benefit of a rapid life cycle, relative to the years needed to establish a mature grapevine. For this reason, it was necessary to establish a scalable *P. syringae* infection assay for grapevine capable of infecting an entire potted vine or single detached organ such as a leaf and maintain that detached organ for the days needed for *P. syringae* to multiply. **The first objective of this work was to develop and optimize a simple, reproducible *P. syringae* infection assay for grapevine to progress understanding of *Vitis* immune response and aid in pathogen resistance improvement and screening. The second goal of this research was to apply this novel assay to determine if *VviERF6L1* overexpression enhanced grapevine resistance to *P. syringae*.**

After various modifications, a previously described *P. syringae* infection assay (Tornero and Dangl, 2001) was optimized for grapevine capable of inoculating a whole plant or a detached leaf. Optimal colony-forming unit (CFU) density from detached grapevine leaf extracts was obtained five days after dipping inoculation with a 0.5 OD culture solution. This technique was also successful for *P. syringae* infection of detached potato leaves and may be modified for other plant species. *VviERF6L1* transcripts significantly increased in response to *P. syringae* infection in detached Cabernet Sauvignon leaves one day after infection. Application of this assay identified *VviERF6L1*

overexpression vines had significantly reduced colony-forming unit (CFU) formation than empty vector control vines, and *VviERF6L1* may play a role in *P. syringae* resistance in grapevine.

4.2 Materials and Methods

Plant materials and growth conditions

Vines were grown under greenhouse conditions at 21-26 ˚C with 20-50% relative humidity and mid-day light intensities of ~1200 μmol $m^{-2}s^{-1}$ including supplemental light from 1000 W high-pressure sodium lamps (16:8 light-dark cycle) placed ~4.5 m above the greenhouse floor. Vines were grown in Stuewe and Son's tree pots TP915R (22.9 cm x 39.4 cm) containing 1:1:1:2 perlite:peat moss:Grow Mulch (Kellogg):washed sand. Each pot contained ~8.0 kg of soil mix and was elevated 7.5 cm off the floor with perforated black plastic platforms. Mature plants were irrigated with tap water weekly, and vines were fertilized with UltraGreen (5:10:10) fertilizer once a month. It is recommended to water vines the night before leaf harvests to insure open stomata for the infection assay. Vines were trained to single shoots. Own-rooted *Vitis vinifera* (L.) cv. Cabernet Sauvignon clone 8.1 (CS) vines were obtained from Sunridge Nursery (California). *VviERF6L1* overexpression lines (L12-3, -11, and -23) and empty vector control (G1) were established at the Mid-Florida Research and Education Center for the Institute of Food and Agricultural Sciences, which is described in detail elsewhere (Toups et al., 2020).

Optimization of *P. syringae* infection assay for *Vitis* leaves

The *Vitis* leaf *P. syringae* infection assay, extraction, and CFU calculation is based on work described previously (Tornero and Dangl, 2001) with changes and optimizations made for grapevine, potato, and other leaves with a dense cuticle or mesophyll for which syringe infiltration is difficult or destructive. All infection and extraction steps are recommended to be performed with sterile technique to minimize contamination. Incubation chambers that consisted of 1.2 L Tupperware and lids containing 200 mL milli-Q water, baths that consisted of 1.2 L Tupperware and lids containing 500 mL DI water, dip containers that consisted of 1.2 L Tupperware and lids, buffers, media, and wire leaf support grids were sterilized and cooled in a laminar flow hood before each round of infection. *P. syringae* virulent isolate DC3000 pathovar Pst and avirulent DC3000 *avrRpt2* were obtained from Dr. Won Gyu Choi and Dr. Patricia Santos at the University of Nevada, Reno. *P. syringae* was cultured from glycerol stock in NYGA + RK broth [5 g peptone, 3 g yeast extract, 20 mL glycerol per 1L, pH 7.0 + 50 mg/L rifampicin and 25 mg/L kanamycin final concentration] for one week with increasing volume and fresh media every two days to obtain 250 mL cultures. The culture was always transferred to fresh media 12-24 hours before leaf inoculation to insure bacteria were in the log phase (Tornero and Dangl, 2001). Results shown here are from the avirulent strain, but both strains function in this system. Cultures were grown at 28 ˚C with shaking at 200 rpm. Five individual cultures were started one week before leaf infection days, to ensure enough bacteria for a successful assay. For the infection, 25 leaves from at least 15 CS vines were cut underwater with a razor blade at the point where the petiole connects to the stem. Leaves of comparable age and size (3rd-6th node from the apical meristem) determined by measuring from the petiole attachment

point on the leaf blade to the mid-leaf point tip were used for all experiments. Abscised leaves were placed in zip block bags containing 0.05% liquid dish soap. Leaves were shaken at max speed (80 rpm) on a back-and-forth table rocker to remove dust and debris. Five leaves were placed in five individual 1.2 L Tupperware (abaxial side down) and rinsed under gently running DI water for one hour to further remove debris from the leaf surface. While the leaves rinsed, 25 incubation chambers were labeled and assembled in a flow hood by placing a sterile wire support grid in the sterile 200 mL of water. Five sterile empty Tupperware containers were filled with 5% bleach (500 mL total volume) in the flow hood. After one hour of rinsing, the leaves were sanitized in 5% bleach for 5 minutes with five leaves per container. The leaves were removed from the bleach, and excess bleach solution was allowed to briefly drip off the leaves before the five leaves were rinsed in 500 mL sterile DI water for 10 minutes. Each set of five leaves were rinsed in a total of three individual 500 mL sterile DI water baths for 10 minutes in each bath to remove and dilute the bleach. In the third bath, ~1 cm of the end of the petiole was excised underwater from each leaf in case of bleach uptake. While leaves were in the sterile water baths, the *P. syringae* cultures were spun down at 4 ˚C for 10 mins at 4500 RPM in a Sorvall RC 5C plus centrifuge from Dupont. Supernatants were decanted, and pellets were dissolved in 3-5 mL sterile $MgCl_2$ Buffer [10 mM $MgCl_2$]. Pellet slurries were combined and mixed in a sterile 50 mL Falcon tube. The optical density (OD) of a ten-fold dilution of the combined *P. syringae* slurry was measured at 600 nm relative to a $MgCl_2$ Buffer blank cuvette using a Nanodrop spectrophotometer (Thermo Scientific NanoDrop 2000a). The *P. syringae* slurry was diluted to 0.5 OD (~ 2.5 x 10^8 CFU/mL) for grapevine leaves (recommended 0.2 OD (~1 x 10^8 CFU/mL (Katagiri et al., 2002)) for potato leaves; optimization may be

required for other species) with $MgCl_2$ Buffer, and 200 mL of the 0.5 OD inoculum was aliquoted in four dip containers. The control dip container and a control vacuum dip container each contained 200 mL $MgCl_2$ Buffer. Each of the five dip containers corresponded to one of the treatments (30 sec infection, 1 min infection, 1 min control, 3 min infection, 1 min -0.05 MPa vacuum infection, 1 min -0.05 vacuum control). Before leaf dipping, Silwet L-77 was added to each dip container to a final concentration of 0.02%. Each leaf was individually placed in a dip container abaxial side up and gently swirled for either 30 sec, 1 min, 3 min, or subjected to a -0.05 MPa vacuum for 1 min. Only a 1 min control dip and vacuum dip were used as quality control for contamination. This assay can also be applied to entire potted plants with the additional steps of sealing the top of the pot to prevent soil loss and covering the vine with a clear plastic bag supported by wires, sticks, or a tomato cage after dipping (data not shown). After treatment, excess dipping solution was allowed to drip from the leaf and each leaf was carefully placed in an incubation chamber abaxial side down on the wire support grid with the petiole dipping into the sterile water. Incubation chambers were closed and placed in a 27 ˚C growth chamber with a 16:8 light-dark cycle with 265 μE $m^{-2}s^{-1}$ light intensity.

Optimization of *P. syringae* infection assay extraction for *Vitis* leaves

On 1, 3, 5, and 7 days after dipping, three leaf discs (6.3 mm diameter) were taken from each leaf and placed in a 2 mL tube containing 1 mL $MgCl_2$ Buffer and 0.02% Tween 20 (different species may require more or less tissue). *P. syringae* was extracted from the leaf discs at 28 ˚C with 400 rpm shaking for 1 hour. After 1 hour, 200 µL of each sample was serially diluted with $MgCl_2$ Buffer in a 96-well plate. The optimal dilution series for

grapevine leaves included 1x, 1/5x, 1/25x, 1/125x, 1/625x, and 1/3,125x for all samples to ensure resultant CFU were countable (different species may require dilution series optimization). These dilutions are referred to as 0, 1, 2, 3, 4, and 5, respectively. Duplicate 20 µL aliquots of each serial dilution of each sample was plated on a gridded NYGA + ½ RK plates [5 g peptone, 3 g yeast extract, 20 mL glycerol, 15 g agar per 1L, pH 7.0 + 25 mg/L rifampicin and 12.5 mg/L kanamycin final concentration]. Each plate contained the serial dilution of a control and *P. syringae* infected sample. Plates were incubated at 28 ˚C for 2 days. Results presented here are from *P. syringae* DC3000 Pst *avrRpt2* infection.

P. syringae infection assay colony-forming unit counting

After 2 days of incubation at 28 ˚C, colonies were counted and recorded for each dilution of each replicate of each serial dilution of each sample. Technical replicate colonies were averaged. Total CFUs were calculated similarly to previous work (Tornero and Dangl, 2001) (Equation 1). The final version of the optimized version of the *P. syringae* infection assay was performed nine times.

Overexpression _VviERF6L1_ vine _P. syringae_ infection assay

All supplies were sterilized, and all work was performed with sterile technique in a flow hood. *P. syringae* was cultured as was described for the optimization of the *P. syringae* infection assay. Six leaves from at least three individual L12-3, L12-11, L12-23 overexpression vines, and G1 empty vector control plants were removed from vines and sanitized as was described for the optimization of the *P. syringae* infection assay with all leaves per line placed in individual baths. Similar leaves were selected as in the

optimization of the *P. syringae* infection assay. Three leaves of each line were dipped in either 0.5 OD *P. syringae* DC3000 *avrRpt2* or $MgCl_2$ Buffer both containing 0.02% Silwet L-77 for one minute with gentle shaking and placed in incubation chambers as described for the optimization of the *P. syringae* infection assay. Incubation chambers were placed in a growth chamber under the same conditions described for the optimization of the *P. syringae* infection assay. Leaf discs were extracted on day 5 after dipping. *P. syringae* was extracted and colonies were counted as in the optimization of the *P. syringae* infection. The *VviERF6L1* overexpression line *P. syringae* infection experiment was repeated for 11 rounds with three leaves treated per line per treatment (mock or *P. syringae* infected). Results presented here are from *P. syringae* DC3000 Pst *avrRpt2* infection.

***P. syringae* vacuum survival**

Five individual *P. syringae* cultures were grown, spun down, and adjusted to 0.5 OD as for the *P. syringae* infection assay, and prepared as for the *P. syringae* infection assay. However, the cultures were not combined. Five 200 mL 0.5 OD *P. syringae* dip containers and five 200 mL control dip containers were prepared. Duplicate 200 μL aliquots of the bacteria solution were serially diluted and plated as for the *syringae* infection assay extraction before vacuuming. Each dip container was subjected to vacuum till -0.05 MPa was reached at which point the vacuum was maintained but not increased. The dip containers were incubated at -0.05 MPa for one minute before the pressure was released. This process was also used in the *P. syringae* infection assay optimization for vacuum treatments. Duplicate 200 μL aliquots of the vacuum treated solutions were serially diluted and plated as for the *syringae* infection assay extraction. This process was repeated for five

vacuuming sessions for each of the five bacterial and control solutions. CFUs were counted as for the *P. syringae* infection assay.

Leaf incubation chamber survival LiCor measurements

Photosynthesis and stomatal conductance were measured with a LiCor LI-64000 Portable Photosynthesis System on detached CS leaves treated with Control conditions described for the *P. syringae* infection assay 1, 3, 5, and 7 days after sterilization and Control treatment. LiCor settings included 25 ˚C block temperature, 400 ppm CO_2 reference, and 1000 μE $m^{-2} s^{-1}$ PAR. Relative humidity ranged from 20-35% when measurements were taken between 10:00 am-12:00 pm in November. Measurements were recorded 2 min after a 2x3 cm head clamp was applied to the leaves. Leaf petioles remained submerged during readings. Sanitization, control mock infection, and LiCor measurements were repeated individually for at least 33 leaves. Inert leaf controls were a dead, dried leaf placed in an incubation chamber in the growth chamber. Photosynthesis and stomatal conductance of these inert control leaves were zero.

RNA-Extraction and RT-qPCR

Four rounds of five CS leaves were treated with *P. syringae* infection or mock infection (Control) as was described for the optimization of the *P. syringae* infection assay. Whole leaves excluding the petiole were harvest on days 1, 3, 5, and 7 and frozen in liquid nitrogen. RT-qPCR was performed as previously described (Cochetel et al., 2020). Briefly, all samples were ground with a mortar and pestle under liquid nitrogen. RNA extraction was performed with a previously described CTAB based extraction and LiCl precipitation

following cleanup with the Spectrum™ Plant Total RNA kit (Sigma-Aldrich). All RNA extractions were treated with RNAse-free DNase I (Qiagen) to remove genomic DNA contamination. Samples were quantified on a nanodrop, and RNA quality was confirmed with gel electrophoresis by loading 250 ng RNA on a 1.2% gel as well as checked for the presence of gDNA with a GoTaq Green-LAR based PCR analyzed with electrophoresis on a 2% gel employing 400 ng of RNA. Primers were designed using NCBI Primer-BLAST. Primer sequences were previously described (Cochetel et al., 2020). Reference genes (*ACT7* and *GAPDH*) were chosen for consistent band intensity under the various experimental conditions determined with a Go-Taq Green-based PCR reaction. *PR1* (F: AGATTTCATTGCCACTTCTTGTTGG and R: GAGTTCTGGGCACAACAGAC) was used as a potential positive control gene for *P. syringae* infection. *VviERF6L1* primers used were F: TCTCAGTCCCTCAGCCCATC and R: GAGGCGTGCGGAGACGA. The PCR reaction included 95 °C for 2 min, 35 cycles of 95 °C for 30 s, 62 °C for 25 s, and 72 °C for 25 s. Primer efficiencies were verified on purified PCR products (Machery-Nagel NucleoSpin® Gel and PCR Clean-up kit) and were considered at 100% for the gene expression calculations. All reactions were performed on a Bio-Rad Real-Time thermal cycler CFX96 with the following protocol: 95 °C for 3 mins; 40 cycles of 95 °C for 10 s, 60 °C for 15 s. Fluorescence was recorded after each cycle and melting curve analysis was performed from 65 °C to 95 °C. Reference genes were selected based on a low coefficient of variation of expression reported in literature and uniform expression for all cDNA samples for each of the above-described experiments.

4.3 Results

The *P. syringae* infection assay was optimized using detached Cabernet Sauvignon (CS) leaves. The CS and *VviERF6L1* overexpression *P. syringae* infection assay data presented here were derived from avirulent *P. syringae* DC3000 Pst *avrRpt2* infection. However, trials were performed using both *P. syringae* DC3000 and *P. syringae* DC3000 Pst *avrRpt2*. Dilutions 1 through 5 correspond to 1x, 1/5x, 1/25x, 1/125x, 1/625x, and 1/3,125x, respectively, and Day 1 was the day after inoculation.

P. syringae was viable after multiple rounds of -0.05 MPa vacuuming

Syringe infiltration of *P. syringae* into grapevine leaves failed due to inefficient spread and leaf damage (data not shown). Vacuum infiltration and dip inoculation were considered as alternative methods to deliver *P. syringae* infection to detached CS leaves. Vacuum infiltration was performed as described previously (Katagiri et al., 2002), but optimized for grapevine leaves. Briefly, leaves were submerged abaxial side up in 200 mL inoculum. A vacuum pressure of -0.05 MPa (~14.75 inches of mercury) was identified as optimal for producing bubbles on both sides of the leaf, indicative of successful infiltration and minimizing leaf damage. A 1-minute incubation at -0.05 MPa was sufficient for downstream *P. syringae* leaf extraction with longer incubation in the vacuum chamber resulting in bacterial lawns upon extraction. The *P. syringae* survived multiple rounds of vacuuming at -0.05 MPa (Fig. 1), and the number of resultant colonies was not significantly different from that of the culture plated before the vacuuming treatment (Fig. 1).

Leaves were considered viable in incubation chambers for up to seven days

A scalable *P. syringae* infection assay capable of infecting whole vines or detached leaves was desirable for grapevine because it takes months to establish propagates and years to establish mature vines. However, it was also necessary any detached organ remain viable for days after infection; previous research performed in Arabidopsis indicates *P. syringae* infection symptoms take about three days to appear in susceptible Arabidopsis plants (Katagiri et al., 2002). To ensure a level of vigor and stomatal conductance for successful *P. syringae* infection of the detached grapevine leaves, CS leaves were sanitized, mock-infected, and placed in incubation chambers with petiole feeding for 1, 3, 5, and 7 days. Leaves in incubation chambers had significantly higher photosynthesis and stomatal conductance than inert leaf controls (zero photosynthesis and stomatal conductance (see Methods)) (Fig. 2). Generally, the photosynthesis and stomatal conductance decreased with increasing time in the incubation chamber, but all values remained significantly higher than zero throughout the seven days (Fig. 2). Leaves remained turgid and green (not quantified).

A *Vitis* leaf *P. syringae* infection protocol was optimized

As expected, as long as bacterial lawns (predominately dilution 0) were not considered, any dilution could be used to accurately calculate CFUs per leaf area (Fig. 3). There was no significant difference between the CFUs per leaf area for any dilution, day, or *P. syringae* infection treatment (Fig. 3). However, Day 1, particularly for lower dilutions and the 30 second *P. syringae* infection treatment generally had lower CFUs than other days and treatments, but this was not significant (Fig. 3). To better identify optimized *P. syringae* infection conditions, the variance between rounds of infection and occurrence of

zero colonies and bacterial lawns were compared across the 95 infection technique-dilution-day combinations to identify conditions with the lowest variance and most countable number of colonies. All *P. syringae* inoculum had a 0.5 OD because lower densities resulted in low colony formation from grapevine leaf extracts. Generally, the variance of the number of colonies was highest for all infection techniques and all extraction days for more concentrated dilutions (e.g. dilution 0 and 1), and the more concentrated dilutions had more occurrences of uncountable bacterial lawns (Fig. 4). Per round of *P. syringae* infection assay optimization with detached CS leaves, the vacuum infiltration method on average had the most occurrences of bacterial lawns for all five dilutions (Fig. 4). Across all infection techniques, the presence of lawns increased with increasing days of incubation. For example, across all infection techniques and dilutions, day 7 of extraction had the highest frequency of bacterial lawns (Fig. 4). There were no instances of lawns on 1-minute dip Controls, but there were a few instances of lawns and contamination on Vacuum Controls (Figs. 4 and 5).

Generally, the variance of the number of colonies was the lowest for all infection techniques and all extraction days for more diluted extracts (e.g. dilution 3 and 4). However, higher levels of dilutions also more frequently yielded zero colonies (Fig. 5). Across all treatments, day 1 extracts had the highest occurrences of zero colonies for all dilutions (Fig. 5). The three-minute infection technique had the highest occurrences of zero colonies across dilutions and extraction days (Fig. 5). Based on these results, the 30-second and 1-minute infection techniques, dilutions 1-4, and days 3 and 5 resulted in the most countable numbers of colonies (Fig. 5).

To further narrow the optimal technique-dilution-day combination for *Vitis* leaves, the variance and average number of colonies were quantified from nine experimental rounds for the 30-second and 1-minute infection techniques for dilutions 1-4 on days 3 and 5 (Table 1). The target range of countable colonies was identified as $5 \leq n \leq 20$ based on literature (Tornero and Dangl, 2001) and the grid size used for plating the extraction dilution series. The 1-minute infection technique with extraction five days after dipping and CFU determination based on the number of colonies present in dilution 3 was the closest infection technique-dilution-day combination to the mean and median colony variance of the combinations in Table 1 and was thereby considered optimal for these CS leaves for this assay. However, protocols in Arabidopsis are flexible with the exact dilution used per round of extraction based on the formation of resultant colonies (Tornero and Dangl, 2001), and either day 3 or day 5 are successful for *P. syringae* extraction from detached CS leaves.

This protocol was also successful for potato leaf *P. syringae* infection (data not shown), but this species required different infection conditions than grapevine. Potato (*Solanum tuberosum* cv. Atlantic) leaves appeared more susceptible to *P. syringae* infection than those of *Vitis* and required infection with lower OD or higher dilution of extracts (data not shown).

VviERF6L1 transcripts increased in CS leaves after one day in response to *P. syringae* treatment

VviERF6L1 transcript abundance was on average ~2-fold higher in *P. syringae* infected leaves than Control mock-infected leaves one day after treatment (Fig. 6). RT-qPCR was

performed on detached CS leaves treated with 1-minute *P. syringae* dip or a 1-minute mock infection Control to determine if *VviERF6L1* was transcriptionally responding to the *P. syringae* infection (Fig. 6). Treated leaves were harvested one, three, five, and seven days after infection. *VviERF6L1* transcript abundance in *P. syringae* infected leaves was not significantly different from Control on any other day of infection than one day after treatment for these detached CS leaves (Fig. 6).

A predicted *PR1* (Vitvi03g01650) paralog was employed as a potential *P. syringae* infection positive control gene because *PR1* transcript abundance increase in response to pathogens (Cameron et al., 1999). Surprisingly, this gene on average had lower expression in response to *P. syringae* infection than the mock-infected samples, but the transcript abundance of this gene was not significantly different from the Control mock infection on any day (Fig. 6). Of note, this gene was also significantly downregulated in OX *VviERF6L1* lines (Toups et al., 2020).

Overexpression of *VviERF6L1* may reduce grapevine susceptibility to *P. syringae*

The *VviERF6L1* overexpression vines had fewer colony-forming units (CFUs) per leaf area than the empty vector control vines (Fig. 6). Based on the results from the optimization of the detached grapevine leaf *P. syringae* infection assay, *VviERF6L1* overexpression lines (L12-3, L12-11, and L12-23) and empty vector control (G1) detached sanitized leaves were treated for one minute with mock Control or *P. syringae* infection. *P. syringae* was extracted from the leaves five days after dipping inoculation. As with the CS Controls from the optimization experiment, all Controls from this experiment generally had no contamination (data not shown); plates with Control colony formation or contamination

were discarded. Unlike the CS *P. syringae* infection assay, which had optimal colonies for CFU determination from dilution 3, the *VviERF6L1* overexpression and G1 leaves had the most countable colonies on dilution 0. Higher dilutions had more occurrences of zero colonies for all vines. Both L12-11 and L12-23 had significantly reduced CFUs per leaf area than G1 (Fig. 6). L12-3 also had on average a lower number of CFUs per leaf area, but this was not significantly different from G1 (Fig. 6).

4.4 Discussion

The *P. syringae* infection assay results are comparable for grapevine and Arabidopsis

This work optimized a *P. syringae* infection assay adaptable for whole vines or detached grapevine leaves. This assay was based on techniques previously described for Arabidopsis, but several changes were made to adapt the method to grapevine. Ten-fold more bacteria were needed during dipping and a smaller serial dilution was used during extract plating to have consistent *P. syringae* colony formation for detached grapevine leaves than was described for Arabidopsis (Tornero and Dangl, 2001). Dip inoculation was determined to be the most effective and least labor-intensive technique for *P. syringae* infection of grapevine (Table 1 and Figs. 3 and 4). Dip inoculation relies on *P. syringae* entry into the stomata, which is controlled by various environmental factors like stress, light (Assmann and Jegla, 2016), and humidity (Carvalho et al., 2016). These factors may affect the infection efficiency of the *P. syringae* infection assay for grapevine leaves presented here. Vacuum infiltration had higher rates of contamination than dip treatment (Figs. 3 and 4)

and more labor was involved in the infection process, but vacuum infiltration appears standard for Arabidopsis (Chen et al., 2000; Liu et al., 2015). Given the results of the detached CS leaf optimization *P. syringae* infection, dipping, and extraction after 3-5 days yielded the most consistent results (Table 1 and Figs. 3 and 4). In the future, this technique may be optimized for additional plant species and used to characterize PAMP-triggered immunity and systemic acquired resistance (SAR) in different grapevine cultivars as was previously performed in Arabidopsis (Liu et al., 2015).

Visually, virulent P. *syringae* infected leaves developed chlorotic spots, necrosis, and in some cases turned red or purple (Fig. 7) presumably due to anthocyanin accumulation in response to coronatine (Af et al., 1992), an isoleucine-jasmonic acid (JA) mimic toxin from *P. syringae* to counteract SA-signaling (B et al., 1994). However, not all leaves showed infection symptoms including Control (Fig. 7) and avirulent infected grapevine leaves, which appeared healthy for numerous samples, coherent with literature (Katagiri et al., 2002).

The CS and *VviERF6L1* overexpression vine *P. syringae* infection assay results presented here (Figs. 3 and 6) were derived from avirulent *P. syringae* DC3000 Pst *avrRpt2* infection because this strain was demonstrated to have higher ethylene production (Guan et al., 2015), and it was hypothesized infection by this strain may result in a more significant response in the *VviERF6L1* overexpression vines. However, this assay should be repeated comparing various *P. syringae* pathovars across *Vitis* species and the *VviERF6L1* overexpression vines.

P. syringae thrives epiphytically in addition to *in folium*. The surfactant in the *P. syringae* dipping solution should have allowed *P. syringae* entry into the intercellular space

in leaves. Epiphytic vs. endophytic *P. syringae* was not quantified here. Re-sanitization of leaf surface as described elsewhere for Arabidopsis (Katagiri et al., 2002) after *P. syringae* infection and incubation followed by extraction would further validate intercellular infection in grapevine leaves. However, Pst DC3000 is a weak epiphyte, and does not survive on leaf epidermis more than 48 hours (Xin and He, 2013); therefore, the *P. syringae* extracted from the grapevine leaves is likely endophytic. Macerating leaf discs may be a further improvement to this assay, releasing more bacteria during extraction as has been performed in some Arabidopsis protocols (Katagiri et al., 2002). However, an hour incubation with shaking was previously shown to be as effective as tissue grinding in Arabidopsis (Tornero and Dangl, 2001).

CFUs from the CS detached leaf optimization of the *P. syringae* infection assay were comparable to extractions from Arabidopsis (Chen et al., 2000; Liu et al., 2015; Tornero and Dangl, 2001) although much lower CFUs were obtained from the *VviERF6L* overexpression vines including the empty vector control. This difference may be attributed to the necessity to count colonies on dilution 0 for the *VviERF6L1* overexpression lines because there were few colonies on higher diluted extracts. However, the results from the *VviERF6L* overexpression vine *P. syringae* infection assay on dilution 0 were consistent for multiple rounds of the experiment (Fig. 6). The assay can be reperformed for the *VviERF6L* overexpression vines using a different dilution series or more tissue for extraction in future experiments.

Alternatively, the differences may be attributed to a thicker cuticle, denser mesophyll, or higher natural resistance Seyval Blanc (the background of the *VviERF6L1* overexpression lines) may have to *P. syringae* than does Arabidopsis or CS. To investigate

this possibility the presence of RPS2 genes were compared between Arabidopsis (Tello-Ruiz et al., 2018), the PN40024 reference genome (Canaguier et al., 2017), and the CS clone-8 v1.0 genome (Chin et al., 2016). Unfortunately, there is no Seyval Blanc genome available for this comparison at this time. *AtRPS2*, the R-gene confirming resistance to the *P. syringae* DC3000 *avrRpt2*, has 76 paralogs in Arabidopsis compared to the 353 orthologs in the PN40024 grapevine genome (Tello-Ruiz et al., 2018). AtRPS2 and the closest grapevine PN40024 ortholog (Vitvi11g00146) share ~66 %ID for protein sequences (Altschul et al., 1990). Only one CS RPS2 ortholog was identified in the diploid CS clone 8 genome v1.0 (Chin et al., 2016) for which the PN RPS2 and CS RPS2 proteins had 100 %ID. Experiments should be performed in the future to identified *P. syringae* susceptible and resistant grapevines by comparing CFUs from different grapevine cultivars and species infected with avirulent or virulent *P. syringae*.

Previously, combining multiple rounds of pathogen assays has been advised against in Arabidopsis due to significant differences between rounds (Tornero and Dangl, 2001). Here, multiple rounds of the *P. syringae* infection assay for the CS and OX *VviERF6L1* detached leaf experiments were combined (Figs. 3 and 6) because there were only small differences between rounds per experiment, and different leaves dipped in the same batch of inoculum should be treated as technical replicates. However, the colonies from these extractions still require validation as *P. syringae,* which can be accomplished by PCR and sequencing using *P. syringae* specific primers (Porotikova et al., 2016) or other methods (Gerin et al., 2019).

The *P. syringae* infection assay presented here can follow *P. syringae* infection progression in the same detached leaf over a series of days. However, the damage inflicted

by removing leaf discs may trigger a JA response and increase *P. syringae* susceptibility (Son et al., 2012). This limitation was minimized by extracting leaf discs from the same leaf region for each leaf on each day during the detached CS leaf optimization to uniformize any JA response in all samples. Alternatively, individual leaves can be used for separate days in any future time-course experiments.

Pathogen resistance is a complex culmination of numerous signals, one of which is *VviERF6L1*

Plant-pathogen interactions are affected by environmental factors as well as plant age (Boyes et al., 2001), and plant responses to bacteria vary for subtle differences in irrigation or airflow (Katagiri et al., 2002). Previous vine exposure to pathogens or abiotic stress may also prime different symptoms and susceptibility (Yakura, 2020). Additionally, numerous phytohormones and signaling network crosstalk determine overall plant susceptibility or resistance to a given pathogen (Guan et al., 2015; Xin and He, 2013). For example, SA and JA are generally considered to act antagonistically although both are essential in biotic stress response (Son et al., 2012). Genes involved in *P. syringae* resistance are mainly associated with SA signaling. SA accumulation can lead to SAR or whole plant resistance to a host of pathogens in response to a localized infection (Chen et al., 2000). Activation of JA-signaling represses SA-signaling and reduces resistance to *P. syringae* (Son et al., 2012). However, JA-signaling is essential for induced systemic resistance (ISR) against *P. syringae*.

Ethylene can also have conflicting roles in plant immune responses (Washington et al., 2016). For example, *ERF1* overexpression enhances *Botrytis cinerea* resistance and

increases *P. syringae* susceptibility (Berrocal-Lobo et al., 2002), but Arabidopsis *ethylene insensitive* 2 (*ein2*) mutants have increased resistance to *P. syringae* and other pathogens (Af et al., 1992). Due to these conflicting signals, it is not surprising there are divergent conclusions for the role of ethylene signaling in plant-pathogen resistance (Broekaert et al., 2006; Glazebrook, 2005; Guan et al., 2015; van Loon et al., 2006). Previously, the role of *VviERF6L* orthologs was demonstrated to have conflicting effects on *P. syringae* susceptibility in Arabidopsis (Fröschel et al., 2019; Moffat et al., 2012). The work presented here supports that of Fröschel *et al*. and concludes overexpression of *VviERF6L1* increases grapevine resistance to *P. syringae* likely by positively regulating SA signaling. The reality of the matter is numerous factors including the plant cultivar, age, organ, and previous exposure to abiotic and biotic stress as well as the pathogen and the specific pathovar infecting a plant effect hormone crosstalk and thereby overall resistance.

In the past century, *P. syringae* has been identified as the source of new diseases on over twenty woody perennial species including grapevine (Gerin et al., 2019). *P. syringae* reduced fruiting by up to 60% in Australian vineyards (Whitelaw-Weckert et al., 2011). Additionally, *P. syringae* infection made grapevine more susceptible to secondary infections from other pathogens (Whitelaw-Weckert et al., 2011). Incidence of *P. syringae* symptoms is on the rise in vineyards all across the world, but the pathogenicity of this bacteria in *Vitis* remains largely uncharacterized. Evidence is already emerging certain cultivars are more resistant than others although this is highly pathovar dependent (Gerin et al., 2019), and this requires further characterization.

This work developed a simple and reproducible *P. syringae* infection assay for grapevine. The *P. syringae* infection assay was capable of inoculating whole vines or

detached leaves. This assay was also effective for *P. syringae* infection of detached potato leaves and may be optimized for other plant species. Implementation of this assay identified overexpression of *VviERF6L1* reduced grapevine susceptibility to *P. syringae*. However, the mechanism by which *VviERF6L1* elicits *P. syringae* resistance remains unknown and requires further elucidation. Mechanisms for *VviERF6L1* prompting *P. syringae* resistance may involve putative *VviERF6L1* transcriptional targets that were previously identified (Toups et al., 2020) and are known to be involved in pathogen response. Additionally, *WRKY33* may be involved in *VviERF6L1*'s role in *P. syringae* resistance. *WRKY33* followed a similar expression pattern as *ERF6Ls* across numerous organs and treatments in *Vitis* (Toups et al., 2020), and WRKY33 activates ACS transcription and ethylene signaling during pathogen response (Li et al., 2012; Mao et al., 2011). The increase in ethylene biosynthesis during pathogen response (Guan et al., 2015), and the increase in *VviERF6L1* transcripts in response to *P. syringae* infection (Fig. 6) provide a possible link between ethylene signaling and *VviERF6L1*. The increase in *VviERF6L1* transcript abundance may be resultant of increased ethylene and part of an ethylene-dependent pathogen resistance response. Overall, *VviERF6L1* provides a promising link between ethylene signaling and pathogen response in grapevine.

4.5 References

Af, B., Rw, I., Jr, E., and Bj, S. (1992). Disease development in ethylene-insensitive Arabidopsis thaliana infected with virulent and avirulent Pseudomonas and Xanthomonas pathogens. Mol. Plant-Microbe Interact. MPMI *5*.

Altschul, S.F., Gish, W., Miller, W., Myers, E.W., and Lipman, D.J. (1990). Basic local alignment search tool. J. Mol. Biol. *215*, 403–410.

Assmann, S.M., and Jegla, T. (2016). Guard cell sensory systems: recent insights on stomatal responses to light, abscisic acid, and CO2. Curr. Opin. Plant Biol. *33*, 157–167.

B, F., Ce, B., Cn, P., and Jg, T. (1994). Arabidopsis Mutants Selected for Resistance to the Phytotoxin Coronatine Are Male Sterile, Insensitive to Methyl Jasmonate, and Resistant to a Bacterial Pathogen. Plant Cell *6*.

Berrocal-Lobo, M., Molina, A., and Solano, R. (2002). Constitutive expression of ETHYLENE-RESPONSE-FACTOR1 in Arabidopsis confers resistance to several necrotrophic fungi. Plant J. Cell Mol. Biol. *29*, 23–32.

Boyes, D.C., Zayed, A.M., Ascenzi, R., McCaskill, A.J., Hoffman, N.E., Davis, K.R., and Görlach, J. (2001). Growth stage-based phenotypic analysis of Arabidopsis: a model for high throughput functional genomics in plants. Plant Cell *13*, 1499–1510.

Broekaert, W.F., Delauré, S.L., De Bolle, M.F.C., and Cammue, B.P.A. (2006). The role of ethylene in host-pathogen interactions. Annu. Rev. Phytopathol. *44*, 393–416.

Cameron, R.K., Paiva, N.L., Lamb, C.J., and Dixon, R.A. (1999). Accumulation of salicylic acid and PR-1 gene transcripts in relation to the systemic acquired resistance (SAR) response induced by Pseudomonas syringae pv. tomato in Arabidopsis. Physiol. Mol. Plant Pathol. *55*, 121–130.

Canaguier, A., Grimplet, J., Di Gaspero, G., Scalabrin, S., Duchêne, E., Choisne, N., Mohellibi, N., Guichard, C., Rombauts, S., Le Clainche, I., et al. (2017). A new version of the grapevine reference genome assembly (12X.v2) and of its annotation (VCost.v3). Genomics Data *14*, 56–62.

Carvalho, D.R.A., Fanourakis, D., Correia, M.J., Monteiro, J.A., Araújo-Alves, J.P.L., Vasconcelos, M.W., Almeida, D.P.F., Heuvelink, E., and Carvalho, S.M.P. (2016). Root-to-shoot ABA signaling does not contribute to genotypic variation in stomatal functioning induced by high relative air humidity. Environ. Exp. Bot. *123*, 13–21.

Chen, Z., Kloek, A.P., Boch, J., Katagiri, F., and Kunkel, B.N. (2000). The *Pseudomonas syringae avrRpt2* Gene Product Promotes Pathogen Virulence from Inside Plant Cells. Mol. Plant-Microbe Interactions® *13*, 1312–1321.

Chin, C.-S., Peluso, P., Sedlazeck, F.J., Nattestad, M., Concepcion, G.T., Clum, A., Dunn, C., O'Malley, R., Figueroa-Balderas, R., Morales-Cruz, A., et al. (2016). Phased diploid genome assembly with single-molecule real-time sequencing. Nat. Methods *13*, 1050–1054.

Cochetel, N., Ghan, R., Toups, H.S., Degu, A., Tillett, R.L., Schlauch, K.A., and Cramer, G.R. (2020). Drought tolerance of the grapevine, Vitis champinii cv. Ramsey, is associated

with higher photosynthesis and greater transcriptomic responsiveness of abscisic acid biosynthesis and signaling. BMC Plant Biol. *20*.

Dangl, J.L., Dietrich, R.A., and Richberg, M.H. (1996). Death Don't Have No Mercy: Cell Death Programs in Plant-Microbe Interactions. Plant Cell *8*, 1793–1807.

Eisenmann, B., Czemmel, S., Ziegler, T., Buchholz, G., Kortekamp, A., Trapp, O., Rausch, T., Dry, I., and Bogs, J. (2019). Rpv3–1 mediated resistance to grapevine downy mildew is associated with specific host transcriptional responses and the accumulation of stilbenes. BMC Plant Biol. *19*.

Fröschel, C., Iven, T., Walper, E., Bachmann, V., Weiste, C., and Dröge-Laser, W. (2019). A Gain-of-Function Screen Reveals Redundant ERF Transcription Factors Providing Opportunities for Resistance Breeding Toward the Vascular Fungal Pathogen Verticillium longisporum. Mol. Plant-Microbe Interact. MPMI *32*, 1095–1109.

Gerin, D., Cariddi, C., de Miccolis Angelini, R. m., Rotolo, C., Dongiovanni, C., Faretra, F., and Pollastro, S. (2019). First Report of Pseudomonas Grapevine Bunch Rot Caused by Pseudomonas syringae pv. syringae. Plant Dis. *103*, 1954–1960.

Glazebrook, J. (2005). Contrasting mechanisms of defense against biotrophic and necrotrophic pathogens. Annu. Rev. Phytopathol. *43*, 205–227.

Goto, S., Sasakura-Shimoda, F., Yamazaki, M., Hayashi, N., Suetsugu, M., Ochiai, H., and Takatsuji, H. (2016). Development of disease-resistant rice by pathogen-responsive expression of WRKY45. Plant Biotechnol. J. *14*, 1127–1138.

Guan, R., Su, J., Meng, X., Li, S., Liu, Y., Xu, J., and Zhang, S. (2015). Multilayered Regulation of Ethylene Induction Plays a Positive Role in Arabidopsis Resistance against Pseudomonas syringae. Plant Physiol. *169*, 299–312.

Hall, B.H., McMahon, R.L., Noble, D., Cottier, E.J., and McLintock, D. (2002). First report of Pseudomonas syringae on grapevines (Vitis vinifera) in South Australia. Australas. Plant Pathol. *31*, 421–422.

Hall, S.J., Dry, I.B., Gopurenko, D., and Whitelaw-Weckert, M.A. (2019). Pseudomonas syringae pv. syringae from cool climate Australian grapevine vineyards: new phylogroup PG02f associated with bacterial inflorescence rot. Plant Pathol. *68*, 312–322.

Katagiri, F., Thilmony, R., and He, S.Y. (2002). The Arabidopsis Thaliana-Pseudomonas Syringae Interaction. Arab. Book Am. Soc. Plant Biol. *1*.

Klingner, A.E., Palleroni, N.J., and Pontis, R.E. (1976). Isolation of Pseudomonas syringae from Lesions on Vitis vinifera. J. Phytopathol. *86*, 107–116.

Li, G., Meng, X., Wang, R., Mao, G., Han, L., Liu, Y., and Zhang, S. (2012). Dual-Level Regulation of ACC Synthase Activity by MPK3/MPK6 Cascade and Its Downstream

WRKY Transcription Factor during Ethylene Induction in Arabidopsis. PLOS Genet. *8*, e1002767.

Li, Q., Hu, A., Qi, J., Dou, W., Qin, X., Zou, X., Xu, L., Chen, S., and He, Y. (2020). CsWAKL08, a pathogen-induced wall-associated receptor-like kinase in sweet orange, confers resistance to citrus bacterial canker via ROS control and JA signaling. Hortic. Res. *7*, 1–15.

Liu, X., Sun, Y., Kørner, C.J., Du, X., Vollmer, M.E., and Pajerowska-Mukhtar, K.M. (2015). Bacterial Leaf Infiltration Assay for Fine Characterization of Plant Defense Responses using the Arabidopsis thaliana-Pseudomonas syringae Pathosystem. J. Vis. Exp. JoVE.

van Loon, L.C., Geraats, B.P.J., and Linthorst, H.J.M. (2006). Ethylene as a modulator of disease resistance in plants. Trends Plant Sci. *11*, 184–191.

Lu, S., Li, Q., Wei, H., Chang, M.-J., Tunlaya-Anukit, S., Kim, H., Liu, J., Song, J., Sun, Y.-H., Yuan, L., et al. (2013). Ptr-miR397a is a negative regulator of laccase genes affecting lignin content in Populus trichocarpa. Proc. Natl. Acad. Sci. *110*, 10848–10853.

Mao, G., Meng, X., Liu, Y., Zheng, Z., Chen, Z., and Zhang, S. (2011). Phosphorylation of a WRKY Transcription Factor by Two Pathogen-Responsive MAPKs Drives Phytoalexin Biosynthesis in Arabidopsis. Plant Cell *23*, 1639–1653.

Melotto, M., Underwood, W., Koczan, J., Nomura, K., and He, S.Y. (2006). Plant stomata function in innate immunity against bacterial invasion. Cell *126*, 969–980.

Moffat, C.S., Ingle, R.A., Wathugala, D.L., Saunders, N.J., Knight, H., and Knight, M.R. (2012). ERF5 and ERF6 Play Redundant Roles as Positive Regulators of JA/Et-Mediated Defense against Botrytis cinerea in Arabidopsis. PLoS ONE *7*.

Morris, C.E., Monteil, C.L., and Berge, O. (2013). The Life History of *Pseudomonas syringae* : Linking Agriculture to Earth System Processes. Annu. Rev. Phytopathol. *51*, 85–104.

Naumann, G., Alfieri, L., Wyser, K., Mentaschi, L., Betts, R.A., Carrao, H., Spinoni, J., Vogt, J., and Feyen, L. (2018). Global Changes in Drought Conditions Under Different Levels of Warming. Geophys. Res. Lett. *45*, 3285–3296.

Pautasso, M., Döring, T.F., Garbelotto, M., Pellis, L., and Jeger, M.J. (2012). Impacts of climate change on plant diseases—opinions and trends. Eur. J. Plant Pathol. *133*, 295–313.

Porotikova, E.V., Dmitrenko, U.D., Atapina, E.E., Volkov, Y.A., Risovannaya, V.I., Stranishevskaya, E.P., Gorislavets, S.M., Kamionskaya, A.M., and Vinogradova, S.V. (2016). First Report of the Bacterial Leaf Spot Caused by Pseudomonas syringae on Grapevine (Vitis vinifera) in Russia. Plant Dis. *101*, 380–380.

Quezada, E.-H., García, G.-X., Arthikala, M.-K., Melappa, G., Lara, M., and Nanjareddy, K. (2019). Cysteine-Rich Receptor-Like Kinase Gene Family Identification in the Phaseolus Genome and Comparative Analysis of Their Expression Profiles Specific to Mycorrhizal and Rhizobial Symbiosis. Genes *10*, 59.

Rienth, M., Crovadore, J., Ghaffari, S., and Lefort, F. (2019). Oregano essential oil vapour prevents Plasmopara viticola infection in grapevine (Vitis Vinifera) and primes plant immunity mechanisms. PLOS ONE *14*.

Savary, S., Willocquet, L., Pethybridge, S.J., Esker, P., McRoberts, N., and Nelson, A. (2019). The global burden of pathogens and pests on major food crops. Nat. Ecol. Evol. *3*, 430–439.

Son, G.H., Wan, J., Kim, H.J., Nguyen, X.C., Chung, W.S., Hong, J.C., and Stacey, G. (2012). Ethylene-Responsive Element-Binding Factor 5, ERF5, Is Involved in Chitin-Induced Innate Immunity Response. Mol. Plant. Microbe Interact. *25*, 48–60.

Tello-Ruiz, M.K., Naithani, S., Stein, J.C., Gupta, P., Campbell, M., Olson, A., Wei, S., Preece, J., Geniza, M.J., Jiao, Y., et al. (2018). Gramene 2018: unifying comparative genomics and pathway resources for plant research. Nucleic Acids Res. *46*, D1181–D1189.

Tornero, P., and Dangl, J.L. (2001). A high-throughput method for quantifying growth of phytopathogenic bacteria in Arabidopsis thaliana. Plant J. *28*, 475–481.

Toups, H.S., Cochetel, N., Gray, D., and Cramer, G.R. (2020). VviERF6Ls: an expanded clade in Vitis responds transcriptionally to abiotic and biotic stresses and berry development. BMC Genomics *21*.

Warmerdam, S., Sterken, M.G., Van Schaik, C., Oortwijn, M.E.P., Lozano-Torres, J.L., Bakker, J., Goverse, A., and Smant, G. (2018). Mediator of tolerance to abiotic stress ERF6 regulates susceptibility of Arabidopsis to Meloidogyne incognita. Mol. Plant Pathol. *20*, 137–152.

Washington, E.J., Mukhtar, M.S., Finkel, O.M., Wan, L., Banfield, M.J., Kieber, J.J., and Dangl, J.L. (2016). Pseudomonas syringae type III effector HopAF1 suppresses plant immunity by targeting methionine recycling to block ethylene induction. Proc. Natl. Acad. Sci. *113*, E3577–E3586.

Whalen, M.C., Innes, R.W., Bent, A.F., and Staskawicz, B.J. (1991). Identification of Pseudomonas syringae pathogens of Arabidopsis and a bacterial locus determining avirulence on both Arabidopsis and soybean. Plant Cell *3*, 49–59.

Whitelaw-Weckert, M.A., Whitelaw, E.S., Rogiers, S.Y., Quirk, L., Clark, A.C., and Huang, C.X. (2011). Bacterial inflorescence rot of grapevine caused by Pseudomonas syringae pv. syringae. Plant Pathol. *60*, 325–337.

Xin, X.-F., and He, S.Y. (2013). Pseudomonas syringae pv. tomato DC3000: A Model Pathogen for Probing Disease Susceptibility and Hormone Signaling in Plants. Annu. Rev. Phytopathol. *51*, 473–498.

Xu, J., and Zhang, S. (2014). Regulation of ethylene biosynthesis and signaling by protein kinases and phosphatases. Mol. Plant.

Xu, J., and Zhang, S. (2015). Mitogen-activated protein kinase cascades in signaling plant growth and development. Trends Plant Sci. *20*, 56–64.

Yakura, H. (2020). Cognitive and Memory Functions in Plant Immunity. Vaccines *8*.

Zhu, Y., Qian, W., and Hua, J. (2010). Temperature Modulates Plant Defense Responses through NB-LRR Proteins. PLOS Pathog. *6*, e1000844.

Zorzatto, C., Machado, J.P.B., Lopes, K.V.G., Nascimento, K.J.T., Pereira, W.A., Brustolini, O.J.B., Reis, P.A.B., Calil, I.P., Deguchi, M., Sachetto-Martins, G., et al. (2015). NIK1-mediated translation suppression functions as a plant antiviral immunity mechanism. Nature *520*, 679–682.

Equations

$$\frac{k\left(\frac{\text{Extraction volume (effective fold dilution)}}{\text{Plated volume}}\right)\left[\left(\#\text{ colonies} * \text{Dilution from plating series}\right)\right]}{\text{Leaf disc SA (or alternatively grams of tissue)}}$$

Equation 1: Colony forming unit calculation. The number of CFUs was determined from the ratio of the extraction volume to the plated volume (k (blue)) multiplied by the number of colonies counted (pink) multiplied by the dilution factor (green) divided by the surface area (SA) of the leaf disc. Modified from original equation description from Tornero et al. 2001.

Tables

Table 1: The top treatment-dilution-day combinations with the lowest variance and most countable number of colonies. The top infection technique-dilution-day combinations ordered from lowest to highest variance and standard deviation (SD). The mean number of colonies (Average) shown to determine "countability". Low average colonies (< 5) indicated in red and high number of countable colonies (> 20) indicated in orange. n = 9 rounds with three leaves per infection technique (Treatment).

Treatment	Dilution	Day	Variance	SD	Average
30 sec	4	3	4.7	2.16794834	3
30 sec	1	3	9.08333333	3.01385689	21.1666667
1 min	4	5	20.8108974	4.56189625	4.96153846
30 sec	3	3	23.4	4.83735465	6.4
1 min	3	3	47.025641	6.85752441	8.76923077
30 sec	4	5	50.4	7.09929574	5
1 min	4	3	130.559524	11.4262646	8.16666667
1 min	3	5	130.668182	11.4310184	11.7272727
1 min	2	3	176.361111	13.2801021	15.1111111
30 sec	3	5	183.285714	13.5383054	11.3571429
1 min	2	5	188.224359	13.7194883	14.1538462
30 sec	2	3	199.340909	14.118814	22.9090909
1 min	1	5	239.455556	15.4743515	27.2
30 sec	2	5	297.818182	17.2574095	21.2727273
30 sec	1	5	327.975	18.1100801	11.25
1 min	1	3	390.229167	19.754219	11.625

Figures

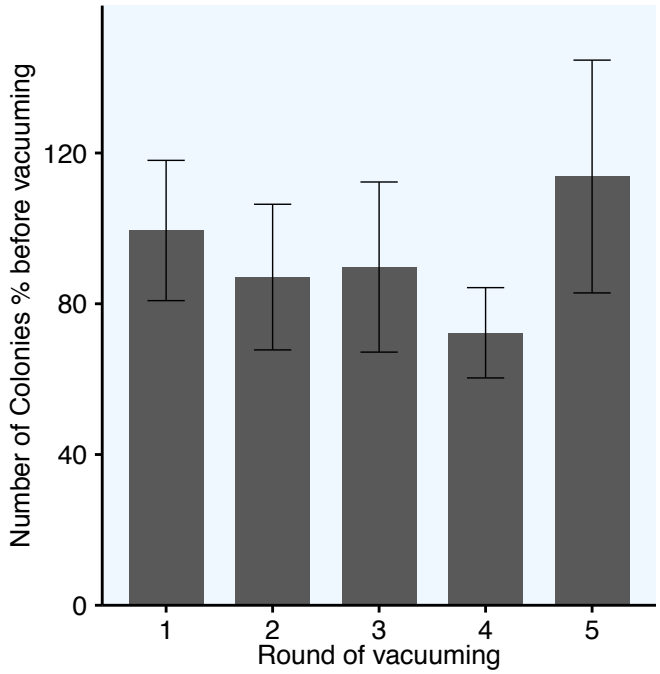

Figure 1: Percent survival of *P. syringae* colonies after multiple rounds of vacuum treatments. The average percentage of colonies grown from 200 μL of vacuum treated *P. syringae* dipping solution after 1, 2, 3, 4, and 5 rounds of vacuuming to -0.05 MPa maintained for one-minute relative to colonies grown from 200 μL of *P. syringae* dipping solution prior to vacuum treatment. Mean ± SE; n = 5. ANOVA ($p \leq 0.05$).

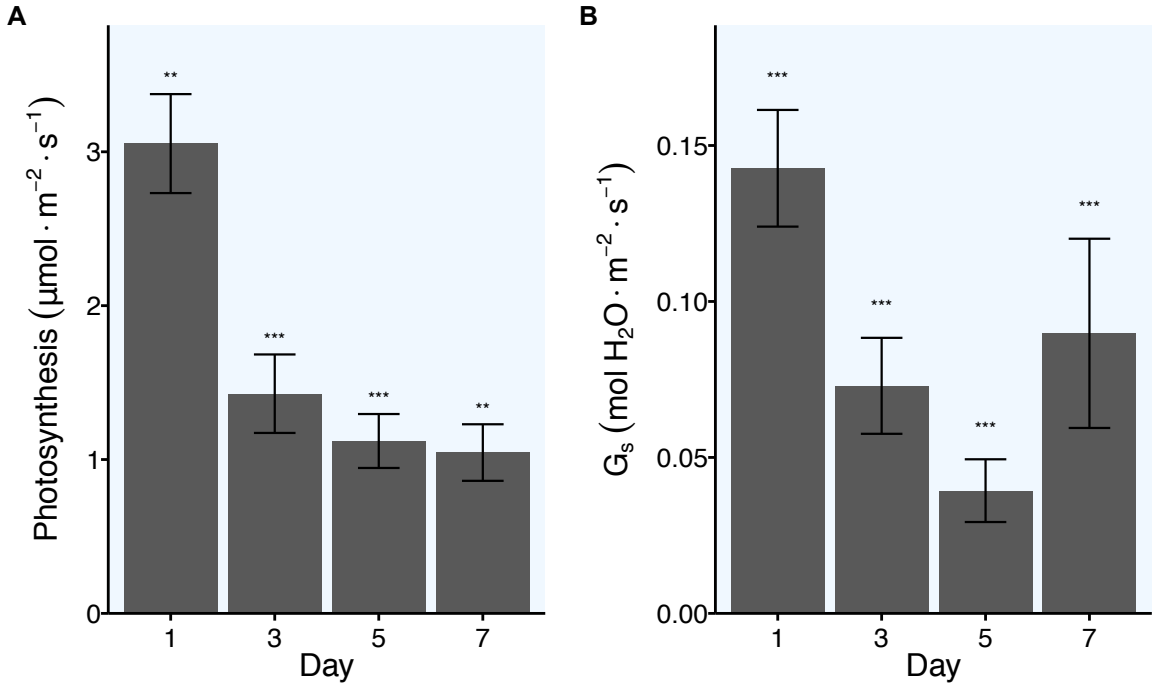

Figure 2: Photosynthesis and Stomatal conductance of detached CS leaves in incubation chambers. The average photosynthesis (μmol ·m^{-2}·s^{-1}) and stomatal conductance (Gs; mol H_2O ·m^{-2}·s^{-1}) of sanitized and mock infected detached CS leaves with petiole feeding in incubation chambers for 1, 3, 5, and 7 days. Mean ± SE; n ≥ 33. ANOVA ($p \leq 0.05$) per day relative to zero photosynthesis and stomatal conductance.

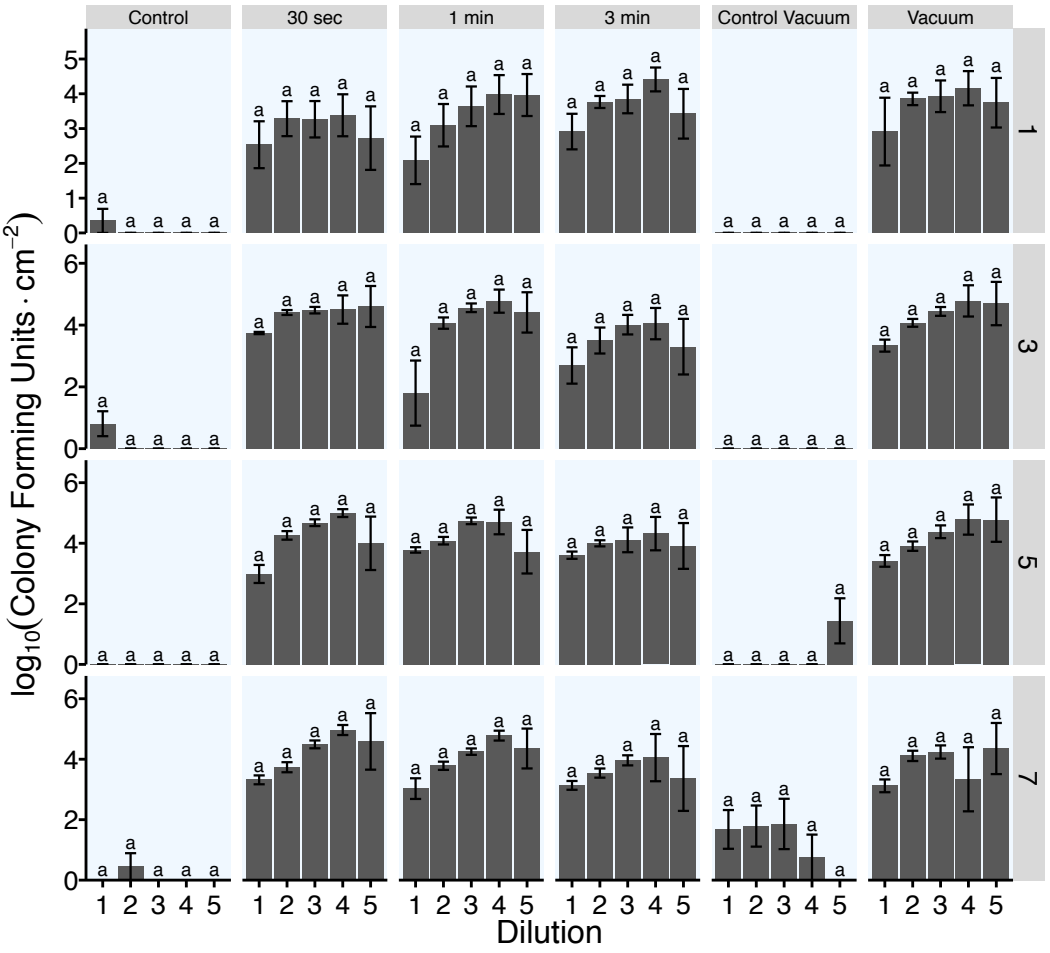

Figure 3: Colony forming units per leaf area of detached CS leaves. The average number of colony forming units per leaf surface area (cm^{-2}) (log_{10} transformed) from dilutions 1-5 on 1, 3, 5, or 7 days after *P. syringae* infection via dipping for 30 seconds, 1 minute, or 3 minutes, or vacuum infiltration at -0.05 MPa for 1 minute or mock infection (dipping/vacuuming in buffer for 1 minute). Dilutions 0, 1, 2, 3, 4, and 5 correspond to 1x, 1/5x, 1/25x, 1/125x, 1/625x, and 1/3,125x *P. syringae* leaf extraction, respectively. Dilution 0 was excluded due to the abundance of bacterial lawns. Mean ± SE; n = 9 rounds of three leaves per treatment per round ANOVA Tukey's HSD ($p \leq 0.05$) letters per treatment.

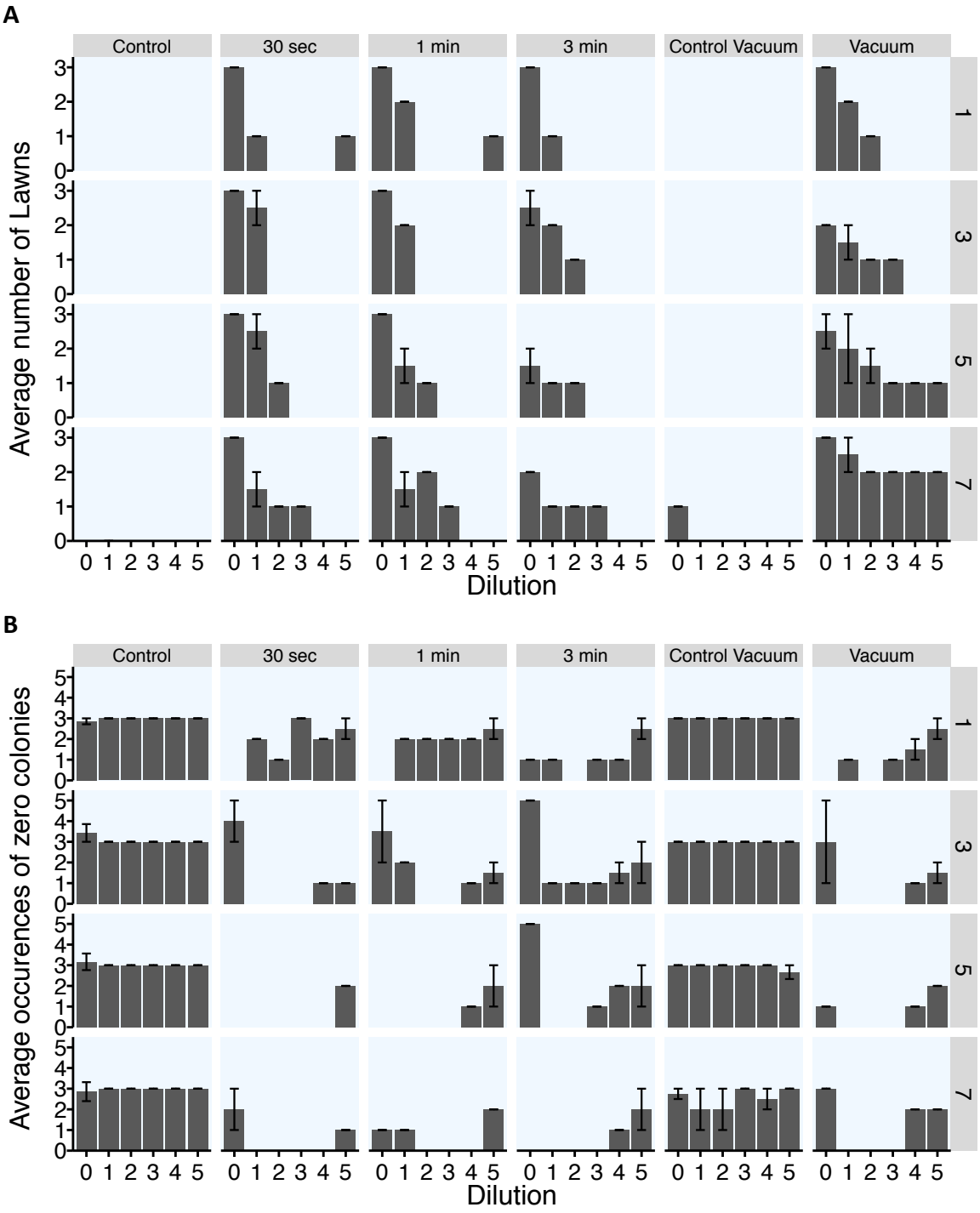

Figure 4: Optimization of extraction dilution series. A) The average number of bacterial lawns per round and **B)** The average number of extractions that did not yield colonies (zero colonies) from *P. syringae* infection assays performed on detached CS leaves treated with 1-minute Control, 30 second *P. syringae* infection, 1-minute *P. syringae* infection, 3-minute *P. syringae* infection, Control vacuum at -0.05 MPa for 1 minute and *P. syringae*

infection Vacuum at -0.05 MPa for 1 minute. Extractions performed 1, 3, 5, and 7 days after treatment. Dilutions 0, 1, 2, 3, 4, and 5 correspond to 1x, 1/5x, 1/25x, 1/125x, 1/625x, and 1/3,125x *P. syringae* leaf extraction, respectively. Mean ± SE; n = 9 rounds of three leaves per treatment per round.

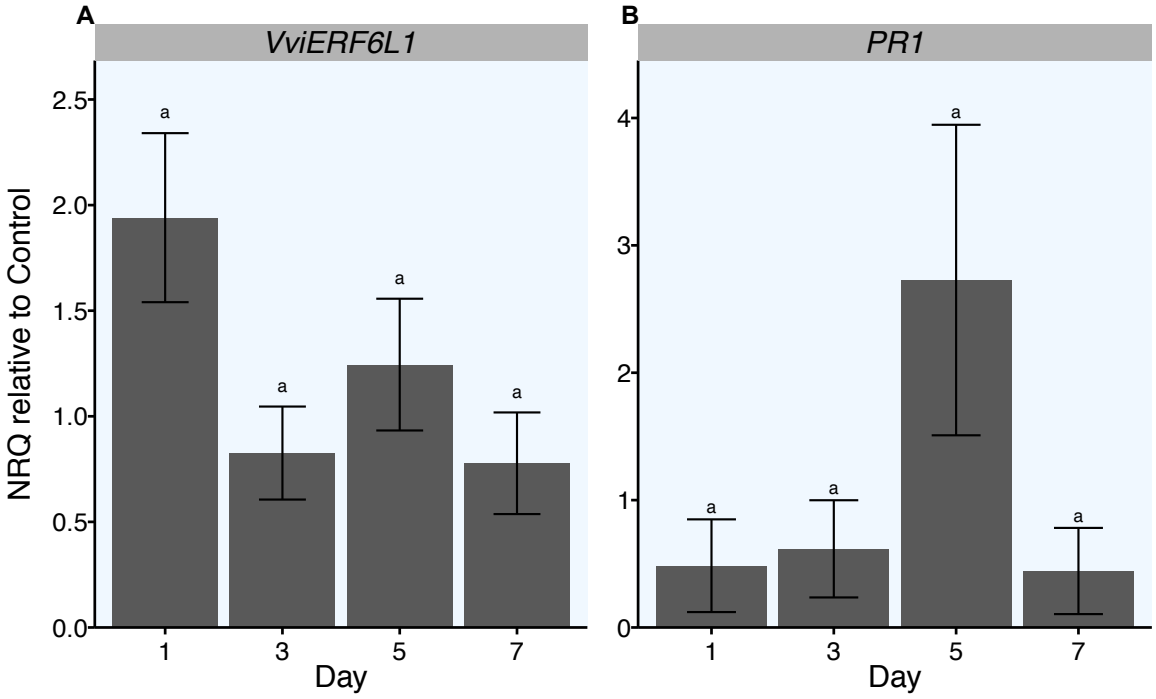

Figure 5: *VviERF6L1* and putative *PR1* relative transcript NRQ after *P. syringae* infection. The relative **A)** *VviERF6L1* and **B)** putative *PR1* transcript abundance (Normalized Relative Quantity; NRQ) relative to Control 1-minute mock infected leaves of sanitized CS leaves treated for 1-minute dip *P. syringae* infection after 1, 3, 5, and 7 days of treatment. Mean ± SE; n = 4. One-way ANOVA Tukey's HSD ($p \leq 0.05$) letters for *P. syringae* infected samples only per gene per day.

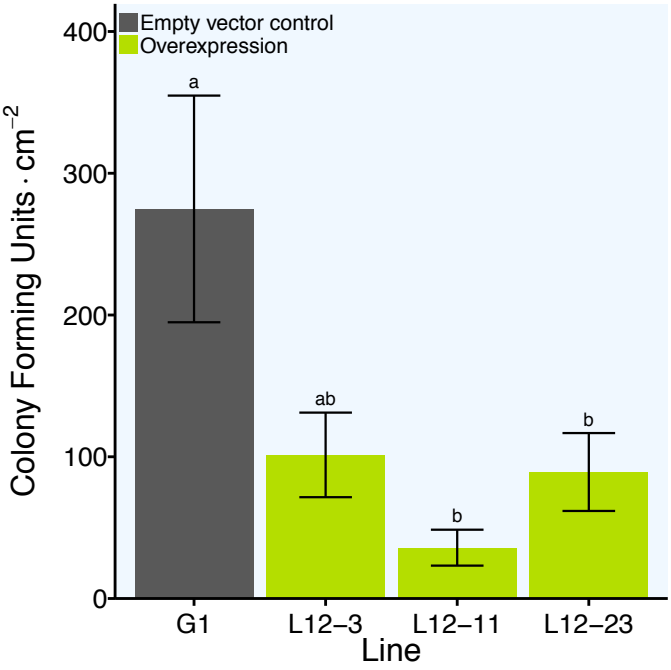

Figure 6: Colony forming units per leaf area of *VviERF6L1* overexpression vines. The average number of colony forming units per leaf surface area (cm^{-2}) from dilution 0 (1x extract) five days after *P. syringae* infection. The three overexpression lines (L12-3, L12-11, and L12-23) are indicated in green, and the G1 empty vector control line is indicated in grey. Mean ± SE; n = 11 rounds of three leaves per treatment per round (only *P. syringae* infected leaves shown). ANOVA Tukey's HSD ($p \leq 0.05$) letters.

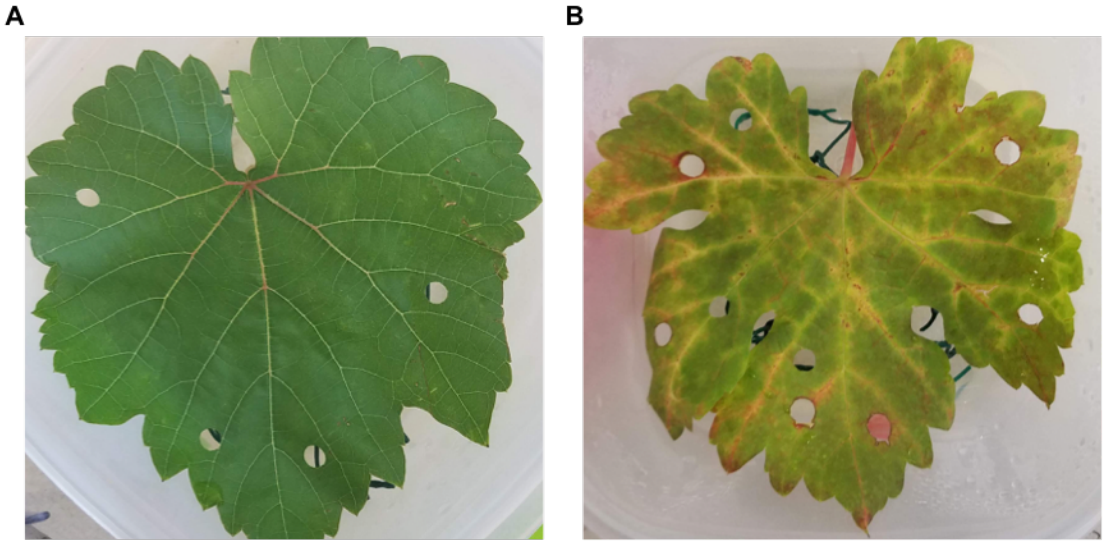

Figure 7: Control and virulent infected grapevine leaves. A) a 1-minute mock infected G1 leaf on day 5 prior to tissue extraction. **B)** a virulent *P. syringae* DC3000 1-minute infected CS leaf on day 5 post-tissue extraction.

CHAPTER 5:

A MULTI-LEVEL ANALYSIS OF ABSCISIC ACID METABOLISM REVEALS SPECIES-SPECIFIC RESPONSES TO WATER DEFICIT IN GRAPEVINE

This chapter is based on a manuscript that is prepared for submission to PLoS ONE.

Toups, H. S., Cochetel, N., Galdamez, K., Deluc, L., Cramer, G. R. A Multi-Level analysis of abscisic acid metabolism reveals species-specific responses to water deficit in grapevine. PLoS ONE, In Preparation, (2021).

5.0 Abstract

Abscisic acid is a phytohormone involved in water deficit response. NCED3 performs the rate-limiting step of abscisic acid biosynthesis and is a key contributor to plant water deficit responses. In this study, *NCED3* transcript accumulation and abscisic acid metabolism were further characterized as key water deficit responses in four *Vitis* species (*Vitis vinifera* (Cabernet Sauvignon), *Vitis champinii* (Ramsey), *Vitis riparia* (Riparia Gloire), and *Vitis vinifera* x *Vitis girdiana* (SC2)) in leaves and roots. The concentrations of abscisic acid and related derivative metabolites increased with water deficit and were dependent upon the grapevine species. RNA-Seq and RT-qPCR data were consistent with the changes in abscisic acid metabolite concentrations. Transcript abundances substantiate *NCED3* as a key gene in the water deficit response; however, NCED3 protein concentrations assayed in western blots were not affected. Major differences in abscisic acid metabolism at the gene, protein, and metabolite levels were detected between leaves and roots in these four species. *NCED3* transcript abundance and abscisic acid concentration in drought-tolerant Ramsey increased earlier and to a higher extent than the other species during long-term, moderate to severe water deficits but were not stimulated as much by short-term, rapid dehydration. In drought-sensitive Riparia, *NCED3* transcript abundance and abscisic acid metabolite concentrations increased to a lower extent than in Ramsey during moderate to severe water deficits. Overall, Grapevine species have distinct abscisic acid metabolism that depends highly on the severity and duration of stress and organ (leaves or roots). This study confirms that abscisic acid metabolism and *NCED3* are part of a core water deficit response in *Vitis* species. Relative quantities of transcripts, proteins, abscisic acid, and derivative metabolites were determined, but many aspects of abscisic acid metabolism and water

deficit responses warrant additional investigation. This study provides a better understanding of how *Vitis* is adapted to dry environments, which may be exploited for future breeding programs.

5.1 Introduction

Drought is a natural climatic event that occurs all across the world (Um et al., 2017) and may become more frequent and severe in the near future (Cabré and Nuñez, 2020; Dai, 2013; Monteverde and De Sales, 2020). For sessile crops, the consequences of severe water deficit (WD) can be devastating. Historically, droughts decreased global crop production by 10% (Lesk et al., 2016). To elicit drought tolerance, intricate and complex WD response signals throughout the plant involving multiple steps of regulation. For example, epigenetic modification and chromatin remodeling allow easier accessibility to dehydration responsive genes like *RESPONSIVE TO DESICCATION 29A* (*RD29A*) (Asensi-Fabado et al., 2017; Kim et al., 2008). Transcriptionally, genes may be transcribed (or not) (Cochetel et al., 2020), alternatively spliced (Chong et al., 2019), and present alternative untranslated region (UTR) isoforms (Lei et al., 2015; Srivastava et al., 2018) or polyadenylation (Chakrabarti et al., 2018). MicroRNAs like miR160 target growth-related auxin response factor transcripts like *ARF10* for degradation (Bouzroud et al., 2018; Pagliarani et al., 2017). siRNAs are another mechanism of regulation that contribute to WD response (Jung et al., 2016). Post-translational modifications can mark enzymes for degradation or activation (Ghimire et al., 2020; Guerra et al., 2015; Hashiguchi and Komatsu, 2016) like the

phosphorylation of SNRK2s, which are critical proteins in the abscisic acid (ABA) signaling pathway (Kobayashi et al., 2005). The numerous steps of regulation ultimately lead to the proteins and metabolites that result in the phenotype of the plant. Understanding WD response in plants continues to expand, but few studies investigate WD response at more than one level of regulation. This work provides a more comprehensive view of core ABA metabolism in response to WD by examining ABA-related transcripts, protein, and metabolites in four distinct *Vitis* species during three different WD experiments in leaves and roots.

ABA is a phytohormone associated with abiotic stress response including WD. ABA signaling is initiated when ABA is perceived by the PYRABACTIN RESISTANCE1/PYR1-LIKE/REGULATORY COMPONENTS OF ABA RECEPTORS (PYR/PYL/RCAR) receptors (Liu et al., 2007; Pandey et al., 2009; Park et al., 2009; Shen et al., 2006) that then interact with PP2Cs allowing the activation of SNRK2s (Mustilli et al., 2002; Nakashima et al., 2009). SNRK2s activate ABA-responsive transcription factors (TFs) including AREB/ABFs (Furihata et al., 2006; Kobayashi et al., 2005; Umezawa et al., 2013; Vlad et al., 2008; Wang et al., 2013; Yoshida et al., 2010) and ABIs (Finkelstein and Lynch, 2000; Finkelstein et al., 2005). Activated TFs bind to cis-acting elements in promoter regions of target genes (Guiltinan et al., 1990; Mundy et al., 1990). This core ABA signaling pathway initiates the transcription of numerous downstream targets including aquaporins (Parent et al., 2009; Wong et al., 2018; Zarrouk et al., 2016), suberin TFs (Cottle and Kolattukudy, 1982; Lippold et al., 2009), galactinol synthases (Li et al., 2020; Taji et al., 2002), and RDs (Abe et al., 2003; Tu et al., 2018) that ultimately result in physiological changes that better allow a plant to survive under adverse conditions.

ABA is synthesized from isoprenoid products of the methylerythritol phosphate (MEP) pathway in the plastid (Rodrı´guez-Concepción and Boronat, 2002). Through a series of desaturation (Bartley et al., 1999; Linden et al., 1994; Ruiz-Sola and Rodríguez-Concepción, 2012) and cyclization reactions (Zeng et al., 2015); ß-carotene is formed and hydroxylated (ß-CAROTENE HYDROXYLASE (BETA-OHASE 2)) into zeaxanthin (Du et al., 2010, 1999). Zeaxanthin is epoxidated (ZEAXANTHIN EPOXIDASE (ZEP/ABA DEFICIENT 1 (ABA1)) into violaxanthin through intermediary antheraxanthin (Eskling et al., 1997; Hieber et al., 2000; Niyogi, 1999). Neoxanthin, synthesized by NEOXANTHIN SYNTHASE (NXS/ABA4), and violaxanthin participate in the rate-limiting step of ABA biosynthesis performed by NINE-CIS-EPOXYCAROTENOID DIOXYGENASE (NCED) (Qin and Zeevaart, 1999; Schwartz, 1997; Tan et al., 1997). The resulting molecule, xanthoxin is transported out of the plastid into the cytoplasm where ABA biosynthesis is completed (Schwartz et al., 1997). XANTHOXIN DEHYDROGENASE (ABA DEFICIENT 2 (ABA2)) protonates the epoxy group of xanthoxin to form ABA aldehyde (González-Guzmán et al., 2002). Finally, ABA aldehyde is oxidized to active ABA by ABA ALDEHYDE OXIDASE (AAO) (Seo et al., 2000) with a molybdenum cofactor sulfurase (ABA DEFICIENT 3 (ABA3)).

ABA is conjugated with UDP-glucose (Xu et al., 2014) to generate an inactive storage form of ABA (Cutler and Krochko, 1999). ABA-GE is formed by the esterification of ABA with UDP-glucose by UDP-glucose glucosyltransferase (UGT) (Lim et al., 2005; Liu et al., 2015). Once conjugated, ABA-GE is stored in the vacuole (Bray and Zeevaart, 1985; Burla et al., 2013; Lehmann and Glund, 1986) and may be present in the endoplasmic

reticulum (Xu et al., 2012). ABA-GE is readily de-esterified to active ABA via ß-d-glucosidases (BG or BGLU) (Lee et al., 2006; Xu et al., 2012).

ABA catabolism is composed of three conduits through ABA hydroxylation to form 7', 8', or 9'-hydroxy ABA (Nambara and Marion-Poll, 2005). ABA hydroxylation is performed by ABA hydroxylases (CYTOCHROME P450 (CYP707A)) (Krochko et al., 1998). 7'-hydroxy ABA (7'OH ABA) is hydroxylated at the C-7' methyl group (Nambara and Marion-Poll, 2005). 8'-hydroxy ABA is isomerized into phaseic acid (PA) (Krochko et al., 1998) and further reduced to dihydrophaseic acid (DPA) (Gillard and Walton, 1976). Neophaseic acid (NeoPA) is formed from 9'-hydroxy ABA and is considered a minor catabolite (Nambara and Marion-Poll, 2005).

ABA is transported throughout the plant (Kuromori et al., 2018). The ABA transporter, ABCG25 (Kuromori et al., 2010), exports ABA from vascular tissue while ABCG40 (Kang et al., 2010) imports ABA into guard cells to elicit stomatal closure during abiotic stress. Other ABA transporters involved in seed/embryo development are ABCG22 (Merilo et al., 2015), ABCG30, and ABCG31 (Kang et al., 2015). More recently NPF4.5 (AIT2) and NPF4.6 (AIT1) (Léran et al., 2020) were also confirmed to transport ABA (Chen et al., 2020).

ABA appears to be a key regulator of physiological and transcriptional responses to water deficit (Cochetel et al., 2020; Ikegami et al., 2009; Ren et al., 2007). Previously, RNA-Sequencing analysis (RNA-Seq) was performed on four diverse *Vitis* species (*Vitis vinifera* cv. Cabernet Sauvignon clone-8 (CS), *Vitis champinii* cv. Ramsey (RA), *Vitis riparia* cv. Riparia Gloire (RI), and *Vitis vinifera* x *Vitis girdiana* hybrid SC2 (SC)) in response to one- and two-weeks of well-watered (Control) and a natural dry-down water

deficit (WD). The stem water potential of moderate WD-treated vines was ~ -0.5 and -0.8 MPa after one and two weeks of treatment, respectively. This experiment paired with an additional one-week severe WD experiment (stem water potential ~ -1.5 MPa), in which these four grapevines experienced stress more severe than the stress level achieved after two weeks of moderate WD.

These species differ in drought tolerance with RA appearing the most drought tolerant and RI the most susceptible (Cochetel et al., 2020). RA retained the highest stomatal conductance, photosynthesis, and stem water potential of the four species under both long-term WD treatments. RI was the first species to shut down photosynthesis and experience stress levels resulting in leaf loss or even vine death in response to moderate and severe long-term WD (Cochetel et al., 2020). Specific and shared transcriptomic responses between the four *Vitis* species were identified. The transcript abundance of many abscisic acid signaling genes like *DEHYDRIN 1* (*DHN1*) were strongly increased by WD with distinct differences between the species in both experiments. A weighted gene co-expression network analysis (WGCNA) identified a water-deficit core gene set with the ABA biosynthesis gene, *NCED3*, as a potential hub in all four species. RA emerged as the most physiologically active and transcriptionally responsive species following WD. **We hypothesized the different transcriptional and physiological responses among the species may have been reflective of differences in ABA metabolism.** However, ABA and ABA-derived metabolite quantification was not presented in the previous study.

To test this hypothesis, prior observations of these four grapevine species' responses to WD and ABA metabolism (Cochetel et al., 2020) were built upon with the addition of ABA and ABA-related metabolite quantification as well as additional WD

experiments. The term "ABA-related metabolites" refers to the group of compounds quantified in this study that are derived from ABA: ABA-GE, PA, DPA, NeoPA, and 7'OH ABA. Although there were numerous differences between the four species, the contrast of drought-tolerant Texan-native RA to susceptible riparian RI will be the focus of the results presented here.

It was expected that ABA and ABA-related metabolite quantification would mirror the transcript abundance of ABA metabolism genes in response to WD, which was found to be true in general. In this study, increased ABA metabolism was confirmed as a key response to WD through quantitative analysis of ABA, ABA-related metabolites (HPLC-MS/MS), ABA metabolism-related transcripts (RNA-Seq and RT-qPCR), and NCED3 protein (western blots) from three experiments in which the species were exposed to varying intensity and duration of WD.

5.2 Materials and Methods

Plant material and growth conditions

Vitis vinifera (L.) cv. Cabernet Sauvignon clone 8 (CS) obtained from Inland Desert Nursery (Benton City, Washington, USA), *Vitis champinii* (RA), *Vitis riparia* (RI), and a *Vitis vinifera* x *girdiana* hybrid (SC2) obtained from the Plant Foundation Services at UC Davis (Davis, CA USA) were grown in a greenhouse. Greenhouse conditions ranged from 21-26 °C, 20-50% relative humidity, and had average mid-day light intensities of 1200 μmoles m^{-2} s^{-1}. Supplemental light was applied using 1000 W high-pressure sodium lamps

to maintain a 16 h light and 8 h dark cycle. Cuttings from mother plants were hydroponically propagated in aerated pH 5.5 water trays. When roots were established, cuttings were transferred to Stuewe and Son's Anderson AB39 pots (0.96 L) consisting of ~1.0 kg Quikrete medium grain sand and 80 g of fritted clay for plants used for RNA-Seq and small pot experiments. Propagates were allowed to acclimate to potting conditions for one month before beginning experiments. Plants were irrigated with Cramer's complete nutrient solution (1.5 mM $Ca(NO_3)_2$, 2 mM KNO_3, 0.6 mM $MgSO_4$, 1 mM KH_2PO_4, 1.5 mM $CaCl_2$, 36 μM Fe^{2+} Sprint 330, 1 μM $MnSO_4$, 0.5 μM $CuSO_4$, 20 μM $ZnSO_4$, 20 μM H_3BO_3, and 0.01 μM $(NH_4)_6Mo_7O_{24}$). Pots were elevated 7.5 cm off the floor on perforated black plastic flats in a random design for species, treatment, and harvest date.

Small pot experiments

After pots were prepared, 100% relative soil water content (RSWC) was measured as the weight of the individual pot two hours after irrigation to the point of saturation (water flowing from the bottom of the pot). Each pot was covered with aluminum foil to minimize evaporation. Experiments performed in the small pots included 1) WD and Control treatments for one- and two-week moderate WD used for RNA-Seq, ABA, and ABA-related metabolite quantification, and physiological measurements 2) one week severe WD and Control treatments to support the original RNA-Seq experiment and quantify *NCED3* transcripts and NCED3 protein as well as ABA (in addition to original measurements reported elsewhere (Cochetel et al., 2020)).

For the original moderate WD RNA-Seq experiment previously described (Cochetel et al., 2020), 3-5 individual CS, RA, RI, and SC vines were subjected to one or

two weeks of moderate water deficit, or well-watered daily complete nutrient solution. The moderate WD was defined by stem water potentials of -0.26 ± 0.02 to -0.32 MPa ± 0.02 after one and two weeks of Control treatment and -0.49 ± 0.04 MPa to -0.82 ± 0.06 MPa after one and two weeks of WD, respectively. At one and two weeks of treatment various measurements were taken (Cochetel et al., 2020). Total plant leaves (excluding petiole) and roots were harvested after one and two weeks of treatment. The sand was removed from root samples by briefly washing in room temperature tap water for 10 seconds and patting dry on paper towels for an additional 10 seconds. Samples were immediately frozen in liquid nitrogen and stored at -80°C. Sand removal from roots was essential for accurate ABA quantification (normalization based on ground dry weight used for extraction).

For the one-week severe WD experiment, 3-5 individual CS, RA, RI, and SC vines were subjected to one week of severe water deficit or watered daily to saturation with a complete nutrient solution. The severe WD was defined by stem water potentials of ~ -1.5 MPa, and stem water potential for Control treated vines similar to that of the moderate WD Controls (~ -0.2 to -0.3 MPa). At one week of treatment, various measurements were taken (Cochetel et al., 2020), and total plant leaves (excluding petiole) and roots were harvested. Sand was removed from roots as in the moderate WD experiment. Samples were immediately frozen in liquid nitrogen and stored at -80°C.

Rapid dehydration experiments

The day before the experiment, the first mature leaf (5-6th node from the apical meristem) of CS, RA, and RI vines were measured from petiole attachment point to the tip of the leaf down the midvein and marked with a tag to ensure leaves of similar developmental stage

and leaf area were used for this experiment. Also, on the day before the experiment, dehydration chambers were prepared. Airtight dehydration chambers (1.2 L Rubbermaid Takealong © container, Newell Rubbermaid, Atlanta, GA, USA) were prepared as before (Hopper et al., 2014), containing 50 mL 333 mM NaCl or DI water (for rapid dehydration and Control treatment, respectively) and a wire support grid. Dehydration chambers were placed in a 27 ˚C growth chamber (~200 μmol $m^{-2}s^{-1}$) to equilibrate overnight. The following day, two hours before solar noon, the marked leaves were cut underwater, weighed, and quickly placed in a dehydration chamber (~30 secs). WD leaves were placed abaxial side up having no contact with the salt solution. Control leaves were placed adaxial side up with petioles dipping into the water to prevent dehydration and provide petiole water-feeding. Five leaves were prepared per species per treatment per round. Leaves were collected after 2, 4, 8, and 24 hours of treatment. At these times three leaves were combined and immediately frozen in liquid nitrogen. These leaves were later used for *NCED3* transcript, NCED3 protein, and ABA quantification. Photosynthesis and stomatal conductance were measured on a fourth leaf using a portable photosynthesis system (LICOR model 6400XT, Lincoln, NE, USA) set at 400 μmol s^{-1} flow rate, 400 μmol mol^{-1} reference CO_2, with a leaf temperature at 27 °C and PAR 1000 μmol m^{-2} s^{-1}. After LICOR measurements, leaf water potential was measured with a Plant Water Status Console (Soilmoisture Equipment Corp., CA, USA) on the same fourth leaf. Water potential measurements were performed by placing the excised leaves in the pressure chamber and slowly increasing the pressure till liquid began to flow from the petiole. The pressure reading of the instant the liquid appeared was recorded. The fourth leaf was placed in a syringe and frozen in liquid nitrogen. Later, the syringe was thawed and 10 μL of leaf liquid was extracted to measure osmotic

potential in triplicate. The osmotic potential was measured with a vapor pressure osmometer (VaPro 5600 EliTechGroup). Turgor was calculated as the difference between leaf water potential and osmotic pressure (Tyree and Hammel, 1972). A fifth leaf was used to measure leaf water content. Water content was calculated as the difference between the leaf fresh weight at harvest and the leaf dry weight divided by the difference between turgid leaf weight and the leaf dry weight (Barrs and Weatherley, 1962). Turgid leaf weight was obtained by submerging a leaf underwater for 24 hours (leaf weight was constant), patting the leaf dry, and weighing the turgid leaf. Leaves were then dried in an oven at 60 ˚C for 48 hours and weighed to determine dry weight. All leaves were weighed before final measurements were performed to determine water loss. This experiment was performed five times with each leaf coming from an individual vine. Three leaves were combined for *NCED3* transcript, NCED3 protein, and ABA quantification per round to have enough material for all measurements.

CS ABA metabolism-related gene identification

ABA metabolism genes were identified with protein basic local alignment search tool (BLASTP) using known ABA metabolism PN40024 protein sequences as a query. Orthologs were confirmed based on the highest total score, E-value, and length. When two BLAST hits were highly similar for the same query, the hits were identified as alleles of the same gene. In total, 46 ABA metabolism genes were identified from the primary (alternative (alt)1) and/or secondary (alt2) CS haplotig sequences. Alleles are referred to as alternatives without a designated haplotype because the phased chromosome-scale assembly was not complete for the CS clone 8 v1.0 genome. Alternative names were

assigned as "alt1" if only 1 paralog was identified based on V3 annotation. Alternatives were assigned as "alt1" and "alt2" when two paralogs were identified with "alt1" corresponding to the primary contig and "alt2" correspond to the haplotig denoted as "P" and "H" respectively in CS gene names. When multiple paralogs were identified corresponding to multiple V3 genes with the same annotation symbol, "alt1_1" and "alt2_1" were named to correspond to CS alleles with the same V3 gene name. Paralogs with only one allele with the same annotation symbol as other V3 genes are indicated as "alt1_2" and "alt1_3".

RNA-Seq Re-analysis

Reads were trimmed as previously described using trimmomatic v0.36 (Bolger et al., 2014) and sample quality was confirmed with FastQC v0.11.5 (Babraham Bioinformatics, 2010). To improve the original analysis, PRJNA516950 was re-analyzed with the CS clone 8 v1.0 genome due to the quality, accessibility, and overlap with the experimental design. After filtering, reads were aligned against the CS genome (Chin et al., 2016) with HISAT2 v2.0.5 (Kim et al., 2015). Counts were obtained with featureCounts v1.5.1 (Liao et al., 2014). Differentially expressed genes with an adjusted p-value ≤ 0.05 were identified with DESeq2 v1.26.0 (Love et al., 2014). Contrasts of interest included comparing each species x week x organ Control and WD as well as comparing WD RA x organ x week to those of CS, RI, and SC. All heatmaps were drawn with ComplexHeatmap v2.2.0 (Gu et al., 2016), dendextend v1.13.4 (Galili, 2015), and circlize v0.4.8 (Gu et al., 2014) to extract contrasts of interest in RStudio.

WGCNA is a correlation network methodology used to 1) identify clusters (modules) of interconnected nodes 2) summarize node profiles of a module using a highly connected hub node (Eigengene) 3) identify significant modules and annotate the network nodes (Langfelder and Horvath, 2008). In this case, the WGCNA was performed to identify genes most connected to Eigengenes that were most associated with WD, [ABA], and [ABA-related metabolites]. ABA metabolism-related genes were the focus of this analysis. WGCNA version 1.41 (Langfelder and Horvath, 2008) was performed per organ as previously described (Cochetel et al., 2020). Topological Overlap Matrix (TOM) was used to detect modules using the DynamicTreecut algorithm with a minimum module size of 30 and a branch merge cut height of 0.25. The module eigengenes were used to evaluate the association among the modules for species, treatments, weeks, and various metabolites with a focus on ABA metabolism-related genes. GO enrichment analysis was performed with TopGO v2.38.1 (Alexa et al., 2006) using biological process terms corresponding to the CS clone 8 v1.0 genome.

ABA quantification

ABA and ABA-related metabolites were quantified with HPLC-MS/MS using a methanol-based extraction as previously described (Gouthu et al., 2013). Briefly, ABA derivative quantification from the one and two weeks of moderate WD, one week of severe WD, and rapid dehydration experiment samples (Control and WD treated) was performed with methanol, formic acid, water (15:1:4) extraction, and deuterated standards. Samples were purified with Oasis® HLB 3.5ml columns (Waters®) and eluted with methanol. Samples

were reconstituted in acetonitrile, water, and formic acid (15:85:0.1) and separated with an Aligent™ Zorbax® Extend C_{18} column (201 x 150 mm; 5 μm) with Opti-Solve® 2-micron guard column (Optimize Technologies™, USA). A binary gradient of LC-MS grade acetonitrile (Thermofisher Scientific) acidified with 0.1% formic acid and HPLC grade water (Thermofisher Scientific) also acidified with 0.1% formic acid were used to resolve ABA derivatives. Mass spectrometry was carried out using multiple reaction monitoring (MRM) using a hybrid triple quadrupole/linear ion trap 4000 QTRAP LC-MS/MS instrument equipped with a Turbo V source (Applied Biosystems™, USA) with a 0.2 mL/min flow rate under the conditions previously described. D6 deuterated ABA (Toronto Research Chemicals) was used as an internal standard for all samples and D4 deuterated ABA (OlChemIm) was used as an extraction efficiency standard for one and two-week moderate and one-week severe WD experiment samples only.

RT-qPCR

RT-qPCR was performed as previously described (Cochetel et al., 2020). Briefly, all samples were ground with a mortar and pestle under liquid nitrogen. RNA extraction was performed with a previously described CTAB based extraction and LiCl precipitation following cleanup with the Spectrum™ Plant Total RNA kit (Sigma-Aldrich). All RNA extractions were treated with RNAse-free DNase I (Qiagen) to remove genomic DNA contamination. Samples were quantified on a nanodrop, and RNA quality was confirmed with gel electrophoresis by loading 250ng RNA on a 1.2% gel as well as checked for the presence of gDNA with a GoTaq Green-LAR based PCR analyzed with electrophoresis on a 2% gel employing 400ng of RNA. Primers were designed using NCBI Primer-BLAST.

Primer sequences were previously described (Cochetel et al., 2020). Reference genes (*ACT7* and *GAPDH*) were chosen for consistent band intensity under the various experimental conditions determined with Go-Taq Green-based PCR reaction. The PCR reaction included 95 °C for 2 min, 35 cycles of 95 °C for 30 s, 62 °C for 25 s, and 72 °C for 25 s. Primer efficiencies were verified on purified PCR products (Machery-Nagel NucleoSpin® Gel and PCR Clean-up kit) and were considered at 100% for the gene expression calculations. All reactions were performed on a Bio-Rad Real-Time thermal cycler CFX96 with the following protocol: 95 °C for 3 mins; 40 cycles of 95 °C for 10 s, 60 °C for 15 s. Fluorescence was recorded after each cycle and melting curve analysis was performed from 65 °C to 95 °C. Reference genes were selected based on a low coefficient of variation of expression reported in literature and uniform expression for all cDNA samples for each of the above-described experiments. *NCED3* transcript abundance for the one week severe WD experiment was previously reported (Cochetel et al., 2020).

Western Blots

Proteins were extracted as previously described with chloroform/methanol (Wessel and Flügge, 1984) for one week severe WD samples and in 2x laemmli buffer for rapid dehydration samples. Total protein extracts were quantified with the Pierce BCA Protein Assay Kit (Thermo Scientific) according to the manufacturer's instructions. Total protein extract (35 μg) was loaded on 12.5% TGX stain-free polyacrylamide gels (BioRad) with 5 μL of precision plus all blue standard ladder (BioRad) and a CS Control IRC (35 μg) spiked with 15.75 ng of NCED3 peptide standard (Pacific Immunology) that acted as a positive control. The inter-run caliber (IRC) (a CS Control leaf sample loaded on every gel for the

severe one-week WD samples and a CS Control two-hour sample for the rapid dehydration samples) had 2 kDa positive control peptides (peptides the antibodies were designed against) added to confirm antibody specificity and activity for each western blot. The addition of the peptides did not interfere with the detection nor quantification of the 67 kDa NCED3 band in the IRC or other samples. Proteins were transferred onto a PVDF membrane (BioRad) using a Trans-Blot Turbo (BioRad) and imaged with a Chemidoc (BioRad) for total protein (Taylor and Posch, 2014). Membranes were blocked and probed with NCED3 (rabbit) primary antibodies (each 1:1000) (a 1:1 mix of antiNCED3.1 and 3.2 (Pacific Immunology)) followed by goat anti-rabbit-HRP (BioRad) secondary antibody (1:1000). Antibody (antiNCED3.1, antiNCED3.2, and antiNCED3.3) target sequences were determined to be NCED3 specific relative to the other CS NCEDs via BLAST, unique from each other, and present in available *Vitis* genomes (PN40024 (Canaguier et al., 2017), CS (Minio et al., 2018), and RI (Girollet et al., 2019)). Antibody detection was linearly related to the amount of protein loaded and deemed to be sufficient for relative quantification of protein amount. ECL-Spray (Advansta) was applied uniformly to the membrane, and the membranes were imaged with a Chemidoc (BioRad) for 12 secs. NCED3 protein in samples was quantified in ImageLab (BioRad) relative to the IRC ran on each gel and normalized to a fragment of total protein free of transfer artifacts from a StainFree membrane image (Taylor and Posch, 2014). Several postulated NCED3 degradation/cleavage products or subunits were also detected as previously (Endo et al., 2008; Kalladan et al., 2019; Tan et al., 2001), but only the 67 kDa band was used for relative quantification. To summarize, relative NCED3 protein abundance was quantified

using western blots with internal NCED3 peptide standards and StainFree membrane normalization using an IRC loaded on each gel (Taylor and Posch, 2014).

Statistical analysis

Statistical analysis was performed comparing multiple means including one-, two-, three-, and four-way ANOVAs after assumptions were met. Non-normal data were box-cox transformed to meet normality and homoscedastic assumptions (Fox, 2020). Post Hoc tests were performed with Tukey's Test HSD for comparisons between species, treatments, and time points after assumptions were met. Asterisks indicate statistical significance from ANOVA (* = $p \leq 0.05$, ** = $p \leq 0.01$, *** = $p \leq 0.001$). Letters indicate statistical significance between the multiple comparisons. The error rate $\alpha = 0.05$ was used in all comparisons. Statistical analyses and all other R-based analyses were performed using R version 3.6.3 in RStudio version 1.2.13335 (R Core Team, 2018).

5.3 Results

Grapevine organs and species differ in ABA and related metabolite concentrations during one and two weeks of moderate WD

ABA and ABA-related metabolites (ABA-GE, PA, DPA, NeoPA, and 7'OH ABA) were quantified (Gouthu et al., 2013) from leaf and root samples (Figs. 1 and 2) collected from a previous experiment (Cochetel et al., 2020). Briefly, CS, RA, RI, and SC were subjected to one- or two weeks of well-watered Control or a natural dry down moderate-water deficit.

The moderate WD was defined by stem water potentials of -0.26 ± 0.02 to -0.32 MPa ± 0.02 after one and two weeks of Control treatment and -0.49 ± 0.04 MPa to -0.82 ± 0.06 MPa after one and two weeks of WD, respectively (Cochetel et al., 2020).

After two weeks of WD, ABA and its related metabolites were significantly more abundant in the leaves and roots of the four species relative to the average control (Figs. 1and 2). The term "significant" will be used in this work to mean statistically significant at a p-value of 0.05 or less. Strikingly, only RA showed an early significant ABA accumulation in response to WD in the leaves after just one week of treatment (Fig. 1 top left panel). RA leaves and roots had 3-fold and 6-fold higher respective average [ABA] than those of the drought-sensitive RI (Fig. 1). After two weeks of treatment, RA retained higher [ABA] compared to RI (and SC), while CS had more variable and intermediate [ABA] (Fig. 1). Unlike in the leaves, the significant accumulation of ABA in the roots at two weeks of WD was not different among the different species. On average for all species, the ABA accumulation at two weeks of WD resulted in 3-fold more ABA in the leaves than roots. As a general rule, [ABA] can be ranked by species during moderate WD as RA > CS > RI > SC in both leaves and roots.

Consistent with [ABA], [ABA-GE] followed similar accumulation patterns as ABA in response to two weeks of WD with RA having higher concentrations in the roots and leaves (Fig. 1). RA was the only species to have significantly higher [ABA-GE] in response to two weeks of WD in the roots (Fig. 1). [ABA-GE] was significantly higher than [ABA] in leaves and lower than [ABA] in the roots (Fig. 1) for all species per treatment per week.

ABA catabolites (7'OH-ABA, NeoPA, PA, and DPA) also demonstrated distinct high accumulations in RA at one week of WD in the roots and both organs after two weeks

of treatment (Fig. 2). The other species had intermediate or lower [ABA catabolites] (Fig. 2). [ABA catabolites] were comparable between the organs at one week of WD, but [ABA catabolites] were generally higher in leaves than roots at two weeks of treatment (Fig. 2). For example, RA had > 10-fold increase in [PA] in leaves relative to roots at two weeks of WD. RA was the only species that had significantly increased concentrations of all four ABA catabolites in both organs in response to WD (Fig. 2).

Like [ABA] and [ABA-GE], all [ABA catabolites] increased in response to the moderate WD with RA > CS > RI ≥ SC (Fig. 2), but there were clear differences in the use of the catabolite pathways in grapevines. As expected, the products of the main ABA catabolic pathway, [DPA] and [PA] (Nambara and Marion-Poll, 2005), were much higher than [7'OH ABA] and [NeoPA] (Fig. 2). Interestingly, [PA] was higher than [DPA] in WD leaves. However, the reverse was true in WD roots, where [DPA] was equivalent to or higher than [PA]. The minor catabolite, NeoPA, had very low concentrations relative to the other catabolites (Fig. 2).

To further understand ABA metabolism in the plant as a whole, the distribution of ABA and ABA-related metabolites was examined for the whole plant. "Total ABA Metabolites" will be defined as the sum of the leaf and root total [ABA] and [ABA-related metabolites] (Supplemental File 1A for whole plant or Supplemental File 1B for individual organ). [ABA] and each [ABA-related metabolite] per organ was also divided by the summed [Total ABA Metabolites] per whole plant to estimate the percentage that each metabolite represented in the whole metabolic pathway (Supplemental File 2).

This approach revealed the same patterns as looking at the [metabolites] individually: RA had an earlier accumulation of [Total ABA Metabolites] at one week of

WD and retained higher [Total ABA Metabolites] than the other species at two weeks of treatment. On a whole plant basis, there were significant increases in [Total ABA Metabolite] by two weeks of treatment (Supplemental File 1A) providing evidence for an increase in ABA biosynthesis along with other metabolism pathways. Total ABA Metabolite distribution at week one of WD was less clear and may indicate that changes in ABA metabolite concentrations were the result of redistribution of ABA (e.g. conjugation, catabolism, and/or transport). Generally, leaves and roots had comparable [Total ABA Metabolites] at one week of treatment, but leaves had 2 to > 10-fold higher [Total ABA Metabolites] than roots at two-weeks of WD. Altogether, ABA metabolism in RA appears to respond earlier and more significantly than in the other species.

ABA-GE represented the major portion of the leaf ABA metabolites in Controls in the first week (Supplemental File 2). However, after one week of WD, RA leaves uniquely had a significant decrease in the proportion of ABA-GE, indicating ABA metabolism was shifted from ABA-GE to other ABA metabolites such as ABA and DPA. The proportion of ABA-GE in WD roots at week two decreased relative to Control in all of the species except for CS, which was proportionately low relative to the other three species (Supplemental File 2). ABA and ABA-GE in the roots, in general, were a much smaller proportion of Total ABA Metabolites than DPA. These changes indicate that ABA metabolism was dependent upon the species, the organ, and the duration of the water deficit.

To further evaluate the range of [ABA] and [ABA metabolites] between the species, the WD:C ratios of [ABA] and [ABA metabolites] were investigated (Fig. 3). ABA and 7'OH ABA had the highest z-scores of all the metabolites quantified (Fig. 3). RI leaves at one week of treatment had the highest score for WD:C ABA-GE (Fig. 3), indicating ABA-

GE may have been accumulating in RI WD leaves at this time. The WD:C ABA-GE score for RA leaves at week one was about two STD lower than the average WD:C ABA metabolite average (Fig. 3), indicating ABA-GE may be deconjugated into active ABA and/or downstream catabolites, supporting similar observations from Supplemental File 2. ABA-GE also had a negative score for the roots of all species in weeks one and two (Fig. 3), possibly reflecting ABA activation through this pathway. 7'OH ABA had the highest scores for RA roots and leaves at week one and RA and CS roots and leaves at week two (Fig. 3) despite 7'OH ABA having lower concentrations than metabolites representing catabolism through 8'OH ABA (PA and DPA). The high z-scores for 7'OH ABA in these select species and organs may indicate these species redistribute a higher portion of ABA catabolism through the 7'OH ABA pathway than the other species in response to WD, but this pathway either catabolizes lower [ABA] than that through 8'OH ABA, PA, and DPA (Fig. 2) or catabolites are further degraded into compounds not quantified here. Alternatively, the high z-scores for 7'OH ABA may be attributed to the large difference between root Control and WD [7'OH ABA] averages at week two in RA and CS that result in a greater fold difference (38-fold difference) than those of [PA] (6-fold difference) and [DPA] (3-fold difference). The differences between the catabolites indicate ABA may be preferentially deactivated by different mechanisms in each species in each organ and with increasing WD stress. For example, at week two, RA was the only species to have positive scores in leaves and roots for PA. Combined with the positive scores for RA leaves and roots 7'OH ABA and RA leaves NeoPA scores at week two of treatment, RA appears to be catabolizing ABA relative to the other species.

One and two weeks of moderate WD significantly increases *NCED3* transcript abundance

To investigate ABA metabolism regulation of the four *Vitis* species in response to WD, a targeted re-analysis of a large RNA-Seq dataset was performed using the annotation of the most recent diploid grapevine genome, CS clone-8 v1.0 (Chin et al., 2016). The original analysis of this dataset was performed with the V2 assembly V2 annotation of the PN40024 reference genome (Cochetel et al., 2020), but re-analysis was warranted with the release of the CS genome that overlapped with the experimental design. CS genes related to ABA metabolism (referred to here as "ABA metabolism-related genes") were identified with the protein basic local alignment search tool (BLASTP) using known ABA metabolism PN40024 protein sequences as a query. In total, 46 ABA metabolism-related genes were identified (Appendix 1). The alleles were classified as alt1 and/or alt2 based on the contig origin of this heterozygous genome (primary or haplotig); no haplotype was attributed because the phased chromosome-scale assembly for this genome was not available at the time (Materials and Methods).

NCED3 (Fig. 4) was the only significantly increased differentially expressed gene (DEG) specifically linked to ABA metabolism in leaves and roots of all four species in response to two weeks WD (Appendix 2). *NCED3* was also the ABA metabolism-related DEG that had the highest average TPM for all WD species' leaves. *NCED3* had the highest expression level of the five annotated *NCEDs* in both leaves and roots at one and two weeks of WD in all species with the highest level of expression in RA (Fig. 4). The other *NCEDs* were lowly expressed (Fig. 4), but *NCED5* and *NCED6* alternatives also had higher expression levels in RA for various organ x time point combinations compared to the other

species (Fig. 4). Overall, *NCED3* appears to be the major ABA metabolism-related gene contributing transcripts to downstream ABA biosynthesis during WD.

RA had ABA metabolism-related DEGs in response to one and two weeks of moderate WD

No ABA metabolism DEG stood out as much as *NCED3* in the WD response, but many other ABA metabolism DEGs were identified (Appendices 3-4) including genes involved in ABA biosynthesis (Appendix 1), deconjugation (Supplemental File 4), and catabolism (Supplemental File 3). RA leaves and roots had the most ABA metabolism DEGs in response to two weeks of WD compared to the other species. For example, in addition to *NCED3*, *NCED5* alt2 had significantly higher transcript abundance in RA WD roots at one week of treatment than those of the other species (Fig. 4 and Appendix 3) while *NPQ1* alt1, *ABA1* alt1, and *AAO3* alt1 were all significantly lower in RA WD leaves at two weeks of WD than those of the other species (Supplemental File 3 and Appendix 3). *BG1* alt1 and alt2 were DEGs in RA WD leaves and roots relative to respective Controls, but neither *BG1* allele was a DEG in the organs of any other species (Appendix 2). Interestingly, *BG1* alt1 transcript abundance was significantly lower in RA leaves and roots at two weeks of WD than those of the other species. At week two, RA WD also had the lowest *BG3* alt1 and BG3 alt 2 transcript abundances in leaves and roots. Finally, *CYP707A1* alt1 had significantly higher transcript abundance in RA WD leaves at two weeks of treatment than those of the other three species (Supplemental File 3 and Appendix 3).

Organs also showed significant differences in specific ABA metabolism DEGs. For example, average *ABA1* alt1 transcript abundance over all treatments, times, and species

was significantly higher in the leaves than the roots. Contrasting to *ABA1* alt1, average *AAO3* alt1 transcript abundance was significantly higher in roots than that in leaves across all species, times, and treatments although lowly expressed. *BG1* alt1, *BG1* alt2, and *CYP707A1* alt1 also had higher average transcript abundance in roots than in leaves across all species, treatments, and times.

One and two weeks of moderate WD significantly increases ABA transport gene transcript abundance

RA had significantly increased *ABCG25* and *ABCG40* transcript abundance relative to other species after two weeks of WD in leaves and roots (Supplemental File 5). *ABCG25* alt1 was about ~4-fold change higher in RA roots than those of the other three species at both time points and significantly higher in RA than CS WD leaves at two weeks of treatment. *ABCG25* alt2 transcript abundance was also significantly higher in RA WD leaves than those of RI and SC at week two (Appendix 3). After one week of WD, RA roots had ~8-fold change increase in *ABCG40* transcripts relative to those of CS, but *ABCG40* was not significantly different in Control vs. WD contrasts for either RA or CS at week one (Appendix 2). ABA transporter genes *ABCG25* alt1 and alt2 and *ABCG40* had significantly higher average transcript abundance in roots than leaves in all species, weeks, and treatments.

ABA metabolite gene transcript abundance may partially explain ABA metabolite concentrations

Multiple ABA metabolism genes had significantly increased transcript abundance similar to the increases observed in ABA metabolites. To more easily compare species response to WD and link [ABA metabolites] to upstream transcripts, the average ratio of WD:C transformed TPM were expressed as a z-score per ABA metabolism gene group (e.g. *NCED3*, *NCED5* alt1 and 2, and *NCED6* alt1 and 2 are all represented in the *NCED* gene group) with darker colors indicating a greater difference from the mean ratio of the ABA metabolism genes (Fig. 5). RA stands out in this comparison, having the highest score for *ß-carotene hydroxylases* (roots weeks one and two), *zeaxanthin epoxidases* (roots weeks one and two), *NCEDs* (leaves and roots weeks one and two), *AAO3s* (leaves week one), *UDP-glucose glucosyltransferases* (leaves and roots week two), *ß-d-glucosidases* (roots week one), and various potential *ABA hydroxylases* (leaves week one and roots weeks one and two) (Fig. 5) that may partially explain the high [ABA] and [ABA-related metabolites] observed in RA. RA also had the lowest scores for *violaxanthin de-epoxidases* (leaves week one), *xanthoxin dehydrogenases* (roots week two), *ß-d-glucosidases* (leaves week two), and *ABA aldehyde oxidases* (leaves and roots week 2) (Fig. 5). The low score and low expression (Fig. 5) of *ß-d-glucosidases,* as well as the high z-score for *UDP-glucose glucosyltransferases* in RA leaves at week two, may explain the high [ABA-GE] observed in RA WD leaves at this time; ABA may be conjugated into ABA-GE but not deconjugated allowing [ABA-GE] to increase. The higher [ABA-GE] in RI WD leaves at week one of treatment relative to the other species (Fig. 5) and the higher score for *ß-d-glucosidase* may indicate ABA-GE is an important source of ABA for RI in earlier WD response. RI and SC had the lowest [catabolites] in the leaves, which is paralleled in the score of the *ABA hydroxylases*.

ABA metabolism genes were correlated with multiple WGCNA modules

WGCNA was performed to identify clusters of genes (modules) associated with the different experimental conditions (organ, time, [ABA] and [ABA-related metabolites]) (Figs. 6 and 7 and Appendix 4, see Materials and Methods). ABA metabolism-related genes were spread across multiple gene modules. In the leaves, 30 WGCNA modules were identified (Fig. 6). WD was positively correlated with five modules; lightyellow, darkgreen, brown, saddlebrown, and green (Fig. 6). Positive correlations were defined by p-value ≤ 0.05 and Pearson's correlation coefficient ≥ 0.25. Generally, the metabolites were positively correlated with the same five modules as WD (Fig. 6). The 46 ABA metabolism genes were spread across 20 different modules in leaves. However, within these modules only lightyellow overlapped with WD, ABA, and the ABA-related metabolites. The lightyellow module contained the greatest number of ABA metabolism genes (seven) including *NCED3* (Eigengene-based connectivity of 0.91), *NCED6* alt1 (0.77), and *NCED6* alt2 (0.70) (Appendix 1). Eigengene-based connectivity (module membership) values are between -1 to 1 and measure the correlation of a gene to the eigengene of a module; the farther the module membership value is from 0, the more connected or hub-like the gene is in the module (Langfelder and Horvath, 2008).

NCED3 was a hub gene in the lightyellow module, being the 15th most correlated gene to the eigengene representing this module (referred to as "rank 15"). Hub genes are highly connected to all other genes in the module. Disruption of hub genes disturbs the gene expression of numerous other genes in a module. *NCED3* was closely connected to ABA signaling genes in this module including the top 1 gene, *HIGHLY ABA INDUCED 1*

(*HAI1*) (VvCabSauv08_P0061F.ver1.0.g440640). Other top genes in the lightyellow module included *RAS-RELATED PROTEIN 18* (*RAB18*) (VvCabSauv08_H0004F_076.ver1.0.g050030; rank 9) (Lång and Palva, 1992), *HOMEOBOX-7* (*HB-7* (VvCabSauv08_P0060F.ver1.0.g439740; rank 12), and *PP2C-8* (VvCabSauv08_P0452F.ver1.0.g610510; rank 14) (Appendix 4). The rank of *NCED3* in the lightyellow module far exceeded that of any other ABA metabolism gene in any module; the second highest ranking gene was *UGT71C4* alt2 (rank 90) in the red module (Appendix 4). In the lightyellow module, *NCED6* alt1 was the second highest ranking ABA metabolism gene (rank 259) (Appendix 4).

In the roots, 34 WGCNA modules were identified (Fig. 7). In total, ten modules were positively correlated (p-value ≤ 0.05 and Pearson's correlation coefficient ≥ 0.25) with WD (Fig. 7). Among the modules positively correlated to WD, four were also positively correlated with 7'OH ABA, ABA, ABA-GE DPA, NeoPA, and PA (Fig. 7 and Appendix 4); royalblue, lightgreen, midnightblue, and pink. The ABA metabolism genes were spread across 20 modules in the roots. The midnightblue module contained the greatest number of ABA metabolism genes (ten) including *NCED3* (0.95), *NCED5* alt2 (0.80), *NCED5* alt1 (0.75), and *NCED6* alt1 (0.65) (Appendix 1). Of all ABA metabolism genes and all root modules, *NCED3* was the only hub gene corresponding to the midnightblue module (rank 19) (Appendix 4). Like in the leaves, *NCED3* was closely connected to ABA signaling genes in the midnightblue module in the roots; these genes included: *RD26* (VvCabSauv08_H0024F_036.ver1.0.g115900; rank 1), *SEVEN IN ABSENTIA OF ARABIDOPSIS 2* (*SINAT2*) (VvCabSauv08_P0027F.ver1.0.g381860; rank 6), *NAC DOMAIN CONTAINING PROTEIN 47* (*NAC047*)

(VvCabSauv08_P0024F.ver1.0.g368680; rank 7), *GALACTINOL SYNTHASE 1* (*GolS1*) (VvCabSauv08_P0018F.ver1.0.g349170 and VvCabSauv08_P0018F.ver1.0.g349150; rank 9 and 10, respectively), and *Hordeum vulgare L. 22 (HVA22E)* (VvCabSauv08_P0095F.ver1.0.g483690, rank 16) (Appendix 4).

To better understand the roles of these genes in the modules, gene ontology enrichment was performed using biological process terms for the brown, green, and lightyellow modules in the leaves and the midnightblue and pink modules in the roots (Appendix 5). These modules were selected for high correlation to WD and the metabolites as well as for the number of ABA metabolism genes contained in each module. The gene ontology (GO) term "response to endogenous stimulus" was enriched in these modules (Appendix 5). All of these modules were enriched for "response to stress" and "response to stimulus" GO terms (Appendix 5). All modules except the green module in the leaf included the "response to abiotic stimuli" GO term (Appendix 5). The lightyellow module in the leaf was enriched for the "biosynthetic process" GO term (Appendix 5), and lightyellow had the highest correlation with *NCED3* and *NCED6* in the leaves (Appendix 4), supporting this grouping. The ABA metabolism gene functions were enriched with GO terms assigned to the modules most correlated with WD and the [metabolites] supporting a link between transcript abundance and [metabolite].

[ABA] increased during severe water deficit, but NCED3 protein abundance did not

To further the understanding of ABA metabolism in the distinct genotypes of this study in response to WD, relative NCED3 protein abundance was quantified (Supplemental File 6 and Appendix 6) in addition to *NCED3* transcripts and [ABA] from another experiment

that was performed previously (Cochetel et al., 2020). Briefly, the four *Vitis* species underwent a natural dry-down for a week that achieved a lower stem water potential (~ -1.5 MPa) than that of vines that experienced the two-week moderate WD treatment (~ -0.8 MPa). RI was majorly impacted by this severe WD; the majority of RI shoots withered and died (Cochetel et al., 2020). Shoots of the other species wilted. Only surviving vines were used in subsequent analyses.

Previously (Cochetel et al., 2020), it was found that *NCED3* transcript abundance (NRQ) was significantly increased in response to WD in all species except for the surviving RI; RA and CS had the highest *NCED3* NRQ in the leaves and roots in response to WD. While CS Control leaves and RA Control and WD leaves had significantly higher relative NCED3 protein than respective roots (Supplemental File 6), unexpectedly there was no significant difference of NCED3 relative protein abundance between the treatments or species (Supplemental File 6) using the 67 kDa band corresponding to the complete NCED3 protein.

[ABA] after one week of severe WD increased and was comparable to those of two weeks of moderate WD (Figs. 1 and 8). The [ABA] of all WD treated leaves, except those of RI were significantly different from respective Control (Fig. 8), which paralleled *NCED3* NRQ (Cochetel et al., 2020). RA leaves had a significantly higher [ABA] than those of RI and SC in response to WD, which was also observed in the *NCED3* NRQ. Additionally, RA was the only species to have significantly higher [ABA] in both the leaves and the roots in response to WD (Fig. 8). The similarity in [ABA] between the week-two moderate and one-week severe WD experiments indicated that ABA metabolism was dependent on severity and duration of WD stress.

Rapid dehydration increases *NCED3* transcript abundance and [ABA] but does not affect NCED3 protein abundance

A WD time course experiment was conducted to examine *NCED3* transcript abundance, relative NCED3 protein abundance, and [ABA] in response to rapid dehydration WD. As all vines from previous experiments were submitted to the same treatments for the same long-term duration, there may have been a limited range of responses revealed in the previous experiments. Transcript abundances can change within seconds/minutes/hours in response to stimulus (Crisp et al., 2017; Kollist, 2019; Pleiss et al., 2007), and the week(s) duration of previous experiments lacked insight into short-term changes. To address the limited range of WD and long-term duration in the previous experiments, a third experiment was performed to expose detached leaves to rapid dehydration or continual petiole irrigation under controlled conditions for 2, 4, 8, and 24 hours. SC was not used in this experiment.

Throughout the rapid dehydration experiment, WD leaves had significantly lower stem water potential and lost significantly more water than Control leaves (Appendix 7). As expected, both stomatal conductance (Gs) and photosynthesis (Ps) were significantly reduced over the course of the WD treatment (Appendix 7). Leaf water potential and calculated turgor pressure (Tyree and Hammel, 1972) were also significantly reduced in the WD treated leaves (Appendix 7) although the osmotic potential was not commonly affected by the short-term rapid dehydration. Per time point per treatment, there was no significant difference between the leaf water potential, indicating all species were experiencing the same level of stress. RA was the only species to significantly maintain Ps

and Gs despite a significant reduction in leaf water potential after two hours of rapid dehydration (Appendix 7).

NCED3 transcript abundance increased for all species in response to the rapid dehydration (Fig. 9). Average RA *NCED3* transcript abundance was highest after two hours of rapid dehydration, but RA rapid dehydration *NCED3* transcripts at two hours of treatment were not significantly different than any other time point of rapid dehydration (Fig. 9 and Appendix 8). *NCED3* NRQ was much lower in RA than CS rapid dehydration leaves (Fig. 9 and Appendix 8). Surprisingly, *NCED3* transcript level stayed constant in RI leaves throughout the rapid dehydration leaves (Fig. 9 and Appendix 8).

[NCED3 protein] (67 kDa corresponding to the complete protein) was not significantly different for any species in Control or rapid dehydration WD at any time point (Supplemental File 6). The NCED3 relative abundance similarity between Control and WD leaves in the rapid dehydration was comparable to those observed in the one-week severe WD experiment.

[ABA] increased in response to short-term rapid dehydration WD (Fig. 9). CS WD experienced a general increase in [ABA] with time like CS WD *NCED3* transcript abundance (Fig. 9). RA WD had the lowest [ABA] of the WD treated species at all times; RA WD was only significantly different from RA Control after 24 hours of treatment (Fig. 9 and Appendix 8). RA [ABA] paralleled RA *NCED3* transcript abundances (Fig. 9), which surprisingly did not increase as much as CS during this short-term WD treatment. RI WD had the highest [ABA] of the WD species at four and eight hours of treatment and steadily increased with time (Fig. 9 and Appendix 8). Of note, RI WD [ABA] did not follow the same trend as RI WD *NCED3* transcript abundance (Fig. 9), which remained relatively

constant throughout the stress. This observation may indicate RI is relying on a different source of ABA (like ABA-GE deconjugation) more than the other species under short-term rapid dehydration. Although the WD species were experiencing the same level and duration of stress and having similar physiological responses (Appendix 7), each species displayed unique ABA metabolism responses via *NCED3* transcript abundance and [ABA] (Fig. 9 and Appendix 8). *NCED3* transcript abundance and [ABA] during short-term rapid dehydration did not display the same responses as the longer-term moderate and severe WD, indicating ABA metabolism is highly dependent not only on organ and species but also on stress severity and duration.

5.4 Discussion

Higher *NCED3* transcript abundance is a core WD response in *Vitis*

Overall, this work highlights differences in transcripts, a protein, and metabolites in the ABA metabolism pathway in two organs of four *Vitis* species in response to WD. Various [ABA] and [ABA metabolites] (Figs. 1-3 and 8-9) were in part explained by corresponding changes in upstream transcript abundances (Figs. 4-7 and Supplemental Files 3-5). Throughout these experiments, *NCED3* stood out as a key WD response gene in both leaves and roots of the four grape species selected for their distinct drought tolerance previously observed (Cochetel et al., 2020; Fort et al., 2017; Pavlousek, 2011; Saritha et al., 2017; Suarez et al., 2019). From the WGCNA, two modules contained the most ABA metabolism genes in the leaves and roots (Appendix 1) and were most correlated to WD and the [ABA-

related metabolites]. *NCED3* was the sole ABA metabolism hub gene (Appendix 4) in these modules. Additionally, *NCED3* transcript abundance increased in all WD experiments described here regardless of severity, duration, organ, and even species. *NCED3* was also identified as a key transcript in WD response previously (Sussmilch et al., 2017) and is well described to increase during water stress in plants (Liu et al., 2016; Qin and Zeevaart, 1999; Tan et al., 1997). In addition to ABA metabolism and signaling genes, the *NCED3*-containing modules include numerous genes involved in plastid function like plastid transkelotases and the chloroplastic 50S ribosome subunit as well as aquaporins, ion transporters, ascorbate oxidase, galactinol synthase, and cysteine and sulfur regulatory genes, which have known associations to ABA (Batool et al., 2018; Bittner et al., 2001; Lamarque et al., 2019; Li et al., 2020) (Appendix 4).

Only one *NCED3* allele was detected in the CS v1.0 and later in the CS v1.1 genome using available protein BLASTP. However, a second allele (VvCabSauv08_v1_Primary000127F: 1106359..1108727) was found with manual curation using only the alternative contig in the CS v1.1 genome. The two *NCED3* alleles share 99% identity determined by Clustal Omega alignment, and therefore the transcript abundance for this gene was representative of both alleles.

Leaves and roots differ in *NCED3* transcript abundance, NCED3 protein levels, [ABA], and [ABA-related metabolite]

The primary site of ABA biosynthesis (leaves versus roots), as well as the initial site and signal to trigger a stress response during WD, has been a controversial topic (Carvalho et al., 2016; Christmann et al., 2007; McAdam et al., 2016). Recently, a small root-sourced

signaling peptide, CLE25, was identified in *Arabidopsis thaliana* that controls stomatal closure via ABA biosynthesis in the leaves (Takahashi et al., 2018). However, there is no orthologous peptide in many species including grapevine, and the subtleties of WD detection in roots and shoots as well as the identities of long-distance signaling molecules (including ABA itself) remains elusive.

Leaves and roots had different levels of ABA metabolism-related transcripts (Figs. 4 and 5 and Supplemental Files 3-5 and Appendices 2-3), NCED3 protein (Supplemental File 6), ABA, and ABA-related metabolites (Figs. 1, 2, 8, and 9) in these experiments. Additionally, the leaf and root *NCED3*-containing modules did not contain the same ABA metabolism genes, indicating a difference in ABA metabolism and signaling in leaves and roots as observed previously in grapevine (Khadka et al., 2019; Rossdeutsch et al., 2016) and other plant species (Gu et al., 2019; Ksouri et al., 2016; Min et al., 2020; Yang et al., 2020). However, whole organs were used for these analyses. Specific cell types like the guard cell (Assmann and Jegla, 2016) or root endodermis (Duan et al., 2013) have specialized responses to ABA and likely have unique regulation of *NCED3* and ABA metabolism, each of which requires further investigation in these grapevines.

In both the moderate and severe WD experiments, leaves generally had a higher abundance of *NCED3* transcripts and [ABA] than roots as was expected (Cornish and Zeevaart, 1985; Correia et al., 2014; Hu et al., 2016; Lovelli et al., 2012; Manzi et al., 2015). Leaves also had higher [NCED3 protein] than roots in the severe WD experiment. The differences in *NCED3* transcripts, NCED3 protein, [ABA], and [ABA-related metabolite] between leaves and roots may reflect different sensitivity to ABA between the organs as implied previously (Correia et al., 2014; Finkelstein, 2013). It is likely the [ABA]

threshold to elicit a specific ABA response is organ-specific (Rattanakon et al., 2016) and may involve ABA and/or ABA-related metabolite transport between organs. Previously, exogenous application of ABA was demonstrated to greatly affect transcriptomic signaling within berries, shoot tips, leaves, roots, and cell culture with no one gene demonstrating the same change in transcript abundance across all organs (Rattanakon et al., 2016). Organ-specific sensitivity to other hormones has also been previously described. For example, exogenous [μM] of auxin stimulates leaf and shoot expansion but inhibits root elongation (Chadwick and Burg, 1967; Evans et al., 1994). Gibberellins similarly demonstrated organ specificity with high concentrations biosynthesized in the stamen from which lower concentrations are transported out to support other floral organ development like the petals (Hu et al., 2008).

ABA, like gibberellins, is biosynthesized (Holbrook et al., 2002; McAdam and Brodribb, 2018; Zhang et al., 1987) and transported throughout a plant (Kuromori et al., 2018). ABA transport from vascular cells into guard cells is well documented with several identified transporters (ABCG40 (Kang et al., 2010), ABCG25 (Kuromori et al., 2010), ABCG22 (Merilo et al., 2015), ABCG30, ABCG31 (Kang et al., 2015), AIT2, and AIT1 (Léran et al., 2020)). There is evidence that root ABA may be in part shoot sourced (Ernst et al., 2010; Goodger and Schachtman, 2010; Ikegami et al., 2009), and ABA transport into the root has been described (Ikegami et al., 2009) in addition to ABA-vascular unloading and transport into guard cells (Kuromori et al., 2010) and endosperm-ABA unloading into the seed embryo (Kang et al., 2015). In the moderate WD experiment, *ABCG25* and *ABCG40* had higher transcript abundance in roots than leaves for all species, treatments, and time points (Supplemental File 5), indicating possible ABA phloem unloading and

ABA transport into the roots. *ABCG25* is predominantly expressed in phloem companion cells in *Arabidopsis thaliana* (Brady et al., 2007; Kuromori et al., 2010), indicating ABA is transported down through the plant. *ABCG25* transcripts accumulated in *Arabidopsis thaliana* roots in response to salt stress (Winter et al., 2007), and when GFP was expressed under a 2.0 kb *AtABCG25* promoter, a signal was observed in the root in the presence of 10 μM ABA (Kuromori et al., 2014). AtABCG40, responsible for importing ABA into guard cells, also plays a role in lateral root development and is expressed in primary and lateral roots in addition to being crucial for stomatal function (Kang et al., 2010).

ABA-GE was highly abundant during the moderate WD (Fig. 1) as was expected (Hansen and Dörffling, 1999). However, ABA-GE transport regulation remains unresolved. Leaves had significantly higher [ABA-GE] than roots in the moderate WD experiment (Fig. 1), but the organs may have different requirements for this metabolite (Acanda et al., 2020; Manzi et al., 2015; Thameur et al., 2011). *BG1* had significantly higher transcript abundance in roots than leaves for the majority of species for both treatments and times in the moderate WD experiment (Supplemental File 5), indicating the possible importance of ABA-GE deconjugation in the roots. Despite low membrane permeability (Baier et al., 1990) and attempts to identify an ABA-GE transporter (Kang et al., 2010), this potential ABA transport pathway remains unsolved. ABA-GE transport may be one source of shoot-derived ABA in roots that has not been well characterized (Kuromori et al., 2018).

Grapevine species differ in physiological and biochemical responses to WD

In these experiments, species had distinct biochemical regulation of ABA. CS generally had the most variable physiological measurements (Cochetel et al., 2020), *NCED3*

transcript abundance, [ABA], and [ABA-related metabolites] in response to the various water deficit experiments. In all experiments, RI quickly closed stomata (Cochetel et al., 2020) and remained at this new homeostasis throughout the WD while having a small increase in ABA metabolite-related transcripts and [ABA] relative to CS and RA. SC demonstrated a similar biochemical response to RI with lower transcript and metabolite levels. In the moderate and severe WD experiments, RA had higher [ABA] in both leaves and roots relative to the other species (Figs. 1, 2, and 8). RA also had the highest *NCED3* transcript abundance in moderate and severe WD treatments (Fig. 4) (Cochetel et al., 2020). Additionally, RA had the highest levels of *NCED3* transcripts (Fig. 4) and [ABA] (Fig. 1) at the earliest time point during the moderate WD, indicating RA may be the most sensitive (earliest to respond) of the species investigated for long-term WD detection. RA maintained higher physiological function during the moderate and severe WD (Cochetel et al., 2020) despite higher levels of ABA than the other species (Figs. 1 and 8). RA also maintained stomatal conductance longer during rapid dehydration (till 2 hours) than the other species despite comparable levels of stress, [ABA], and *NCED3* transcript abundance at this time. These observations indicate RA may be less sensitive to [ABA] over time in terms of physiological response (like stomatal closure) or RA may be enacting changes that better allow RA to function under WD (e.g. suberization or modified hydraulic conductance) relative to the other species as described in wheat (Guóth et al., 2009; Thameur et al., 2011) and other plants (Mamrutha et al., 2017; Mohamed et al., 2020; Tombesi et al., 2015). Several aquaporin genes display differential and unique responses to water deficit in RA leaves (Appendix 2). Genes involved in cysteine biosynthesis and metabolism are also constitutively higher in the roots of RA (Cochetel et al., 2020); thus,

linking the gene expression and physiological responses to known ABA effectors that were not investigated here. The physiological and sensitive transcriptomic response that occurs at milder longer-term WD in RA indicates RA may be able to take advantage of moderate or longer-term WD by maintaining open stomata longer than the other species despite decreasing water availability.

Drought tolerance is the ability of a vine to sustain physiological activity while minimizing or repairing damage during WD (Gambetta, 2016). The drought tolerance of plants is associated with stomatal behaviors in response to WD and resultant use or preservation of available water. Grapevine responses to WD are characterized as belonging to a spectrum of stomatal reactions in WD ranging from isohydric to anisohydric (Sade and Moshelion, 2014). Isohydric species maintain a relatively constant leaf water potential through early stomatal closure during WD (Tardieu and Simonneau, 1998) like RI. Anisohydric species experience decreasing leaf water potential and maintain open stomata during WD (Tardieu and Simonneau, 1998) like RA. It is possible the iso- and aniso-hydric behaviors are controlled by different mechanisms (chemical and/or hydraulic regulation) altogether, by different mechanisms for different WD severities (moderate versus severe), or by different mechanisms at different time points (initial versus long-term) during a drought (Tardieu and Simonneau, 1998). Isohydric behavior is often considered advantageous for conferring drought tolerance (Gerzon et al., 2015; Sade and Moshelion, 2014; Schultz, 2003; Tardieu and Simonneau, 1998). However, by the definition of drought tolerance (Gambetta, 2016), it may be worth reconsidering the association of isohydric grapevines with drought tolerance in favor of connection to drought avoidance. A vine that can maintain stomatal aperture (i.e. anisohydric), photosynthesis, and other physiological

functions under decreasing water availability like RA may be considered more drought tolerant than a vine that shuts down early when experiencing stress like RI. Overall, ABA biosynthesis appeared to be a WD response that differentiated the species. The time frames investigated in these experiments emphasize the ABA metabolism and WD response of the different species depends on the duration and severity of stress. WD experiments must be designed and compared to each other very carefully for this reason. More time points should be investigated in the future to better understand differences in short- and long-term WD and the transition between them in terms of ABA metabolism.

The rapid dehydration response varies and is inconsistent with previous dehydration responses

Previously, a similar rapid dehydration experiment was performed (Hopper et al., 2014). The average water lost at two (-0.139 ± 0.022 g) and four (-0.122 ± 0.012 g) hours of rapid dehydration treatment were comparable to the previous experiment after two (~ -0.1 g) and three (~ -0.14 g) hours of a similar rapid dehydration treatment. However, in a second similar rapid dehydration experiment where microarray transcript quantification was performed, but water loss was not quantified, *NCED3* transcript abundance showed different expression patterns in CS, RA, and RI than were observed here (Hopper et al., 2016). These differences may be real or due to different transcriptomic technologies. Microarray data are often subject to cross-hybridization of the probes and can be less reliable, such as the probe for *NCED3* (VIT_19s0093g00550), which may cross-hybridize (Ghan et al., 2015). The [ABA] curve of RI in the current rapid dehydration assay mirrored that of the *NCED3* transcript curve that was previously observed and was expected in this

experiment. The minor increase in RA and RI *NCED3* transcript abundance at 24 hours of treatment was the most distinct difference between this and the previous experiment. In addition to the differences in technology, this distinction may be a result of differences in the age of leaves selected, the time of year, time of day, or even different experiences the plants had with WD in the past (Walter et al., 2011). Control *NCED3* transcript abundance was comparable for all species and time points between this and previous experiments.

NCED3 protein concentration was not changed by WD

Despite differences in ABA biosynthesis transcripts and [ABA], [NCED3 protein] was generally constant for all species, treatments, and time points. Few studies consider NCED3 protein levels (Endo et al., 2008; Hu et al., 2016; Kalladan et al., 2019). It is possible NCED3 protein sequence variation (Appendix 6) contributes to the observed differences in ABA accumulation in the species or NCED3 may have distinctive activity in the different species like in Arabidopsis accessions (Kalladan et al., 2019). In peanut, authors mention increased ABA with a parallel increase in NCED3 protein (Liu et al., 2016), and in Arabidopsis lower NCED3 correlated to lower [ABA] in at least one transgenic line (Kalladan et al., 2019), but this correlation was not observed in grapevine under these WD experiments using the 67 kDa complete NCED3 protein. This relationship may be organ, stress, or time-specific. NCED3 activity has previously been screened (Schwartz et al., 2003), but a correlation between transcripts and protein was not made.

Previous proteomic studies investigating highly WD responsive proteins have not yet singled out NCED3 (Alvarez et al., 2013; Chen et al., 2019; Lima et al., 2019; Riccardi

et al., 2004; Tamburino et al., 2017), despite the importance of NCED3 in WD response and ABA metabolism. Recently, an *Arabidopsis thaliana* proteome database was released examining gene expression and [protein] across organs (Mergner et al., 2020a) and development (Mergner et al., 2020b), but no such resource has been developed for abiotic stress response yet. It is also likely post-translational modifications including cleavage play an important role in NCED3 activity (Endo et al., 2008), but NCED3 post-translational modifications are not well described at this time (Cruz et al., 2019). To the best of the author's knowledge, no other study examining transcript, protein, and metabolite concentrations has been performed in grapevine that includes NCED3 and ABA at this time.

Other factors and regulatory mechanisms may impact ABA metabolism

Three levels of ABA regulation were examined in this study. However, numerous other steps may impact [ABA], [ABA-related metabolite], and the physiological responses a plant has to WD. For these reasons, the response of a plant to a short, long, moderate, or severe WD may be vastly different. Many levels of the biochemical regulation of WD response and ABA biosynthesis require characterization. NCED3 has uncharacterized phosphorylation and other potential post-translational modifications that may affect activity or localization (Endo et al., 2008; Heazlewood et al., 2008; Tan et al., 2001). NCED3 may also interact with other proteins with unknown consequences. Alternative splicing and alternative 3'UTR usage may affect transcript function, lifetime, and localization may potentially significantly impact or optimize a WD response based on the severity and duration of the stress (Chakrabarti et al., 2018; Potenza et al., 2015; Vitulo et

al., 2014). Signal peptides like CLE25 (Takahashi et al., 2018), miRNA (Pagliarani et al., 2017), siRNA (Jung et al., 2016), and other regulatory molecules likely play important roles in ABA metabolism and WD response and require further investigation.

Lastly, grafting interactions may affect ABA metabolism, signaling, sensitivity, and physiological responses to WD. Traditionally, grapevines are cultivated by grafting a desirable fruit-bearing scion onto an adventitious rootstock selected based on environmental conditions. Grafting enables desirable traits of a rootstock like disease resistance or salt tolerance to be conferred to the scion (Albacete et al., 2015). Previously, grafting was not found to affect the physiological response of grapevine to a short WD (Barrios-Masias et al., 2019). However, grafting has indisputable effects on both the rootstock and scion (Cookson et al., 2013; Holbrook et al., 2002; Kundariya et al., 2020; Pagliarani et al., 2017), and the molecular effects grafting may have on ABA metabolism and WD response remain unresolved.

In conclusion, ABA biochemistry was investigated at three levels of regulation (transcript, protein, and metabolite) across three experiments of varying severity and duration in the leaves and roots of four grapevine species. RNA-Seq analysis and metabolite quantification demonstrated ABA metabolism was a major WD response. ABA-related metabolites could in part be explained by upstream ABA metabolism-related gene transcript abundances. Gene expression profiling, DEA, WGCNA, GO enrichment analysis, and RT-qPCR supported *NCED3* as a key WD response gene. *NCED3* was a highly expressed DEG in response to WD in leaves and roots of all four species. *NCED3* was also the only ABA metabolism-related gene identified as a hub gene in WGCNA modules corresponding both to WD and the ABA-related metabolites. Finally, *NCED3* was

supported as a hub gene in GO by the presence of biosynthetic and abiotic stress response GO terms in the WD and metabolite correlated modules. Western blots demonstrated NCED3 protein abundance did not appear to change in response to WD, indicating that protein activity may be different from protein abundance. There was unique and specific ABA metabolism regulation and WD response that occurred in the leaves and roots. Grapevine species demonstrated a spectrum of physiological, biochemical, and metabolic responses to different WD conditions. These responses depended on the duration and severity of WD. RA responded earlier to long-term WD with higher *NCED3* transcripts and [ABA] while maintaining physiological activity longer at the cost of water availability. During long-term WD, RI generally experienced a smaller increase of *NCED3* transcripts and [ABA], which were maintained at a constant level throughout the stress in parallel with quick closing stomata. *NCED3* transcript abundance did not mirror [ABA] in all species during short-term WD, indicating the species have distinct ABA metabolism responses to different WD severities and durations. Thus, this study shows that ABA metabolism and regulation in grapevine species is variable and complex. Additional studies are needed to further elucidate the regulation of ABA metabolism to produce better more drought-tolerant crops.

5.5 References

Abe, H., Urao, T., Ito, T., Seki, M., Shinozaki, K., and Yamaguchi-Shinozaki, K. (2003). Arabidopsis AtMYC2 (bHLH) and AtMYB2 (MYB) Function as Transcriptional Activators in Abscisic Acid Signaling. Plant Cell *15*, 63–78.

Acanda, Y., Martínez, Ó., Prado, M.J., González, M.V., and Rey, M. (2020). Changes in abscisic acid metabolism in relation to the maturation of grapevine (Vitis vinifera L., cv. Mencía) somatic embryos. BMC Plant Biol. *20*, 487.

Albacete, A., Martínez-Andújar, C., Martínez-Pérez, A., Thompson, A.J., Dodd, I.C., and Pérez-Alfocea, F. (2015). Unravelling rootstock×scion interactions to improve food security. J. Exp. Bot. *66*, 2211–2226.

Alexa, A., Rahnenführer, J., and Lengauer, T. (2006). Improved scoring of functional groups from gene expression data by decorrelating GO graph structure. Bioinformatics *22*, 1600–1607.

Alvarez, S., Roy Choudhury, S., Hicks, L.M., and Pandey, S. (2013). Quantitative Proteomics-Based Analysis Supports a Significant Role of GTG Proteins in Regulation of ABA Response in Arabidopsis Roots. J. Proteome Res. *12*, 1487–1501.

Asensi-Fabado, M.-A., Amtmann, A., and Perrella, G. (2017). Plant responses to abiotic stress: The chromatin context of transcriptional regulation. Biochim. Biophys. Acta BBA - Gene Regul. Mech. *1860*, 106–122.

Assmann, S.M., and Jegla, T. (2016). Guard cell sensory systems: recent insights on stomatal responses to light, abscisic acid, and CO2. Curr. Opin. Plant Biol. *33*, 157–167.

Babraham Bioinformatics (2010). Babraham Bioinformatics - FastQC A Quality Control tool for High Throughput Sequence Data.

Baier, M., Gimmler, H., and Hartung, W. (1990). The Permeability of the Guard Cell Plasma Membrane and Tonoplast. J. Exp. Bot. *41*, 351–358.

Barrios-Masias, F.H., Knipfer, T., Walker, M.A., and McElrone, A.J. (2019). Differences in hydraulic traits of grapevine rootstocks are not conferred to a common Vitis vinifera scion. Funct. Plant Biol. *46*, 228–235.

Barrs, H.D., and Weatherley, P.E. (1962). A Re-Examination of the Relative Turgidity Technique for Estimating Water Deficits in Leaves. Aust. J. Biol. Sci. *15*, 413–428.

Bartley, G.E., Scolnik, P.A., and Beyer, P. (1999). Two Arabidopsis thaliana carotene desaturases, phytoene desaturase and zeta-carotene desaturase, expressed in Escherichia coli, catalyze a poly-cis pathway to yield pro-lycopene. Eur. J. Biochem. *259*, 396–403.

Batool, S., Uslu, V.V., Rajab, H., Ahmad, N., Waadt, R., Geiger, D., Malagoli, M., Xiang, C.-B., Hedrich, R., Rennenberg, H., et al. (2018). Sulfate is Incorporated into Cysteine to Trigger ABA Production and Stomatal Closure. Plant Cell *30*, 2973–2987.

Bittner, F., Oreb, M., and Mendel, R.R. (2001). ABA3 is a molybdenum cofactor sulfurase required for activation of aldehyde oxidase and xanthine dehydrogenase in Arabidopsis thaliana. J. Biol. Chem. *276*, 40381–40384.

Bolger, A.M., Lohse, M., and Usadel, B. (2014). Trimmomatic: a flexible trimmer for Illumina sequence data. Bioinformatics *30*, 2114–2120.

Bouzroud, S., Gouiaa, S., Hu, N., Bernadac, A., Mila, I., Bendaou, N., Smouni, A., Bouzayen, M., and Zouine, M. (2018). Auxin Response Factors (ARFs) are potential mediators of auxin action in tomato response to biotic and abiotic stress (Solanum lycopersicum). PLoS ONE *13*.

Brady, S.M., Orlando, D.A., Lee, J.-Y., Wang, J.Y., Koch, J., Dinneny, J.R., Mace, D., Ohler, U., and Benfey, P.N. (2007). A High-Resolution Root Spatiotemporal Map Reveals Dominant Expression Patterns. Sci. New Ser. *318*, 801–806.

Bray, E.A., and Zeevaart, J.A.D. (1985). The Compartmentation of Abscisic Acid and β-d-Glucopyranosyl Abscisate in Mesophyll Cells. Plant Physiol. *79*, 719–722.

Burla, B., Pfrunder, S., Nagy, R., Francisco, R.M., Lee, Y., and Martinoia, E. (2013). Vacuolar Transport of Abscisic Acid Glucosyl Ester Is Mediated by ATP-Binding Cassette and Proton-Antiport Mechanisms in Arabidopsis. Plant Physiol. *163*, 1446–1458.

Cabré, F., and Nuñez, M. (2020). Impacts of climate change on viticulture in Argentina. Reg. Environ. Change *20*, 12.

Canaguier, A., Grimplet, J., Di Gaspero, G., Scalabrin, S., Duchêne, E., Choisne, N., Mohellibi, N., Guichard, C., Rombauts, S., Le Clainche, I., et al. (2017). A new version of the grapevine reference genome assembly (12X.v2) and of its annotation (VCost.v3). Genomics Data *14*, 56–62.

Carvalho, D.R.A., Fanourakis, D., Correia, M.J., Monteiro, J.A., Araújo-Alves, J.P.L., Vasconcelos, M.W., Almeida, D.P.F., Heuvelink, E., and Carvalho, S.M.P. (2016). Root-to-shoot ABA signaling does not contribute to genotypic variation in stomatal functioning induced by high relative air humidity. Environ. Exp. Bot. *123*, 13–21.

Chadwick, A.V., and Burg, S.P. (1967). An Explanation of the Inhibition of Root Growth Caused by Indole-3-Acetic Acid. Plant Physiol. *42*, 415–420.

Chakrabarti, M., Dinkins, R.D., and Hunt, A.G. (2018). Genome-wide atlas of alternative polyadenylation in the forage legume red clover. Sci. Rep. *8*, 11379.

Chen, K., Li, G.-J., Bressan, R.A., Song, C.-P., Zhu, J.-K., and Zhao, Y. (2020). Abscisic acid dynamics, signaling, and functions in plants. J. Integr. Plant Biol. *62*, 25–54.

Chen, Z., Xu, J., Wang, F., Wang, L., and Xu, Z. (2019). Morpho-physiological and proteomic responses to water stress in two contrasting tobacco varieties. Sci. Rep. *9*, 18523.

Chin, C.-S., Peluso, P., Sedlazeck, F.J., Nattestad, M., Concepcion, G.T., Clum, A., Dunn, C., O'Malley, R., Figueroa-Balderas, R., Morales-Cruz, A., et al. (2016). Phased diploid

genome assembly with single-molecule real-time sequencing. Nat. Methods *13*, 1050–1054.

Chong, G.L., Foo, M.H., Lin, W.-D., Wong, M.M., and Verslues, P.E. (2019). Highly ABA-Induced 1 (HAI1)-Interacting protein HIN1 and drought acclimation-enhanced splicing efficiency at intron retention sites. Proc. Natl. Acad. Sci. *116*, 22376–22385.

Christmann, A., Weiler, E.W., Steudle, E., and Grill, E. (2007). A hydraulic signal in root-to-shoot signalling of water shortage: Hydraulic signalling of water shortage. Plant J. *52*, 167–174.

Cochetel, N., Ghan, R., Toups, H.S., Degu, A., Tillett, R.L., Schlauch, K.A., and Cramer, G.R. (2020). Drought tolerance of the grapevine, Vitis champinii cv. Ramsey, is associated with higher photosynthesis and greater transcriptomic responsiveness of abscisic acid biosynthesis and signaling. BMC Plant Biol. *20*.

Cookson, S.J., Clemente Moreno, M.J., Hevin, C., Nyamba Mendome, L.Z., Delrot, S., Trossat-Magnin, C., and Ollat, N. (2013). Graft union formation in grapevine induces transcriptional changes related to cell wall modification, wounding, hormone signalling, and secondary metabolism. J. Exp. Bot. *64*, 2997–3008.

Cornish, K., and Zeevaart, J.A. (1985). Abscisic Acid Accumulation by Roots of Xanthium strumarium L. and Lycopersicon esculentum Mill. in Relation to Water Stress. Plant Physiol. *79*, 653–658.

Correia, B., Pintó-Marijuan, M., Castro, B.B., Brossa, R., López-Carbonell, M., and Pinto, G. (2014). Hormonal dynamics during recovery from drought in two Eucalyptus globulus genotypes: from root to leaf. Plant Physiol. Biochem. PPB *82*, 151–160.

Cottle, W., and Kolattukudy, P.E. (1982). Abscisic Acid Stimulation of Suberization. Plant Physiol. *70*, 775–780.

Crisp, P.A., Ganguly, D.R., Smith, A.B., Murray, K.D., Estavillo, G.M., Searle, I., Ford, E., Bogdanović, O., Lister, R., Borevitz, J.O., et al. (2017). Rapid Recovery Gene Downregulation during Excess-Light Stress and Recovery in Arabidopsis. Plant Cell *29*, 1836–1863.

Cruz, E.R., Nguyen, H., Nguyen, T., and Wallace, I.S. (2019). Functional analysis tools for post-translational modification: a post-translational modification database for analysis of proteins and metabolic pathways. Plant J. *99*, 1003–1013.

Cutler, A.J., and Krochko, J.E. (1999). Formation and breakdown of ABA. Trends Plant Sci. *4*, 472–478.

Dai, A. (2013). Increasing drought under global warming in observations and models. Nat. Clim. Change *3*, 52–58.

Du, H., Wang, N., Cui, F., Li, X., Xiao, J., and Xiong, L. (2010). Characterization of the β-Carotene Hydroxylase Gene DSM2 Conferring Drought and Oxidative Stress Resistance by Increasing Xanthophylls and Abscisic Acid Synthesis in Rice. Plant Physiol. *154*, 1304–1318.

Duan, L., Dietrich, D., Ng, C.H., Chan, P.M.Y., Bhalerao, R., Bennett, M.J., and Dinneny, J.R. (2013). Endodermal ABA Signaling Promotes Lateral Root Quiescence during Salt Stress in *Arabidopsis* Seedlings. Plant Cell *25*, 324–341.

Endo, A., Sawada, Y., Takahashi, H., Okamoto, M., Ikegami, K., Koiwai, H., Seo, M., Toyomasu, T., Mitsuhashi, W., Shinozaki, K., et al. (2008). Drought Induction of Arabidopsis 9-cis-Epoxycarotenoid Dioxygenase Occurs in Vascular Parenchyma Cells. PLANT Physiol. *147*, 1984–1993.

Ernst, L., Goodger, J.Q.D., Alvarez, S., Marsh, E.L., Berla, B., Lockhart, E., Jung, J., Li, P., Bohnert, H.J., and Schachtman, D.P. (2010). Sulphate as a xylem-borne chemical signal precedes the expression of ABA biosynthetic genes in maize roots. J. Exp. Bot. *61*, 3395–3405.

Eskling, M., Arvidsson, P.-O., and Åkerlund, H.-E. (1997). The xanthophyll cycle, its regulation and components. Physiol. Plant. *100*, 806–816.

Evans, M.L., Ishikawa, H., and Estelle, M.A. (1994). Responses of Arabidopsis roots to auxin studied with high temporal resolution: Comparison of wild type and auxin-response mutants. Planta *194*, 215–222.

Finkelstein, R. (2013). Abscisic Acid Synthesis and Response. Arab. Book Am. Soc. Plant Biol. *11*.

Finkelstein, R.R., and Lynch, T.J. (2000). The Arabidopsis Abscisic Acid Response Gene ABI5 Encodes a Basic Leucine Zipper Transcription Factor. Plant Cell *12*, 599–609.

Finkelstein, R., Gampala, S.S.L., Lynch, T.J., Thomas, T.L., and Rock, C.D. (2005). Redundant and Distinct Functions of the ABA Response Loci ABA-INSENSITIVE(ABI)5 and ABRE-BINDING FACTOR (ABF)3. Plant Mol. Biol. *59*, 253–267.

Fort, K., Fraga, J., Grossi, D., and Walker, M.A. (2017). Early Measures of Drought Tolerance in Four Grape Rootstocks. J. Am. Soc. Hortic. Sci. *142*, 36–46.

Fox, J. (2020). An R Companion to Applied Regression (Thousand Oaks CA: Sage).

Furihata, T., Maruyama, K., Fujita, Y., Umezawa, T., Yoshida, R., Shinozaki, K., and Yamaguchi-Shinozaki, K. (2006). Abscisic acid-dependent multisite phosphorylation regulates the activity of a transcription activator AREB1. Proc. Natl. Acad. Sci. U. S. A. *103*, 1988–1993.

Galili, T. (2015). dendextend: an R package for visualizing, adjusting and comparing trees of hierarchical clustering. Bioinformatics *31*, 3718–3720.

Gambetta, G.A. (2016). Water Stress and Grape Physiology in the Context of Global Climate Change. J. Wine Econ. *11*, 168–180.

Gerzon, E., Biton, I., Yaniv, Y., Zemach, H., Netzer, Y., Schwartz, A., Fait, A., and Ben-Ari, G. (2015). Grapevine Anatomy as a Possible Determinant of Isohydric or Anisohydric Behavior. Am. J. Enol. Vitic. *66*, 340–347.

Ghan, R., Van Sluyter, S.C., Hochberg, U., Degu, A., Hopper, D.W., Tillet, R.L., Schlauch, K.A., Haynes, P.A., Fait, A., and Cramer, G.R. (2015). Five omic technologies are concordant in differentiating the biochemical characteristics of the berries of five grapevine (Vitis vinifera L.) cultivars. BMC Genomics *16*, 946.

Ghimire, S., Tang, X., Zhang, N., Liu, W., and Si, H. (2020). SUMO and SUMOylation in plant abiotic stress. Plant Growth Regul.

Gillard, D.F., and Walton, D.C. (1976). Abscisic Acid Metabolism by a Cell-free Preparation from Echinocystis lobata Liquid Endosperm. Plant Physiol *58*, 6.

Girollet, N., Rubio, B., Lopez-Roques, C., Valière, S., Ollat, N., and Bert, P.-F. (2019). De novo phased assembly of the Vitis riparia grape genome. Sci. Data *6*, 1–8.

González-Guzmán, M., Apostolova, N., Bellés, J.M., Barrero, J.M., Piqueras, P., Ponce, M.R., Micol, J.L., Serrano, R., and Rodríguez, P.L. (2002). The Short-Chain Alcohol Dehydrogenase ABA2 Catalyzes the Conversion of Xanthoxin to Abscisic Aldehyde. Plant Cell *14*, 1833–1846.

Goodger, J.Q., and Schachtman, D.P. (2010). Re-examining the role of ABA as the primary long-distance signal produced by water-stressed roots. Plant Signal. Behav. *5*, 1298–1301.

Gouthu, S., Morre, J., Maier, C.S., and Deluc, L.G. (2013). An Analytical Method to Quantify Three Plant Hormone Families in Grape Berry Using Liquid Chromatography and Multiple Reaction Monitoring Mass Spectrometry. In Phytochemicals, Plant Growth, and the Environment, D.R. Gang, ed. (New York, NY: Springer New York), pp. 19–36.

Gu, H., Yang, Y., Xing, M., Yue, C., Wei, F., Zhang, Y., Zhao, W., and Huang, J. (2019). Physiological and transcriptome analyses of Opisthopappus taihangensis in response to drought stress. Cell Biosci. *9*, 56.

Gu, Z., Gu, L., Eils, R., Schlesner, M., and Brors, B. (2014). circlize implements and enhances circular visualization in R. Bioinformatics *30*, 2811–2812.

Gu, Z., Eils, R., and Schlesner, M. (2016). Complex heatmaps reveal patterns and correlations in multidimensional genomic data. Bioinforma. Oxf. Engl. *32*, 2847–2849.

Guerra, D., Crosatti, C., Khoshro, H.H., Mastrangelo, A.M., Mica, E., and Mazzucotelli, E. (2015). Post-transcriptional and post-translational regulations of drought and heat response in plants: a spider's web of mechanisms. Front. Plant Sci. *6*.

Guiltinan, M.J., Marcotte, W.R., and Quatrano, R.S. (1990). A plant leucine zipper protein that recognizes an abscisic acid response element. Science *250*, 267–271.

Guóth, A., Tari, I., Gallé, Á., Csiszár, J., Pécsváradi, A., Cseuz, L., and Erdei, L. (2009). Comparison of the Drought Stress Responses of Tolerant and Sensitive Wheat Cultivars During Grain Filling: Changes in Flag Leaf Photosynthetic Activity, ABA Levels, and Grain Yield. J. Plant Growth Regul. *28*, 167–176.

Hansen, H., and Dörffling, K. (1999). Changes of free and conjugated abscisic acid and phaseic acid in xylem sap of drought-stressed sunflower plants. J. Exp. Bot. *50*, 1599–1605.

Hashiguchi, A., and Komatsu, S. (2016). Impact of Post-Translational Modifications of Crop Proteins under Abiotic Stress. Proteomes *4*.

Heazlewood, J.L., Durek, P., Hummel, J., Selbig, J., Weckwerth, W., Walther, D., and Schulze, W.X. (2008). PhosPhAt : a database of phosphorylation sites in Arabidopsis thaliana and a plant-specific phosphorylation site predictor. Nucleic Acids Res. *36*, D1015–D1021.

Hieber, A.D., Bugos, R.C., and Yamamoto, H.Y. (2000). Plant lipocalins: violaxanthin de-epoxidase and zeaxanthin epoxidase. Biochim. Biophys. Acta BBA - Protein Struct. Mol. Enzymol. *1482*, 84–91.

Holbrook, N.M., Shashidhar, V.R., James, R.A., and Munns, R. (2002). Stomatal control in tomato with ABA-deficient roots: response of grafted plants to soil drying. J. Exp. Bot. *53*, 1503–1514.

Hopper, D.W., Ghan, R., and Cramer, G.R. (2014). A rapid dehydration leaf assay reveals stomatal response differences in grapevine genotypes. Hortic. Res. *1*.

Hopper, D.W., Ghan, R., Schlauch, K.A., and Cramer, G.R. (2016). Transcriptomic network analyses of leaf dehydration responses identify highly connected ABA and ethylene signaling hubs in three grapevine species differing in drought tolerance. BMC Plant Biol. *16*.

Hu, B., Cao, J., Ge, K., and Li, L. (2016). The site of water stress governs the pattern of ABA synthesis and transport in peanut. Sci. Rep. *6*, 32143.

Hu, J., Mitchum, M.G., Barnaby, N., Ayele, B.T., Ogawa, M., Nam, E., Lai, W.-C., Hanada, A., Alonso, J.M., Ecker, J.R., et al. (2008). Potential Sites of Bioactive Gibberellin Production during Reproductive Growth in Arabidopsis. Plant Cell *20*, 320–336.

Ikegami, K., Okamoto, M., Seo, M., and Koshiba, T. (2009). Activation of abscisic acid biosynthesis in the leaves of Arabidopsis thaliana in response to water deficit. J. Plant Res. *122*, 235–243.

Jung, I., Ahn, H., Shin, S.-J., Kim, J., Kwon, H.-B., Jung, W., and Kim, S. (2016). Clustering and evolutionary analysis of small RNAs identify regulatory siRNA clusters induced under drought stress in rice. BMC Syst. Biol. *10*, 115.

Kalladan, R., Lasky, J.R., Sharma, S., Kumar, M.N., Juenger, T.E., Marais, D.L.D., and Verslues, P.E. (2019). Natural Variation in 9-Cis-Epoxycartenoid Dioxygenase 3 and ABA Accumulation. Plant Physiol. *179*, 1620–1631.

Kang, J., Hwang, J.-U., Lee, M., Kim, Y.-Y., Assmann, S.M., Martinoia, E., and Lee, Y. (2010). PDR-type ABC transporter mediates cellular uptake of the phytohormone abscisic acid. Proc. Natl. Acad. Sci. *107*, 2355–2360.

Kang, J., Yim, S., Choi, H., Kim, A., Lee, K.P., Lopez-Molina, L., Martinoia, E., and Lee, Y. (2015). Abscisic acid transporters cooperate to control seed germination. Nat. Commun. *6*, 8113.

Khadka, V.S., Vaughn, K., Xie, J., Swaminathan, P., Ma, Q., Cramer, G.R., and Fennell, A.Y. (2019). Transcriptomic response is more sensitive to water deficit in shoots than roots of Vitis riparia (Michx.). BMC Plant Biol. *19*, 72.

Kim, D., Langmead, B., and Salzberg, S.L. (2015). HISAT: a fast spliced aligner with low memory requirements. Nat. Methods *12*, 357–360.

Kim, J.-M., To, T.K., Ishida, J., Morosawa, T., Kawashima, M., Matsui, A., Toyoda, T., Kimura, H., Shinozaki, K., and Seki, M. (2008). Alterations of Lysine Modifications on the Histone H3 N-Tail under Drought Stress Conditions in Arabidopsis thaliana. Plant Cell Physiol. *49*, 1580–1588.

Kobayashi, Y., Murata, M., Minami, H., Yamamoto, S., Kagaya, Y., Hobo, T., Yamamoto, A., and Hattori, T. (2005). Abscisic acid-activated SNRK2 protein kinases function in the gene-regulation pathway of ABA signal transduction by phosphorylating ABA response element-binding factors. Plant J. *44*, 939–949.

Kollist, H. (2019). Rapid Responses to Abiotic Stress: Priming the Landscape for the Signal Transduction Network. Trends Plant Sci *24*, 13.

Krochko, J.E., Abrams, G.D., Loewen, M.K., Abrams, S.R., and Cutler, A.J. (1998). (+)-Abscisic Acid 8′-Hydroxylase Is a Cytochrome P450 Monooxygenase. Plant Physiol. *118*, 849–860.

Ksouri, N., Jiménez, S., Wells, C.E., Contreras-Moreira, B., and Gogorcena, Y. (2016). Transcriptional Responses in Root and Leaf of Prunus persica under Drought Stress Using RNA Sequencing. Front. Plant Sci. *7*.

Kundariya, H., Yang, X., Morton, K., Sanchez, R., Axtell, M.J., Hutton, S.F., Fromm, M., and Mackenzie, S.A. (2020). MSH1-induced heritable enhanced growth vigor through grafting is associated with the RdDM pathway in plants. Nat. Commun. *11*, 1–14.

Kuromori, T., Miyaji, T., Yabuuchi, H., Shimizu, H., Sugimoto, E., Kamiya, A., Moriyama, Y., and Shinozaki, K. (2010). ABC transporter AtABCG25 is involved in abscisic acid transport and responses. Proc. Natl. Acad. Sci. *107*, 2361–2366.

Kuromori, T., Sugimoto, E., and Shinozaki, K. (2014). Intertissue Signal Transfer of Abscisic Acid from Vascular Cells to Guard Cells. PLANT Physiol. *164*, 1587–1592.

Kuromori, T., Seo, M., and Shinozaki, K. (2018). ABA Transport and Plant Water Stress Responses. Trends Plant Sci. *23*, 513–522.

Lamarque, L.J., Delzon, S., Toups, H., Gravel, A.-I., Corso, D., Badel, E., Burlett, R., Charrier, G., Cochard, H., Jansen, S., et al. (2019). Over-accumulation of abscisic acid in transgenic tomato plants increases the risk of hydraulic failure. Plant Cell Environ.

Lång, V., and Palva, E.T. (1992). The expression of a rab-related gene, rab18, is induced by abscisic acid during the cold acclimation process of Arabidopsis thaliana (L.) Heynh. Plant Mol. Biol. *20*, 951–962.

Langfelder, P., and Horvath, S. (2008). WGCNA: an R package for weighted correlation network analysis. BMC Bioinformatics *9*, 559.

Lee, K.H., Piao, H.L., Kim, H.-Y., Choi, S.M., Jiang, F., Hartung, W., Hwang, I., Kwak, J.M., Lee, I.-J., and Hwang, I. (2006). Activation of Glucosidase via Stress-Induced Polymerization Rapidly Increases Active Pools of Abscisic Acid. Cell *126*, 1109–1120.

Lehmann, H., and Glund, K. (1986). Abscisic acid metabolism-vacuolar/extravacuolar distribution of metabolites. Planta *168*, 559–562.

Lei, L., Shi, J., Chen, J., Zhang, M., Sun, S., Xie, S., Li, X., Zeng, B., Peng, L., Hauck, A., et al. (2015). Ribosome profiling reveals dynamic translational landscape in maize seedlings under drought stress. Plant J. *84*, 1206–1218.

Léran, S., Noguero, M., Corratgé-Faillie, C., Boursiac, Y., Brachet, C., and Lacombe, B. (2020). Functional Characterization of the Arabidopsis Abscisic Acid Transporters NPF4.5 and NPF4.6 in Xenopus Oocytes. Front. Plant Sci. *11*.

Lesk, C., Rowhani, P., and Ramankutty, N. (2016). Influence of extreme weather disasters on global crop production. Nature *529*, 84–87.

Li, T., Zhang, Y., Liu, Y., Li, X., Hao, G., Han, Q., Dirk, L.M.A., Downie, A.B., Ruan, Y.-L., Wang, J., et al. (2020). Raffinose synthase enhances drought tolerance through raffinose synthesis or galactinol hydrolysis in maize and *Arabidopsis* plants. J. Biol. Chem. *295*, 8064–8077.

Liao, Y., Smyth, G.K., and Shi, W. (2014). featureCounts: an efficient general purpose program for assigning sequence reads to genomic features. Bioinforma. Oxf. Engl. *30*, 923–930.

Lim, E.-K., Doucet, C.J., Hou, B., Jackson, R.G., Abrams, S.R., and Bowles, D.J. (2005). Resolution of (+)-abscisic acid using an Arabidopsis glycosyltransferase. Tetrahedron Asymmetry *16*, 143–147.

Lima, L.L., Balbi, B.P., Mesquita, R.O., Silva, J.C.F. da, Coutinho, F.S., Carmo, F.M.S., Vital, C.E., Mehta, A., Loureiro, M.E., Fontes, E.P.B., et al. (2019). Proteomic and Metabolomic Analysis of a Drought Tolerant Soybean Cultivar from Brazilian Savanna. Crop Breed. Genet. Genomics *1*.

Linden, H., Misawa, N., Saito, T., and Sandmann, G. (1994). A novel carotenoid biosynthesis gene coding for zeta-carotene desaturase: functional expression, sequence and phylogenetic origin. Plant Mol. Biol. *24*, 369–379.

Lippold, F., Sanchez, D.H., Musialak, M., Schlereth, A., Scheible, W.-R., Hincha, D.K., and Udvardi, M.K. (2009). AtMyb41 Regulates Transcriptional and Metabolic Responses to Osmotic Stress in Arabidopsis. Plant Physiol. *149*, 1761–1772.

Liu, S., Li, M., Su, L., Ge, K., Li, L., Li, X., Liu, X., and Li, L. (2016). Negative feedback regulation of ABA biosynthesis in peanut (Arachis hypogaea): a transcription factor complex inhibits AhNCED1 expression during water stress. Sci. Rep. *6*, 37943.

Liu, X., Yue, Y., Li, B., Nie, Y., Li, W., Wu, W.-H., and Ma, L. (2007). A G Protein-Coupled Receptor Is a Plasma Membrane Receptor for the Plant Hormone Abscisic Acid. Science *315*, 1712–1716.

Liu, Z., Yan, J.-P., Li, D.-K., Luo, Q., Yan, Q., Liu, Z.-B., Ye, L.-M., Wang, J.-M., Li, X.-F., and Yang, Y. (2015). UDP-Glucosyltransferase71C5, a Major Glucosyltransferase, Mediates Abscisic Acid Homeostasis in Arabidopsis. Plant Physiol. *167*, 1659–1670.

Love, M.I., Huber, W., and Anders, S. (2014). Moderated estimation of fold change and dispersion for RNA-seq data with DESeq2. Genome Biol. *15*.

Lovelli, S., Scopa, A., Perniola, M., Di Tommaso, T., and Sofo, A. (2012). Abscisic acid root and leaf concentration in relation to biomass partitioning in salinized tomato plants. J. Plant Physiol. *169*, 226–233.

Mamrutha, H.M., Nataraja, K.N., Rama, N., Kosma, D.K., Mogili, T., Lakshmi, K.J., Kumar, M.U., and Jenks, M.A. (2017). Leaf surface wax composition of genetically diverse mulberry (Morus sp.) genotypes and its close association with expression of genes involved in wax metabolism. Curr. Sci. *112*, 759–766.

Manzi, M., Lado, J., Rodrigo, M.J., Zacarías, L., Arbona, V., and Gómez-Cadenas, A. (2015). Root ABA Accumulation in Long-Term Water-Stressed Plants is Sustained by Hormone Transport from Aerial Organs. Plant Cell Physiol. *56*, 2457–2466.

McAdam, S.A.M., and Brodribb, T.J. (2018). Mesophyll Cells Are the Main Site of Abscisic Acid Biosynthesis in Water-Stressed Leaves. Plant Physiol. *177*, 911–917.

McAdam, S.A.M., Manzi, M., Ross, J.J., Brodribb, T.J., and Gómez-Cadenas, A. (2016). Uprooting an abscisic acid paradigm: Shoots are the primary source. Plant Signal. Behav. *11*, e1169359.

Mergner, J., Frejno, M., List, M., Papacek, M., Chen, X., Chaudhary, A., Samaras, P., Richter, S., Shikata, H., Messerer, M., et al. (2020a). Mass-spectrometry-based draft of the Arabidopsis proteome. Nature *579*, 409–414.

Mergner, J., Frejno, M., Messerer, M., Lang, D., Samaras, P., Wilhelm, M., Mayer, K.F.X., Schwechheimer, C., and Kuster, B. (2020b). Proteomic and transcriptomic profiling of aerial organ development in Arabidopsis. Sci. Data *7*, 334.

Merilo, E., Jalakas, P., Laanemets, K., Mohammadi, O., Hõrak, H., Kollist, H., and Brosché, M. (2015). Abscisic Acid Transport and Homeostasis in the Context of Stomatal Regulation. Mol. Plant *8*, 1321–1333.

Min, X., Lin, X., NDAYAMBAZA, B., Wang, Y., and Liu, W. (2020). Coordinated mechanisms of leaves and roots in response to drought stress underlying full-length transcriptome profiling in Vicia sativa L. BMC Plant Biol. *20*, 165.

Minio, A., Massonnet, M., Vondras, A., Figueroa-Balderas, R., Blanco-Ulate, B., and Cantu, D. (2018). Iso-Seq allows genome-independent transcriptome profiling of grape berry development (Genomics).

Mohamed, I.A.A., Shalby, N., Bai, C., Qin, M., Agami, R.A., Jie, K., Wang, B., and Zhou, G. (2020). Stomatal and Photosynthetic Traits Are Associated with Investigating Sodium Chloride Tolerance of Brassica napus L. Cultivars. Plants *9*.

Monteverde, C., and De Sales, F. (2020). Impacts of global warming on southern California's winegrape climate suitability. Adv. Clim. Change Res. *11*, 279–293.

Mundy, J., Yamaguchi-Shinozaki, K., and Chua, N.H. (1990). Nuclear proteins bind conserved elements in the abscisic acid-responsive promoter of a rice rab gene. Proc. Natl. Acad. Sci. *87*, 1406–1410.

Mustilli, A.-C., Merlot, S., Vavasseur, A., Fenzi, F., and Giraudat, J. (2002). Arabidopsis OST1 Protein Kinase Mediates the Regulation of Stomatal Aperture by Abscisic Acid and Acts Upstream of Reactive Oxygen Species Production. Plant Cell *14*, 3089–3099.

Nakashima, K., Fujita, Y., Kanamori, N., Katagiri, T., Umezawa, T., Kidokoro, S., Maruyama, K., Yoshida, T., Ishiyama, K., Kobayashi, M., et al. (2009). Three Arabidopsis SnRK2 Protein Kinases, SRK2D/SnRK2.2, SRK2E/SnRK2.6/OST1 and SRK2I/SnRK2.3, Involved in ABA Signaling are Essential for the Control of Seed Development and Dormancy. Plant Cell Physiol. *50*, 1345–1363.

Nambara, E., and Marion-Poll, A. (2005). ABSCISIC ACID BIOSYNTHESIS AND CATABOLISM. Annu. Rev. Plant Biol. *56*, 165–185.

Niyogi, K.K. (1999). PHOTOPROTECTION REVISITED: Genetic and Molecular Approaches. Annu. Rev. Plant Physiol. Plant Mol. Biol. *50*, 333–359.

Pagliarani, C., Vitali, M., Ferrero, M., Vitulo, N., Incarbone, M., Lovisolo, C., Valle, G., and Schubert, A. (2017). The Accumulation of miRNAs Differentially Modulated by Drought Stress Is Affected by Grafting in Grapevine. Plant Physiol. *173*, 2180–2195.

Pandey, S., Nelson, D.C., and Assmann, S.M. (2009). Two Novel GPCR-Type G Proteins Are Abscisic Acid Receptors in Arabidopsis. Cell *136*, 136–148.

Parent, B., Hachez, C., Redondo, E., Simonneau, T., Chaumont, F., and Tardieu, F. (2009). Drought and Abscisic Acid Effects on Aquaporin Content Translate into Changes in Hydraulic Conductivity and Leaf Growth Rate: A Trans-Scale Approach. Plant Physiol. *149*, 2000–2012.

Park, S.-Y., Fung, P., Nishimura, N., Jensen, D.R., Fujii, H., Zhao, Y., Lumba, S., Santiago, J., Rodrigues, A., Chow, T. -f. F., et al. (2009). Abscisic Acid Inhibits Type 2C Protein Phosphatases via the PYR/PYL Family of START Proteins. Science 1173041.

Pavlousek, P. (2011). Evaluation of drought tolerance of new grapevine rootstock hybrids. J. Environ. Biol. *32*, 543–549.

Pleiss, J.A., Whitworth, G.B., Bergkessel, M., and Guthrie, C. (2007). Rapid, Transcript-Specific Changes in Splicing in Response to Environmental Stress. Mol. Cell *27*, 928–937.

Potenza, E., Racchi, M.L., Sterck, L., Coller, E., Asquini, E., Tosatto, S.C.E., Velasco, R., Van de Peer, Y., and Cestaro, A. (2015). Exploration of alternative splicing events in ten different grapevine cultivars. BMC Genomics *16*.

Qin, X., and Zeevaart, J.A.D. (1999). The 9-cis-epoxycarotenoid cleavage reaction is the key regulatory step of abscisic acid biosynthesis in water-stressed bean. Proc. Natl. Acad. Sci. *96*, 15354–15361.

R Core Team (2018). R: The R Project for Statistical Computing.

Rattanakon, S., Ghan, R., Gambetta, G.A., Deluc, L.G., Schlauch, K.A., and Cramer, G.R. (2016). Abscisic acid transcriptomic signaling varies with grapevine organ. BMC Plant Biol. *16*.

Ren, H., Gao, Z., Chen, L., Wei, K., Liu, J., Fan, Y., Davies, W.J., Jia, W., and Zhang, J. (2007). Dynamic analysis of ABA accumulation in relation to the rate of ABA catabolism in maize tissues under water deficit. J. Exp. Bot. *58*, 211–219.

Riccardi, F., Gazeau, P., Jacquemot, M.-P., Vincent, D., and Zivy, M. (2004). Deciphering genetic variations of proteome responses to water deficit in maize leaves. Plant Physiol. Biochem. *42*, 1003–1011.

Rodríguez-Concepción, M., and Boronat, A. (2002). Elucidation of the Methylerythritol Phosphate Pathway for Isoprenoid Biosynthesis in Bacteria and Plastids. A Metabolic Milestone Achieved through Genomics. Plant Physiol. *130*, 1079–1089.

Rossdeutsch, L., Edwards, E., Cookson, S.J., Barrieu, F., Gambetta, G.A., Delrot, S., and Ollat, N. (2016). ABA-mediated responses to water deficit separate grapevine genotypes by their genetic background. BMC Plant Biol. *16*, 91.

Ruiz-Sola, M.Á., and Rodríguez-Concepción, M. (2012). Carotenoid Biosynthesis in Arabidopsis: A Colorful Pathway. Arab. Book Am. Soc. Plant Biol. *10*.

Sade, N., and Moshelion, M. (2014). The dynamic isohydric–anisohydric behavior of plants upon fruit development: taking a risk for the next generation. Tree Physiol. *34*, 1199–1202.

Saritha, K., Vijaya, D., Srinivas Rao, B., and Padma, M. (2017). Relative Salt Tolerance of Different Grape Rootstocks to Different Chloride Salts. Int. J. Curr. Microbiol. Appl. Sci. *6*, 24–33.

Schultz, H.R. (2003). Differences in hydraulic architecture account for near-isohydric and anisohydric behaviour of two field-grown Vitis vinifera L. cultivars during drought. Plant Cell Environ. *26*, 1393–1405.

Schwartz, S.H. (1997). Specific Oxidative Cleavage of Carotenoids by VP14 of Maize. Science *276*, 1872–1874.

Schwartz, S.H., Léon-Kloosterziel, K.M., Koornneef, M., and Zeevaart, J.A. (1997). Biochemical characterization of the aba2 and aba3 mutants in Arabidopsis thaliana. Plant Physiol. *114*, 161–166.

Schwartz, S.H., Qin, X., and Zeevaart, J.A.D. (2003). Elucidation of the Indirect Pathway of Abscisic Acid Biosynthesis by Mutants, Genes, and Enzymes. Plant Physiol. *131*, 1591–1601.

Seo, M., Peeters, A.J.M., Koiwai, H., Oritani, T., Marion-Poll, A., Zeevaart, J.A.D., Koornneef, M., Kamiya, Y., and Koshiba, T. (2000). The Arabidopsis aldehyde oxidase 3 (AAO3) gene product catalyzes the final step in abscisic acid biosynthesis in leaves. Proc. Natl. Acad. Sci. U. S. A. *97*, 12908–12913.

Shen, Y.-Y., Wang, X.-F., Wu, F.-Q., Du, S.-Y., Cao, Z., Shang, Y., Wang, X.-L., Peng, C.-C., Yu, X.-C., Zhu, S.-Y., et al. (2006). The Mg-chelatase H subunit is an abscisic acid receptor. Nature *443*, 823–826.

Srivastava, A.K., Lu, Y., Zinta, G., Lang, Z., and Zhu, J.-K. (2018). UTR dependent control of gene expression in plants. Trends Plant Sci. *23*, 248–259.

Suarez, D.L., Celis, N., Anderson, R.G., and Sandhu, D. (2019). Grape Rootstock Response to Salinity, Water and Combined Salinity and Water Stresses. Agronomy *9*, 321.

Sussmilch, F.C., Brodribb, T.J., and McAdam, S.A.M. (2017). Up-regulation of NCED3 and ABA biosynthesis occur within minutes of a decrease in leaf turgor but AHK1 is not required. J. Exp. Bot. *68*, 2913–2918.

Taji, T., Ohsumi, C., Iuchi, S., Seki, M., Kasuga, M., Kobayashi, M., Yamaguchi-Shinozaki, K., and Shinozaki, K. (2002). Important roles of drought- and cold-inducible genes for galactinol synthase in stress tolerance in Arabidopsis thaliana. Plant J. *29*, 417–426.

Takahashi, F., Suzuki, T., Osakabe, Y., Betsuyaku, S., Kondo, Y., Dohmae, N., Fukuda, H., Yamaguchi-Shinozaki, K., and Shinozaki, K. (2018). A small peptide modulates stomatal control via abscisic acid in long-distance signalling. Nature *556*, 235–238.

Tamburino, R., Vitale, M., Ruggiero, A., Sassi, M., Sannino, L., Arena, S., Costa, A., Batelli, G., Zambrano, N., Scaloni, A., et al. (2017). Chloroplast proteome response to drought stress and recovery in tomato (Solanum lycopersicum L.). BMC Plant Biol. *17*, 40.

Tan, B.C., Schwartz, S.H., Zeevaart, J.A.D., and McCarty, D.R. (1997). Genetic control of abscisic acid biosynthesis in maize. Proc. Natl. Acad. Sci. *94*, 12235–12240.

Tan, B.-C., Cline, K., and McCarty, D.R. (2001). Localization and targeting of the VP14 epoxy-carotenoid dioxygenase to chloroplast membranes. Plant J. *27*, 373–382.

Tardieu, F., and Simonneau, T. (1998). Variability among species of stomatal control under fluctuating soil water status and evaporative demand: modelling isohydric and anisohydric behaviours. J. Exp. Bot. *49*, 419–432.

Taylor, S.C., and Posch, A. (2014). The Design of a Quantitative Western Blot Experiment (Hindawi).

Thameur, A., Ferchichi, A., and López-Carbonell, M. (2011). Quantification of free and conjugated abscisic acid in five genotypes of barley (Hordeum vulgare L.) under water stress conditions. South Afr. J. Bot. *77*, 222–228.

Tombesi, S., Nardini, A., Frioni, T., Soccolini, M., Zadra, C., Farinelli, D., Poni, S., and Palliotti, A. (2015). Stomatal closure is induced by hydraulic signals and maintained by ABA in drought-stressed grapevine. Sci. Rep. *5*, 12449.

Tu, M., Wang, X., Zhu, Y., Wang, D., Zhang, X., Cui, Y., Li, Y., Gao, M., Li, Z., Wang, Y., et al. (2018). VlbZIP30 of grapevine functions in dehydration tolerance via the abscisic acid core signaling pathway. Hortic. Res. *5*, 1–15.

Tyree, M.T., and Hammel, H.T. (1972). The Measurement of the Turgor Pressure and the Water Relations of Plants by the Pressure-bomb Technique. J. Exp. Bot. *23*, 267–282.

Um, M.-J., Kim, Y., Park, D., and Kim, J. (2017). Effects of different reference periods on drought index (SPEI) estimations from 1901 to 2014. Hydrol. Earth Syst. Sci. *21*, 4989–5007.

Umezawa, T., Sugiyama, N., Takahashi, F., Anderson, J.C., Ishihama, Y., Peck, S.C., and Shinozaki, K. (2013). Genetics and Phosphoproteomics Reveal a Protein Phosphorylation Network in the Abscisic Acid Signaling Pathway in Arabidopsis thaliana. Sci. Signal. *6*, rs8–rs8.

Vitulo, N., Forcato, C., Carpinelli, E.C., Telatin, A., Campagna, D., D'Angelo, M., Zimbello, R., Corso, M., Vannozzi, A., Bonghi, C., et al. (2014). A deep survey of alternative splicing in grape reveals changes in the splicing machinery related to tissue, stress condition and genotype. BMC Plant Biol. *14*.

Vlad, F., Turk, B.E., Peynot, P., Leung, J., and Merlot, S. (2008). A versatile strategy to define the phosphorylation preferences of plant protein kinases and screen for putative substrates. Plant J. *55*, 104–117.

Walter, J., Nagy, L., Hein, R., Rascher, U., Beierkuhnlein, C., Willner, E., and Jentsch, A. (2011). Do plants remember drought? Hints towards a drought-memory in grasses. Environ. Exp. Bot. *71*, 34–40.

Wang, P., Xue, L., Batelli, G., Lee, S., Hou, Y.-J., Van Oosten, M.J., Zhang, H., Tao, W.A., and Zhu, J.-K. (2013). Quantitative phosphoproteomics identifies SnRK2 protein kinase substrates and reveals the effectors of abscisic acid action. Proc. Natl. Acad. Sci. U. S. A. *110*, 11205–11210.

Wessel, D., and Flügge, U.I. (1984). A method for the quantitative recovery of protein in dilute solution in the presence of detergents and lipids. Anal. Biochem. *138*, 141–143.

Winter, D., Vinegar, B., Nahal, H., Ammar, R., Wilson, G.V., and Provart, N.J. (2007). An "Electronic Fluorescent Pictograph" Browser for Exploring and Analyzing Large-Scale Biological Data Sets. PLoS ONE *2*, e718.

Wong, D.C.J., Zhang, L., Merlin, I., Castellarin, S.D., and Gambetta, G.A. (2018). Structure and transcriptional regulation of the major intrinsic protein gene family in grapevine. BMC Genomics *19*, 248.

Xu, Z.-Y., Lee, K.H., Dong, T., Jeong, J.C., Jin, J.B., Kanno, Y., Kim, D.H., Kim, S.Y., Seo, M., Bressan, R.A., et al. (2012). A Vacuolar β-Glucosidase Homolog That Possesses

Glucose-Conjugated Abscisic Acid Hydrolyzing Activity Plays an Important Role in Osmotic Stress Responses in Arabidopsis. Plant Cell *24*, 2184–2199.

Xu, Z.-Y., Yoo, Y.-J., and Hwang, I. (2014). ABA Conjugates and Their Physiological Roles in Plant Cells. In Abscisic Acid: Metabolism, Transport and Signaling, D.-P. Zhang, ed. (Dordrecht: Springer Netherlands), pp. 77–87.

Yang, Y., Guo, Y., Zhong, J., Zhang, T., Li, D., Ba, T., Xu, T., Chang, L., Zhang, Q., and Sun, M. (2020). Root Physiological Traits and Transcriptome Analyses Reveal that Root Zone Water Retention Confers Drought Tolerance to Opisthopappus taihangensis. Sci. Rep. *10*, 2627.

Yoshida, T., Fujita, Y., Sayama, H., Kidokoro, S., Maruyama, K., Mizoi, J., Shinozaki, K., and Yamaguchi-Shinozaki, K. (2010). AREB1, AREB2, and ABF3 are master transcription factors that cooperatively regulate ABRE-dependent ABA signaling involved in drought stress tolerance and require ABA for full activation. Plant J. *61*, 672–685.

Zarrouk, O., Garcia-Tejero, I., Pinto, C., Genebra, T., Sabir, F., Prista, C., David, T.S., Loureiro-Dias, M.C., and Chave, M.M. (2016). Aquaporins isoforms in cv. Touriga Nacional grapevine under water stress and recovery—Regulation of expression in leaves and roots. Agric. Water Manag. *164*, 167–175.

Zeng, J., Wang, C., Chen, X., Zang, M., Yuan, C., Wang, X., Wang, Q., Li, M., Li, X., Chen, L., et al. (2015). The lycopene β-cyclase plays a significant role in provitamin A biosynthesis in wheat endosperm. BMC Plant Biol. *15*.

Zhang, J., Schurr, U., and Davies, W.J. (1987). Control of Stomatal Behaviour by Abscisic Acid which Apparently Originates in the Roots. J. Exp. Bot. *38*, 1174–1181.

(1999). The zeaxanthin biosynthesis enzyme ^{2}-carotene hydroxylase is involved in myxoxanthophyll synthesis in Synechocystis sp. PCC 6803. FEBS Lett. *454*, 247–251.

Figures

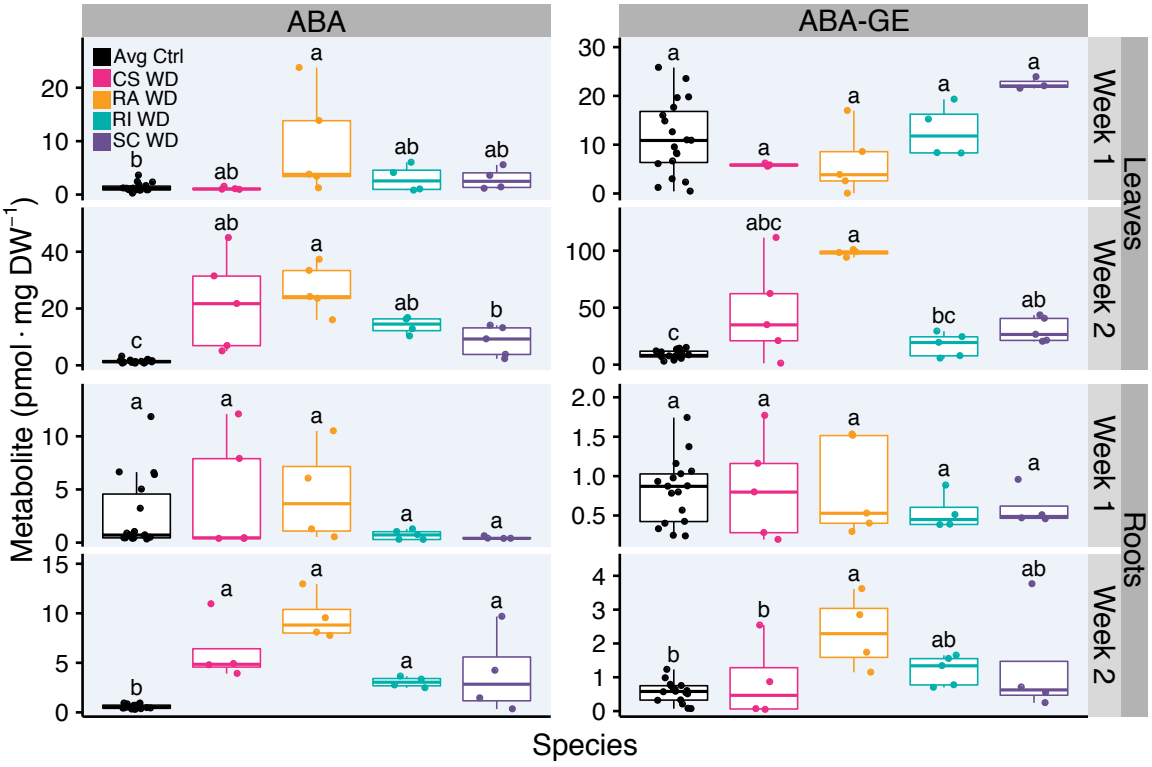

Figure 1: ABA and ABA-GE concentrations after one- and two-weeks of moderate WD. ABA (left) and ABA-GE (right) concentrations (pmol·mg DW^{-1}) in leaves (top) and roots (bottom) after one- and two-weeks of Control (Ctrl) or WD treatment. Control represented for all species per organ per time; there was no significant difference between Control species per organ per week. Two-way ANOVA Tukey's HSD ($p \leq 0.05$) letters for each metabolite per organ per week. Black corresponds the Control values for all species. Pink, orange, blue and purple correspond to CS, RA, RI, and SC respectively. Each point represents an individual measurement. n = three-five individual vines.

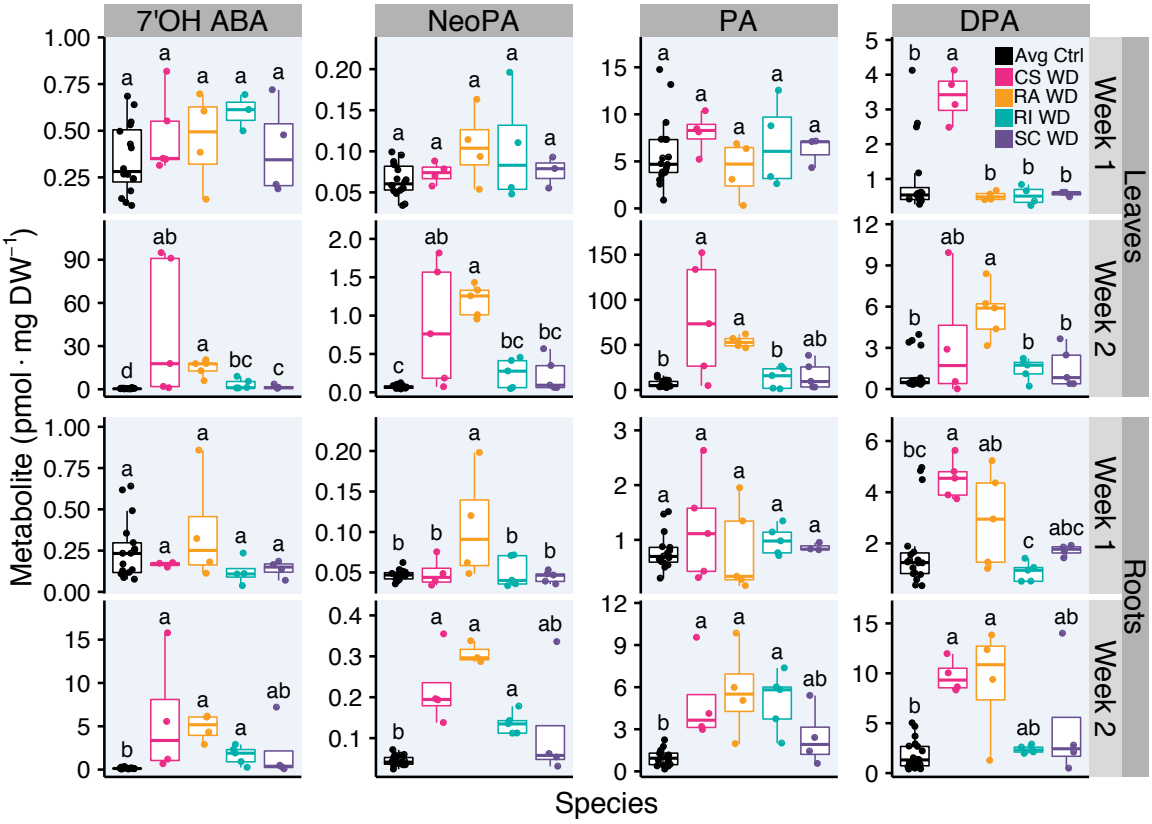

Figure 2: ABA catabolite concentrations after one- and two-weeks of moderate WD. 7'OH ABA, NeoPA, PA, and DPA (left to right) concentrations (pmol·mg DW^{-1}) in leaves (top) and roots (bottom) after one- and two-weeks of Control (Ctrl) or WD treatment. Control represented for all species per organ per time; there was no significant difference between Controls per species per organ per week. Two-way ANOVA Tukey's HSD ($p \leq 0.05$) letters for each metabolite per organ per week. Black corresponds the Control values for all species. Pink, orange, blue and purple correspond to CS, RA, RI, and SC respectively. Each point represents an individual measurement. n = three-five individual vines.

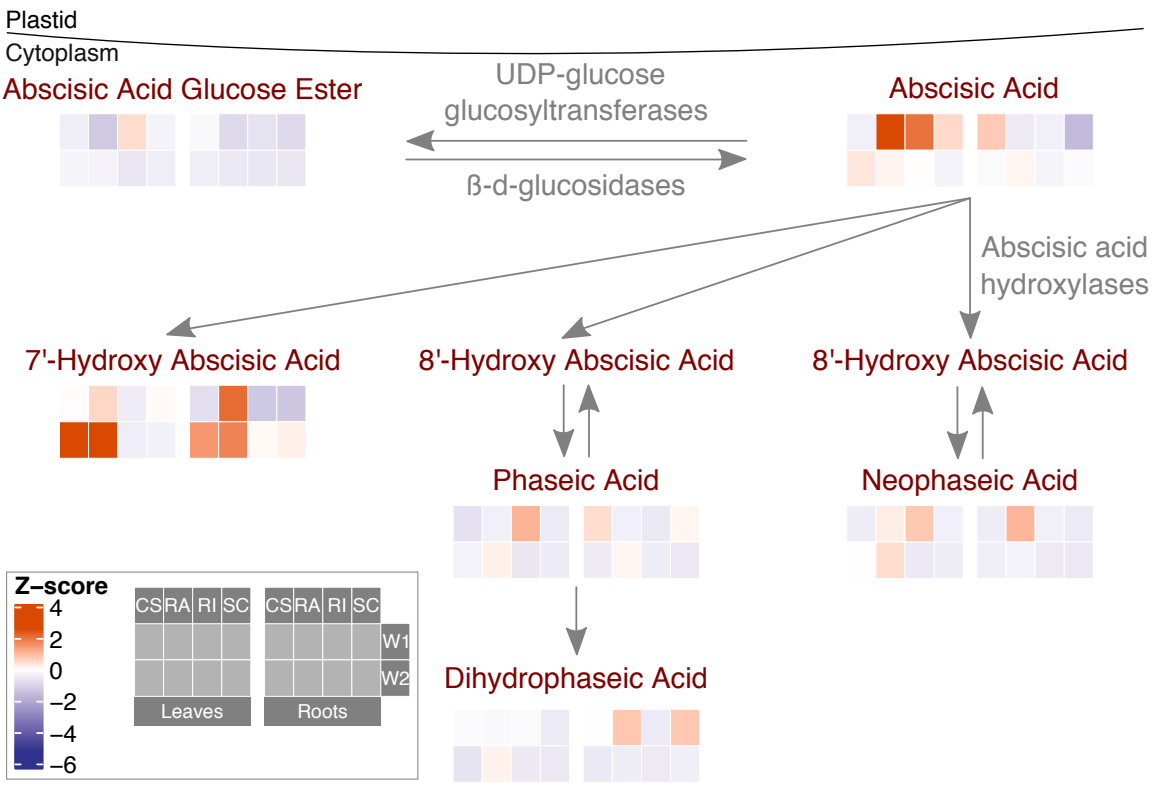

Figure 3: Average relative ABA metabolite concentrations after moderate WD. Heatmap representation of the average ratio of ABA box-cox transformed metabolite concentrations (WD:C) in leaves (left) and roots (right) after one- (top) and two-weeks (bottom) treatment in the four *Vitis* species (CS, RA, RI, SC from left to right per organ). Z-scores calculated for all metabolites and conditions as a group with red corresponding to higher and blue corresponding to lower scores. ABA metabolites in red and corresponding genes in grey. Cellular location indicated in black.

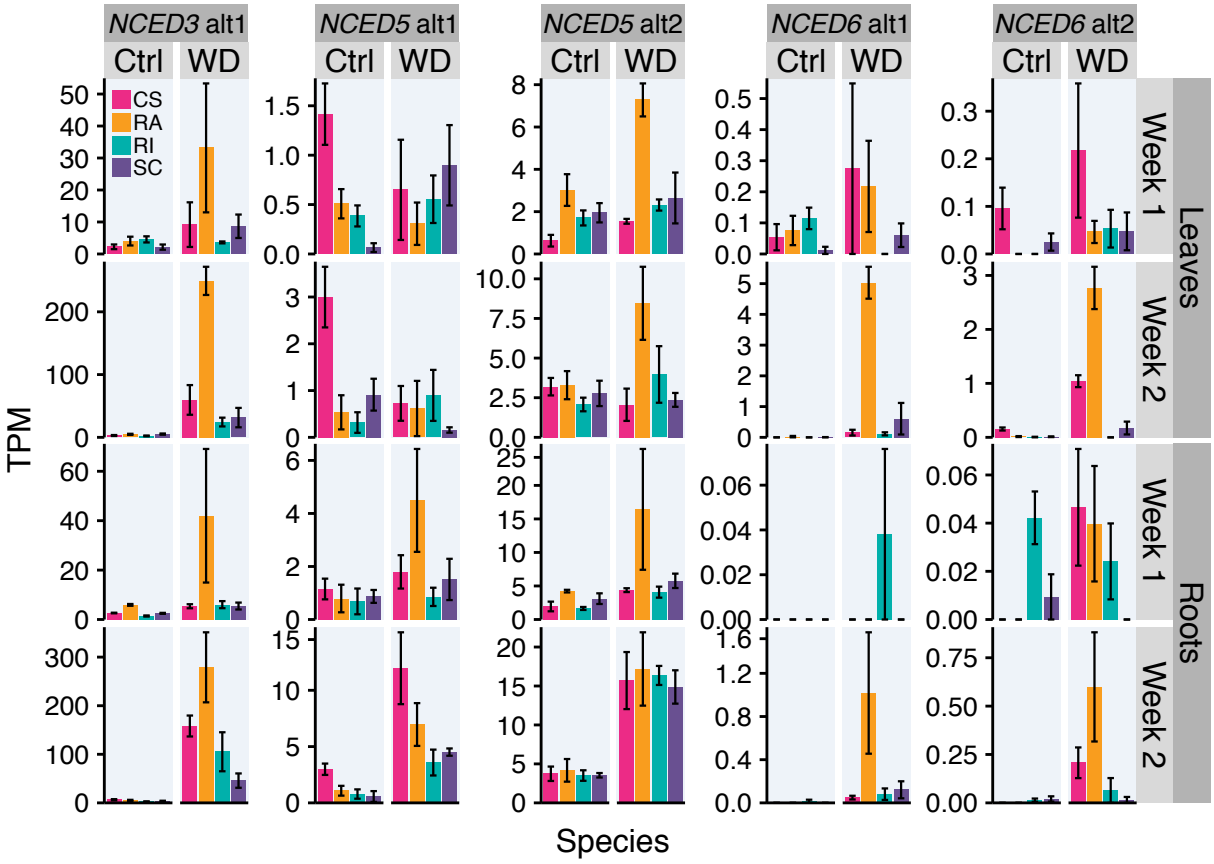

Figure 4: *NCED* transcript abundance after one- and two-weeks of moderate WD. *NCED3*, *NCED5* alt1 and alt2, *NCED6* alt1 and alt2 (left to right) expression represented as TPM after one- (top) and two-weeks (bottom) of Control (Ctrl) (left) or WD (right) treatment in leaves (top) and roots (bottom). Pink, orange, blue and purple correspond to CS, RA, RI, and SC respectively. Mean ± SE, n = three-five individual vines.

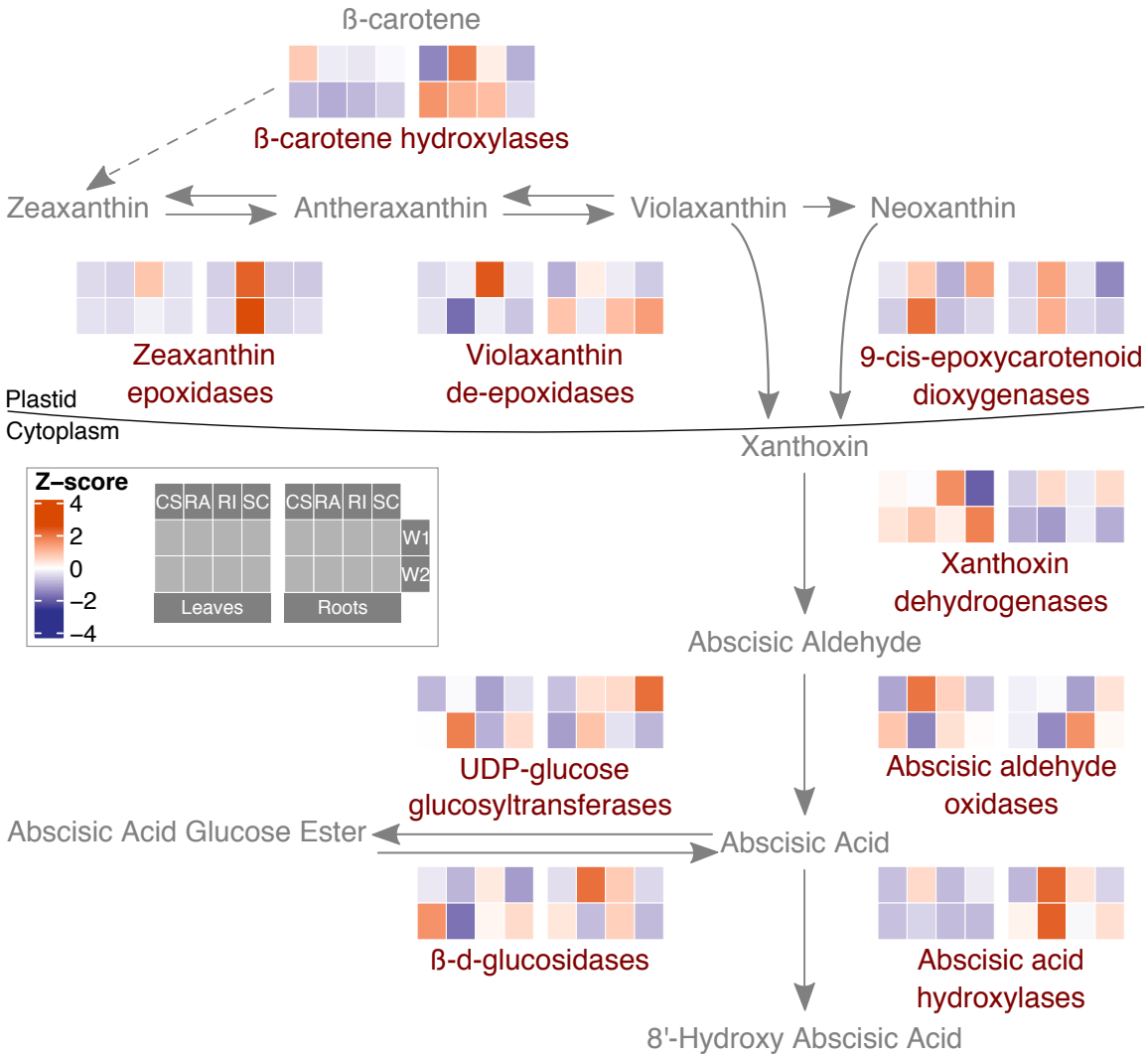

Figure 5: Average relative ABA metabolite gene transcript abundance after moderate WD. Heatmap representation of the average ratio of $\log_2$ box-cox transformed ABA metabolite gene TPM (WD:C) in leaves (left) and roots (right) after one- (top) and two-weeks (bottom) treatment in the four *Vitis* species (CS, RA, RI, SC from left to right per organ). Z-scores calculated for all per gene group (average of multiple paralogs) for all conditions with red corresponding to higher and blue corresponding to lower scores. ABA metabolite genes in red and resultant metabolites in grey. Cellular location indicated in black.

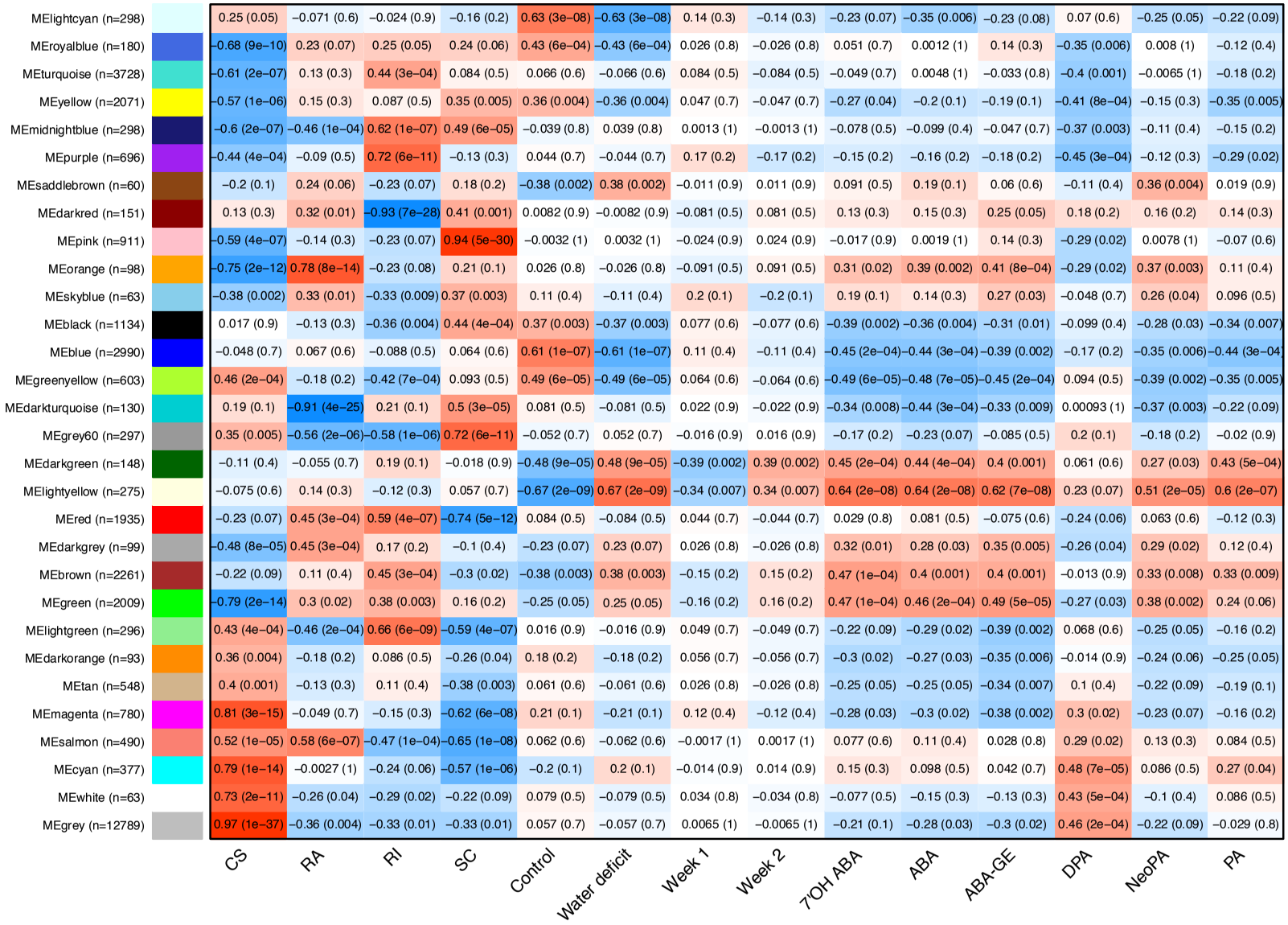
MElightcyan (n=298) 0.25 (0.05) −0.071 (0.6) −0.024 (0.9) −0.16 (0.2) 0.63 (3e−08) −0.63 (3e−08) 0.14 (0.3) −0.14 (0.3) −0.23 (0.07) −0.35 (0.006) −0.23 (0.08) 0.07 (0.6) −0.25 (0.05) −0.22 (0.09)
MEroyalblue (n=180) −0.68 (9e−10) 0.23 (0.07) 0.25 (0.05) 0.24 (0.06) 0.43 (6e−04) −0.43 (6e−04) 0.026 (0.8) −0.026 (0.8) 0.051 (0.7) 0.0012 (1) 0.14 (0.3) −0.35 (0.006) 0.008 (1) −0.12 (0.4)
MEturquoise (n=3728) −0.61 (2e−07) 0.13 (0.3) 0.44 (3e−04) 0.084 (0.5) 0.066 (0.6) −0.066 (0.6) 0.084 (0.5) −0.084 (0.5) −0.049 (0.7) 0.0048 (1) −0.033 (0.8) −0.4 (0.001) −0.0065 (1) −0.18 (0.2)
MEyellow (n=2071) −0.57 (1e−06) 0.15 (0.3) 0.087 (0.5) 0.35 (0.005) 0.36 (0.004) −0.36 (0.004) 0.047 (0.7) −0.047 (0.7) −0.27 (0.04) −0.2 (0.1) −0.19 (0.1) −0.41 (8e−04) −0.15 (0.3) −0.35 (0.005)
MEmidnightblue (n=298) −0.6 (2e−07) −0.46 (1e−04) 0.62 (1e−07) 0.49 (6e−05) −0.039 (0.8) 0.039 (0.8) 0.0013 (1) −0.0013 (1) −0.078 (0.5) −0.099 (0.4) −0.047 (0.7) −0.37 (0.003) −0.11 (0.4) −0.15 (0.2)
MEpurple (n=696) −0.44 (4e−04) −0.09 (0.5) 0.72 (6e−11) −0.13 (0.3) 0.044 (0.7) −0.044 (0.7) 0.17 (0.2) −0.17 (0.2) −0.15 (0.2) −0.16 (0.2) −0.18 (0.2) −0.45 (3e−04) −0.12 (0.3) −0.29 (0.02)
MEsaddlebrown (n=60) −0.2 (0.1) 0.24 (0.06) −0.23 (0.07) 0.18 (0.2) −0.38 (0.002) 0.38 (0.002) −0.011 (0.9) 0.011 (0.9) 0.091 (0.5) 0.19 (0.1) 0.06 (0.6) −0.11 (0.4) 0.36 (0.004) 0.019 (0.9)
MEdarkred (n=151) 0.13 (0.3) 0.32 (0.01) −0.93 (7e−28) 0.41 (0.001) 0.0082 (0.9) −0.0082 (0.9) −0.081 (0.5) 0.081 (0.5) 0.13 (0.3) 0.15 (0.3) 0.25 (0.05) 0.18 (0.2) 0.16 (0.2) 0.14 (0.3)
MEpink (n=911) −0.59 (4e−07) −0.14 (0.3) −0.23 (0.07) 0.94 (5e−30) −0.0032 (1) 0.0032 (1) −0.024 (0.9) 0.024 (0.9) −0.017 (0.9) 0.0019 (1) 0.14 (0.3) −0.29 (0.02) 0.0078 (1) −0.07 (0.6)
MEorange (n=98) −0.75 (2e−12) 0.78 (8e−14) −0.23 (0.08) 0.21 (0.1) 0.026 (0.8) −0.026 (0.8) −0.091 (0.5) 0.091 (0.5) 0.31 (0.02) 0.39 (0.002) 0.41 (8e−04) −0.29 (0.02) 0.37 (0.003) 0.11 (0.4)
MEskyblue (n=63) −0.38 (0.002) 0.33 (0.01) −0.33 (0.009) 0.37 (0.003) 0.11 (0.4) −0.11 (0.4) 0.2 (0.1) −0.2 (0.1) 0.19 (0.1) 0.14 (0.3) 0.27 (0.03) −0.048 (0.7) 0.26 (0.04) 0.096 (0.5)
MEblack (n=1134) 0.017 (0.9) −0.13 (0.3) −0.36 (0.004) 0.44 (4e−04) 0.37 (0.003) −0.37 (0.003) 0.077 (0.6) −0.077 (0.6) −0.39 (0.002) −0.36 (0.004) −0.31 (0.01) −0.099 (0.4) −0.28 (0.03) −0.34 (0.007)
MEblue (n=2990) −0.048 (0.7) 0.067 (0.6) −0.088 (0.5) 0.064 (0.6) 0.61 (1e−07) −0.61 (1e−07) 0.11 (0.4) −0.11 (0.4) −0.45 (2e−04) −0.44 (3e−04) −0.39 (0.002) −0.17 (0.2) −0.35 (0.006) −0.44 (3e−04)
MEgreenyellow (n=603) 0.46 (2e−04) −0.18 (0.2) −0.42 (7e−04) 0.093 (0.5) 0.49 (6e−05) −0.49 (6e−05) 0.064 (0.6) −0.064 (0.6) −0.49 (6e−05) −0.48 (7e−05) −0.45 (2e−04) 0.094 (0.5) −0.39 (0.002) −0.35 (0.005)
MEdarkturquoise (n=130) 0.19 (0.1) −0.91 (4e−25) 0.21 (0.1) 0.5 (3e−05) 0.081 (0.5) −0.081 (0.5) 0.022 (0.9) −0.022 (0.9) −0.34 (0.008) −0.44 (3e−04) −0.33 (0.009) 0.00093 (1) −0.37 (0.003) −0.22 (0.09)
MEgrey60 (n=297) 0.35 (0.005) −0.56 (2e−06) −0.58 (1e−06) 0.72 (6e−11) −0.052 (0.7) 0.052 (0.7) −0.016 (0.9) 0.016 (0.9) −0.17 (0.2) −0.23 (0.07) −0.085 (0.5) 0.2 (0.1) −0.18 (0.2) −0.02 (0.9)
MEdarkgreen (n=148) −0.11 (0.4) −0.055 (0.7) 0.19 (0.1) −0.018 (0.9) −0.48 (9e−05) 0.48 (9e−05) −0.39 (0.002) 0.39 (0.002) 0.45 (2e−04) 0.44 (4e−04) 0.4 (0.001) 0.061 (0.6) 0.27 (0.03) 0.43 (5e−04)
MElightyellow (n=275) −0.075 (0.6) 0.14 (0.3) −0.12 (0.3) 0.057 (0.7) −0.67 (2e−09) 0.67 (2e−09) −0.34 (0.007) 0.34 (0.007) 0.64 (2e−08) 0.64 (2e−08) 0.62 (7e−08) 0.23 (0.07) 0.51 (2e−05) 0.6 (2e−07)
MEred (n=1935) −0.23 (0.07) 0.45 (3e−04) 0.59 (4e−07) −0.74 (5e−12) 0.084 (0.5) −0.084 (0.5) 0.044 (0.7) −0.044 (0.7) 0.029 (0.8) 0.081 (0.5) −0.075 (0.6) −0.24 (0.06) 0.063 (0.6) −0.12 (0.3)
MEdarkgrey (n=99) −0.48 (8e−05) 0.45 (3e−04) 0.17 (0.2) −0.1 (0.4) −0.23 (0.07) 0.23 (0.07) 0.026 (0.8) −0.026 (0.8) 0.32 (0.01) 0.28 (0.03) 0.35 (0.005) −0.26 (0.04) 0.29 (0.02) 0.12 (0.4)
MEbrown (n=2261) −0.22 (0.09) 0.11 (0.4) 0.45 (3e−04) −0.3 (0.02) −0.38 (0.003) 0.38 (0.003) −0.15 (0.2) 0.15 (0.2) 0.47 (1e−04) 0.4 (0.001) 0.4 (0.001) −0.013 (0.9) 0.33 (0.008) 0.33 (0.009)
MEgreen (n=2009) −0.79 (2e−14) 0.3 (0.02) 0.38 (0.003) 0.16 (0.2) −0.25 (0.05) 0.25 (0.05) −0.16 (0.2) 0.16 (0.2) 0.47 (1e−04) 0.46 (2e−04) 0.49 (5e−05) −0.27 (0.03) 0.38 (0.002) 0.24 (0.06)
MElightgreen (n=296) 0.43 (4e−04) −0.46 (2e−04) 0.66 (6e−09) −0.59 (4e−07) 0.016 (0.9) −0.016 (0.9) 0.049 (0.7) −0.049 (0.7) −0.22 (0.09) −0.29 (0.02) −0.39 (0.002) 0.068 (0.6) −0.25 (0.05) −0.16 (0.2)
MEdarkorange (n=93) 0.36 (0.004) −0.18 (0.2) 0.086 (0.5) −0.26 (0.04) 0.18 (0.2) −0.18 (0.2) 0.056 (0.7) −0.056 (0.7) −0.3 (0.02) −0.27 (0.03) −0.35 (0.006) −0.014 (0.9) −0.24 (0.06) −0.25 (0.05)
MEtan (n=548) 0.4 (0.001) −0.13 (0.3) 0.11 (0.4) −0.38 (0.003) 0.061 (0.6) −0.061 (0.6) 0.026 (0.8) −0.026 (0.8) −0.25 (0.05) −0.25 (0.05) −0.34 (0.007) 0.1 (0.4) −0.22 (0.09) −0.19 (0.1)
MEmagenta (n=780) 0.81 (3e−15) −0.049 (0.7) −0.15 (0.3) −0.62 (6e−08) 0.21 (0.1) −0.21 (0.1) 0.12 (0.4) −0.12 (0.4) −0.28 (0.03) −0.3 (0.02) −0.38 (0.002) 0.3 (0.02) −0.23 (0.07) −0.16 (0.2)
MEsalmon (n=490) 0.52 (1e−05) 0.58 (6e−07) −0.47 (1e−04) −0.65 (1e−08) 0.062 (0.6) −0.062 (0.6) −0.0017 (1) 0.0017 (1) 0.077 (0.6) 0.11 (0.4) 0.028 (0.8) 0.29 (0.02) 0.13 (0.3) 0.084 (0.5)
MEcyan (n=377) 0.79 (1e−14) −0.0027 (1) −0.24 (0.06) −0.57 (1e−06) −0.2 (0.1) 0.2 (0.1) −0.014 (0.9) 0.014 (0.9) 0.15 (0.3) 0.098 (0.5) 0.042 (0.7) 0.48 (7e−05) 0.086 (0.5) 0.27 (0.04)
MEwhite (n=63) 0.73 (2e−11) −0.26 (0.04) −0.29 (0.02) −0.22 (0.09) 0.079 (0.5) −0.079 (0.5) 0.034 (0.8) −0.034 (0.8) −0.077 (0.5) −0.15 (0.3) −0.13 (0.3) 0.43 (5e−04) −0.1 (0.4) 0.086 (0.5)
MEgrey (n=12789) 0.97 (1e−37) −0.36 (0.004) −0.33 (0.01) −0.33 (0.01) 0.057 (0.7) −0.057 (0.7) 0.0065 (1) −0.0065 (1) −0.21 (0.1) −0.28 (0.03) −0.3 (0.02) 0.46 (2e−04) −0.22 (0.09) −0.029 (0.8)
CS
RA
RI
SC
Control
Water deficit
Week 1
Week 2
7'OH ABA
ABA
ABA-GE
DPA
NeoPA
PA

Figure 6: WGCNA of the leaves. Heatmap representation of the association of modules and experimental conditions for the leaf samples. Experimental conditions listed in columns and modules in rows. Module eigengene Pearson's correlation coefficient and p-value (in parenthesis) listed for each module per each experimental condition. Cell colors range from high correlation (red) to negative correlation (blue). Number of genes in each module represented by n in parenthesis after module name.

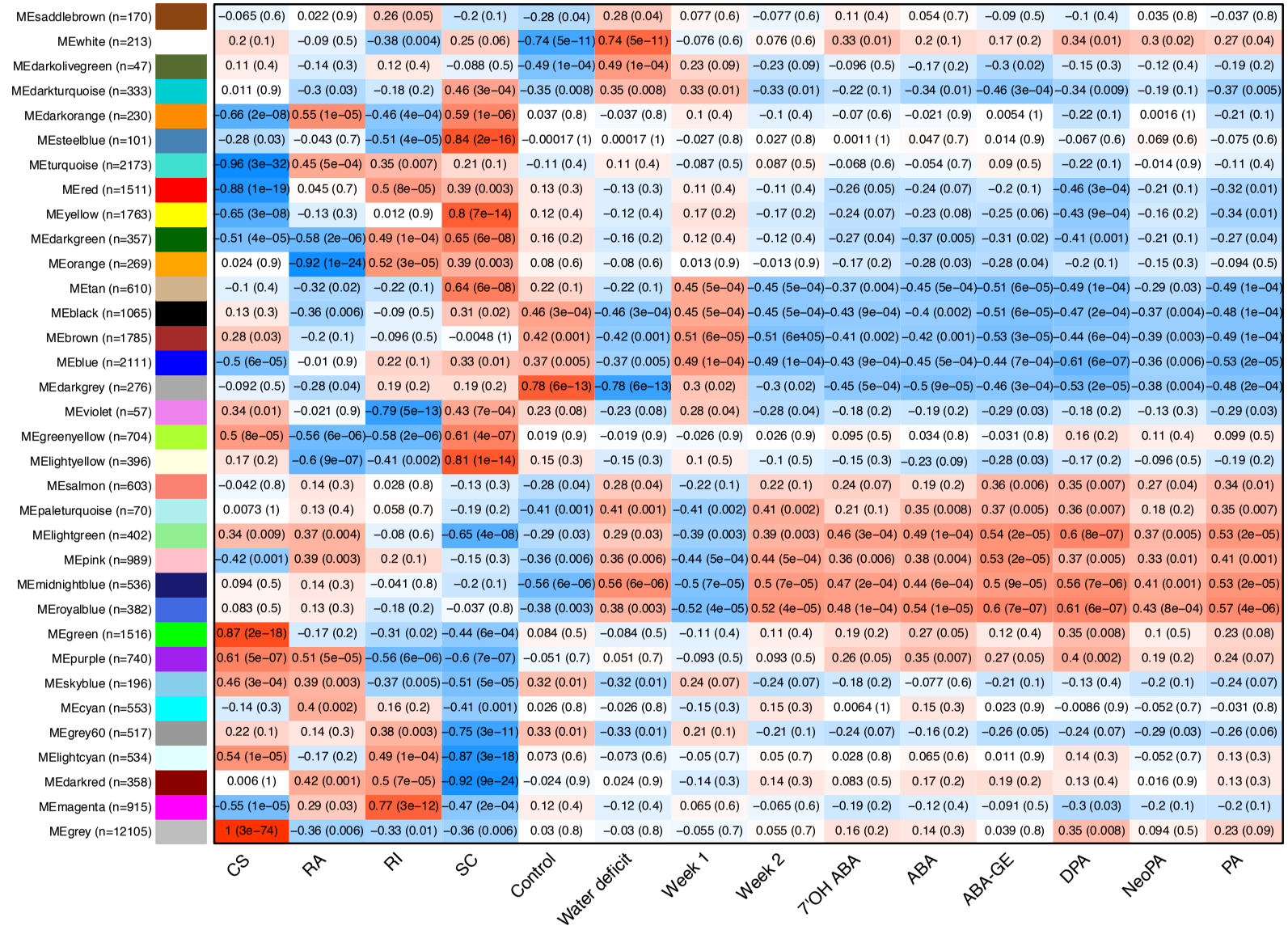
MEsaddlebrown (n=170) −0.065 (0.6) 0.022 (0.9) 0.26 (0.05) −0.2 (0.1) −0.28 (0.04) 0.28 (0.04) 0.077 (0.6) −0.077 (0.6) 0.11 (0.4) 0.054 (0.7) −0.09 (0.5) −0.1 (0.4) 0.035 (0.8) −0.037 (0.8)
MEwhite (n=213) 0.2 (0.1) −0.09 (0.5) −0.38 (0.004) 0.25 (0.06) −0.74 (5e−11) 0.74 (5e−11) −0.076 (0.6) 0.076 (0.6) 0.33 (0.01) 0.2 (0.1) 0.17 (0.2) 0.34 (0.01) 0.3 (0.02) 0.27 (0.04)
MEdarkolivegreen (n=47) 0.11 (0.4) −0.14 (0.3) 0.12 (0.4) −0.088 (0.5) −0.49 (1e−04) 0.49 (1e−04) 0.23 (0.09) −0.23 (0.09) −0.096 (0.5) −0.17 (0.2) −0.3 (0.02) −0.15 (0.3) −0.12 (0.4) −0.19 (0.2)
MEdarkturquoise (n=333) 0.011 (0.9) −0.3 (0.03) −0.18 (0.2) 0.46 (3e−04) −0.35 (0.008) 0.35 (0.008) 0.33 (0.01) −0.33 (0.01) −0.22 (0.1) −0.34 (0.01) −0.46 (3e−04) −0.34 (0.009) −0.19 (0.1) −0.37 (0.005)
MEdarkorange (n=230) −0.66 (2e−08) 0.55 (1e−05) −0.46 (4e−04) 0.59 (1e−06) 0.037 (0.8) −0.037 (0.8) 0.1 (0.4) −0.1 (0.4) −0.07 (0.6) −0.021 (0.9) 0.0054 (1) −0.22 (0.1) 0.0016 (1) −0.21 (0.1)
MEsteelblue (n=101) −0.28 (0.03) −0.043 (0.7) −0.51 (4e−05) 0.84 (2e−16) −0.00017 (1) 0.00017 (1) −0.027 (0.8) 0.027 (0.8) 0.0011 (1) 0.047 (0.7) 0.014 (0.9) −0.067 (0.6) 0.069 (0.6) −0.075 (0.6)
MEturquoise (n=2173) −0.96 (3e−32) 0.45 (5e−04) 0.35 (0.007) 0.21 (0.1) −0.11 (0.4) 0.11 (0.4) −0.087 (0.5) 0.087 (0.5) −0.068 (0.6) −0.054 (0.7) 0.09 (0.5) −0.22 (0.1) −0.014 (0.9) −0.11 (0.4)
MEred (n=1511) −0.88 (1e−19) 0.045 (0.7) 0.5 (8e−05) 0.39 (0.003) 0.13 (0.3) −0.13 (0.3) 0.11 (0.4) −0.11 (0.4) −0.26 (0.05) −0.24 (0.07) −0.2 (0.1) −0.46 (3e−04) −0.21 (0.1) −0.32 (0.01)
MEyellow (n=1763) −0.65 (3e−08) −0.13 (0.3) 0.012 (0.9) 0.8 (7e−14) 0.12 (0.4) −0.12 (0.4) 0.17 (0.2) −0.17 (0.2) −0.24 (0.07) −0.23 (0.08) −0.25 (0.06) −0.43 (9e−04) −0.16 (0.2) −0.34 (0.01)
MEdarkgreen (n=357) −0.51 (4e−05) −0.58 (2e−06) 0.49 (1e−04) 0.65 (6e−08) 0.16 (0.2) −0.16 (0.2) 0.12 (0.4) −0.12 (0.4) −0.27 (0.04) −0.37 (0.005) −0.31 (0.02) −0.41 (0.001) −0.21 (0.1) −0.27 (0.04)
MEorange (n=269) 0.024 (0.9) −0.92 (1e−24) 0.52 (3e−05) 0.39 (0.003) 0.08 (0.6) −0.08 (0.6) 0.013 (0.9) −0.013 (0.9) −0.17 (0.2) −0.28 (0.03) −0.28 (0.04) −0.2 (0.1) −0.15 (0.3) −0.094 (0.5)
MEtan (n=610) −0.1 (0.4) −0.32 (0.02) −0.22 (0.1) 0.64 (6e−08) 0.22 (0.1) −0.22 (0.1) 0.45 (5e−04) −0.45 (5e−04) −0.37 (0.004) −0.45 (5e−04) −0.51 (6e−05) −0.49 (1e−04) −0.29 (0.03) −0.49 (1e−04)
MEblack (n=1065) 0.13 (0.3) −0.36 (0.006) −0.09 (0.5) 0.31 (0.02) 0.46 (3e−04) −0.46 (3e−04) 0.45 (5e−04) −0.45 (5e−04) −0.43 (9e−04) −0.4 (0.002) −0.51 (6e−05) −0.47 (2e−04) −0.37 (0.004) −0.48 (1e−04)
MEbrown (n=1785) 0.28 (0.03) −0.2 (0.1) −0.096 (0.5) −0.0048 (1) 0.42 (0.001) −0.42 (0.001) 0.51 (6e−05) −0.51 (6e−05) −0.41 (0.002) −0.42 (0.001) −0.53 (3e−05) −0.44 (6e−04) −0.39 (0.003) −0.49 (1e−04)
MEblue (n=2111) −0.5 (6e−05) −0.01 (0.9) 0.22 (0.1) 0.33 (0.01) 0.37 (0.005) −0.37 (0.005) 0.49 (1e−04) −0.49 (1e−04) −0.43 (9e−04) −0.45 (5e−04) −0.44 (7e−04) −0.61 (6e−07) −0.36 (0.006) −0.53 (2e−05)
MEdarkgrey (n=276) −0.092 (0.5) −0.28 (0.04) 0.19 (0.2) 0.19 (0.2) 0.78 (6e−13) −0.78 (6e−13) 0.3 (0.02) −0.3 (0.02) −0.45 (5e−04) −0.5 (9e−05) −0.46 (3e−04) −0.53 (2e−05) −0.38 (0.004) −0.48 (2e−04)
MEviolet (n=57) 0.34 (0.01) −0.021 (0.9) −0.79 (5e−13) 0.43 (7e−04) 0.23 (0.08) −0.23 (0.08) 0.28 (0.04) −0.28 (0.04) −0.18 (0.2) −0.19 (0.2) −0.29 (0.03) −0.18 (0.2) −0.13 (0.3) −0.29 (0.03)
MEgreenyellow (n=704) 0.5 (8e−05) −0.56 (6e−06) −0.58 (2e−06) 0.61 (4e−07) 0.019 (0.9) −0.019 (0.9) −0.026 (0.9) 0.026 (0.9) 0.095 (0.5) 0.034 (0.8) −0.031 (0.8) 0.16 (0.2) 0.11 (0.4) 0.099 (0.5)
MElightyellow (n=396) 0.17 (0.2) −0.6 (9e−07) −0.41 (0.002) 0.81 (1e−14) 0.15 (0.3) −0.15 (0.3) 0.1 (0.5) −0.1 (0.5) −0.15 (0.3) −0.23 (0.09) −0.28 (0.03) −0.17 (0.2) −0.096 (0.5) −0.19 (0.2)
MEsalmon (n=603) −0.042 (0.8) 0.14 (0.3) 0.028 (0.8) −0.13 (0.3) −0.28 (0.04) 0.28 (0.04) −0.22 (0.1) 0.22 (0.1) 0.24 (0.07) 0.19 (0.2) 0.36 (0.006) 0.35 (0.007) 0.27 (0.04) 0.34 (0.01)
MEpaleturquoise (n=70) 0.0073 (1) 0.13 (0.4) 0.058 (0.7) −0.19 (0.2) −0.41 (0.001) 0.41 (0.001) −0.41 (0.002) 0.41 (0.002) 0.21 (0.1) 0.35 (0.008) 0.37 (0.005) 0.36 (0.007) 0.18 (0.2) 0.35 (0.007)
MElightgreen (n=402) 0.34 (0.009) 0.37 (0.004) −0.08 (0.6) −0.65 (4e−08) −0.29 (0.03) 0.29 (0.03) −0.39 (0.003) 0.39 (0.003) 0.46 (3e−04) 0.49 (1e−04) 0.54 (2e−05) 0.6 (8e−07) 0.37 (0.005) 0.53 (2e−05)
MEpink (n=989) −0.42 (0.001) 0.39 (0.003) 0.2 (0.1) −0.15 (0.3) −0.36 (0.006) 0.36 (0.006) −0.44 (5e−04) 0.44 (5e−04) 0.36 (0.006) 0.38 (0.004) 0.53 (2e−05) 0.37 (0.005) 0.33 (0.01) 0.41 (0.001)
MEmidnightblue (n=536) 0.094 (0.5) 0.14 (0.3) −0.041 (0.8) −0.2 (0.1) −0.56 (6e−06) 0.56 (6e−06) −0.5 (7e−05) 0.5 (7e−05) 0.47 (2e−04) 0.44 (6e−04) 0.5 (9e−05) 0.56 (7e−06) 0.41 (0.001) 0.53 (2e−05)
MEroyalblue (n=382) 0.083 (0.5) 0.13 (0.3) −0.18 (0.2) −0.037 (0.8) −0.38 (0.003) 0.38 (0.003) −0.52 (4e−05) 0.52 (4e−05) 0.48 (1e−04) 0.54 (1e−05) 0.6 (7e−07) 0.61 (6e−07) 0.43 (8e−04) 0.57 (4e−06)
MEgreen (n=1516) 0.87 (2e−18) −0.17 (0.2) −0.31 (0.02) −0.44 (6e−04) 0.084 (0.5) −0.084 (0.5) −0.11 (0.4) 0.11 (0.4) 0.19 (0.2) 0.27 (0.05) 0.12 (0.4) 0.35 (0.008) 0.1 (0.5) 0.23 (0.08)
MEpurple (n=740) 0.61 (5e−07) 0.51 (5e−05) −0.56 (6e−06) −0.6 (7e−07) −0.051 (0.7) 0.051 (0.7) −0.093 (0.5) 0.093 (0.5) 0.26 (0.05) 0.35 (0.007) 0.27 (0.05) 0.4 (0.002) 0.19 (0.2) 0.24 (0.07)
MEskyblue (n=196) 0.46 (3e−04) 0.39 (0.003) −0.37 (0.005) −0.51 (5e−05) 0.32 (0.01) −0.32 (0.01) 0.24 (0.07) −0.24 (0.07) −0.18 (0.2) −0.077 (0.6) −0.21 (0.1) −0.13 (0.4) −0.2 (0.1) −0.24 (0.07)
MEcyan (n=553) −0.14 (0.3) 0.4 (0.002) 0.16 (0.2) −0.41 (0.001) 0.026 (0.8) −0.026 (0.8) −0.15 (0.3) 0.15 (0.3) 0.0064 (1) 0.15 (0.3) 0.023 (0.9) −0.0086 (0.9) −0.052 (0.7) −0.031 (0.8)
MEgrey60 (n=517) 0.22 (0.1) 0.14 (0.3) 0.38 (0.003) −0.75 (3e−11) 0.33 (0.01) −0.33 (0.01) 0.21 (0.1) −0.21 (0.1) −0.24 (0.07) −0.16 (0.2) −0.26 (0.05) −0.24 (0.07) −0.29 (0.03) −0.26 (0.06)
MElightcyan (n=534) 0.54 (1e−05) −0.17 (0.2) 0.49 (1e−04) −0.87 (3e−18) 0.073 (0.6) −0.073 (0.6) −0.05 (0.7) 0.05 (0.7) 0.028 (0.8) 0.065 (0.6) 0.011 (0.9) 0.14 (0.3) −0.052 (0.7) 0.13 (0.3)
MEdarkred (n=358) 0.006 (1) 0.42 (0.001) 0.5 (7e−05) −0.92 (9e−24) −0.024 (0.9) 0.024 (0.9) −0.14 (0.3) 0.14 (0.3) 0.083 (0.5) 0.17 (0.2) 0.19 (0.2) 0.13 (0.4) 0.016 (0.9) 0.13 (0.3)
MEmagenta (n=915) −0.55 (1e−05) 0.29 (0.03) 0.77 (3e−12) −0.47 (2e−04) 0.12 (0.4) −0.12 (0.4) 0.065 (0.6) −0.065 (0.6) −0.19 (0.2) −0.12 (0.4) −0.091 (0.5) −0.3 (0.03) −0.2 (0.1) −0.2 (0.1)
MEgrey (n=12105) 1 (3e−74) −0.36 (0.006) −0.33 (0.01) −0.36 (0.006) 0.03 (0.8) −0.03 (0.8) −0.055 (0.7) 0.055 (0.7) 0.16 (0.2) 0.14 (0.3) 0.039 (0.8) 0.35 (0.008) 0.094 (0.5) 0.23 (0.09)
CS
RA
RI
SC
Control
Water deficit
Week 1
Week 2
7'OH ABA
ABA
ABA-GE
DPA
NeoPA
PA

Figure 7: WGCNA of the roots. Heatmap representation of the association of modules and experimental conditions for the root samples. Experimental conditions listed in columns and modules in rows. Module eigengene Pearson's correlation coefficient and p-value (in parenthesis) listed for each module per each experimental condition. Cell colors range from high correlation (red) to negative correlation (blue). Number of genes in each module represented by n in parenthesis after module name.

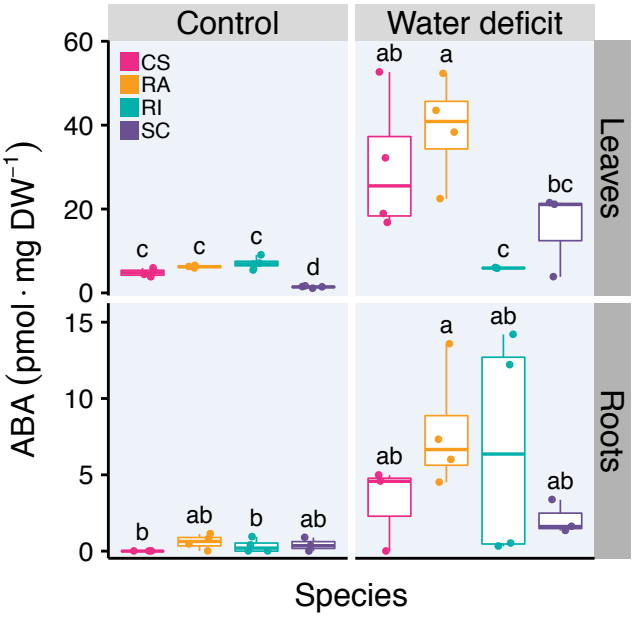

Figure 8: ABA concentrations after one-week of severe WD. ABA concentrations (pmol·mg DW^{-1}) in leaves (top) and roots (bottom) after one-week of Control (left) or WD (right) treatment. Two-way ANOVA Tukey's HSD ($p \leq 0.05$) letters for each metabolite per organ per week. Pink, orange, blue and purple correspond to CS, RA, RI, and SC respectively. Each point represents an individual measurement. n = three-five individual vines.

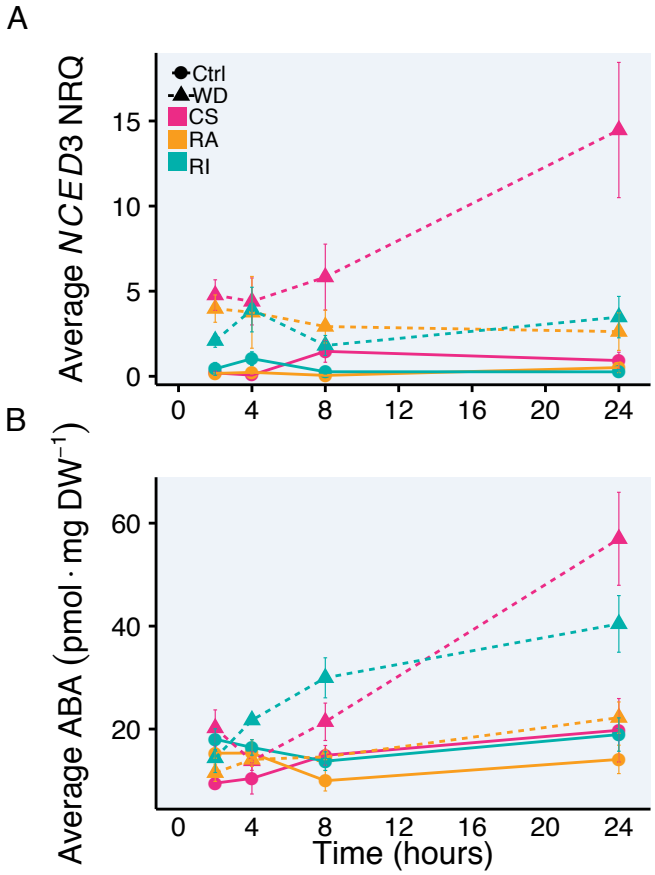

Figure 9: *NCED3* transcript NRQ and ABA concentrations after severe rapid dehydration. A) Relative *NCED3* transcript abundance (NRQ) and **B**) ABA concentrations (pmol·mg DW^{-1}) in leaves after 2, 4, 8, and 24 hours of Control (solid line and circles) or rapid dehydration WD (dotted line and triangles) treatment. Two-way ANOVA Tukey's HSD ($p \leq 0.05$) letters for each metabolite per organ per week. Pink, orange, blue and purple correspond to CS, RA, RI, and SC respectively. Mean ± SE, n = three-five individual vines.

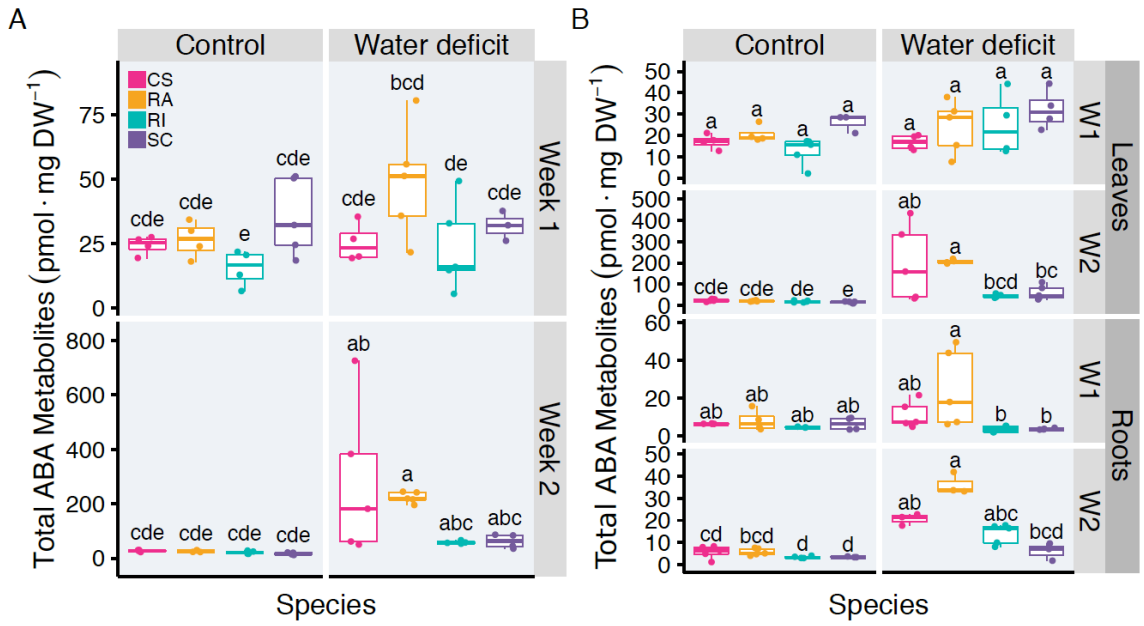

Supplemental File 1: Summed total whole plant ABA metabolite concentration and summed total whole plant ABA metabolite concentration per organ after one- and two-weeks of moderate WD. A) Combined ABA, ABA-GE, 7'OH ABA, NeoPA, PA, and DPA concentrations from both leaves and roots (Total ABA Metabolites (pmol·mg DW^{-1})) referred to as summed total of whole plant ABA metabolites after one- (top) and two-weeks (bottom) of Control (left) or WD (right) treatment. Three-way ANOVA Tukey's HSD ($p \leq 0.05$). B) Combined ABA, ABA-GE, 7'OH ABA, NeoPA, PA, and DPA concentrations (Total ABA Metabolites (pmol·mg DW^{-1})) for leaves (top) and roots (bottom) after one- (top) and two-weeks (bottom) of Control (left) or WD (right) treatment. Two-way ANOVA Tukey's HSD ($p \leq 0.05$) letters per organ per week. Pink, orange, blue and purple correspond to CS, RA, RI, and SC respectively. Each point represents an individual measurement. n = three-five individual vines.

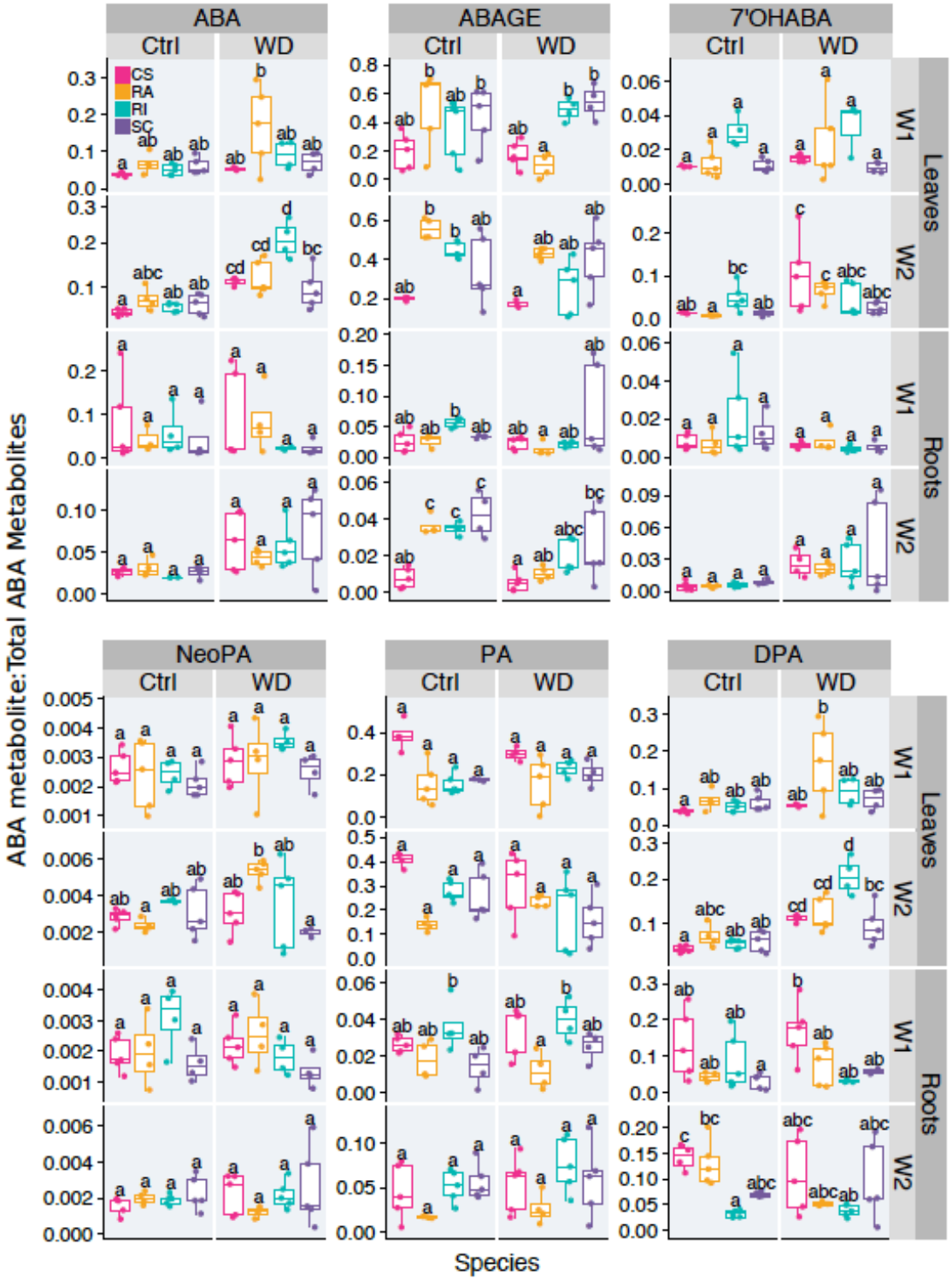

Supplemental File 2: ABA metabolite distribution relative to total whole plant ABA metabolites per organ after one- and two-weeks of moderate WD. ABA, ABA-GE,

7’OH ABA (left to right top), NeoPA, PA, and DPA (left to right bottom) ratio relative to summed total of whole plant ABA metabolites in leaves (top) and roots (bottom) after one- and two-weeks of Control (Ctrl) or WD treatment. Two-way ANOVA Tukey’s HSD ($p \leq 0.05$) letters for each metabolite per organ per week. Pink, orange, blue and purple correspond to CS, RA, RI, and SC respectively. Each point represents an individual measurement. n = three-five individual vines.

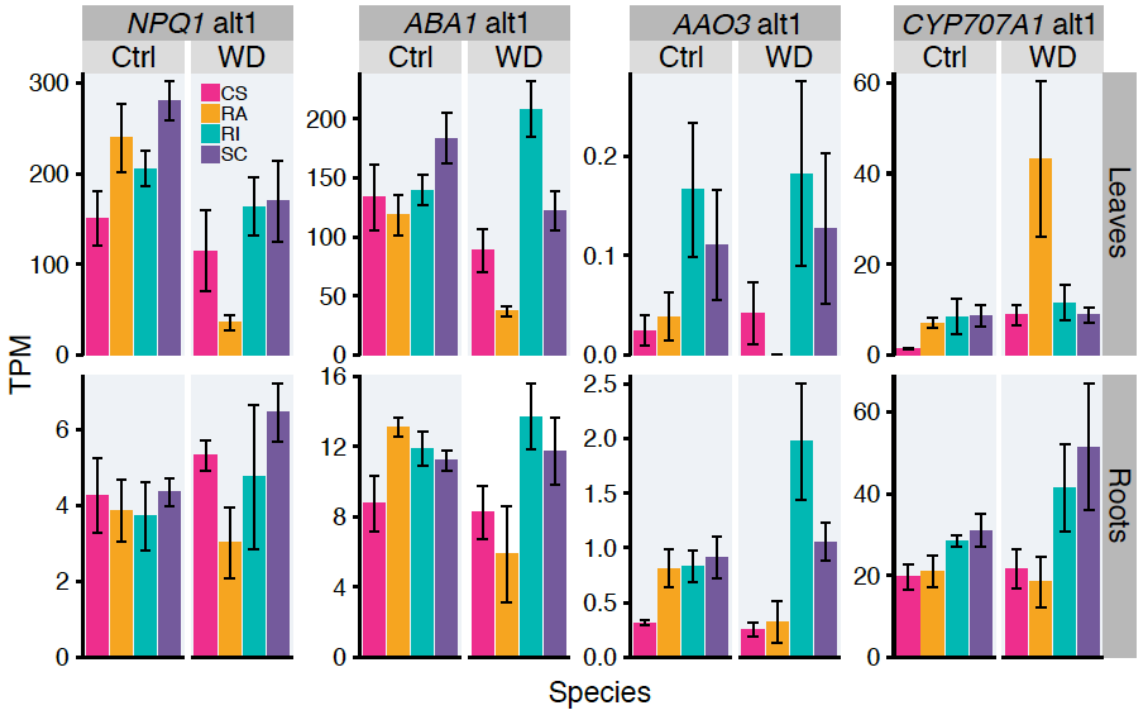

Supplemental File 3: Differentially expressed ABA metabolism genes in RA WD W2 leaves and roots. *NPQ1* alt1, *ABA1* alt1, *AAO3* alt1, and *CYP707A1* alt1 (left to right) expression represented as TPM after two-weeks of Control (Ctrl) (left) or WD (right) treatment in leaves (top) and roots (bottom). Pink, orange, blue and purple correspond to CS, RA, RI, and SC respectively. Mean ± SE, n = three-five individual vines.

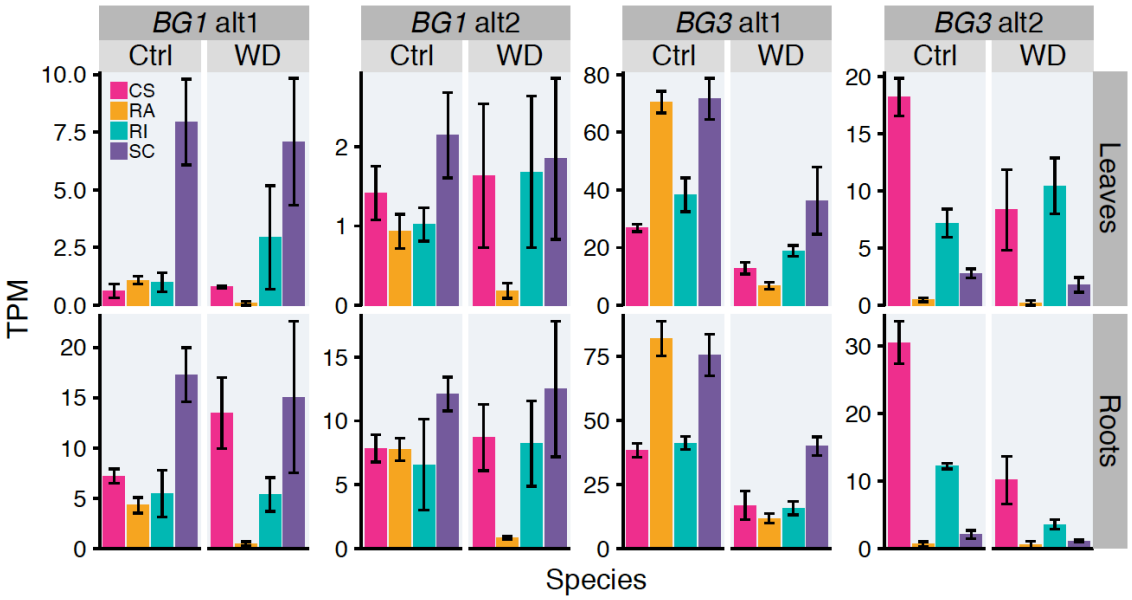

Supplemental File 4: *BG1* and *BG3* transcript abundance after one- and two-weeks of moderate WD. *BG1* alt1 and alt2 and *BG3* alt1 and alt2 (left to right) expression represented as TPM after two-weeks of Control (Ctrl) (left) or WD (right) treatment in leaves (top) and roots (bottom). Pink, orange, blue and purple correspond to CS, RA, RI, and SC respectively. Mean ± SE, n = three-five individual vines.

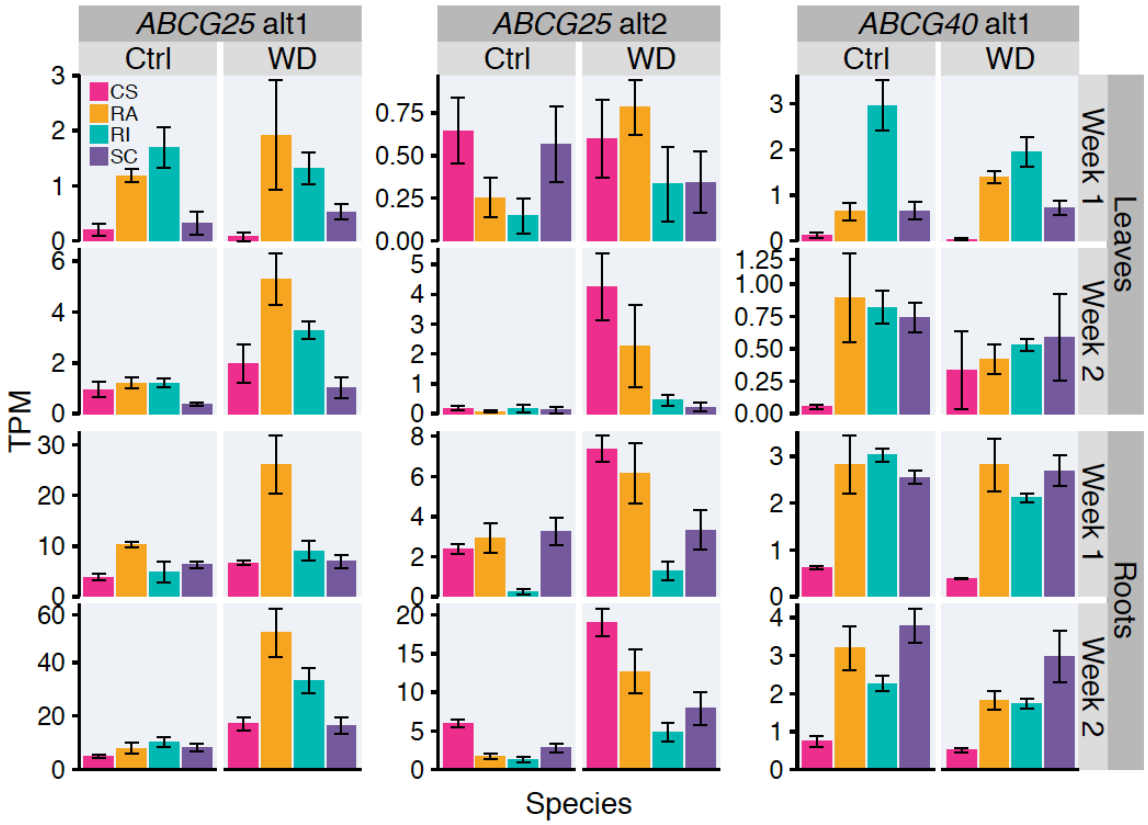

Supplemental File 5: *ABCG* transcript abundance after one- and two-weeks of moderate WD. *ABCG25* alt1 and alt2, and *ABCG40* alt1 (left to right) expression represented as TPM after one- (top) and two-weeks (bottom) of Control (Ctrl) (left) or WD (right) treatment in leaves (top) and roots (bottom). Pink, orange, blue and purple correspond to CS, RA, RI, and SC respectively. Mean ± SE, n = three-five individual vines.

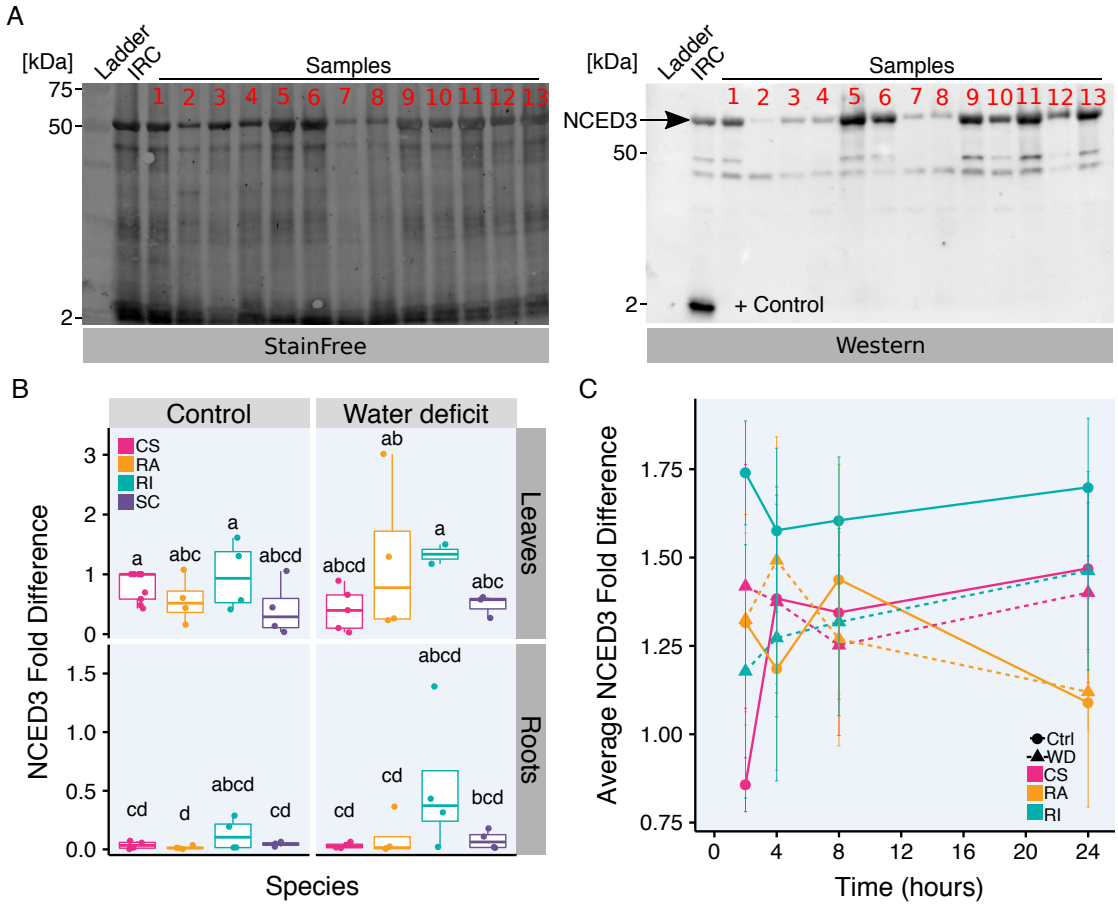

Supplemental File 6: One-week severe water deficit and rapid dehydration NCED3 Western blots. A) Representative example of StainFree membrane and representative example of antiNCED3 probed Western Blot. Each gel was loaded with ladder (relevant ladder kDa bands indicated), IRC (35 μg CS Control sample + antiNCED3 target peptide (2 kDa) as a positive control), and 13 samples (35 μg total protein extract). Samples 1-4 are RA Control leaves. Samples 5-8 are RA WD leaves. Samples 9-11 are RI Control leaves. Samples 12-13 are RI WD leaves. Samples varied per gel. All samples were run on 3-4 individual gels. Western blots were normalized to a range of total protein on the StainFree membrane image excluding imperfections. Samples were normalized to the same IRC on each gel using 67 kDa band corresponding to NCED3 to quantify relative NCED3 protein fold difference. Additional NCED3 Western blot bands may correspond to NCED3 subunits. **B**) Relative NCED3 fold difference after one-week Control (left) or severe WD (right) in leaves (top) and roots (bottom). Samples are the same as in **A**). 2-way ANOVA Tukey's HSD ($p < 0.05$) letters for each metabolite per organ per week. Each point represents an individual measurement. n = three-five individual vines. **C**) Average relative NCED3 fold difference after 2, 4, 8, or 24 hours Control (Ctrl) (solid line and circles) or rapid dehydration WD (dotted line and triangles) relative to CS Control leaf IRC loaded on each gel. 2-way ANOVA Tukey's HSD ($p < 0.05$) no significant difference for each

metabolite per organ per week. Mean ± SE, n = three-five individual leaves. Pink, orange, blue and purple correspond to CS, RA, RI, and SC respectively.

CHAPTER 6
CONCLUSION

Summary of research and developed methods

Previous work identified two genes (*VviERF6L1* and *NCED3*) in grapevine involved in abiotic stress response and ABA signaling that required further investigation and characterization (Cochetel et al., 2020; Cramer et al., 2014; Rattanakon et al., 2016). These genes were hypothesized to function as hub genes or genes highly connected to numerous other genes the disruption of which would impact signaling in various ABA-dependent responses. Specifically, *VviERF6L1* was hypothesized to function as a pleiotropic abiotic stress hub gene in *Vitis*. *NCED3* transcript accumulation and ABA biosynthesis were hypothesized to be a core water deficit response reflective of cultivar-specific drought tolerance during abiotic stress. To test these hypotheses, multi-level analyses of DNA, RNA, protein, and metabolite quantification in diverse *Vitis* species including *Vitis vinifera* cv. Cabernet Sauvignon (CS), *Vitis champinii* cv. Ramsey (RA), *Vitis riparia* cv. Riparia Gloire (RI), and *Vitis vinifera* x *Vitis girdiana* cv. SC2 (SC) were performed.

Before focusing on the genes of interest individually, ABA response elements (ABREs) were annotated for all Pinot Noir (PN40024) reference genome promoter regions using a bioinformatics approach to further substantiate the abiotic stress responses of *VviERF6L1*, *NCED3,* and other genes that were previously observed (Cochetel et al., 2020; Cramer et al., 2014; Rattanakon et al., 2016). ABREs were hypothesized to be highly abundant (more so than was previously reported (Wong et al., 2017)) in grapevine promoter regions. Using a more comprehensive set of ABREs than before (Wong et al., 2017), extensive promoter regions (-3,000 bp), and the new v3 PN40024 genome, ABREs were confirmed to be highly abundant in the grapevine reference genome. At least one ABRE

was present in the majority of all promoter regions. The presence of various ABREs in the *ERF6L1* and *NCED3* promoter regions supported the hypothesis that these genes were involved in ABA signaling and partially explained previous transcriptional responses observed in response to abiotic stresses.

ERF6Ls were previously identified as a novel clade in grapevine hypothesized to be involved in ABA and ethylene signaling, berry development, cold, and water deficit responses (Cramer et al., 2014; Hopper et al., 2016). Meta-data analysis of publicly available microarray and RNA-Seq data series confirmed the *VviERF6L* clade to transcriptionally respond to numerous stimuli including water deficit, cold, salinity, pathogen infection, wounding, and berry ripening (Toups et al., 2020). *VviERF6Ls* were expressed in many tissues including leaves, roots, and berries. However, the hypothesis that *VviERF6L1* was a hub gene was not supported, and *VviERF6Ls* were generally lowly (although significantly) differentially expressed during abiotic stress responses. Some of the highest differential expression of *VviERF6Ls* was in response to pathogens and wounding (Toups et al., 2020).

The hypothesis of *VviERF6L1* function in grapevine was revised to *VviERF6L1* increases resistance to certain pathogens, and the challenge became identifying the specific pathogens those may be. This new hypothesis was based on differentially expressed genes in *VviERF6L1* overexpression vines all being involved in pathogen response, and pathogen response cis-acting elements like the WBOXATNPR1 in the *VviERF6L1* promoter region (Toups et al., 2020). This hypothesis was also supported by known effects of *ERF5* and *ERF6 Arabidopsis thaliana* orthologs on pathogen susceptibility (Moffat et al., 2012; Son et al., 2012). To test the functional role of *VviERF6L1* in pathogen response, the

susceptibility of *VviERF6L1* overexpression vines to *Pseudomonas syringae* was compared to that of empty vector control vines. A grapevine-optimized *P. syringae* infection assay was established. Using this novel assay, *VviERF6L1* was demonstrated to have significantly higher transcript abundance in response to *P. syringae* than mock inoculation early during infection in detached Cabernet Sauvignon leaves. Additionally, *VviERF6L1* overexpression vines had significantly fewer colony-forming units during *P. syringae* infection and thereby higher resistance than empty vector control vines. These experiments supported the hypothesis that *VviERF6L1* increases grapevine tolerance to *P. syringae*. Additional studies are ongoing in collaboration with Dr. Lance Cadle Davidson at Cornell University to investigate potential roles of *VviERF6L1* for mildew resistance in grapevine.

To test the hypothesis that *NINE-CIS-EPOXYCAROTENOID DIOXYGENASE* (*NCED3)* is a hub gene in response to water deficit, *NCED3* transcripts, NCED3 protein, and ABA concentration were quantified in the leaves and roots of four *Vitis* species in response to three different water deficit severities using RNA-Seq, RT-qPCR, western blots, and HPLC-MS/MS. Not only was *NCED3* identified as a hub gene, but *NCED3* was identified as the only ABA metabolism gene that was a hub gene in water deficit response, supporting this hypothesis. *NCED3* transcript accumulation and ABA metabolism (particularly ABA biosynthesis) were validated as a major part of the core water deficit responses in the four *Vitis* species. However, ABA metabolism was highly dependent on species, organ, stress severity, and stress duration during water deficit. The ABA concentration and *NCED3* transcript abundance reflected previously described physiological responses (Cochetel et al., 2020) with more drought-tolerant grapevines

having higher ABA concentrations earlier in water deficit treatment. Overall, the drought-tolerant Texan grapevine, RA, was found to respond earlier and more sensitively during longer-term moderate and severe water deficits than the other more water deficit sensitive species like RI.

This research incorporated the novel aspect of quantifying ABA biosynthesis at the gene (*NCED3* transcript abundance), protein (NCED3 protein abundance), and metabolite (ABA concentration) levels in grapevine. It was hypothesized *NCED3* transcripts would mirror NCED3 protein abundance that in turn would correlate to ABA concentration during water deficit. Interestingly, *NCED3* transcript abundance paralleled ABA concentration, but this similarity was not maintained for NCED3 protein. It is well-established transcript abundance does not always equate to protein abundance (Greenbaum et al., 2003; Jia et al., 2018; Liu and Aebersold, 2016; Liu et al., 2016; Perl et al., 2017). However, it was surprising that NCED3 protein abundance did not significantly change in response to water deficit. Although NCED3 protein quantification with western blots did not support the hypothesis that *NCED3* transcripts correlate with NCED3 protein under water deficit conditions, different water deficit conditions or more sensitive protein quantification techniques may reveal a different pattern in future experiments.

Future research directions

The ABRE containing promoter sequences may be utilized to identify novel motifs associated with ABA signaling and abiotic stress response (Bailey et al., 2009). Many novel and uncharacterized genes were also identified in this analysis, having higher

numbers of ABREs in respective promoter regions that may provide valuable targets for future studies to improve grapevine breeding programs and abiotic stress tolerance. Genes containing ABREs provide a valuable resource for marker-assisted breeding programs to use in the future to improve drought or abiotic stress tolerance. Additionally, clustering of genes with numerous ABREs, such as was observed on chromosome 18 in the PN40024 genome, may be used to identify an ABA response locus in grapevine.

Further pathogen studies should be implemented to investigate the role not only of *VviERF6L1* but the whole *VviERF6L* clade in pathogen response. Development of a multi-*erf6l* knockdown vine would be particularly useful for furthering the functional characterization of this highly conserved clade. This work identified *VviERF6L1* plays a role in pathogen response likely through salicylic acid, but it is unclear if *ERF6Ls* are also involved in jasmonic acid-dependent pathogen and pest response, and the link to ethylene is still unclear. Additionally, the grapevine-optimized *P. syringae* infection assay can be used to characterize the susceptibility of different grapevine cultivars and species to *P. syringae* to identify resistant vines. Further research may be performed to investigate the compounding effects of abiotic and biotic stress on grapevine as well as the potential preclusion to secondary infections following *P. syringae* infection in grapevine (Whitelaw-Weckert et al., 2011).

The importance and role of *NCED3* in ABA biosynthesis and abiotic stress response is widely studied in plants (Beardsell and Cohen, 1975; Cheng et al., 2014; Nambara and Marion-Poll, 2005), but very few studies have investigated the NCED3 protein let alone related it to *NCED3* transcript and ABA abundances. Additionally, the ABA metabolism of these four grapevines was not characterized before this work. The

Western blots performed to quantify NCED3 protein abundance may have not been sensitive enough to observe subtle differences in protein content, and further work should be performed to understand how NCED3 is regulated at the protein level during water deficit and other abiotic stresses in grapevine and other plant species. NCED3 protein concentration may be better determined using ELISAs (Engvall and Perlmann, 1971) or LC-MS/MS. NCED3 also has putative post-translational modifications (Cruz et al., 2019) that require further understanding.

Concluding remarks

The work performed throughout this dissertation contributed publicly available RNA-Seq data, annotation of grapevine ABREs, and a grapevine-optimized *P. syringae* infection assay to the scientific community. These contributions can be implemented in future studies and experiments. The goal of this dissertation was to improve the characterization of *VviERF6Ls* and *NCED3* in grapevine by testing the hypothesis that these genes were hubs in ABA signaling and abiotic stress response. Although only *NCED3* was supported as a hub gene, these analyses brought new insight into the roles of these genes during abiotic and biotic stress as well as ABA signaling in different grapevine species. *VviERF6L1* was determined to enhance grapevine resistance to *P. syringae*, and *NCED3* was validated as a core part of water deficit response across *Vitis* species.

References

Bailey, T.L., Boden, M., Buske, F.A., Frith, M., Grant, C.E., Clementi, L., Ren, J., Li, W.W., and Noble, W.S. (2009). MEME Suite: tools for motif discovery and searching. Nucleic Acids Res. *37*, W202–W208.

Beardsell, M.F., and Cohen, D. (1975). Relationships between Leaf Water Status, Abscisic Acid Levels, and Stomatal Resistance in Maize and Sorghum. PLANT Physiol. *56*, 207–212.

Cheng, Z.J., Zhao, X.Y., Shao, X.X., Wang, F., Zhou, C., Liu, Y.G., Zhang, Y., and Zhang, X.S. (2014). Abscisic Acid Regulates Early Seed Development in Arabidopsis by ABI5-Mediated Transcription of SHORT HYPOCOTYL UNDER BLUE1[C][W][OPEN]. Plant Cell *26*, 1053–1068.

Cochetel, N., Ghan, R., Toups, H.S., Degu, A., Tillett, R.L., Schlauch, K.A., and Cramer, G.R. (2020). Drought tolerance of the grapevine, Vitis champinii cv. Ramsey, is associated with higher photosynthesis and greater transcriptomic responsiveness of abscisic acid biosynthesis and signaling. BMC Plant Biol. *20*.

Cramer, G.R., Ghan, R., Schlauch, K.A., Tillett, R.L., Heymann, H., Ferrarini, A., Delledonne, M., Zenoni, S., Fasoli, M., and Pezzotti, M. (2014). Transcriptomic analysis of the late stages of grapevine (Vitis vinifera cv. Cabernet Sauvignon) berry ripening reveals significant induction of ethylene signaling and flavor pathways in the skin. BMC Plant Biol. *14*.

Cruz, E.R., Nguyen, H., Nguyen, T., and Wallace, I.S. (2019). Functional analysis tools for post-translational modification: a post-translational modification database for analysis of proteins and metabolic pathways. Plant J. *99*, 1003–1013.

Engvall, E., and Perlmann, P. (1971). Enzyme-linked immunosorbent assay (ELISA) quantitative assay of immunoglobulin G. Immunochemistry *8*, 871–874.

Greenbaum, D., Colangelo, C., Williams, K., and Gerstein, M. (2003). Comparing protein abundance and mRNA expression levels on a genomic scale. Genome Biol. *4*, 117.

Hopper, D.W., Ghan, R., Schlauch, K.A., and Cramer, G.R. (2016). Transcriptomic network analyses of leaf dehydration responses identify highly connected ABA and ethylene signaling hubs in three grapevine species differing in drought tolerance. BMC Plant Biol. *16*.

Jia, H., Sun, W., Li, M., and Zhang, Z. (2018). Integrated Analysis of Protein Abundance, Transcript Level, and Tissue Diversity To Reveal Developmental Regulation of Maize. J. Proteome Res. *17*, 822–833.

Liu, Y., and Aebersold, R. (2016). The interdependence of transcript and protein abundance: new data–new complexities. Mol. Syst. Biol. *12*.

Liu, Y., Beyer, A., and Aebersold, R. (2016). On the Dependency of Cellular Protein Levels on mRNA Abundance. Cell *165*, 535–550.

Moffat, C.S., Ingle, R.A., Wathugala, D.L., Saunders, N.J., Knight, H., and Knight, M.R. (2012). ERF5 and ERF6 Play Redundant Roles as Positive Regulators of JA/Et-Mediated Defense against Botrytis cinerea in Arabidopsis. PLoS ONE *7*.

Nambara, E., and Marion-Poll, A. (2005). Abscisic acid biosynthesis and catabolism. Annu. Rev. Plant Biol. *56*, 165–185.

Perl, K., Ushakov, K., Pozniak, Y., Yizhar-Barnea, O., Bhonker, Y., Shivatzki, S., Geiger, T., Avraham, K.B., and Shamir, R. (2017). Reduced changes in protein compared to mRNA levels across non-proliferating tissues. BMC Genomics *18*, 305.

Rattanakon, S., Ghan, R., Gambetta, G.A., Deluc, L.G., Schlauch, K.A., and Cramer, G.R. (2016). Abscisic acid transcriptomic signaling varies with grapevine organ. BMC Plant Biol. *16*.

Son, G.H., Wan, J., Kim, H.J., Nguyen, X.C., Chung, W.S., Hong, J.C., and Stacey, G. (2012). Ethylene-Responsive Element-Binding Factor 5, ERF5, Is Involved in Chitin-Induced Innate Immunity Response. Mol. Plant. Microbe Interact. *25*, 48–60.

Toups, H.S., Cochetel, N., Gray, D., and Cramer, G.R. (2020). VviERF6Ls: an expanded clade in Vitis responds transcriptionally to abiotic and biotic stresses and berry development. BMC Genomics *21*.

Whitelaw-Weckert, M.A., Whitelaw, E.S., Rogiers, S.Y., Quirk, L., Clark, A.C., and Huang, C.X. (2011). Bacterial inflorescence rot of grapevine caused by Pseudomonas syringae pv. syringae. Plant Pathol. *60*, 325–337.

Wong, D.C.J., Lopez Gutierrez, R., Gambetta, G.A., and Castellarin, S.D. (2017). Genome-wide analysis of cis-regulatory element structure and discovery of motif-driven gene co-expression networks in grapevine. DNA Res. Int. J. Rapid Publ. Rep. Genes Genomes *24*, 311–326.

APPENDICES

CHAPTER 2: ABRES IN PN40024 GRAPEVINE REFERENCE GENOME PROMOTER REGIONS

Appendix 1: Coordinates of all annotated ABREs in the PN40024 grapevine reference genome. The ABRE variant, gene name, start and stop coordinates, length and strand of each ABRE present in the PN40024 grapevine reference genome. Number of total ABREs summarized per gene, number of total ABRE variants, and consensus ABRE occurrences.

CHAPTER 3: VviERF6LS: AN EXPANDED CLADE IN VITIS RESPONDS TRANSCRIPTIONALLY TO ABIOTIC AND BIOTIC STRESSES AND BERRY DEVELOPMENT

Appendix 1: PN40024 and Cabernet Sauvignon (CS) VviERF6L protein motif consensus sequences. Motif number (given based on E-value ranking), amino acid sequence, conservation (E-value), and length (amino acid residues) of the nine highly conserved protein motifs in PN40024 and CS VviERF6L proteins.

Appendix 2: PN40024 VviERF6L protein motif coordinates including consensus motif, and VviERF6L specific motif sequence, start and stop residue positions.

Appendix 3: PN40024 VviERF6L ERF domain percent identity with closest *Arabidopsis thaliana* ERF domain ortholog.

Appendix 4: Cabernet Sauvignon (CS) *VviERF6L* protein motif coordinates including start position, motif number and consensus motif.

Appendix 5: Percent identity of PN40024 and Cabernet Sauvignon (CS) VviERF6L protein motifs.

Appendix 6: Cabernet Sauvignon (CS) *VviERF6L* gene names, protein sequences and protein length. Average length of all 26 at bottom.

Appendix 7: PN40024, CS, CA, and CH *VviERF6Ls* and all PN40024 VviERF protein sequences used to create phylogenetic tree.

Appendix 8: PN40224 *VviERF6L* putative promoter region (-3000 bp) motif coordinates. Motif name, start site relative to transcription start site, sequence, PLACE identification number, Vitis gene name, and corresponding *VviERF6L* name are given.

Appendix 9: PN40024 *VviERF6L* promoter (-3000 bp) motif frequency. Including motif name, frequency in each *VviERF6L* denoted by common and gene names.

Appendix 10: Expression of *VviERF6Ls* across grapevine tissues and organs from the grapevine expression Atlas.

Appendix 11: Meta-data analysis of microarrays and RNA-seq series downloaded from NCBI GEO and SRA and investigated for VviERF6L expression.

Appendix 12: Annotation and number of cross hybridizing *VviERF6L* probes.

Appendix 13: Differential expression analysis contrasts of interest for PRJNA516950. Including contrast number (arbitrarily assigned), species, treatment, organ, and week for both sample groups being compared.

Appendix 14: List of genes co-expressed with *VviERF6L* clade in four out of five data series. Gene ID and corresponding annotation. The four RNA-Seq data series the genes were co-expressed with the *VviERF6L* clade is listed.

Appendix 15: Fold increase of *VviERF6L12* expression relative to average expression of all other *VviERF6Ls*. Expression value of *VviERF6L12* and average value of all other *VviERF6Ls* across all conditions for each data series with each data series' respective units. Fold increase of *VviERF6L12* expression taken as ratio of *VviERF6L12* expression relative to average expression value of all other *VviERF6Ls* across all conditions per data series.

Appendix 16: Morphological phenotyping measurements taken that were not statistically significant between OX VviERF6L1 and empty vector control lines. Measurements were collected over the span of three weeks to 3 years. Data were tested for significant differences between empty vector control line (G1) and overexpression lines (L12-1, 2, 3, 11, and 23). Assumptions were met for tests used to determine significance.

Appendix 17: Annotations of differentially expressed genes in three *VviERF6L1* overexpression lines relative to empty vector control.

Appendix 18: Primers used for RT-qPCR analysis. Primers were designed using primer 3 and NCBI's primer design tool. Primers were designed to be specific for genes of interest and respectful of RT-qPCR settings and specifications.

CHAPTER 5: A MULTI-LEVEL ANALYSIS OF ABSCISIC ACID METABOLISM REVEALS SPECIES-SPECIFIC RESPONSES TO WATER DEFICIT IN GRAPEVINE

Appendix 1: ABA biosynthesis, conjugation, and catabolism genes. Cabernet Sauvignon (CS) clone 8 v1.0, PN40024 V2 genome V3 annotation, and PN40024 V2 genome V2 annotation IDs listed with corresponding gene symbol, alternative, ABA related metabolic process, gene description, and leaf and root WGCNA module with the highest Eigengene value. Annotation listed from ORCAE PN40024 orthologs. Green and blue correspond to Eigengene values ≥ 0.8 in the leaves and roots respectively. Alternative were assigned as "alt1" if only 1 paralog was identified based on V3 annotation. Alternatives were assigned as "alt1" and "alt2" when two paralogs were identified with "alt1" corresponding to the primary contig and "alt2" correspond to the haplotig denoted as "P" and "H" respectively in CS gene names. When multiple paralogs were identified corresponding to multiple V3 genes with the same annotation symbol, "alt1_1" and "alt2_1" were named to correspond to CS alleles with the same V3 gene name. Paralogs with only one allele with the same annotation symbol as other V3 genes are indicated as "alt1_2" and "alt1_3".

Appendix 2: WD vs. Control (Ctrl) differential expression analysis results per genotype per organ per week. Each tab contains the results from a single differential expression analysis contrast. Contrasts are listed alphabetically by genotype and organ and numerically by week. Leaves are abbreviated as L. Roots are abbreviated as R. Control is abbreviated at Ctrl. Other abbreviations are consistent with the text. ABA metabolism genes are at the top of each contrast. Significantly differentially expressed ABA metabolite genes are denoted in blue and paired with relevant gene symbol and metabolic process (biosynthesis, conjugation, catabolism, or transport). Preliminary annotation of ABA metabolite genes and alt assignment is in Appendix 2.

Appendix 3: RA WD vs. CS, RI, and SC WD differential expression analysis results per organ per week. Each tab contains the results from a single differential expression analysis contrast. Contrasts are listed alphabetically by genotype and organ and numerically by week. Leaves are abbreviated as L. Roots are abbreviated as R. Other abbreviations are consistent with the text. ABA metabolism genes are at the top of each contrast. Significantly differentially expressed ABA metabolite genes are denoted in blue and paired with relevant gene symbol and metabolic process (biosynthesis, conjugation, catabolism, or transport). Preliminary annotation of ABA metabolite genes and alt assignment is in Appendix 2.

Appendix 4: Gene module Eigengene values for leaves and roots. For each gene (rows), the kME and p-values are presented for each module (columns). The second columns contains annotation information for each gene.

Appendix 5: Gene ontology of leaf and root WD and ABA metabolite positively correlated gene modules. GO ID, Term, total genes annotated with a GO ID, number of genes that were significantly linked to a GO ID out of the top 500 most correlated genes selected for gene ontology for each gene module of interest, expected number of genes that would be linked to a GO ID, and Fisher statistic stated for each module of interest. Modules of interest are listed per tab with relevant organ and module color from Figs. 8 and 9 and Supplemental File 4.

Appendix 6: antiNCED3 sequences and target information. antiNCED3 target gene name, target size (kD), target sequence, and target sequence length (AA). Cys- indicates a non-coding cysteine added for production purposes.

Appendix 7: Physiological measurements performed on rapid dehydration leaves. Stem water potential [Ψstem (Mpa)], solute pressure [Ψs (Mpa)], turgor pressure [Ψp (Mpa)], stomatal conductance [Gs (mol H2O·m-2 ·s-1)], photosynthesis [Ps (μmol·m-2 ·s-1)], and water content (%) averaged for all times and genotypes for Control (Ctrl) and WD (mean ± SE). Three-way ANOVA p-values displayed (p-value < 0.05 considered *), n = three-five individual leaves.

Appendix 8: NCED3 NRQ and ABA concentration statistics for rapid dehydration. Two-way ANOVA was per time point on species and treatment for NCED3 NRQ and ABA concentration followed by Tukey's HSD. Control abbreviated as Ctrl. Two-way ANOVA Tukey's HSD ($p < 0.05$) letters. There was no significant difference for any genotype, treatment, or time point for NCED3 fold difference.